PROCEEDINGS OF THE ELEVENTH WORKSHOP

ON

GENERAL RELATIVITY AND GRAVITATION

in JAPAN

WASEDA UNIVERSITY, TOKYO, JAPAN

JANUARY 9 – 12, 2002

Edited by

Jun-ichirou Koga, Kei-ichi Maeda,
Takashi Nakamura, Kenji Tomita

PREFACE

The eleventh workshop on General Relativity and Gravitation was held at the International Conference Center of Waseda University from January 9th to 12th, 2002. The main purpose of this workshop was to review the latest developments in General Relativity and gravitation. The topics covered also include particle physics, astrophysics and cosmology. A further purpose was to promote lively and stimulating interaction between researchers working in these fields.

The workshop was organized as an international conference. There were 79 talks totally, among which are 13 talks from overseas. All of the 9 invited talks and the 3 semi-invited talks were given in English, and so were most of the contributed talks as well. The workshop was quite successful with more than 150 participants. We wish to thank all the participants for their contribution to the workshop.

We would like to thank Mrs.Yokota, the secretary at the Department of Physics, Kyoto University, for her devoted transaction of various official works. We are also grateful to the graduate students of the astrophysics group in Waseda University for their cooperation in management of the workshop. The workshop would not have been successful without their help. This workshop was financially supported by Monbukagakusho Grant-in-Aid for Scientific Research, No.12440063 and Grant-in-Aid for Creative Scientific Research, No.09NP0801.

Program (Table of Contents)

Thursday, January 10

Morning Session I (Chairman: K. Tomita)

Morning Session II (Chairman: M. Shibata)

Afternoon Session I (Chairman: Y. Kojima)

Friday, January 11

* manuscript not available

Black-Hole Accretion Flow: Recent Topics

S. Mineshige[1]

Yukawa Institute, Kyoto University, Sakyo-ku, Kyoto 606-8502, Japan

R. Takahashi[2]

Department of Astronomy, Kyoto University, Sakyo-ku, Kyoto 606-8502, Japan

Abstract

Recent progress in the theoretical understanding of black-hole accretion flow is overviewed with special emphasis on the roles of magnetic fields. Topics include X-ray spectral variation of Cyg X-1, spatial inhomogeneity and temporal variations found in simulated MHD flow, resolving black hole environments with future space radio interferometer mission, and supercritical accretion flow.

1 Introduction: Variability of Black Holes

Accretion flow onto black holes (BHs) seems to be one of the most important physics to understand the various activities and formation processes of astrophysical objects. Many theoretical and observational developments have been made in the last decade, although there still remain fundamental questions, such as the structure of adiabatic accretion flow, role of magnetic fields, jet formation mechanisms, and the properties of super-critical accretion. Especially, recent theoretical efforts are rather focused on the role of convection, outflow, and magnetic fields in forming disk structure, spectra, and variability. We, here, pick up several topics and discuss future direction of the research of black-hole astronomy.

To get a good insight into these problems, a proto-type BH candidate, Cygnus X-1, is still useful to investigate, since for this object many observational studies have been performed mostly in X-ray bands. It is in this object that aperiodic X-ray fluctuations were found [23]. It is now widely known that complex variability patterns are one of the most prominent observational features of black-hole objects, e.g., Galactic BH candidates and active galactic nuclei. The power-spectral densities (PSDs) show something like $1/f$ fluctuations, which are rather intriguing. Such variability properties should contain the important physics involved with accretion flow into BHs. Hence, many efforts have been devoted so far to quantify these variability patterns appearing in the PSDs and to explain these fundamental observational facts. Yet, its origin is not completely clear.

Here, we utilize a potentially powerful method to analyze time-variable data; the technique of the superposed shot. If we have a close look at the X-ray intensity variations of Cyg X-1, we notice rather spiky features (referred to as shots) to be present on the timescale of several sec. By summing up only large events, by aligning their peaks, we can obtain a sort of the average variation patterns and spectral variations. Such a technique has been developed by Negoro and his collaborators [22]. The results of his recent analysis [21] are summarized in figure 1.

The upper panel shows an average time profile of the shots of Cyg X-1 in the 1.2–58.4 keV band obtained by superposing 872 large shots (with peak intensity of exceeding twice its average). Surprisingly, the shot profile is rather smooth and, more importantly, is rather symmetric in time with respect to the peak epoch. The profile is well represented by double exponential models; i.e., exponential functions with two time constants; one about 0.1 s and the other several sec. The deviations from the best-fit double exponential model are illustrated in the middle panel of figure 1. Even more interesting is the hardness ratio (7.3–14.6 keV/1.2–7.3 keV) variation of the excess shot (shot component subtracted by the mean flux), which is depicted in the bottom panel of figure 1. It clearly exhibits a soft spectrum before the peak intensity, and a rapid hardening in $\ll 0.1$ s around the peak, followed by complex changes.

[1] E-mail:minesige@yukawa.kyoto-u.ac.jp
[2] E-mail: rohta@kusastro.kyoto-u.ac.jp

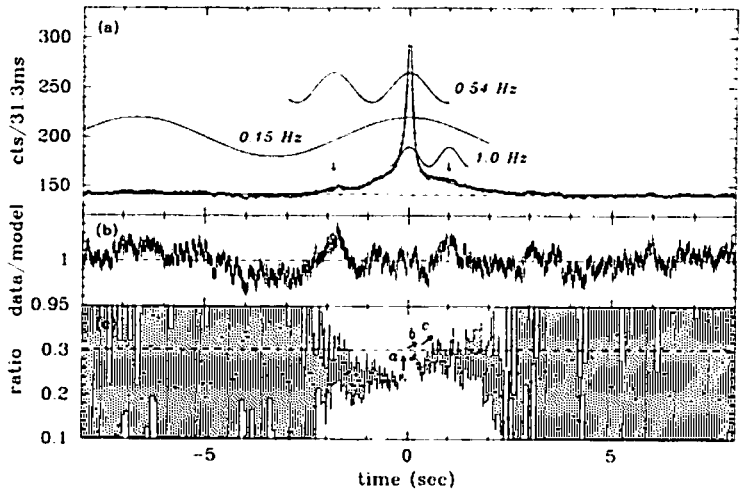

Figure 1: The variability properties of the superposed shot obtained based on the *Ginga* data of Cyg X-1 [21]. (a) Average time profile of the shots. (b) The ratio of the observed counts to that expected by the best-fit two-exponential model. (c) The hardness ratio variations. The dashed line is the averaged hardness ratio.

An important discovery is that our current analysis strongly points the presence of two (or more) physical timescales involved with X-ray variability: $\tau \simeq 0.1 - 1$ s, on which shot profile rises and decays, and $\tau < 10$ ms, on which a spectral hardening occurs around the shot peak. We should caution that the hard X-ray peak does not significantly lag behind the soft X-ray peak even within a shorter time resolution of ~ 2 ms of the RXTE [4]. From the theoretical points of view, it is very difficult to explain both different timescales simultaneously by means of a single physical mechanism, since usually one physical mechanism has one typical timescale.

Figure 2 schematically illustrates the distinction between the variation patterns which usual models predict and those obtained by our data analyses. We thus reject the hot spot model and Compton cloud model in their original forms. In the Compton-cloud model, for example, hard photons come out later, since they should be Compton up-scattered by hot electrons before leaving the cloud, thus the peak of harder photons being systematically delayed behind that of softer ones, in contradiction with what we observe. In other words, these models predict comparable hardening timescale to the shot (intensity variation) timescales (few sec). Rather, we suggest that the relatively long shot timescales could be somehow related to accretion timescales, while the short one could be due to magnetic reconnection. Note that time symmetric light curves are reproduced in terms of time-dependent ADAF model [18] (see also [11] for more detailed discussion.) Such features are consistent with the view of MHD accretion flow discussed in the next section.

2 Diversity of Flows in Adiabatic Regimes

2.1 ADAF, ADIOS, and CDAF

Next, we turn the subject to the theoretical investigations regarding the three-dimensional (3D) structure of hot accretion flow. Here, 'hot' accretion flows refer to the ones which seem to appear in the adiabatic (cooling-inefficient) regimes of flow. Note that such hot flow contrasts with the so-called standard disk, in which radiative cooling is substantial. Recently, multi-dimensional simulations have been intensively performed and a new paradigm of CDAF (convection-dominated accretion flow) has emerged in the adiabatic accretion regimes, in addition to the 'classical' ADAF [9] models (see [20] for a review). The original optically thin ADAF model has been constructed in a vertically one-zone approximation and the resultant differential equations with respect to r (radial distance to the center) are solved either by

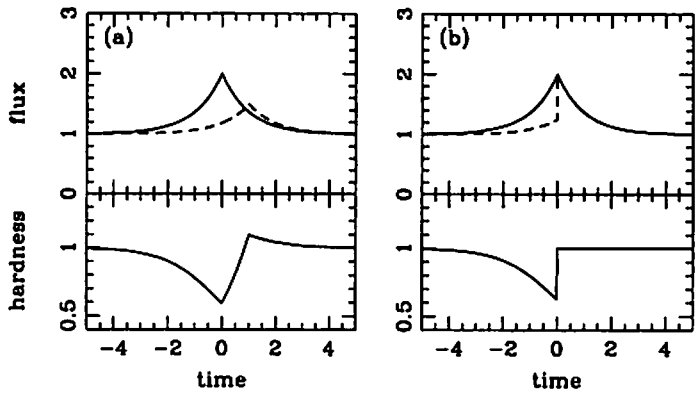

Figure 2: Schematic light curves (upper) and hardness ratios (lower) of the two models for hard time lag: (a) delayed hard X-ray peak, (b) abrupt hardening at the peak. The solid and dashed lines in the upper represent soft and hard fluxes. It is easy to produce case (a) profile with physical models, but the observations point the case (b) [21].

the self-similar technique or numerically. Recently made 2D/3D, adiabatic hydrodynamical simulations, however, revealed distinct forms of accretion flows. Igumenshchev & Abramowicz [10], for example, claimed that nearly one-dimensional ADAF appears only when the viscosity parameter α is moderate, $0.01 < \alpha \leq 0.1$. When α is smaller, large-scale circulation or convection occurs and it largely modifies the flow structure. For example, the density profile is significantly flatter than in ADAF (see table 1). Such flow is called as convection-dominated accretion flow (CDAF). If α is large ($\alpha \sim 1$), on the other hand, strong outflows result. Again, the density profile is distinct, slightly flatter than in ADAF (table 1). Blandford & Begelman [3] elucidate such flows known and named ADIOS (advection dominated inflows and outflows).

The critical test of these flows are to examine their spectral properties. Figure 3 displays the typical ADAF (left) and CDAF (right) spectra calculated in a similar way to that of Ball et al. [2]. Distinct spectra of these flow models are due to their different density profiles (see table 1): they are $\rho \propto (r/r_{\rm S})^{-p}$ with $p = 1.5$ (ADAF) and $p = 0.5$ (CDAF), respectively, In this plot, we took the same proportionality constant, ρ_0, determined by the adopted mass-accretion rate (see below), $\dot{M}$, in the case of ADAF also in CDAF, so, figure 3 can be used only for demonstration purpose. The other adopted parameters are: the inner-edge radius is $1.0\ r_{\rm S}$ (with $r_{\rm S}$ being the Schwarzschild radius), the outer-edge radius is $10^{2.5}\ r_{\rm S}$, the mass-flow rate is $\log \dot{m} \equiv \log(\dot{M}c^2/L_{\rm E}) = -3.29$ (with $L_{\rm E}$ being the Eddington luminosity), the mass of black hole is $M_{\rm BH} = 10^8 M_\odot$, the ion temperature profile is $10^{12}(r/r_{\rm S})^{-1.0}$ K, the electron temperature profile is $10^{10}(r/r_{\rm S})^{-0.6}$ K, and magnetic field strengths are taken to be the equipartition values; i.e., $B^2 \propto (r/r_{\rm S})^{-(1+p)}$. Note that the results are rather insensitive to the black-hole masses.

In the case of ADAF, emission from the innermost ring dominates over the contribution from the outer parts at all wavelengths because of its steeper density profiles. Note that the density profile of $\rho \propto r^{-3/2}$ leads to the bremsstrahlung emissivity of $dE \propto \rho^2 T^{1/2} r^2 dr \propto r^{-1.5} dr$. In the case of CDAF, in contrast,

Table 1: ADAF, CDAF, and MHD flow

accretion mode	$\rho(r)$	$T(r)$	$v_r(r)$	$B^2(r)$
ADAF	$\propto r^{-\frac{3}{2}}$	$\propto r^{-1}$	$\propto r^{-\frac{1}{2}}$	...
outflow	$\propto r^{-1}$	$\propto r^{-1}$	$\propto r^{-1}$	...
CDAF	$\propto r^{-\frac{1}{2}}$	$\propto r^{-1}$	$\propto r^{-\frac{3}{2}}$	...
MHD flow	$\propto r^{-0.5}$	$\propto r^{-1.0}$	$\propto r^{-1.5}$	$\propto r^{-1.5}$

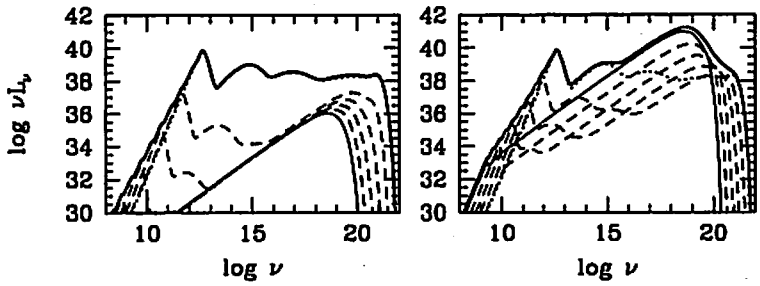

Figure 3: Typical ADAF (upper left) and CDAF (upper right) spectra, together with that of MHD flow (lower). For model parameters, see text. The thick solid line represents the total spectra, while thin solid, dashed, and dotted lines represent the contributions from the outermost, middle, and innermost rings, respectively. The MHD flow spectrum is more like that of CDAF.

X-ray emission comes mainly from the outer parts due to its somewhat flatter density profile ($\rho \propto r^{-1/2}$ yields $dE \propto r^{0.5}dr$). This is well demonstrated in figure 3. We also understand that bremsstrahlung is a dominant process in CDAF even in X-rays, while Compton up-scattering of synchrotron emission is more important in ADAF. These distinctive features should be paid attention when we compare with the observation.

2.2 MHD accretion flow

Hydrodynamical simulations are, however, of limited use here, since the magnitude of the viscosity (or magnetic field strengths) is treated as a free parameter there, although it cannot be so but should be determined in accordance with magnetic field amplifications within the disk. In other words, magnetohydrodynamical (MHD) simulations are indispensable. What is then about the case of MHD flow? Machida et al. [16] have analyzed the flow patterns within the simulated 3D MHD flow [15], finding large-scale convective motions dominating in accretion flows. Further, they also already noted similar density and temperature profiles of MHD flow to those of CDAF (see table 2). Therefore, the spectra should be more like that of CDAF (see figure 3) and not like that of ADAF.

Then, a serious problem arises; namely, such MHD flow models cannot account for the observations of Cyg X–1 during its hard state in the two senses: (1) CDAF predicts rather flat ($f_\nu \propto \nu^0$) spectrum due to Bremsstrahlung, unless we assume significant electron heating as well as ion heating [2] but the observations clearly show a power-law decline (e.g. $f_\nu \propto \nu^{-0.7}$) in X-ray ranges. (2) Rapid variability seems to arise via time-dependent processes probably associated with magnetic flares in the innermost region (see §1), but X-ray emission from the inner part of CDAF is negligible (figure 3). Radiation from the outer parts cannot show rapid variations as are observed (§1).

In view of these arguments, ADAF looks better as a model for the hard state of Cyg X–1, since then we expect rapidly fluctuating X-ray emission by Compton up-scattering of seed synchrotron photons produced in intermittent magnetic flares occurring in the innermost part. Then, what is a loophole?

The key to resolving this issue might be sought in the detailed reconnection physics. Here we address a question as to whether the dissipated magnetic energy by reconnection goes directly to plasma or radiation. So far, all the MHD simulations postulate no radiative cooling (since we are now concerned with the adiabatic accretion regimes), but if dissipated energy could be radiated away by enhanced emissivity as a consequence of magnetic reconnection, entropy production in electrons would be largely reduced, leading to a suppression of convective motions. Then, MHD flow structure would be more like that of ADAF, and not CDAF, thus explaining both of the spectral shape and the presence of X-ray variability in the Cyg X–1 data. This is still a hypothesis, thus requiring further study.

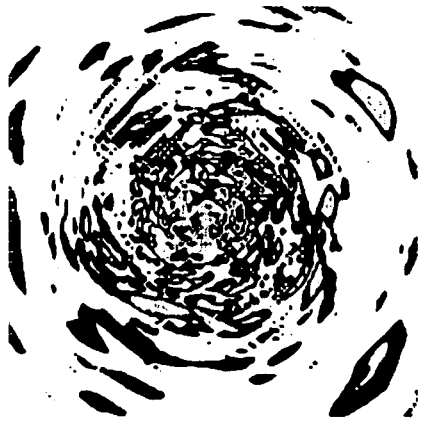

Figure 4: The contours of j/ρ (current density/matter density) values on the equatorial plane of the simulated MHD flow [12]. Note that this quantity is a good indicator for occurrence of magnetic reconnection.

2.3 Role of magnetic fields

Let us, here, summarize the various roles of magnetic fields in accretion flows.

- source of viscosity,
- disk corona (and ADAF) heating,
- cause of flares, producing variability,
- source of radiation via synchrotron,
- jet & outflow formation.

These processes have been successively simulated through global MHD simulations of the inner accretion disk by several groups of researchers [15,6,7]. They have found that magnetic fields can be amplified sufficiently enough to explain the observations; the estimated viscosity parameters are in a range of $0.01 < \alpha < 1.0$. Large corona can be constructed by MHD processes. Also, it is possible to produce aperiodic variability, which seems to be closely related spatial inhomogeneous (probably fractal) structure (see figure 4).

It is of great importance to stress that large magnetic-field strength is expected in ADAF/corona than in standard-type disks for the following reason: In the standard disk, gravitational energy is efficiently converted to radiation energy. On the other hand, magnetic field energy is suppressed below gas energy (but not by many orders below), since otherwise magnetic fields will leave the system in forms of bubbles. We thus obtain an equality,

$$E_{\rm mag} \leq E_{\rm gas} \ll E_{\rm grav} \sim E_{\rm rad}. \tag{1}$$

This situation is just like the solar photosphere. From the observational point of view, therefore, magnetic fields are not very important.

In ADAF/corona, in contrast, gravitational energy turns into fluid energy with little being radiated away. Again, magnetic energy is comparable to (but a bit less than) the gas energy. Thus, we have an equality,

$$E_{\rm mag} \leq E_{\rm gas} \sim E_{\rm grav} \gg E_{\rm rad}. \tag{2}$$

The situation is more like X-ray images of the solar coronae, in which magnetic fields are known to form filamentary (or loop) structure emerging from below the photosphere. This is the main reason why magnetic fields are likely to produce observable effects in the hard state of BHs.

Finally, we point out an exciting possibility of mapping a relativist disk by using a future space VLBI mission. The target is M87, which seems to harbor a supermassive black hole with a mass of $\sim 2.5 \times 10^9 M_\odot$. Surprisingly, a next-generation space VLBI mission is expected to achieve a superb angular resolution, down to 10 micro-arcsec, which corresponds to only 3 $r_{\rm S}$ in the case of M87 located at the distance of $\sim$ 16 Mpc. We calculate the expected disk image by the ray-shooting method, fully

Figure 5: Expected appearance of a relativistic disk in the radio map. To incorporate the finite beam-size effect, the image has been smoothed by the Gaussian filter with the smoothing length of 1 r_S. (From Takahashi & Mineshige, in preparation.)

considering relativistic effects (including Doppler boosting and gravitational lensing effects by the central black hole, see [5]). We then smooth the image in accordance with a finite beam size, and display the result in figure 5. This is the case of a non-rotating black hole and the inclination angle is set to be 80°. Obviously, we will be able to prove the presence of a 'black hole' at the center. This sort of map may be obtained in the near future, definitely within 20 years!!

3 Super-Critical Accretion Flow

Finally, we touch on the recent interesting issue of ultra-luminous compact X-ray sources (ULXs) successively found in the arms of nearby spiral galaxies. Some of these seem to exhibit large luminosities, comparable to the Eddington luminosity. Then the theory predicts that photon trapping is substantial. Such a flow is well modeled by the slim disk [1].

Let us summarize the striking results obtained by the fully relativistic calculations of the slim disk [17] (see also table 2). First, for the cases with Schwarzschild BHs the inner-edge radius of the disk *decreases* from 3 r_S to $\sim r_S$ as luminosity goes up to $L \sim L_E$. Second, for both cases of disks around Schwarzschild and Kerr BHs, radial temperature profiles become flatter as L increases, from $T \propto r^{-3/4}$ in the standard regime to $T \propto r^{-1/2}$ in the slim-disk regime. At $L \sim L_E$, the disks around Schwarzschild and Kerr BHs look quite similar.

Accordingly, accretion disk spectra differ from those expected by the simple standard-disk theory. To make direct comparison with the observations, we performed spectral fitting to the theoretical spectra based on the disk-blackbody model [19]. The free parameters are r_{in}, the (apparent) inner-edge radius of the disk, and T_{in}, the maximum temperature. There are many effects affecting the fitting results.

Table 2: Standard disk and slim disk ($m_1 \equiv M_{BH}/10\ M_\odot$)

disk model	standard disk	slim disk
disk inner edge (r_{in})	$= 3\ r_S$	$\leq 2\ r_S$
maximum temperature (T_{in})	$\sim 1\ m_1^{-\frac{1}{4}}$ keV	$\sim 2\ m_1^{-\frac{1}{4}}$ keV
temperature profile	$\propto r^{-\frac{3}{4}}$	$\propto r^{-\frac{1}{2}}$

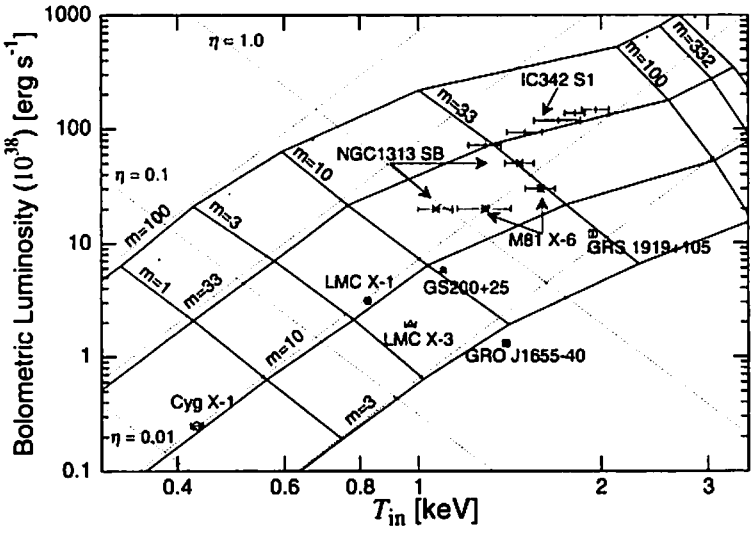

Figure 6: X-ray H-R diagram of X-ray sources [26]. Solid lines represent the constant M (black-hole mass) and constant $\dot{M}$ loci according to our model, while dotted lines are the same but based on the standard accretion disk (SSD) theory. Some observational data of ULXs and Galactic BH candidates are also plotted.

Gravitational lensing and self-shielding of the radiation from the innermost parts by the outer parts tend to increase the size of the emission region, since for the latter the innermost part with smaller size is obscured and thus instead the surrounding part with a bit larger size is now most visible in X-rays. Conversely, projection, Doppler boosting, and Compton scattering tend to decrease $r_{\rm in}$. In large inclination systems, therefore, self-shielding and Doppler boosting operate in the opposite ways. The situations are rather complex. Caution is needed when interpreting the fitting results of the observational spectra.

Let us check what observations tell. Figure 6 shows the interesting results taken from [26]. This is the $T_{\rm in}$-L diagram and the solid lines represent the calculated loci of constant BH mass or constant mass accretion rate. Also, the observational data points of BH candidates, including ultra-luminous compact X-ray sources (ULXs), are plotted. We wish to pay particular attention to the temporal behavior of IC 342, which evolves along the line of the theoretically predicted track; namely, it clearly shows decrease in $r_{\rm in}$ with increase of L. For comparison, we also plot the constant-$r_{\rm in}$ lines with straight dotted lines. The fact of decreasing $r_{\rm in}$ at large L indicates that IC 342 should have near-critical accretion flow. This also provides a good example that even if the estimated inner-edge radius is below 3 $r_{\rm S}$ the BH may not be an extreme Kerr hole.

The theoretical study of such near- or super-Eddington sources have just started. Interaction between radiation and matter has been a big concern and still remains an open question. We need fully 2D/3D radiation hydrodynamics to establish 2D/3D relativistic slim disk models. Internal Compton scattering in multi-dimension and evaluations of photon trapping effects are also important to consider.

Another interesting issue is the fate of radiation pressure-dominated disk. According to the standard-disk model, the hottest part which is dominated by radiation pressure is violently thermally unstable. How such a disk evolves is still an open question. Possibilities are (1) relaxation oscillations leading to quasi-periodic bursting behavior [8,24]; (2) soft-to-hard transition which may occur when the viscosity parameter (α) is large [25]; and (3) strongly clumped disk [13]. Observations of some sources, such as GRS1915+105, show bursting behavior, thus supporting the possibility (1), while it is also possible that

only an upper part of the disk undergoes transitions to produce coronae transiently [14]. We expect more observational evidence to accumulate in the next decade.

References

[1] M.A. Abramowicz, B. Czerny, J.-P. Lasota, E. and Szuszkiewicz: Astrophys. J. **332** (1988) 646

[2] G.H. Ball, R. Narayan, and E. Quataert: Astrophys. J. **552** (2001) 221

[3] R.D. Blandford and M.C. Begelman: Mon. Not. Roy. Astron. Soc. MNRAS **303** (1999) L1

[4] Y.X. Feng, T.P. Li, L. Chen: Astrophys. J. **514** (1999) 373

[5] J. Fukue and T. Yokoyama Pub. Astron. Soc. Japan **40** (1988) 15

[6] J.F. Hawley, S.A. Balbus, and J.M. Stone: Astrophys. J. **554** (2001) L49

[7] J.F. Hawley and J.H. Krolik: Astrophys. J. **548** (2001) 348

[8] F. Honma, R. Matsumoto, and S. Kato, Pub. Astron. Soc. Japan **43** (1991) 147

[9] S. Ichimaru, Astrophys. J. **214** (1977) 840

[10] V. Igumenshchev and M.A. Abramowicz, Astrophys. J. Supple. **130** (2000) 463

[11] S. Kato, J. Fukue, and S. Mineshige, *Black-Hole Accretion Disks* (Kyoto Univ. Press, 1998), Chap. 10

[12] T. Kawaguchi, S. Mineshige, M. Machida, R. Matsumoto, and K. Shibata, Pub. Astr. Soc. Japan **52** (2000) L1

[13] J. Krolik, Astrophys. J. **498** (1998) L13

[14] A. Kubota, Ph.D. Thesis, University of Tokyo (2001)

[15] M. Machida, M.R. Hayashi and R. Matsumoto, Astrophys. J. **532** (2000) L67

[16] M. Machida, R. Matsumoto, and S. Mineshige: Pub. Astr. Soc. Japan **53** (2001) L1

[17] T. Manmoto and S. Mineshige, 2001, in preparation

[18] T. Manmoto, M. Takeuchi, S. Mineshige, R. Matsumoto, and H. Negoro, Astrophys. J. **464** (1996) L135

[19] K. Mitsuda *et al.* Pub. Astron. Soc. Japan **36** (1984) 741

[20] R. Narayan, in *Lighthouses of the Universe*, (MPI 2001), in press

[21] H. Negoro, S. Kitamoto, and S. Mineshige: Astrophys. J. **554** (2001) 528

[22] H. Negoro, S. Miyamoto, and S. Kitamoto: Astrophys. J. **423** (1994) L127

[23] M. Oda *et al.* Astrophys. J. **166** (1971) L1

[24] E. Szuszkiewicz and J.C. Miller, Mon. Not. Roy. Astron. Soc.**298** (1998) 888

[25] M. Takeuchi and S. Mineshige, Astrophys. J. **505** (1998) L19

[26] K. Watarai, T. Mizuno, and S. Mineshige, Astrophys. J. **549** (2001) L77

A Numerical Study of the Axisymmetric Pulsar Magnetosphere

Jun Ogura[1]

Department of Physics, Hiroshima University,
Higashi-Hiroshima, Hiroshima 739-8526, Japan

Abstract

A large number of papers has been written down about the theoretical work of pulsar magnetosphere. The issues still reminds open, although roughly 30 years have passed. Recently Contopoulos et.al. numerically constructed global smooth magnetosphere. we study the natures of the magnetosphere and the current distribution.

1 Introduction

A pulsar was identified as a rotating neutron star in the earliest days of pulsar research[1]. The rotating energies continuously transfered to the nebulae around the pulsar. This general picture is established, but the details of the mechanism are not clear. Extraction of rotating energy, and the transformation toward the surrounding matter are of great significance. These mechanisms may be relevant not only to pulsars, but also to AGN and gamma ray burster.

The model of magnetosphere is important for the understanding of the physical pictures. The simplest model is an aligned rotator one. Goldreich and Julian[2] examined the aligned model in vacuum. They consider the magnetic fields due to a dipole moment of the star. However, when we consider the plasma flow, the magnetic field should be modified significantly. In addition to the poloidal field which is expressed by a flax function, there is a toroidal magnetic field $B_\phi = A(\Psi)/R$. The equation governing the magnetosphere is reduced to a coupled equation between A and Ψ. The function Ψ may be determined by assuming A. Some authors examined special case, $A = \text{const}$ [3] and $A \propto \Psi$ [4]. The basic equation becomes linear partial differential one for these cases. However, the solutions have singularities elsewhere in the magnetosphere. Contopoulos, Kazanas & Fendt[5] recently showed continuous and smooth solution from the stellar surface to the wind region across the light cylinder. In this paper, we extend their work.

2 Model and Basic Equations

2.1 Pulsar equation

We show a basic equation governing the plasma motion in rotating magnetosphere under the ideal MHD condition $\vec{E} \cdot \vec{B} = 0$. This condition is a good approximation except a small region such as gaps. Since the inertial, gravitational and pressure forces are negligible, the force balance is given by

$$\rho_e \vec{E} + \frac{\vec{J}}{c} \times \vec{B} = 0, \tag{1}$$

where the charge density ρ_e is given by

$$\rho_e = \nabla \cdot \vec{E}/4\pi. \tag{2}$$

is the electric charge density in the magnetosphere.

For axially symmetric magnetic field, it is convenient to use the flux function Ψ. The poloidal magnetic field B_p is given by

[1] E-mail:ogura@theo.phys.sci.hiroshima-u.ac.jp

$$\vec{B}_P = \frac{\nabla\Psi \times \vec{\phi}}{R}, \tag{3}$$

where we used a cylindrical coordinate system (R, ϕ, Z). The azimuthal magnetic field B_ϕ is defined by

$$B_\phi = \frac{A(\Psi)}{R}, \tag{4}$$

where $A(\Psi)$ is related with poloidal current density through the Maxwell equation.

Finally, the electric field is given by

$$\vec{E} = \frac{R\Omega}{c}\vec{B}_p \times \vec{\phi}, \tag{5}$$

where Ω is the angular velocity of rotation of a star, onto which the magnetosphere is anchored.

Using eqs.(2)-(5) into eq.(1), we have the pulsar equation [6, 7]

$$(1-x^2)\left(\frac{\partial^2\Psi}{\partial x^2} - \frac{1}{x}\frac{\partial\Psi}{\partial x} + \frac{\partial^2\Psi}{\partial z^2}\right) - 2x\frac{\partial\Psi}{\partial x} = -R_{LC}AA'(\Psi), \tag{6}$$

where we have introduced the convenient notation $x \equiv R/R_{LC}$ and $z \equiv Z/R_{LC}$, with $/R_{LC} \equiv c/\Omega$, light cylinder.

2.2 Iteration scheme

Nothing has been specified the function A so far. Corresponding to this function, the magnetic fields are calculated. It is not clear whether there is a singularity or kink elsewhere. Assuming A, the elliptic equation (6) can be solved both for the interior $x < 1$ and the exterior $x > 1$. The both function at the light cylinder $\Psi(x = 1^+, z)$ and $\Psi(x = 1^-, z)$ are mismatched in general. If one is lucky enough, one has the connect distribution A and magnetic field.

Contopoulos et.al. [5] have set out to obtain the solution of the force-free rotating dipole magnetosphere in all space, without kinks or discontinuities on or around the light cylinder, using the following relaxation-type technique.

1. Chose some initial trial electric current distribution $A(\Psi)$.
2. Solve the eq.(6) both inside and outside.
3. Redefine the distribution of $A(\Psi)$ by iteration as follows, at the light cylinder.
4. Repeat steps 1 3 until the field line connects smoothly.

The new distribution of $A(\Psi)$ is given by

$$AA'_{new}(\Psi) = \mu_1 AA'_{in}(\Psi_{in}) + \mu_2 AA'_{out}(\Psi_{out}) + \mu_3(\Psi_{in} - \Psi_{out}), \tag{7}$$

at the light cylinder, where

$$\Psi = \frac{1}{2}[\Psi_{in} + \Psi_{out}], \tag{8}$$

with weight factors $\mu_1 + \mu_2 = 1$ and $\mu_3 < 1$.

In order to be able to solve the problem all the way to infinity, we rescaled our x and z variables as $X_{in} = x$, $Z_{in} = z/(1+z)$, $X_{out} = (x-1)/x$, and $Z_{out} = z/(1+z)$.

The boundary conditions are

$$\Psi(X_{in}=0) = 0, \tag{9}$$

$$\partial_{X_{in}}\Psi(X_{in}=1) = \frac{AA'}{2}, \tag{10}$$

$$\partial_{Z_{in}}\Psi(Z_{in}=0) = 0, \tag{11}$$

$$\Psi(Z_{in}=1) = 0, \tag{12}$$

$$\Psi(\text{around the origin}) = \left(\frac{m}{R_{LC}}\right)\frac{x^2}{(x^2+z^2)^{3/2}}, \tag{13}$$

in inside the light cylinder, and

$$\partial_{X_{out}}\Psi(X_{out}=0) = \frac{AA'}{2}, \tag{14}$$

$$\Psi(X_{out}=1) = 0, \tag{15}$$

$$\Psi(Z_{out}=0) = \Psi_{open}, \tag{16}$$

$$\Psi(Z_{out}=1) = 0, \tag{17}$$

in outside of one, where m is the dipole magnetic moment and Ψ_{open} is given by the value of $\Psi(X_{in}=1, Z_{in}=0)$. Our result is shown in Fig.1 which is confirmed with Contopoulos et.al[5].

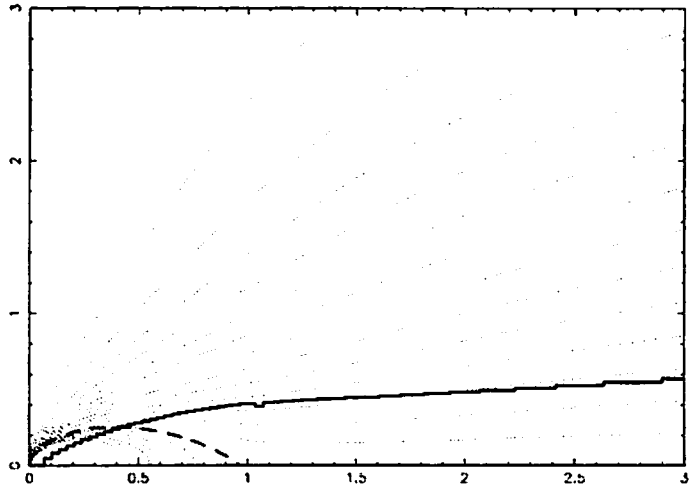

Figure 1: The structure of aligned rotating magnetosphere, which is almost consistent with Contopoulos et.al [5]. The horizontal line is the direction of x, and the vertical line is the direction of z. We can see the magnetic field line is connected smoothly through the light-cylinder($x=1$). The doted lines represent flux surfaces in intervals of $0.1\Psi_{pc}$, with $\Psi=0$ along the axis. The dashed field line is the last open field line corresponding to $\Psi_{open}=1.38\Psi_{pc}$. The solid line shows the null surface where $\rho_e=0$.

3 Plasma Flow

Since the magnetosphere was calculated, we can see the distribution of plasma. The plasma moves only along the magnetic field. The velocity of the plasma is given by

$$\vec{v} = \kappa\vec{B} + R\Omega\vec{\phi}, \tag{18}$$

where the second term is purely corotating velocity component. In the steady state configuration, the current density is given by the Maxwell equation as

$$\partial_t \vec{E} = \vec{\nabla} \times \vec{B} - 4\pi \vec{J} = 0. \tag{19}$$

If $\vec{J} = \rho_e \vec{v}$, the function κ is determined as

$$\kappa = \frac{A'(\Psi)}{4\pi\rho_e}, \tag{20}$$

is given by (18),(19), and MHD condition $\vec{E} = -\vec{v} \times \vec{B}$.

Fig.2 shows the current distribution in the magnetosphere where the electric current is defined as $\vec{J} = \rho_e \vec{v}$. The main electric current stream outward from the dipole polar cap, and is distributed along the inner open field lines. A small amount of return current flows along the boundary between the last open field (dotted) line and the dashed-dotted line. The plasma flow in the closed line has no poloidal component of velocity.

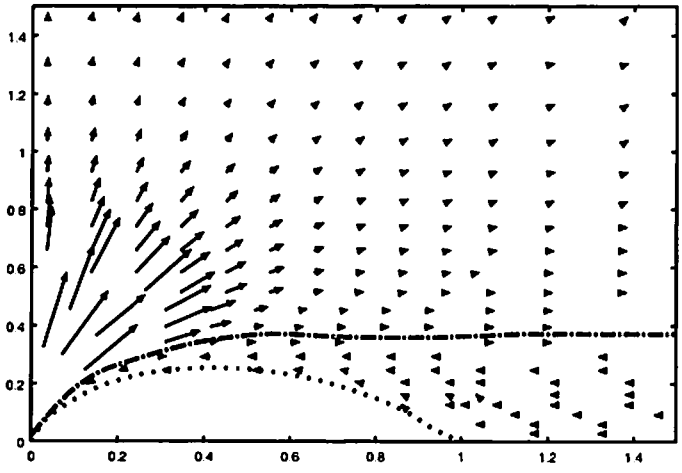

Figure 2: The current distribution on the x-z plane. The size of arrow means the amount of the current. The dotted line represents the last open field. The dash-dotted separates the outflow region to return current region.

4 Current distribution

The current distribution A' along the specified field line is shown in Fig.3. The result obviously shows outflow current is dominated. We have calculated several times from different initial current distribution, but have the same final one. The final functions converged at moment, we do not know that the solution is unique. There is no proof at all. Therefore it is very important to check whether alternative distribution exists or not.

References

[1] T. Gold, Nature **218** (1968) 731

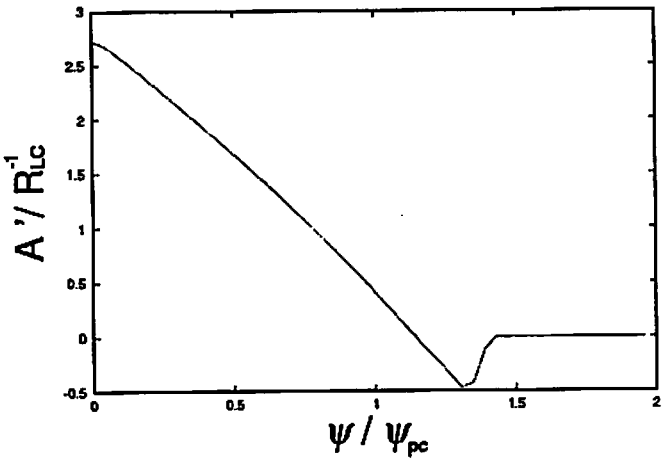

Figure 3: Derivative of vector potential A' along the open field line $\Psi = \Psi_{pc}$, which corresponds with the electric current distribution.

[2] P. Goldreich, W.J. Julian, ApJ, **157** (1969) 869

[3] F.C. Michel, ApJ **180** (1973) 207

[4] F.C. Michel, ApJ **197** (1975) 193

[5] I. Contopoulos, D. Kazanas, and C. Fendt, ApJ **511** (1999) 351

[6] E.T. Scharleman and R.V. Wagoner, ApJ **182** (1973) 951

[7] F.C. Michel, ApJ **180** (1973) L133

[8] F.C. Michel, ApJ **192** (1974) 713

General Relativistic Analysis of Particle Acceleration in Pulsar Magnetosphere

Nobuyuki Sakai[1]

Faculty of Education, Yamagata University, Yamagata 990-8560

Shinpei Shibata[2]

Faculty of Science, Yamagata University, Yamagata 990-8560

Abstract

We reconstruct a 3+1 formalism of general relativistic electromagnetism, and derive the equations of motion of charged particles in pulsar magnetosphere, taking account of the inclination between the rotation axis and the magnetic axis. We analyze particle acceleration in the polar cap, finding that gravity changes its dynamics significantly.

1 Introduction

The origin of radio emission from pulsars remains a great mystery. One of the likely scenarios is that particles are accelerated along open magnetic field lines, γ-rays emit, and electron-positron pair production occur subsequently. The process of particle acceleration has been intensively studied in flat spacetime [1]. The field-aligned electric field is driven by deviation of the space charge from Goldrich-Julian charge density, which is determined by the magnetic field geometry. Therefore, general relativistic effects on the field geometry are crucial for the formation of the field-aligned electric field and particle acceleration.

Muslimov & Tsygan initiated the general relativistic analysis of electromagnetic fields around a pulsar [3]; they solve Maxwell equations on the assumption that the particles move with the light speed. Shibata showed, however, their assumption is not always true [2]. Later Mestel included the equations of motion of particles in general relativistic electromagnetic equations [4]. Here we derive the basic equations more rigorously and generally: we correct Mestel's equation and extend it to include the inclination angle between the magnetic axis and the rotation angle.

2 3+1 Electromagnetic Equations

The basic equations are general relativistic Maxwell equations coupled to the equation of motion of a charged particle:

$$\mathcal{F}^{\mu\nu}{}_{;\nu} = 4\pi\mathcal{J}^{\mu}, \quad \mathcal{F}_{[\mu\nu;\lambda]} = 0, \quad m\frac{Dv^{\mu}}{D\tau} = e\mathcal{F}^{\mu\nu}v_{\nu}. \tag{1}$$

In order to apply these equations to a specific case, it is convenient to rewrite them in a 3+1 form. Such a method was discussed by Landau & Lifshitz [5] and Thorne & Macdonald [6]. For the purpose of our study, we combine and modify the two methods: we adopt the ADM formalism to decompose a spacetime and electromagnetic fields into a 3+1 form as in [6], and write down 3+1 electromagnetic equations in a straightforward manner as in [5].

We adopt the metric used in the ADM formalism,

$$ds^2 = -\alpha^2 dt^2 + q_{ij}(dx^i + \beta^i dt)(dx^j + \beta^j dt), \tag{2}$$

and introduce the fiducial observers with the 4-velocity,

$$u_{\mu} = (-\alpha, 0, 0, 0), \quad (\mu = 0, 1, 2, 3), \tag{3}$$

[1]E-mail: sakai@ke-sci.kj.yamagata-u.ac.jp
[2]E-mail: shibata@sci.kj.yamagata-u.ac.jp

which defines a series of spacelike hypersurfaces $\Sigma(t)$ orthogonal to u^μ. We define the projection tensor, which projects any 4D vector or tensor onto $\Sigma(t)$, as

$$h^{\mu\nu} \equiv g^{\mu\nu} + u^\mu u^\nu. \tag{4}$$

With u^μ and $h_{\mu\nu}$ we decompose the electromagnetic field $\mathcal{F}^{\mu\nu}$ and the charge-current vector J^μ into the electric field $\boldsymbol{E}$, the magnetic field $\boldsymbol{B}$, the charge density ρ and the current density $\boldsymbol{J}$ [6]:

$$\mathcal{F}^{\mu\nu} = u^\mu E^\nu - u^\nu E^\mu + \epsilon^{\mu\nu\lambda\sigma} u_\lambda B_\sigma, \quad \mathcal{J}^\mu = \rho u^\mu + J^\mu, \tag{5}$$

where $\epsilon^{\mu\nu\lambda\sigma}$ is the Levi-Civita tensor with $\epsilon^{0123} = 1/\sqrt{-g}$. Substituting (5) into the basic equations (1) and the continuity equation $\mathcal{J}^\mu_{;\mu} = 0$, we obtain the 3+1 expression of the basic equations:

$$\mathrm{div}\boldsymbol{B} = 0, \tag{6}$$

$$\frac{1}{\sqrt{q}}\partial_t(\sqrt{q}B^i) + [\mathrm{rot}(\alpha\boldsymbol{E} + \boldsymbol{\beta}\times\boldsymbol{B})]^i = 0, \quad (i = 1,2,3), \tag{7}$$

$$\mathrm{div}\boldsymbol{E} = 4\pi\rho, \tag{8}$$

$$-\frac{1}{\sqrt{q}}\partial_t(\sqrt{q}E^i) + [\mathrm{rot}(\alpha\boldsymbol{B} + \boldsymbol{\beta}\times\boldsymbol{E})]^i = 4\pi\alpha J^i, \tag{9}$$

$$\frac{1}{\sqrt{q}}\partial_t(\sqrt{q}\rho) + \mathrm{div}(\alpha\boldsymbol{J}) = 0, \tag{10}$$

$$\frac{d}{d\tau}\{\gamma(-\alpha + \boldsymbol{\beta}\cdot\boldsymbol{V})\} - \gamma^2\left\{-\frac{\partial_0\alpha}{\alpha} + \frac{\partial_0 q_{ij}}{2}V^iV^j + \frac{\boldsymbol{V}\cdot\partial_0\boldsymbol{\beta}}{\alpha}\right\} = \frac{e}{m}\frac{\gamma}{\alpha}\boldsymbol{E}\cdot\boldsymbol{V}, \tag{11}$$

$$\frac{d}{d\tau}(\gamma V_i) - \gamma^2\left\{-\frac{\partial_i\alpha}{\alpha} + \frac{\partial_i q_{jk}}{2}V^jV^k + \frac{\boldsymbol{V}\cdot\partial_i\boldsymbol{\beta}}{\alpha}\right\} = \frac{e}{m}\gamma\left[\boldsymbol{E} + \boldsymbol{V}\times\boldsymbol{B} - (\boldsymbol{E}\cdot\boldsymbol{V})\frac{\boldsymbol{\beta}}{\alpha}\right]_i. \tag{12}$$

Here inner product, cross product, divergence and rotation are defined as

$$\boldsymbol{Q}\cdot\boldsymbol{P} \equiv Q_iP^i, \quad [\boldsymbol{Q}\times\boldsymbol{P}]^i \equiv \epsilon^{ijk}Q_jP_k, \quad \mathrm{div}\ \boldsymbol{P} \equiv \frac{1}{\sqrt{q}}\partial_i(\sqrt{q}P^i), \quad [\mathrm{rot}\ \boldsymbol{P}]^i \equiv \epsilon^{ijk}\partial_jP_k, \tag{13}$$

where ϵ^{ijk} is the spatial Levi-Civita tensor with $\epsilon^{123} = 1/\sqrt{q}$. The Lorentz factor γ and the 3-velocity vector V^i are defined as

$$\gamma \equiv -v^\mu u_\mu = \alpha v^0, \quad V^i \equiv \frac{v^\mu h^i_\mu}{\gamma} = \frac{v^i + \beta^i v^0}{\gamma}. \tag{14}$$

3 Electromagnetic Equations in Pulsar Magnetosphere

We assume that the spacetime outside a neutron star is stationary, axisymmetric and vacuum. Up to first order in the slow-rotation approximation, the spacetime is described by the metric,

$$\hat{\alpha}^2 = F(\hat{r}) \equiv 1 - \frac{r_g}{r}, \quad \hat{\beta}^{\hat{\varphi}} = \omega(\hat{r}) \equiv \frac{2J}{\hat{r}^3}, \quad \hat{q}_{ij} = \mathrm{diag}(F^{-1}(\hat{r}),\ \hat{r}^2,\ \hat{r}^2\sin\hat{\theta}), \tag{15}$$

where r_g and J are the gravitational radius and the angular momentum of the star, respectively, and we have adopted the spherical coordinates $(\hat{t},\ \hat{r},\ \hat{\theta},\ \hat{\varphi})$ so that $\hat{\theta} = 0$ accords with the rotation axis.

In order to work with the "magnetic coordinates" $(t,\ r,\ \theta,\ \varphi)$, where the magnetic dipole axis accords with $\theta = 0$ [3], we introduce the "corotating coordinates" as $\hat{\varphi} \to \hat{\varphi} - \Omega\hat{t}$, where Ω is the angular velocity of the star [5]. Supposing the magnetic axis is $\hat{\theta} = \chi$, $\hat{\varphi} = 0$, the coordinate transformation from the corotating coordinate to the magnetic coordinate is given by

$$\begin{aligned}
&\hat{x} = \hat{r}\sin\hat{\theta}\cos\hat{\varphi}, \quad \hat{y} = \hat{r}\sin\hat{\theta}\sin\hat{\varphi}, \quad \hat{z} = \hat{r}\cos\hat{\theta},\\
&x = \hat{x}\cos\chi + \hat{z}\sin\chi, \quad y = \hat{y}, \quad z = -\hat{x}\sin\chi + \hat{z}\cos\chi,\\
&x = r\sin\theta\cos\varphi, \quad y = r\sin\theta\sin\varphi, \quad z = r\cos\theta.
\end{aligned} \tag{16}$$

The shift vector in (15) is, accordingly, transformed into

$$\beta^r = 0, \quad \beta^\theta = -\sin\chi\sin\varphi(\Omega-\omega), \quad \beta^\varphi = (\cos\chi - \cot\theta\cos\varphi\sin\chi)(\Omega-\omega), \tag{17}$$

while the lapse function and the spatial metric remain unchanged: $\alpha^2(r) = F(r)$, $q_{rr} = F^{-1}(r)$.

We analyze the basic equations (6)-(12) with the metric (17). First, we suppose that the magnetic field distortion due to the external currents is negligibly small. Then the magnetic field is governed by (6) and (9) with $\boldsymbol{J} = 0$: $\mathrm{div}\boldsymbol{B} = 0$ and $\mathrm{rot}(\alpha\boldsymbol{B}) = 0$. We adopt the dipole-like solution [7, 3]:

$$B_{(r)} \equiv \frac{B^r}{\sqrt{F}} = B_0\frac{f(r)}{f(r_*)}\left(\frac{r_*}{r}\right)^3\cos\theta, \quad f(r) \equiv -3\left(\frac{r}{r_g}\right)^3\left[\ln F(r) + \frac{r_g}{r}\left(1+\frac{r_g}{2r}\right)\right], \tag{18}$$

$$B_{(\theta)} \equiv r^2B^\theta = \frac{B_0}{2}\frac{\sqrt{F}}{f(r_*)}\left[-2f(r) + 3F^{-1}(r)\right]\left(\frac{r_*}{r}\right)^3, \tag{19}$$

where $r = r_*$ denotes the star surface.

Equation (7) is satisfied if there exists a potential Φ such as

$$\alpha\boldsymbol{E} + \boldsymbol{\beta}\times\boldsymbol{B} = -\nabla\Phi. \tag{20}$$

Substituting (20) into the other of Maxwell equations (8), we obtain

$$\mathrm{div}\left(\frac{\nabla\Phi}{\alpha}\right) = 4\pi(-\rho + \rho_{GJ}), \quad 4\pi\rho_{GJ} \equiv -\mathrm{div}\left(\frac{\boldsymbol{\beta}}{\alpha}\times\boldsymbol{B}\right). \tag{21}$$

Let us consider the flow of charged particles. In the case under consideration, magnetic field dominates over electric field, where particles are at the lowest landau level and the inertial drift motion across the magnetic field is negligible. Therefore, we may regard that particles go along with magnetic field lines:

$$\boldsymbol{V} = \kappa\boldsymbol{B}, \quad \boldsymbol{J} = \rho\boldsymbol{V} = \rho\kappa\boldsymbol{B}, \tag{22}$$

where κ is a scalar function. Then continuity equation (10) implies [3, 4]

$$\alpha\rho\kappa = \frac{\sqrt{F}\rho V}{B} = \text{constant on magnetic field lines.} \tag{23}$$

One of the equations of motion (11), supposing $B_\varphi = E_\varphi = 0$, reduces to

$$\frac{d}{d\tau}(\sqrt{F}\gamma) = \frac{e}{m}\frac{1}{F}\frac{d\Phi}{d\tau}. \tag{24}$$

The other equation (12) need not be solved because the spatial trajectory is determined by (22).

Finally, we consider boundary conditions. We assume that the star crust is a perfect conductor, and hence particles on the surface do not suffer Lorentz force. This ideal MHD condition is given by $\nabla\Phi = 0$, from (12) and (20) with ignoring the small term $(\boldsymbol{E}\cdot\boldsymbol{V})\beta/\alpha$. We also assume that there exists a closed magnetic lines, where the ideal MHD condition holds. Therefore, our boundary conditions are $\Phi = \nabla\Phi = 0$ at $r = r_*$, and on the boundary surface defined by the "last open field lines", $\theta = \theta_c(r)$.

4 Particle Acceleration in the Polar Cap

We are interested in the "polar cap" region, $\theta < \theta_c(r)$, where particle acceleration may occur. For simplicity, we restrict ourselves to the region near the magnetic pole just above the surface, where the following approximations hold: (i) $\theta_c(r) \approx$ constant, (ii) $\theta \ll 1$ (we take its first order), and (iii) d/dr along the particle trajectory $\approx \partial/\partial r$. The assumption (i) and the boundary condition $\Phi(\theta_c) = 0$ imply that Φ can be expanded as

$$\Phi = \sum_{l,m}\bar{\Phi}(r)Y_{lm}(\theta,\varphi), \quad l = n\frac{\theta_c}{\pi}, \quad (n = 0, 1, 2, \ldots). \tag{25}$$

In our analysis below, we take only the $n = 0$ (homogeneous) or $n = 1$ (lowest) mode.

Using the normalized variables [2],

$$j \equiv -\frac{2\pi\sqrt{F}J}{\Omega B} = \text{constant}, \quad \phi \equiv \frac{e}{m}\Phi, \quad s \equiv \sqrt{\frac{2\Omega B_0 e}{m}}r, \tag{26}$$

we rewrite (8) and (12) as

$$\frac{\sqrt{F}}{s^2}\frac{d}{ds}\left(s^2\frac{d\phi}{ds}\right) - \frac{l(l+1)}{\sqrt{F}s^2}\phi = \frac{B}{B_0\sqrt{F}}\left(\frac{j}{V} - \bar{j}\right), \quad \bar{j} \equiv \left(1 - \frac{\omega}{\Omega}\right)(\cos\chi + \theta\cos\varphi\sin\chi), \tag{27}$$

$$\frac{d}{ds}(\sqrt{F}\gamma) = \frac{1}{F}\frac{d\phi}{ds}. \tag{28}$$

The particle trajectory is given by integrating $d\theta/dr = B^r/B^\theta$, resulting in $\theta(s) \approx \theta_*\sqrt{s/s_*}$ for $\theta \ll 1$. In the following analysis we fix some of the parameters: $r_* = 10$km, ($s_* = 2.5 \times 10^5$), $r_g = 2$km, $\Omega = 2\pi$ s^{-1}, $\omega_*/\Omega = 0.1$, $\theta_c = \sqrt{\Omega r_*/c}$ ($\pi/\theta_c = 217$), $\chi = 30°$ and $\gamma_* = 1.0001$.

We can argue the behavior of particles by looking at the "force term" (LHS) of (27). If $j > \bar{j}$, the force term always positive; $d\gamma/ds$ increases monotonically. If $j < \bar{j}$, on the other hand, the force term takes both positive and negative, depending on V, and hence oscillating behavior is expected. Numerical integration of (27) and (28) verifies this argument, as shown in Fig. 1. If we set $r_g = \omega = 0$ (no gravity) and $\chi = 0$ (no inclination), we reproduce Shibata's result, $\bar{j} = 1$ [2]. The expression of $\bar{j}$ in (27) indicates that both effects of gravity and of inclination reduce $\bar{j}$, or equivalently, the critical value of j. An qualitative difference from the result for the flat spacetime is that in the case of $j < \bar{j}$ oscillation does not always continue to infinity but the particle velocity becomes $V = 0$ at some point, beyond which one cannot integrate the equations. A stationary solution is nonexistent in this case.

Next, we consider the dynamics for $\bar{j} \approx \bar{j}_{cr}$. To see the approximate behavior, we expand $\bar{j}$ with ξ, defined as $s = s_*(1 + \xi)$, up to the first order, resulting in

$$\bar{j} = \bar{j}_*\,|1 + C\xi|, \quad C \equiv \frac{3\omega_*}{\Omega} + \frac{\theta_*}{2}\cos\varphi\tan\chi. \tag{29}$$

This shows that $\bar{j}$ increases or decreases according to the sign of C. In the absence of gravity ($\omega_* = 0$), its sign depends simply on whether $\cos\varphi > 0$ (toward curvature) or $\cos\varphi < 0$ (away curvature), as claimed in [2]. He showed, for example, that particles are accelerated after oscillation along away curvature lines if j is slightly less than 1. The effect of gravity changes this behavior. If we take $\omega_*/\Omega = 0.1$ typically, C can be negative only if $\theta_* > 0.6|\sec\varphi|\cot\chi > 0.6\cot\chi$ even for away curvature. Unless χ is large enough, in most small-θ region, $\bar{j}$ simply increases and acceleration after oscillation cannot occur. This argument is confirmed by the numerical result in Fig. 2.

Finally, we discuss the effect of fluctuations of Φ in the non-radial direction, $l(l+1)\phi/\sqrt{F}s^2$. Because ϕ is positive, this term acts as an "accelerator". We consider two cases: (a) $n = 0$ and (b) $n = 1$. In Case (a) we find the solution where particles reach $\gamma \approx 10^6$ but ϕ and γ remain finite. This condition is required to make particle energy large enough to cause creation of electron-positron pairs with finite electric field. In Case (b), on the other hand, due to the effect of the linear term of ϕ, we have not found such a solution. We will report a detailed analysis elsewhere.

References

[1] See, e.g, [2] and references therein.

[2] S. Shibata, MNRAS 287 (1997) 262.

[3] A.G. Muslimov & A.I. Tsygan, MNRAS 255 (1992) 61.

[4] L. Mestel, ASP Conference Series 105 (1996) 417.

[5] L.D. Landau & E.M. Lifshitz, *The Classical Theory of Fields* (Pergamon, 1975).

[6] K.S. Thorne & D. Macdonald, MNRAS 198 (1982) 339.

[7] V.L. Ginzburg & L.M. Ozenoi, Sov. Phys. JETP **20** (1965) 689.

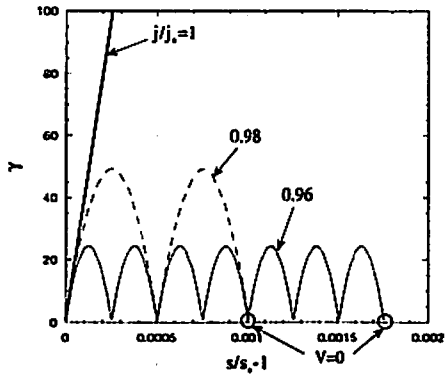

Figure 1: Spatial distribution of γ along magnetic field lines. We choose $\theta = 0$, (which leads $\bar{j}_* = 0.81$), and $n = 1$. γ oscillates or increases monotonically according to j. In this case oscillation eventually stops with V approaching zero, in contrast with the non-gravity case.

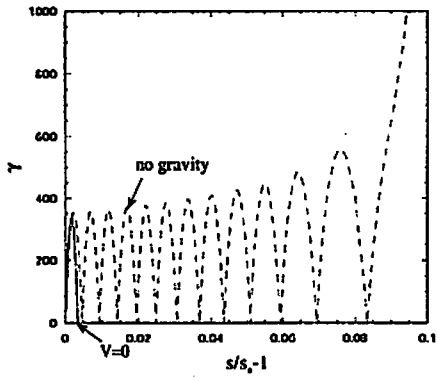

Figure 2: Spatial distribution of γ along "away" field lines. We choose $\theta_* = 5°$, $\varphi = 180°$, (which leads $\bar{j}_* = 0.822$), $j/\bar{j}_* = 0.997$ and $n = 1$. Gravity changes particle dynamics drastically.

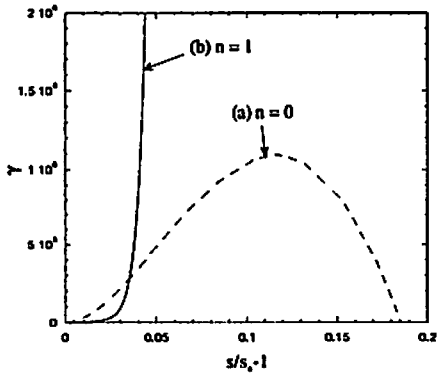

Figure 3: We choose the same parameters except for $j/\bar{j}_* = 1.01$ and n: (a) $n = 0$ and (b) $n = 1$. The angular fluctuation term accelerates a particle.

Grad-Shafranov equation in noncircular axisymmetric stationary spacetimes

Kunihito Ioka,[1] Misao Sasaki[2]

Department of Earth and Space Science, Osaka University, Toyonaka 560-0043, Japan

Abstract

We obtain the Grad-Shafranov equation, that is, a equation to which the basic equations for the axisymmetric stationary ideal magnethydrodynamic system are reduced, in the noncircular spacetimes.

1 INTRODUCTION

Recently a new class of pulsars has been recognized, which is called magnetar. Magnetars are super strongly magnetized neutron stars, whose magnetic fields are greater than the quantum critical field $B_{cr} = m_e^2 c^3/eh \sim 4.4 \times 10^{13}$ G. The ratio of the magnetic field to the gravitational energy can be estimated as

$$\delta \sim \frac{(B^2/8\pi)(4\pi R^3/3)}{GM^2/R} \sim 10^{-4} \left(\frac{B}{2\times 10^{16}\mathrm{G}}\right)^2 \left(\frac{R}{10^6\mathrm{cm}}\right)^4 \left(\frac{M}{1.4M_\odot}\right)^{-2}. \quad (1)$$

Therefore the magnetic fields of $\gtrsim 10^{16}$ G may be important for the deformation of the neutron star (e.g., [9]). The deformation of the neutron star is relevant to the precession of the neutron star, the gravitational wave emission, the oscillation of the neutron star and so on.

In order to model magnetars, we have to consider the equilibrium configuration of magnetized stars in the general relativistic magnetohydrodynamics (MHD). In this respect, we have to take the electromagnetic energy into account in the source of the gravitational field, and have to solve the configuration of the electromagnetic fields and the matter in a curved spacetime. So far several works have been devoted to the equilibrium of the magnetized stars in axisymmetric stationary spacetimes [3, 4]. However these works consider only poloidal magnetic field for simplicity. Indeed the poloidal field is compatible with the circularity of the spacetime. The stress-energy tensor is said to be circular or nonconvective if

$$\eta_\mu T^{\mu|\nu} \eta^\alpha \xi^{\beta|} = 0, \quad \xi_\mu T^{\mu|\nu} \eta^\alpha \xi^{\beta|} = 0, \quad (2)$$

where $\eta = \partial/\partial t$ and $\xi = \partial/\partial\varphi$ are two Killing vectors associated with stationarity and axisymmetry, respectively. This conditions are equivalent to the absence of the momentum currents in the meridional planes orthogonal to two Killing vectors. In the case of a fluid, this means that there is no convective motion but only circular motion around the axis of symmetry. Papapetrou [14] and Carter [6, 7] have shown that when the stress-energy tensor is circular, there exists a family of two-surfaces everywhere orthogonal to the plane defined by the two Killing vectors. In other words, one may choose coordinates (t, x^1, x^2, φ) such that $\eta = \partial/\partial t$, $\xi = \partial/\partial\varphi$ and the metric components g_{01}, g_{02}, g_{31}, g_{32} are identically zero. As a consequence the problem is simplified dramatically. However the toroidal field violates the circularity condition. Thus in order to study the magnetars in general, we have to consider the noncircular case.

The problem can be divided into two parts. The first part is to solve the Einstein equation for given stress-energy tensor. And the second is to solve the configuration of matter and electromagnetic fields in a curved spacetime. The formalism to solve the Einstein equation in the axisymmetric stationary spacetime is developed by Maeda et al. [11], Sasaki [15], and Gourgoulhon & Bonazzola [8]. So here we focus our attention on the second problem to solve the equation of motion of matter and electromagnetic fields in a curved spacetime.

[1] E-mail:ioka@vega.ess.sci.osaka-u.ac.jp
[2] E-mail:misao@vega.ess.sci.osaka-u.ac.jp

It is well known that the basic equations for the axisymmetric stationary ideal MHD system can be reduced to a single second-order, nonlinear partial differential equation, so called the Grad-Shafranov (GS) equation, in the Newtonian case [10], the Schwarzschild spacetime case [12] and the Kerr spacetime case [13]. However, as far as we know, the GS equation for the noncircular spacetimes has never been given explicitly. The purpose of this paper is to derive the GS equation explicitly in the general (i.e., noncircular) axisymmetric stationary spacetimes.

Greek indices run from 0 to 3, small Latin indices from 1 to 3 and capital Latin indices from 1 to 2.

2 BASIC EQUATIONS AND CONSERVATION LAWS

The basic equations governing the general relativistic ideal MHD are as follows. The first equation is the baryon conservation,

$$(\rho_b u^\mu)_{;\mu} = u^\mu \rho_{b,\mu} + \rho_b u^\mu{}_{;\mu} = 0, \tag{3}$$

where ρ_b is the rest mass density and u^μ is the fluid 4-velocity ($u_\mu u^\mu = -1$). The second equations are the equations of motion, which give the conservation of the fluid energy,

$$u^\mu \rho_{,\mu} + (\rho + p) u^\mu{}_{;\mu} = 0, \tag{4}$$

and the Euler equations,

$$(\rho + p) u^\mu{}_{;\nu} u^\nu + (g^{\mu\nu} + u^\mu u^\nu) p_{,\nu} - F^{\mu\nu} J_\nu = 0, \tag{5}$$

where ρ, p and J^μ are the fluid energy density, pressure and the electric current 4-vector, respectively. From Eqs. (3) and (4) we have the relation,

$$\mu := \frac{d\rho}{d\rho_b} = \frac{\rho + p}{\rho_b}, \tag{6}$$

where μ is the specific enthalpy (per unit mass). The third equations are the Maxwell equations,

$$F_{[\alpha\beta;\gamma]} = 0, \quad F^{\mu\nu}{}_{;\nu} = 4\pi J^\mu, \tag{7}$$

where the Maxwell field strength tensor $F_{\mu\nu}$ is given by the vector potential A_μ as $F_{\mu\nu} = A_{\mu,\nu} - A_{\nu,\mu}$. The electric and magnetic fields referred to the flow u^α are defined as

$$E_\mu = F_{\mu\nu} u^\nu, \quad B_\mu = \frac{1}{2} \epsilon_{\mu\nu\alpha\beta} u^\nu F^{\alpha\beta} \tag{8}$$

where $\epsilon_{\mu\nu\alpha\beta}$ is the Levi-Civita antisymmetric tensor. Note that the inversion of the above equations is given by $F_{\mu\nu} = u_\mu E_\nu - u_\nu E_\mu + \epsilon_{\mu\nu\alpha\beta} u^\alpha B^\beta$ with $E_\mu u^\mu = B_\mu u^\mu = 0$. Since the ideal MHD assumes the perfect conductivity, the fourth equation is the frozen-in condition,

$$E_\mu \;=\; F_{\mu\nu} u^\nu = 0. \tag{9}$$

The final equation is the equation of state, $p = p(\rho_b, \rho)$.

Our purpose is to solve the above basic equations under axisymmetry and stationarity. Bekenstein and Oron [1] have shown that the axisymmetric stationary system has four quantities conserved on each flowline. Conserved quantities are the magnetic flux per unit particle flux $[C(\Psi)]$, the 'angular velocity' of the magnetic field line $[\Omega(\Psi)]$, the total energy $[E(\Psi)]$ and the total angular momentum $[L(\Psi)]$, where the flowline is characterized by the flux function Ψ. A toroidal component of the vector potential $A_\mu \xi^\mu = A_3$ can play the role of the flux function Ψ when we choose the gauge such that $A_{\mu,\nu} \eta^\nu = A_{\mu,0} = 0$ and $A_{\mu,\nu} \xi^\nu = A_{\mu,3} = 0$ since we can proof $u^\mu (\xi^\nu A_\nu)_{,\mu} = 0$. Here we use the fact that the Lie derivatives of all physical quantities along the Killing vectors must vanishes, $\mathcal{L}_\xi u^\mu = \xi^\nu u^\mu{}_{;\nu} - u^\nu \xi^\mu{}_{;\nu} = 0$.

According to Bekenstein and Oron [1, 2], we can show that

$$F_{03} \;=\; 0, \quad F_{0A} = \Omega(\Psi) F_{A3}, \tag{10}$$

$$F_{31} \;=\; \Psi_{,1} = C\sqrt{-g}\rho_b u^2, \quad F_{23} = -\Psi_{,2} = C\sqrt{-g}\rho_b u^1, \quad F_{12} = C\sqrt{-g}\rho_b (u^3 - \Omega u^0), \tag{11}$$

where $\Omega(\Psi)$ and $C(\Psi)$ are conserved along each flowline. The above equations are effectively the first integrals of the Maxwell equations (7). It is useful to rewrite the above equations as $B^\mu = -C\rho_b\left[(u_0+\Omega u_3)u^\mu + \eta^\mu + \Omega\xi^\mu\right]$. Note that the conserved function $\Omega(\Psi)$ is the Ψ-derivative of the electric potential, $\Omega(\Psi) = -dA_0/d\Psi$. In addition we can show that $E(\Psi)$, $L(\Psi)$ and $D(\Psi)$ are also conserved along flowlines where

$$-D = \mu(u_0+\Omega u_3), \quad -E = \chi u_0 + C(u_0+\Omega u_3)\frac{B_0}{4\pi}, \quad L = \chi u_3 + C(u_0+\Omega u_3)\frac{B_3}{4\pi}, \tag{12}$$

where $\chi = \mu + B^2/4\pi\rho_b$. The above equations are effectively the first integrals of the Euler equations (5). We can find the relation $D = E - \Omega L$, which together with (12) implies that $B^2/\rho_b + C(B_0 + \Omega B_3) = 0$. Note that the conserved functions $\Omega(\Psi)$, $C(\Psi)$, $E(\Psi)$ and $L(\Psi)$ are given by hand.

3 GS EQUATION

The GS equation is the Euler equation in the transfield direction, so that our aim is to factorize the derivative of the flux function from the Euler equation. With Eq. (6), the Euler equation (5) can be written as

$$\rho_b(\mu u_{\mu;\nu}u^\nu + \mu_{,\mu} + u_\mu u^\nu \mu_{,\nu}) - F_{\mu\nu}J^\nu = 0. \tag{13}$$

The 1-component of the first term can be transformed as

$$\begin{aligned}
& \rho_b(\mu u_{1;\mu}u^\mu + \mu_{,1} + \rho_b u_1 u^\mu \mu_{,\mu}) \\
= \;& \rho_b u^2(\mu u_{1;2} + u_1\mu_{,2}) + \rho_b(\mu u_{1;0}u^0 + \mu u_{1;1}u^1 + \mu u_{1;3}u^3) + \rho_b\mu_{,1}(1 + u_1u^1) \\
= \;& \rho_b u^2(\mu u_{1;2} + u_1\mu_{,2}) + \rho_b(\mu u_{1;0}u^0 + \mu u_{1;1}u^1 + \mu u_{1;3}u^3) + \rho_b\mu_{,1}(-u_0u^0 - u_2u^2 - u_3u^3) \\
= \;& \rho_b u^2(\mu u_{1;2} + u_1\mu_{,2} - u_2\mu_{,1}) + \rho_b\mu u_{1;1}u^1 + \rho_b\mu u_{1;0}u^0 + \rho_b\mu u_{1;3}u^3 \\
- \;& \rho_b u^0(\mu u_0)_{,1} + \rho_b\mu u^0(u_{0;1} + \Gamma^\mu_{01}u_\mu) - \rho_b u^3(\mu u_3)_{,1} + \rho_b\mu u^3(u_{3;1} + \Gamma^\mu_{31}u_\mu) \\
= \;& \rho_b u^2(\mu u_{1;2} + u_1\mu_{,2} - u_2\mu_{,1}) - \rho_b\mu u_{2;1}u^2 - \rho_b u^0(\mu u_0)_{,1} - \rho_b u^3(\mu u_3)_{,1} \\
= \;& \rho_b u^2(\mu u_{1;2} - \mu u_{2;1} + u_1\mu_{,2} - u_2\mu_{,1}) - \rho_b u^0(\mu u_0)_{,1} - \rho_b u^3(\mu u_3)_{,1},
\end{aligned} \tag{14}$$

The second term of Eq. (13) can be transformed as

$$-F_{1\mu}J^\mu = -\frac{1}{4\pi\sqrt{-g}}\Psi_{,1}\left[\Omega(\sqrt{-g}F^{0A})_{,A} - (\sqrt{-g}F^{3A})_{,A}\right] + \frac{1}{4\pi\sqrt{-g}}F_{12}(\sqrt{-g}F^{12})_{,1}. \tag{15}$$

Since $F^{12} = -(-g)^{-1/2}u_0B_3 + (-g)^{-1/2}u_3B_0$, the second term of the above equation is given by

$$\begin{aligned}
\frac{1}{4\pi\sqrt{-g}}F_{12}(\sqrt{-g}F^{12})_{,1} &= -\frac{1}{4\pi}C\rho_b(u^3 - \Omega u^0)(u_0B_3 - u_3B_0)_{,1} \\
&= -\rho_b u^0\left[-\frac{1}{4\pi}C\Omega(u_0B_3 - u_3B_0)\right]_{,1} - \rho_b u^3\left[\frac{1}{4\pi}C(u_0B_3 - u_3B_0)\right]_{,1} \\
&- \frac{1}{4\pi}\rho_b u^0(u_0B_3 - u_3B_0)(C\Omega)'\Psi_{,1} + \frac{1}{4\pi}\rho_b u^3(u_0B_3 - u_3B_0)C'\Psi_{,1}.
\end{aligned} \tag{16}$$

From Eqs. (14), (15) and (16) with Eqs. (12), we find that the Euler equation (13) can be transformed as $f_{GS}\Psi_{,1} = 0$. A similar calculation can be applied to the 2-component, and we can factorize the derivative of the flux function Ψ as $f_{GS}\Psi_{,2} = 0$. Then the GS equation is given by $f_{GS} = 0$ where

$$\begin{aligned}
f_{GS} &= \frac{1}{C\sqrt{-g}}\left[(\mu u_1)_{,2} - (\mu u_2)_{,1}\right] + \frac{1}{4\pi\sqrt{-g}}\left[\left(\sqrt{-g}F^{3A}\right)_{,A} - \Omega\left(\sqrt{-g}F^{0A}\right)_{,A}\right] \\
&+ \rho_b u^0\left[E' - \frac{1}{4\pi}\left(u_0B_3 - u_3B_0\right)\left(C\Omega\right)'\right] - \rho_b u^3\left[L' - \frac{1}{4\pi}\left(u_0B_3 - u_3B_0\right)C'\right] = 0.
\end{aligned} \tag{17}$$

This is a second-order, nonlinear partial differential equation for the flux function Ψ but it is not so clear since the flux function appears implicitly.

If we use the (2+1)+1 formalism ([8], see Sec. A), we have the GS equation as

$$f_{GS} = \frac{1}{NMC}\epsilon^{AB}(\mu U_{\perp A})_{||B} + \rho_b(u_\Omega + \Theta u_\Theta)\left[E' - Z(C\Omega)'\right] - \rho_b(u_\Theta + \Omega u_\Omega)\left[L' - ZC'\right]$$
$$+ \frac{1}{4\pi NM}\left[\left(NMF^{3A}\right)_{||A} - \Omega\left(NMF^{0A}\right)_{||A}\right] = 0 \tag{18}$$

where Θ, $u_\perp{}^\mu$, u_Ω and u_Θ are given in Sec. B, and

$$U_\perp{}^A = -\frac{1}{NMC\rho_b}\epsilon^{AB}\Psi_{,B} - (u_\Omega + \Theta u_\Theta)N_\perp{}^A - (u_\Theta + \Omega u_\Omega)M_\perp{}^A, \tag{19}$$

$$Z = \frac{1}{4\pi}(u_0 B_3 - u_3 B_0) = \frac{1}{4\pi}C\rho_b u_\Theta(1 + \Theta\Omega)\left[\eta_\mu\eta^\mu\xi_\nu\xi^\nu - (\eta_\mu\xi^\mu)^2\right], \tag{20}$$

$$F^{0A} = \left(g^{0B}g^{A0} - g^{00}g^{AB}\right)\Omega\Psi_{,B} + \left(g^{03}g^{AB} - g^{0B}g^{A3}\right)\Psi_{,B} + \left(g^{01}g^{A2} - g^{02}g^{A1}\right)F_{12}$$
$$= \frac{1}{N^2}\left[H^{AB} + \frac{M_\perp{}^A M_\perp{}^B}{M^2}\right]\Omega\Psi_{,B} - \frac{1}{N^2}\left[N^\varphi H^{AB} - \frac{M_\perp{}^A N_\perp{}^B}{M^2}\right]\Psi_{,B}$$
$$- \left[\left(\frac{N_\perp{}^B + N^\varphi M_\perp{}^B}{N^2}\right)\epsilon_B{}^A + \frac{M_\perp{}^A N_\perp{}^B M_\perp{}^C \epsilon_{BC}}{N^2M^2}\right]\frac{F_{12}}{\sqrt{H}}, \tag{21}$$

$$F^{3A} = \left(g^{3B}g^{A0} - g^{30}g^{AB}\right)\Omega\Psi_{,B} + \left(g^{33}g^{AB} - g^{3B}g^{A3}\right)\Psi_{,B} + \left(g^{31}g^{A2} - g^{32}g^{A1}\right)F_{12}$$
$$= \frac{1}{N^2}\left[N^\varphi H^{AB} - \frac{N_\perp{}^A M_\perp{}^B}{M^2}\right]\Omega\Psi_{,B} + \left[\left(\frac{1}{M^2} - \left(\frac{N^\varphi}{N}\right)^2\right)H^{AB} - \frac{N_\perp{}^A N_\perp{}^B}{N^2M^2}\right]\Psi_{,B}$$
$$+ \left[\left\{\left(\frac{1}{M^2} - \left(\frac{N^\varphi}{N}\right)^2\right)M_\perp{}^B - \frac{N^\varphi N_\perp{}^B}{N^2}\right\}\epsilon_B{}^A + \frac{N_\perp{}^A N_\perp{}^B M_\perp{}^C \epsilon_{BC}}{N^2M^2}\right]\frac{F_{12}}{\sqrt{H}}, \tag{22}$$

$$\frac{F_{12}}{\sqrt{H}} = C\rho_b NM(u^3 - \Omega u^0) = C\rho_b NM u_\Theta(1 - \Omega\Theta). \tag{23}$$

acknowledgments

This work was supported in part by Grant-in-Aid for Scientific Research of the Japanese Ministry of Education, Culture, Sports, Science and Technology, No.00660.

A $(2+1)+1$ DECOMPOSITION

Let n_μ be the unit timelike 4-vector orthogonal to t = const hypersurface Σ_t and oriented in the direction of increasing t, $n_\mu = -Nt_{,\mu}$, where $n_\mu n^\mu = -1$. The 3-metric induced by $g_{\mu\nu}$ on Σ_t is given by $h_{\mu\nu} = g_{\mu\nu} + n_\mu n_\nu$. Let m_μ be the 4-vector field defined by $m_\mu = Mh_\mu{}^\nu\varphi_{,\nu} = M\varphi_{|\mu}$ where $m_\mu m^\mu = 1$. The induced 2-metric on $\Sigma_{t\varphi}$ is given by $H_{\mu\nu}$ where

$$g_{\mu\nu} = -n_\mu n_\nu + h_{\mu\nu} = -n_\mu n_\nu + m_\mu m_\nu + H_{\mu\nu}. \tag{24}$$

Note that $\sqrt{-g} = N\sqrt{h} = NM\sqrt{H}$. Then any vector can be decomposed into the directions of n_μ, m_μ and the others. The Killing vectors are decomposed as

$$\eta^\mu = Nn^\mu - N^\mu = Nn^\mu - MN^\varphi m^\mu - N_\perp{}^\mu, \quad \xi^\mu = Mm^\mu - M_\perp{}^\mu. \tag{25}$$

The component expressions are $n_\mu = (-N, 0, 0, 0)$, $n^\mu = \left(1/N, N^1/N, N^2/N, N^3/N\right)$, $m_\mu = (-MN^\varphi, 0, 0, M)$, $m^\mu = \left(0, M^1/M, M^2/M, 1/M\right)$ and

$$\begin{pmatrix} g_{00} & g_{0j} \\ g_{i0} & g_{ij} \end{pmatrix} = \begin{pmatrix} N_kN^k - N^2 & -N_j \\ -N_i & h_{ij} \end{pmatrix}, \quad \begin{pmatrix} g^{00} & g^{0j} \\ g^{i0} & g^{ij} \end{pmatrix} = \begin{pmatrix} -\frac{1}{N^2} & -\frac{N^j}{N^2} \\ -\frac{N^i}{N^2} & h^{ij} - \frac{N^iN^j}{N^2} \end{pmatrix} \tag{26}$$

$$\begin{pmatrix} h_{AB} & h_{A3} \\ h_{3B} & h_{33} \end{pmatrix} = \begin{pmatrix} H_{AB} & -M_{\perp A} \\ -M_{\perp B} & M^2 + M_{\perp A}M_\perp{}^A \end{pmatrix}, \quad \begin{pmatrix} h^{AB} & h^{A3} \\ h^{3B} & h^{33} \end{pmatrix} = \begin{pmatrix} H^{AB} + \frac{M_\perp{}^A M_\perp{}^B}{M^2} & \frac{M_\perp{}^A}{M^2} \\ \frac{M_\perp{}^B}{M^2} & \frac{1}{M^2} \end{pmatrix} \tag{27}$$

B INVERSION

All physical quantities can be derived from the flux function Ψ and the conserved functions $C(\Psi)$, $\Omega(\Psi)$, $E(\Psi)$ and $L(\Psi)$ when the metric $g_{\mu\nu}$ is known. Let us derive all physical quantities explicitly in this section [5]. First we decompose the fluid 4-velocity as

$$u^\mu = u_\Omega(\eta^\mu + \Omega\xi^\mu) + u_\Theta(\xi^\mu + \Theta\eta^\mu) + {u_\perp}^\mu, \tag{28}$$

where $(\eta^\mu + \Omega\xi^\mu)$ is orthogonal to $(\xi^\mu + \Theta\eta^\mu)$ so that $\Theta = -\xi_\mu(\eta^\mu + \Omega\xi^\mu)/\eta_\mu(\eta^\mu + \Omega\xi^\mu)$. With Eqs. (12), the coefficients of the 4-velocity are derived as

$$u_\Omega = \frac{E - \Omega L}{A_\Omega \mu} = \frac{D}{A_\Omega \mu}, \quad u_\Theta = -\frac{(L - \Theta E)}{A_\Theta \mu}\left(\frac{4\pi\mu}{A_\Omega C^2 \rho_b}\right)\left(1 - \frac{4\pi\mu}{A_\Omega C^2 \rho_b}\right)^{-1}, \tag{29}$$

where $4\pi\mu/(A_\Omega C^2\rho_b) = 4\pi\mu\rho_b(A_\Omega {u_\Omega}^2 - 1)/B^2 := {M_a}^2$ is the square of the effective Alfvén Mach number M_a, $A_\Omega = -(\eta_\mu + \Omega\xi_\mu)(\eta^\mu + \Omega\xi^\mu)$ and $A_\Theta = (\xi_\mu + \Theta\eta_\mu)(\xi^\mu + \Theta\eta^\mu)$. With Eqs. (11), the other terms of the 4-velocity are derived as

$${u_\perp}^\mu = -\frac{1}{NMC\rho_b}\epsilon^{\mu\nu}\Psi_{,\nu}, \tag{30}$$

where the antisymmetric tensor is given by $\epsilon_{\mu\nu} = \epsilon_{\mu\nu\alpha\beta}n^\alpha m^\beta$. The magnetic fields are derived from $B^\mu = C\rho_b\,[A_\Omega u_\Omega u^\mu - (\eta^\mu + \Omega\xi^\mu)]$. From the relation $u_\mu u^\mu = -1$ we have

$$-\frac{D^2}{A_\Omega \mu^2} + \frac{(4\pi)^2(L - \Theta E)^2}{{A_\Omega}^2 A_\Theta C^4 \rho_b^2}\left(1 - \frac{4\pi\mu}{A_\Omega C^2\rho_b}\right)^{-2} + \frac{H^{AB}\Psi_{,A}\Psi_{,B}}{N^2M^2C^2\rho_b^2} = -1, \tag{31}$$

which is the equation for ρ_b (or μ or ρ) with Eqs. (6) and the equation of state.

References

[1] J. D. Bekenstein and E. Oron, Phys. Rev. **D 18**, 1809 (1978).

[2] J. D. Bekenstein and E. Oron, Phys. Rev. **D 19**, 2827 (1979)

[3] S. Bonazzola, E. Gourgoulhon, M. Salgado, and J. A. Marck, Astron. Astrophys. **278**, 421 (1993).

[4] M. Bocquet, S. Bonazzola, E. Gourgoulhon, and J. Novak, Astron. Astrophys. **301**, 757, (1995).

[5] M. Camenzind, Astron. Astrophys. **162**, 32 (1986).

[6] B. Carter, J. Math. Phys. **10**, 70 (1969).

[7] B. Carter, in *Black Holes—Les Houches* 1972, edited by C. DeWitt and B. S. DeWitt (Gordon and Breach, New York, 1973).

[8] E. Gourgoulhon, and S. Bonazzola, Phys. Rev. **D 48**, 2635 (1993).

[9] K. Ioka, Mon. Not. R. Astron. Soc. **327**, 639 (2001).

[10] R. V. E. Lovelace, C. Mehanian, C. M. Mobarry, and M. E. Sulkanen, Astrophys. J. **62**, 1 (1986).

[11] K. Maeda, M. Sasaki, T. Nakamura, and S. Miyama, Prog. Theor. Phys. **63**, 719 (1980).

[12] C. M. Mobarry, and R. V. E. Lovelace, Astrophys. J. **309**, 455 (1986).

[13] S. Nitta, M. Takahashi, and A. Tomimatsu, Phys. Rev. **D 44**, 2295 (1991).

[14] A. Papapetrou, Ann. Inst. H. Poincaré A **4**, 83 (1966).

[15] M. Sasaki, in *Problems of Collapse and Numerical Relativity*, edited by D. Bancel and M. Signore (Reidel, Dordrecht, 1984)

Slowly decaying tails of massive scalar fields in black hole spacetimes

Hiroko Koyama [1] and Akira Tomimatsu [2]

Department of Physics, Nagoya University, Nagoya, Aichi, 464-8602, Japan

Abstract

We study the dominant late-time behaviors of massive scalar fields in static and spherically symmetric spacetimes. Considering the field evolution in the far zone where the gravitational field is weak, we show under which conditions the massive field oscillates with an amplitude that decays slowly as $t^{-5/6}$ at very late times, as previously found in (say) the Schwarzschild case. Our conclusion is that this long-lived oscillating tail is generally observed at timelike infinity in black hole spacetimes, while it may not be able to survive if the central object is a normal star. We also discuss that such a remarkable backscattering effect is absent for the field near the null cone at larger spatial distances.

1 Introduction

One of the most remarkable features of wave dynamics in curved spacetimes is tails. Scalar, electromagnetic and gravitational fields in curved spacetimes do not, in general, propagate entirely along the null cone, but are accompanied by 'tails' which propagate in the interior of the null cone. This implies that at late times waves do not cut off sharply but rather die off in tails.

In particular, it has been well established that the late-time evolution of massless scalar fields propagating in black-hole spacetimes is dominated by an inverse power-law behavior, as was first analyzed by Price [1]. In a brilliant work, Leaver [2] demonstrated that late-time tails can be associated with the existence of a branch cut in the Green's function for the wave propagation problem. Gundlach et.al. [3] showed that power-law tails also characterize the late-time evolution of radiative fields at future null infinity, while the decay rate is different from that of timelike infinity. Furthermore, it has been shown that power-law tails are a genuine feature of gravitational collapse Late-time tails develop even when no horizon is present in the background, which means that power-law tails should be present in perturbations of stars, or after the implosion and subsequent explosion of a massless field which does not result in black hole formation. The existence of these tails was demonstrated in full non-linear numerical simulations of the spherically symmetric collapse of a self-gravitational massless scalar field.

When the scalar field has a non-zero mass, the tail behaviors are quite different from massless ones. For example, as is well known, the tails exist even in Minkowski spacetimes, which is related to the fact that different frequencies forming a massive wave packet have different phase velocities[5]. If the background spacetime is curved, it is expected that interesting features peculiar to massive fields develop through the scattering due to the spacetime curvature.

Recently it was pointed out that the late-time tails of massive scalar fields in Reissner-Nordström spacetime are quite different from massless fields in the existence of the intermediate late time tails [6](see also [7]). If the Compton wave length m^{-1} of a massive field is much longer than the horizon radius of a black hole with the mass M, namely $mM \ll 1$, each multiple moment ψ of the field evolves into the oscillatory inverse power-law behavior

$$\psi \sim t^{-l-3/2}\sin(mt), \tag{1}$$

at intermediate late times. It is clear from (1) that massive fields decay slower than massless ones, and waves with peculiar frequency ω quite close to m mainly contribute to massive tail, while the

[1] E-mail:hiroko@allegro.phys.nagoya-u.ac.jp
[2] E-mail:atomi@allegro.phys.nagoya-u.ac.jp

dominant contribution to massless tails should be evaluated in the zero-frequency limit $\omega \to 0$. Though the oscillatory power-law form (1) has been numerically verified at intermediate late times, $mM \ll mt \ll 1/(mM)^2$, it should be noted that the intermediate tails are not the final asymptotic behaviors; Another wave pattern can dominate at very late times, when it still remains very difficult to determine numerically the exact decay rate [6, 7]. In the previous paper [8], we have analytically found that the transition from the intermediate behavior to the asymptotic one occurs in nearly extreme Reissner-Nordström background. The oscillatory inverse power-law behavior of the dominant asymptotic tail is approximately given by

$$\psi \sim t^{-5/6}\sin(mt), \tag{2}$$

independently of the multiple moment l, and the decay becomes slower than the intermediate ones. Then, the similar result for the decay rate has been obtained by considering massive scalar fields in Schwarzschild background (in the limited cases that $mM \ll 1$ or $mM \gg 1$, where M is the black-hole mass) [9] and massive Dirac fields in Kerr-Newman backgrounds [10]. Asymptotic behaviors of massive scalar fields in dilaton black-hole backgrounds have been also discussed [11].

These results given in [8, 9, 10] suggest that massive fields in black hole backgrounds decay as $t^{-5/6}$ generally at very late times. So it is an interesting subject to study how universally such a slowly decaying tail develops. It has been numerically shown [4] that a power-law tail develops even when the collapsing massless scalar field fails to produce a black hole. This is an evidence for the late-time tail to be a direct consequence of wave scattering in far distant regions. In this paper we prove that the decay law $t^{-5/6}$ of massive scalar fields can be essentially determined by the analysis in the far zone where the gravitational field is weak. However, we can also derive the conditions for the tails with the decay rate of $t^{-5/6}$ to dominate as an asymptotic behavior. Considering the physical interpretation of the conditions, we can claim that any spherically symmetric black holes generate the same asymptotic tails, while the conditions may not be satisfied if the central object is a normal star.

In Sec.2 we introduce the Green's function analysis to investigate the time evolution of a massive scalar field in any static, spherically symmetric spacetimes. In Sec.3 we consider the approximation valid in the far zone, and we find the conditions for the tail with the decay rate of $t^{-5/6}$ to develop. The final section is devoted to discussion , which contains a comment that the tail with the decay rate of $t^{-5/6}$ can develop also in rotating black hole spacetimes.

2 Green's function analysis

2.1 Massive scalar fields in spherically symmetric spacetimes

We consider the evolution of a massive scalar field in a static spherically symmetric background with the asymptotically flat metric given by

$$ds^2 = -f(r)dt^2 + h(r)dr^2 + r^2(d\theta^2 + \sin^2\theta d\varphi^2). \tag{3}$$

Here we do not assume the metric to be a solution of the vacuum or electrovac Einstein equations. The scalar field Φ with the mass m satisfies the wave equation

$$\Box\Phi = m^2\Phi. \tag{4}$$

Resolving the field into spherical harmonics

$$\Phi = \frac{\psi^l(t,r)}{r}Y_{l,m}(\theta,\varphi), \tag{5}$$

hereafter we omit the index l of ψ^l for simplicity, and we obtain a wave equation for each multiple moment

$$\left[\frac{\partial^2}{\partial t^2} - \frac{\partial^2}{\partial r_*^2} + V(r)\right]\psi = 0, \tag{6}$$

where r_* is the Wheeler tortoise coordinate.

The time evolution of the radial function ψ is given by

$$\psi(r_*,t) = \int [G(r_*,r'_*;t)\psi_t(r'_*,0) + G_t(r_*,r'_*;t)\psi(r'_*,0)]dr'_* \tag{7}$$

for $t \geq 0$, where the retarded Green's function G is defined as

$$\left[\frac{\partial^2}{\partial t^2} - \frac{\partial^2}{\partial r_*^2} + V\right] G(r_*,r'_*;t) = \delta(t)\delta(r_* - r'_*). \tag{8}$$

The Fourier inversion formula is

$$G(r_*,r'_*;t) = -\frac{1}{2\pi}\int_{-\infty+ic}^{\infty+ic} \tilde{G}(r_*,r'_*;\omega)e^{-i\omega t}d\omega, \tag{9}$$

where c is some positive constant. Now the Fourier component of the Green's function $\tilde{G}(r_*,r'_*;\omega)$ is expressed in terms of two linearly independent solutions for the homogeneous equation. The boundary condition for the basic solution $\tilde{\psi}_1$ is that it should be well behaved on the event horizon if the central object is a black hole, and at $r = 0$ otherwise. On the other hand, the other basic basic solution $\tilde{\psi}_2$ is required to be well behaved at spatial infinity, $r \to \infty$. Using these two solutions, $\tilde{G}(r_*,r'_*;\omega)$ can be written by

$$\tilde{G}(r_*,r'_*;\omega) = \frac{1}{W(\omega)}\begin{cases} \tilde{\psi}_1(r'_*,\omega)\tilde{\psi}_2(r_*,\omega) & , \quad r_* > r'_* \\ \tilde{\psi}_1(r_*,\omega)\tilde{\psi}_2(r'_*,\omega) & , \quad r_* < r'_*, \end{cases} \tag{10}$$

where $W(\omega)$ is the Wronskian defined by

$$W(\omega) = \tilde{\psi}_1\tilde{\psi}_{2,r_*} - \tilde{\psi}_{1,r_*}\tilde{\psi}_2. \tag{11}$$

The integrand in (9) has branch points at $\omega = \pm m$. Considering the branch points, one may change the integration path in (9). As will be shown later, the late-time tails are generated owing to the existence of a branch cut (in $\tilde{\psi}_2$) placed along the interval $-m \leq \omega \leq m$.

2.2 The analysis in a region far from the gravitational source

It has been found in the previous papers [8, 9, 10, 11] that the oscillatory power-law tails of massive scalar fields whose decay rate is $t^{-5/6}$ dominate at asymptotically late times in black-hole spacetimes. In this paper we show that the decay law can be simply derived by considering wave modes only in a far distant region, as a generic behaviors observed in any black hole spacetime.

For that purpose, we assume

$$\frac{r}{M} \gg 1, \tag{12}$$

where M is the gravitational mass of a background field. Expanding (6) as a power series in M/r and neglecting terms of order $O[(M/r)^3]$ and higher, we obtain the approximated form

$$\frac{\partial^2\tilde{\psi}}{\partial r^2} - U\tilde{\psi} = 0, \tag{13}$$

where

$$U = (m^2 - \omega^2) - \frac{2M\omega^2}{r} + \frac{2M'(m^2-\omega^2)}{r} - \frac{\lambda^2 - \frac{1}{4}}{r^2}. \tag{14}$$

The coefficient λ in (14) depends on the multiple moment l and the other parameters M, M', Q and Q'. For example, in the case of Reissner-Nordström background with mass M and charge Q, we have

$$\lambda = \sqrt{\left(l+\frac{1}{2}\right)^2 + 4m^2M^2 - 12\omega^2M^2 - m^2Q^2 + 2\omega^2Q^2}. \tag{15}$$

We keep the term of order of $O(M^2/r^{-2})$ in (13), in order to confirm that the decay rate of asymptotic timelike tails found in [8, 9, 10, 11] is independent of λ. Introducing the variable defined as

$$x = 2\varpi r, \tag{16}$$

where $\varpi = \sqrt{m^2 - \omega^2}$, (13) is rewritten by

$$\left[\frac{d^2}{dx^2} - \frac{1}{4} + \frac{\kappa}{x} - \frac{\lambda^2 - 1/4}{x^2}\right]\tilde{\psi} = 0, \tag{17}$$

where κ is

$$\kappa = \frac{Mm^2}{\varpi} - (M + M')\varpi. \tag{18}$$

3 The conditions for the slowly decaying tails to develop

Our aim is now to show that the tail with the power-law decay of $t^{-5/6}$ is a generic asymptotic behavior in black-hole spacetimes by using the wave modes satisfying (13). One may claim that the inner boundary condition to determine $\tilde{\psi}_1$ is missed if the analysis is limited to the range (12). Hence, we treat $\tilde{\psi}_1$ as a general solution for (13) and reveal a condition which allows the excitation of the asymptotic power-law tail. Fortunately we will be able to prove that such a condition is always satisfied if the event horizon exist in the background spacetime.

First, let us give $\tilde{\psi}_2$, by requiring that it damps exponentially for $|\omega| < m$ and to be purely outgoing for $|\omega| > m$ at spatial infinity. The outer boundary condition leads to

$$\tilde{\psi}_2(\varpi, r) = W_{\kappa,\lambda}(x), \tag{19}$$

where $W_{\kappa,\lambda}(x)$ is the Whittaker function [12]. Note that $W_{\kappa,\lambda}(x)$ is a many-valued function of ϖ, and there is a cut in $\tilde{\psi}_2$. The late-time tail is generated by the contribution from the branch cut in $\tilde{\psi}_2$, while $\tilde{\psi}_1$ is a one-valued function of ϖ, as was shown in [8, 9]. This is because the late-time tail is a consequence of backscattering. b In the following we will clarify under what kind of conditions for a and b the power-law tail with the decay rate of $t^{-5/6}$ asymptotically dominates.

In the far distant region $\tilde{\psi}_1$ is approximated by

$$\tilde{\psi}_1 \simeq Ae^{i2\sqrt{\kappa x}} + Be^{-i2\sqrt{\kappa x}}, \tag{20}$$

where A and B are

$$A = \pi^{-1/2}\kappa^{-1/4}x^{1/4}(2\lambda)e^{-i\pi/4}\left\{\kappa^{-\lambda}a\Gamma(2\lambda)e^{-i\pi\lambda} - \kappa^{\lambda}b\Gamma(-2\lambda)e^{i\pi\lambda}\right\} \tag{21}$$

and

$$B = \pi^{-1/2}\kappa^{-1/4}x^{1/4}(2\lambda)e^{-i\pi/4}\left\{\kappa^{-\lambda}a\Gamma(2\lambda)e^{i\pi\lambda} - \kappa^{\lambda}b\Gamma(-2\lambda)e^{-i\pi\lambda}\right\}, \tag{22}$$

respectively. In this region, independently of λ, the mode clearly shows a wave behavior with the amplitudes $|A|$ and $|B|$ corresponding to the outgoing and ingoing parts for $\omega > 0$, while $|A|$ and $|B|$ correspond to the ingoing and outgoing parts for $\omega < 0$. We find the conditions for the slowly decaying tail as $t^{-5/6}$ to develop are equivalent with the inequalities

$$|B| \gtrless |A| \tag{23}$$

for $\omega \gtrless 0$ respectively. Therefore, it is sufficient to consider the inequalities (23) independently of λ, as the conditions for the tail with the decay rate of $t^{-5/6}$ to dominate at late times. (23) means *the amplitude of ingoing waves for $\tilde{\psi}_1$ is larger than that of outgoing waves* in the far distant region.

The origin of the slowly decaying tail as $t^{-5/6}$ of a massive scalar field can be considered a resonance by cooperation between dispersion and backscattering. It is a common feature when the scalar field has a nonzero mass that in far distant regions the effective potential (14) is a monotonously increasing function with r and the radial mode shows a wave behavior. If the central object is a black hole, the conditions (23) are surely satisfied because of the existence of the event horizon. So, we can conclude that this long-lived oscillating tail is generally observed in arbitrary spherical symmetric black-hole spacetimes.

4 Discussion

We have found that whether the tail with the decay rate of $t^{-5/6}$ develops at very late times can be judged relevantly by wave modes only in far distant regions. Then, even when the central object is a rotating black hole, only the parameters M' and λ in the effective potential (14) will be changed in far distant regions. Since these are not relevant to the conditions (23), the same tail behaviors are expected to dominate also in Kerr spacetimes.

Finally we comment about late-time tail behaviors when the central object is a normal star like as a neutron star or a boson star. If the expression of $\tilde{\psi}_1$ is assumed to be extended to the region $r \leq M$, then we must require $\tilde{\psi}_1$ to be regular at $r = 0$. This leads to the equality $|A| = |B|$ which means that the amplitude of outgoing is equivalent with that of ingoing. Then the tail with the decay rate of $t^{-5/6}$ never develops. Though this extension may not be valid, we can expect the equality $|A| = |B|$ to be valid, unless some absorption of waves occurs in the inner region. This is a future problem to be checked by giving a background gravitational field with a regular center.

References

[1] R. H. Price, Phys. Rev. D **5**, 2419 (1972).

[2] E W. Leaver, Phys. Rev. D **34**, 384 (1986).

[3] C. Gundlach, R H. Price, and J.Pullin, Phys. Rev. D**49**, 883 (1994).

[4] C. Gundlach, R H. Price, and J.Pullin, Phys. Rev. D**49**, 890 (1994).

[5] P.M. Morse and H. Feshbach, *Methods of Theoretical Physics* (McGraw-Hill, New York, 1953).

[6] S. Hod and T. Piran, Phys. Rev. D **58**, 044018 (1998).

[7] L. M. Burko, *Abstracts of plenary talks and contributed papers*, 15th International Conference on General Relativity and Gravitation, Pune, 1997, p. 143, unpublished.

[8] H. Koyama and A. Tomimatsu, Phys. Rev. D **63**, 064032 (2001).

[9] H. Koyama and A. Tomimatsu, Phys. Rev. D **64**, 044014 (2001).

[10] F. Finster, N. Kamran, J. Smoller and S-T Yau, gr-qc/0107094.

[11] R. Moderski and M. Rogatko, Phys.Rev. D **64**, 044024 (2001).

[12] *Handbook of Mathematical Functions*, edited by M. Abramowitz and I.A. Stegun (Dover, New York, 1970).

[13] H. Koyama and A. Tomimatsu, gr-qc/0112075, to appear in Phys.Rev. D.

Discovery and Observation of Intermediate Massive Black Hole

T.G. Tsuru[1] H. Matsumoto
Department of Physics, Kyoto University, Kitashirakawa, Sakyo, Kyoto 606-8502, Japan

S.Matsushita
Submillimeter Array, Harvard-Smithonian Center for Astrophysics, P.O. Box 824, Hilo, HI 96721-0824, USA

R.Kawabe
National Astronomical Observatory, Osawa, Mitaka 181-8588, Japan

T.Harashima
Toyokawa, Minolta Co., Ltd., 2-41, Koumyou-cho, Toyokawa 442-8570, Japan

F.Iwamuro, T.Maihara
Department of Astrophysics, Kyoto University, Kitashirakawa, Sakyo, Kyoto 606-8502, Japan

T.Ebisuzaki
Advanced Computer Center, RIKEN, 2-1, Hirosawa, Wako 351-0198, Japan

J.Makino
Department of Astronomy, University of Tokyo, 7-3-1, Hongo, Bunkyo, Tokyo 113-0033, Japan

Abstract

By using ASCA and Chandra, we discovered a new type of black hole, intermediate massive black hole (IMBH), at the off-center position in the starburst galaxy M82. We also found and expanding molecular super bubble (EMSB) surrounding the IMBH with Nobeyama Millimeter Array. One of the seven star clusters which we detected with Subaru Telescope observation was identified with the IMBH within the absolute position accuracy. The results suggest the IMBH was formed in the starburst activity $10^6 \sim 10^7$ yrs ago. We also introduce a new formation scenario of SMBH through the merging of IMBHs which fall into galaxy center by the dynamical friction.

1 Introduction

The existence of two types of black holes (BHs) has been known, so far. One is the stellar mass black hole, whose mass is $\sim 10 M_\odot$. A representative of this type is well-known Cyg X-1. This type of BH is born from a supernova due to the gravitational collapse of a high mass star. The other type is so-called super massive black hole (SMBH), which is found at the center of almost all the galaxies. The mass of a SMBH exceeds $\sim 10^6 M_\odot$ and sometimes reaches $\sim 10^9 M_\odot$, which is same as the mass of a small galaxy. Some of them, about $\sim 1\%$ to $\sim 10\%$, have activities and are observed as active galactic nuclei (AGN) and QSO in many wave lengths.

Evolution of X-ray luminosity function of AGN detected with X-ray deep surveys indicates that a SMBH was very active in the early Universe of $z = 2 - 5$ but is inactive at present[1]. The discovery that the mass of a SMBH is proportional to the bulge mass proves that the origin of a SMBH connects with the galaxy formation in spite that the SMBH is a very local existence at a galactic center[2].

After the big bang, the universe cooled down once and it was recombined from plasma state to neutral state at the redshift of ~ 1000. After that, the birth of first star and galaxy formation were made at the redshifts between 1000 and 10. At the redshift between 10 and 5, the whole universe was heated up and re-ionized, again. The energy source of this big event is thought to be UV lights from QSOs containing SMBH. Therefore, SMBH should have been formed at the same time or just after the galaxy formation.

[1] E-mail:tsuru@cr.scphys.kyoto-u.ac.jp

Thus, SMBH and AGN have been playing very important roles in the evolution of the universe and galaxy. However, the formation mechanism of SMBH is still mystery. Since the mass of a SMBH is very high, it can not be formed at once, but it should have been growing up little by little. If it is the case, the baby of a SMBH should be found in a young galaxy. Then, we search for a baby SMBH in observe a young galaxy, that is starburst galaxy.

Starburst galaxy is thought to be a galaxy in which burst star formation is occurring at galactic nucleus. In the case of M82 galaxy, which is a prototype of starburst galaxy, the star formation rate is $\sim 10^4$ times higher than the value in our galaxy. Burst star formation causes very high supernova rate and burst formation of stellar mass black holes. Inter stellar matter heated up by the supernovae finally escapes from the gravity of galaxy and galactic wind is formed. The starburst galaxy is thought to be a prototype of young galaxy in the early universe. Among them, M82 galaxy is the most famous and the nearest starburst galaxy and has been investigated in many wavelengths. Then, we observed M82 galaxy with X-ray, IR, and radio.

2 X-ray Observation

2.1 ASCA

We made X-ray observations of M82 with two epoch making X-ray satellites. One is Japanese X-ray satellite ASCA, which was the first X-ray CCD mission and enabled hard X-ray imaging observation above 2keV due to the multi thin foil mirrors. The other is Chandra X-ray observatory launched in 1999. The image resolution reaches about one arcsec, which is almost same as the one of Subaru telescope.

Figure 1 shows the X-ray spectrum of M82 obtained with ASCA [3]. The spectrum is well fitted with two optically thin thermal plasma components with the temperatures of $kT = 0.32$, 0.95keV and a hard component, whose absorption and temperature are $N_{\rm H} = 1.9 \times 10^{22}{\rm cm}^{-2}$ and $kT = 13.8$keV, respectively. Imaging analysis revealed that the two optically thin thermal plasma components are significantly extended. On the other hand, the hard component is point-like within the ASCA resolution.

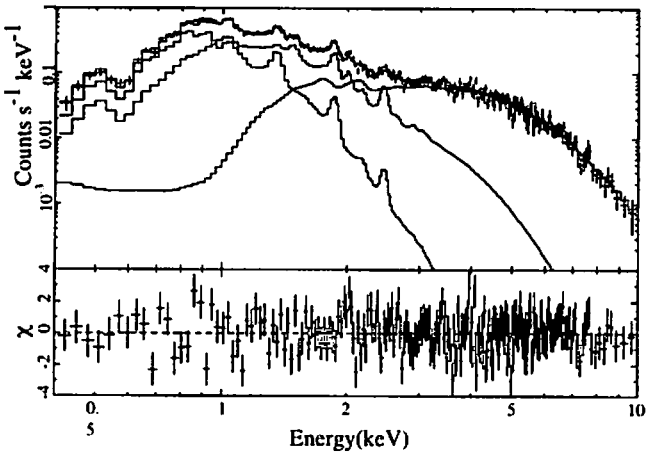

Figure 1: ASCA SIS0+1 (X-ray CCD) spectrum obtained within a 6'.0 radius from the center of M82 and the best-fit model[3].

If the hard component originates in an actual point source, it should have time variability. Thus, we made monitoring observation with ASCA. The monitoring observation was made at 9 exposures with each exposure time of 10ksec spanning over a half year.

The left panel of figure 2 shows the long term light curves of 0.7-1.5keV and 3-10keV bands obtained with GIS onboard on ASCA[4, 5]. There is significant time variability in 3-10keV, in spite that the counting rate in 0.7-1.5keV band is stable through the monitoring observation. Adding to the long term

variability, we found short time variability in 3-10keV band within a day, which is shown in the right panel of figure 2. This is a direct evidence for the existence of a high luminous BH in M82.

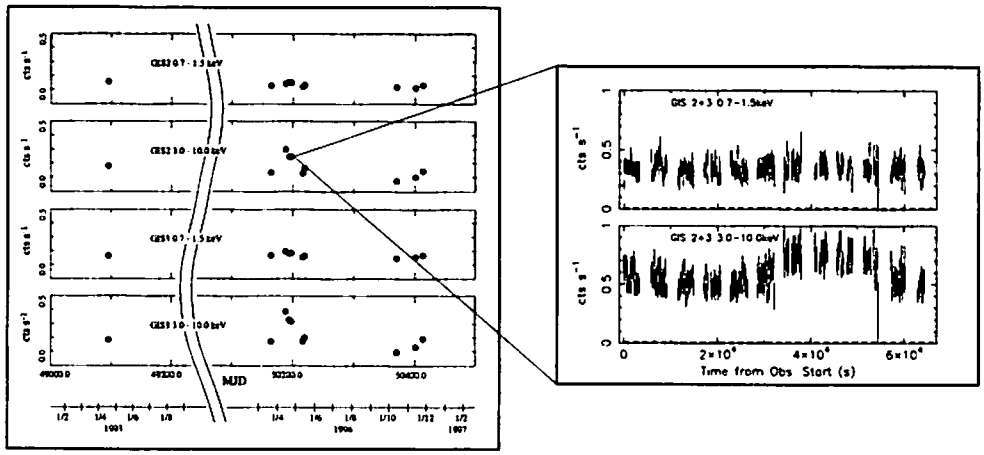

Figure 2: Long (left) and short (right) term light curves at the energy bands of 0.7-1.5keV and 3-10keV obtained with ASCA GIS2 and 3[4].

2.2 Chandra

In order to investigate the precise position of the BH in M82, we made observation with Chandra X-ray observatory. The exposures were made twice and we found about ten sources near the galactic center shown in the left panel of figure 3, most of which were time variable[6, 7]. No X-ray source is found at the galaxy center of M82. Among the X-ray sources detected, only the brightest source No.7 can explain the X-ray luminosity of the time variable source we found with ASCA (see the right panel of figure 3). Thus, we concluded that the source No.7 is the BH discovered with ASCA.

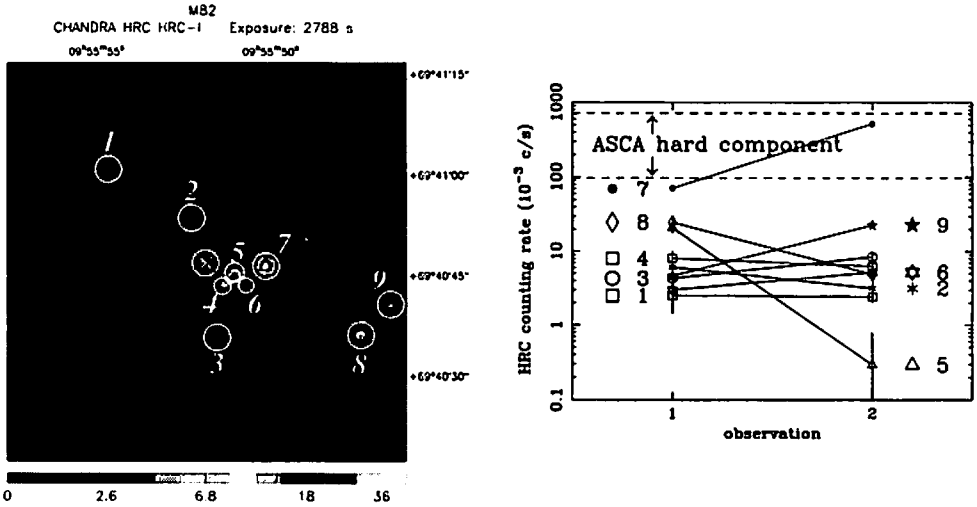

Figure 3: Chandra HRC image of the center region of M82 obtained in the 1st exposure (left)[6]. The light curves of point sources detected from the HRC observation (right).

2.3 Summary of X-ray Observation

The discussion and summary of X-ray observations are given in this section [6]. The source No.7 has time variability of 3hr with high X-ray luminosity as shown in the ASCA light curve, which immediately concludes that the source is an X-ray luminous BH. The mass accretion onto the BH by its gravity is made against the radiation pressure from the source. Then, the lower limit on the mass of the BH can be obtained from the following inequality (Eddington Limit),

$$M_{\rm BH} > \frac{\sigma_{\rm T} L_{\rm X}}{4\pi c G m_{\rm p}}, \tag{1}$$

where $M_{\rm BH}$, $L_{\rm X}$, $\sigma_{\rm T}$ are the BH mass, X-ray luminosity and Thomson cross section. The lower limit on the BH mass is obtained to be $700 M_{\odot}$, which is too heavy as a stellar mass BH. Thus, the source No.7 is not stellar mass BH. Chandra observation revealed that the source No.7 is located at galactic off-center, 170 pc apart from the M82 dynamical center. SMBH known so far is always located at a galactic center. Then, it is concluded that the source No.7 is not SMBH, either. Since the mass of M82 within 170pc from the galactic center is estimated to be $\sim 10^7 M_{\odot}$, the mass of source No.7 is lower than $10^7 M_{\odot}$, otherwise its position should have been the dynamical center. Although we do not go into detail in this paper, the mass of the source No.7 should be lower than $\sim 10^6 M_{\odot}$ from the discussion of the dynamical friction. Then, the mass of the source No.7 is lower than the mass of a SMBH. Thus, from the two significant natures of its mass and position, we concluded that the source No.7 is a new type of BH and named it Intermediate Massive Black Hole (IMBH).

3 Near IR and Radio Observation

3.1 Subaru Telescope

Next, we made observation with Subaru Telescope, 8.2m optical an infrared telescope on Mauna Kea. Subaru Telescope has the largest single-piece mirror in the world. Figure 4 shows K'-band image of central region of M82 with Subaru Telescope[8]. We detected many young star clusters in the center region of M82. Adding to this, we found that one of the star clusters has the consistent position with the one of the IMBH within the position accuracy (see figure 4). Then, we concluded that the IMBH is located in the star cluster.

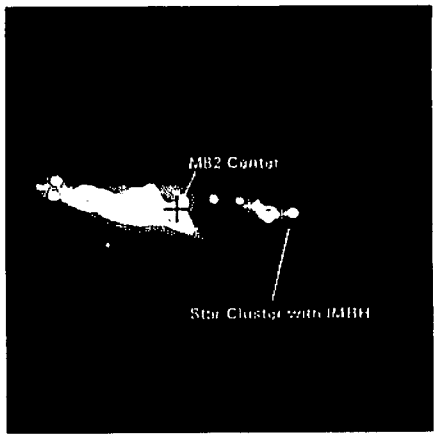

Figure 4: Near IR (K'-band) image of the center region of M82 obtained with CISCO of Subaru Telescope.

3.2 Nobeyama Millimeter Array

We made radio observation with Nobeyama Millimeter Array (NMA) located in Nagano prefecture. NMA is an interferometer with 6 10m antennas and enables imaging and spectroscopy observation of molecular clouds. The left panels of figure 5 shows the radio image of carbon monoxide (CO) in M82 obtained with NMA[9]. We next obtained a position velocity map (P-V map) along this line. P-V map is velocity distribution of the molecular cloud as a function of position. As shown in the left bottom panel of figure 5, we found a peculiar structure. In the normal case, a spiral galaxy is rigidly rotating. Therefore, a straight line is expected in the P-V map (see figure 5). On the other hand, the peculiar structure found in M82 indicates the existence of an expanding molecular supper bubble (EMSB).

The right panel of figure 5 shows the radio image of the EMSB, we discovered. The EMSB is located at galactic off-center and its kinetic energy reaches $\sim 10^{55}$ergs, which is equivalent with $\sim 10^4$ SNe. We estimated the age of $\sim 10^6$ yrs from the size and the expanding velocity of EMSB. These results suggest that a burst star formation and $\sim 10^4$ SNe explosions occurred $\sim 10^6$ yrs ago at galactic off-center position. From the comparison with X-ray image, we found that the IMBH is located at the center of the EMSB.

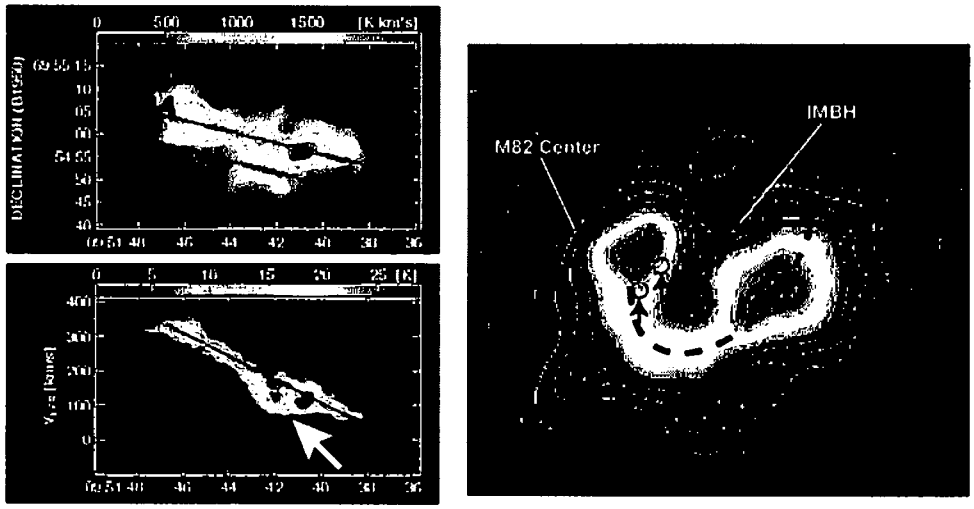

Figure 5: Left: Radio image (top), P-V map (bottom) of CO in the center region of M82 obtained with Nobeyama Millimeter Array [9]. White arrow in the P-V map indicates the peculiar expanding structure newly discovered with our observation. Right: Expanding Molecular Super Bubble in M82. The three arrows indicate the positions of the source No.4, 5 and 6 in the left panel of figure3.

Observational results and discussion give above are summarized here. We discovered a new type of black hole, IMBH, located at galactic off-center, whose mass is within the range from 10^3 to $10^{6-7}M_{\odot}$. We also discovered an EMSB formed by 10^4 SNe at 10^6 yrs ago. The IMBH is located at center of EMSB and in a young star cluster. From these results, we concluded that the IMBH was born from starburst activity forming the EMSB.

4 Formation Scenario of SMBH and Galaxy Evolution

From the observational results shown above, we introduced a new formation scenario of IMBH and SMBH[10]. The scenario is based on N-body simulation with the GRAPE computer, which is special purpose computer designed for gravitational N-body simulation. The 6th generation of GRAPE reaches 100 Tflops. Figure 6, 7 and 8 show the schematic view of our scenario.

Phase 1: Formation of IMBH

1. In the beginning of the galaxy formation, starburst starts and many star clusters are formed from the gravitationally collapsed molecular clouds in the primordial galaxy. In a star cluster, high mass and low mass stars are born.
2. The high mass stars sink into the core of the star cluster by dynamical friction.
3. Since the cross section of the high mass star is significantly large, the merging of high mass stars occurs in the core of the star cluster and a single very massive star is born.
4. The very massive star immediately collapses into a BH with hundreds solar mass, which is the baby of an IMBH.
5. The baby IMBH swallows the surrounding stars and ambient gas, then grows up to be an IMBH.

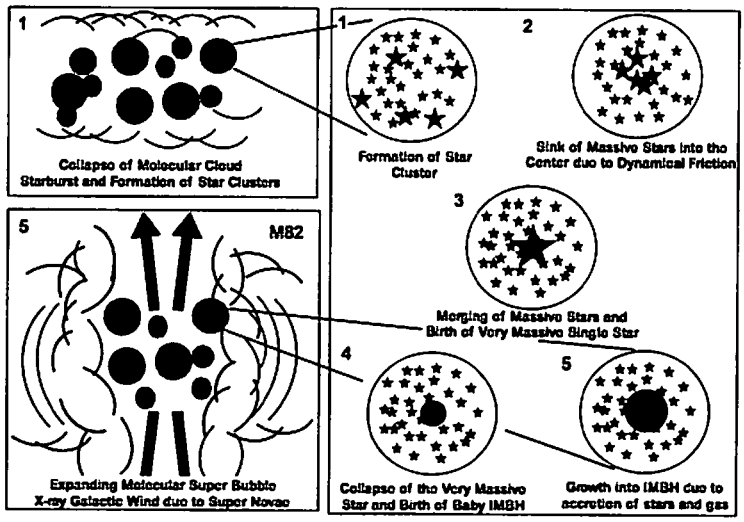

Figure 6: Formation scenario of IMBH and SMBH (Phase 1).

During the phase 1, other remaining high mass stars which did not merge explode as supernovae. As a result, the inter stellar matter is heated up or swept by the shock wave from supernovae, then galactic wind and EMSB are formed.

Phase 2: Formation of SMBH and AGN

6. At the end of starburst in the phase 1, an IMBH is born only in a star cluster with a high density core. Then, a high mass star cluster contains an IMBH but a low mass star cluster does not.
7. High mass star clusters start sinking toward the galactic center by dynamical friction, again. The high mass star clusters also convey IMBHs into the galactic center. On the other hand, low mass star clusters are blown off toward the halo.
8. The high mass star clusters merge each others in the galactic center region. On the other hand, the IMBHs conveyed by the star clusters continue sinking into the galactic center.
9. The merging of IMBHs occurs by radiating gravitational wave, and a single SMBH is finally born.
10. Due to the accretion of surrounding stars and ambient gas, the SMBH becomes active in radiation and jet. Thus, the SMBH is observed as an AGN in the early universe. On the other hand, the remnant of merged star clusters forms the bulge structure of the galaxy. The low mass star clusters blown off to the halo come to be globular clusters at present.

Phase 3: From an AGN to Quiet Galaxy

11. All the surrounding stars and ambient gas are finally consumed by the AGN, then the SMBH stops its activity and becomes quiet. This is quiet galaxy at present such as Andromeda Galaxy and our Galaxy.

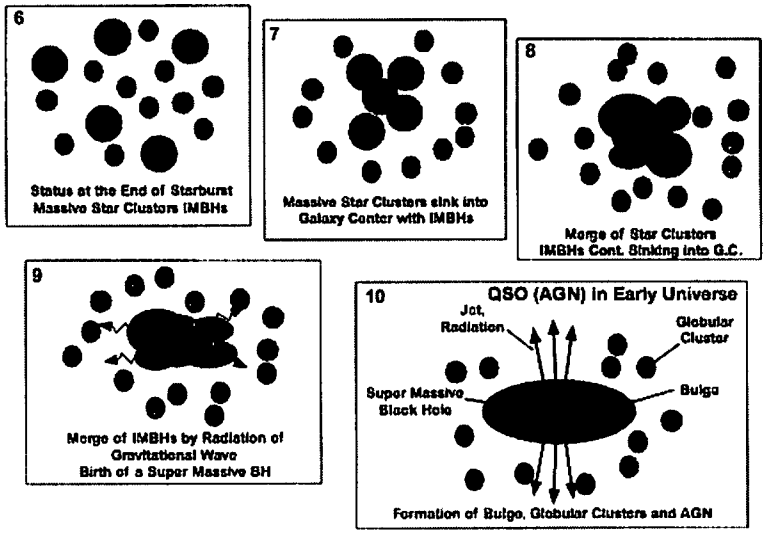

Figure 7: Formation scenario of IMBH and SMBH (Phase 2).

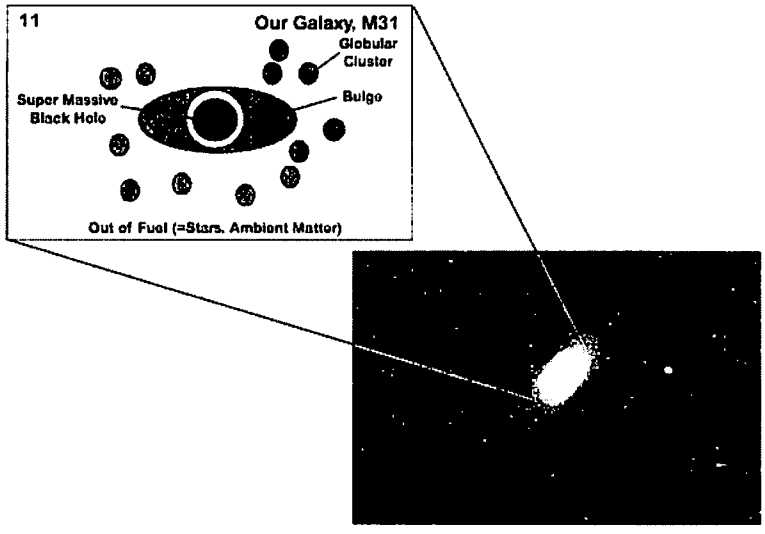

Figure 8: Formation scenario of IMBH and SMBH (Phase 3).

5 On-going and Future Projects

The scenario stated above explains not only the formation of SMBH but also the evolution of a galaxy. However, it is still just a scenario. Then, we are making further studies on the birth of SMBH and

evolution of galaxy. We have two on-going projects. A wide range is still allowed for the mass of IMBH in M82. Then, the first project is the determination of the mass of the IMBH in M82 with the IRCS Echelle spectrometer of Subaru Telescope.

The second project is the search for the 2nd M82. Recently, two groups have reported the detection of candidates for IMBHs with Chandra observation. One is done in the starburst galaxy NGC3628. Chandra detected a bright source at galactic off-center[11]. In spite that the X-ray luminosity of the source is a factor of 10 lower than the IMBH in M82, the situation is very similar. The other one is from the Chandra observation of the "Antennae" galaxies NGC4038 and 4039. The two galaxies of NGC4038 and 4039 are merging each other and strong starburst is going on. Several X-ray sources with luminosities of $\sim 10^{40}$ergs s^{-1} were detected from Chandra observation[12]. These two studies are concentrated on X-ray observation. However, we think that multi-wave lengths observation is essential to figure out the birth of IMBH and SMBH. Then, we are observing another promising starburst galaxy NGC2146 with X-ray and radio bands, as we made to M82. The radio observation was already done and our Chandra monitoring observation in the summer of 2002 is scheduled.

After the on-going projects, I (TGT) would like to go into these two future projects with Astro-E2 satellite, which is scheduled to be launched in Feb. 2005. First one is the study of the galactic wind. In the early phase of galaxy evolution, galaxy is thought to have been injecting a large amount of energy into intergalactic space as a form of galactic wind with metal enriched high temperature plasmas. Therefore, it should have played important roles in the evolution of the universe and galaxy. The second is the study of BH itself and general relativity. ASCA discovered gravitational redshifted iron K-emission line from AGN and gave the first direct observational evidence for the existence of Kerr BH[13, 14]. This is the beginning of observational study on the black hole itself as a real existence and spacetime geometry close to the black hole, which will be further pushed up by the observation of the fine structure of the emission lines with Astro-E2.

References

[1] Miyaji,T., Hasinger,G., Schmidt,M., A&A **369**, 49.

[2] Gebhardt,K., et al. ApJL **539**, L13.

[3] Tsuru,T.G. et al. PASJ **49**, 619.

[4] Matsumoto,H., Tsuru,T. 1999, PASJ, **51**, 321

[5] Ptak,A. et al. 1999, ApJ, **517**, L85

[6] Matsumoto,H. et al. 2001, ApJL, **547**, L25

[7] Kaaret,P. et al. 2001, MNRAS, **321**, L29

[8] Harashima,T. et al. 2002, in preparation

[9] Matsushita,S. et al. 2000, ApJL, **545**, L107

[10] Ebisuzaki,T. et al. 2001, ApJL, **562**, L19

[11] Strickland,D.K., et al. 2001, ApJ, **560**, 707

[12] Fabbiano,G., et al. 2001, ApJ, **554**, 1035

[13] Tanaka,Y., et al. 1995, Nature, **375**, 659

[14] Iwasawa,K., et al. 1997, MNRAS, **282**, 1038

Japanese References

天文月報 1999年9月号

パリティ 2001年5月号

日本物理学会誌 2001年6月号

Are intermediate-mass Black Holes really the "Missing links" between stellar and supermassive black holes? — A view from a stellar dynamicist.

Junichiro Makino[1]

Department of Astronomy,
School of Science, The University of Tokyo
7-3-1 Hongo, Bunkyo-ku, Tokyo 113-0033, Japan

Abstract

Recently, an "intermediate mass" black hole (IMBH) was found in the central region of galaxy M82 through observations made by ASCA, Chandra and SUBARU. This is the first finding of a black hole with the mass more than 100 solar mass but significantly less than 1 million solar mass, and, as such, has completely changed our understanding of the formation process of massive blackholes. We describe our new scenario in which IMBHs serve as the "missing link" between stellar-mass and supermassive black holes. IMBHs first form in young compact star clusters through runaway merging of massive stars. While these IMBHs are forming, the host star clusters sink toward the galactic nucleus through dynamical friction, and upon evaporation deposit their IMBHs near the galactic center. The IMBHs then form binaries and eventually merge via gravitational radiation, forming a supermassive BH.

1 Introduction

It is now well established that the central engines of QSO and AGN activities are supermassive black holes (SMBHs) which lie at the very center of galaxies (see, e.g., [11]). In addition, there is rapidly growing evidence for SMBHs in the centers of many galaxies (for a review, see [10]). Although relatively few galaxies show conclusive evidences for central black holes, even fewer galaxies exist for which observations indicate that a central SMBH does not exist [9].

Even so, how these SMBHs are formed is not at all understood. Our theoretical understanding has not advanced much beyond the scenarios described by Rees [25, 26] in the early 1980s. In his famous diagram, Rees draw basically two scenarios in which SMBH are formed from massive gas clouds. The first one is direct monolithic collapse, the second is via the formation of a star cluster, with subsequent runaway collisions leading to BH formation.

However, numerical studies have demonstrated that either scenario is not likely. Let us consider the first scenario. If we perform one-dimensional simulation of the spherically-symmetric collapse, we can easily form SMBHs from initial gas clouds. However, in reality there are always non-spherical perturbations such as rotations, external tidal field and small-scale structures. Any of these prevents the formation of single massive BH, since at some point non-spherical collapse leads to fission. The final outcome of the gravitational collapse of massive gas clouds is most likely a cluster of stars, not a single SMBH.

How about the second scenario? Can we form SMBHs from star clusters? If the cluster is compact enough, through thermal evolution the central core of the cluster would shrink and become relativistic. However, in order for sizable fraction of the cluster mass to become relativistic, the velocity dispersion of the cluster must be very high right from the beginning, since the velocity dispersion goes up only very slowly as the collapse proceeds. In the case of the self-similar collapse, we have

$$\rho_c \propto r_c^{-2.23} \tag{1}$$

where ρ_c and r_c are the central density and the core radius. From the virial theorem, we have $v_c \propto r_c^{-0.12}$, where v_c is the central velocity dispersion. Thus, it is clearly impossible to form a relativistic core from

[1] E-mail:makino@astron.s.u-tokyo.ac.jp

usual dynamical evolution of a stellar system. In practice, long before the core becomes relativistic, the self-similar collapse would be halted by the energy production from binary stars formed through three-body interaction.

A different possibility to form BH in a star cluster is through merging of stars or stellar-mass BHs in close encounters. If there is a fair number of massive stars initially in the cluster, they might directly evolve into stellar-mass BHs. At the time of the formation, they are not the most massive objects in the cluster. However, in a relatively short time, they become the most massive object, since stars which are more massive than stellar-mass BHs will become neutron stars through Type II supernovae. The BHs then sink to the cluster core through dynamical friction, and might form a compact core of BHs. Here again the velocity dispersion is not large. In fact, for the core of the massive object, the velocity dispersion can be lower than the velocity dispersion of the cluster as a whole. A massive BH cannot be formed even from a core made of stellar mass BHs.

However, as we stated above, the collapse of the core is halted by the formation of binary stars, which transfer their gravitational binding energy to kinetic energies of other stars (BHs) in the core through binary-single star scattering. Such scattering events, on average, result in the increase of the binding energy of the binary, and therefore the orbit of the binary shrinks. If the orbit can shrink sufficiently that the timescale of the gravitational wave radiation becomes short enough, a BH binary would merge. However, recent N-body simulations [23] have demonstrated that practically all of these black-hole binaries are ejected from the cluster by recoil of interactions with other BHs before they merge through gravitational radiation. Thus, it is unlikely that BHs grow through merging in star clusters. In fact, Portegies Zwart and McMillan [23] argued that this is the reason why we do not see any massive BH at the centers of globular clusters.

There are a variety of other theories and scenarios to form SMBHs. Since there are so many of them, here we decline even from just listing some of them. All theories so far proposed share one common shortcomming. There is no observational support. Of course, this is not the fault of any theorist. Just that no one has ever seen an SMBH in its making.

2 IMBHs in M82

M82 is one of the nearest starburst galaxies, and its central activity has attracted the interest of observers. Matsumoto and Tsuru [16] observed the central region with ASCA X-ray satellite, and found a pointlike source which showed short-time variation and AGN-like spectrum. The Eddington mass was around 400 $M_\odot$.

Matsushita *et al.* [18] observed the same region with Nobeyama Millimeter Array and found a huge expanding shell of the molecular gas. They estimated the age and kinetic energy of the shell to be around 1 Myr and 10^{55} erg, suggesting that a strong starburst took place a few Myr ago.

From these two observations, Taniguchi *et al.* [28] proposed that an IMBH of the mass around $10^3 M_\odot$ had been formed through the merging of compact objects formed by Type II Supernovae (SNe). The energy of the expanding shell implies 10^4 SNe. So there are more than enough compact objects to form an IMBH. Difficulty, however, is how we can let that many of compact objects to merge in such a short time. As we have discussed in some details in section 1, compact objects in a star cluster are not likely to merge with each other.

Recent high-resolution observations in X-ray and Infrared have completely changed our view of M82.

Matsushita and Tsuru [17] have identified nine bright compact X-ray sources in the central region of M82 using recent Chandra data. The brightest source (No. 7 in their Table 1) had a luminosity of 9×10^{40}erg/s in Jan 2000, corresponding to a BH with a minimum mass of $700 M_\odot$ (assuming the Eddington luminosity). It probably consists of a single compact object, as its X-ray flux shows rapid time variation [17]. This object is bright enough to explain the pointlike source observed by ASCA ([16]). Among the eight other sources, at least three (5, 8 and 9) have Eddington masses greater than $30 M_\odot$.

Chandra results add quite a bit more information to what was already known by ASCA and NMA. First of all, the pointlike X-ray source is really a collection of point sources, but most of the luminosity comes from a single source. Second, this brightest source, with Eddington mass of $700 M_\odot$ is not at the dynamical center of M82 but at the center of the expanding gas shell. Thus, it is quite unlikely that

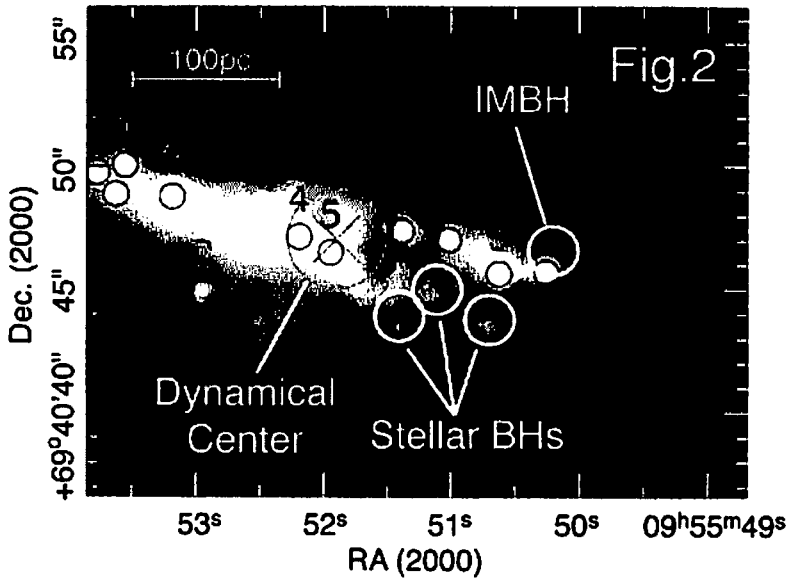

Figure 1: IR (K' band) image of the central region of M82 by SUBARU IRCS. black dots are candidates of star clusters and white circles are the locations of bright X-ray point sources found by Chandra. Courtesy of Dr. Iwamuro.

these two are unrelated, but it is still unclear how we can form an IMBH from large number of compact objects.

The key to understand the relation between the starburst and the IMBH was brought to us by SUBARU. Harashima *et al.* [6] observed the same region in the IR (J, H, and K'-band) using the CISCO instrument on the SUBARU telescope [6]. They identified a number of young compact star clusters. At least four of them coincide with the X-ray sources within the positional uncertainties of Chandra and SUBARU. The other five Chandra X-ray sources are far outside the central starburst region of M82. Even so, two of them coincide with infrared sources in the 2MASS point source catalog. The logical conclusion from these observations is that most of the Chandra X-ray sources, including the brightest one with an Eddington mass of $700M_{\odot}$, were formed in star clusters.

Therefore, we now "know" for sure that an IMBH (or its candidate) is formed in a young and bright cluster. Nevertheless, we also know that it is unlikely that an IMBH is formed through merging of compact objects in a star cluster, no matter how massive and how compact the star cluster is (except for the case where we have really relativistic cluster). Clearly, some of the assumptions we made must be wrong.

3 IMBH formation through runaway growth

One candidate of the wrong assumption is that merging would occur after massive stars become compact remnants. This assumption is okay for globular clusters, where the timescale of the dynamical friction for the most massive stars is much longer than the lifetime of massive stars. Typical relaxation time of present-day globular clusters is 1 Gyrs or longer, and therefore the dynamical friction timescale of a 100 $M_{\odot}$ star is around 10 Myr, since the dynamical friction timescale is proportional to the inverse of the mass. Mergings are most likely to occur at the core of the cluster, where the number density of the stars is the highest. If the most massive stars experiences SNe before they can sink to the core by dynamical friction, it is reasonable to assume that the core of the cluster will be dominated by compact remnants.

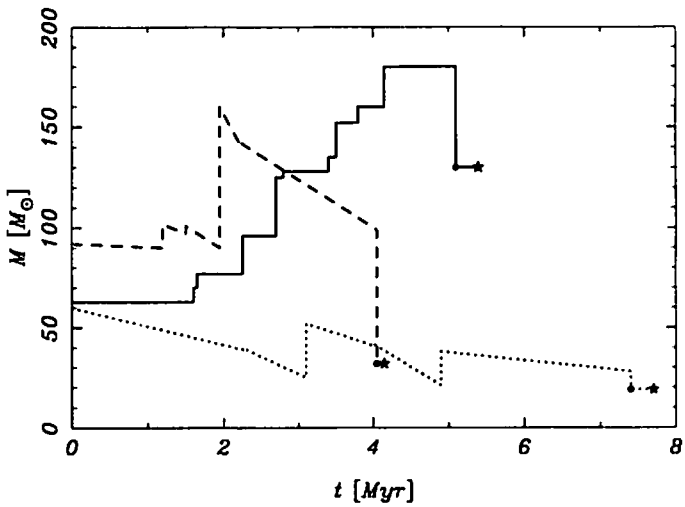

Figure 2: The growth of the most massive star in model clusters, in simulations by Portegies Zwart *et al.* [21]. The horizontal axis is time in Myrs and the vertical axis the mass in unit of the Solar mass. Solid curve shows the result of the run with no mass loss during the main sequence phase. Dashed and dotted curves are with different assumptions on mass loss. Figure kindly provided by Dr. Portegies Zwart.

However, the star clusters in M82 are young, having experienced SNe just a few Myrs ago, and yet the IMBH is there. So we should consider the possibility that massive stars sink to the core before they go SNe, and merge with each other.

Massive stars in star clusters have higher merging rates than less massive cluster members (or field stars) because of their larger geometrical cross sections and a stronger gravitational focusing, and concentration to the core by dynamical friction in the cluster. In addition, complex resonances in binary-single star encounters contribute to a significant increase in merging rate of massive stars [8, 20]. If these effects are strong enough, we expect that the "merging instability" [12], or runaway growth of the most massive star, will occur in the cluster core. In fact, N-body simulations carried out by Portegies Zwart *et al.* [21] have demonstrated that runaway merging can take place in a systems containing $\sim$ 12,000 stars, before stellar evolution eliminates the most massive stars. In their calculation, almost all merging events took place during resonant three-body interactions. Stars are assumed to always merge when physically collide in their calculation. This assumption is generally okay since the velocity dispersion of the cluster is not very large, 30 km/s or less. We can regard encounters essentially parabolic, even in the cases in which they occur during three-body interactions.

In one case, the most massive star experienced more than ten collisions and reached a mass of around $200M_\odot$ before evolving into a supernova. There is considerable uncertainty as to how much mass would remain as a BH after the supernova explosion of such a massive star, but it is quite likely that the remnant BH would still be one of the most massive objects in the cluster, and that the runaway merging process would continue. There is also significant uncertainty concerning the rate of mass loss in the main sequence phase, which has very strong effect on the final mass of the runaway merger. However, even in the case where the mass loss is large, the runaway merger would still be the most massive star in the cluster, and therefore the resulted BH would be one of the most massive stars in the cluster.

In order for the runaway merging to occur, dynamical friction timescale for the most massive stars must be short enough that they can sink to the center during their lifetime of several Myr. The dynamical friction timescale may be expressed as follows [equation 7-26 in [3]]:

$$t_{\rm fric} = \frac{1.17}{\log\Lambda}\frac{r^2 v_c}{Gm} \simeq 2.7\times10^7 \left(\frac{r}{1{\rm pc}}\right)^2 \left(\frac{r_h}{10{\rm pc}}\right)^{-1/2} \left(\frac{M}{10^6 M_\odot}\right)^{1/2} \left(\frac{20M_\odot}{m}\right) {\rm yr}, \qquad (2)$$

where $\log\Lambda$ is the Coulomb logarithm, G is the gravitational constant, v_c is the local velocity dispersion, r is the distance from the center of the cluster, r_h and M are the half-mass radius and the total mass of the cluster, and m is the mass of the star. Here, it is assumed that the background stellar distribution is that of the singular isothermal sphere. Thus, if the cluster has a very large core, the above equation underestimates the timescale for stars in the core. Such a large core, however, is probably unlikely.

In the following, we consider how dynamical friction works in the cluster found in M82. From the infrared luminosity, Harashima *et al.* [6] estimate that the total mass of the cluster is $\sim 5\times10^6 M_\odot$. They also estimated the seeing-corrected radius of the cluster as 5 pc, which is most likely a good estimate of r_h. For $r = 0.5\mathrm{pc} \sim 0.1 r_h$, a volume which contains about 5% of the total cluster mass, the dynamical friction timescale is less than 10 Myr. We therefore conclude that a significant fraction of the most massive stars sink to the cluster center and undergo runaway merging before exploding as supernovae.

Note that it is much harder to let runaway merging to occur in a typical globular cluster with the size of 10 pc and mass of $5\times10^5 M_\odot$. Here again, massive stars within the distance around $r = 0.5\mathrm{pc} \sim 0.05 r_h$ might participate in the runaway merging, but the total mass in this region is a factor of 30 smaller than that in our cluster in M82. Thus, very roughly speaking, typical number of merging events would also be smaller by a factor of 30.

After the BH has become much more massive than other cluster members, it forms a cusp near the cluster center [1], and continues to swallow other stars. Unfortunately, no realistic simulations of this phase of the evolution are available. Marchant and Shapiro [19] performed Monte-Carlo simulations of this stage for a simplified cluster containing 3×10^5 solar-mass stars and one 50 solar-mass seed BH.

This initial condition itself is rather unrealistic, since the underlying assumption is that a BH can be formed through the self similar collapse of globular cluster. Even so, we can use their result to predict what would occur to a seed BH in our star cluster in M82.

They found that the BH mass jumped to over $10^3 M_\odot$ (0.3% of the cluster mass) almost immediately after they put the BH into the system. After this initial rapid growth, a slower phase ensued, with a doubling timescale comparable to the relaxation time of the cluster. Their result should be regarded as a lower limit on the BH growth rate, since realistic effects, in particular the presence of a mass spectrum, would greatly enhance the accretion rate. Taking these effects into account, it seems safe to suppose that 0.1% of the total cluster mass accretes to form a $\sim 5000 M_\odot$ central BH in a few Myr.

As stated above, there are more than 10 bright star clusters in the vicinity of the IMBH host cluster in M82, some of them apparently hosting small BHs. Their age is around 10 Myr [6]. Also, the starburst in M82 is a long-duration event, having started at least 200 Myr ago [5]. If we assume that clusters form at a constant rate, we conclude that around 200 clusters have been formed. We believe it is safe to assume that around one hundred clusters similar to our host cluster have formed in total, and that a considerable fraction of them host IMBHs.

4 Building up the central SMBH

It seems we have at least one plausible theoretical model for the formation of IMBHs in young and compact star clusters near the center of a starburst galaxy. It is also quite likely many other such IMBHs are formed during the starburst. Thus, if we can let these IMBHs sink to the center and merge with each other, we can make massive central BHs, of the mass $10^5 M_\odot$ or more.

It is rather easy to bring IMBHs down to the center of the galaxy. The host cluster would sink toward the center of the galaxy, by the same dynamical friction mechanism which brought massive stars within the cluster to the center of the cluster.

Rewriting equation (2) using appropriate scaling for this case, we find that the timescale on which the cluster sinks to the galactic center via dynamical friction is

$$t_{\mathrm{fric}} \simeq 6\times10^8 \left(\frac{r}{1\mathrm{kpc}}\right)^2 \left(\frac{v_c}{100\mathrm{kms}^{-1}}\right) \left(\frac{5\times10^6 M_\odot}{m}\right) \mathrm{yr}. \quad (3)$$

Clusters initially within 1 kpc of the galactic center can therefore reach the center within one Gyr. Note that an IMBH can reach the galactic center only if its host cluster can sink to the center before it evaporates. If the cluster dissolves before significant orbital decay occurs, the timescale for the IMBH to fall to the center increases greatly.

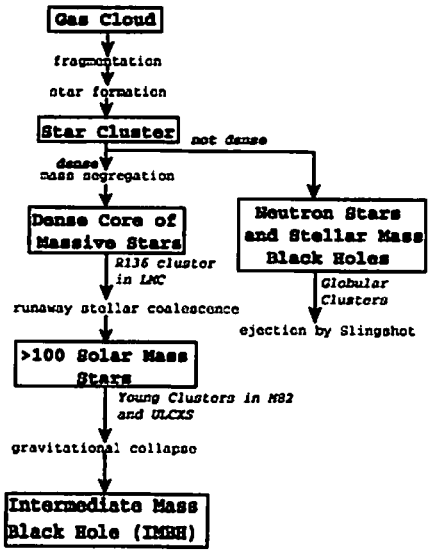

Figure 3: Schematic diagram of the formation process of an intermediate-mass black hole (IMBH). From Ebisuzaki *et al.*[4].

Evaporation is driven partly by thermal relaxation and partly by stellar mass loss. Portegies Zwart *et al.* [22] estimated that the evaporation timescale for a tidally limited compact star cluster is around 2-3 half-mass relaxation times, which is of the order of a few Gyr for our star clusters.

As the cluster sinks toward the center, the tidal field of the parent galaxy becomes stronger and the mass loss rate becomes higher. However, for a thermally well-relaxed cluster, this effect is relatively small since the cluster has almost isothermal cusp within the half-mass radius. In this case, very roughly speaking, the mass within the Roche lobe is proportional to the distance to the galactic center. Thus, even if we take into account the effect of enhanced mass loss, the timescale of orbital decay becomes shorter as the cluster sinks, and it will deposit the central BH to the very center of the galaxy. At this time, the entire cluster must have been dissolved.

The next, and final, question is whether multiple IMBHs at the center of the galaxy can merge or not. The evolution of massive binary black holes was first discussed by Begelman *et al.* [2]. They took into account dynamical friction from field stars and energy loss via gravitational radiation. They found that the merging timescale depends strongly on mass, and for a very massive BH with a mass of $10^8 M_\odot$ in which they were interested, merging took much longer than a Hubble time.

A binary BH evolve much in the same way as a binary star in a dense star cluster evolve, through interaction with other stars. In the case of a binary star, interactions with other stars results in a roughly linear growth of the binding energy, since interaction cross section σ is proportional to the inverse of the semi-major axis a in the regime of strong gravitational focusing. The average amount of the increase of the binding energy E is around $0.4E$ (see Spitzer [27]).

In the case of usual binary stars in a star cluster, this process continues until two components merge through collision or the binary itself is ejected from the cluster through the recoil of three-body encounter. Most of the increase of the binding energy is carried away by the third star, but the center-of-mass motion of the binary also receives kinetic energy. If the resulted velocity is larger than the escape velocity, they escape from the cluster.

In the case of massive BH binary, however, the evolution is more complex. First, the binary would not escape from the galaxy through interaction with usual field stars, simply because the binary is far more massive. In practice, since the BH binary is so much more massive than field stars, the random velocity of the BH binary is very small and the BH binary can be regarded as staying at the center of

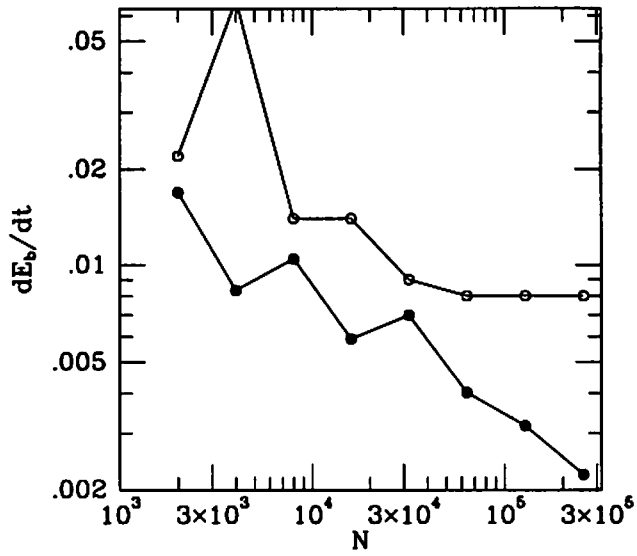

Figure 4: The time evolution of the energy of the BH binary for runs with N = 2k (bottom) to 256k (top). Thin curves represent 2k (solid), 4k (short dashed), 8k (long dashed) and 16k (dot dashed) runs. Thick curves represent 32k (solid), 64k (short dashed), 128k (long dashed) and 256k (dot dashed) runs. From Makino [14].

the galaxy.

However, this fact that the BH binary stays at the center causes a different problem. The BH binary evolves through close encounters with other stars. In the case of a usual binary in a star cluster, the random velocity of the center of mass motion of the binary is comparable to that of field stars and the binary can interact with any other stars in the core. However, the BH binary can interact only with stars with the angular momentum small enough to approach to BH binary. Once all the stars with low angular momentum are expelled, the evolution of the binary would stop. The stars would then slowly diffuse into orbits with low angular momentum through two-body relaxation. Begelman *et al.* [2] estimated the evolution timescale of black hole binary and concluded that the timescale is much longer than the Hubble time, for the case of supermassive BH binary ($\sim 10^8 M_\odot$) in elliptical galaxies. This is the so-called "loss-cone depletion" effect, which also limit the growth timescale of a single BH in a cluster or a galactic center.

However, whether this loss-cone depletion actually occur or not is still an open question. Recent extensive numerical simulations [13, 14, 24] have shown that the hardening of the BH binary through dynamical friction is in fact several orders of magnitude faster than the prediction from loss-cone arguments. Though the number of particles employed (up to 256k) was not large enough to model SMBH binaries, it was certainly large enough to model evolution of IMBH binaries. With 256k particles, the mass ratio between the BH particles and field particles is 2560, which directly corresponds to the case of IMBH.

In Makino [14], I simulated the evolution of binary BHs formed in the mergings of two identical spherical galaxies both of which containing central BHs. Thus, the intention of my simulation was to model the evolution of BH binaries formed in the merging of elliptical galaxies which already contain massive central BHs. However, we can interpret results obtained in these simulations to predict the fate of IMBHs which are brought to the center of the parent galaxy by sinking star clusters.

For all simulations, I set the BH mass as 1% of the initial total mass of the galaxy. For standard runs, initial galaxy model is the King model with $W_0 = 7$.

Figure 4 shows the evolution of the binding energy of the binary, for standard runs with a wide range

of number of particles. The system of unit is "Heggie" unit [7], where $M = G = -4E = 1$. Here, M is the total mass of one galaxy, G is the gravitational constant and E is the total energy of the galaxy. In this unit, $t_c = 2\sqrt{2}$ is the standard half-mass crossing time. We let two galaxies collide from a parabolic orbit. Therefore the initial total energy of the entire system is $2E = -0.5$.

We can see that the evolution of the binding energy of the BH binary is rather fast, reaching to the binding energy comparable to the total energy of the system in 10 crossing time or so.

The timescale of the gravitational radiation is given by

$$t_{\rm GR} = 2 \times 10^{15} g(e) \left(\frac{M_{\rm BH}}{10^4 M_\odot}\right)^{-3} \left(\frac{a}{0.001{\rm pc}}\right)^4 \quad {\rm yr}, \tag{4}$$

with $g(e)$ given by

$$\begin{aligned} g(e) &= \frac{(1-e^2)^{7/2}}{1+(73/24)e^2+(37/96)e^4} \\ &\simeq 2(1-e)^{7/2} \quad (e \sim 1). \end{aligned} \tag{5}$$

which, in our unit,

$$t_{\rm GR} = 1.2 \times 10^8 g(e) \left(\frac{M_{\rm BH}}{10^4 M_\odot}\right) \left(\frac{v_c}{150{\rm km/s}}\right)^{-8} E_b^{-4} \quad {\rm yr}. \tag{6}$$

Here, v_c is the velocity dispersion of the stars in physical unit and E_b is the binding energy of the binary BH in our unit. Thus, if the binding energy of the BH binary can reach around $E_b = 3$ in our unit, BHs would merge through gravitational wave radiation in about 1 Myrs. If the orbit is somewhat eccentric, the timescale would be much shorter.

The dynamical timescale in our unit is translated to the physical unit by the following relation.

$$t_c = 1.7 \times 10^4 \left(\frac{M_{\rm BH}}{10^4 M_\odot}\right) \left(\frac{v_c}{150{\rm km/s}}\right)^{-3} \quad {\rm yr}. \tag{7}$$

Within several hundred time units, E_b would reach unity. Thus, the merging timescale of an IMBH binary would be several Myrs.

If the timescale of the merging is shorter than the typical time interval at which star clusters containing IMBHs reach the center, we can conclude that BHs would merge and grow. However, several Myrs is not quite short enough, since several tens of IMBHs might reach to the center with 100 Myrs or so. What would happen if third BH falls in before two BHs merge?

One possibility is that at least the third BH is ejected through interaction with the binary, as it is in the case of binaries in star clusters. However, there is one difference. The potential well of the parent galaxy is much deeper than that of a typical star cluster. Therefore, the BH binary becomes very tightly bound before it can escape from the galaxy. The typical orbital velocity of the binary components when they escape from the parent galaxy (or cluster) is around $10v_c$, where v_c is the central velocity dispersion of the galaxy. The gravitational wave timescale is still very long, if we assume a circular orbit. However, here we almost certainly know that the eccentricity is high. The most conservative estimate would be to assume that eccentricity e follows the thermal equilibrium, where $f(e) = 2e$. In this case, average eccentricity is 0.7, for which $t_{\rm GR}$ is almost two orders of magnitude shorter than that for the circular binary. In practice, the effect of eccentricity is much larger, for the following two reasons. First, the binary would experience more than one encounters with the third BH before ejection. Therefore, the expected value for the maximum eccentricity is significantly higher than the average value of 0.7. Second, it is known that the actual distribution of the eccentricity after strong interaction with the third BH is biased to higher eccentricity than the thermal distribution. Makino and Ebisuzaki [15] analyzed the first effect, and concluded that effective merger timescale by gravitational wave radiation is about 3×10^3 times shorter than that for a circular binary.

Thus, when there are three IMBHs at the center of the galaxy, we can expect that in most cases two of them would merge through gravitational wave radiation. In almost all cases where the merging would take place, it would be between two most massive ones. The fate of the least massive one is difficult to

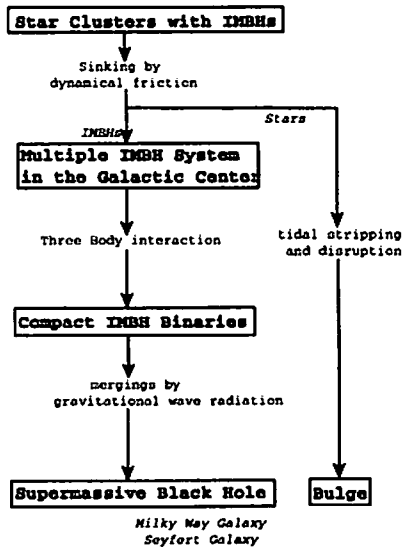

Figure 5: Schematic diagram of the formation of supermassive black holes from star clusters containing intermediate-mass BHs (IMBHs). From Ebisuzaki *et al.*[4].

predict. In some cases it may be ejected from the galaxy. In other cases they would remain in the galaxy when the two other BHs merge, and form the binary again.

Once one BH has become more massive than typical infalling BHs, it becomes extremely unlikely that it will be ejected, since the recoil velocity from three-body interactions is inversely proportional to the mass (because of momentum conservation). Thus, even though some of the infalling BHs might be ejected by the slingshot mechanism, the central BH will continue to grow.

5 Discussion

In this paper, we have discussed the implications for our understanding of the SMBH formation mechanism of the recent discovery of an IMBH in M82. Our conclusion is that the IMBH found in M82 plays the role of "missing link" between stellar-mass BHs and SMBHs.

Our proposed scenario is a rather complicated two-stage one. In the first stage, the seed BH is formed through merging of massive stars in a young and compact star cluster, which is formed during a nuclear starburst. This seed BH grows further by mergings with other massive stars in the cluster, and eventually becomes IMBH similar to what was found in M82.

In the second stage, the parent cluster of IMBH sink to the center of the galaxy through dynamical friction, and deposits the IMBH to the center of the galaxy. If the starburst resulted in the formation of many clusters, fairly large number of IMBHs would be brought to the galactic center. These IMBHs would merge either through dynamical friction from field stars or through three-body interaction of three BHs.

In both stages, two stellar-dynamical mechanisms play essential roles: dynamical friction and three-body interaction. Dynamical friction brings the massive stars (stage 1) or star cluster (stage 2) to the center. Three-body interaction of massive objects increases the chance of merging.

Clearly, the view presented here is biased by the fact I am a stellar dynamicist, and the scenario discussed in this paper ignores many other physics which might play important roles. Here we just list a few of them. First of all, we ignore completely the possible effect of the gas in star cluster or galaxy center. In the case of the star cluster, gas dynamics would not be very important since the potential well

of the cluster is not deep enough to trap gas. However, for galactic center the gas would certainly play important role, and most likely effect of the presence of gas is to greatly accelerate the merging of binary BH [2]. Other important astrophysical processes include the evolution and final fate of massive stars and the outcome of the close encounter of IMBH and massive main-sequence stars.

From the side of the theoretical study, the largest uncertainty is in the stellar evolution. Both the study of the "microphysics", namely the evolution of massive stars and merger outcome, and the "macrophysics", where we study the sensitivity of the outcome to the assumptions in microphysics, will be important.

A more important question is to what degree we can regard M82 as "typical". Certainly, M82 is not a normal galaxy, because it is a nearby starburst galaxy. Most of galaxies might have experienced a period of very high star formation rate when they were young, but whether the scenario we discussed here is applicable to such young galaxies is something we cannot answer now.

On the other hand, it seems that our scenario fits rather well into the standard cosmological scenario in which structures are formed "bottom up". In the bottom-up scenario, galaxies are formed through merging of a number of gas-rich protogalaxies. In such merging events, large fraction of the gas would be swept to the center of the merger product, as has been demonstrated by a number of simulations of merging and galaxy formations. Thus, nuclear starburst is a quite natural outcome expected from the bottom-up scenario, and compact star clusters which is similar to what is observed in M82 may be a common feature of such nuclear starburst.

A rather different question is whether we can form the supermassive galaxies in elliptical galaxies and QSOs with the proposed scenario. My personal opinion is that it's a bit unlikely, simply because QSOs do have massive accretion disks and high accretion rate (otherwise they are not luminous). Clearly, the gas accretion is the primary mechanism for the growth of supermassive BHs. If we consider that ellipticals are formed through merging of smaller galaxies, we would expect similar infall of gas as in the case of nuclear starbursts. So why in some cases nuclear starbursts occur, and in other cases the gas directly reach to the vicinity of central black holes? One possible explanation is that the presence of the massive BH itself prevents the star formation, either through strong gravitational field or through UV radiation.

To summarize, the finding of IMBH in M82 opens up the possibility of the understanding of the formation process of massive BHs with, at least, some observational evidences and constraints. We described one scenario which seems plausible. However, our scenario is certainly not the only possibility and there many problems yet to be solved.

I'd like to thank Toshi Ebisuzaki, Takeshi G. Tsuru, Yoko Funato, Sachiko K. Okumura, Satoshi Matsushita, Piet Hut, Steve McMillan, Simon Portegies Zwart and a number of other people for invaluable discussions. This work is supported in part by the Research for the Future Program of Japan Society for the Promotion of Science (JSPS-RFTP97P01102).

References

[1] J. N. Bahcall and R. A. Wolf, The Astrophysical Journal **209** (1976) 21.

[2] M. C. Begelman, R. D. Blandford, and M. J. Rees, Nature **287** (1980) 307.

[3] J. Binney and S. Tremaine, *Galactic Dynamics*, (Princeton University Press, Princeton, 1987).

[4] T. Ebisuzaki, J. Makino, T. Go Tsuru, Y. Funato, S. Portegies Zwart, P. Hut, S. McMillan, S. Matsushita, H. Matsumoto and R. Kawabe, The Astrophysical Journal Letters **562** (2001) L19.

[5] R. de Grijs, R. W. O'Connell, and J. S. Gallagher, The Astronomical Journal **121** (2001) 768.

[6] T. Harashima, et al., in preparation (2002)

[7] , D. C. Heggie and R. D. Mathieu, in *The Use of Supercomputers in Stellar Dynamics*, eds P. Hut and S. McMillan, (Springer, New York, 1986), p 233.

[8] P. Hut and S. Inagaki, The Astrophysical Journal **298** (1985) 502.

[9] J. Kormendy and R. D. McClure, The Astronomical Journal **105** (1993) 1793.

[10] J. Kormendy and D. Richstone, Annual Review of Astronomy and Astrophysics **33** (1995) 581.

[11] J. H. Krolick. *Active galactic nuclei: from the central black hole to the galactic environment* (Princeton University Press, Princeton, 1999).

[12] H. M. Lee, The Astrophysical Journal **319** (1987) 801.

[13] J. Makino, T. Fukushige, S. K. Okumura, and T. Ebisuzaki, Publications of Astronomical Society of Japan **45** (1993) 303.

[14] J. Makino, The Astrophysical Journal **478** (1997) 58.

[15] , J. Makino and T. Ebisuzaki, The Astrophysical Journal **436** (1994) 607.

[16] H. Matsumoto and T. G. Tsuru, Publications of Astronomical Society of Japan **51** (1999) 321.

[17] H. Matsumoto,T. G. Tsuru, K. Koyama, H. Awaki, C. R. Canizares, N. Kawai, S. Matsushita, and R. Kawabe, The Astrophysical Journal **547** (2001) L25.

[18] S. Matsushita, R. Kawabe, H. Matsumoto, T. G. Tsuru, K. Kohno, K. Morita, S. K. Okumura, and B. Vila-Vilar, The Astrophysical Journal Letters **545** (2000) L107.

[19] A. B. Marchant, and S. L. Shapiro, The Astrophysical Journal **239** (1980) 685.

[20] S. L. W. McMillan, The Astrophysical Journal **306** (1986) 552.

[21] S. F. Portegies Zwart, J. Makino, S. L. W. McMillan, and P. Hut, Astronomy and Astrophysics **348** (1999) 117.

[22] S. F. Portegies Zwart, J. Makino, S. L. W. McMillan, S. and P. Hut, The Astrophysical Journal **546** (2001) L101. Astronomy and Astrophysics**348** (1999) 117.

[23] S. F. Portegies Zwart, and S. L. W. McMillan, S. L. W., The Astrophysical Journal **528** (2000) L17.

[24] G. D. Quinlan and L. Hernquist, New Astronomy **2** (1997) 533.

[25] M. J. Rees, The Observatory **98** (1978) 210.

[26] M. J. Rees, Annual Review of Astronomy and Astrophysics **22** (1984) 471.

[27] , L. Spitzer, Jr., *Dynamical Evolution of Globular Clusters*, (Princeton University Press, Princeton, New Jersey, 1987).

[28] Y. Taniguchi, Y. Shioya, T. G. Tsuru, and S. Ikeuchi, Publications of Astronomical Society of Japan **52** (2000) 533.

Radiation-Hydrodynamical Growth of Supermassive Black Holes and QSO Formation

Masayuki Umemura[1]

Center for Computational Physics, University of Tsukuba
Tsukuba, Ibaraki, 305-8577, Japan

Abstract

As a novel mechanism to build up a supermassive black hole, the radiation drag by the intense radiation from a starburst in a bulge is considered. It is found that the putative correlation between black hole mass and bulge mass is basically determined by a fundamental constant, that is, the energy conversion efficiency for nuclear fusion of hydrogen to helium, $\epsilon = 0.007$. Based upon the present radiation hydrodynamical model for the formation of supermassive black holes, a scenario for the QSO formation is proposed in relation to ultraluminous infrared galaxies and narrow line type I AGNs.

1 Introduction

The recent discovery of high redshift quasars (Fan et al. 2001) implies that the formation of supermassive black holes proceeded in less than 10^9 yr. Also, the recent compilation of the kinematical data of galactic centers in both active galaxies and inactive ones has shown that a central 'massive dark object' (MDO), which is the nomenclature for a black hole (BH) candidate, correlates with the properties of galactic bulges. The demography of MDOs have revealed the following relations:

1) The BH mass exhibits a linear relation to the bulge mass with the ratio of

$$f_{\rm BH} \equiv \frac{M_{\rm BH}}{M_{\rm bulge}} = 0.001 - 0.006 \tag{1}$$

as a median value (Kormendy & Richstone 1995; Richstone et al. 1998; Magorrian et al. 1998; Gebhardt et al. 2000a; Ferrarese & Merritt 2000; Merritt & Ferrarese 2001a).

2) The BH mass correlates with the velocity dispersion of bulge stars with a power-law relation as $M_{\rm BH} \propto \sigma^n$, $n = 3.75$ (Gebhardt et al. 2000b) or 4.72 (Ferrarese & Merritt 2000; Merritt & Ferrarese 2001a, b).

3) The $f_{\rm BH}$ tends to grow with the age of youngest stars in a bulge until 10^9 yr (Merrifield et al. 2000).

4) In disk galaxies, the mass ratio is significantly smaller than 0.01 if the disk stars are included (Salucci 2000; Sarzi et al. 2001).

5) For quasars the $f_{\rm BH}$ is of a similar level to that for elliptical galaxies (Laor 1998).

6) The $f_{\rm BH}$ in Seyfert 1 galaxies is not well converged, which may be considerably smaller than 0.01 (Wandel 1999; Gebhardt et al. 2000a) or similar to that for ellipticals (McLure 2001), while the BH mass-to-velocity dispersion relation in Seyfert 1 galaxies seems to hold good in a similar way to elliptical galaxies (Gebhardt et al. 2000a; Nelson 2000).

On the other hand, the observations of the X-ray emission (Brandt et al. 1997) or Paα lines (Veilleux, Sanders, & Kim 1999) intrinsic for active nuclei have been detected in roughly one forth of ultraluminous infrared galaxies (ULIRGs). Furhtermore, it has been revealed that QSO host galaxies are mostly luminous and well evolved early-type galaxies (McLeod & Rieke 1995; Bahcall et al. 1997; Hooper, Impey, & Foltz 1997; McLeod, Rieke, & Storrie-Lombardi 1999; Brotherton et al. 1999; Kirhakos et al. 1999; McLure et al. 1999; McLure, Dunlop, & Kukula 2000). These observations lead to the paradigm proposed by Sanders et al. (1988) that ULIRGs could evolve into QSOs. Comprehensively judging from all these findings on QSO hosts and supermassive BHs, it is likely that the formation of a QSO, a bulge, and a supermassive BH is mutually related.

[1] E-mail:umemura@rccp.tsukuba.ac.jp

Some theoretical models have been hitherto considered to explain the BH-to-bulge correlations, e.g., hydrodynamical ones including a wind-regulation model (Silk & Rees 1998) or an inside-out accretion model (Adams, Graff, & Richstone 2001), and self-interacting dark matter model (Ostriker 2000). But, little has been elucidated regarding the physics on the angular momentum transfer which is inevitable for BH formation, since the rotation barrier by the tidal spin up in a growing density fluctuation is given by

$$\frac{R_{\rm barr}}{R_{\rm Sch}} \approx 10^7 \left(\frac{M_b}{10^8 M_\odot}\right)^{-2/3} \left(\frac{\lambda}{0.05}\right)^2 (1+z)^{-1} \tag{2}$$

in units of the Schwarzshild radius $R_{\rm Sch}$, where M_b is the baryonic mass, z is the cosmological redshift, and λ is the spin parameter which provides the ratio of circular velocity to velocity dispersion of dark matter (Sasaki & Umemura 1996). Here, R_{barr} is estimated by $R_{barr} = j_b(z)^2/GM_b$, where j_b is the specific angular momentum given by $j_b \simeq R_{\rm max}\sigma\lambda$ with $R_{\rm max}$ being the maximum expansion radius of the fluctuation. Furthermore, required mechanisms for BH formation must work effectively in a spheroidal system like a bulge. The α-viscosity or non-axisymmetric gravitational instabilities would effectively transfer angular momentum once a disk-like system forms, but they are not likely to work in a spheroidal system.

In this paper, as a potential mechanism in a spheroidal system, the relativistic drag force by the radiation from bulge stars is considered, and the BH-to-bulge ratio is derived with incorporating radiation hydrodynamics jointly with simple stellar evolution in a bulge. As a result, the BH-to-bulge ratio is basically determined by the energy conversion efficiency for nuclear fusion of hydrogen to helium, $\epsilon = 0.007$. Also, in relation to BH growth, a scenario for quasar formation is addressed.

2 Formation of Supermassive Black Holes

2.1 Mass Accretion due to Radiation Drag

A radiation hydrodynamical model which could account for the putative correlations between supermassive BHs and bulges is recently proposed by Umemura (2001), where the relativistic drag force by the radiation from bulge stars is considered. The radiation drag can extract angular momentum from gas and allow the gas to accrete onto the center (Umemura, Fukue, & Mineshige 1997, 1998; Fukue, Umemura, & Mineshige 1997). For the total luminosity L_* of a uniform bulge, the radiation energy density is given by

$$E \simeq L_*/cR^2, \tag{3}$$

where c is the light speed and R is the radius of the bulge. Then, the angular momentum loss rate by the radiation drag is given by

$$d\ln J/dt \simeq -\chi E/c, \tag{4}$$

where J is the total angular momentum of gaseous component and χ is the mass extinction coefficient which is given by $\chi = \kappa_d/\rho$ with dust absorption coefficient κ_d and gas density ρ. Therefore, in an optically-thin regime,

$$d\ln J/dt \simeq -\frac{\tau L_*}{c^2 M_g}, \tag{5}$$

where τ is the total optical depth of the system and M_g is the total mass of gas. In an optically-thick regime, the radiation drag efficiency is saturated due to the conservation of the photon number (Tsuribe & Umemura 1997). Thus, an expression of the angular momentum loss rate which includes both regimes is given by

$$d\ln J/dt \simeq -\frac{L_*}{c^2 M_g}(1-{\rm e}^{-\tau}). \tag{6}$$

In practice, it is likely that optically-thin surface layers are stripped from optically-thick clumpy clouds by the radiation drag, and the stripped gas losing angular momentum accretes onto the center (Kawakatu & Umemura 2002). Since the radiative cooling is effective in the surface layers, the accretion is likely

to proceed in an isothermal fashion until an optically-thick massive dark object forms. Then, the mass accretion rate is estimated to be

$$\dot{M} = -M_g \frac{d\ln J}{dt} \simeq \frac{L_*}{c^2}(1 - e^{-\tau}). \tag{7}$$

In an optically-thick regime, this gives simply

$$\dot{M} = \frac{L_*}{c^2}, \tag{8}$$

which is numerically

$$\dot{M} = 0.1 M_\odot \mathrm{yr}^{-1} \left(\frac{L_*}{10^{12} L_\odot}\right). \tag{9}$$

This rate is comparable to the Eddington mass accretion rate for a black hole with $10^8 M_\odot$, that is,

$$\dot{M}_{\rm Edd} = 0.2 M_\odot \mathrm{yr}^{-1} \eta^{-1} \left(\frac{M_{\rm BH}}{10^8 M_\odot}\right), \tag{10}$$

where η is the energy conversion efficiency. Unless otherwise stated, $\eta = 0.42$ for an extreme Kerr black hole is assumed. The timescale of radiation drag-induced mass accretion is

$$t_{\rm drag} \simeq \frac{c^2 R^2}{\chi L_*} = 8.6 \times 10^7 \mathrm{yr} R_{\rm kpc}^2 \left(\frac{L_*}{10^{12} L_\odot}\right)^{-1} \left(\frac{Z}{Z_\odot}\right)^{-1}, \tag{11}$$

where $R_{\rm kpc} = R/\mathrm{kpc}$ and Z is the metallicity of gas. It is noted that the gas which is more abundant in metals accretes in a shorter timescale, because the extinction is predominantly given by the dust opacity. For the moment, an optically-thick stage is considered. Due to the mass accretion induced by the radiation drag, a massive dark object (MDO) forms at the center on bulge. Then, the mass of MDO is estimated by

$$M_{\rm MDO} = \int_0^t \dot{M} dt \simeq \int_0^t L_*/c^2 dt. \tag{12}$$

Next, we employ a simplest analytic model for bulge evolution. The star formation rate is assumed to be a Schmidt law, $S(t) = k f_g$. If we invoke the instantaneous recycling approximation, the star formation rate is given by

$$\dot{M}_*/M_b = k e^{-\alpha k t}, \tag{13}$$

where α is the net efficiency of the conversion into stars after subtracting the mass loss. The radiation energy emitted by a main sequence star is 0.14ϵ to the rest mass energy of the star, $m_* c^2$, where ϵ is the energy conversion efficiency of nuclear fusion from hydrogen to helium, which is 0.007. Thus, the luminosity of the bulge is estimated to be

$$L_* = 0.14 \epsilon k e^{-\alpha k t} M_b c^2. \tag{14}$$

By substituting this in (12),

$$M_{\rm MDO} = 0.14 \epsilon \alpha^{-1} M_b (1 - e^{-\alpha k t}). \tag{15}$$

The term $M_b(1 - e^{-\alpha k t})$ represents just the stellar mass in the system which is $M_{\rm bulge}$ observationally. As a consequence, the MDO mass to bulge mass ratio is given by

$$\frac{M_{\rm MDO}}{M_{\rm bulge}} = 0.14 \epsilon \alpha^{-1} = 0.002 \alpha_{0.5}^{-1}, \tag{16}$$

where $\alpha_{0.5} = \alpha/0.5$. It should be noted that the final mass is basically determined by ϵ. This is just comparable to the observed ratio.

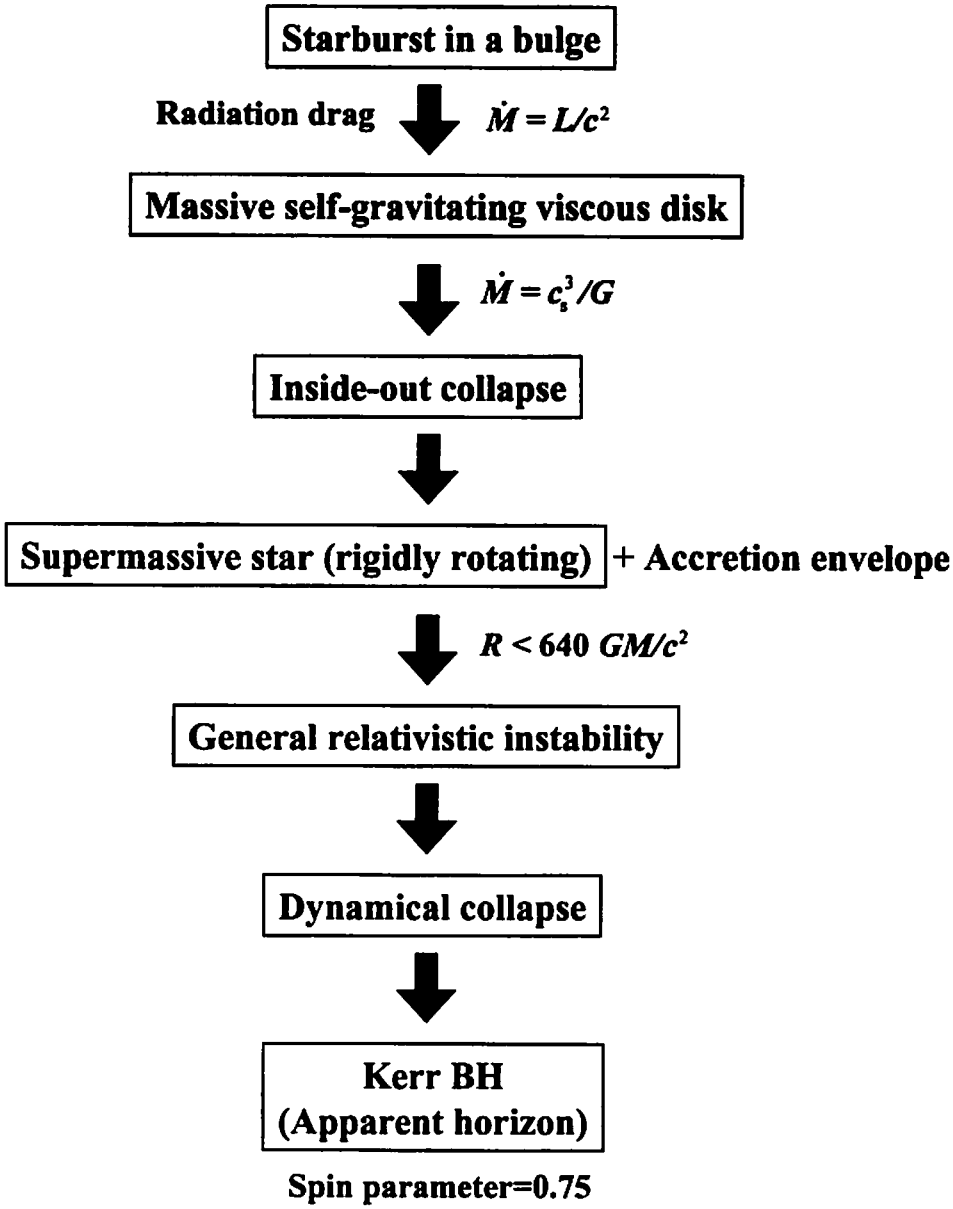

Figure 1: A picture for the formation of a supermassive black hole from a galactic scale to a horizon. The radiation from a starburst in a bulge exerts the radiation drag onto dusty interstellar gas. Resultantly, the interstellar gas sheds angular momentum and accrete onto the center to form a massive dark object (MDO). The MDO is equivalent to a massive self-gravitating viscous disk. This disk undergoes the inside-out viscous collapse to form a rigidly rotating supermassive star with accretion envelope. A rigidly rotating supermassive star becomes subject to the general relativistic instability. Then, the supermassive star collapse dynamically and eventually a Kerr black hole is born.

2.2 Towards the Horizon

In the above, the prediction for the MDO-to-bulge mass relation is made in the context of radiation drag-induced mass accretion. However, the MDO itself is not a supermassive black hole, because the radiation drag is not likely to remove the angular momentum thoroughly, but some residual angular momentum will terminate the radial contraction. Hence, we should consider the further collapse of the MDO through other physical mechanisms.

In the MDO, the viscosity is expected to work effectively because the timescale for viscous accretion is given by $j/\alpha_{\rm v}c_s^2$, where j is the specific angular momentum, $\alpha_{\rm v}$ is the viscous parameter, and c_s is the sound velocity. Thus, the MDO is likely to be a massive self-gravitating viscous disk. For a self-gravitating viscous disk, some self-similar solutions are known to give an inside-out disk collapse (Mineshige & Umemura 1996; Mineshige & Umemura 1997; Tsuribe 1999). In particular, Tsuribe (1999) provided a convenient formula for the inside-out mass accretion rate,

$$\dot{M}_a = \frac{3\alpha_{\rm v}c_s^3}{QG}, \tag{17}$$

where Q is the Toomre's Q which is $\kappa c_s/\pi G\Sigma$ for the epicycle frequency κ and the surface density Σ. Tsuribe (1999) has found a solution of stable accretion with $Q \approx 2$. The critical accretion rate is given by

$$\dot{M}_a \simeq \frac{c_s^3}{G} = 0.24 M_\odot {\rm yr}^{-1} \left(\frac{T}{10^4\ {\rm K}}\right)^{3/2}. \tag{18}$$

This rate is again comparable to the Eddington mass accretion rate for a black hole with $10^8 M_\odot$ [see (20)] if $T \approx 10^4$K. Through this inside-out collapse, a central core grows. The core is expected to be a rigidly rotating supermassive star because the viscous transfer of angular momentum works to smear out any differential rotation in a self-gravitating system.

The equilibrium configuration and the stability of a rigidly rotating supermassive star has been scrutinized by Baumgarte & Shapiro (1999). They found that a rotating supermassive star becomes unstable for $R < 640/GM/c^2$. As for the dynamical collapse of a rotating supermassive star, Saijo et al. (2002) performed post-Newtonian calculations and found that if a rotating supermassive star is in rigid rotation, it can collapse towards the horizon scale without undergoing bar-mode instability. The final stage of the collapse was investigated by Shibata (2002) with a full general relativistic approach and the emergence of an apparent horizon of a Kerr black hole was shown. The resultant spin parameter of the black hole is around 0.75.

Hence, a massive dark object formed by radiation drag-induced mass accretion could evolve into a supermassive Kerr black hole through the inside-out viscous collapse and the general relativistic instability. The present picture for the formation of a supermassive black hole is summarized in Figure 1.

3 QSO Formation

3.1 Warm Regime

In this section, the QSO formation is addressed based on the radiation-hydrodynamical formation of supermassive BHs. In the present picture, the MDO includes not only a central supermassive BH but also a massive accreting disk. Since the mass accretion onto a BH is limited by the inside-out viscous accretion, the BH mass grows according to

$$M_{\rm BH} = \dot{M}_a t. \tag{19}$$

The viscous accretion rate is sensitively dependent on the disk temperature. Under an intense starburst, the disk is exposed to strong ultraviolet radiation. Then, the disk could be heated up to 10^4K, although the detail is dependent on the dust extinction and radiative cooling. Here, we call the disk accretion with 10^4K a warm regime.

Since the MDO mass is given by (15), it exceeds $M_{\rm BH}$ in an early stage and stays greater than $M_{\rm BH}$ until a time $t_{\rm cross}$ when (19) equals (15). After $t_{\rm cross}$, the BH mass must be limited by (15). The timescale $t_{\rm cross}$ is estimated to be $t_{\rm cross} \approx 10^9$yr.

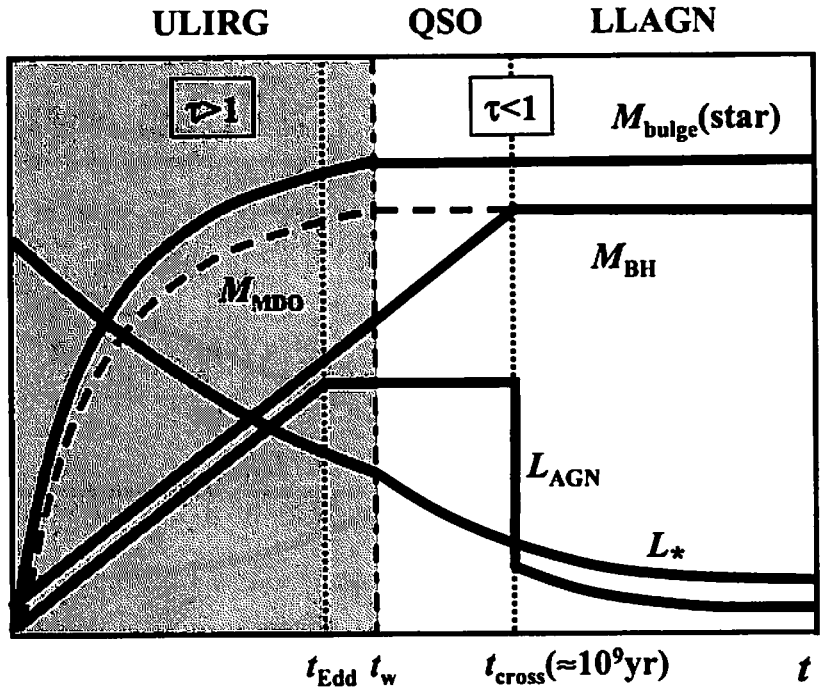

Figure 2: Schematic sketch of the QSO formation in the *warm* regime ($T_{disk} \approx 10^4$K). The abscissa is time and the ordinate is arbitrary. M_{bulge} is the mass of stellar component in the bulge. M_{MDO} is the mass of the massive dark object (MDO). M_{BH} is the mass of the supermassive BH. L_* and L_{AGN} are the bulge luminosity and the black hole accretion luminosity, respectively.

However, before t_{cross} the interstellar gas may be brown out by a galactic wind. Kodama & Arimoto (1997) argued that the color-magnitude relation of bulges can be reproduced if a galactic wind sweeps away the gas at the epoch of a few 10^8 yr. After the galactic wind epoch t_w, the bulge would evolve passively without the star formation episodes.

With considering t_{cross} and t_w, we propose a possible scenario for the QSO formation, which is schematically shown in Figure 2. Here, the system is assumed to be optically thick before t_w and become transparent at t_w. At $t < t_w$, the mass of stellar component in the bulge, M_{bulge}, increases with continuous star formation and the MDO mass (M_{MDO}) grows in proportion to M_{bulge} by radiation drag-induced mass accretion. The bulge luminosity (L_*) gradually decreases with decaying star formation rate according to the consumption of gaseous materials. This optically-thick bright phase may correspond to a ULIRG. In this picture, a ULIRG harbors a more or less active nucleus. At t_w, the radiation drag-induced mass accretion practically stops owing to the reduced efficiency of radiation drag due to the small optical depth. But, M_{MDO} is still greater than M_{BH} and thus M_{BH} continues to grow until t_{cross}.

The AGN activity is regulated by the viscous mass accretion rate. However, if the accretion rate exceeds the Eddington rate, the emergent luminosity is saturated around the Eddington luminosity due to the photon trapping effects (e.g. Ohsuga et al. 2002). The Eddington rate is given by

$$\dot{M}_{Edd} \equiv M_{BH}/t_{Edd}, \tag{20}$$

where t_{Edd} is the Eddington time-scale which is $t_{Edd} = 1.9 \times 10^8$yr for the adopted energy conversion efficiency. Super-Eddington accretion disk leads to a so-called slim accretion disk (Abramowicz et al. 1988). Recently, a slim disk is considered for the model of narrow line Syfert 1 galaxies (NLS1s) (e.g. see Mineshige et al. 2000 and references therein). NLS1s are thought to be the early stage of black hole growth (Mathur 2000). NLS1s have a characteristic property in X-ray spectrum that NLS1s exhibit strong soft X-ray excess and show large photon indices (Boller, Brandt, & Fink 1996). If (20) is combined

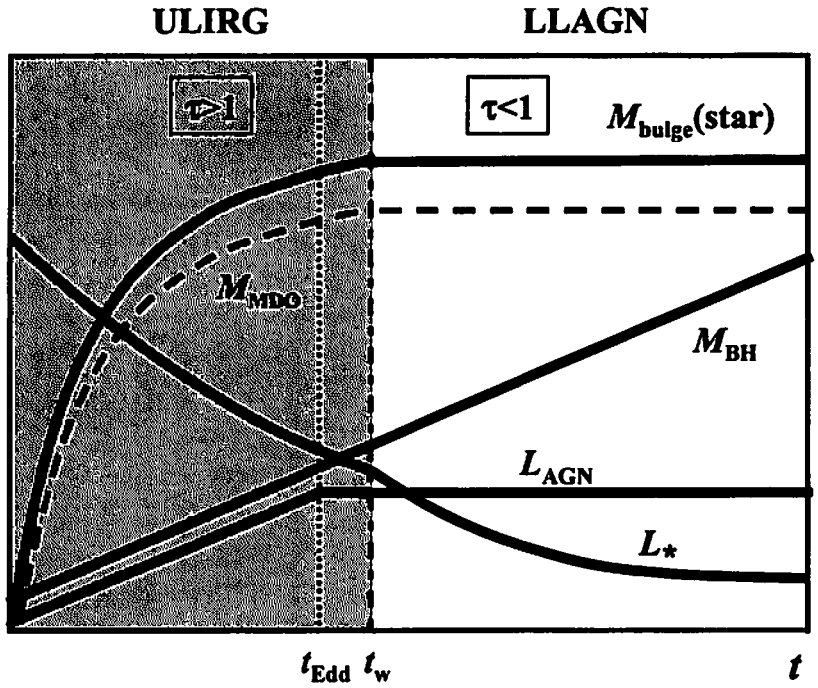

Figure 3: Schematic sketch of the QSO formation in the *cold* regime ($T_{\rm disk} \approx 10^2$K). The abscissa is time and the ordinate is arbitrary. $M_{\rm bulge}$ is the mass of stellar component in the bulge. $M_{\rm MDO}$ is the mass of the massive dark object (MDO). $M_{\rm BH}$ is the mass of the supermassive BH. L_* and $L_{\rm AGN}$ are the bulge luminosity and the black hole accretion luminosity, respectively.

with (19), then we have

$$\frac{\dot{M}_a}{\dot{M}_{\rm Edd}} = \frac{t}{t_{\rm Edd}}. \tag{21}$$

Hence, if $t < t_{\rm Edd}$, then the accretion rate is super-Eddington. This early pahse may correspond to narrow line type I quasar (NLQSO1). Although the nucleus in this phase is embedded in optically thick interstellar medium, X-ray observations of ULIRGs might reveal this super-Eddington phase.

After $t_{\rm Edd}$, AGN luminosity is just determined by $\dot{M}_a$, which is constant if the disk is isothermal. At $t_{\rm cross}$, all gas of the MDO falls onto the BH and then

$$\frac{M_{\rm BH}}{M_{\rm bulge}} = 0.002\alpha_{0.5}^{-1} \tag{22}$$

is achieved. Simultaneously, the AGN luminosity ($L_{\rm AGN}$) drops abruptly, because the radiation drag-induced accretion becomes weak in the optically-thin passive evolution phase and also the energy conversion efficiency of an ADAF (advection-dominated accretion flow) is proportional to $\dot{M}/\dot{M}_{\rm Edd}$. Such a nucleus would be a low luminosity AGN (LLAGN) as suggested by Kawaguchi & Aoki (2001).

As a result, there is time delay between L_* and $L_{\rm AGN}$, and the AGN is in high luminosity state between $t_{\rm Edd}$ and $t_{\rm cross}$. This luminous phase of AGN may correspond to the QSO phenomenun. The duration of the QSO phase is several times 10^8yr. Finally, $M_{\rm BH}/M_{\rm bulge}$ is predicted to increase with $L_{\rm AGN}$ or age until $t_{\rm cross}$ and with the metallicity of the gas.

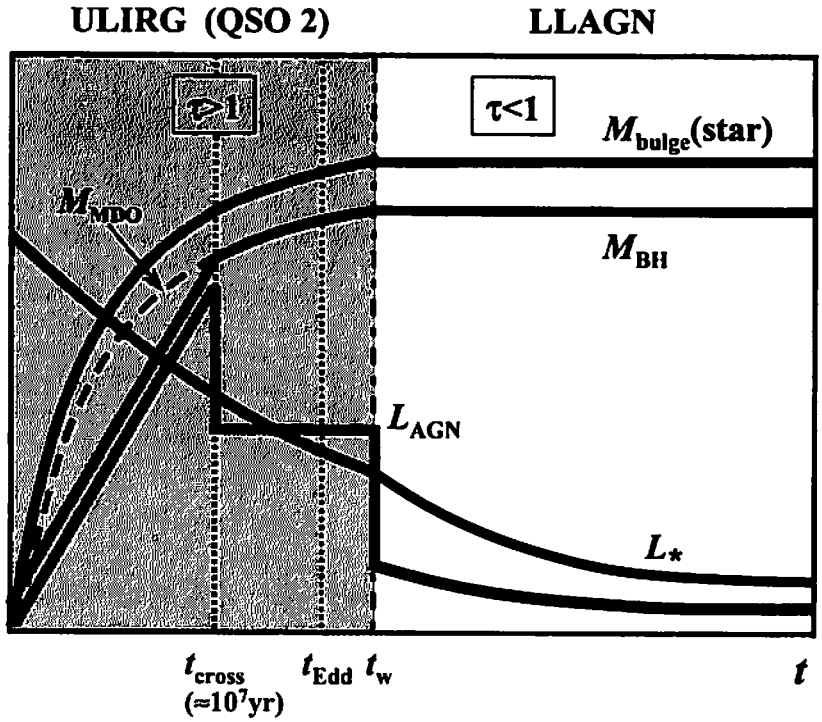

Figure 4: Schematic sketch of the QSO formation in the *hot* regime ($T_{disk} \approx 10^6$K). The abscissa is time and the ordinate is arbitrary. M_{bulge} is the mass of stellar component in the bulge. M_{MDO} is the mass of the massive dark object (MDO). M_{BH} is the mass of the supermassive BH. L_* and L_{AGN} are the bulge luminosity and the black hole accretion luminosity, respectively.

3.2 Cold and Hot Regimes

So far, the disk temperature is assumed to be around 10^4K. But, the disk could be much cooler due to the dust cooling (*cold* regime), or could have a large velocity dispersion due to the turbulent motion (*hot* regime). Here, we consider the QSO formation in the cold and hot regimes.

In the cold regime (Fig. 3), the growth of BH is quite slow, and t_{cross} becomes longer than 10^{10}yr. Hence, a luminous phase of AGN does not appear. Also, the the BH-to-bulge mass ratio is expected to be considerably smaller than $f_{BH} = 0.001$. Thus, this cold regime fails to account for the QSO formation and the BH-to-bulge mass ratio.

In contrast, the BH grows quickly in $\sim 10^7$yr in the hot regime (Fig. 4). A very luminous AGN appear in optically-thick phase. This may correspond to type II QSOs. However, in optically-thin phase, the AGN fades out due to the exhaustion of the fuel. Hence, again the hot regime fails to explain the normal QSOs. But, the BH-to-bulge mass ratio can be realized.

In conclusion, to account for the QSO phenomenun, the warm regime seems most favorable.

4 Discussion

If the BH accretion causes the nuclear activity, one should add the further radiative mass accretion induced by the nuclear luminosity L_{AGN}. Finally, the BH mass to bulge mass ratio is predicted as

$$M_{BH}/M_{bulge} = 0.14\varepsilon\alpha^{-1}(1-\eta)^{-1} = 0.003\alpha_{0.5}^{-1}. \quad (23)$$

If the BH mass is determined by the present mechanism, the BH mass to velocity dispersion relation is naturally understood in the context of a cold dark matter (CDM) cosmology. Supposing the bulge is

a virialized system, then $GM_{\rm tot}/R = \sigma^2$ and

$$R \approx 0.5 R_{\rm max} \propto M_{\rm tot}^{1/3}(1+z_{\rm max})^{-1}, \tag{24}$$

where $R_{\rm max}$ is the radius at the maximum expansion epoch $z_{\rm max}$. If a CDM cosmology is assumed, then

$$(1+z_{\rm max}) \propto M_b^{-\beta}, \tag{25}$$

where $\beta \simeq 1/6$ around $M_b = 10^{12} M_\odot$, almost regardless of the cosmological parameters (Bunn & White 1997). Combining all these relations, we find $M_{\rm BH} \propto \sigma^n$ with $n = 6/(2-3\beta)$, which is 4 for $\beta = 1/6$. This result is just corresponding to the inferred relation between the BH mass and the stellar velocity dispersion.

The radiation drag efficiency would be strongly subject to the effect of geometrical dilution (Umemura, Fukue, & Mineshige 1998). If the system is spherical, the emitted photons are effectively consumed within the system, whereas a large fraction of photons can escape from a disk-like system and thus the drag efficiency is considerably reduced. This may be the reason why $f_{\rm BH}$ is observed to be significantly smaller than 0.01.

References

[1] Abramowicz, M. A., Czerny, B., Lasota, J. P. & Szuszkiewicz, 1988, ApJ, 332, 646

[2] Adams, F. C., Graff, D. S., & Richstone, D. O. 2001, ApJ, 551, L31

[3] Bahcall, J. N., et al. 1997, ApJ, 479, 642

[4] Baumgarte, T. W., & Shapiro, S. L. 1999, ApJ, 526, 941

[5] Boller, Th, Brandt, W. N. & Fink, H. 1996, A&A, 305, 53

[6] Brandt, W. N., et al. 1997, MNRAS, 290, 617

[7] Brotherton, M. S., et al. 1999, ApJ, 520, L87

[8] Bunn, E. F., & White, M. 1997, ApJ, 480, 6

[9] Davies, R. L., et al. 1983, ApJ, 266, 41

[10] Fan, X. et al. 2001, AJ, 122, 2833

[11] Ferrarese, L., & Merritt, D. 2000, ApJ, 539, L9

[12] Fukue, J., Umemura, M., & Mineshige, S. 1997, PASJ, 49, 673

[13] Gebhardt, K., et al. 2000a, ApJ, 539, L13

[14] Gebhardt, K., et al. 2000b, ApJ, 543, L5

[15] Haehnelt, M. G., & Rees, M. J. 1993, MNRAS, 263, 168

[16] Hooper, E. J., Impey, C. D., & Foltz, C. B. 1997, ApJ, 480, L95

[17] Kawaguchi, T., & Aoki, K. 2001, preprint

[18] Kawakatu, N. & Umemura, M. 2002, MNRAS, 329, 572

[19] Kirhakos, S., et al. 1999, ApJ, 520, 67

[20] Kodama, T., & Arimoto, N. 1997, A&A, 320, 41

[21] Kormendy, J., & Richstone, D. 1995, ARAA, 33, 581

[22] Krolik, J. H. 2001, ApJ, in press (astro-ph/0012134)

[23] Laor, A. 1998, ApJ, 505, L83

[24] Laor, A. 2001, ApJ, in press (astro-ph/0101405)

[25] Magorrian, J., et al. 1998, AJ, 115, 2285

[26] Mathur, S. 2000, MNRAS, 314, L17

[27] McLeod, K. K., & Rieke, G. H. 1995, ApJ, 454, L77

[28] McLure, R. J. 2001, in this volume

[29] McLure, R. J., Dunlop, J. S., & Kukula, M. J. 2000, MNRAS, 318, 693

[30] McLure, R. J., et al. 1999, MNRAS, 308, 377

[31] Merrifield, M. R., Forbes, Duncan A., & Terlevich, A. I. 2000, MNRAS, 313, L29

[32] Merritt, D., & Ferrarese, L. 2001a, MNRAS, 320, L30

[33] Merritt, D., & Ferrarese, L. 2001b, ApJ, 547, 140

[34] Mineshige, S., Kawaguchi, T., Takeuchi, M. & Hayashida, K. 2000, PASJ, 52, 499

[35] Mineshige, S. & Umemura, M. 1996, ApJ, 469, L49

[36] Mineshige, S. & Umemura, M. 1997, ApJ, 480, 167

[37] Nelson, C. H. 2000, ApJ, 544, L91

[38] Ohsuga, K, Mineshige, S., Mori, M. & Umemura, M. 2002, ApJ submitted.

[39] Ostriker, J. P. 2000, Phys. Rev. Lett., 84, 5258

[40] Richstone, D., et al. 1998, Nature, 395A, 14

[41] Saijyo, M., Baumgarte, T. W., Shapiro, S. L., & Shibata, M. 2002, ApJ, in press

[42] Salucci, P., et al. 2000, MNRAS, 317, 488

[43] Sanders, D. B., et al. 1988, ApJ, 325, 74

[44] Sarzi, M., et al. 2001, ApJ, 550, 65

[45] Sasaki, S. & Umemura, M. 1996, ApJ, 462, 104

[46] Shibata, M. 2002, preprint

[47] Silk, J., & Rees, M. 1998, A&A, 331, L1

[48] Tsuribe, T. 1999, ApJ, 527, 102

[49] Tsuribe, T., & Umemura, M. 1997, ApJ, 486, 48

[50] Umemura, M. 2001, ApJ, 560, L29

[51] Umemura, M., Fukue, J., & Mineshige, S. 1997, ApJ, 479, L97

[52] Umemura, M., Fukue, J., & Mineshige, S. 1998, MNRAS, 299, 1123

[53] Veilleux, S., Sanders, D. B., & Kim, D.-C. 1999, ApJ, 522, 139

[54] Wandel, A. 1999, ApJ, 519, L39

The Growth of a Supermassive Black Hole and NLQSO

Nozomu Kawakatu[1] Masayuki Umemura[2]

Center for Computational Physics, University of Tsukuba, Tsukuba, Ibaraki, 305-8577, Japan

Masao Mori[3]

Department of law, University of senshu, tama-ku, kawasaki, 214-8580, Japan

Abstract

Based on the radiation drag model for the BH growth as well as the chemical evolution of the host galaxy, we have constructed the coevolution model of a QSO BH and the host galaxy. As a result, it is found that the luminosity in a QSO phase is changed from the host-dominant phase to the AGN-dominant phase in the timescale of a few 10^8 years. Also, according to the prediction for the properties in the early phase of QSO, we discuss a unified scenario for the evolution of an elliptical galaxies.

1 Introduction

Recent X-ray and optical observations indicate that active galactic nuclei (AGN) are divided into two subclasses by the way of black hole (BH) growth; one is the rapidly growing phase, and the other is slow growing phase [28, 5, 27]. As for the Seyfert 1 galaxies (Sy1s), it has been known that Sy1s are divided into two subclasses according to the broad emission line width, $V_{\rm BLR}$. Sy1s with $V_{\rm BLR}$ less than 2000km/s are called narrow line Sy1s (NLSy1s), the others with broader line width are called broad line Sy1s(BLSy1s). Then, NLSy1s correspond to the rapidly growing phase of BH. On the other hand, BLSy1s correspond to the slow growing phase of BH. Moreover, according to these observations, it has been suggested that NLSy1s may be Sy1s in the early stage of their evolution [19]. As for QSOs, it seems to be expected that there exists the rapidly growing phase of QSO BHs by the analogy with NLSy1s. But, QSOs in the early phase have not been observed and all QSOs have been observed on the slow growing phase of QSO BHs so far.

The recent further high quality observations of galactic center have shown that the estimated mass of a central "massive dark object"(MDO), which is the nomenclature for a supermassive BH candidate, does correlate with the mass of galactic bulges; the mass ratio of the BH to the bulge is 0.001-0.006 as a median value [16, 29, 18, 17, 9, 7, 26, 22, 23, 33]. (It is noted that the bulge means a whole galaxy for an elliptical galaxy.) In addition, a lot of recent efforts have revealed that QSO host galaxies are mostly luminous and well-evolved early-type galaxies [20, 3, 10, 21, 4, 14, 25, 24]. These findings, combined with the BH-to-bulge relations, suggest that the formation of a supermassive BH, a host galaxy, and a QSO is mutually related. But, a physical link between the formation of a supermassive BH and the formation and evolution of a host galaxy is an open question.

Recently, as a potential mechanism to work in a spheroidal system, Umemura [31] has considered the effects of radiation drag, and it has been found that this mechanism really works efficiently in a clumpy interstellar medium (ISM) [11]. But, in previous our work the effect of the realistic chemical evolution specified of the host galaxy has not been considered. Thus, the relation between a QSO BH and host has not been physically up to now . Hence, in order to reveal the formation and evolution of QSOs and clarify whether QSOs in the early phase correspond to the observed objects or not, it is important to predict observable features of the rapidly growing phase of QSO BHs. Here, based on the radiation drag

[1] E-mail:kawakatu@rccp.tsukuba.ac.jp
[2] E-mail:umemura@rccp.tsukuba.ac.jp
[3] E-mail:mmori@isc.senshu-u.ac.jp

model with incorporating the effect of the chemical evolution, we construct a model for coevolution of a QSO BH and the host. The purpose of this paper is to clarify the relationship between a BH growth and the QSO host evolution and to predict the physical properties of QSOs in the early phase.

2 Coevolution model

First, we build up the BH growth model. Then, we suppose a simple two-component system that consists of a spheroidal stellar bulge and inhomogeneous optically-thick ISM within it. In the radiation drag model, it is likely that optically thin surface layers are stripped from optically thick clumpy clouds by the radiation drag, and the stripped gas losing angular momentum accretes on to a central massive object. Then, the mass of an MDO, $M_{\rm MDO}$, which is the total mass of dusty ISM assembled to the central massive object, is given by

$$M_{\rm MDO} = \eta_{\rm drag} \int_0^{t_{\rm w}} \frac{L_{\rm bulge}}{c^2} dt \simeq 0.3\epsilon M_{\rm bulge}, \tag{1}$$

where $L_{\rm bulge}$ is the bulge luminosity, $\eta_{\rm drag}$ is found to be maximally 0.34 in the optically thick limit, $t_{\rm w}$ is a galactic wind timescale, and ϵ is the energy conversion efficiency of nuclear fusion from hydrogen to helium, which is 0.007 [31, 11].

In this model, we should distinguish BH mass from the mass of an MDO although the mass of an MDO is often regarded as BH mass from an observational point of view. Supposing the mass accretion driven by the viscosity on to the BH horizon is limited by an order of Eddington rate, the BH mass grows according to

$$M_{\rm BH} = M_0 e^{\nu t/t_{\rm Edd}}, \tag{2}$$

where ν is the ratio of BH accretion rate to the Eddington rate, $\nu = \dot{M}_{\rm BH}/\dot{M}_{\rm Edd}$, which is about 0.1 for QSOs, and $t_{\rm Edd}$ is the Eddington timescale, $t_{\rm Edd} = 1.9 \times 10^8$yr. Here M_0 is the mass of a seed BH, which could be an early formed massive BH with $\sim 10^5 M_\odot$ [32, 30].

Next, we construct the model for QSO evolution. To treat the realistic chemical evolution, we use an evolutionary spectral synthesis code 'PEGASE' [8]. In this paper, we consider a giant elliptical galaxy as a host galaxy to study the process of the evolution to QSOs. Then, we employ the galactic wind model because it can reproduce the color-magnitude relation of a present-day elliptical galaxy [1]. Thereby, we can estimate the evolution of the physical properties of QSO host, such as mass, luminosity, color and metallicity.

3 QSO BH - QSO host relation

Based on this coevolution model, the evolution of the mass of stellar component in the bulge ($M_{\rm bulge}$), the mass of MDO ($M_{\rm MDO}$) and the mass of the supermassive BH ($M_{\rm BH}$) in Figure 1 are shown, assuming that the Eddington ratio is constant ($\nu = 1$). The BH mass reaches $M_{\rm MDO}$ at a time $t_{\rm cross}$ when $M_{\rm MDO} = M_{\rm BH}$. As seen in Figure 1, during $t < t_{\rm cross}$, the BH mass fraction $f_{\rm BH}$ increases with time. At $t > t_{\rm cross}$, almost all of the MDO matter has fallen onto the central BH, and therefore the BH fraction is saturated to $f_{\rm BH} = M_{\rm MDO}/M_{\rm bulge} \simeq 0.001$. This is just comparable to the observed ratio.

Recently, it has been argued that color-magnitude relation of bulges can be reproduced if a galactic wind sweeps away the gas at a wind epoch $t_{\rm w}$, which is a few 10^8yr [15]. Since the bulge luminosity decreases as shown in Figure 2, which shows the evolution of luminosity, the phase at $t < t_{\rm w}$ is a bright, optically thick phase, which may correspond to a ultraluminous infrared galaxy (ULIRG) phase. Even at $t > t_{\rm w}$, $M_{\rm BH}$ continues to grow until $t_{\rm cross}$ and therefore the AGN brightens with time if the Eddington ratio is constant (see Figure 1, 2). This optically thin phase may correspond to a QSO phase ($t_{\rm w} \leq t \leq t_{\rm cross}$). After the AGN luminosity ($L_{\rm AGN}$) exhibits a peak at $t_{\rm cross}$, it fades out abruptly. The later fading nucleus could be a low luminosity AGN (LLAGN) [2, 13]. As seen from Figure 2, it is found that QSO phase can be divided into two phases.; one is the host luminosity-dominant phase, and the other is the AGN luminosity-dominant phase. However, a remarkable point is that all QSOs have been observed to be on the latter phase so far. Thus, it is important that our model can predict the exsistence of the early

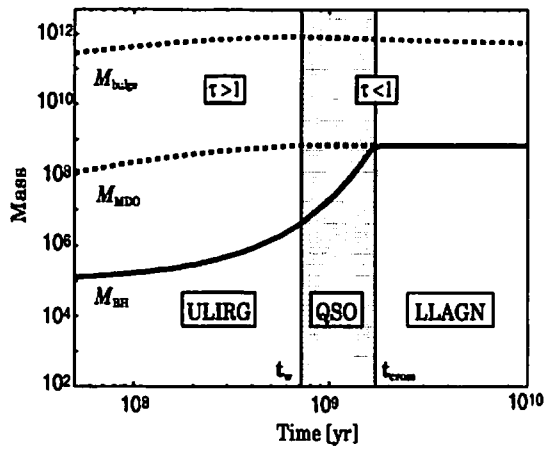

Figure 1: BH growth, assuming $M_0 = 10^5 M_\odot$ and $\nu = 1.0$. The abscissa is time in units of yr. The ordinate is mass in units of $M_\odot$. $M_{\rm bulge}$ is the mass of stellar component in bulge. $M_{\rm MDO}$ is the mass of MDO. $M_{\rm BH}$ is the mass of the supermassive BH. $t_{\rm w}$ is the galactic wind timescale. $t_{\rm cross}$ is defined so that $M_{\rm MDO} = M_{\rm BH}$. The optically thin phase ($t_{\rm w} \leq t \leq t_{\rm cross}$), which is the hatched area, corresponds to a QSO phase. The optically thick phase ($t < t_{\rm w}$) corresponds to a ULIRG phase. The phase of low mass accretion rate corresponds to a low luminosity AGN (LLAGN).

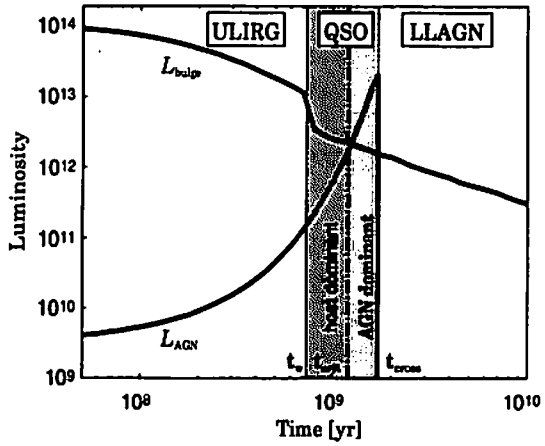

Figure 2: AGN luminosity and bulge one as a function of time. The ordinate is the luminosity in units of $L_\odot$. $t_{\rm cross}$ is the time when $L_{\rm bulge} = L_{\rm AGN}$. Here, we assume that $L_{\rm AGN}$ is Eddington luminosity. QSO phase can be divided into two phases; one is the host luminosity-dominant phase, which is dark hatched area ($t_{\rm w} \leq t \leq t_{\rm crit}$) and the other is the AGN luminosity-dominant phase, which is light hatched area ($t_{\rm crit} \leq t \leq t_{\rm cross}$). The life time of both phases are comparable to each other, which is about 10^8yr.

stage of QSO, which is the host-luminosity dominant phase, although the host-dominated QSOs have not been observed. In Figure 2, it is also shown that the life time of both phases are comparable to each other, which is about 10^8yr and the luminosity of hard X-ray is $L_X = 10^{10} - 5 \times 10^{11} L_\odot$ if $L_X = 0.1 L_{AGN}$ [6] in the early phase. Finally, comparing the properties of both phases, we show the broad emission line width, the color of the QSO host galaxy. As for the broad emission line width, which coresponds to the velocity, V_{BLR}, we use the empirical law to estimate the its evolution. As a result, the circular velocity of broad line clouds (V_{BLR}) is given by $V_{BLR} \simeq (GM_{BH}/r_{BLR})^{1/2} = 1700(M_{BH}/10^8 M_\odot)^{1/4}$km/s, where r_{BLR} is the size of BLR. Then, it is found that the broad emission line width in the early phase of QSOs is less than 1500km/s. Next, we show the color at the rest frame in Figure 3. As seen in Figure 3, it is

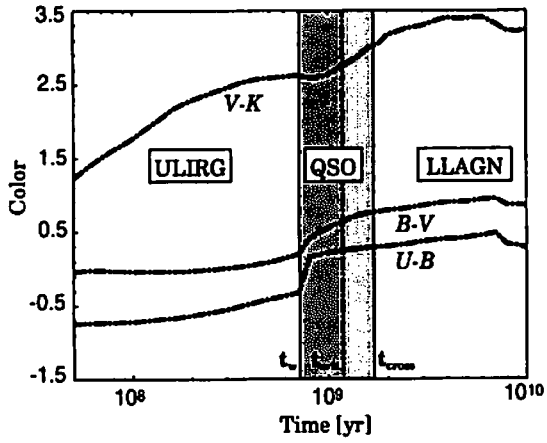

Figure 3: U-B,B-V and V-K color at the rest frame as a function of time. The ordinate is the U-B,B-V and V-K color. For B-V, QSO host in the early phase is about 0.5 magnitude bluer than that in the late phase. This is an important observable feature that can distinguish two phases.

found that U-B color of the early phase QSO hosts can not be distinguished from that of the late phase because the massive stars in host galaxies have declined at about 10^9 yr. Also, it is shown that B-V color of QSO hosts in the early phase can be about 0.5 magnitude bluer than that in the late phase. Then, this may be an important observable feature that distinguishs the early phase of QSO from the late phase of one. Moreover, Figure 3 denotes that V-K color of QSO hosts in the early phase can be about 0.2 magnitude bluer than that in the late phase. But, this may not be the observable feature because V-K regime corresponds to the far infrared at high redshift.

4 Conclusions

Based on the radiation drag model for the BH growth and the realistic chemical evolution model of the QSO host, we have constructed the coevolution model for a QSO BH and the host galaxy. Then, we have investigated the relationship between a QSO BH and the host physically, and also predicted the properties of QSO in the early phase. The followings have been found. i) The luminosity in a QSO phase is changed from the host-dominant phase to the AGN-dominant phase in the timescale of a few 10^8 years. ii) The width of broad emission line of the early phase is narrower, which is less than 1500km/s. iii) The QSO host in the early phase is about 0.5 magnitude bluer in rest B-V color. Hence, this may be the observable feature that distinguishes the early phase of QSO from the late phase unlike other color (U-B,V-K). iv) The X-ray luminosity is $L_X = 10^{10} - 5 \times 10^{11} L_\odot$ if $L_X = 0.1 L_{AGN}$.

From these properties, some observed objects (e.g., a radio galaxy, an ULIRG with AGN activity and a type II QSO) may be considered as the candidates of a QSO in the early phase. Then, we propose the unified scenario for the evolution of elliptical galaxy (ULIRG - QSO(galaxy) - QSO(AGN) - LLAGN) based on a radiation-hydrodynamical model [12].

References

[1] Arimoto, N., & Yoshii, Y. 1987, A&A, 173, 23

[2] Awaki, H., et al. 2001, PASJ, 53, 647

[3] Bahcall, J.N., et al. 1997, ApJ, 479, 642

[4] Brotherton, M.S., et al. 1999, ApJ, 520, L87

[5] Boller, Th., Brandt, W.N., & Fink, H. 1996, A&A, 305, 53

[6] Elvis, M., et al. 1994, ApJS, 95, 1

[7] Ferrarese, L., & Merritt, D. 2000, ApJ, 539, L9

[8] Fioc, M., & Rocca-Volmerrange, B. 1997, A&A, 326, 950

[9] Gebhardt K. et al., 2000, ApJ, 543, L5

[10] Hooper, E.J., Impey, C.D., & Foltz, C.B. 1997, ApJ, 480, L95

[11] Kawakatu, N., Umemura, M. 2002, MNRAS, 329,572

[12] Kawakatu, N., Umemura, M. & Mori, M. 2002, in preparation

[13] Kawaguchi, T., & Aoki, K. 2001, PASJ, submitted

[14] Kirhakos, S., Bahcall, J.N., Schneider, D.P., & Kristian, J. 1999, ApJ, 520, 67

[15] Kodama, T., & Arimoto, N. 1997, A&A, 320, 41

[16] Kormendy, J., & Richstone, D. 1995, ARA&A, 33, 581

[17] Laor, A. 1998, ApJ, 505, L83

[18] Magorrian, J., et al. 1998, AJ, 115, 2285

[19] Mathur, S. 2000, MNRAS, 314, L17

[20] McLeod, K.K., & Rieke, G.H. 1995, ApJ, 454, L77

[21] McLeod, K.K., Rieke, G.H., & Storrie-Lombardi, L.J. 1999, ApJ, 511, L67

[22] McLure, R.J., & Dunlop, J.S. 2001a, preprint (astro-ph/0108417)

[23] ———. 2001b, MNRAS, 327, 199

[24] McLure, R.J., Dunlop, J.S., & Kukula, M.J. 2000, MNRAS, 318, 693

[25] McLure, R.J., Kukula, M.J., Dunlop, J.S., Baum, S.A., O'Dea, C.P., & Hughes, D.H. 1999, MNRAS, 308, 377

[26] Merritt, D., & Ferrarese L. 2001, MNRAS, 320, L30

[27] Mineshige, S., Kawaguchi, T., Takeuchi, M., & Hayashida, K. 2000, PASJ, 52, 499

[28] Pounds, K.A., Done, C., & Osbore J.P. 1995, MNRAS, 277, L5

[29] Richstone, D., et al. 1998, Nature, 395A, 14

[30] Shibata, M. 2001, preprint

[31] Umemura, M. 2001, ApJ, 560, L29

[32] Umemura, M., Loeb, A., & Turner, E.L. 1993, ApJ, 419, 459

[33] Wandel, A. 2001, ApJ, preprint (astro-ph/0108461)

Supermassive Star Collapse: (3+1) Post–Newtonian Simulation

Motoyuki Saijo [1] [(a)] , Thomas W. Baumgarte [2] [(b)], Stuart L. Shapiro [3] [(a),(c)] and Masaru Shibata [4] [(d)]

[(a)] *Department of Physics, University of Illinois at Urbana-Champaign, Urbana, Illinois 61801-3080, U.S.A.*

[(b)] *Department of Physics and Astronomy, Bowdoin College, 8800 College Station Brunswick, Maine 04011-8488, U.S.A.*

[(c)] *Department of Astronomy and NCSA, University of Illinois at Urbana-Champaign, Urbana, Illinois 61801, U.S.A.*

[(d)] *Graduate School of Arts and Sciences, University of Tokyo, Komaba, Meguro, Tokyo 153-8902, Japan*

Abstract

We study the gravitational collapse of a rotating supermassive star by means of a (3+1) hydrodynamical simulation in a post-Newtonian approximation of general relativity. We evolve a uniformly rotating supermassive star from the onset of radial instability at $R_p/M = 411$, where R_p is the proper polar radius of the star and M is the total mass-energy, to the point at which the post-Newtonian approximation breaks down. We introduce a scale factor and a "comoving" coordinate to handle the large variation in radius during the collapse and focus on the central core of the supermassive star. We find that the collapse is likely to form a supermassive black hole coherently, with almost all of the matter falling into the hole, leaving very little ejected matter to form a disk. In the absence of nonaxisymmetric bar formation, the collapse of a uniformly rotating supermassive star does not lead to appreciable quasi-periodic gravitational wave emission by the time our integrations terminate. However, the coherent nature of the implosion suggests that rotating supermassive star collapse will be a promising source of gravitational wave bursts. We also expect that, following black hole formation, long wavelength quasi-periodic waves will result from quasi-normal ringing. These waves may be detectable by the Laser Interferometer Space Antenna (LISA).

1 Introduction

There is increasing evidence that supermassive black holes (SMBHs) exist at the center of all galaxies, and that they are the sources which power active galactic nuclei and quasars. Large numbers of observations are provided by the Hubble space telescope suggesting that SMBHs exist in galaxies such as M31 ($3 \times 10^7 M_\odot$), M87 ($1 \sim 2 \times 10^9 M_\odot$) and our own galaxy ($2.5 \times 10^6 M_\odot$) (see for example, Ref. [1] for a brief overview).

Although evidence of the existence of SMBHs is compelling, the actual formation process of these objects is still uncertain [2]. Several different scenarios have been proposed, some based on stellar dynamics, others on gas hydrodynamics, and still others which combine the processes. At present, there is no definitive observation as yet which confirms or rules out any one of these scenarios.

Here we focus on the collapse of a supermassive star (SMS). Baumgarte and Shapiro [3] investigated the equilibrium, stability and quasi-static evolution of a SMS with uniform rotation. They showed that the nondimensional ratios R_p/M, T/W and J/M^2 for all critical configurations at the onset of collapse are universal numbers, independent of the history or mass of the star. Here R_p is the proper polar radius,

[1] Electronic address: saijo@astro.physics.uiuc.edu
[2] Electronic address: tbaumgar@bowdoin.edu
[3] Electronic address: shapiro@astro.physics.uiuc.edu
[4] Electronic address: shibata@provence.c.u-tokyo.ac.jp

M is the gravitational mass (total mass-energy), T is the rotational kinetic energy, W is the gravitational binding energy and J is the angular momentum. They also pointed out the possibility of bar formation during catastrophic collapse prior to black hole (BH) formation, assuming that the collapse is nearly homologous ($T/W \propto 1/R_p$). New and Shapiro [4] later investigated the quasi-static evolution of a SMS with differential rotation, assuming negligible viscosity and magnetic fields. They showed that in this case, bar formation prior to the onset of relativistic instability is inevitable. The investigation of supermassive objects is one of the primary observational missions for space-based detection of gravitational waves. Potential sources of high signal to noise events in the frequency range ($10^{-4} \sim 10^{-1}$ Hz) include quasi-periodic waves arising from nonaxisymmetric bars in collapsing SMSs and the inspiral of binary SMBHs. In addition, the nonspherical collapse of rotating SMSs to SMBHs could be a significant source of burst and quasi-normal ringing radiation. In this paper we tract the collapse of a SMS by numerical simulation to investigate some of these possibilities.

We take our initial stellar model to be a marginally unstable SMS star near the critical point, $R_p/M \sim 430$. We treat the gas adiabatically, since for sufficiently massive stars neither photon nor neutrino losses are dynamically significant. We take the adiabatic index to be 4/3, appropriate for a radiation-pressure dominated SMS, and construct a critical, uniformly rotating polytrope with index $n \approx 3$ for our starting point. Our goal is to determine the final outcome of the collapse. We want to address the following questions: Does a SMBH definitely form following the catastrophic collapse? Is the collapse coherent or does the central region collapse first, followed by the gradual accretion of the envelope? Does the collapsing configuration fragment? Does a disk form? Does a rotating bar form during the collapse?

We use a post-Newtonian (PN) hybrid hydrodynamical code in (3+1) dimensions to tract SMS collapse. Our adopted hybrid scheme is relativistically exact for static spherical spacetimes. The onset of radial instability occurs when $T/W \ll 0.1$, so our initial equilibrium spacetime is very nearly spherical. Locating the onset of radial instability in a SMS requires the presence of nonlinear gravitation to at least 2PN order [3, 5]. For these reasons, the nonlinearity captured in our hybrid scheme, which extends beyond 1PN, is essential to treat this problem. Of course, it is necessary to use a fully general relativistic code to follow the final implosion of the matter into a black hole (BH) and to reliably determine the gravitational waveforms. However, a fully relativistic (3+1) code capable of handling the large dynamic range spanned by SMS collapse is not yet available. Fortunately, since our initial configuration is nearly Newtonian, we can use our hybrid scheme to track most of the implosion up to the point where the formation of a BH is likely. Our hybrid scheme is also adequate to address most of the questions raised above, at least in a preliminary fashion.

This paper is organized as follows. In Sec. 2 we present the basic equations of our PN formulation in "comoving" coordinates. We discuss our numerical results for rotating SMS collapse in Sec. 3. In Sec. 4 we summarize our findings. Throughout this paper, we use geometrized units ($G = c = 1$) and adopt Cartesian coordinates (x, y, z) with the coordinate time t. Greek and Latin indices run over (t, x, y, z) and (x, y, z), respectively. A more detailed discussion is presented in Ref. [6].

2 (3+1) PN Relativistic Hydrodynamics in "Comoving" Coordinates

In this section, we briefly derive the (3+1) hybrid PN relativistic hydrodynamic equations in "comoving" coordinates. We solve the fully relativistic equations for hydrodynamics, but neglect some higher-order dynamical PN terms in the Einstein field equations. Note that this approximation gives the exact solution for a static spherical spacetime. To track the collapse over the vast dynamic range from $\gtrsim 410M$ down to a few M and to investigate the central core at late times, we require a suitable comoving coordinate system. Such a coordinate choice is possible because in Newtonian gravity, an $n = 3$ spherical polytrope collapses homologously. Therefore, we can construct a "comoving" frame, subtracting the mean "Hubble" flow from the local velocity, to follow most of the collapse with sufficient grid resolution.

We write the PN line element in "comoving" coordinates as

$$ds^2 = (-\hat{\alpha}^2 + \hat{\beta}_k \hat{\beta}^k)dt^2 + 2\hat{\beta}_k d\hat{x}^k dt + \hat{a}^2 \hat{\psi}^4 \delta_{ij} d\hat{x}^i d\hat{x}^j, \quad (1)$$

where α is the lapse function, β^k is the shift vector, ψ is the conformal factor, respectively. Note that $\hat{A}$

will represent the quantity A as measured in "comoving" coordinates. Among the geometric quantities, we only need to adjust the shift vector [6].

In the "comoving" frame, the continuity equation, energy equation, and Euler equation with Γ-law equation of state including artificial viscosity for a perfect fluid are written as

$$\frac{\partial(\hat{a}^3\rho_*)}{\partial t} + \frac{\partial}{\partial \hat{x}^i}(\hat{a}^3\rho_*\hat{v}^i) = 0, \tag{2}$$

$$\frac{\partial(\hat{a}^3 e_*)}{\partial t} + \frac{\partial}{\partial \hat{x}^i}(\hat{a}^3 e_*\hat{v}^i) = -\frac{\hat{a}^3}{\Gamma}(\rho\epsilon)^{-1+1/\Gamma}P_{\rm vis}\frac{\partial}{\partial \hat{x}^i}(\alpha\hat{u}^t\psi^6\hat{v}^i), \tag{3}$$

$$\frac{\partial}{\partial t}(\hat{a}^2\rho_*\tilde{\hat{u}}_i) + \frac{\partial}{\partial \hat{x}^j}(\hat{a}^2\rho_*\tilde{\hat{u}}_i\hat{v}^j) = -\hat{a}^2\alpha\psi^6\frac{\partial}{\partial \hat{x}^i}(P + P_{\rm vis}) - \hat{a}^2\rho_*\tilde{\hat{u}}^t\frac{\partial\alpha}{\partial \hat{x}^i} + \hat{a}^2\rho_*\tilde{\hat{u}}_j\frac{\partial \hat{W}^j}{\partial \hat{x}^i}$$
$$+2\hat{a}^2\rho_*\frac{1+\Gamma\epsilon}{\hat{u}^t\psi}[(\alpha\hat{u}^t)^2 - 1]\frac{\partial\psi}{\partial \hat{x}^i}, \tag{4}$$

where $\hat{a}$ is the scale factor, ρ is the rest-mass density, ρ_* is the coordinate rest mass density, v^i is a 3-velocity, e_* is a coordinate energy density, u^i is a 4-velocity, $\tilde{u}^i = (1+\Gamma\epsilon)u^i$, $P_{\rm vis}$ is the artificial viscosity pressure, P is a pressure.

Gravitational field equations in the PN approximation are derived from the Hamiltonian constraint, momentum constraint and the maximal time-slicing condition. The equations in the comoving frame are written as

$$\hat{\Delta}\psi = -2\pi\hat{a}^2\psi^5\hat{\rho}_{\rm H}, \tag{5}$$

$$\hat{\Delta}(\alpha\psi) = 2\pi\alpha\hat{a}^2\psi^5(\hat{\rho}_{\rm H} + 2\hat{S}), \tag{6}$$

$$\delta_{ij}\hat{\Delta}\hat{\beta}^j + \frac{1}{3}\hat{\partial}_i\hat{\partial}_j\hat{\beta}^j = 16\pi\alpha\hat{J}_i, \tag{7}$$

$$\hat{W}^i \equiv \hat{\beta}^i - H\hat{x}^i, \tag{8}$$

where $\hat{\rho}_{\rm H} = n_\mu n_\nu \hat{T}^{\mu\nu}$, $\hat{J}_i = -n_\mu \hat{h}_{i\nu}\hat{T}^{\mu\nu}$, $\hat{S} = \hat{h}^i_\mu \hat{h}_{i\nu}\hat{T}^{\mu\nu}$, $n_\mu = (-\alpha, 0, 0, 0)$, $\hat{h}_{\mu\nu} = \hat{g}_{\mu\nu} + n_\mu n_\nu$, and $\hat{\Delta}$ is the flat Laplacian measured in the "comoving" frame, $H \equiv \dot{\hat{a}}/\hat{a}$. Note that the quantity $\hat{W}^i$ subtracts the Hubble flow from $\hat{\beta}^i$ (see Ref. [6] for details).

3 Uniformly Rotating SMS Collapse

Consider an overview of SMS evolution. Cooling and contraction of a rotating SMS will ultimately spin it up to the mass-shedding limit. After that, the SMS contracts secularly along the mass-shedding sequence as it cools, slowly losing mass and maintaining uniform rotation via viscosity and/or magnetic braking [5]. Upon reaching the onset of radial instability, the star will collapse catastrophically and form a BH, or a flattened rotating disk, or some combination thereof. It is this catastrophic collapse which we wish to follow with our dynamical code.

We slightly decrease the pressure and initiate the collapse. We install a triaxial density perturbation to provide the seed for bar formation, should the physical situation lead to unstable growth. We evolve the rotating SMS up to the point at which the PN approximation breaks down.

We show the density profile in the equatorial plane in Figure 1 and in the meridional plane in Figure 2. The ability of our scale factor implementation to resolve the matter distribution even as it becomes increasingly compact during the implosion is evident from these snapshots. We find no indication of the formation of a circumstellar disk with significant mass by the termination of our simulation. In fact, the fraction of the rest mass outside a sphere of radius $r/M_0 = 7.0$ is 26% and outside the sphere of $r/M_0 = 28.0$ is 10%. Accordingly, most of the mass is concentrated in the center and is collapsing inward when we terminate our integration. Note that by employing a density cutoff, we are not reliably resolving the very outermost region. But we note that even with a cutoff, M_0 is conserved to 96% accuracy (Fig. 10 of Ref. [6]). We thus conclude that the rotation cannot provide sufficient centrifugal support in the bulk of the envelope to counter gravity and form a disk with more than 10% of the total mass. Though our computation is terminated when the lapse drops below $\alpha_c \sim 0.3$, we can still infer the final fate of

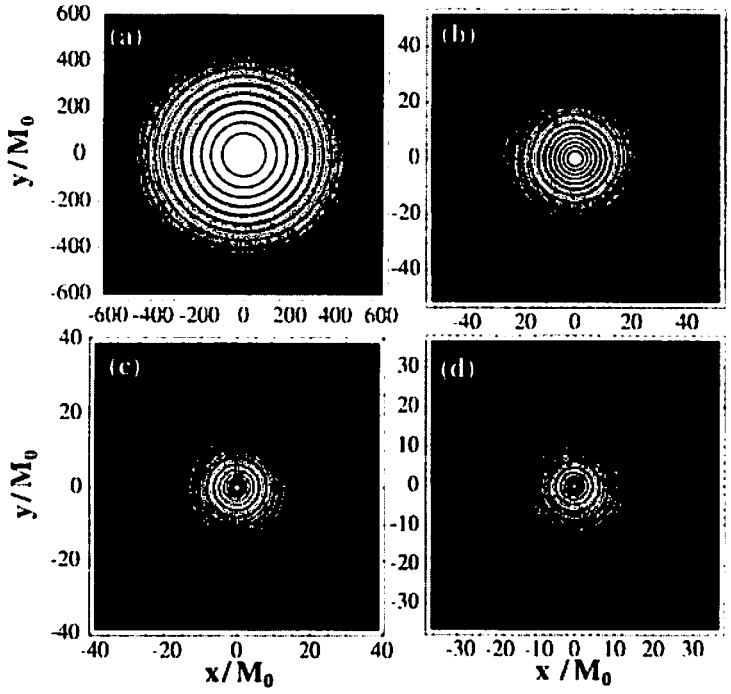

Figure 1: Density contours ρ_* in the equatorial plane at selected times during rotating SMS collapse. Snapshots are plotted at $(t/t_D,\ \rho_c^*,\ d)$ = (a) $(5.0628 \times 10^{-4},\ 8.254 \times 10^{-9},\ 10^{-7})$, (b) $(2.50259,\ 1.225 \times 10^{-4},\ 10^{-5})$, (c) $(2.05360,\ 8.328 \times 10^{-3},\ 5.585 \times 10^{-7})$, (d) $(2.50405,\ 3.425 \times 10^{-2},\ 1.357 \times 10^{-7})$, respectively. The contour lines denote densities $\rho^* = \rho_c^* \times d^{(1-i/16)}$ $(i = 1, \cdots, 15)$.

the collapse from examination of the velocity profile of the star (Fig. 2; see also Fig. 16 of Ref. [6]). The growth of an appreciable inward radial component of the velocity field strongly suggests that immediately after the time we terminate the integrations, the bulk of the matter will cross the event horizon of the nascent BH in a dynamical timescale as measured at the center of the star.

Though the newly formed BH acquires the bulk of the mass in a coherent implosion, it does not obtain all of the mass and angular momentum. Lingering gaseous fragments in the outermost envelope containing negligible mass but nonnegligible angular momentum are not followed in our simulation, which focuses on the imploding massive bulk of the star. These fragments may accrete on a longer timescale (or even escape), but we cannot track their evolution with our current calculation.

If all of the initial mass-energy and angular momentum are consumed by the final BH, it will be rapidly rotating with $a/M \approx 1$. Although we cannot follow the final formation and growth of the BH, our PN simulations suggest that the final a/M may be slightly lower, due to the loss of angular momentum carried by gas orbiting near the equator (see Shibata and Shapiro [7]).

4 Conclusion

We follow rotating SMS collapse from the onset of radial collapse at $R_p/M_0 \sim 411$ to the point where the PN approximation breaks down ($R_p/M_0 \sim 8$). The challenge of covering this large a dynamic range is met by introducing a scale factor and a "comoving" coordinate system which takes advantage of the homologous nature of the initial collapse.

Collapse of a uniformly rotating, relativistically unstable SMS is coherent and leads to the formation of a SMBH containing the bulk of the mass of the progenitor star. We find no evidence of bars prior to BH formation, so that the collapse is largely axisymmetric. As a result, little angular momentum can

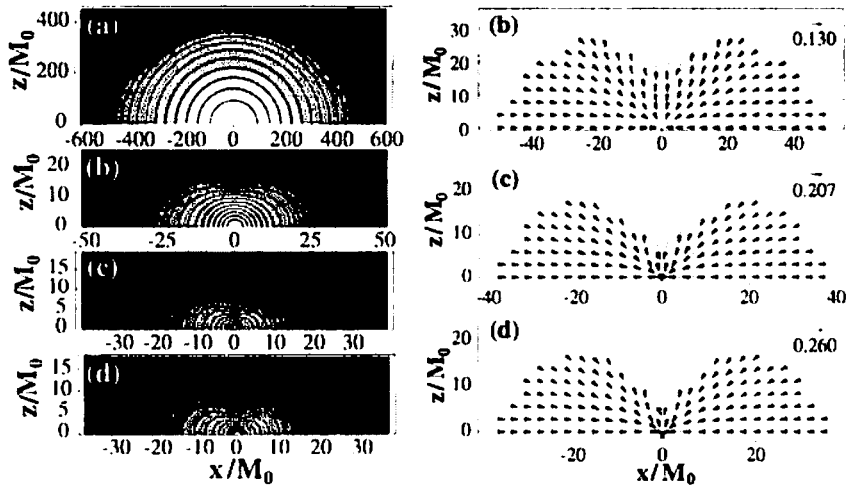

Figure 2: Density contours ρ_* in the meridional plane at selected times during rotating SMS collapse (left panel). The times, the central densities and contour levels are the same as in Fig. 1. Velocity field in the equatorial plane at selected times during rotating SMS collapse (right panel). The times are the same as in Fig. 1.

be radiated away by gravitational waves. From the coherent, axisymmetric nature of the implosion we conclude that the collapse of a SMS, rotating uniformly at the onset of collapse, is a promising source of gravitational wave bursts. In the absence of bar formation, SMS collapse will not produce quasi-periodic waves prior to SMBH formation. However, such waves will be generated by the nascent BH via quasi-normal mode ringing.

Our (3+1) hybrid PN calculations offer a first glance at SMS collapse. An improved description will require several refinements to our computational scheme. First, it will be necessary to employ a fully relativistic treatment of Einstein's field equations to explore the final dynamical phase of collapse once a BH has formed.

Secondly, our computation would benefit significantly from the nested grid method to handle the large dynamic range characterizing SMS collapse. It is difficult to follow the small amount of matter in the equatorial plane that is supported by centrifugal forces while the bulk of the matter collapses. The nested grid method may provide one means of concentrating computational resources on the central region of the star while simultaneously resolving the low density outermost regions.

References

[1] E. D. Macchetto, Astron. Space Sci. **269-270**, 269 (2001).

[2] M. J. Rees, in *Black Holes in Binaries and Galactic Nuclei*, edited by L. Kaper, E. P. J. van den Heurel, and P. A. Woudt (Springer-Verlag, New York, 2001), p. 351.

[3] T. W. Baumgarte and S. L. Shapiro, Astrophys. J. **526**, 941 (1999).

[4] K. C. B. New and S. L. Shapiro, Astrophys. J. **548**, 439 (2001).

[5] Ya. B. Zel'dovich, and I. D. Novikov, Stars and Relativity, translated by E. Arlock, edited by K. S. Thorne and W. D. Arnett (Univ. Chicago Press, Chicago, 1967).

[6] M. Saijo, T. W. Baumgarte, S. L. Shapiro, and M. Shibata, Astrophys. J. **569**, in press (2002) (astro-ph/0202112).

[7] M. Shibata and S. L. Shapiro, in preparation.

The shape of the K_α line of iron as the evidence of the black hole existence

Alexander F. Zakharov[1]

Institute of Theoretical and Experimental Physics,
25, B.Cheremushkinskaya st., Moscow, 117259, Russia

Serge V. Repin[2]

Space Research Institute, 84/32,
Profsoyuznaya st., Moscow, 117810, Russia

Abstract

Observations of Seyfert galaxies in X-ray region reveal the wide emissive lines in their spectra, which can arise in inner parts of accretion disks, where the effects of General Relativity (GR) must be counted. A spectrum of a solitary emission line of a hot spot in Kerr accretion disk is simulated, depending on the radial coordinate r and the angular momentum $a = J/M$ of a black hole, under the assumption of equatorial circular motion of a hot spot. It is shown that the characteristic two-peak line profile with the sharp edges arises at a large distance, (about $r \approx (3-10)\, r_g$). The inner regions emit the line, which is observed with one maximum and extremely wide red wing. High accuracy future spectral observations, being carried out, could detect the angular momentum a of the black hole.

The general status of black holes described in a number of papers (see, for example [1, 2, 3] and references therein). As it was emphasized in these reviews the most solid evidence for an existence of black holes comes from observations of some Seyfert galaxies because we need a strong gravitational field approximation to interpret these observational data, so probably we observe manifestations radiation processes from the vicinity of the black hole horizon (these regions are located inside the Schwarzschild black hole horizon, but outside the Kerr black hole horizon, thus we should conclude that we have manifestations of rotational black holes).

Recent observations of Seyfert galaxies in X-ray band [4, 5, 6, 7, 8, 9] reveal the existence of wide iron K_α line (6.4 keV) in their spectra along with a number of other weaker lines (Ne X, Si XIII,XIV, S XIV-XVI, Ar XVII,XVIII, Ca XIX, etc.). The line width corresponds to the velocity of the matter motion of tens of thousands kilometers per second, reaching the maximum value $v \approx 80000 - 100000$ km/s [5] for the galaxy MCG-6-30-15 and $v \approx 48000$ km/s [10] for MCG-5-23-16. In some cases the line has characteristic two-peak profile [5, 11] with a high "blue" maximum and the low "red" one and the long red wing, which gradually drops to the background level.

For individual objects, where the existence of the black holes is assumed, a strong variability of X-ray brightness was registered [12], as well as the rapid changes of the line profile (Yaqoob et al.[11], NGC 7413) and the quasiperiodic oscillations ([13], GRC 1915+105).

The large amount of observational data requires its comprehension, theoretical simulation and interpretation. The numerical simulations of the accretion disk spectrum under GR assumptions has been reported in the paper [14]. In the paper [15] the observational manifestations of GR effects are considered in X-ray binaries. Different physical models of the origin of a wide emissive iron K_α line in the nuclei of Seyfert galaxies are analyzed in the papers [16, 17].

The numerical approach, applied here based on the method, described earlier in papers [18, 19, 20, 21].

Many astrophysical processes, where the great energy release is observed, are assumed to be connected with the black holes. Because the main part of the astronomical objects, such as the stars and galaxies,

[1]E-mail: zakharov@vitep5.itep.ru
[2]E-mail: repin@mx.iki.rssi.ru

possesses the proper rotation, then there are no doubts that the black holes, both stellar and supermassive, possess the intrinsic proper rotation too.

The stationary black holes are described by the Kerr metric [22]:

$$ds^2 = -\frac{\Delta}{\rho^2}\left(dt - a\sin^2\theta d\phi\right)^2 + +\frac{\sin^2\theta}{\rho^2}\left[\left(r^2+a^2\right)d\phi - adt\right]^2 + \frac{\rho^2}{\Delta}dr^2 + \rho^2 d\theta^2, \quad (1)$$

where

$$\rho^2 = r^2 + a^2\cos^2\theta, \quad \Delta = r^2 - 2Mr + a^2. \quad (2)$$

The equations geodesics however can be simplified if we will use the complete set of the first integrals which were found by Carter [23]: $E = p_t$ is the particle energy at infinity, $L_z = p_\phi$ is z-component of its angular momentum, $m = p_i p^i$ is the particle mass and Q is the Carter's separation constant [23]:

$$Q = p_\theta^2 + \cos^2\theta\left[a^2\left(m^2 - E^2\right) + L_z^2/\sin^2\theta\right]. \quad (3)$$

As shown by Zakharov [24, 18], the equations of photon motion can be reduced to

$$\frac{dt'}{d\sigma} = -a\left(a\sin^2\theta - \xi\right) + \frac{r^2+a^2}{\Delta}\left(r^2 + a^2 - \xi a\right), \quad (4)$$

$$\frac{dr}{d\sigma} = r_1, \quad (5)$$

$$\frac{dr_1}{d\sigma} = 2r^3 + \left(a^2 - \xi^2 - \eta\right)r + (a-\xi) + \eta, \quad (6)$$

$$\frac{d\theta}{d\sigma} = \theta_1, \quad (7)$$

$$\frac{d\theta_1}{d\sigma} = \cos\theta\left(\frac{\xi^2}{\sin^3\theta} - a^2\sin\theta\right), \quad (8)$$

$$\frac{d\phi}{d\sigma} = -\left(a - \frac{\xi}{\sin^2\theta}\right) + \frac{a}{\Delta}\left(r^2 + a^2 - \xi a\right), \quad (9)$$

where $\eta = Q/M^2E^2$ and $\xi = L_z/ME$ are the Chandrasekhar's constants [25], which should be derived from the initial conditions in the disk plane; r and a are the appropriate dimensionless variables. The system (4)-(9) has also two integrals,

$$\epsilon_1 \equiv r_1^2 - r^4 - \left(a^2 - \xi^2 - \eta\right)r^2 - 2\left[(a-\xi)^2 + \eta\right]r + a^2\eta = 0, \quad (10)$$

$$\epsilon_2 \equiv \theta_1^2 - \eta - \cos^2\theta\left(a^2 - \frac{\xi^2}{\sin^2\theta}\right) = 0, \quad (11)$$

which can be used for the precision control. This method differs from the approach which was developed in papers [26, 27, 28, 29].

We assume that the hot spot emits isotropically distributed quanta in the local frame. First, one should define the Chandrasekhar's constants for each quantum and then integrate the system (4)-(9) to either the infinity or the events horizon, depending on the constants values.

The trajectories classification, depending on the Chandrasekhar's constants can be found in the papers [30, 31]. The details of simulation and initial conditions can be found in papers [18, 21].

The simulated spectrum of a hot spot for $a = 0.9$, $\theta = 60°$ and different radius values is shown in Fig. 1. The proper quantum energy (in co-moving frame) is set to unity. The observer at infinity registers then the characteristic two-peak profile, where the "blue" peak is higher than the "red" one and the center is shifted to the left. Some spectrum jugging near its minimum is explained by pure statistical reasons and has no the physical nature.

As far as the radius diminishes the spectrum is enhanced, i.e. increases the residual between the maximum and minimum quanta energy, registered by far observer. For example, for $a = 0.9$, $r = 1.2\,r_g$ and $\theta = 60°$, where r_g has its standard form $r_g = 2kM/c^2$, i.e. in the vicinity of the marginally stable orbit, the quanta, flown out to the distant observer, may differ 5 times in their energy. The red maximum

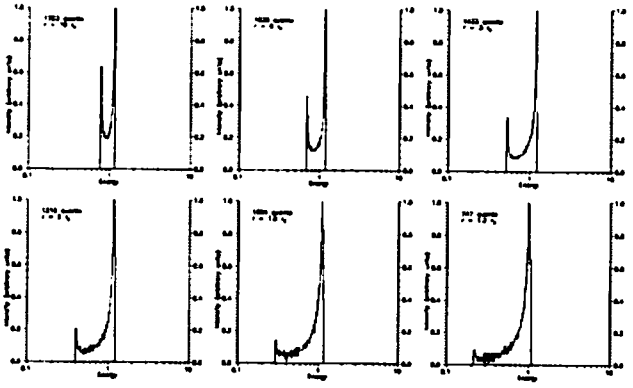

Figure 1: Spectrum of a hot spot for $a = 0.9$, $\theta = 60°$ and different values of the radial coordinate. The marginally stable orbit lays at $r = 1.16\, r_g$.

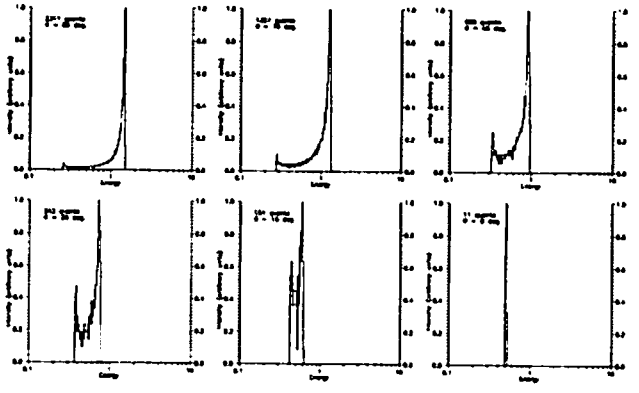

Figure 2: Spectrum of a hot spot for $a = 0.9$, $r = 1.5\, r_g$ and different θ angle values.

decreases its height with diminishing the radius and at $r < 2\, r_g$ becomes almost undistinguishable. It is interesting to note that the spectrum has very sharp edges, both red and blue. Thus, for $a = 0.9$, $r = 3\, r_g$, $\theta = 60°$ the distant observer has registered 1433 quanta of 20417 isotropically emitted; 127 of them ($\approx$ 9%) drop to the interval $1.184 < E < 1.202$ (blue maximum) and 43 quanta drop to $0.525 < E < 0.533$ (red maximum), whereas no one quantum has the energy $E < 0.518$ or $E > 1.236$.

A spectrum of a hot spot for $a = 0.9$, $r = 1.5\, r_g$ and different θ values is shown on Fig. 2. The spectrum for $\theta = 60°$ and the same a and r values is included in Fig. 1 and should be added to the current figure too. As it follows from the figure, the spectrum critically depends on the disk inclination angle. For large θ values, when the line of sight slips almost along the disk plane, the spectrum is strongly stretched, its red maximum is essentially absent, but the blue one appears narrow and very high. The red wing is strongly stretched because of the Doppler effect, so that the observer registers the quanta with 5 times energy difference. As far as the θ angle diminishes the spectrum grows narrow and changes the shape: its red maximum first appears and then gradually increases its height. At $\theta = 0°$ both maxima merge to each other and the spectrum looks like the δ-function. It is evident since all the points of the emitting ring are equal in their conditions with respect to the observer. The frequency of registered quanta in that case is 2 time lower than the frequency of the emitted ones. A fall in frequency consists here in two effects, acting in the same direction: the transversal Doppler effect and the gravitational red shift.

The strong variability of Seyfert galaxies in X-ray does not contradict the assumption, that we observe

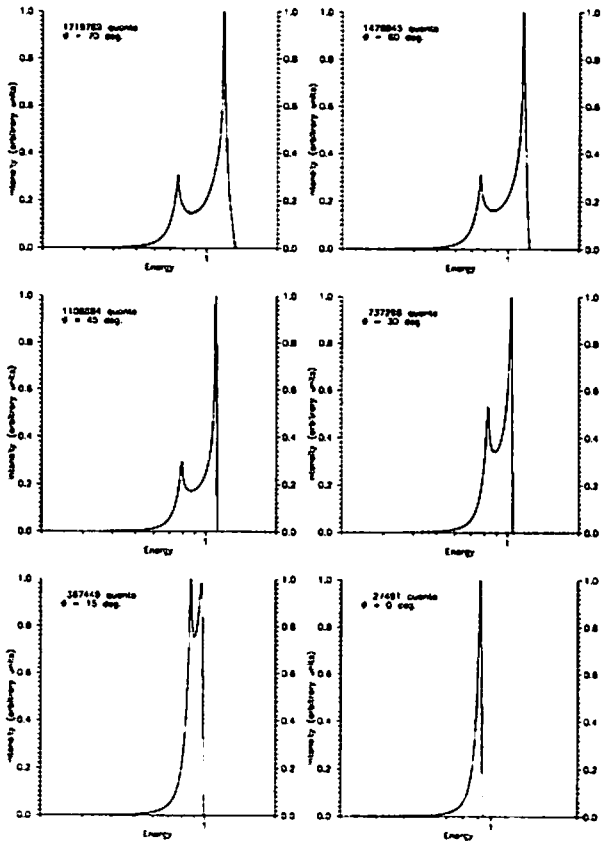

Figure 3: The spectral line shape for different values of θ angle. The emitting region is the wide ring and its inner boundary is the last stable orbit (for rotational parameter $a = 0.9$ this r-value is equal to $r = 1.16\,r_g$), its outer boundary corresponds to $r = 10\,r_g$.

the emission of the hot spots from the inner region of accretion disk, which can decay or grow dim, going towards a horizon as time passes. The spectrum dynamics is understood qualitatively by reference to Fig. 1, considered sequentially from top to bottom. It was considered the case of a wide accretion disk [32] and it was shown that the shape of the spectral line retains its type with two peaks [32] (see Fig.3). It is noted that the inner parts give the essential contribution into red wing of spectrum. and on the physical nature of a hot spot and are not discussed here.

The assumption can be checked out in long-term systematic X-ray observations with high time resolution of such Seyfert galaxies as NGC 1068, NCG 2110, MCG-6-30-15, NGC 4507, etc., where K_α line is sharply defined. The observations could confirm the existence of multiple spots, which motion and dynamics lead to X-ray variability in intensity and spectrum.

This work was supported in part by Russian Foundation for Basic Research (project N 00-02-16108). AFZ would like to thank organizers of the The 11th Workshop on General Relativity and Gravitation for inviting to this conference and giving him the opportunity to present the results of recent efforts.

References

[1] A.F. Zakharov, in *"Fundamental problems of high energy physics and field theory"* (Proceedings of the XXIII Workshop on High Energy Physics and Field Theory), ed. by I.V.Filimonova and V.A.

Petrov, (Institute for High Energy Physics, Protvino, 2000) p. 169.

[2] V.P. Frolov, I.D. Novikov, *Physics - Uspekhi* **44**, (2001) 291.

[3] E.P. Liang, *Physics Reports* **302** (1998) 69.

[4] A.C. Fabian *et al.*, *MNRAS* **277** (1995) L11.

[5] Y. Tanaka, *et al.*, *Nature* **375** (1995) 659.

[6] K. Nandra *et al.*, *ApJ* **476** (1997) 70.

[7] K. Nandra *et al.*, *ApJ* **477** (1997) 602.

[8] A. Malizia *et al.*, *ApJSS* **113** (1997) 311.

[9] R.M. Sambruna *et al.*, *ApJ* **495** (1998) 749.

[10] K.A. Weawer, J.H. Krolik, E.A. Pier, *ApJ* **498** (1998) 213.

[11] T. Yaqoob *et al.*, *ApJ* **490** (1997) L25.

[12] J.W. Sulentic, P. Marziani, M. Calvani, *ApJ* **497** (1998) L65.

[13] B. Paul *et al.*, *ApJ* **492** (1998) L63.

[14] B.C. Bromley, K. Chen, W.A. Miller, *ApJ* **475** (1997) 57.

[15] W. Cui, S.N. Zhang, W. Chen, *ApJ* **492** (1998) L53.

[16] J.M. Sulentic *et al.*, *ApJ* **501** (1998) 54.

[17] A.C. Fabian, in *"Relativistic Astrophysics"* (Proceedings of the XXth Texas Symposium), ed. by J.C.Wheeler and H. Martel, (American Institute of Physics, AIP Conference Proceedings, vol. 586, New York, 2001) p. 643.

[18] A.F. Zakharov, *MNRAS* **269** (1998) 283.

[19] A.F. Zakharov, Preprint MPA **755**, 1993.

[20] A.F. Zakharov, in *"Annals for the 17th Texas Symposium on Relativistic Astrophysics"*, (The New York Academy of Sciences, 1995) **759**, p. 550.

[21] A.F. Zakharov, S.V. Repin, *AZh* **76** (1999) 803.

[22] C.W. Misner, K.S. Thorne, J.A. Wheeler, *"Gravitation"* W.H.Freeman and Company, San Francisco, 1973.

[23] B. Carter, *Phys. Rev.* **D174** (1968) 1559.

[24] A.F. Zakharov, *AZh* 1991, **35** (1991) 145.

[25] S. Chandrasekhar, *"Mathematical Theory of Black Holes"* (Clarendon Press, Oxford, 1983).

[26] C.T. Cunningham, *ApJ* **202** (1975) 788.

[27] C.T. Cunningham, J.M. Bardeen, *ApJ* **183** (1973) 237.

[28] V. Karas, D. Vokrouhlický, A.G.Polnarev, *MNRAS* **259** (1992) 569.

[29] K.P. Rauch, R.D. Blandford, *Caltech Preprint*, GRP-334, 1993.

[30] A.F. Zakharov, *ZhETPh* **91** (1986) 3.

[31] A.F. Zakharov, *ZhETPh* **95** (1989) 385.

[32] A.F. Zakharov, S.V. Repin, *AZh* **79** (2002) 88.

Stability of Self-Similar Solutions with Perfect Fluids

Tomohiro Harada[1]

Department of Physics, Waseda University,
Shinjuku, Tokyo, 169-8555, Japan

Abstract

Self-similar solutions may play important roles in the future asymptotic behavior of expanding universe and/or in the final stage of gravitational collapse. We do full-order stability analysis of self-similar solutions with perfect fluids in general relativity against the so-called kink mode. We find that a wide class of self-similar solutions are unstable. This instability affects the nature of self-similar solutions as attractors or critical solutions.

1 Introduction

The most widely researched self-similar system in general relativity is a spherically symmetric self-similar spacetime with a perfect fluid. The existence of such solutions requires the equation of state to be of the form $P = k\rho$ if it is barotropic.

It has been conjectured that self-similar solutions may play important roles in gravitational collapse and/or in cosmological situations. Indeed, critical phenomena [1, 2, 3] and convergence phenomena [4, 5] provide good examples for that conjecture. For Newtonian self-similar solutions of isothermal gas, which is obtained as a limit $k \to 0$, Ori and Piran [6] pointed out the existence of kink instability in a wide class of self-similar solutions. Here, the analysis is generalized to fully general relativistic case. See [7] for details. We adopt units such that $G = c = 1$.

2 Basic Equations

2.1 Einstein's Equations

The line element in a spherically symmetric spacetime is given by

$$ds^2 = -e^{\sigma(t,r)}dt^2 + e^{\omega(t,r)}dr^2 + R^2(t,r)(d\theta^2 + \sin^2\theta d\phi^2). \tag{1}$$

We consider a perfect fluid as a matter field

$$T^{\mu\nu} = (\rho + P)u^\mu u^\nu + Pg^{\mu\nu}, \tag{2}$$

with the equation of state

$$P = k\rho. \tag{3}$$

and we assume $0 < k < 1$. We adopt the comoving coordinates. We define dimensionless functions such as

$$\eta \equiv 8\pi r^2\rho. \quad S \equiv \frac{R}{r}. \quad M \equiv \frac{2m}{r}. \quad y \equiv \frac{M}{\eta S^3}. \tag{4}$$

where $m(t,r)$ is called Misner-Sharp mass. It is often more convenient to use the following coordinates:

$$\tau \equiv -\ln|t|. \quad z \equiv \ln\left|\frac{r}{t}\right|. \tag{5}$$

We also define a velocity function V. The V is the velocity of the z = const curve relative to the fluid element, which is written as

$$V^2 = e^{2z+\omega-\sigma}. \tag{6}$$

[1] E-mail:harada@gravity.phys.waseda.ac.jp

We impose Einstein's field equations. Then, σ and ω are integrated as

$$e^{\sigma} = a_{\sigma}(t)(\eta e^{-2z})^{-\frac{2k}{1+k}}, \quad e^{\omega} = a_{\omega}(r)\eta^{-\frac{2}{1+k}} S^{-4}, \tag{7}$$

where $a_{\sigma}(t)$ and $a_{\omega}(r)$ can be made constant using the rescaling freedom of t and r. Using the dimensionless variables, Einstein's equations are reduced to the following partially differential equations (PDE's):

$$M + M' = \eta S^2 (S + S'), \tag{8}$$

$$\dot{M} + M' = -k\eta S^2 (\dot{S} + S'), \tag{9}$$

$$\begin{aligned} &\ddot{S} + 2\dot{S}' + S'' + \left[\frac{k}{1+k}\left(\frac{\dot{\eta}}{\eta} + \frac{\eta'}{\eta} - 2\right) + 1\right](\dot{S} + S') \\ = \; & -\frac{k}{1+k} e^{\sigma-\omega-2z}\left(\frac{\eta'}{\eta} - 2\right)(S + S') - \frac{1}{2} e^{\sigma-2z}\frac{M + k\eta S^3}{S^2}, \end{aligned} \tag{10}$$

and

$$\frac{M}{S} = 1 + e^{-\sigma+2z}(\dot{S} + S')^2 - e^{-\omega}(S + S')^2, \tag{11}$$

where three of the above four equations are independent.

2.2 Self-similarity

For self-similar solutions, we assume that all dimensionless quantities depend only on z. Then, from equations (8)-(11), we obtain the following ordinary differential equations (ODE's):

$$M' = \frac{k}{1+k}\frac{1-y}{y} M, \tag{12}$$

$$S' = -\frac{1-y}{1+k} S, \tag{13}$$

$$\eta' = \left[2(1-y) - 2\frac{ky - \frac{1}{4}(1+k)^2 e^{\omega}\eta}{V^2 - k}\right]\eta, \tag{14}$$

and constraint equation

$$V^2(1-y)^2 - (k+y)^2 + (1+k)^2 e^{\omega} S^{-2}(1 - y\eta S^2) = 0. \tag{15}$$

3 Sonic points

The sonic point is defined by

$$V^2 = k, \tag{16}$$

that is, V is equal to the sound speed. At the sonic point, the system of the ODE's (12)-(14) is singular. The regularity requires

$$ky - \frac{1}{4}(1+k)^2 e^{\omega}\eta = 0. \tag{17}$$

From these equations, we can find that sonic points are parametrized by one parameter y_s, where y_s is the value of y at the sonic point.

We introduce new independent variable u which is defined as

$$-\frac{dz}{du} = V^2 - k. \tag{18}$$

Using u in place of z, a sonic point turns out to be a critical point (or a singular point) of the resultant system of the ODE's. A critical point is classified by the behavior of solutions around the point. Then, we can obtain the linearized ODE's in the matrix form. This matrix has two generically nonzero eigenvalues $\lambda_{\pm}$ ($\lambda_- \leq \lambda_+$). These two eigenvalues $\lambda_{\pm}$ are associated with the corresponding eigenvectors, respectively.

The sonic points are classified into saddles, nondegenerate nodes, degenerate nodes and foci with these two eigenvalues. The focal sonic point is unphysical.

The eigenvectors correspond to the two allowed directions along which solutions cross the sonic point. It can be seen that, along the allowed directions $\pm$,

$$\frac{V'}{V} = \frac{1}{2} \mp \frac{\sqrt{D}}{2(1+k)}, \tag{19}$$

where D, which must be nonnegative, is given by some polynomial of k and y_s and hereafter the upper and lower signs denote the +ve and −ve directions, respectively.

4 Kink Instability

4.1 Equations for kink mode

We consider perturbations which satisfy the following conditions: (1) The initial perturbations vanish inside (outside) the sonic point for $t < 0$ ($t > 0$). (2) M, S and η are continuous everywhere. (3) η' is discontinuous at the sonic point, although it has definite one-sided values.

We denote the full order perturbations as

$$\delta S(\tau, z) = S(\tau, z) - S_b(z), \quad \delta M(\tau, z) = M(\tau, z) - M_b(z), \quad \delta\eta(\tau, z) = \eta(\tau, z) - \eta_b(z), \tag{20}$$

where M_b, S_b and η_b denote the background self-similar solution. Hereafter we often omit the subscript 'b'. By conditions (1)-(3), the perturbations satisfy $\delta M = 0, \delta S = 0, \delta\eta = 0, \delta M' = 0, \delta S' = 0, \delta\eta' \neq 0$ at the sonic point at initial moment $\tau = \tau_0$, where the prime denotes the derivative with respect to z on the perturbed side. The evolution of the initially unperturbed region is completely described by the background self-similar solution.

From equations (8)-(11), after a rather lengthy calculation, we obtain the following equation:

$$\frac{\delta\dot{V}'}{V} - \left[1 - 2\left(\frac{V'}{V}\right)_b\right]\frac{\delta V'}{V} + \left(\frac{\delta V'}{V}\right)^2 = 0. \tag{21}$$

4.2 Stability analysis

If we linearize equation (21), we can obtain

$$\frac{\delta V'}{V} = \text{const} \cdot e^{\alpha\tau}, \tag{22}$$

where

$$\alpha \equiv 1 - 2\left(\frac{V'}{V}\right)_b. \tag{23}$$

In fact, equation (21) is easily integrated. Putting $X \equiv \delta V'/V$, we rewrite equation (21) as

$$\dot{X} - \alpha X + X^2 = 0. \tag{24}$$

There are two stationary solutions $X = 0$ and $X = \alpha$. General solutions are the following:

$$X = \frac{\alpha}{1 - \exp(-\alpha\tau + \text{const})}, \quad \text{for} \quad \alpha \neq 0 \tag{25}$$

$$X = \frac{1}{\tau + \text{const}}, \quad \text{for} \quad \alpha = 0 \tag{26}$$

4.2.1 $D > 0$ case

First, we consider $\alpha > 0$. It can be seen that, as τ increases, X blows up to $-\infty$ at some finite moment $\tau \to \tau_d - 0 > \tau_0$ for an initial value $X_0 < 0$, where

$$\tau_d \equiv \tau_0 + \frac{1}{\alpha} \ln \left(1 - \frac{\alpha}{X_0} \right), \tag{27}$$

while X monotonically approaches α for $X_0 > 0$. Next, we consider $\alpha < 0$. It can be seen that, as τ increases, X monotonically approaches 0 for $X_0 > \alpha$, while X blows up to $-\infty$ at some finite moment $\tau = \tau_d - 0 > \tau_0$ for $X_0 < \alpha$. Actually these two analyses under two different backgrounds are only apparently different local pictures of nonlinear dynamics. This case corresponds to a nondegenerate node or saddle. The global dynamical behavior of the perturbation is schematically depicted in figure 1 (a).

4.2.2 $D = 0$ case

We consider $\alpha = 0$. It can be seen that, as τ increases, X diverges to $-\infty$ at some finite moment $\tau \to \tau_d$, where

$$\tau_d \equiv \tau_0 - \frac{1}{X_0}, \tag{28}$$

for $X_0 < 0$, while X approaches 0 for $X_0 > 0$. This case corresponds to a degenerate node for which $D = 0$ and $(V''/V)_b = 1/2$. The global behavior is depicted in figure 1 (b).

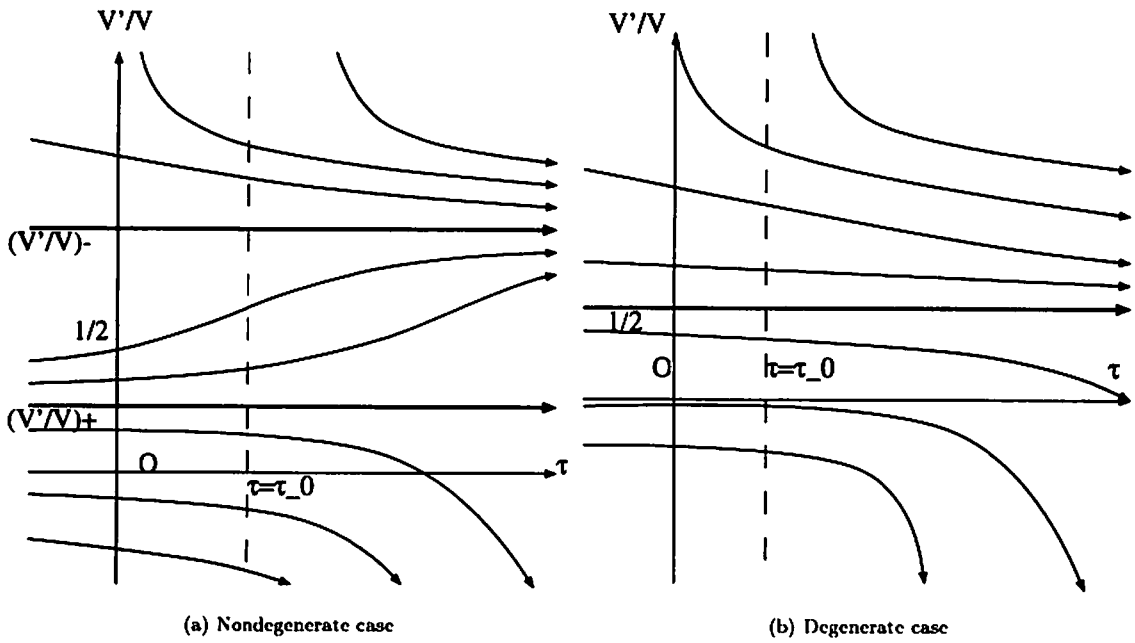

(a) Nondegenerate case (b) Degenerate case

Figure 1: Dynamical behavior of the kink mode (a) for a nondegenerate case and (b) for a degenerate case.

4.3 Stability criterion

We define instability as the blow up of density gradient in finite time interval. The obtained criterion is summarized in table 1. The present criterion for stability should be considered as a necessary condition for stability, while the criterion for instability should be considered as a sufficient condition for instability.

Table 1: Stability for the kink mode and the class of sonic points

t	Primary node	Secondary node	Degenerate node	Saddle: +	Saddle: −
> 0	Stable	Unstable	Unstable	Stable	Unstable
< 0	Unstable	Stable	Unstable	Unstable	Stable

5 Applications

The class of the sonic point of each known self-similar solution has been researched by several authors. Here we only present the obtained stability of known solutions with the nature of the sonic points.

The expanding flat Friedmann solution is unstable against the kink mode for $1/3 \leq k < 1$. The collapsing flat Friedmann solution is also unstable for $0 < k \leq 1/3$ against the kink mode. The expanding flat Friedmann solution for $0 < k < 1/3$ and the collapsing flat Friedmann solution for $1/3 < k < 1$ do not suffer kink instability.

The static self-similar solution is unstable for $0 < k < 1$.

Nonanalytic self-similar solutions are all unstable for $t < 0$. For $t > 0$, nonanalytic self-similar solutions do not suffer kink instability.

The Larson-Penston (attractor) solution is stable for the kink mode for $0 < k \lesssim 0.036$, while it is unstable for $0.036 \lesssim k$. It is important that the kink mode does not affect the nature of the Larson-Penston solution as an attractor for $0 < k \lesssim 0.036$, while it does for $0.036 \lesssim k$.

The kink mode does not affect the critical nature of the Evans-Coleman (critical) solution for $0 < k \lesssim 0.89$, while the Evans-Coleman solution suffers the kink instability for $0.89 \lesssim k$. Since the critical solution is assumed to have a single unstable mode, the Evans-Coleman solution for $0.89 \lesssim k$ cannot be a critical solution.

6 Summary

A wide class of self-similar solutions are unstable against the kink mode. The development of this instability will result in the formation of a shock wave. The implications are that the Larson-Penston (attractor) solution loses its attractive nature for $0.036 \lesssim k$, that the Evans-Coleman (critical) solution loses its critical nature for $0.89 \lesssim k$ and that the flat Friedmann universe suffers kink instability for $1/3 \leq k < 1$.

References

[1] C.R. Evans and J.S. Coleman, Phys. Rev. Lett. **72** (1994) 1782.

[2] T. Koike, T. Hara and S. Adachi, Phys. Rev. Lett. **74** (1995) 5170.

[3] D.W. Neilsen and M.W. Choptuik, Class. Quantum Grav. **17** (2000) 733; Class. Quantum Grav. **17** (2000) 761.

[4] T. Harada, Phys. Rev. D **58** (1998) 104015.

[5] T. Harada and H. Maeda, Phys. Rev. D **63** (2001) 084022.

[6] A. Ori and T. Piran, MNRAS **234** (1988) 821.

[7] T. Harada, Class. Quantum Grav. **18** (2001) 4549.

Incompatibility of Kinematic Self-Similarity with Polytropic Equation of State

Hideki Maeda[a 1], Tomohiro Harada[b 2], Hideo Iguchi[c 3], and Naoya Okuyama[d 4]

[a,b,d] *Department of Physics, Waseda University, Shinjuku, Tokyo, 169-8555, Japan*

[c] *Department of Physics, Tokyo Institute of Technology, Oh-Okayama, Meguro, Tokyo, 152, Japan*

Abstract

We have investigated spherically symmetric spacetimes which contain a perfect fluid obeying the polytropic equation of state and admit a kinematic self-similar vector of the second kind which is neither parallel nor orthogonal to the fluid flow. We have assumed two kinds of polytropic equation of state in general relativity and shown that such spacetimes must be vacuum spacetimes.

1 Introduction

In general relativity self-similarity is defined by the existence of a homothetic Killing vector field [1]. In Newtonian gravity, self-similarity in the polytropic case differs from that in the isothermal case in having the different form of the dimensionless variable since the sound speed is not constant in the polytropic case. The dimensionless variable is $c_s t/r$ in the isothermal case ($p = c_s^2 \rho$), while that is $[\sqrt{K} t^{2-\gamma}]/[G^{(\gamma-1)/2} r]$ in the polytropic case ($p = K\rho^\gamma$). In general relativity, there exists a natural generalization of homothety called *kinematic self-similarity* which is defined by the existence of a kinematic self-similar vector field [2]. The natural counterpart of the self-similarity in the Newtonian polytropic case is the kinematic self-similarity of the second kind.

In this paper we study the spacetimes which admit a kinematic self-similar vector field of the second kind and contain a perfect fluid obeying the polytropic equation of state. We assume two kinds of polytropic equation of state in general relativity and show that there is no non-trivial kinematic self-similar solutions of the second kind obeying the polytropic equation of state with positive pressure. In this paper we adopt the $c = 1$ unit.

2 Spherically Symmetric Spacetime and Kinematic Self-Similarity

The line element in a spherically symmetric spacetime is given by

$$ds^2 = -e^{2\Phi(t,r)}dt^2 + e^{2\Psi(t,r)}dr^2 + R(t,r)^2 d\Omega^2, \tag{1}$$

where $d\Omega^2 = d\theta^2 + \sin^2\theta d\varphi^2$. We consider a perfect fluid as a matter field

$$T_{\mu\nu} = p(t,r)g_{\mu\nu} + (\mu(t,r) + p(t,r))U_\mu U_\nu, \tag{2}$$

$$U_\mu = (-e^\Phi, 0, 0, 0). \tag{3}$$

Here we adopt the comoving coordinates. Then the Einstein equations and the equations of motion for the perfect fluid are reduced to the following simple form:

[1] E-mail:hideki@gravity.phys.waseda.ac.jp
[2] E-mail:harada@gravity.phys.waseda.ac.jp
[3] E-mail:iguchi@th.phys.titech.ac.jp
[4] E-mail:okuyama@gravity.phys.waseda.ac.jp

$$\Phi_r = -\frac{p_r}{\mu + p}, \tag{4}$$

$$\Psi_t = -\frac{\mu_t}{\mu + p} - \frac{2R_t}{R}, \tag{5}$$

$$m_r = 4\pi\mu R_r R^2, \tag{6}$$

$$m_t = -4\pi p R_t R^2, \tag{7}$$

$$0 = -R_{tr} + \Phi_r R_t + \Psi_t R_r, \tag{8}$$

$$m = \frac{1}{2G} R(1 + e^{-2\Phi} {R_t}^2 - e^{-2\Psi} {R_r}^2), \tag{9}$$

where $m(t, r)$ is called the Misner-Sharp mass. In this paper, we assume two kinds of polytropic equation of state in general relativity. One is

$$p = K\mu^\gamma, \tag{10}$$

where K and γ are constants and the other [3] is

$$\begin{cases} p = Kn^\gamma, \\ \mu = m_b n + \dfrac{p}{\gamma - 1}. \end{cases} \tag{11}$$

where the constant m_b is the mean baryon mass and $n(t, r)$ is baryon number density. We call the first one the equation of state (I) and the second the equation of state (II). Here we assume that $K \neq 0$ and $\gamma \neq 0, 1$. It is noted that the sound speed of the matter obeying the equation of state (II) does not become faster than the speed of light since the equation of state (II) is approximated to the equation of state $p = (\gamma - 1)\mu$ in the high (low) density region for $\gamma > 1$ ($\gamma < 1$) although the sound speed of the matter obeying the equation of state (I) become faster than the speed of light in the high (low) density region for $\gamma > 1$ ($\gamma < 1$).

A kinematic self-similarity vector ξ satisfies the conditon

$$\mathcal{L}_\xi h_{\mu\nu} = 2h_{\mu\nu}, \quad \mathcal{L}_\xi U_\mu = \alpha U_\mu, \tag{12}$$

where $h_{\mu\nu} = g_{\mu\nu} + U_\mu U_\nu$ is the projection tensor, $\mathcal{L}_\xi$ denotes Lie differentiation along ξ and α is a constant [2, 4]. The similarity transformation is characterized by α which is referred to as the similarity index. Here we treat only the case that $\alpha \neq 0, 1$, corresponding to self-similarity of the second kind, and a kinematic self-similar vector is neither parallel nor orthogonal to the fluid flow (these cases are treated in [5]). Self-similarity implies that the metric functions can be written as

$$R = rS(\xi), \quad \Phi = \Phi(\xi), \quad \Psi = \Psi(\xi), \tag{13}$$

where $\xi = r/(\alpha t)^{1/\alpha}$ is the self-similar variable. The Einstein equations imply that the quantities m, μ and p must be of the form

$$2Gm = r\left(M_1(\xi) + \frac{r^2}{t^2} M_2(\xi)\right), \tag{14}$$

$$8\pi G\mu = \frac{1}{r^2}\left(W_1(\xi) + \frac{r^2}{t^2} W_2(\xi)\right), \tag{15}$$

$$8\pi G p = \frac{1}{r^2}\left(P_1(\xi) + \frac{r^2}{t^2} P_2(\xi)\right), \tag{16}$$

and a set of ordinary differential equations resluts by demanding that the Einstein equations and the equations of motion of the matter field are satisfied for the different terms separately. The resulting equations for a perfect fluid (4)-(9) reduce to the following:

$$
\begin{aligned}
M_1 + M_1' &= W_1 S^2 (S + S'), && (17)\\
3M_2 + M_2' &= W_2 S^2 (S + S'), && (18)\\
M_1' &= -P_1 S^2 S', && (19)\\
2\alpha M_2 + M_2' &= -P_2 S^2 S', && (20)\\
M_1 &= S[1 - e^{-2\Psi}(S + S')^2], && (21)\\
\alpha^2 M_2 &= S S'^2 e^{-2\Phi}, && (22)\\
(P_1 + W_1)\Phi' &= 2P_1 - P_1', && (23)\\
(P_2 + W_2)\Phi' &= -P_2', && (24)\\
W_1' S &= -(P_1 + W_1)(\Psi' S + 2S'), && (25)\\
(2\alpha W_2 + W_2')S &= -(P_2 + W_2)(\Psi' S + 2S'), && (26)\\
S'' + S' &= S'\Phi' + (S + S')\Psi', && (27)
\end{aligned}
$$

where the prime denotes the deviation with respect to $\ln \xi$.

3 No Go Theorem

The following theorem is proved.

Theorem (No Go Theorem for Kinematic Self-Similarity of the Second Kind with Polytropic Equation of State).
Let the $(\mathcal{M}^4, g)$ be a spherically symmetric spacetime which
a) *admits a kinematic self-similar vector of the second kind ξ^μ which is neither parallel nor orthogonal to the fluid flow; and*
b) *satisfies the Einstein equations for a perfect fluid with positive pressure obeying the equation of state* (I) *for $\gamma \neq 1$ or* (II).
Then $(\mathcal{M}^4, g)$ is the Minkowski spacetime for any positive α or the Schwarzschild spacetime for $\alpha = 3/2$.

Proof. We assume that the spacetime is not a vacuum spacetime and lead to a contradiction. When a perfect fluid obeys the equation of state (I), we find from equations (15) and (16) that

$$\alpha = \gamma, \quad P_1 = W_2 = 0, \quad P_2 = \frac{K}{(8\pi G)^{\gamma-1}\alpha^2} \xi^{-2\gamma} W_1^\gamma \quad \text{(case (A))}, \tag{28}$$

or

$$\alpha = \frac{1}{\gamma}, \quad P_2 = W_1 = 0, \quad P_1 = \frac{K\alpha^{2/\alpha}}{(8\pi G)^{\gamma-1}} \xi^2 W_2^\gamma \quad \text{(case (B))}. \tag{29}$$

When a perfect fluid obeys the equation of state (II), we find from equation (15) and (16) that

$$\alpha = \gamma, \quad P_1 = 0, \quad P_2 = \frac{K}{m_b^\gamma (8\pi G)^{\gamma-1}\alpha^2} \xi^{-2\gamma} W_1^\gamma = (\gamma - 1) W_2 \quad \text{(case (C))}, \tag{30}$$

or

$$\alpha = \frac{1}{\gamma}, \quad P_2 = 0, \quad P_1 = \frac{K\alpha^{2/\alpha}}{m_b^\gamma (8\pi G)^{\gamma-1}} \xi^2 W_2^\gamma = (\gamma - 1) W_1 \quad \text{(case (D))}. \tag{31}$$

In case(A), $\Phi' = 0$ can be obtained from equation (23) and then P_2 must be constant from equation (24). On the other hand, $\Psi' S + 2S = 0$ can be obtained from equation (26) and then W_1 must be constant from equation (25). These contradict to equation (28), and therefore this spacetime must be a vacuum spacetime.

In case(B), $\Phi' = 0$ can be obtained from equation (24) and then $P_1 \propto \xi^2$ can be obtained from equation (23). On the other hand, $\Psi' S + 2S = 0$ can be obtained from equation (25) and then $W_2 \propto \xi^{-2\alpha}$ can be obtained from equation (26). These contradict to equation (29), and therefore this spacetime must be a vacuum spacetime.

In case(C), $\Phi' = 0$ can be obtained from equation (23) and then P_2 must be constant from equation (24). Equation (30) gives that $W_1 \propto \xi^2$. On the other hand, M_1 must be constant since equation (19), and then $M_1 S' = 0$ can be obtained with differentiating equation (21) and using equation (27). When $M_1 = 0$, equation (17) gives that $S + S' = 0$, however this contradicts to equation (21). When $S' = 0$, equation (17) results in that W_1 must be constant, however this is a contradiction. Then it can be concluded that this spacetime is a vacuum spacetime.

In case(D), $\Phi' = 0$ can be obtained from equation (24) and then $P_1 \propto \xi^2$ can be obtained from equation (23). Equation (31) gives that $P_1 = (\gamma - 1) W_1 \propto \xi^2$ and W_2 must be constant. On the other hand, $M_1' S = M_1 S'$ can be obtained with differentiating equation (21) and using equation (27) which means that $M_1 = 0$ or $M_1'/M_1 = S'/S$. When $M_1 = 0$, equation (17) gives that $S + S' = 0$, however this contradicts to equation (21). When $M_1'/M_1 = S'/S$, $S'(P_1 + W_1)(S + S') = 0$ can be obtained from equations (17) and (19) which means that $S' = 0$ or $S + S' = 0$ since $\gamma \neq 0$ here. When $S' = 0 = M_1'$, W_1 must be constant from equation (17), however this is a contradiction. When $S' + S = 0$, equation (21) gives that $M_1 = S$, and then $P_1 = -1/S^2$ can be obtained from equation (19) which means negative pressure. This is a contradiction, and therefore it can be concluded that this spacetime is a vacuum spacetime.

From Birkhoff's theorem, this spacetime is the Minkowski spacetime or the Schwarzschild spacetime. The Schwarzschild spacetime can be obtained only for $\alpha = 3/2$ in which case equations (18) and (20) are degenerated. The Schwarzschild black hole in Lemaitre's coordinates is written as

$$ds^2 = -dt^2 + r_g^{\frac{2}{3}} \left(\frac{dR^2}{\left[\frac{3}{2}(R-t)\right]^{\frac{2}{3}}} + \left[\frac{3}{2}(R-t)\right]^{\frac{4}{3}} d\Omega^2 \right), \tag{32}$$

with $3/2(R-t) = r_g$ being the Schwarzschild radius. Changing the radial coordinate as $R = r^{3/2}$,

$$ds^2 = -dt^2 + r_g^{\frac{2}{3}} \left(\frac{9/4 dr^2}{\left[\frac{3}{2}(1 - t/r^{\frac{3}{2}})\right]^{\frac{2}{3}}} + r^2 \left[\frac{3}{2}(1 - t/r^{\frac{3}{2}})\right]^{\frac{4}{3}} d\Omega^2 \right), \tag{33}$$

can be obtained. ■

4 Summary

We have shown that there is no non-trivial spherically symmetric solution that contains a perfect fluid with positive pressure obeying the polytropic equation of state and admits a kinematic self-similar vector of the second kind which is neither parallel nor orthogonal to the fluid flow. In order to show the whole picture of the generic collapse of the polytrope gas, the full numerical simulations of gravitational collapse will have to be done.

References

[1] A.H. Cahill and M.E. Taub, Commun. Math. Phys. **21**, 1 (1971).

[2] B. Carter and R.N. Henriksen, Ann. Physique Supp. 14, 47 (1989); B. Carter and R.N. Henriksen, J. Math. Phys. 32, 2580 (1991).

[3] S.L. Shapiro and S.A. Teukolsky, *Black Holes, White Dwarfs, and Newtron Stars* (Wiley, 1983).

[4] A.A. Coley, Class. Quantum Grav. 14, 87-118 (1997); P.M. Benoit and A.A. Coley, Class. Quantum Grav. 15, 2397-2414 (1998).

[5] H. Maeda, T. Harada, H. Iguchi and N. Okuyama, in preparation.

Gravitational Radiation Reaction
- *Present Status and Future prospect* -

Yasushi Mino[1]

Department of Physics, Washington University, Campus Box 1105,
One Brookings Dr., St.Louis, MO 63130-4899, USA

Abstract

In this talk, we review the present study of the gravitational self-force problem, and discuss the possible direction of the future investigation.

1 Introduction

A space-based project LISA was proposed, which has an extremely long base line as a perticular feature[1]. Recently, ESA and NASA signed a letter of understanding to construct and fly LISA jointly, and the development of LISA's detector technology is now vigorously underway. For the success of this project, we have to establish the theoretical tools to identify astrophysical parameters of gravitational-waves sources from the detected gravitational waves. Among possible astrophysical sources, binary systems of supermassive blackholes (thought to exist at galactic centers) and solar-mass compact objects (like blackholes, neutron stars, white dwarfs) are indentified to be the most promising targets of LISA as their event rates are expected to be large enough[1].

As the supermassive blackhole dominates the gravitational field, we consider to approximate such binary systems by the linear perturbation to a Kerr blackhole. For the mathematical simplicity, we use a point particle as a compact object inspiralling to the background blackhole, which induces the perturbation. Once an orbit of the point particle is given, there is a method to calculate the observable waveform. Therefore, the remaining problem is to establish a method of calculating the orbital evolution of the particle, which is efficient enough for the realistic application to the gravitational-wave data analysis.

For this purpose, we consider to calclulate the self-force acting on the particle. Here we encounter the divergence of the self-field and we need a regularization calculation to extract out the physically meaningful finite part corresponding to the self-force. The regularization scheme was discussed in Ref.[2] using the harmonic gauge condition. Schematically the reaction force is given by

$$F_\alpha(\tau_0) \;=\; \lim_{x\to z(\tau_0)} F_\alpha[h^{\rm tail}_{\mu\nu}](x)\,, \qquad F_\alpha[h^{\rm tail}_{\mu\nu}](x) \;=\; F_\alpha[h^{\rm full}_{\mu\nu}](x) - F_\alpha[h^{\rm dir}_{\mu\nu}](x)\,, \quad (x\neq z(\tau))\,, \tag{1}$$

where z is the orbit of the particle with the proper time τ, and τ_0 is the time of the orbital point which we calculate the force. $h^{\rm tail}_{\mu\nu}$ is the tail part of the metric perturbation induced by the point particle, and is regular at the coincidence limit $x\to z(\tau)$. $h^{\rm full}_{\mu\nu}$ is the full metric perturbation induced by the point particle, and $h^{\rm dir}_{\mu\nu}$ is its direct part as defined in Refs.[2], both of which diverge at the coincidence limit $x\to z(\tau)$. $F_\alpha[...]$ is a tensor operator on the metric pertubation, and is defined as

$$F_\alpha[h_{\mu\nu}] \;=\; -m\left(h_{\alpha\beta;\gamma} - \frac{1}{2}h_{\beta\gamma;\alpha}\right)V^\beta V^\gamma\,. \tag{2}$$

V^α is a vector defined on the field point x, which coincides the four velocity $v^\alpha(\tau_0)$ when we take the coincidence limit $x\to z(\tau_0)$.

Because of the divergence of the full part and the direct part, it is a non-trivial task to perform the subtraction, which we call the '*Subtraction Problem*'. We shall discuss the present status to this problem in Sec.2. The self-force in the linear gravitational perturbation is a gauge dependent vector, therefore, one has to fix the gauge appropriately in evaluating both the full metric perturbation and its direct part before calculating the force, which we call the '*Gauge Problem*'. We shall discuss the present possible idea to this problem in Sec.3.

[1] E-mail:mino@wugrav.wustl.edu

At present, the most successful investigation in the self-force problem is done only when the background is a Schwarzschild blackhole. We shall conclude in Sec.4 with a future possible direction of the investigation when the background is a Kerr blackhole.

2 Subtraction Problem

As a target of LISA, binary systems are astrophysically expected to have fairly large eccentricity[1]. For such orbits, numerical calculation seems unavoidable. Since divergence is hard to deal with numerically, we consider to replace the divergence of the full part and the direct part by an infinite sum of finite terms under a certain expansion rule as

$$F_\alpha[h^{\rm full/dir}_{\mu\nu}](x) \;=\; \lim_{N\to\infty}\sum_n^N F_\alpha^{\rm full/dir(n)}(x)\,. \tag{3}$$

When we apply the same expansion rule to the tail part as

$$F_\alpha[h^{\rm tail}_{\mu\nu}](x) \;=\; \lim_{N\to\infty}\sum_n^N F_\alpha^{\rm tail(n)}(x)\,, \qquad F_\alpha^{\rm tail(n)} \;=\; F_\alpha^{\rm full(n)} - F_\alpha^{\rm dir(n)}\,, \tag{4}$$

this becomes a convergent expansion, and one can exchange the infinity limit of the summation $N\to\infty$ and the coincidence limit $x\to z(\tau_0)$. Thence, we finally have

$$F_\alpha(\tau_0) \;=\; \lim_{N\to\infty}\sum_n^N\left\{F_\alpha^{\rm full(n)}(z(\tau_0)) - F_\alpha^{\rm dir(n)}(z(\tau_0))\right\}. \tag{5}$$

Though it is possible to derive each term of the full part numerically, it is still impossible to calculate all terms. In this sense, all we can do is the approximated calculation of Eq.5. The problem to obtain a result of better accuracy with a limited computational power, is called the '*Convergence Problem*'.

As a possible rule to provide an infinite expansion of the fields, there were proposed two approaches; power expansion[4] and mode decomposition[3], which we shall summarize below.

2.1 Power Expansion Approach

In this approach, we first evaluate the full part and the direct part at $x^\alpha(r)=\{t_0,r,\theta_0,\phi_0\}$ in the Boyer-Lindquist coordinate system, where $z^\alpha(\tau_0)=\{t_0,r_0,\theta_0,\phi_0\}$ is the location of the particle. Here the radius r is taken at the neighborhood of r_0, thence, we can implement the Taylor expansion[2]. Because these fields become singular at $r=r_0$, we can consider the expansion with the negative power of r at $r_0<r<\infty$ or the expansion with the positive power of $r-r_H$ at $r_H<r<r_0$, where r_H is the radius of the (outer) horizon as

$$F_\alpha[h^{\rm full}_{\mu\nu}](x(r)) \;=\; \begin{cases} \lim_{K\to\infty}\sum_k^K F_\alpha^{{\rm full}(k,-)} r^{-k}\,, & (r_0<r<\infty)\,, \\ \lim_{K\to\infty}\sum_k^K F_\alpha^{{\rm full}(k,+)}(r-r_H)^k\,, & (r_H<r<r_0)\,, \end{cases} \tag{6}$$

$$F_\alpha[h^{\rm dir}_{\mu\nu}](x(r)) \;=\; \begin{cases} \lim_{K\to\infty}\sum_k^K F_\alpha^{{\rm dir}(k,-)} r^{-k}\,, & (r_0<r<\infty)\,, \\ \lim_{K\to\infty}\sum_k^K F_\alpha^{{\rm dir}(k,+)}(r-r_H)^k\,, & (r_H<r<r_0)\,. \end{cases} \tag{7}$$

At present, the fully relativistic calculation of the direct part for the arbitrary orbit has been done for a Schwarzschild background in Ref.[4], using the local expansion technique of the direct part[3]. We

[2]Precisely speaking, we define the 'Power Expansion' as a technique to replace radial homogeneous functions with a finite number of power of radius r under a given precision[5], and it might have a wider applicability besides the self-force problem.

When we use this technique for the regularization calculation as described here, we encounter a problem; the power indices become non-integer, and the resulting full part cannot be a correct Taylor expansion. Ref.[4] discuss the prescription to obtain the correct Taylor expansion.

[3]Some detail of the local expansion technique is discussed in Ref.[3]. Comparing the mode decomposition approach, the direct part can easily be derived.

consider that we can simply extend the calculation to the case of a Kerr blackground. Meanwhile, the calculation of the full part has been derived only for the circular orbit in Ref.[4] under a post-Newtonian expansion approximation. Therefore, we stil have two problems here; the generalization of the orbit and the fully relativistic calculation Lastly, we comment that the convergence behavior is not good in this approach.

2.2 Mode decomposition Approach

In this approach, we first evaluate the full part and the direct part at $x^\alpha = \{t_0, r, \theta, \phi\}$.

We decompose the full part by the tensor spherical/spheroidal harmonics $Y^{(\ell m)A}_{\alpha\beta}(\theta,\phi)$ as

$$h^{\rm full}_{\mu\nu}(x) = \lim_{L\to\infty}\sum_{\ell=0}^{L}\sum_{m=-\ell}^{\ell}\sum_{A} h^{\rm full}_{(\ell m)A}(t,r)Y^{(\ell m)A}_{\mu\nu}(\theta,\phi)\,. \tag{8}$$

Then we have a decoupled equations for the mode coefficients $h^{\rm full}_{(\ell m)A}(t,r)$, which we can evaluate numerically.

Contrary to the full part, the direct part is defined only at the neighborhood of the particle's orbit[2], which is insufficient for the mode decomposition in the exact sense. In the regularization calculation (1), we take the coincidence limit $x \to z(\tau_0)$ after the subtraction. thence, only the part non-vanishing in the coincidence limit makes a contribution to the final result. With the local coordinate expansion technique in Ref.[3], one evaluate this part of the direct part by the background coordinates, then one can decompose it by the mode-decomposition formula[3] as

$$h^{\rm dir}_{\mu\nu}(x) = \lim_{L\to\infty}\sum_{\ell=0}^{L}\sum_{m=-\ell}^{\ell}\sum_{A} h^{\rm dir}_{(\ell m)A}(r)Y^{(\ell m)A}_{\mu\nu}(\theta,\phi)\,. \tag{9}$$

This approach has made a most successful progress when the background is a Schwarzschild blackhole[3]. Ref.[3] has derived a quite general formula to decompose all the typical terms under the local coordinate expansion. However, the extention to a Kerr case is still a problem.

The convergence problem of this approach is not yet solved, however, the solution seems to be promising[8]. The direct part in this approach have an ambiguity in adding a vanishing term. Using this freedom, one can re-define the tail part such that it has a good convergence behavior.

3 Gauge Problem

The regularization scheme (1) is defined in the harmonic gauge condition, and the more important thing is that we have the analytic description of the direct part only in the harmonic gauge condition. However, we do not have a systematic method to calculate the metric perturbation in the harmonic gauge like Regge-Wheeler formalism[11] or Chrzanovsky formalism[12][4].

In the following subsection, we shall describe some possible ideas for a systematic and efficient calculation of the full part, Starting from a systematic method in calculating the metric perturbation, such as Regge-Wheeler formalism[11] and Chrzanovsky formalism[12]. We may have two approaches to this problem; local harmonic gauge approach and gauge invariant approach, which we shall discuss below.

3.1 Local Harmonic Gauge Approach

The strategy here is to calculate the Green function of the metric perturbation which satisfies the harmonic gauge condition at the neighborhood of the particle. Under the Fourier-Harmonic decomposition, the

[4] An idea to calculate the metric perturbation in the harmonic gauge is proposed when the background is a Schwarzschild blackhole[10].

Green function[5] can be constructed by the sum of homogeneous solutions as

$$G^{\rm full}_{\mu\nu\mu'\nu'}(x,x') = \sum_{(\ell m\omega)AA'} \mathcal{G}_{(\ell m\omega)AA'}(r,r')Y^{(\ell m\omega)A}(\theta\phi)Y^{(\ell m\omega)A'*}(\theta'\phi')e^{-i\omega(t-t')}, \tag{10}$$

$$\mathcal{G}_{(\ell m\omega)AA'}(r,r') = \left(h^{up}_{(\ell m\omega)A}(r)h^{in*}_{(\ell m\omega)A}(r')\theta(r-r') + h^{in}_{(\ell m\omega)A}(r)h^{up*}_{(\ell m\omega)A}(r')\theta(r'-r) \right), \tag{11}$$

thence, the problem is how to calculate the homogeneous metric perturbation in the harmonic gauge condition.

By the power expansion technique we can replace the radial homogeneous Regge-Wheeler/Teukolsky functions with a finite number of power of the radius r under a given order of precision[5]. Then we obtain the homogeneous metric perturbation in the Regge-Wheeler gauge[11] or in the radiation gauge[12], whose radial dependence has a fairly simple analytical structure. Because of its simplicity, the calculation of the gauge transformation is possible at the neighborhood of the particle[13].

We, however, note that there may remain another gauge problem. When integrating the equation of the gauge transformation, we cannot take into account the boundary condition as we have an approximated source term just around the particle, thence, an unknown homogeneous gauge mode might be added to the final result.

3.2 Gauge invariant Approach

This approach is established only in a Schwarzschild background for the 'gauge invariant property' of the Regge-Wheeler gauge condition. We, therefore, focus on the case when the background is approximated by a Schwarzschild blackhole.

The genuity of the Regge-Wheeler gauge condition is its gauge invariant nature under the spherical harmonic decomposition. Once a metric perturbation of an unknown gauge condition is given as

$$h_{\mu\nu}(x) = \sum_{\ell m,A} h_{(\ell m)A}(t,r)Y^{(\ell m)A}_{\mu\nu}(\theta,\phi), \tag{12}$$

one can uniquely calculate the gauge transformation vector $\xi^{\rm RW}_\mu$ by a linear differential operation of the mode coefficients of (12) as

$$\xi^{\rm RW}_\mu[{\rm h}](x) = \sum_{\ell m,A} \xi^{\rm RW}_{(\ell m)A}[h_{(\ell m)A'}](t,r)Y^{(\ell m)A}_{\mu}(\theta,\phi). \tag{13}$$

We note that this is purely a property of a gauge transformation and it hold even when $h_{\mu\nu}$ does not satisfy the Einstein equation.

Using the gauge invariant property of the Regge-Wheeler gauge, we define a metric perturbation in the hybrid gauge condition[6] as

$$h^{\rm H-RW}_{\mu\nu}(x) = h^{\rm H}_{\mu\nu}(x) + \nabla_{(\mu}\xi^{\rm RW}_{\nu)}[{\rm h}^{\rm tail,H}](x), \tag{14}$$

where $h^{\rm H}_{\mu\nu}$ is the full metric perturbation in the harmonic gauge, and ${\rm h}^{\rm tail,H}_{\mu\nu}$ is its tail part.

We note that we have a freedom to add a finite gauge transformation to the full part in the regularization scheme (1)[14]. One can prove that $\xi^{\rm RW}_\nu[{\rm h}^{\rm tail,H}](x)$ is finite around the orbit, and we can use the hybrid gauge condition in (1) as

$$F^{\rm H-RW}_\alpha(\tau_0) = \lim_{x\to z(\tau_0)} F_\alpha[h^{\rm tail,RW}_{\mu\nu}](x), \tag{15}$$

$$\begin{aligned} h^{\rm tail,RW}_{\mu\nu}(x) &= h^{\rm H-RW}_{\mu\nu}(x) - h^{\rm dir,H}_{\mu\nu}(x) \\ &= h^{\rm RW}_{\mu\nu}(x) - \left(h^{\rm dir,H}_{\mu\nu}(x) + \nabla_{(\mu}\xi^{\rm RW}_{\nu)}[{\rm h}^{\rm dir,H}](x)\right), \quad (x \neq z(\tau)), \end{aligned} \tag{16}$$

where $h^{\rm RW}_{\mu\nu}$ is the full metric perturbation in the Regge-Wheeler gauge condition. As the divergent part is determined only by the direct part derived in Ref.[2], we have a modified regularization scheme which only used the conventional perturbation calculation.

[5]The special feature of the (quasi-)harmonic gauge condition is that there is no 'local term' in the radial Green function, i.e. the term proportional to $\delta(r-r')$, which is in contrast to the Regge-Wheeler/radiation gauge condition.

[6]The name 'Hybrid gauge' comes from the talk by L. Barack at Capra 4[14]

4 Conclusion and Future Prospect

In this talk, we review our present understanding of the gravitational self-force problem. We pointed out some new problems to be solved; the convergence problem in the regularization calculation, and the problem for an efficient calculation method of the full part.

As for subtraction problem, we discuss two proposed expansion methods; the power expansion method and the mode decomposition method. The power expansion method is effective for the Green function regularization under the Fourier-Harmonic decomposition, whereas the mode decomposition method applies both to the field regularization and to the Green function regularization. We also note that the mode decomposition method is simpler in calculating the full part (besides tha gauge problem), and has more prospect in solving the convergence problem. Therefore, we conclude that the mode decomposition approach seems to be advantageous in the present study of these approaches.

As for the gauge problem, we discuss two possible approaches in adapting the conventional formalism of the metric perturbation for the regularization calculation; the local-harmonic gauge method and the gauge invariant method. The advantage of the local harmonic gauge method is that it is applicable to a Kerr case, however, the calculation is expected to be very complicated. The gauge invariant method adopt a well-defined gauge condition in whole the background spacetime, however, the calculation method is established only when the background is a Schwarzschild blackhole. We conclude that we still need more study in both approaches.

References

[1] See the LISA webpage: http://lisa.jpl.nasa.gov/ .

[2] Y. Mino, M. Sasaki and T. Tanaka, Phys. Rev. **D55**, 3457 (1997), and in Prog. Theor. Phys. Supp. **128** (1997), and T. C. Quinn and R. M. Wald,Phys. Rev. **D60**, 064009 (1999).

[3] L. Barack, Y. Mino, H. Nakano, A. Ori and M. Sasaki, gr-qc/0111011, accepted for Phys. Rev. Lett., and Y. Mino, H. Nakano and M. Sasaki, gr-qc/0111074.

[4] Y. Mino and H. Nakano, Prog. Theor. Phys. **100**(1998)507, H. Nakano, Y. Mino, M. Sasaki, Prog. Theor. Phys. **106**(2001)339.

[5] Y. Mino, in preparation.

[6] S. Mano, H. Suzuki and E. Takasugi, Prog. Theor. Phys. **95**(1996)1079, and Prog. Theor. Phys. **96**(1996)549, and S. Mano and E. Takasugi, Prog. Theor. Phys. **97**(1997)213.

[7] Y. Mino, (unpublished).

[8] private communication with A. Ori, and L. Barack.

[9] L. Barack, Phys. Rev. **D62**(2000)084027, and L. Barack, and A. Ori, Phys. Rev. **D61**(2000)061502.

[10] L. Barack, Phys. Rev. **D64**(2001)084021.

[11] F. J. Zerilli, Phys. Rev. **D2**(1970)2141.

[12] P. L. Chrzanowski, Phys. Rev. D 11(1975)2042.

[13] Y. Mino, talk in 3rd Capra Ranch Meeting (June 2-9, 2000, US),
http://www.tapir.caltech.edu/~capra3/Proceedings/mino/index.html
and, Y.Mino, talk in the 4th Capra Ranch Meeting (28 - 31 May 2001, Golm, Germany),
http://www.aei-potsdam.mpg.de/ lousto/CAPRA/PROCEEDINGS/Mino/Mino.html .

[14] L. Barack and A. Ori, Phys. Rev. **D64**(2001)124003, and L. Barack, talk in the 4th Capra Ranch Meeting (28 - 31 May 2001, Golm, Germany),
http://www.aei-potsdam.mpg.de/ lousto/CAPRA/PROCEEDINGS/Barack/Barack.html .

Covariant Self-force Regularization of a Particle Orbiting a Schwarzschild Black Hole

— Mode Decomposition Regularization —

Hiroyuki Nakano,[1] Misao Sasaki[2]

Department of Earth and Space Science, Graduate School of Science, Osaka University, Toyonaka, Osaka 560-0043, Japan

Yasushi Mino[3]

Department of Physics, Washington University, Campus Box 1105, One Brookings Dr., St. Louis, MO 63130-4899, USA

Abstract

Covariant structure of the self-force of a particle in a general curved background has been made clear in the cases of scalar, electromagnetic, and gravitational charges. In this paper, we propose a practical method to calculate the self-force of a particle orbiting a Schwarzschild black hole.

1 Introduction

For a particle carrying a scalar, electromagnetic or gravitational charge, the field configuration of the corresponding type varies in time as it moves around a black hole. To the lowest order in the charge, the particle motion follows a geodesic in the black hole background in the absence of external force fields. However, a part of the time-varying field becomes radiation near the future null infinity or future horizon and carries the energy-momentum away from the system, and a part of it is scattered by the background curvature and comes back to the location of the particle. Hence the motion of the particle is affected in the next order. The force exerted by the back-scattered self-field is called the local reaction force or simply the self-force. To establish a calculational strategy of this force is our ultimate goal.

When we attempt to calculate the reaction force on a point charge (particle), we encounter the divergence of the force. Hence, it is necessary to extract out the physically meaningful finite part of the force. Since the force is a vector by definition with respect to a background space-time, and any vector depends on the choice of coordinates in a covariant manner, the finite reaction force should be given covariantly. The covariant structure of the reaction force was investigated in the scalar case in [1], in the electromagnetic case in [2], and in the gravitational case in [3, 4]. In these investigations, the divergent part of the force was found to be described solely with the local geometrical quantities, whereas the finite part that contributes to the equation of motion was found to be given by the tail part which is due to the curvature scattering of the self-field.

Since the tail part depends non-locally on the geometry of the background spacetime, it is almost impossible to calculate it directly. However, for a certain class of spacetimes such as Schwarzschild/Kerr geometries, there is a way to calculate the full field generated by a point charge. Considering a field point slightly off the particle trajectory, it is then possible to obtain the tail part by subtracting the locally given divergent part from the full field. Thus denoting the field by ${}_s\phi$ for the scalar ($s = 0$), electromagnetic ($s = 1$) or gravitational ($s = 2$) case, with its spacetime indices suppressed, the reaction force is schematically given by

$$F_\alpha(\tau_0) = \lim_{x \to z(\tau_0)} F_\alpha[{}_s\phi^{\rm tail}](x), \quad F_\alpha[{}_s\phi^{\rm tail}](x) = F_\alpha[{}_s\phi^{\rm full}](x) - F_\alpha[{}_s\phi^{\rm dir}](x), \quad (x \neq z(\tau)), \tag{1}$$

[1] E-mail:denden@vega.ess.sci.osaka-u.ac.jp
[2] E-mail:misao@vega.ess.sci.osaka-u.ac.jp
[3] E-mail:mino@wugrav.wustl.edu

where z is the orbit of the particle with the proper time τ, and τ_0 is the proper time at the orbital point at which we calculate the force. The symbol ${}_s\phi^{\rm tail}$ stands for the tail field induced by the particle which is regular in the coincidence limit $x \to z(\tau)$, ${}_s\phi^{\rm full}$ for the full field, and ${}_s\phi^{\rm dir}$ for the direct part as defined in Refs.[1, 2, 3, 4]. Both ${}_s\phi^{\rm full}$ and ${}_s\phi^{\rm dir}$ diverge in the coincidence limit $x \to z(\tau)$. $F_\alpha[...]$ is a tensor operator on the field, and is defined as

$$F_\alpha[{}_s\phi] = \begin{cases} qP_\alpha{}^\beta \nabla_\beta \phi & (s=0), \\ eP_\alpha{}^\beta(\phi_{\gamma;\beta} - \phi_{\beta;\gamma})V^\gamma & (s=1), \\ -mP_\alpha{}^\beta \left(\phi_{\beta\gamma;\delta} - \frac{1}{2}g_{\beta\gamma}\phi^\epsilon{}_{;\delta} - \frac{1}{2}\phi_{\gamma\delta;\beta} + \frac{1}{4}g_{\gamma\delta}\phi^\epsilon{}_{;\beta}\right) V^\gamma V^\delta & (s=2), \end{cases} \tag{2}$$

where $P_\alpha{}^\beta = \delta_\alpha{}^\beta + V_\alpha V^\beta$ is the projection tensor with V^α being an appropriate extension of the four velocity $v^\alpha(\tau_0)$ off the orbital point.

In practice, it is a non-trivial task to perform the subtraction of the direct part, which we call the '*Subtraction Problem*'. It should be noted, however, that solving the subtraction problem is not enough when one deals with the gravitational case. In the scalar or electromagnetic case, the reaction force is a gauge-invariant notion. In contrast, the reaction force in the gravitational case depends on the gauge choice. Therefore, one evaluates the full metric perturbation and its direct part in the same gauge before calculating the force. We call this the '*Gauge Problem*', which seems to be a very difficult problem to solve. We do not discuss the possible solution of the gauge problem in this paper, but leave it for future work. In this paper, as a first step, we consider the case that the background is approximated by the Schwarzschild blackhole and use the Boyer-Lindquist coordinates,

$$ds^2 = -\left(1 - \frac{2M}{r}\right)dt^2 + \left(1 - \frac{2M}{r}\right)^{-1} dr^2 + r^2\left(d\theta^2 + \sin^2\theta d\phi^2\right). \tag{3}$$

We use the notation that $x = \{t, r, \theta, \phi\}$ stands for a field point, and $z(\tau_0) = z_0 = \{t_0, r_0, \theta, \phi\}$ for an orbital point. Here we focus on the scalar case. The mode decomposition regularization of the electromagnetic and gravitational cases are differed in our paper [6].

2 Mode decomposition regularization

We call the regularization calculation using the spherical harmonic expansion by the mode decomposition regularization. In this section, we briefly describe the regularization procedure in this approach.

The harmonic decomposition is defined by the analytic structure of the field on the two-sphere. However both the direct field and the full field have a divergence on the sphere including the particle location, the mode decomposition is ill-defined on that sphere. Therefore, we perform the harmonic decomposition of the direct and full fields on a sphere which does not include, but sufficiently close to the orbit. The steps in the mode decomposition regularization are as follows.

1) We evaluate both the full field and the direct field at

$$x = \{t, r, \theta, \phi\}, \tag{4}$$

where we do not take the coincidence limit of either t or r

2) We decompose the full force and direct force into infinite harmonic series as

$$F_\alpha[{}_s\phi^{\rm full}](x) = \sum_{\ell m} F_\alpha^{\ell m}[{}_s\phi^{\rm full}](x), \quad F_\alpha[{}_s\phi^{\rm dir}](x) = \sum_{\ell m} F_\alpha^{\ell m}[{}_s\phi^{\rm dir}](x), \tag{5}$$

where $F_\alpha[{}_s\phi^{\rm full/dir}](x)$ are expanded in terms of the spherical harmonics $Y_{\ell m}(\theta, \phi)$ with the coefficients dependent on t and r. For the direct part, the harmonic expansion is done by extending the locally defined direct force over to the whole two-sphere in a way that correctly reproduces the divergent behavior around the orbital point z_0 up to the finite term.

3) We subtract the direct part from the full part in each ℓ, m mode to obtain

$$F_\alpha^{\ell m}[{}_s\phi^{\rm tail}] = (F_\alpha^{\ell m}[{}_s\phi^{\rm full}] - F_\alpha^{\ell m}[{}_s\phi^{\rm dir}]). \tag{6}$$

The we take the coincidence limit $x \to z_0$. Here we note that one can exchange the order of the procedure, i.e., first take the coincidence limit and then subtract, provided the mode coefficients are finite in the coincidence limit.

4) Finally, by taking the sum over the modes, we obtain the self-force as

$$F_\alpha(\tau_0) = \sum_{\ell m} F_\alpha^{\ell m}[{}_s\phi^{\rm tail}](z_0). \tag{7}$$

It should be noted that because of the divergence of the full force and direct force along a timelike orbit, the mode coefficients of the full force and the direct force are not uniquely defined when we take the coincidence limit in 3). However, the tail force is regular along the orbit[1, 2, 3, 4], and it is uniquely defined. Therefore we expect the non-uniqueness of the direct force does not cause a problem as long as the coincidence limit is taken consistentlly for both the full force and the direct force.

3 Decomposition of the direct part

3.1 Local coordinate expansion

Though we have the covariant form of the local bi-tensor expansion of the direct part, it is not useful for the derivation of the infinite series expansion of it until we evaluate it in a specific coordinate system. Here we discuss the method to evaluate the bi-tensors in a general regular coordinate system.

We derive the direct part of the force with the local bi-tensor expansion using the equal-time condition,

$$0 = \left[\frac{d}{d\tau}\sigma(x, z(\tau))\right]_{\tau=\tau_{\rm eq}(x)}. \tag{8}$$

We define the extension of the four-velocity off the orbit by $V^\alpha(x) := \bar{g}_{\alpha\bar{\alpha}}(x, z_{\rm eq})v^{\bar{\alpha}}_{\rm eq}$, where $\bar{g}_{\alpha\bar{\alpha}}$ is the parallel displacement bi-vector, $z_{\rm eq} = z(\tau_{\rm eq}(x))$, and $v^{\bar{\alpha}}_{\rm eq} = dz^{\bar{\alpha}}/d\tau|_{\tau=\tau_{\rm eq}(x)}$. Using the formulas in Ref. [2, 3], we have

$$F_\alpha[\phi^{\rm dir}](x) = q\bar{g}_\alpha{}^{\bar{\alpha}}(x, z_{\rm eq})\frac{1}{\epsilon^3\kappa}\left\{\sigma_{;\bar{\alpha}}(x, z_{\rm eq}) + \frac{1}{3}\epsilon^2 R_{\bar{\alpha}\bar{\beta}\bar{\gamma}\bar{\delta}}(z_{\rm eq})v^{\bar{\beta}}_{\rm eq}\sigma^{;\bar{\gamma}}(x, z_{\rm eq})v^{\bar{\delta}}_{\rm eq}\right\} + O(y), \tag{9}$$

$$\epsilon = \sqrt{2\sigma(x, z_{\rm eq})}, \quad \kappa = \sqrt{-\sigma_{\bar{\alpha}\bar{\beta}}(x, z_{\rm eq})v^{\bar{\alpha}}_{\rm eq}v^{\bar{\beta}}_{\rm eq}}. \tag{10}$$

3.2 Harmonic decomposition of the direct part

Without loss of generality, we may assume that the particle is located at $\theta_0 = \pi/2$, $\phi_0 = 0$ at time t_0. Since the Fourier modes are independent of the spherical harmonics, we may take the field point to lie on the hypersurface $t = t_0$. That is, we consider the local coordinate expansion of the direct force at a point $\{t_0, r, \theta, \phi\}$ near the particle localtion $\{t_0, r_0, \pi/2, 0\}$. The local expansion of the direct force on the Boyer-Lindquist coordinates can be done in such a way that it consists of terms of the form,

$$\frac{R^{n_1}\Theta^{n_2}\phi^{n_3}}{\xi^{2n_4+1}}, \tag{11}$$

where n_1, n_2, n_3, n_4 are non-negative integers, and

$$\xi := \sqrt{2}r_0\left(a - \cos\tilde{\theta} + \frac{b}{2}(\phi - \phi')^2\right)^{1/2}, \quad R := r - r_0, \quad \Theta := \theta - \frac{\pi}{2}, \tag{12}$$

$$a := 1 + \frac{1}{2r_0^2}\frac{r_0^2}{r_0^2 + \mathcal{L}^2}\frac{r_0^2}{(r_0 - 2M)^2}\mathcal{E}^2R^2, \quad b := \frac{\mathcal{L}^2}{r_0^2}, \quad \phi' := -\frac{\mathcal{L}}{r_0^2 + \mathcal{L}^2}u_r R, \tag{13}$$

where $\mathcal{E} := -g_{tt}dt/d\tau$, $\mathcal{L} := g_{\phi\phi}d\phi/d\tau$, and $u_r := g_{rr}dr/d\tau$, and $\tilde{\theta}$ is the relative angle between (θ,ϕ) and $(\pi/2,\phi')$. Since the orbit always remains on the equatorial plane, the force is symmetric under the transformation $\theta \to \pi - \theta$, which implies there is no term proportional to odd powers of Θ. Hence we only need to consider the case of n_2 being an even number in the general form given by Eq. (11). Then the factor Θ^{n_2} may be eliminated by expressing Θ^2 in terms of ξ, R and ϕ, and we are left with terms of the form,

$$\frac{R^{n_1}\phi^{n_3}}{\xi^{2n_4+1}}\,. \tag{14}$$

Explicitly, we find

$$\begin{aligned} F_r^{\rm dir} &= q\Bigg(\frac{\mathcal{L}^2}{r_0(r_0-2M)}\frac{R}{\xi^3} - \frac{r_0^2\mathcal{E}^2}{(r_0-2M)^2}\frac{R}{\xi^3} - \mathcal{L}u_r\frac{\phi}{\xi^3} - \frac{1}{2}\frac{2r_0^2+\mathcal{L}^2}{r_0^3}\frac{1}{\xi} + \frac{1}{2}\frac{\mathcal{E}^2}{r_0-2M}\frac{1}{\xi} \\ &\quad + \frac{1}{2}\frac{(3r_0^2+4\mathcal{L}^2)\mathcal{L}^2}{r_0^3}\frac{\phi^2}{\xi^3} - \frac{2\mathcal{E}^2\mathcal{L}^2}{r_0-2M}\frac{\phi^2}{\xi^3} - \frac{3}{2}\frac{(r_0^2+\mathcal{L}^2)\mathcal{L}^4}{r_0^3}\frac{\phi^4}{\xi^5} + \frac{3}{2}\frac{\mathcal{E}^2\mathcal{L}^4}{r_0-2M}\frac{\phi^4}{\xi^5}\Bigg), \end{aligned} \tag{15}$$

where $F_\alpha^{\rm dir} = F_\alpha[\phi^{\rm dir}]$. The other components of the direct force are derived in the same way. After the decomposition, we can take the radial coincidence limit $r \to r_0$.

4 Regularization Counter Terms

In this section, we present the mode decomposition of the direct force, and compare the resulting regularization counter terms with those obtained by Barack and Ori[11] in their mode-sum regularization scheme (MSRS)[7]. Barack and Ori define the regularization counter terms as

$$\lim_{x\to z_0} F_{\alpha l}^{\rm dir} = A_\alpha L + B_\alpha + C_\alpha/L + O(L^{-2})\,. \quad D_\alpha = \sum_{l=0}^{\infty}\left[\lim_{x\to z_0} F_{\alpha l}^{\rm dir} - A_\alpha L - B_\alpha - C_\alpha/L\right]. \tag{16}$$

where $F_{\alpha l}^{\rm dir}$ is the multipole l-mode of $F_\alpha^{\rm dir}$, $L = \ell + 1/2$, and A_α, B_α and C_α are independent of L. The A_α term is to subract the quadratic divergence, the B_α term the linear divergence, and the C_α term the logarithmic divergence. The D_α term is the remaining finite contribution of the direct force to By the detail analysis, we find $C_\alpha = D_\alpha = 0$ in agreement with Barack and Ori[7].

4.1 The A-term

The A-term describes the quadratic divergent terms of the direct force. Thus we consider the most divergent terms of the direct force, R/ξ^3 and ϕ/ξ^3. The term ϕ/ξ^3 may be replaced as R/ξ^3. The essential fact is that this is odd in R. This leads to the harmonic coefficients proportional to sign(R). We obtain

$$A_t = {\rm sign}(R)\frac{q^2}{r^2}\frac{r_0-2M}{r_0}\frac{u_r}{1-\mathcal{L}^2/r_0^2}\,, \quad A_r = -{\rm sign}(R)\frac{q^2}{r^2}\frac{r_0}{r_0-2M}\frac{\mathcal{E}}{1-\mathcal{L}^2/r_0^2}\,, \quad A_\phi = 0\,. \tag{17}$$

These A-terms vanish when averaged over both limits $R \to \pm 0$.

4.2 The B-term

The linearly divergent terms are described by the B-term, which are of the form, ϕ^{2n}/ξ^{2n+1}. We find in terms of the hypergeometric functions as

$$B_t = -\frac{(r_0-2M)\mathcal{E}u_r}{2r_0^3}F\left(\frac{3}{2},\frac{3}{2};1;-\frac{\mathcal{L}^2}{r_0^2}\right), \tag{18}$$

$$B_r = \frac{(r_0-2M)u_r^2}{2r_0^3}F\left(\frac{3}{2},\frac{3}{2};1;-\frac{\mathcal{L}^2}{r_0^2}\right) - \frac{1}{2r_0^2}\left(F\left(\frac{1}{2},\frac{1}{2};1;-\frac{\mathcal{L}^2}{r_0^2}\right) + \frac{\mathcal{L}^2}{2r_0^2}F\left(\frac{3}{2},\frac{3}{2};2;-\frac{\mathcal{L}^2}{r_0^2}\right)\right), \tag{19}$$

$$B_\phi = \frac{(r_0-2M)\mathcal{L}u_r}{16r_0^3}\left(8F\left(\frac{3}{2},\frac{3}{2};1;-\frac{\mathcal{L}^2}{r_0^2}\right) - 4F\left(\frac{3}{2},\frac{3}{2};2;-\frac{\mathcal{L}^2}{r_0^2}\right) + \frac{9\mathcal{L}^2}{r_0^2}F\left(\frac{5}{2},\frac{5}{2};3;-\frac{\mathcal{L}^2}{r_0^2}\right)\right). \tag{20}$$

The above results for the A and B-terms perfectly agree with the results obtained by Barack and Ori in a quite different fashion[10, 11].

5 Conclusion and Discussion

In this paper, we have only discussed a possible approach to the subtraction problem. We have introduced a regularization method which utilizes the spherical-harmonic decomposition, and have derived the direct part of the self-force, which turns out to be independent of the spin s of the field under consideration. The harmonic decomposition of this direct part has been carried out, and the regularization counter terms for the self-force have been derived for a general geodesic orbit. We have found our result agrees completely with the result obtained by Barack and Ori[11] in their mode-sum regularization scheme (MSRS) [7].

It is worthwhile to point out that the gauge problem in the gravitational case seems far more serious than the subtraction problem. What we know at the moment is that the gravitational self-force is described by the tail part of the metric perturbation induced by a particle[3, 4]. However this is justified only in the harmonic gauge, while the full metric perturbation can be obtained only in the Regge-Wheeler gauge or in the radiation gauge where the identification of the tail part is highly non-trivial. A prescription to identify the tail part of the metric perturbation has been proposed in [8], but it needs to be verified. The gauge problem for the non-radiative monopole and dipole components of the metric perturbation which are not obtainable in the Teukolsky formalism seems to stand as additional serious obstacle. Possible resolutions for the gauge problem are under investigation [13].

Acknowledgements

We thank all the members of the theoretical astrophysics group at Osaka university for useful conversations. Special thanks are due to T. Tanaka, H. Tagoshi and N. Sago for invaluable discussions. The author(HN) is supported by Research Fellowships of the Japan Society for the Promotion of Science for Young Scientists, No. 2397.

References

[1] T. C. Quinn, Phys. Rev. **D62**, 064029 (2000).

[2] B. S. DeWitt and R. W. Brehme, Ann. Phys. (N.Y.) **9**, 220 (1960).

[3] Y. Mino, M. Sasaki and T. Tanaka, Phys. Rev. **D55**, 3457 (1997), and in Prog. Theor. Phys. Supp. **128** (1997).

[4] T. C. Quinn and R. M. Wald, Phys. Rev. **D60**, 064009 (1999).

[5] S. Mano, H. Suzuki and E. Takasugi, Prog. Theor. Phys. **95**, 1079 (1996).

[6] Y. Mino, H. Nakano and Sasaki, gr-qc/0111074 (2001).

[7] L. Barack and A. Ori, Phys. Rev. **D61**, 061502 (2000), and L. Barack, Phys. Rev. **D62**, 084027 (2000).

[8] H. Nakano and M. Sasaki, Prog. Theor. Phys. **105**, 197 (2001) [gr-qc/0010036].

[9] H. Nakano, Y. Mino and M. Sasaki, Prog. Theor. Phys. **106**, 339 (2001) [gr-qc/0104012]

[10] L. Barack, Y. Mino, H. Nakano, A. Ori and M. Sasaki, gr-qc/0111001 (2001).

[11] L. Barack and A. Ori, in preparation.

[12] L. Barack and A. Ori, Phys. Rev. **D64**, 124003 (2001).

[13] N. Sago, H. Nakano and M. Sasaki, in preparation.

Gravitational Self-Force of a Particle Orbiting a Schwarzschild Black Hole
— Gauge Transformation —

Norichika Sago, [1] Hiroyuki Nakano, [2] Misao Sasaki [3]

Department of Earth and Space Science, Graduate School of Science
Osaka University, Toyonaka OSAKA 560-0043, Japan

Abstract

To obtain the self-force on a particle moving in the curved spacetime, we consider the regularization for the metric perturbation induced by the particle. It's known that, under harmonic gauge conditions, we can divide the metric perturbation into a regular tail part and the singular direct part. This singular part does not contribute to the motion of the particle. Thus we can obtain the regularized perturbation by subtracting the singular part from the full field. The singular part can be given locally in the harmonic gauge. Here, in order to obtain the full field in the harmonic gauge, we consider the gauge transformation from the Regge-Wheeler gauge, in which we already have the solution of the field equation, to the harmonic gauge.

1 Introduction

When we consider a point particle (mass μ) moving around a black hole with mass M, its trajectory deviates from the geodesic of the background metric because of the self-force of the particle. In order to know the particle's trajectory precisely, we need to obtain the self-force and solve the equation of motion. The self-force can be given in terms of the perturbations of the gravitational field, $h_{\mu\nu}$, where we consider up to $O(\mu/M)$. The self-force has a divergence at the location of the particle because the gravitational field diverges. Therefore we have to introduce an appropriate regularization. Under the harmonic gauge condition, the full field can be divided into two parts[1]: One is the called the tail part, which has regular behavior. The other one is called the direct part, which is singular at the location of the particle and has no effect on the motion. The tail part is obtained by subtracting the direct part from the full field. To carry out this procedure, we face two problems. One is the '*Subtraction Problem*', which is discussed in Ref.[2]. The other one is the '*Gauge Problem*'. We consider the latter here.

In performing the subtraction to obtain the regularized field, the full field and the direct part must be evaluated in the harmonic gauge because the self-force has the gauge dependence and the concept of the tail part and direct part is defined only in the harmonic gauge. The direct part can be evaluated locally in the harmonic gauge. For the full field, however, we can calculate it only in the Regge-Wheeler (RW) gauge or the radiation gauge[3, 4, 5], not in the harmonic gauge. So we consider the gauge transformation between the harmonic gauge and RW or radiation gauge.

For an infinitesimal gauge transformation,

$$x^\mu \to x'^\mu = x^\mu - \xi^\mu,$$

the change of the self-force can be given:

$$\delta F^\mu = -\mu[(g^{\mu\alpha} + u^\mu u^\alpha)\ddot{\xi}_\lambda + R^\mu_{\alpha\lambda\nu} u^\alpha \xi^\lambda u^\nu], \tag{1}$$

where the overdot denotes the covariant differentiation with respect to the proper time of the particle, u^α is the four-velocity of the particle. If ξ^α has a sufficiently regular behavior, the direct part of the full force has no change by the transformation and we can regard (1) as the change of the self-force[6].

[1] E-mail:sago@vega.ess.sci.osaka-u.ac.jp
[2] E-mail:denden@vega.ess.sci.osaka-u.ac.jp
[3] E-mail:misao@vega.ess.sci.osaka-u.ac.jp

However when we consider the transformation between the harmonic gauge and the RW gauge, ξ^α is singular around the location of the particle. In this case, we can divide ξ^α into two parts. One part is the singular part $\xi^\alpha_{\rm sing}$, which causes the singular change of the bare-force. The other one is the regular part $\xi^\alpha_{\rm reg}$, which is the rest of ξ^α and does give only a change to the self-force. As we will see, we find that $\xi^\alpha_{\rm sing}$ consists of the direct part of the metric perturbation. If we can obtain it, we can evaluate $\xi^\alpha_{\rm reg}$, except for the degree of freedom of the homogeneous solutions. Here, as a first step, we consider the problem at the first post Newtonian order and report the result.

2 Gauge Transformation from the Regge-Wheeler Gauge to the Harmonic Gauge

Here, we consider the metric perturbation in the Schwarzschild background:

$$h_{\mu\nu} = g_{\mu\nu} - g^{(\rm b)}_{\mu\nu}, \tag{2}$$

where $g^{(\rm b)}_{\mu\nu}$ is the Schwarzschild metric by the Boyer-Lindquist coordinates,

$$g^{(\rm b)}_{\mu\nu}dx^\mu dx^\nu = -f(r)dt^2 + f(r)^{-1}dr^2 + r^2(d\theta^2 + \sin^2\theta d\phi^2), \qquad f(r) = 1 - \frac{2M}{r}. \tag{3}$$

Next, we consider the transformation from RW gauge to harmonic gauge:

$$x^\mu_{\rm RW} \rightarrow x^\mu_{\rm H} = x^\mu_{\rm RW} + \xi^\mu, \tag{4}$$

$$h^{\rm RW}_{\mu\nu} \rightarrow h^{\rm H}_{\mu\nu} = h^{\rm RW}_{\mu\nu} - \xi_{\mu;\nu} - \xi_{\nu;\mu}, \tag{5}$$

where ξ^μ is the infinitesimal displacement vector of the gauge transformation. The indices, H and RW denote the harmonic and RW gauge respectively.

By substituting (5) into the harmonic gauge condition $\bar{h}^{\rm H}_{\mu\nu}{}^{;\mu} = 0$, we obtain the equation for ξ^μ:

$$\xi^\mu{}_{;\nu}{}^{;\nu} = \bar{h}^{\mu\nu}_{{\rm RW};\nu}, \qquad \bar{h}_{\mu\nu} = h_{\mu\nu} - \frac{1}{2}g^{(\rm b)}_{\mu\nu}h. \tag{6}$$

According to the 'mode decomposition regularization method'[2], we rewrite ξ^μ, $h_{\mu\nu}$ in the Fourier-harmonic expansion form. For simplicity, in the following, we consider only the odd part, which has the odd parity $(-1)^{\ell+1}$:

$$\xi_\mu = \int d\omega \sum_{\ell m} \frac{i}{2}\Lambda_{\ell m\omega}(r)\left(0, 0, \frac{-1}{\sin\theta}\partial_\phi Y_{\ell m}(\theta,\phi), \sin\theta\partial_\theta Y_{\ell m}(\theta,\phi)\right)e^{-i\omega t}, \tag{7}$$

$$h_{\mu\nu} = \int d\omega \sum_{\ell m} \frac{\sqrt{2\ell(\ell+1)}}{r}e^{-i\omega t} \times \left[-h_{0\ell m\omega}(r)c^{(0)}_{\ell m\mu\nu} + ih_{1\ell m\omega}(r)c_{\ell m\mu\nu} + \frac{\sqrt{(\ell-1)(\ell+2)}}{r}h_{2\ell m\omega}(r)d_{\ell m\mu\nu}\right], \tag{8}$$

where $c^{(0)}_{\ell m\mu\nu}$,$c_{\ell m\mu\nu}$, $d_{\ell m\mu\nu}$ are harmonic tensor with odd parity[4]. By substituting Eqs. (7), (8) into Eq. (6), we obtain the equation for $\Lambda_{\ell m\omega}(r)$ in the following form:

$$\mathcal{L}\Lambda_{\ell m\omega}(r) = -4iR_{\ell m\omega}(r) - \frac{32\pi r^2}{\sqrt{2\ell(\ell+1)(\ell-1)(\ell+2)}}D_{\ell m\omega}(r), \tag{9}$$

where $R_{\ell m\omega}(r)$ is the Regge-Wheeler gauge invariant variable, $D_{\ell m\omega}(r)$ is the Fourier-harmonic coefficient of the stress-energy tensor and

$$\mathcal{L} \equiv f(r)\frac{d^2}{dr^2} + f'(r)\frac{d}{dr} + \left(\frac{\omega^2}{f(r)} - \frac{\ell(\ell+1)}{r^2}\right).$$

If we can solve this equation, we can perform the gauge transformation from the RW gauge and obtain the metric perturbation in the harmonic gauge. As we mentioned previously, however, ξ^α has the singular behavior at the location of the particle. It is difficult to solve Eq.(9) directly because of the singularity of $\Lambda_{\ell m\omega}(r)$. To avoid this difficulty, we consider the following procedure:
From (5), we obtain the relation between the harmonic coefficients of the metric perturbation and displacement vector:

$$h^{\rm H}_{2\ell m\omega}(r) - h^{\rm RW}_{2\ell m\omega}(r) = \Lambda_{\ell m\omega}(r).$$

Since $h^{\rm RW}_{2\ell m\omega} = 0$ in the RW gauge, we find that $\Lambda_{\ell m\omega}(r) = h^{\rm H}_{2\ell m\omega}(r)$. Noting that $h^{\rm H}_{2\ell m\omega}$ can be divided into the regular part and the singular part, that is, the tail part and the direct part:

$$h^{\rm H}_{2\ell m\omega}(r) = h^{\rm H,tail}_{2\ell m\omega}(r) + h^{\rm H,dir}_{2\ell m\omega}(r), \tag{10}$$

then we can regard $\Lambda^{\rm sing}_{\ell m\omega}(r) = h^{\rm H,dir}_{2\ell m\omega}(r)$. Thus we can evaluate $\Lambda^{\rm sing}_{\ell m\omega}(r)$ from the direct part of the metric perturbation. Furthermore, substituting this into (9), we obtain:

$$\mathcal{L}\Lambda^{\rm reg}_{\ell m\omega}(r) = -\mathcal{L}h^{\rm H,dir}_{2\ell m\omega}(r) - 4iR_{\ell m\omega}(r) - \frac{32\pi r^2 D_{\ell m\omega}(r)}{\sqrt{2\ell(\ell+1)(\ell-1)(\ell+2)}}. \tag{11}$$

As we will see in the next section, we can evaluate each term on the right hand side of (11). If the right hand side of (11), regarded as the source term, is finite as a whole, it means $\Lambda^{\rm reg}_{\ell m\omega}(r)$ is regular, we can analyze $\Lambda^{\rm reg}_{\ell m\omega}(r)$ by expanding it around the location of the particle in the local coordinates.

3 Evaluation of the singular part

Here, we evaluate each term on the right hand side of (11) in the case of the point particle and investigate their behavior.

• $D_{\ell m\omega}(r)$ term

For a point particle, $D_{\ell m}(t,r)$ is given in the following form:

$$D_{\ell m}(t,r) = \frac{-i\mu\delta(r-r_0)}{\dot{t}_0\sqrt{\frac{1}{2}\ell(\ell+1)(\ell-1)(\ell+2)}}\left[\frac{1}{2}\left(\dot{\theta}_0^2 - \sin^2\theta_0\dot{\phi}_0^2\right)\frac{X^*_{\ell m}(\theta_0,\phi_0)}{\sin\theta_0} - \sin\theta_0\dot{\phi}_0\dot{\theta}_0 W^*_{\ell m}(\theta_0,\phi_0)\right], \tag{12}$$

where $z(\tau) = (t_0(\tau), r_0(\tau), \theta_0(\tau), \phi_0(\tau))$ represents the orbital point and

$$X_{\ell m}(\theta,\phi) = 2\frac{\partial}{\partial\phi}\left(\frac{\partial}{\partial\theta} - \cot\theta\right)Y_{\ell m}(\theta,\phi), \tag{13}$$

$$W_{\ell m}(\theta,\phi) = \left(\frac{\partial^2}{\partial\theta^2} - \cot\theta\frac{\partial}{\partial\theta} - \frac{1}{\sin^2\theta}\frac{\partial^2}{\partial\phi^2}\right)Y_{\ell m}(\theta,\phi). \tag{14}$$

Performing the inverse Fourier transformation, we can obtain $D_{\ell m\omega}(r)$:

$$D_{\ell m\omega}(r) = \frac{1}{2\pi}\int dt D_{\ell m}(t,r)e^{i\omega t}. \tag{15}$$

• $R_{\ell m\omega}(r)$ term

We can obtain $R_{\ell m\omega}(r)$ by solving the RW equation:

$$\frac{d^2R_{\ell m\omega}(r)}{dr_*^2} + [\omega^2 - V_\ell(r)]R_{\ell m\omega}(r) = \frac{8\pi i r f(r)}{\sqrt{\frac{1}{2}\ell(\ell+1)(\ell-1)(\ell+2)}}\left[\frac{d}{dr}[f(r)D_{\ell m\omega}(r)] - \frac{f(r)}{r}\sqrt{(\ell-1)(\ell+2)}Q_{\ell m\omega}(r)\right], \tag{16}$$

$$V_\ell(r) = \left(1-\frac{2M}{r}\right)\left(\frac{\ell(\ell+1)}{r^2} - \frac{6M}{r^3}\right), \tag{17}$$

where $dr = f(r)dr_*$ and $Q_{\ell m\omega}$ is one of the harmonic coefficient of the stress-energy tensor. We can construct the Green function for (16) from the homogeneous solutions, which can be obtained by the method of Mano et al. [7]. Using this, we obtain $R_{\ell m\omega}(r)$.

• $h^{\rm H,dir}_{2\ell m\omega}(r)$ term

From (8), we can obtain $h^{\rm H,dir}_{2\ell m\omega}(r)$ in terms of the direct part of the metric perturbation:

$$h^{\rm H,dir}_{2\ell m\omega} = \frac{\sqrt{2}r^2}{\sqrt{\ell(\ell+1)(\ell-1)(\ell+2)}} \int dt d\Omega \eta^{\mu\lambda}\eta^{\nu\rho} h^{\rm H,dir}_{\mu\nu} \bar{d}^*_{\ell m\lambda\rho}, \tag{18}$$

where $\eta^{\mu\nu} = {\rm diag}(-1, 1, 1/r^2, 1/r^2\sin^2\theta)$. The components of $h^{\rm H,dir}_{\mu\nu}$ are given locally around the location of the particle in the following form [1]:

$$h^{\rm H,dir}_{\mu\nu} = \frac{4m\bar{g}_{\alpha(\mu}(x,z)\bar{g}_{\nu)\beta}(x,z)}{\sigma(x,z)} \dot{z}^\alpha_0 \dot{z}^\beta_0 \sqrt{\Delta(x,z)} \Big|_{\tau=\tau_{\rm ret}}, \tag{19}$$

where $\sigma(x,z)$ is the bi-scalar of half the squared geodesic distance, $\Delta(x,z)$ is the generalized van Vleck-Morette determinant and $\bar{g}_{\alpha\mu}(x, z_{\rm ret})$ is the parallel displacement bi-vector. To evaluate these, we expand $\sigma(x,z)$, $\Delta(x,z)$ and $\bar{g}_{\alpha\mu}(x, z_{\rm ret})$ around the location of the particle in the local coordinates [2].

For example, we consider the case of a particle moving in a circular orbit ($r_0 = $ const., $\theta_0 = \frac{\pi}{2}$) and investigate the behavior of the right hand side of (11). In this case, each term can be given in the following form:

$$D_{\ell m\omega}(r) = \frac{im\dot{\phi}_0^2}{i_0\sqrt{2\ell(\ell-1)(\ell+1)(\ell+2)}} \delta(r-r_0)\delta(\omega - m\omega_0) X^*_{\ell m}(\theta_0, \phi_0), \tag{20}$$

$$R_{\ell m\omega}(r) = \frac{32\pi i m\dot{\phi}_0^2 X^*_{\ell m}(\theta_0,\phi_0)\delta(\omega-m\omega_0)}{i_0\ell(\ell+1)(\ell-1)(\ell+2)(2\ell+1)} \left[(\ell-1)\frac{r^{\ell+1}}{r_0^\ell}\theta(r_0-r) - (\ell+2)\frac{r_0^{\ell+1}}{r^\ell}\theta(r-r_0)\right], \tag{21}$$

$$\mathcal{L}h^{\rm H,dir}_{2\ell m\omega} = -\frac{16\pi i m\dot{\phi}_0^2 r_0^2}{i_0\ell(\ell+1)(\ell-1)(\ell+2)} \delta(r-r_0)\delta(\omega-m\omega_0) X^*_{\ell m}(\theta_0,\phi_0), \tag{22}$$

where $\omega_0 = \frac{d\phi_0}{dt} = $ const. and we considered up to the first post Newtonian order. Substituting these into (11), we find that the most singular parts in $\mathcal{L}h^{\rm H,dir}_{2\ell m\omega}$ and $D_{\ell m\omega}$ offset each other.

4 Summary

To obtain the full field in the harmonic gauge, we considered the gauge transformation from the Regge-Wheeler gauge to the harmonic gauge. But the displacement vector ξ^μ has singular behavior around the location of the particle. Then we tried to divide ξ^μ into two parts, regular and singular. Noting the relation between the metric perturbation and the displacement vector, we assumed that the singular part of ξ^μ consists of the direct part of the metric perturbations. To see the regularity of the rest of ξ^μ, $\xi^\alpha_{\rm reg}$, we investigate the source term of the equation for it. We find that the most singular part of the source term vanishes. But this is not sufficient to show that the source term is finite and $\xi^\alpha_{\rm reg}$ is regular. We need to take into account the higher order terms. Furthermore it is necessary to solve the equation for the tail part in order that we obtain the metric perturbation in the harmonic gauge, which is our first aim. This issue is left for future study.

5 Acknowledgements

We would like to thank Y.Mino and T.Tanaka for fruitful discussions. We also appreciate a number of support by all the members of the theoretical astrophysics group at Osaka university.

References

[1] Y. Mino, M. Sasaki and T. Tanaka, Phys. Rev. D **55** 3457 (1997).

[2] Y. Mino, H. Nakano and M. Sasaki, qc/0111074.

[3] T. Regge and J. A. Wheeler, Phys. Rev. **108**, 1063 (1957).

[4] F. J. Zerilli, Phys. Rev. D **2**, 2141 (1970).

[5] S. A. Teukolsky, Astrophys. J. **185**, 635 (1973).

[6] L. Barack and A. Ori, Phys. Rev. D **64** 124003 (2001).

[7] S. Mano, H. Suzuki and E. Takasugi, Prog. Theor. Phys. **96**, 549 (1996).

Search for Gravitational Waves from Inspiraling Compact Binaries using interferometer data

Hideyuki Tagoshi

Department of Earth and Space Science,
Osaka University, Toyonaka, Osaka 560-0043, Japan

and TAMA collaboration

Abstract

We analysed the data from the TAMA300 detector and the LISM detector taken in 2001. We searched for gravitational waves from inspiraling compact binaries using matched filtering. The mass range searched is from $1M_\odot$ to $2M_\odot$. The initial results of the analysis are reported.

1 Introduction

The TAMA300 detector is a laser interferometric gravitational wave detector which is located in the campus of NAO, Mitaka, Tokyo. It is a Fabry-Perot-Michelson interferometer with arm length of 300m. The LISM detector is also a Fabry-Perot-Michelson interferometer with arm length of 20m. It is located in the Kamioka mine, Gifu, and it is operated now as a project of ICRR, Univ. of Tokyo.

The TAMA300 detector became ready to operate in the summer of 1999[1]. Since then, several data taking has been performed[2]. It performed a long data taking from August 1th to September 20th, 2001, and more than 1100 hours of data were taken. This data taking is called TAMA DT6. The best sensitivity was about $5 \times 10^{-21}[1/\sqrt{\mathrm{Hz}}]$ around 800Hz. The LISM detector performed a coincident run with TAMA300 during Aug. 1 to 23, and Sep. 3 to 17. The total amount of data was about 780 hours. The best sensitivity was about $6 \times 10^{-20}[1/\sqrt{\mathrm{Hz}}]$ around 800Hz. Both detector showed a good stability, and the data can be used for the physical study like gravitational wave event search. Considering the amount of data, it is a unique chance to experience coincidence analysis using the real interferometer data, since the coincident run by two or more interferometer detectors was not performed for such long duration in the past.

In this paper, we report initial results of the inspiraling compact binaries event search. Based on this work, we also perform a coincident event search, which initial results is reported by H.Takahashi in this volume [3].

2 Inspiraling binaries

Gravitational waves from inspiraling compact binaries, consisting of neutron stars with mass $\sim 1.4M_\odot$ or black holes, have been considered to be the most promising target for laser interferometers. These compact binaries can be produced as a consequence of normal stellar evolution of binaries. It has been also suggested that MACHOs in our Galactic halo may be primordial black holes with mass $\sim 0.5M_\odot$. If so, it is reasonable to expect that some of them are in binaries which coalesce due to the gravitational radiation reaction[4].

Because the amount of data is very large compared to the data taken by TAMA300 during the last two years, we decided to search for the mass range between $1M_\odot$ and $2M_\odot$ first, by the matched filtering method with a one step parameter search algorithm. Much wider mass range will be perform separately by a computationally more efficient matched filtering algorithm called hierarchical search algorithm.

3 Matched filtering

We denote the strain equivalent one-sided power spectrum density of the noise by $S_n(f)$. In order to calculate the expected wave forms, which are called *templates*, we used restricted post-Newtonian wave forms of order 2.5, in which the phase evolution was correctly taken into account up to the 2.5 post-Newtonian order, but the amplitude was evaluated by using the quadrupole formula. As for the 2.5 post-Newtonian phase evolution, we used formulas derived by Blanchet et al.[6] We did not include the effect of spin angular momentum of each star.

When the gravitational wave passes through the interferometer, it produces a relative difference ΔL between the two arm lengths L. The gravitational wave strain amplitude is defined by $\Delta L = Lh(t)$. The wave form $h(t)$ is calculated by combining two independent modes of the gravitational wave and the antenna pattern of the interferometer as

$$h(t) = \mathcal{A}[h_c(t - t_c)\ \cos\alpha + h_s(t - t_c)\ \sin\alpha], \tag{1}$$

where t_c is the coalescence time, and $h_c(t)$ and $h_s(t)$ are the two independent templates with the phase difference $\pi/2$. To construct filters, we need the Fourier transforms of $h_c(t)$ and $h_s(t)$. They were computed directly by using the stationary phase approximation. The parameters to distinguish the wave forms are the amplitude $\mathcal{A}$, the two masses m_1, m_2, the coalescence time t_c and the phase α.

We denote the data from the detector as $s(t)$. We define a filtered unnormalised signal-to-noise ratio ρ after the maximization over α as

$$\rho = \sqrt{(s,h_c)^2 + (s,h_s)^2}, \tag{2}$$

$$(a,b) \equiv 2\int_{-\infty}^{\infty} df \frac{\tilde{a}(f)\tilde{b}^*(f)}{S_n(|f|)}, \tag{3}$$

where $\tilde{a}(f)$ denotes the Fourier transform of $a(t)$ and the asterisk denotes the complex conjugation. This ρ has an expectation value $\sqrt{2}$ in the presence of only Gaussian noise. Thus, the signal-to-noise ratio, SNR, is given by SNR$= \rho/\sqrt{2}$.

The real interferometer data contains non-stationary and non-Gaussian noise. In order to remove the influence of such noise, we introduced a χ^2 test of the time-frequency behaviour of the signal [7]. We divide each template into n mutually independent pieces in the frequency domain, chosen so that the expected contribution to ρ from each frequency band is approximately equal. For two template polarizations $h_c(t)$ and $h_s(t)$, we calculate χ^2 by summing the square of the deviation of each value of ρ from the expected value[8]. This quantity must satisfy the χ^2-statistics with $2n-2$ degrees of freedom, as long as the data consists of Gaussian noise plus chirp signals. However, there was a strong tendency that an event with large χ^2 has a large value of ρ. Thus, by applying a threshold to the χ^2 value, we can reduce the number of fake events without significantly losing the detectability of real events. For convenience, we use a reduced χ^2 which is defined as $\chi^2/(2n-2)$. In the current analysis, we chose $n = 16$.

In order to search for the mass parameter, we prepare a mesh in the mass parameter space. There is a novel way to describe The mass parameter space can be described by a geometrical language[9]. Tanaka and Tagoshi[10] found that the parameter space is described approximately as a flat Euclidian space, and that we can introduce useful mass parameters which simplifies the algorithm to determine the mesh points. The spacing of the mesh points was determined so as not to lose more than 3 % of signal-to-noise due to the mismatch between actual mass parameters and those at mesh points.

The parameter space defined by using our new mass parameters turned out to contain about 200 to 1000 templates for the TAMA300 data, and about 200 to 600 templates for LISM data. Typical number of template is 700 for TAMA300 and 400 for LISM.

4 Matched filtering algorithm

In this section, we briefly describe the one step matched filtering algorithm which are used for TAMA300 and LISM data analysis. We introduced some techniques which are given by Tanaka and Tagoshi[10] for a two step matched filtering algorithm. But we do not explain them here.

The time sequential voltage data from the interferometers are divided into small length of data with length of 52 seconds. Each peace of data have overlap portion with 3.2 seconds. The data are Fourier transformed, and are applied the transfer function to transform the voltage data into strain equivalent data. The method to calibrate the data was explained in [5]. We then calculate Eqs. (2) and (3) for a mass parameter on the mesh point. For each 25 ms of the coalescing time t_c, we search for t_c which realize the maximum value of ρ. If the value is $\rho > 7$, we calculate the value of χ^2 which correspond to the t_c. The same calculation are performed for other mass parameters. All the results are stored so that we can perform analysis of the event search with criterion to identify the events which may be different from the one described below.

In this initial analysis, we search for the mass parameter which realize the maximum of ρ for each 25 ms of t_c. All the information of the events are recorded in the event lists.

5 Results and Discussion

Our analysis was done with 9 Compaq Alpha machines, and also with 12 Intel Pentium4 machines in our laboratory at Osaka University. The matched filtering codes are written in C language, and are MPI parallelled.

Among the TAMA DT6 data, we analysed 1039 hours of data. Other portion of data are unlocked, or some adjustment are made. The portion of data which For the LISM data, we have only analysed the data from the last two weeks. The length analysed is 322 hours.

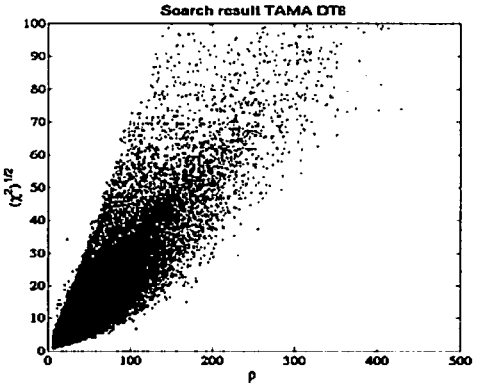

Figure 1:

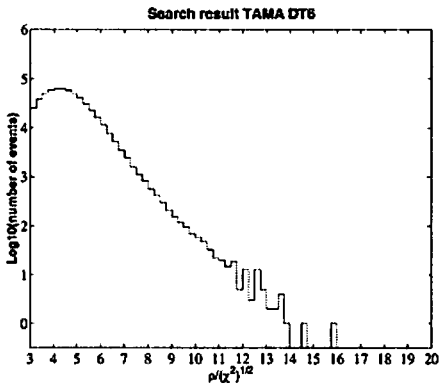

Figure 2:

In Fig. 1, we show scatter plots of $(\rho, \sqrt{\chi^2})$ of events for TAMA results. We see a correlation between ρ and $\sqrt{\chi^2}$. In Fig. 2, we plot the histogram of $\rho/\sqrt{\chi^2}$. We can show from simulations, that by setting a threshold to the value of $\rho/\sqrt{\chi^2}$ of the events, and identify events which $\rho/\sqrt{\chi^2}$ exceed the threshold as the candidate real events, we can obtain reasonable event detection efficiency. Fig. 3 and 4 are results of the LISM data. Fig. 2 and 4 can be used to set the threshold.

In this analysis, we did not see events which exceed the tail of noise distribution significantly. In such cases, we estimate the limit to the upper limit to the event rate. Using 1000 hours of data, we will be able to obtain an upper limit to the event rate about 0.004 events/hours (C.L.=90%). This number should be compared to the value obtained by previous analysis of laser interferometers data, e.g. Caltech 40m detector's results[11]: 0.17/hours ($1M_\odot \sim 3M\odot$), TAMA DT2 results[12]: 0.59/hours ($0.3M_\odot \sim 10M\odot$), TAMA DT4 results[13]: 0.02/hours ($0.3M_\odot \sim 6M\odot$).

We will also perform simulation of Galactic binaries events to set upper limit to the event rate in our Galaxies.

Note that these value are based on the matched filtering analysis by using only one detector's data independently. By performing coincident analysis, it is expected that we will obtain upper limit to the event rate which has different meaning from the results of one detector case, and would be more stringent. We will work on these in the near future.

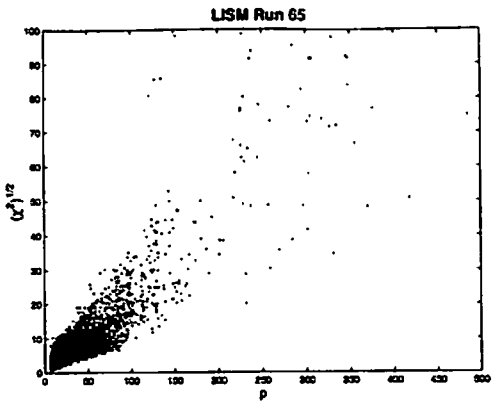

Figure 3:

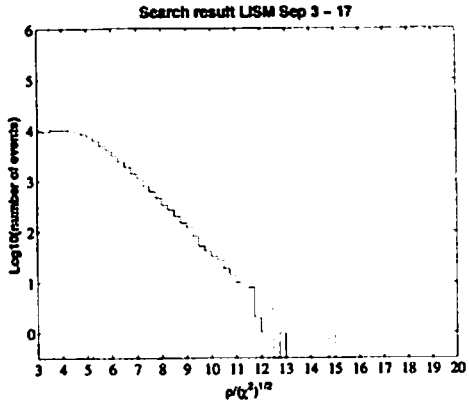

Figure 4:

Acknowledgements

This work was supported by Monukagakusho Grant-in-Aid for Creative Basic Research 09NP0801. This work was also supported in part by Monbukagakusho Grant-in-Aid 11740150, 12640269.

References

[1] For details about the first data taking of TAMA300 project, see *Gravitational Wave Detection II, (Proceedings of the 2nd TAMA workshop on Gravitational Wave Detection)*, (Univ. Acad. Press, Tokyo, 2000).

[2] M. Ando et al., Phys. Rev. Lett. **86**, 3950 (2001).

[3] H.Takahashi et al., in this volume.

[4] T. Nakamura, M. Sasaki, T. Tanaka, and K.S. Thorne, Astrophys. J. Lett. **487**, L139 (1997).

[5] S.Telada et al., in Ref.1.

[6] L. Blanchet, T. Damour, B. Iyer, C.M. Will, and A.G. Wiseman, Phys. Rev. Lett. **74**, 3515 (1995); L. Blanchet, Phys. Rev. **D54**, 1417 (1996).

[7] B. Allen et al. Phys. Rev. Lett. **83**, 1498 (1999).

[8] B. Allen et al. "GRASP software package", release 1.9.4, section 6.24, http://www.lsc-group.phys.uwm.edu/~ballen/grasp-distribution/ .

[9] B.J. Owen, Phys. Rev. **D53**, 6749 (1996).

[10] T. Tanaka, and H. Tagoshi, Phys. Rev. **D62**, 082001 (2000).

[11] This value are compiled from the results of Ref.7.

[12] H.Tagoshi et al., Phys. Rev. **D63**, 062001 (2001).

[13] H.Tagoshi et al., in preparation.

The coincident event search using TAMA300 and LISM data

Hirotaka Takahashi[1]

Graduate School of Science and Technology , Niigata University , Ikarashi , Niigata 950-2181 , Japan

Hideyuki Tagoshi

Theoretical Astrophysics Department of Earth and Space Science , Osaka University, Toyonaka, Osaka 560-0043, Japan

and The TAMA Collaboration

Abstract

We performed a coincident event search for inspiraling compact binaries using TAMA300 and LISM data taken in the summer of 2001. We have not observed significant coincident events.

1 Introduction

Several laser interferometric gravitational wave(GW) detectors are now under the construction.These include LIGO [1],VIRGO [2], GEO600 [3],and TAMA300 [4].

In Japan,there are two laser interferometric gravitational wave detectors.One is the TAMA300 detector.The TAMA300 is an interferometric GW detector with $300m$ baseline length located at Mitaka campus of the National Astronomical Observatory in Tokyo($35.68°N, 139.54°E$).The other is the LISM detector which is operated mainly by people in ICRR (Univ. of Tokyo).It is an interferometric GW detector with $20m$ baseline length located at Kamioka mine,Gifu ($36.25°N, 137.18°E$).

The TAMA300 and LISM observed during August 1st and September 20th,2001(JST). (Data Taking 6) The best sensitivity of the TAMA300 was about $5 \times 10^{-21}/\sqrt{Hz}$ around $900Hz$. 1038 hours of data was taken during Data Taking 6. The best sensitivity of the LISM was about $6.5 \times 10^{-20}/\sqrt{Hz}$ around $700Hz$. 777 hours of data was taken during that period.

In the past,very little work has devoted to develop the coincident analysis using real data of two or more laser interferometers. A coincident analysis of bursts events in a pair of laser interferometers has been performed by D. Nicholson et al. [5]. They do not use the matched filtering techniques. we perform a coincident analysis based on matched filter using real interferometers(TAMA300 and LISM) data.

2 Inspiral compact binaries

Gravitational waves from inspiral compact binaries,consisting of neutron stars or black hole, have been considered to be the most promising target for laser interferometers because expected event rate of NS-NS merger is a few within $200Mpc/year$ and their waveforms can be theoretically calculated to a very high accuracy.

[1]E-mail:hirotaka@astro.sc.niigata-u.ac.jp

3 Onestep Search

We assume that the time-sequential data of the detector outputs $s(t)$ consists of a signal plus noise $n(t)$. We also assume that the waveform of the signal is predicted theoretically with sufficiently good accuracy.Hence the signal is supposed to be identical to one of the templates except for the normalization of it's amplitude.

To characterize the detector noise ,we define one-sided power spectrum density $S_n(f)$ by

$$S_n(f) = 2\int_{-\infty}^{\infty} < n(t)n(t+\tau) > e^{2\pi i f\tau} d\tau \tag{1}$$

where $< >$ represents the operation of taking the statical average.

We adopt the templates calculated by using the post-Newtonian approximation of of general relativity[6]. We use a simplified version of the post-Newtonian templates in which the phase evolution is calculated 2.5 post-Newtonian order, but the amplitude evolution contains only the lowest Newtonian quadrupole contribution.We also use the stationary phase approximation.

The parameters consist of the coalescing time t_c,the total mass $M(\equiv m_1 + m_2)$,the mass ratio $\eta(\equiv m_1 m_2/M^2)$,and the spin parameters.(We have neglected the spin effects at 2.5 PN order.) In this analysis,we did not take account of the effect of spin angular momentum.The templates corresponding to a given set of the parameters are represented in Fourier space two independent templates $\tilde{h}_c$ and $\tilde{h}_s$[7] as $\tilde{h}(f) = \tilde{h}_c(f)\cos\phi_c + \tilde{h}_s(f)\sin\phi_c$ where ϕ_c is the phase of wave.

Here we define outputs of matched filter as

$$\rho(m_1, m_2, t_c, \cdots) \equiv 2\int_{-\infty}^{\infty} \frac{\tilde{s}(f)\tilde{h}^*(f)}{S_h(f)} df = (s|h) \tag{2}$$

where $*$ means the operation of taking the complex conjugate.In equation (2),we can analytically take the maximization over ϕ_c.

$$\rho = \sqrt{(s|h_c)^2 + (s|h_s)^2} \tag{3}$$

This ρ has an expectation value $\sqrt{2}$ in the presence of Gaussian noise.Thus ,the Signal-to-Noise Ratio (SNR) is given by $SNR = \rho/\sqrt{2}$

Analyzing the real data,we found that the noise contained a large amount of non-stationary and non-Gaussian noise whose statistical properties have not been understood well yet.In order to remove the influence of such noise,we introduce a χ^2 test [8].In this paper,we do not explain a χ^2 test in detail which was explained by the Tanaka and Tagoshi [7].

We searched the parameter space of $1.0M_\odot \leq m_1, m_2 \leq 2.0M_\odot$.In this parameter spaces,we prepared a mesh.The mesh points define templates used for search.The mesh separation is determined so that maximum loss of SNR becomes less than 3%.We use the Tanaka-Tagoshi coordinates. Using geometrical arguments,Tanaka and Tagoshi[7] introduced a new parameterization of masses that simplifies algorithm to determine the mesh points. The parameter space defined by using the Tanaka-Tagoshi coordinates turned out to contain $200 \sim 1000$ templates with the TAMA300.

We independently performed onestep search using TAMA300 and LISM data.As a results of onestep search,we obtain ρ and χ^2 as functions of masses and coalescing time t_c.In each small interval of coalescing time Δt_c,we looked for an event which had the maximum ρ. In this search,we choose $\Delta t_c \sim 3.2sec$.If the events which had the maximum ρ were $\rho > 7$,we wrote the events on TAMA(LISM) event lists.

4 Coincident event search

In this search,the parameters on which the waveforms depend are $\theta^i = (A, t_c, \phi_c, \mathcal{M}, \eta)$ where A and $\mathcal{M} \equiv M\eta^{3/5}$ are the amplitude of waveform and the chirp mass respectively. If the events are 'true' gravitational waves,they should have the same intrinsic parameters in the both detectors. However, we may observe real events with different parameters by the effects of detector noise. Therefore we have to determine the allowed parameter windows. The parameter windows were determined to satisfy the following criterion.

Criterion : *If the probability that events are the same real events is less than* 0.1%,*we reject it from coincident event list.*

4.1 t_c - veto

The distance between the TAMA300 and the LISM is $\sim 220km$.Therefore,the maximum delay of GW signal arrival time is $\Delta t_{cdist} \sim 0.73msec.$ Moreover,the parameter-estimation errors of t_c by the effects of detector noise Δt_{cnoise}were determined by using Fisher Information Matrix[9].We defined the time window which satisfy criterion as $\Delta t_c^{window} = \Delta t_{cdist} + \Delta t_{cnoise}$. If the parameters $t_c^{tama,lism}$ observed in both detectors satisfy

$$|t_c^{tama} - t_c^{lism}| < \Delta t_c^{window} \tag{4}$$

we write the candidate GW events on coincident event lists.

4.2 mass - veto

The parameter-estimation errors of mass parameters by the effects of detector noise$\Delta\mathcal{M}$,$\Delta\eta$ were determined by using Fisher Information Matrix.We defined the time window which satisfy criterion as $\Delta\mathcal{M}$,$\Delta\eta$. If the parameters $\mathcal{M}_{tama,lism}$,$\eta_{tama,lism}$ observed in both detectors satisfy

$$|\mathcal{M}_{tama} - \mathcal{M}_{lism}| < \Delta\mathcal{M} \tag{5}$$

$$|\eta_{tama} - \eta_{lism}| < \Delta\eta \tag{6}$$

we write the candidate GW events on coincident event lists.

4.3 ρ - veto

The parameter-estimation errors of ρ by the effects of the LISM detector noise $\Delta\rho_{noise}^{lism}$ were determined by using Fisher Information Matrix.If ρ_{lism} satisfy

$$\rho_{tama}r - \Delta\rho_{lism} \leq \rho_{lism} \leq \rho_{tama}r - \Delta\rho_{lism}\ , \quad \overline{\left(\frac{\rho_{lism}}{\rho_{tama}}\right)} \equiv r \tag{7}$$

we write the candidate GW events on coincident event lists.

5 Results

The total length of data used for onestep search was $\sim 322hours$. As a result of the onestep search,we obtain the independent TAMA(LISM) events lists.In order to perform the coincident event search,we extracted the TAMA (LISM)events lists for common lock parts($\sim 245hours$).As a result,there are the 1580707 (142465) candidate GW events with the TAMA300(LISM) (Table 1). Over these candidate GW events,we performed the t_c-veto.As a results, there are the 124 candidate GW events.Moreover,over the events that survived t_c-veto,we performed the mass-veto.As a results,there are the 17 candidate GW events.Fig.1 shows the ρ distribution of coincident events that pass the t_c and mass-veto. Over the events that survived the t_c and mass-veto,we performed the ρ-veto.As a result,there are no significant GW events.

	Results of onestep search	after t_c -veto	after t_c and mass -veto	after t_c ,mass and ρ-veto
TAMA	1580707	124	17	0
LISM	142465			

Table 1: Results of coincident event search.

6 Discussion

We performed a coincident event search for inspiraling compact binaries using TAMA300 and LISM data.

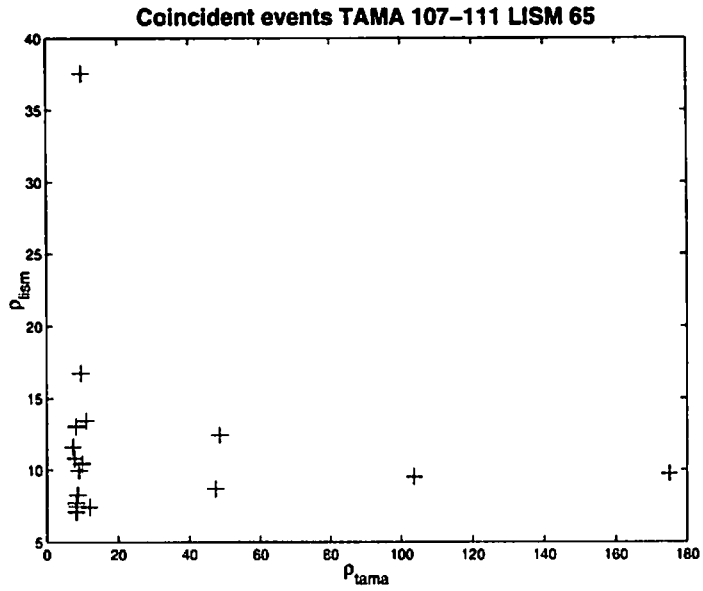

Figure 1: ρ scatter plots of coincident events passing the t_c and mass-veto.

In the future work,we will evaluate the accidental coincident rate. And even in the case if there are no significant events,we can obtain upper limit to the event rate in the data using e.g. Poisson statistics. It is also important that we understand the detection efficiency of this methods using Monte-Carlo simulations. Moreover,we compare upper limit to the event rate concluded single detector analysis with upper limit to the event rate concluded coincident analysis.

References

[1] A. Abramovici et al.,sience **256**,325 (1992).

[2] B. Caron et al. ,in *Gravitaional Wave Experiments*, edited by E. Coccia,G. Pizzella, and F. Ronga,(World Scientific, Singapore,1995).

[3] K. Danzmann et al.,in *Gravitaional Wave Experiments*, edited by E. Coccia,G. Pizzella, and F. Ronga,(World Scientific, Singapore,1995).

[4] k. Tsubono,in *Gravitational Wave Experiments*, edited by E. Coccia,G. Pizzella, and F. Ronga,(World Scientific, Singapore,1995).

[5] D. Nicholson et al.,Phys.Lett.A,218 (1996).

[6] L. Blanchet et al.,Phys. Rev. Lett. **74**,3515 (1995).

[7] T. Tanaka and H. Tagoshi,Phys.Rev.D **62**,082001.(2000)

[8] B. Allen et al.,Phys.Rev.Lett. **62**,1489 .(1999)

[9] C. Cutler and É. E. Flanagan,Phys.Rev.D **49**,082001.(1994)

Direct Measurement of the Acceleration of the Universe using 0.1Hz Band Laser Interferometer Gravitational Wave Antenna in Space

Naoki Seto[1]

Department of Earth and Space Science, Osaka University, Toyonaka 560-0043, Japan

Seiji Kawamura[2]

National Astronomical Observatory, Mitaka 181-8588, Japan

Takashi Nakamura[3]

Yukawa Institute for Theoretical Physics, Kyoto University, Sakyo-ku, Kyoto 606-8502, Japan

Abstract

It may be possible to construct a laser interferometer gravitational wave antenna in space with $h_{rms} \sim 10^{-27}$ at $f \sim 0.1$Hz in this century. We show possible specification of this antenna which we call DECIGO. Using this antenna we show that 1) typically 10^5 ($10^4 \sim 10^6$) chirp signals of coalescing binary neutron stars per year may be detected with S/N $\sim 10^4$. 2) We can directly measure the acceleration of the universe by ten years observation of binary neutron stars. 3) The stochastic gravitational waves of $\Omega_{GW} \gtrsim 10^{-20}$ predicted by the inflation may be detected by correlation analysis for which effects of the recent cosmic acceleration would become highly important. Our formula for phase shift due to accelerating motion might be also applied for binary sources of LISA. This proceeding is based on Ref.[1].

1 Specification of DECIGO

The sensitivity of a space antenna with an arm length of 1/10 of LISA [2] and yet the same assumption of the technology level, such as a laser power of 1 W, the optics of 30 cm, etc. will be 4×10^{-21}Hz$^{-1/2}$ around 0.1 Hz in terms of strain, a factor of 10 better than the planned LISA sensitivity around 0.1 Hz (see also http://www.physics.montana.edu/maggie for a project named MAGGIE around this band). The sensitivity could be improved by a factor of 1000 for the next generation of a space antenna with more sophisticated technologies such as implementation of higher-power lasers and larger optics in order to increase the effective laser power available on the detectors, and thus to reduce the shot noise. The ultimate sensitivity of a space antenna in the far future could be, however, 3×10^{-27} around 0.1 Hz in terms of strain, assuming the quantum limit sensitivity for a 100 kg mass and an arm length of 1/10 of LISA. We name this detector DECIGO (DECi hertz Interferometer Gravitational wave Observatory). This requires an enormous amount of effective laser power, and also requires that the other noise sources, such as gravity gradient noise, thermal noise, practical noise, etc. should be all suppressed below the quantum noise. Here we assume that such an antenna may be available by the end of this century, although we note that within the next five years or so NASA will begin serious discussions of a follow-on to the planned NASA/ESA LISA mission, so DECIGO technology may be achieved sooner. Note here that when the pioneering efforts to detect the gravitational waves started in the last century using resonant type detectors as well as laser interferometers, few people expected the present achievement

[1] E-mail:seto@vega.ess.sci.osaka-u.ac.jp
[2] E-mail:seiji.kawamura@nao.ac.jp
[3] E-mail:takashi@yukawa.kyoto-u.ac.jp

in resonant type detectors. Therefore all the experimentalists and the theorists on gravitational waves should not be restricted to the present levels of the detectors. Our point of view in this note is believing the proverb " Necessity is the mother of the invention" so that we argue why a detector like DECIGO is necessary to measure some important parameters in cosmology.

The sensitivity of DECIGO, which is optimized at 0.1 Hz, is assumed to be limited only by radiation pressure noise below 0.1 Hz and shot noise above 0.1 Hz. The contributions of the two noise sources are equal to each other at 0.1Hz, giving the quantum limit sensitivity at this frequency. The radiation pressure noise has a frequency dependence of $\propto f^{-2}$ (in units of $\mathrm{Hz}^{-1/2}$) because of the inertia of the mass, while the shot noise has a dependence of approximately $\propto f^{1}$ (in units of $\mathrm{Hz}^{-1/2}$) because of the signal canceling effect due to the long arm length. In figure 1 we show sensitivity of various detectors and characteristic amplitude h_c for a chirping NS-NS binary at $z = 1$.

2 Direct Measurement of the Acceleration of the Universe

Recent distance measurements for high-redshift supernovae suggest that the expansion of our universe is accelerating [3] which means that the equation of the state of the universe is dominated by "dark energy" with $\rho + 3p < 0$. *SuperNova / Acceleration Probe* (SNAP, http://lbl.gov) project will observe ~ 2000 Type Ia supernovae per year up to the redshift $z \sim 1.7$ so that we may get the accurate luminosity distance $d_L(z)$ in near future. Gravitational wave would be also a powerful tool to determine $d_L(z)$ [4].

From accurate $d_L(z)$ one may think that it is possible to determine the energy density $\rho(z)$ and the pressure $p(z)$ as functions of the redshift. However as shown by Weinberg [5] and Nakamura & Chiba [6], $\rho(z)$ and $p(z)$ can not be determined uniquely from $d_L(z)$ but they depend on one free parameter Ω_{k0} (the spatial curvature).

Recent measurement of the first peak of the anisotropy of CMB is consistent with a flat universe ($\Omega_{k0} = 0$) for primordially scale-invariant spectrum predicted by slow-roll inflation under the assumption of Λ cosmology. However it is important to determine the curvature of the universe irrespective of the theoretical assumption on the equation of the state and the primordial spectra also. In other words an independent determination of Ω_{k0} is indispensable since Ω_{k0} is by far the important parameter. As discussed in [6], the direct measurement of the cosmic acceleration [7] can be used for this purpose. Here we point out that the gravitational waves from the coalescing binary neutron stars at $z \sim 1$ observed by DECIGO may be used to determine Ω_{k0}. Even in the worst case the redundancy is important to confirm such an important finding as the dark energy.

Cosmic Acceleration.—

A Cosmic Acceleration.— We consider the propagation of gravitational wave in our isotropic and homogeneous universe. The metric is given by $ds^2 = -dt^2 + a(t)^2(dx^2 + r(x)^2(d\theta^2 + \sin^2\theta d\phi^2))$, where $a(t)$ is the scale factor and $a(t)r(x)$ represents the angular distance. The relation between the observed time of the gravitational waves t_o at $x = 0$ and the emitted time t_e at the fixed comoving coordinate x is given by $\int_{t_e}^{t_o} \frac{dt}{a(t)} = x = const.$ Then we have $dt_o/dt_e = a_o/a_e = (1 + z)$ and

$$\frac{d^2t_o}{dt_e^2} = (1 + z)a_e^{-1}(\partial_t a(t_o) - \partial_t a(t_e)) \equiv g_{cos}(z) = (1 + z)((1 + z)H_0 - H(z)), \tag{1}$$

where $H(z)$ is the Hubble parameter at the redshift z and H_0 is the present Hubble parameter. For an emitter at the cosmological distance $z \gtrsim 1$ we have $g_{cos}(z) \sim O(t_0^{-1})$ where t_0 is the age of universe $t_0 \sim 3 \times 10^{17}$ sec. From above equations we have $\Delta t_o = \Delta t_e(1+z) + \frac{g_{cos}(z)}{2}\Delta t_e^2 + \cdots$, where Δt_o and Δt_e are the arrival time at the observer and the time at the emitter, respectively. When we observe the gravitational waves from the cosmological distance, we have $\Delta t_o = \Delta T + X(z)\Delta T^2 + \cdots$, with $X(z) \equiv g_{cos}(z)/2(1+z)^2$, where $\Delta T = (1 + z)\Delta t_e$ is the arrival time neglecting the cosmic acceleration/deceleration (the second term). Now for $\Delta T \sim 10^9$ sec, the time lag of the arrival time due to the cosmic acceleration/deceleration amounts to the order of second $\sim 10^{18}/(3 \times 10^{17}) \sim 1$ [sec]. From Eq. (1), if $X(z)$ is positive, then $\partial_t a(t_o) > \partial_t a(t_e)$. This clearly means that our universe is accelerating. Therefore the value of this time lag is the direct evidence for the acceleration/deceleration of the universe.

As shown in [6], if the accurate value of $X(z)$ at a single point z_s is available it is possible to determine Ω_{k0} as $\Omega_{k0} = \{1 - (dr(z_s)/dz)^2(1 + z_s)^2(H_0 - 2X(z_s))^2\}\{r(z_s)^2H_0^2\}^{-1}$, where we have assumed that the

quantity $r(z) \equiv d_L(z)/(1+z)$ is obtained accurately, *e.g.*, by SNAP. Even if the accurate values of $X(z)$ are not available for any points, we may apply the maximal likelihood method to determine Ω_{k0}. Using the value of Ω_{k0} thus determined, we can obtain the equation of state of our universe without any theoretical assumption on its matter content [6].

B Evolution of Phase of Gravitational Waves from Coalescing Binary at Cosmological Distance.—

Let us study an inspiraling compact binary system that evolves secularly by radiating gravitational wave [8]. For simplicity we study a circular orbit and evaluate the gravitational wave amplitude and the energy loss rate by Newtonian quadrupole formula. We basically follow analysis of Cutler & Flanagan [8] but properly take into account of effects of accelerating motion. The Fourier transform $\tilde{h}(f) = \int_{-\infty}^{\infty} e^{2\pi i f t} h(t) dt$ for the wave $h(t)$ is evaluated using the stationary phase approximation as $\tilde{h}(f) = K d_L(z)^{-1} M_c^{5/6} f^{-7/6} \exp[i\Phi(f)]$, where K is determined by the angular position and the orientation of the binary relative to the detector, and M_c is the chirp mass of the system. Keeping the first order term of the coefficient $X(z)$, the phase $\Phi(f)$ of the gravitational wave becomes

$$\Phi(f) = 2\pi f t_c - \phi_c - \frac{\pi}{4} + \frac{3}{4}(8\pi M_{cz} f)^{-5/3} - \frac{25}{32768} X(z) f^{-13/3} M_{cz}^{-10/3} \pi^{-13/3}, \tag{2}$$

where t_c and ϕ_c are integral constants and $M_{cz} = M_c(1+z)$ is the redshifted chirp mass.

If we include the post-Newtonian (PN) effects up to P$^{1.5}$N-order, the term $3/4(8\pi M_{cz} f)^{-5/3}$ in eq.(2) should be modified as $\frac{3}{4}(8\pi M_{cz} f)^{-5/3}\left[1 + \frac{20}{9}\left(\frac{743}{336} + \frac{11\mu}{4M_c}\right)x + (4\beta - 16\pi)x^{3/2}\cdots\right]$, where $x \equiv (\pi M_t f(1+z))^{2/3} = O(v^2/c^2)$ is the PN expansion parameter with M_t being the total mass of the binaries. The term proportional to β in P$^{1.5}$N order ($\propto x^{3/2}$) is caused by the spin effect [8, 9]. In general P^{N}N contribution depends on the frequency f as $O(f^{(-5+2N)/3})$ and is largely different from the dependence $f^{-13/3}$ caused by the cosmic acceleration. This difference is very preferable for the actual signal analysis.

C the estimation error.—

For the circular orbit of the binary neutron stars (NSs) of mass M_1 and M_2 with the separation a at the redshift z, the frequency of the gravitational waves f is given by $f = 0.1\mathrm{Hz}(1+z)^{-1}(M_t/2.8M_\odot)^{1/2} \times (a/15500\mathrm{km})^{-3/2}$. The coalescing time t_c, the number of cycles N_{cycle} and the characteristic amplitude of the waves h_c are given by

$$t_c = 7(1+z)(M_1/1.4M_\odot)^{-1}(M_2/1.4M_\odot)^{-1}(M_t/2.8M_\odot)^{-1}(a/15500\mathrm{km})^4\mathrm{yr} \tag{3}$$

$$N_{cycle} = 1.66\times10^7(M_1/1.4M_\odot)^{-1}(M_2/1.4M_\odot)^{-1}\times(M_t/2.8M_\odot)^{-1/2}(a/15500\mathrm{km})^{5/2} \tag{4}$$

$$h_c = 1.45\times10^{-23}(1+z)^{5/6}(M_c/1.2M_\odot)^{5/6}(f/0.1\mathrm{Hz})^{-1/6}(d_L/10\mathrm{Gpc})^{-1} \tag{5}$$

Let us evaluate how accurately we can fit the parameter $X(z)$. We take six parameters $\lambda_i = \{A, M_{cz}, \mu_z, t_c, \phi_c, M_{cz}^{-10/3}X(z)\}$ in the matched filtering analysis up to 1PN-order for the phase $\Phi(f)$ and Newtonian order for the amplitude [8]. Here A is the amplitude of signal $K d_L(z)^{-1} M_c^{5/6}$ in the previous subsection and μ_z is the redshifted reduced mass $\mu_z = (1+z)M_1M_2/M_t$. As the chirp mass M_{cz} can be determined quite accurately, we simply put $\Delta X(z) = \Delta\left\{M_{cz}^{-10/3}X(z)\right\}/M_{cz}^{-10/3}$. For simplicity we fix the redshift of sources at $z=1$ and calculate S/N and the error ΔX for equal mass binaries with various integration time Δt before coalescence. We use the effective factor $1/\sqrt{5}$ for reduction of antenna sensitivity due to its rotation [2]. For the present analysis we neglect the binary confusion noise since double White Dwarf binaries do not exist at frequency $f \gtrsim 0.1$Hz [2].

We found that we can detect NS-NS binaries at $z=1$ with $S/N \simeq 20000$ and $\Delta X/t_0^{-1} \simeq 7.0\times10^{-3}$ for integration time $\Delta t = 16$yr ($N_{cycle} \sim 10^7$ orbital cycles), and $S/N \simeq 10000$ and $\Delta X/t_0^{-1} \simeq 1.26$ for $\Delta t = 1$yr (see Fig.2]). With this detector it would be possible to determine $X(z)$ and obtain the information of the cosmic acceleration quite accurately. With $\Delta T = 16$yr we have the estimation error for the redshifted masses as $\Delta M_{cz}/M_{cz} = 1.5\times10^{-11}$, $\Delta\mu_z/\mu_z = 4.2\times10^{-8}$ and for the wave amplitude $\Delta A/A \sim (S/N)^{-1} = 5\times10^{-5}$. Although the more detailed study is needed to estimate the error of the binary inclination angle, it is expected that the luminosity distance d_L can be determined accurately so that the redshift z can be determined using the inverse function $z = d_L^{-1}(\mathrm{distance})$ of the accurate luminosity distance from *e.g.* SNAP. As a result we can know two (not redshifted) masses M_1 and M_2

for $\sim 10^5$ binaries per year up to $z = 1$ [10]. This will be large enough to establish the mass function of NS which would bring us important implications for the equation of the state of the high density matter and the explosion mechanisms of TypeII supernovae.

As the S/N and the estimation error scale as $S/N \propto h_{rms}^{-1}$ and $\Delta X \propto h_{rms}$, we can attain $\Delta X/t_0^{-1} \simeq 7.0$ for the integration time $T = 16$yr using a less sensitive detector with $h_{rms} \sim 10^{-24}$ (1000 times worse). Even though the error bar ΔX is fairly large for this detector, the likelihood analysis would be an efficient approach to study the cosmic acceleration. Considering the estimated cosmological coalescence rate of NS-NS binaries ($\gtrsim 2 \times (10\mathrm{Gpc}/350\mathrm{Mpc})^3 \sim 10^5\mathrm{yr}^{-1}$) [10], we may expect the decrease of the estimation error ΔX roughly by a factor of $\sim 1/300 = 1/\sqrt{10^5}$.

D Acceleration in the Very Early Universe.—

In the inflationary phase there was an extremely rapid acceleration of the universe. In this phase the gravitational waves were generated by quantum fluctuation [11]. With CMB quadrupole anisotropies measured by COBE, the slow-roll inflation model predicts a constraint on the stochastic background $\Omega_{GW} \lesssim 10^{-15} - 10^{-16}$ at $f \sim 0.1$Hz [12]. Ungarelli and Vecchio [13] discussed that the strain sensitivity $h_{rms} \sim 10^{-24}$ is the required level at $f \sim 0.1$Hz for detecting $\Omega_{GW} \sim 10^{-16}$ by correlating two detectors for decades. It is important to note that the band $f > 0.1$ Hz is free from stochastic backgrounds generated by White Dwarf binaries. The radiation from neutron stars binaries is present in this band and it is indispensable to remove their contributions accurately from data stream, where effects of the cosmic acceleration would be highly important. Thus measurement of the present-day cosmic acceleration is closely related to detection of the primordial gravitational wave background that is one of the most interesting targets in cosmology. If DECIGO with $h_{rms} \sim 2 \times 10^{-27}$ at $f \sim 0.1$Hz is available we can detect the primordial gravitational waves background even if the energy density is extremely low $\Omega_{GW} \sim 10^{-20}$ by correlating two detectors for a decade.

Confusion noise due to NS-NS (or NS-BH, BH-BH) binaries might be important in the band $f \sim 0.1$Hz. Ungarelli and Vecchio [13] investigated the critical frequency f_g where we can, in principle, remove signal from individual NS-NS binaries by matched filtering analysis and the observed window becomes transparent to the primordial stochastic background. They roughly estimated $f_g \sim 0.1$Hz where the number of binaries per frequency bin ($\sim 10^{-8}$Hz) is less than one. But binaries around $f \sim f_g \sim 0.1$ chirp significantly within observing time scale and the situation would be more complicated than monochromatic sources [2]. Although more detailed analysis is needed, a much smaller NS-NS coalescence rate than $\sim 10^5\mathrm{yr}^{-1}$ might be required for our analysis to be valid.

3 Discussions

The determination of the angular position of the source is crucial for matching the phase [2]. The phase modulation at the orbital radius 1AU corresponds to $2\mathrm{AU}/c \sim 1000$[sec]. Thus, in order to match the phase within the accuracy of 0.1[sec] we need to determine the angular position with precision $\sim 0.1/1000$ [rad] $\sim 20''$. In the matched filtering analysis we can simultaneously fit parameters of the angular position as well as the relative acceleration between the source and the barycenter of the solar system. Due to their correlation in the Fisher matrix, the measured acceleration would be somewhat degraded if we cannot determine the angular position by other observational methods. Using the gravitational wave alone, we can, in advance, specify the coalescence time and the angular position of the source within some error box. If coalescence of NS-NS binaries would release the optical signal (*e.g.* Gamma Ray Bursts as proposed by [14]) we may measure the angular position accurately by pointing telescopes toward the error box at the expected coalescence time from the chirp signal. Therefore we have not tried to fit the angular position of the source in the matched filtering method [2]. We might also determine the redshift of the source by using optical information of host galaxies.

Let us discuss the effects of the local motion g_{local} of the emitter on the second derivative d^2t_o/dt_e^2. As the effect of bulk motion of galaxy is much smaller than cosmological effect, we estimate the internal acceleration within the galaxy based on the observational result of NS-NS binary PSR 1913+16. As shown in Table 1 of [15], the dominant contribution of its acceleration $\ddot{x}$ comes from the global Galactic potential field and has time scale $c/\ddot{x} \sim 10t_0(R_e/10\mathrm{kpc})(V_{rot}/200\mathrm{kms}^{-1})$ that can be comparable to the cosmic signal g_{cos} where R_e is the effective radius of the acceleration and V_{rot} is galactic rotation

velocity. However the contamination of local effect g_{local} can be reduced by taking the statistical average of many binaries as $\langle g_{cos} + g_{local} \rangle = \langle g_{cos} \rangle$. We also note that the cosmological change in phase of a coalescing binary [given by the last term in Eq. (3)] may have other applications, and may under certain circumstances be observable by the planned LISA mission.

References

[1] N. Seto, S. Kawamura & T. Nakamura, Phys. Rev. Lett. **87**, 221103 (2001).

[2] P. L. Bender *et al.*, *LISA Pre-Phase A Report*, Second edition, July 1998

[3] A. G. Riess *et al.* Astron. J. **116**, 1009 (1998); S. Perlmutter *et al.* Astrophys. J. **517**, 565 (1999)

[4] B. F. Schutz, Nature **323**, 310 (1986); B. F. Schutz, Class. Quant. Grav. **6**, 1761 (1989).

[5] S. Weinberg, Astrophys. J. **161**, L233 (1970)

[6] T. Nakamura and T. Chiba, Mon. Not. Roy. Astron. Soc. **306**, 696 (1999); T. Chiba and T. Nakamura, Phys. Rev. D **62**, 121301 (2000).

[7] A. Loeb, Astrophys. J. **499**, L111 (1998).

[8] C. Cutler and E. E. Flanagan, Phys. Rev. D **49** 2658 (1994).

[9] C. Cutler *et al.*, Phys. Rev. Lett. **70**, 2984 (1993); L. Blanchet *et al.*, Phys. Rev. Lett. **74**, 3515 (1995).

[10] V. Kalogera *et al.*, Astrophys. J. **556**, 346 (2001). astro-ph/0012038.

[11] M. Maggiore, Phys. Rept. **331**, 283 (2000)

[12] M. S. Turner, Phys. Rev. D **55**, 435 (1997);

[13] C. Ungarelli and A. Vecchio. Phys. Rev. D **63**, 064030 (2001)

[14] B. Paczynski, Astrophys. J. **308**, L43 (1986).

[15] T. Damour, and J. H. Taylor, Astrophys. J. **366**, 501 (1991).

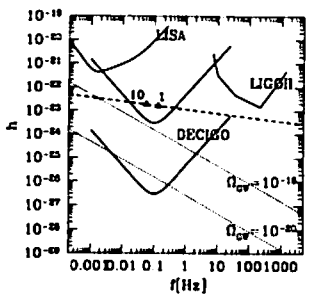

Figure 1: Sensitivity (effectively S/N=1) for various detectors (LISA, DECIGO, LIGOII and a detector 10^3 times less sensitive than DECIGO) in the form of h_{rms} (solid lines). The dashed line represents evolution of the characteristic amplitude h_c for NS-NS binary at $z = 1$ (filled triangles; wave frequencies at 1yr and 10 yr before coalescence). The dotted lines represent the required sensitivity for detecting stochastic background with $\Omega_{GW} = 10^{-16}$ and $\Omega_{GW} = 10^{-20}$ by ten years correlation analysis (S/N=1).

How accurately can the positions of the Galactic binaries be determined by LISA ?

Ryuichi Takahashi[1]

Department of Physics, Kyoto University,
Kyoto 606-8502, Japan

Naoki Seto[2]

Department of Earth and Space Science, Osaka University,
Toyonaka 560-0043, Japan

Abstract

We calculate how accurately the positions of the short-period binaries (10^{-4} Hz $\lesssim f \lesssim 10^{-2}$ Hz) will be determined from the gravitational wave signals by LISA. We analyze LISA's measurement accuracy for all source parameters, including effects of the chirp signal $\dot{f}$ and the long time observation T_{obs}. It turns out that the chirp signal should be included in the matured filtering at higher frequencies $f \gtrsim 10^{-3}$ Hz for solar mass binaries. We find that the distance to the chirping binary is determined within $\sim 20\%$ (normalized by signal-to-noise ratio equals 10) at best. The fitting formulae of the estimation errors as a function of f and T_{obs} are also obtained.

1 Introduction

The Laser Interferometer space Antenna (LISA) would establish gravitational wave astronomy at low frequency band (10^{-4} Hz $\lesssim f \lesssim 10^{-1}$ Hz). It would bring us essentially new information of the Universe [1]. For example gravitational waves from merging super massive black holes (SMBHs) would be detected with significant signal-to-noise ratio (SNR) $\gtrsim 10^3$, though event rate of such merging is highly unknown (*e.g.* [2]). Galactic binaries are promising sources of LISA [3, 4, 5]. Gravitational waves from some existing binaries (*e.g.* X-ray binary 4U1820-30) would be detected with $SNR > 5$ by one year integration [1]. In addition more than thousands of close white dwarf binaries (CWDBs) are expected to exist in LISA band. Our target in this article is these Galactic binaries. We examine how accurately information of binaries can be extracted from gravitational waves observed by LISA.

Cutler (1998) studied the estimation errors for binary parameters with special attention to the angular variables such as direction and orientation of binaries (see also [7, 8, 9]). He used approximation that emitted gravitational waves would be monochromatic, namely neglected the effects of the chirp signal $\dot{f}$. But wave frequency or the chirp signal are fundamental quantities for gravitational wave astronomy. From the measured chirp signal $\dot{f}$ we can estimate the so called chirp mass $M_c = M_1^{3/5} M_2^{3/5} (M_1 + M_2)^{-1/5}$ (M_1, M_2: masses of two stars) for a binary whose orbital evolution is determined by gravitational radiation reaction. Furthermore the distance to the binary could be obtained from the chirp signal $\dot{f}$ and the amplitude of the wave signal [10]. The frequency f also contains important information. One of the authors (Seto 2001) pointed out that signature of the periastron advance could be detected in gravitational waves from an eccentric binary by measuring its wave frequencies preciously. If this method works well, we can estimate the total mass $M_{total} = M_1 + M_2$ of the binary beside the chirp mass, and consequently each mass of the binary is obtained separately.

Estimation errors for fitting parameters complicatedly correlate to each other and depend largely on observational situations. For example longer observation period would improve not only signal to noise ratio but also resolution of the frequency space. Note that the latter is crucial for reducing Galactic binary

[1] E-mail:takahasi@tap.scphys.kyoto-u.ac.jp
[2] E-mail:seto@vega.ess.sci.osaka-u.ac.jp

confusion noise at $\sim 10^{-3}$Hz, as the number of resolved binaries increases [12]. At LISA age it would become an interesting challenge to optically identify the binaries whose gravitational waves are detected by LISA. We also discuss impacts of these observational efforts for estimation of binary parameters.

This article is organized as follows. In §2 we briefly discuss the gravitational waveforms of chirping binaries and parameter extraction. In §3 we numerically evaluate the parameter estimation errors. §4 is devoted to summary.

2 Gravitational Waveforms and Parameter Extraction

2.1 Gravitational Waveforms

We study the short-period (10^{-4} Hz $\lesssim f \lesssim$ 10^{-2} Hz) binaries such as the close white dwarf binaries (CWDBs) or the neutron star binaries (NBs) in the Galaxy [5]. We only discuss binaries with circular orbits. This is an excellent approximation for CWDBs, as their orbits are circularized by strong tidal interaction.

The chirping gravitational waveform is given with the use of quadrupole approximation [13] as

$$\begin{aligned} h_+(t) &= A\cos\left[2\pi\left(f+\frac{1}{2}\dot{f}t\right)t+\phi_D(t)+\phi_0\right]\times\left[1+\left(\hat{L}\cdot\hat{n}\right)^2\right], \\ h_\times(t) &= -2A\sin\left[2\pi\left(f+\frac{1}{2}\dot{f}t\right)t+\phi_D(t)+\phi_0\right]\times\left(\hat{L}\cdot\hat{n}\right), \end{aligned} \tag{1}$$

where $\hat{L}$ (given by $\bar{\theta}_L, \bar{\phi}_L$) is the unit vector in the direction of the binary's orbital angular momentum, $\hat{n}$ (given by $\bar{\theta}_S, \bar{\phi}_S$) is the unit vector toward the binary and ϕ_0 is an integral constant. These angular variables with bars are defined in a fixed barycenter frame of the solar system. The frequency f and the time variation of the frequency $\dot{f}$ in Eq.(1) are assumed to be constant. We set $\dot{f} = 0$ for the monochromatic waveform which is studied in Cutler(1998). When gravitational radiation reaction dominates evolution of the binary as in the case of CWDBs or NBs, the chirp signal $\dot{f}$ is given as $\dot{f} = (96\pi^{8/3}/5)f^{11/3}M_c^{5/3}$. The amplitude A in Eq.(1) is given in terms of the wave frequency f, chirp signal $\dot{f}$ and the distance D

$$A = \frac{5}{96\pi^2}\frac{\dot{f}}{f^3 D}. \tag{2}$$

Thus we could determine the distance D, if we could measure three observables f, $\dot{f}$ and A [10]. The term $\phi_D(t)$ in Eq.(1) is caused by annual revolution of LISA around the Sun and called the Doppler phase. Its explicit form is given by

$$\phi_D(t) = 2\pi f R\sin\bar{\theta}_S\cos\left[\bar{\phi}(t)-\bar{\phi}_S\right], \tag{3}$$

where $R = 1$ AU and $\bar{\phi}(t) = 2\pi t/T$ ($T = 1$yr) is the direction of LISA in the fixed barycenter frame.

The signals $h_{I,II}(t)$ from a binary are written as $h_{I,II}(t) = (\sqrt{3}/2)(F^+_{I,II}(t)h_+(t) + F^\times_{I,II}(t)h_\times(t))$, where $F^{+,\times}_{I,II}(t)$ are the pattern functions which depend on the source's angular parameters ($\hat{L}$ and $\hat{n}$) and detector's configuration. Further discussion and details about the pattern functions are seen in Cutler (1998).

2.2 Parameter Extraction

We assume that the signal $h_\alpha(t)$ is characterized by some unknown parameters γ_i (eight parameters in the present case: $(A, f, \dot{f}, \phi_0, \bar{\theta}_S, \bar{\phi}_S, \bar{\theta}_L, \bar{\phi}_L)$). In the matched filtering analysis [14] the variance-covariance matrix of the parameter estimation error $\Delta\gamma_i$ is given by inverse of the Fisher information matrix Γ_{ij} as $\langle\Delta\gamma_i\Delta\gamma_j\rangle = \left(\Gamma^{-1}\right)_{ij}$.

For a quasi-monochromatic binary ($\dot{f}T_{obs} \ll f$) the noise spectrum $S_n(f)$ is nearly constant in the frequency region swept by the binary and the Fisher matrix simply becomes [6]

$$\Gamma_{ij} = \frac{2}{S_n(f)}\sum_{\alpha=I,II}\int_0^{T_{obs}} dt\,\frac{\partial h_\alpha(t)}{\partial\gamma_i}\frac{\partial h_\alpha(t)}{\partial\gamma_j}. \tag{4}$$

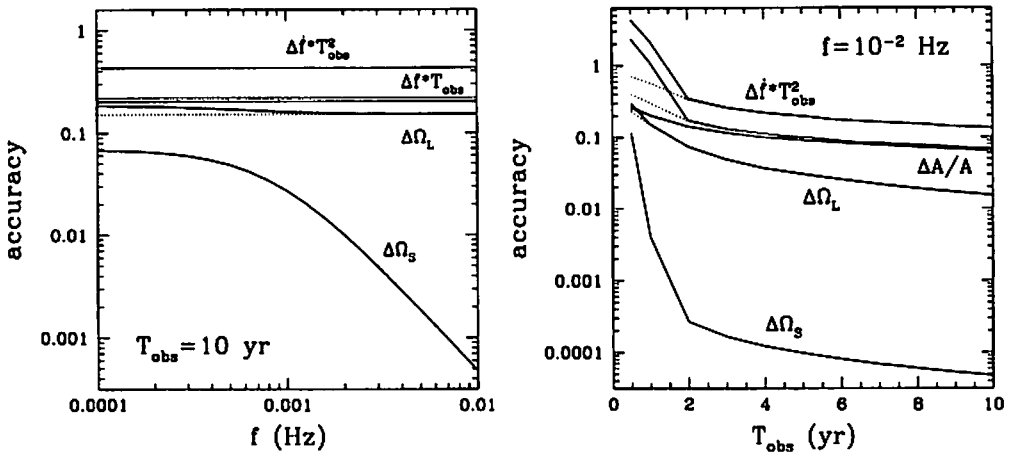

Figure 1: LISA's measurement accuracy for the binaries as a function of the frequency f (left) and observational period T_{obs} (right), under a typical case ($\cos\bar{\theta}_S = 0.3, \bar{\phi}_S = 5.0, \cos\bar{\theta}_L = -0.2, \bar{\phi}_L = 4.0$). These lines correspond to $\Delta\dot{f}, \Delta f, \Delta A, \Delta\Omega_L, \Delta\Omega_S$ from top to bottom. The accuracies are normalized to $SNR = 10$ at 1 (10)yr observation for the right (left) figure. The dotted lines represent the case source positions are known in advance.

The error boxes for the angular parameters $\hat{L}$ and $\hat{n}$ become ellipse in the celestial sphere due to the correlation of two parameters θ and ϕ. In this article we represent the estimation errors for direction and orientation of binaries in the form defined in Cutler (1998) as follows

$$\Delta\Omega = 2\pi\sqrt{\langle\Delta\mu^2\rangle\langle\Delta\phi^2\rangle - \langle\Delta\mu\Delta\phi\rangle^2}, \tag{5}$$

where we have defined $\mu = \cos\theta$. In the same manner the signal to noise ratio (SNR) is given by

$$(SNR)^2 = \frac{2}{S_n(f)} \sum_{\alpha=I,II} \int_0^{T_{obs}} dt\ h_\alpha(t) h_\alpha(t). \tag{6}$$

From equations (4) and (6) it is apparent that the expressions for the estimation errors $\langle\Delta\gamma_i\Delta\gamma_j\rangle$ do not depend on the noise spectrum $S_n(f)$ when they are normalized by the signal-to-noise ratio [6]. In this article we extensively use this normalization method.

3 Results

3.1 General Behavior

We have numerically evaluate parameter estimation errors for various quasi-monochromatic binaries. In this subsection we show results for a typical example with a fixed set of angular parameters at $\cos\bar{\theta}_S = 0.3, \bar{\phi}_S = 5.0, \cos\bar{\theta}_L = -0.2$ and $\bar{\phi}_L = 4.0$. We made figure 1 to clearly demonstrate dependence on wave frequency f (left figure) and observation period T_{obs} (right figure). All results are normalized by $SNR = 10$ after integration period $T_{obs} = 1(10)$ yr for the right(left) figure. The solid lines are results for fitting all the eight parameters. The dotted lines represent the case when the angular position $(\theta_S, \bar{\phi}_S)$ are removed from the fitting parameters. For observation $T_{obs} \gtrsim 2$ yr the difference between the solid and the dotted lines is very small especially for ΔA, Δf and $\Delta\dot{f}$. Their asymptotic time dependence are given

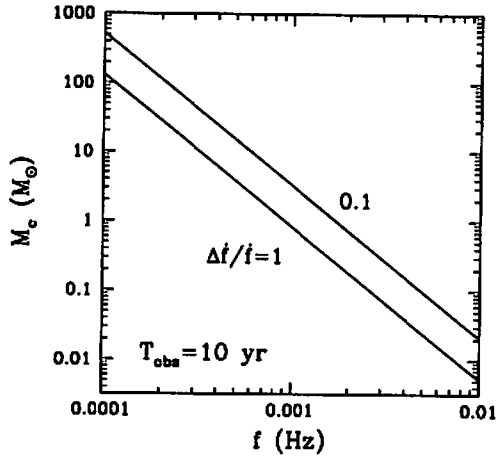

Figure 2: Contours of $\Delta\dot{f}/\dot{f}$ in the parameter space f and m_c. In the region of $\Delta\dot{f}/\dot{f} \lesssim 1$, effects of the chirp signal should not be ignored. In the region of $\Delta\dot{f}/\dot{f} \lesssim 0.1$, the LISA's distance determination accuracy is $\Delta D/D \sim 0.2\,(SNR/10)^{-1}$.

as $\Delta A \propto T_{obs}^{-1/2}$, $\Delta f \propto T_{obs}^{-3/2}$, $\Delta\dot{f} \propto T_{obs}^{-5/2}$, and $\Delta\Omega_{S,L} \propto SNR^{-1} \propto T_{obs}^{-1}$. This fact means that the cross correlation between the source's angular position $(\bar{\theta}_S, \bar{\phi}_S)$ and the other parameters $(A, f, \dot{f}, \phi_0, \bar{\theta}_L, \bar{\phi}_L)$ becomes very small for $T_{obs} \gtrsim 2$ yr. In other words, Fisher information matrix Γ_{ij} becomes diagonalized to the two parts which are the source angular position $(\bar{\theta}_S, \bar{\phi}_S)$ components and the other. We also find that the accuracy of the estimation does not strongly depend on the frequency except for the angular resolution $\Delta\Omega_S$. The angular position of the higher-frequency sources is determined from the periodic Doppler phase which is proportional to the frequency f (see Eq.(3)). Thus Fisher matrix is $\Gamma_{ij} \propto f^2$ for the $(\bar{\theta}_S, \bar{\phi}_S)$ components (see Eq.4) and $\Delta\Omega_S \propto f^{-2}$.

In Fig.2 we plot the contours of $\Delta\dot{f}/\dot{f}$ in the parameter space f and M_c for $T_{obs} = 10$ yr. In the region of $\Delta\dot{f}/\dot{f} \lesssim 1$, the parameter $\dot{f}$ should be included in the matured filtering, but the simple prescription $\dot{f} = 0$ would be better at $\Delta\dot{f}/\dot{f} \gtrsim 1$ since the expected signal would be completely buried in error. The chirp signal $\dot{f}$ is essential to determine the distance D. From the simple relation $A = 5\dot{f}/96\pi^2 f^3 D$, the estimation error for distance D is roughly evaluated as $\Delta D/D \simeq \Delta A/A + \Delta\dot{f}/\dot{f}$. So in the region of $\Delta\dot{f}/\dot{f} \lesssim 0.1$ the distance determination accuracy is $\Delta D/D \sim 0.2(SNR/10)^{-1}$ (see Fig.1).

3.2 Statistical Analysis

In this subsection we present statistical results for their various combinations at the asymptotic region $T_{obs} \gtrsim 2$yr. We have made 100 realizations of $\hat{n}$ and $\hat{L}$ that are distributed randomly on celestial spheres. Then we calculate the estimation errors Δf and $\Delta\dot{f}$ for each binaries normalized by $SNR = 10$ with $T_{obs} = 10$yr. We find that theses errors depend very weakly (less than 10% scatter) on the directions $\hat{n}$ and $\hat{L}$. We calculate their mean values and obtain results given in the following forms

$$\Delta f = 0.22\left(\frac{SNR}{10}\right)^{-1} T_{obs}^{-1}, \tag{7}$$

$$\Delta\dot{f} = 0.43\left(\frac{SNR}{10}\right)^{-1} T_{obs}^{-2}. \tag{8}$$

Note that these results do not depend on the frequency f and would be useful for quantitative analysis of quasi-monochromatic binaries with $T_{obs} \gtrsim 2$yr.

We have also studied the estimation errors $\Delta\Omega_S$, $\Delta\Omega_L$ and $\Delta A/A$. The distributions for the latter two have very large scatters. This is because the Fisher matrix elements relating to the orbital direction $\hat{L}$ become singular at the highly symmetric configuration $\hat{n} = \pm\hat{L}$ and the estimation of the amplitude A is closely related to the inclination. For majority of realizations with $|\hat{n}\cdot\hat{L}| \lesssim 0.8$ we have typically $\Delta A/A \simeq 0.2(SNR/10)^{-1}$. To determine the source direction $\hat{n}$ we can use the information of the Doppler phase in addition to the annual amplitude modulation caused by LISA's rotation. Thus the error $\Delta\Omega_S$ does not show such a bad behavior. For the above 100 realization at $f = 0.01$Hz with $SNR = 10$ and $T_{obs} = 10$yr we have $1.3\times10^{-4}\text{sr} \le \Delta\Omega_S \le 3.7\times10^{-3}\text{sr}$ and the mean value $\Delta\Omega_S = 7.1\times10^{-4}$. Therefore the following relation roughly gives the estimation error for the source direction with $T_{obs} \ge 2$yr

$$\Delta\Omega_S \sim 7.1\times10^{-4}\left(\frac{SNR}{10}\right)^{-2}\left(\frac{f}{10^{-2}\text{Hz}}\right)^{-2}\text{sr}, \tag{9}$$

at $f \gtrsim 2\times10^{-3}$Hz where the Doppler phase becomes more important than the annual amplitude due to the rotation of LISA.

4 Summary

We calculate LISA's measurement accuracy for the short-period binaries (10^{-4} Hz $\lesssim f \lesssim 10^{-2}$ Hz), including the effects of chirp signal $\dot{f}$ and the duration of observation T_{obs}. It turns out that the chirp signal should be included in the matured filtering at $f \gtrsim 2\times10^{-3}(M_c/1M_\odot)^{-5/11}(T_{obs}/10\text{yr})^{-6/11}$ Hz. The distance to the chirping binary is determined within $\sim 20\%$ $(SNR/10)^{-1}$ at best. We obtain the fitting formulae of the estimation errors for the source parameters (such as frequency f, chirp signal $\dot{f}$, amplitude A, angular position Ω_S and distance D) as a function of f and T_{obs}($\gtrsim$ 2 yr). We find that for $T_{obs} \gtrsim$ 2 yr the cross correlation between the angular position $(\bar{\theta}_S, \bar{\phi}_S)$ and the others become negligible. The estimation errors Δf and $\Delta\dot{f}$ are independent of the frequency f and do not strongly depend on the source's position and orientation.

References

[1] Bender, P.L. *et al.* , *LISA Pre-Phase A Report*, Second Edition, July 1998.

[2] Haehnelt, M.G., MNRAS, **269**, 199, (1994)

[3] Mironovskii, V. N. 1965, Soviet Astronomy, **9**, 752

[4] Evans, C. R., Iben, I. J., & Smarr, L. 1987, ApJ, **323**, 129

[5] Hils, D., Bender, P.L. & Webbink, R.F., ApJ, **369**, 271, (1991).

[6] Cutler, C., Phys. Rev. D **57**, 7089, (1998).

[7] Vecchino, A. & Cutler, C., in Folkner, W.M., editor, *Laser Interferometer Space Antenna, Second International LISA Symposium on the Detection and Observation of Gravitational Waves in Space*, AIP Conference Proceedings, Vol.456, p101, (1998).

[8] Moore, T.M. & Hellings, R.W., gr-qc/9910116, (1999).

[9] Hughes, S.A., astro-ph/018483, (2001).

[10] Schutz, B.F., Nature **323**, 310, (1986).

[11] Seto, N., Phys. Rev. Lett., **87**, 251101, (2001).

[12] Seto, N., submitted to MNRAS, (2002).

[13] Peters, P.C., Phys. Rev. **136**, B1224, (1964).

[14] Finn, L.S., Phys. Rev. D **46**, 5236, (1992).

Reconstruction of the initial power spectra from CMB anisotropy

Makoto Matsumiya,[1] Misao Sasaki,[2] Jun'ichi Yokoyama[3]

Department of Earth and Space Science, Graduate School of Science, Osaka University, Toyonaka, 560-0043, Japan

Abstract

We investigate the possibility of reconstructing the initial spectrum of density fluctuations from the cosmic microwave background (CMB) anisotropy. As a first step toward this program, we consider a spatially flat, CDM dominated universe. In this case, it is shown that, with a good accuracy, the initial spectrum satisfies a first order differential equation with the source determined by the CMB angular correlation function. The equation is found to contain singularities arising from zeros of the acoustic oscillations in the transfer functions. Nevertheless, we find these singularities are not fatal, and the equation can be solved nicely. We test our method by considering simple analytic forms for the transfer functions. We find the initial spectrum is reproduced within 5% accuracy even for a spectrum, that has a sharp spike.

1 Introduction

The cosmic microwave background (CMB) anisotropy provides us with a great deal of information of the primordial fluctuations, and it is considered to be a powerful tool for studying the early universe [1].

In most of previous investigations, when cosmological model parameters are estimated from the observational data by likelihood analysis, the initial spectrum is assumed to have a power-law shape [2]. It is true that a conventional slow-roll inflation model, that has now become a 'standard model', gives a power-law spectrum which is almost scale-invariant[3]. However, when analyzing the observed CMB anisotropy, it is much more desirable, and probably much healthier, to constrain the initial spectrum solely by observed data without any theoretical prejudices. For example, even within the context of inflationary cosmology, a variety of generation mechanisms for non-scale-invariant perturbations have been proposed [4]. In this connection, recently several authors have discussed extraction of non-power law features from the CMB observations [5], where the initial spectrum is allowed to have a piece-wise power-law shape.

We approach this issue in an entirely different way, namely, by formulating an inverse problem as faithful as possible. Such an approach will be eventually needed if we seriously want to constrain the initial power spectrum solely from observations of the CMB anisotropy. An approach to this inversion problem has been discussed recently [6].

As a first step, we consider a simple situation in which the transfer functions that relate the input power spectrum $P(k)$ of the gravitational potential to the output CMB angular correlation function $C(\theta)$ are given analytically. This is certainly a toy model. However, it has almost all the essential features a realistic model would have. In particular, unlike [6], our model takes account of not only the Sachs-Wolfe (SW) effect but also the Doppler effect . The latter, which gives rise to zero points in the transfer functions, is the main cause of the difficulty in this inversion problem.

The advantage of adopting this simple situation is that our method of inversion, which we shall develop below may be easily tested at various stages of calculations. Since our primary concern here is to formulate the inversion problem, we fix the cosmological parameters and do not study the dependence of $P(k)$ upon them.

[1] E-mail:matumiya@vega.ess.sci.osaka-u.ac.jp
[2] E-mail:misao@vega.ess.sci.osaka-u.ac.jp
[3] E-mail:yokoyama@vega.ess.sci.osaka-u.ac.jp

2 Basic Equations

Each Fourier mode of temperature perturbations, $\Theta(\eta, k)$, obeys the Boltzmann equation [7],

$$\dot{\Theta} + ik\mu(\Theta + \Psi) = -\dot{\Phi} + \dot{\tau}[\Theta_0 - \Theta - \frac{1}{10}\Theta_2 P_2(\mu) - i\mu V_b], \tag{1}$$

where the dot denotes a derivative with respect to the conformal time η, k is the comoving wave number, $\mu = k^{-1}\boldsymbol{k}\cdot\boldsymbol{\gamma}$, $\dot{\tau}$ is the differential Thomson optical depth and V_b is the bulk velocity of baryons. Ψ and Φ are the gauge-invariant Newtonian potential and spatial curvature perturbation, respectively[7].

Integrating Eq. (1), we obtain

$$(\Theta + \Psi)(\eta_0, k, \mu) = \int_0^{\eta_0} \left\{[\Theta_0 + \Psi - i\mu V_b]\mathcal{V}(\eta) + (\dot{\Psi} - \dot{\Phi})e^{-\tau(\eta)}\right\} e^{ik\mu(\eta-\eta_0)} d\eta, \tag{2}$$

where η_0 is the conformal time today and $\mathcal{V}(\eta)$ is the visibility function given by

$$\mathcal{V}(\eta) = \dot{\tau}(\eta)e^{-\tau(\eta)}; \quad \tau(\eta) = \int_\eta^{\eta_0} \dot{\tau}(\eta')d\eta'. \tag{3}$$

We have neglected the quadrupole term on the right hand side of Eq. (1) since its contribution is negligible in the tight coupling approximation. The visibility function has a sharp peak around the last scattering time η_* so that we assume that recombination occurs instantaneously at $\eta = \eta_*$. Then, the multipole moments of each k mode is approximately given by

$$\begin{aligned}\Theta_l(\eta_0, k) &= (\Theta_0 + \Psi)(\eta_*, k)(2l+1)j_l(kd) + \Theta_1(\eta_*, k)(2l+1)j_l'(kd) \\ &\quad +(2l+1)\int_{\eta_*}^{\eta_0} d\eta' \frac{\partial}{\partial\eta'}(\Psi(\eta', k) - \Phi(\eta', k))j_l(k\eta_0 - k\eta'),\end{aligned} \tag{4}$$

where $d = \eta_0 - \eta_*$ is a conformal distance from the present epoch to the last scattering surface (LSS).

Conventionally, C_l is expressed as

$$\frac{2l+1}{4\pi}C_l = \frac{1}{2\pi^2}\int_0^\infty dk\, k^2 \frac{|\Theta_l(\eta_0, k)|^2}{2l+1}. \tag{5}$$

From Eqs. (4) and (5), we find

$$C_l = \frac{2}{\pi}\int_0^\infty dk\, k^2 \left[(\Theta_0 + \Psi)(\eta_*)j_l(kd) + \Theta_1(\eta_*)j_l'(kd)\right]^2. \tag{6}$$

The angular correlation function is calculated from Eq. (6). Here, we define r by

$$r = 2d\sin\frac{\theta}{2}. \tag{7}$$

This is the spatial distance between two points on the last scattering surface which are observed with the angular separation θ. Since the thickness of the LSS is neglected in Eq. (4), there is a one-to-one correspondence between the observed temperature anisotropy and the perturbation variables on the LSS. Using the relation,

$$\sum_{l=0}^{\infty}(2l+1)P_l(\cos\theta)j_l^2(kd) = \frac{\sin kr}{kr}, \tag{8}$$

the angular correlation function $C(r)$ is given by

$$\begin{aligned}C(r) &= \frac{1}{2\pi^2}\int_0^\infty dk\, k^2 \left[|\Theta_0 + \Psi|^2 \frac{\sin kr}{kr} + \frac{|\Theta_1|^2}{k^2r^2}\left(\frac{\sin kr}{kr} - \cos kr\right)\right. \\ &\quad +\frac{(\Theta_0 + \Psi)\Theta_1}{kd}\left(-\frac{\sin kr}{kr} + \cos kr\right) \\ &\quad \left.+\frac{|\Theta_1|^2}{4k^2d^2}\left(\frac{\sin kr}{kr} - \cos kr - kr\sin kr\right)\right].\end{aligned} \tag{9}$$

We can generally express the relation between $C(r)$ and the initial spectrum as

$$C(r) = \int_0^\infty K(k,r)P(k)dk, \tag{10}$$

where we normalize the initial condition in terms of the curvature perturbation $\Phi(\eta = 0, k)$ and define $P(k) \equiv \langle|\Phi(0,k)|^2\rangle$.

3 Inversion Method

In the above discussion, we have tacitly assumed that r runs from zero to infinity. In reality, however, r is bounded in the finite range $0 \leq r \leq 2d$. Furthermore, it is observationally impossible to determine $C(r)$ on large scales due to the statistical ambiguity, *i.e.*, the cosmic variance. However, the scales which we are interested in are $r \ll d$ and it is expected that modes with $k \geq 1/d$ have little effect on these scales. We therefore neglect the terms proportional to $1/d$ and $1/d^2$ in Eq. (9). In this limit, after a little calculation, we have

$$\tilde{C}(r) \equiv 3rC(r) + r^2C'(r) = \frac{1}{2\pi^2}\int_0^\infty dk\, P(k)\left\{F(k)k^2r\cos kr + (2F(k) + G(k))k\sin kr\right\}. \tag{11}$$

where we have defined

$$\begin{aligned} F(k)P(k) &= |(\Theta_0 + \Psi)(k)|^2, \\ G(k)P(k) &= |\Theta_1(k)|^2, \end{aligned} \tag{12}$$

for notational simplicity. Integrating by parts and employing the Fourier sine formula, we obtain

$$-Fk^2P' + (-F'k + G)kP = 4\pi\int_0^\infty \tilde{C}(r)\sin krdr\,. \tag{13}$$

This is a first order differential equation. We discuss a method for solving this equation in the rest of this section.

We now give the expressions for $F(k)$ and $G(k)$ explicitly in order to examine the properties of Eq. (13), and to verify if thus obtained solution correctly reproduces the original spectrum. For a given model, $F(k)$ and $G(k)$ are determined by the coupled Einstein-fluid equations which are to be solved numerically. However, in order to understand the property of Eq. (13) and to establish a method which we can apply to general cases, we analyse a toy model in which $F(k)$ and $G(k)$ are given analytically.

The solutions are given by

$$\begin{aligned} [\Theta_0 + \Psi](\eta) &= \frac{1}{3}\Phi(0)\cos(kc_s\eta), \\ \Theta_1(\eta) &= c_s\Phi(0)\sin(kc_s\eta), \end{aligned} \tag{14}$$

where $c_s = 1/\sqrt{3}$ and we take the adiabatic initial condition as $\Theta_0(0) = \Psi(0)/3 = -\Phi(0)/3$ and $\Theta_1(0) = 0$. From Eq. (13), we obtain

$$-\frac{1}{9}\cos^2 kr_*k^2P' + \left(\frac{2}{9}kr_*\cos kr_*\sin kr_* + \frac{1}{3}\sin^2 kr_*\right)kP = S(k)\,, \tag{15}$$

where $r_* = c_s\eta_*$ and

$$S(k) = 4\pi\int_0^\infty \tilde{C}(r)\sin kr\,dr\,. \tag{16}$$

Now let us describe our method. Eq. (15) has singularities at $kr_* = (n+1/2)\pi$ which cause difficulties when we solve it numerically. We can, however, determine the values of $P(k)$ at these singularities if we

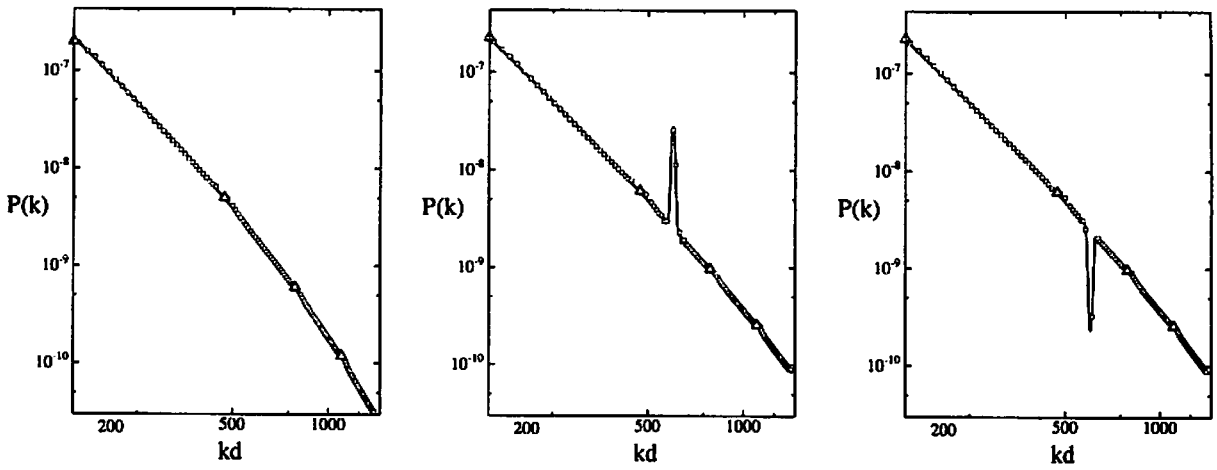

Figure 1: The original spectra (the solid curves) and the reconstructed spectra (the boxes and triangles). The left panel shows the case of the double power-law spectrum given by Eq. (18) and the middle and the right panels show the single power-law spectra with a sharp peak ($s = +1$) and a dip ($s = -1$), respectively, given by Eq. (19). The triangles show the locations of the singular points. We stopped the numerical integrations in the vicinity of the singularities when the relative error exceeded 10%.

assume that the derivative of $P(k)$ is finite. Then the first term on the left-hand side of Eq. (15) vanishes at $kr_* = (n + \frac{1}{2})\pi$, and the values of $P(k)$ at these singularities are given by

$$P\left[k = \left(n + \frac{1}{2}\right)\frac{\pi}{r_*}\right] = \frac{3r_*}{(n + \frac{1}{2})\pi} S\left[k = \left(n + \frac{1}{2}\right)\frac{\pi}{r_*}\right]. \tag{17}$$

Once these values are given, we can solve Eq. (15) by expanding it around the singularities. We search the true solution which connect the adjacent singularities using the shooting method. We solve the equation until the 5th singularity, $kd = 450\pi$, for the following two cases of the original spectra:

$$P(k) = \frac{(kd)^{-3}}{1 + (k/k_s)^p} \exp(-k/k_0), \tag{18}$$

$$P(k) = (kd)^{-3}\left[1 + A\exp\left\{-\frac{(kd - k_p d)^2}{\sigma}\right\}\right]^s \exp(-k/k_0)\,; \quad s = \pm 1\,. \tag{19}$$

The first one is a double power-law spectrum and the second is a single power-law spectrum with a spiky structure, either with a peak ($s = +1$) or a dip ($s = -1$). The results for the choice of the parameters as $p = 2$, $A = 10$, $k_p d = 600$, $\sigma = 10$ and $k_0 d = 1000$ are shown in Fig. 1. We find our method reproduces the original spectra with a good accuracy. In particular, even if the spectrum has a sharp peak or a dip, we can resolve such a local structure using this method. The numerical solution diverges as it approaches the singularities (indicated by the triangles), but the relative error except for the regions close to the singularities is below 5%.

Finally, it is worthwhile to comment that the presence of the singularities in the differential equation (13) may be regarded as an advantage, since the values of $P(k)$ at the singularities can be estimated without solving the differential equation. In particular, if there is a good reason to believe that the spectrum should be a smoothly varying function, a qualitative feature of the spectrum can be obtained at once. For example, in the case of the double power-law spectrum (18), one can see that the original spectrum can be approximately recovered by simply interpolating between the adjacent triangles shown in Fig. 1.

4 Conclusion

We have considered the problem of reconstructing the initial power spectrum of metric perturbation $P(k)$ from C_l data. As a first step, we have investigated a simple case, namely, the Einstein-de Sitter universe with negligible baryons and negligible thickness of the LSS. In this toy model, the relation between the initial spectrum and the angular correlation function is expressed in terms of an integral equation. We have shown that this equation can be transformed to a first order differential equation for $P(k)$. The resulting equation is found to have singularities that comé from the acoustic oscillations of photons, hence their presence is inevitable in any cosmological models not restricted to our simple model. Fortunately, however, the presence of these singularities turns out to be not only harmless but rather advantageous. We have found our method can reproduce the original spectrum with a good accuracy even for a spectrum with a sharp, spiky structure.

The method presented here is applicable only to the Einstein-de Sitter universe in which the ISW effect is negligible. The ISW effect gives an important contribution even in a flat universe model if the cosmological constant is present. Such a model, called the ΛCDM model is preferred by recent observations[8]. Our next step is to include the ISW effect in our method which is currently under study.

References

[1] M. J. White, D. Scott and J. Silk, Ann. Rev. Astron. Astrophys. **32**, 319 (1994); W. Hu, N. Sugiyama and J. Silk, Nature **386**, 37 (1997).

[2] J. R. Bond *et al.* Phys. Rev. Lett. **72**, 13 (1994); L. Knox, Phys. Rev. D **52**, 4307 (1995); G. Jungman, M. Kamionkowski, A. Kosowski and D. N. Spergel, Phys. Rev. D **54**, 1332 (1995); J. R. Bond, G. Efstathiou and M. Tegmark, Mon. Not. R. Astron. Soc. **291**, L33 (1997); D. J. Eisenstein, W. Hu and M. Tegmark, Astrophys. J. **518**, 2 (1999).

[3] S. W. Hawking, Phys. Lett. **115B**, 295 (1982); A. A. Starobinsky, *ibid* **117B**, 175 (1982); A. H. Guth and S-Y. Pi, Phys. Rev. Lett. **49**, 1110 (1982).

[4] A. D. Linde, Phys. Lett. **158B**, 375 (1985); L. A. Kofman and A. D. Linde, Nucl. Phys. **B282**, 555 (1987); J. Silk and M. S. Turner, Phys. Rev. D **35**, 419 (1987); H. M. Hodges and G. R. Blumenthal, Phys. Rev. D. **42**, 3329 (1990); J. Yokoyama and Y. Suto, Astrophys. J. **379**, 427 (1991); M. Sasaki and J. Yokoyama, Phys. Rev. **744**, 970 (1991); A. A. Starobinsky, JETP Lett. **55**, 489 (1992); [Pisma Zh. Eksp. Teor. Fiz. **55** (1992) 477]; J. Yokoyama, Astron. Astrophys. **318**, 673 (1997); J. Yokoyama, Phys. Rev. D **58**, 083510 (1998);**59**, 107303 (1999); S. M. Leach and A. R. Liddle, Phys. Rev. D **63**, 043508 (2001) [arXiv:astro-ph/0010082]; S. M. Leach, M. Sasaki, D. Wands and A. R. Liddle, Phys. Rev. D **64**, 023512 (2001) [arXiv:astro-ph/0101406].

[5] T. Souradeep et. al., astro-ph/9802262; Y. Wang, D. N. Spergel and M. A. Strauss, astro-ph/9812291; Y. Wang, D. N. Spergel and M. A. Strauss, Astrophys. J. **510**, 20 (1999); S. Hannestad, Phys. Rev. D **63**, 043009 (2001).

[6] A. Berera and P. A. Martin, Inverse Problems **15**, 1393 (1999).

[7] H. Kodama and M. Sasaki, Prog. Theor. Phys. Supp. **78**, 1 (1984); H. Kodama and M. Sasaki, Int. J. Mod. Phys. A **1**, 265 (1986); H. Kodama and M. Sasaki, Int. J. Mod. Phys. A **2**, 491 (1987).

[8] A. G. Riess *et al.* [Supernova Search Team Collaboration], Astron. J. **116**, 1009 (1998) [arXiv:astro-ph/9805201]; S. Perlmutter *et al.* [Supernova Cosmology Project Collaboration], Astrophys. J. **517**, 565 (1999) [arXiv:astro-ph/9812133].

A multi-component model for galaxy formation and evolution

Benoit Semelin, [1]

Department of Physics, Waseda University, Shinjuku, Tokyo, 169-8555, Japan

Françoise Combes,[2]

DEMIRM, Observatoire de Paris, 77 av Denfert-Rochereau, 75014, Paris, France

Abstract

Disk galaxies are highly complex systems where gas, stars and dark matter interact through many processes: star formation, stellar wind, supernovae explosions, and more. We present a numerical model in which the warm and cold gas components follow different dynamics. The diffuse warm ($T > 10^4$ K) gas is treated as a fluid through a SPH code, while the cold fragmented gas (i.e. the molecular clouds), is treated with a sticky particle scheme. The following processes are included: heating/cooling of the gas, star formation, supernovae feedback, stellar massloss and metal enrichment. We compute the formation and evolution of Milky Way type galaxies over 2 Gyr. We obtain exponential density profiles for the baryonic components, and study the sensitivity of the baryonic matter composition to variations of the main physical parameters.

1 Introduction

The dynamics of galactic disks is the sum of many contributions. Understanding and accounting for the most important of these contributions is a necessary step toward building consistent numerical models, able to follow the formation and evolution of galaxies.

The main ingredient is gravity, which drives the dynamics both at large scale (global rotation equilibrium) and at smaller scales (spiral arms, formation of cold gas clumps, etc...). This part of the dynamics is well handled in grid simulations by FFT method, and in N-body simulations by the treecode method [1]. Both methods compute gravity at a cost growing as $\sim N \ln(N)$ where N is the number of dynamic degrees of liberty. However, gravity alone is not sufficient to model the evolution of the interstellar medium (ISM), which is essential to the dynamics of spiral galaxies. The ISM is a dissipative system which behaves as a fluid to some extend. Consequently, it is usual to introduce it in simulations as a continuous fluid in Eulerian grid codes or through the SPH algorithm in N-body codes [2].

There has also been a steady effort to include the most relevant physical processes linking the different matter components: dark matter, stars and gas. First, and foremost for the gas dynamics, are the heating and cooling processes. Heating comes in from UV radiations emitted by galactic and extragalactic sources [3]. Radiative cooling of the gas arises from many microscopic phenomena, and is usually quantified using values from interpolation tables (e.g. [4]). Star formation comes next when the gas has cooled down into molecular clouds. It is usually treated using local physical criteria such as Jeans instability (e.g. [5]), or/and a local Schmidt law [6]. The effect of supernovae thermal and kinetic energy input in the gas has also been studied ([7], [8]). The stellar reinjection of gas in the ISM through winds or supernovae explosions has been included too ([9], [10]), showing that the instantaneous recycling approximation used to compute the evolution of the metallicity can be improved on.

[1] E-mail:semelin@gravity.phys.waseda.ac.jp
[2] E-mail:Francoise.Combes@obspm.fr

To model the gas has a continuous fluid, is not an obvious choice. Although it appears reasonable in the case of the diffuse warm gas ($T > 10^4$K), it is not so for the cold fragmented state found in molecular clouds. Indeed simulations of galactic disks usually have a mass resolution of $10^5 - 10^6 M_\odot$, and the cold gas particles represent large portions of giant molecular clouds, which are actually fragmented and self-gravitating. This is far from the ideal gas description of SPH codes. Moreover these particle-clouds behave as ballistic particles encountering inelastic collisions with other clouds, rather than as a continuous fluid. For these reasons, it appears important implement different dynamics for the warm diffuse gas and the cold fragmented gas. Some work in this direction has been done by Noguchi [11], using a sticky particle scheme, or by Andersen & Burkert [12], who have developed a collisional fluid model for the cold gas.

In this work, we present a N-body numerical model for galaxy formation and evolution which takes into account dark matter, stars, and two gas components with different dynamics, the warm and the cold gas. We implement all the physical processes mentioned above, including a realistic massloss scheme. The model is applied to the formation of a Milky Way type galaxy from a pure gas disk.

2 Some details on the implementation

Four types of particles are included in the simulation: dark matter, star, warm gas (SPH particles) and cold gas (sticky particles). The gravity contribution is computed in a tree algorithm with a $\theta = 0.8$ opening criterion. The SPH hydrodynamics is computed for the ideal gas equation of state:

$$P = (\gamma - 1)\rho u \qquad \left(\gamma = \frac{5}{3}\right)$$

We use a spline function for the kernel [13] and make an arithmetic average of the adaptative smoothing lengths to compute the SPH quantities. We follow the time update scheme of smoothing lengths proposed by Hernquist & Katz [2] and we use the viscosity described in [14].

Radiative cooling is implemented by interpolation in the table from Sutherland & Dopita [4]. We also include the most basic model for the UV heating: a constant value of $\sim 10^{-24}$ erg s^{-1}, which mainly accounts for extra-galactic sources. It has been noted by many authors (e.g. [15]) that in dense region, the cooling time of the gas can become much shorter than the dynamical cooling time. Moreover, the cooling factor Λ changes by several orders of magnitude in the temperature range 10 000 K - 20 000 K. To obtain a stable integration of the thermal behavior, we first use an integral scheme comparable to Thomas & Couchman to compute Λ. Then, if the local internal energy variation within one time step is larger than 1/4 of the current value, we damp it to 1/4 (a similar method is used by Weil et al. [16]). When warm gas temperature falls down to 11 000K, the chosen temperature for the transition, the particle is transformed into a cold gas particle.

Star formation occurs in the cold gas phase only, without further conditions. We use a local Schmidt law:

$$\frac{d\rho_{\rm star}}{dt} = C\ \rho_{\rm gas}^n, \qquad (\text{ n=1.5 in ref. model}).$$

The constant C, which depends on the star formation efficiency, is adjusted to produce physical overall star formation rates. Supernovae feedback is taken into consideration. We use a typical lower estimate of 10^{48} erg per solar mass of formed star. The thermal energy is deposited on a few (2 or 3) neighbors. Thermal damping prevents it to be instantaneously radiated. A small kinetic part (a few %) is also imparted to all the neighboring gas particles.

Stellar winds and supernovae explosions return over 40 % of the star mass to the ISM over a few Gyr. A continuous stellar massloss rate was proposed by Jungwiert et al. [10], based on integration over usual Initial Mass Functions. We implement a similar simple version:

$$\frac{dM_{\rm gas}}{dt} = M_{\rm star}\frac{c}{(t - t_{\rm birth} + T_0)},$$

with c=0.055 and $T = 5$ Myr. The gas released by the stars is enriched using a constant value for the yield $y = 0.02$.

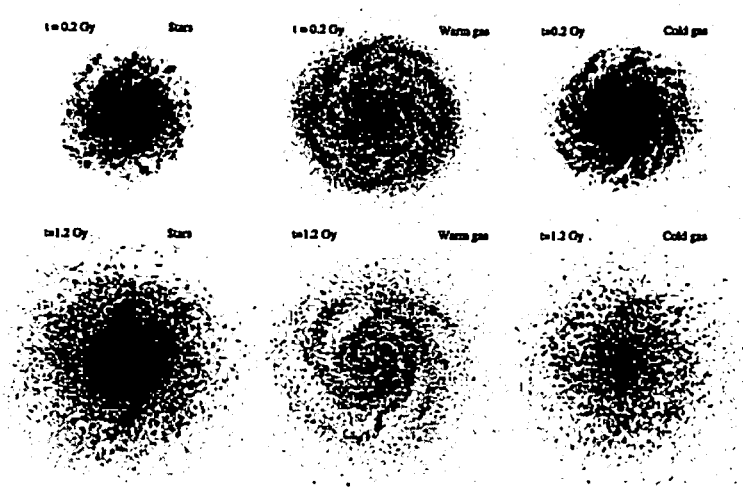

Fig 1: Reference simulation. Configuration of the three baryonic phases after 200 Myr (top) and after 1.2 Gyr (bottom).

3 Reference simulation

All simulations start from a gaseous disk within a dark matter halo. The dark matter is distributed in a Plummer sphere with a typical radius of r_{dm} = 5 Kpc. The total mass of the halo is $M_{dm} = 1.7\,10^{11} M_{\odot}$. The distribution is truncated at 5 r_{dm}.

Initially, all the baryonic matter is in the form of warm gas at a temperature of 15000 K. It is distributed within a Miyamoto-Nagai disk [17], with typical radius r_{bm} = 5 Kpc, and typical thickness z_{bm} = 0.3 Kpc. The total mass of the baryonic matter is $M_{bm} = 5.7\,10^{10} M_{\odot}$. This choice results in a stable disk. The angular speed is computed to provided rotational support and the velocity dispersions have the usual relations to the surface density and epicyclic frequency. Our setting produces a Toomre stability criterion Q = 5 in the center of the disk and Q = 2 at the edge. In all the models we use 10^4 dark matter particles and 510^4 baryonic particles. The softening of the gravity for baryonic particles is 30 pc and 300 pc for dark matter particles. We compute the evolution over 2 Gyr with a time step of 1 Myr.

Fig. 1 presents a face-on view of the three components at 0.2 Gyr and 1.2 Gyr. An interesting feature is that clusters of stars form at the edge of the disk in the early evolution, and later merge in the central part. This phenomenon is present for a large range of parameters and, as noted by Noguchi [11], may be the mechanism of the bulge formation. Usual features such as spiral arms are also present. We observe a strong depletion of the gas phase after 1.2 Gyr. This is quantified in Fig 2. The thermal equilibrium between warm and hot gas is almost instantaneously reached. Then, both phases are depleted through star formation. The evolution slows down after the first Gyr. After 2 Gyr the total gas content is $\sim$ 20 %. In Fig. 3, the surface density profiles of the baryonic components are plotted. The stellar disk profile is exponential with a typical radius of 2 Kpc. The warm gas disk is also exponential but with a larger typical radius of 10 Kpc. Cold gas falls in between. The rotation curve (not plotted), is rather flat between 5 Kpc and 15 Kpc, at a value of 250 km s^{-1}. This set of diagnoses suggests a rather realistic galactic disk.

4 Composition of the baryonic matter: effect of various processes

We have made several runs for the simulation, changing some of the most relevant parameters for the mass equilibrium between the baryonic phases. The characteristics of each run and corresponding composition of the baryonic matter are presented in the table.

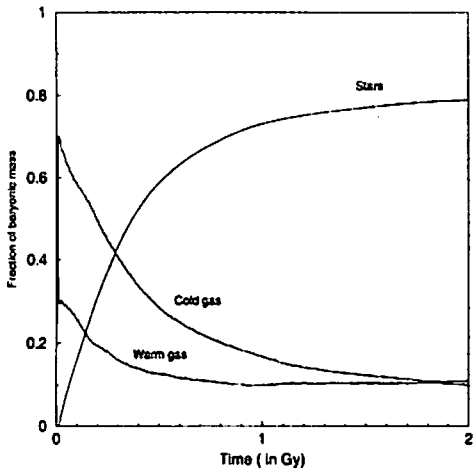

Fig 2: Evolution of the composition of the baryonic matter. The mass fraction of each of the three components is plotted against time.

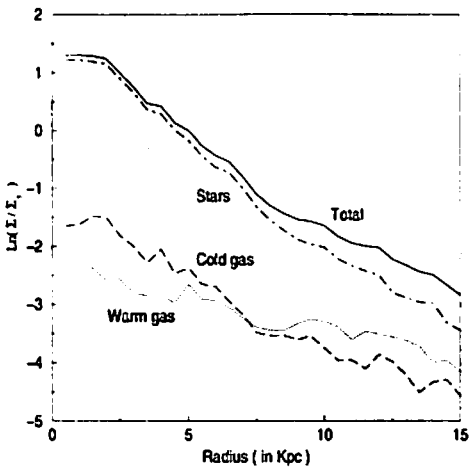

Fig 3: Surface density profiles of the various baryonic components of the disk as functions of the radius. The density scale is logarithmic. The profile are roughly exponential with 10 kpc typical radius for the warm gas, and 2 kpc for the stars.

Model	At 0.5 Gyr			At 2. Gyr		
	Stars	Warm gas	Cold Gas	Stars	Warm gas	Cold gas
1: Reference model	58.7 %	12.5 %	28.8 %	78.9 %	10.9 %	10.2 %
2: Schmidt law n=1	53.7 %	13.3 %	33 %	84.8 %	10.3 %	4.9 %
3: No stellar massloss	65.4 %	11.8 %	22.8 %	86.2 %	8.7 %	5.1 %
4: No SN feedback	58 %	7.6 %	34.4 %	77.5 %	4.9 %	17.6 %
5: Thermal SN feedback	61.2 %	11.3 %	27.5 %	79.5 %	10.4 %	10.1 %
6: High SN feedback	61.4 %	13.2 %	25.4 %	78.5 %	11.2 %	10.3 %

The effect of changing the index from 1.5 to 1 in the Schmidt law is the expected one. Initially, when the gas is dense, the star formation rate is smaller, but it catches up later when the gas density decreases, and the final amount of star formed is larger. The effect of switching off the stellar massloss, which transfers matter from stars to hot gas is more unexpected: the cold gas phase gets depleted. Indeed, the different density dependence of the heating and cooling processes actually creates a density threshold ρ_c below which the warm gas stops cooling. The warm gas density is close ρ_c after 0.5 Gyr in the reference simulation, this is why it stops decreasing (see Fig 2.). Stopping the input from stellar massloss does not affect the threshold; warm gas settles at ρ_c and the transfer to the cold gas stops. Since cold gas keeps forming star, it is soon depleted. On the other hand, the three runs with varying feedback from supernovae explosions show that thermal feedback, which heats up cold gas into warm gas, is actually able to keep the warm gas density somewhat above the critical density, as we can deduce from the smaller warm gas mass at t= 2 Gyr when no feedback is present.

5 Conclusions

We have presented a numerical model for disk galaxy formation which includes several components with different dynamics: dark matter and stars follow collisionless gravitational dynamics, warm gas evolves as a dissipative fluid (SPH method), and cold gas is treated with collisional cloud-particles (sticky particle scheme). Heating, cooling, star formation, SN feedback and stellar massloss are taken into account. We have computed the evolution over 2 Gyr of a typical spiral galaxy, starting from a 100 % warm gas disk. The model produces reasonable and stable values for such properties as baryonic mass composition,

surface density profile, or rotation curve. The influence of several physical processes on the baryonic matter composition is studied. The mass composition responds to these processes without showing strong instability.

Complementary studies prove that intergalactic gas accretion is needed to produce a star formation rate that does not decrease too strongly with time, compared with observations. Our aim in future works is to include the accretion consistently in our model.

References

[1] Barnes, J. E. & Hut, P. 1986, Nature, 324

[2] Hernquist, L., & Katz, N. 1989, ApJS, 70, 419

[3] Gerritsen, J. P. E., & Icke, V. 1997, A&A, 325, 972

[4] Sutherland, R. S., & Dopita, M. A. 1993, ApJS, 88, 253

[5] Steinmetz M., & Muller, E. 1994, A&A, 281, L97

[6] Katz, N. 1992, ApJ, 391, 502

[7] Mihos, J. C., & Hernquist, L. 1994, ApJ, 437, 611

[8] Thacker, R. J., & Couchman, H. M. P. 2000, ApJ, 545, 728

[9] Lia, C., Portinari, L., and Carrora, G. 2001, to appear in MNRAS, astro-ph/0111084

[10] Jungwiert, B., Combes, F., & Palous, J. 2001, A&A, 376, 85

[11] Noguchi, M. 1999, ApJ, 514, 77

[12] Andersen, R.-P., & Burkert, A. 2000, ApJ, 531, 296

[13] Monaghan, J. J., & Latanzio, J. C. 1985, A&A, 149, 135

[14] Monaghan, J. J. 1992. Ann. Rev. A&A, 30, 543

[15] Thomas, P. A., & Couchman, H. M. P. 1992, MNRAS, 257, 11

[16] Weil, M. L., Eke, V. R.,& Efstathiou, G. 1998, MNRAS, 300, 773

[17] Miyamoto, M., & Nagai, R. 1975, Publ. Astron. Soc. Japan, 27, 533

Inhomogeneities in Newtonian Cosmology and its Backreaction to the Evolution of the Universe

Takayuki Tatekawa,[1] Momoko Suda,[2] Kei-ichi Maeda,[3]

Department of Physics, Waseda University, Shinjuku, Tokyo, 169-8555, Japan

Hiroto Kubotani[4]

Faculty of Engineering, Kanagawa University, Yokohama, Kanagawa, 221-8686, Japan

Abstract

We study an effect of inhomogeneity of density distribution of the Universe. We propose a new Lagrangian perturbation theory with a backreaction effect by inhomogeneity. The inhomogeneity affects the expansion rate in a local domain and its own growing rate. We numerically analyze a one-dimensional plane-symmetric model, and calculate the probability distribution functions (PDFs) of several observed variables to discuss those statistical properties.

1 Introduction

The present Universe shows a variety of structures. How such a structure is formed in the evolution of the Universe? One of the most plausible explanations is that the nonlinear dynamics of a self-gravitating system provides such a scale-free structure during the evolution of the Universe. As for a perturbation approach, however, it is just an approximation and will break down in a nonlinear regime, although the Lagrangian approach would be better if we are interested in density perturbations. This is just because a density fluctuation δ and a peculiar velocity $\mathbf{v}$ are perturbed quantities in the Eulerian approach[1], while a displacement of particles from uniform distribution is assumed to be small in the Lagrangian approach[2, 3]. The Lagrangian approach is confirmed to be better than the Eulerian approach by comparison of exact solutions in several cases. Therefore, we will adopt the Lagrangian approximation in this paper and discuss about how to improve it.

In the standard approach of Newtonian cosmology, the global cosmological parameters such as Hubble expansion rate and mean density are given first by a solution of the Einstein equations, i.e. the so-called Friedmann-Robertson-Walker (FRW) universe, which is an isotropic and homogeneous spacetime. According to observation, however, a local structure in the Universe is definitely not homogeneous and isotropic. In the standard approach, the density averaged over the whole space (or a horizon scale) is assumed to be the energy density of the FRW spacetime. However, here the problems of how to average inhomogeneous matter fluid and how to define an averaged isotropic and homogeneous spacetime are arisen. We discuss averaging procedure in local domain, which is smaller than Horizon scale, relativistic effect may not be so important. Therefore in this paper, in order to avoid such a difficulty, we discuss only an averaging procedure in the Newtonian framework.

Proposing a averaging procedure, which is defined by spatial average of physical quantities, Buchert and Ehlers lead the averaged Raychaudhuri's equation[4]. The equation describes how the averaged expansion rate of domain with a finite volume evolves. This equation has an additional term, which we call a 'backreaction term' of inhomogeneities on averaged expansion. Then, Buchert, Kerscher, and Sicka estimated the backreaction term using the conventional Lagrangian perturbation approach[5]. They first

[1] E-mail:tatekawa@gravity.phys.waseda.ac.jp
[2] E-mail:suda@gravity.phys.waseda.ac.jp
[3] E-mail:maeda@gravity.phys.waseda.ac.jp
[4] E-mail:kubotani@cpsun3.b6.kanagawa-u.ac.jp

consider density perturbations in Einstein-de Sitter (E-dS) Universe, then calculated the backreaction term and solved the averaged Raychaudhuri's equation. They showed difference between a cosmological parameter such as Hubble expansion rate in their averaged model and that of the E-dS model. Although they included a backreaction term to estimate the averaged variables in a local domain, they used the perturbed quantities from the E-dS Universe. In other words, they have not take into account a backreaction on the evolution of density perturbations.

Here we improve their approach, i.e. we include a backreaction effect to averaged expansion rate and solve the averaged Raychaudhuri's equation (the generalized Friedmann's equation) with evolution equation of perturbations in the averaged domain [6]. In an averaged domain, the averaged density is either higher or lower than that of the E-dS universe. This difference will change the evolution of density perturbations. In fact, if the domain is overdense, growth rate of perturbations behaves as that in the closed universe, While, if it is underdense, it is just like a solution in the open universe.

2 Averaging of inhomogeneity

2.1 The generalized Friedmann equation

In the Newtonian cosmology, the expansion of a domain is influenced by inhomogeneity inside the domain. Such an effect may be evaluated by spatial integration of field variables in the Lagrangian domain, which evolves with matter fluid. Hence in this paper we study fields averaged over a simply-connected spatial Lagrangian domain $\mathcal{D}$ at time t, which evolved out of the initial domain $\mathcal{D}_i$ at time t_i. The locally averaged scale factor $a_{\mathcal{D}}$, depending on the content, shape and location of the domain $\mathcal{D}$, is defined by the volume of domain $V_{\mathcal{D}}(t) = |\mathcal{D}|$ and its initial volume $V_{\mathcal{D}_i} = |\mathcal{D}_i|$ as

$$a_{\mathcal{D}}(t) \equiv \left(\frac{V_{\mathcal{D}}(t)}{V_{\mathcal{D}_i}}\right)^{1/3} . \tag{1}$$

We define a spatial averaging for any rank tensor field $\mathcal{A} = \{A_{ij\cdots}(\mathbf{r},t)\}$ by the volume integral normalized by the volume of the domain as

$$\langle \mathcal{A} \rangle_{\mathcal{D}}(t) \equiv \frac{1}{V_{\mathcal{D}}(t)} \int_{\mathcal{D}} \mathrm{d}^3 r \, \mathcal{A}(\mathbf{r},t) . \tag{2}$$

Using this averaging, we can derive the generalized Friedmann equation[4]:

$$3\frac{\ddot{a}_{\mathcal{D}}}{a_{\mathcal{D}}} + 4\pi G \langle \rho \rangle_{\mathcal{D}} - \Lambda = Q_{\mathcal{D}} , \tag{3}$$

where $Q_{\mathcal{D}}$ means backreaction term.

$$Q_{\mathcal{D}} \equiv \frac{2}{3}\left(\langle \theta^2 \rangle_{\mathcal{D}} - \langle \theta \rangle_{\mathcal{D}}^2\right) + 2\left(\langle \omega^2 \rangle_{\mathcal{D}} - \langle \sigma^2 \rangle_{\mathcal{D}}\right) \tag{4}$$

On the other hand, we also derive the consistent equations for the Lagrangian perturbations with the backreaction term $Q_{\mathcal{D}}$.

$$\nabla_{\mathbf{x}_b} \cdot \left(\ddot{\mathbf{S}}_b + 2\frac{\dot{a}_b}{a_b}\dot{\mathbf{S}}_b\right) = -4\pi G\rho_b(J_b^{-1} - 1) - Q_b . \tag{5}$$

$$\nabla_{\mathbf{x}_b} \times \left(\ddot{\mathbf{S}}_b + 2\frac{\dot{a}_b}{a_b}\dot{\mathbf{S}}_b\right) = 0 , \tag{6}$$

where S means Lagrangian displacement vector.

3 Effect of inhomogeneity

Here, we study a simple model to show new aspect in our approach. We assume a plane-symmetric 1-dimensional model. The Lagrangian perturbation is given by

$$\nabla_q \psi = \mathrm{S(q)} = b(t)(s(q_1), 0, 0) \, . \tag{7}$$

In the conventional Lagrangian approximation, ZA gives an exact solution in a plane-symmetric case. However, it does not take into account a backreaction effect of inhomogeneity on the Hubble expansion. Since our approach includes the backreaction effect, we will analyze this simple one-dimensional model and compare our results with those by ZA. We also look at a difference of the backreaction term estimated by the conventional Lagrangian approach [5].

As for initial conditions, we adopt a power law spectrum with the index $n = 1$:

$$P_i(k) \propto k \, . \tag{8}$$

We also introduce a cutoff at small scale, which wave number is $k_{cut} = 1024 k_0$, where $k_0 = 2\pi/L$. We set that the initial time is $a = 1$. Then the amplitude of fluctuation is chosen so that the first shell-crossing occurs at $a \simeq 1000$. The number of grids is $N = 2^{16}$ and we use a periodic boundary condition. We take an ensemble average over 500 samples, which initial conditions are given by random Gaussian. In our approach, since we do not know where we are living, we study its statistical properties. In particular, we will see the scale dependence of the averaged variables and the probability distribution of the Hubble parameter, deceleration parameter, and pair-wise velocity.

3.1 Hubble parameter

First we analyze the expansion rate of local domain. If we fix the Hubble parameter H_0 by local observation in a domain $\mathcal{D}$, the most probable value of H_0 is given by the averaged expansion rate of the domain, which is $\langle\theta\rangle_{\mathcal{D}}/3$. We solve Eq. (3) for $a_{\mathcal{D}}$ with a backreaction due to inhomogeneity. If we are living in an underdense region on average, the expansion rate will be faster than the Hubble one for the whole universe. While, if we stay in an overdense region, the rate will be slower than the global Hubble one. If our domain is small, the deviation from H_0 gets large. For example, the dispersion of the Hubble parameter is about 1.2 % for the $l = 128$-grid domain, while 0.66 % for the$l = 256$-grid domain. The dispersion of our model is consistent with the result by Shi and Turner[7].

3.2 Density fluctuation

Next we show the PDF of density fluctuations. In the Eulerian linear approximation, if initial data is given by random Gaussian distribution, the PDF of density fluctuations will remain its Gaussian form during evolution. On the other hand, in the Lagrangian approximation, there appears a nonlinear effect. In fact, Kofman et al shows that the PDF approaches to a log-normal function rather than a Gaussian function in the cases of the Lagrangian approximation[9] and N-body simulation[8].

Here we analyze the PDF of density fluctuations using our approximation. The results are shown in Fig.1. From comparison with the result of ZA, the void region (i.e. an underdense region; $\delta < 0$) is found in higher probability in our approximation. Especially, if the size of a domain is smaller, the difference gets larger. On the other hand, the probability to find an overdense region ($\delta > 0$) decreases in our approximation.

The reason is very simple: During evolution, an overdense region shrinks and a nonlinear structure is formed as the Zel'dovich's pancake. On the other hand, an underdense region expands. Therefore, although the initial volumes of overdense underdense regions are the same, the volume of the latter gets larger than that of the former in a nonlinear stage. In addition to this Lagrangian nonlinear effect, we take into account a backreaction effect. This effect enhances expansion of an underdense region and contraction of an overdense region. As a result, the above difference between ZA and our approximation appears.

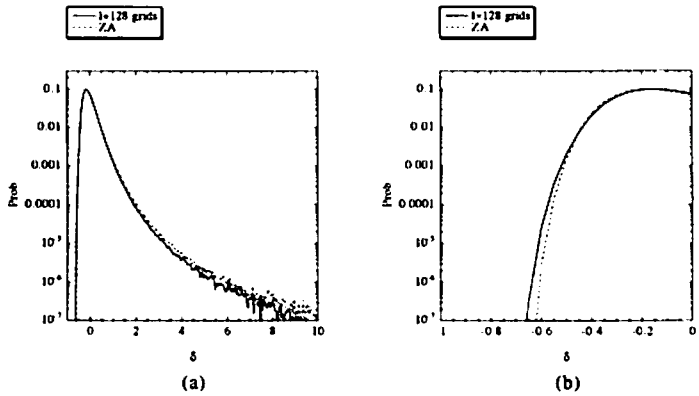

Figure 1: The PDF of density fluctuation at $a = 900$ for $l = 128$-grid domain and that with the ZA. The probability to find an overdense region for $l = 128$-grid domain is less than that with the ZA (a). On the other hand, the probability for an underdense region increases for $l = 128$-grid domain (b).

3.3 Deceleration parameter q

Another interesting observable variable is a deceleration parameter. The recent observation of type Ia supernova may suggest an acceleration of the Universe[10]. Although this result may naively suggest an existence of dark energy such as a cosmological constant Λ, we could find some effective model without dark energy which explain the observation. Then we shall estimate a deceleration parameter averaged in a local domain here.

We define local deceleration parameter $q_{\mathcal{D}}$ as

$$q_{\mathcal{D}} \equiv -\frac{a_{\mathcal{D}}\ddot{a}_{\mathcal{D}}}{\dot{a}_{\mathcal{D}}^2}\,, \tag{9}$$

which can be evaluated by Eq. (3) and $H_{\mathcal{D}}$. Buchert et al.[5] showed the evolution of deceleration parameter for the ZA. Although our approach includes a backreaction consistently, our analysis shows that a deviation of $q_{\mathcal{D}}$ does not get so large. The difference of $q_{\mathcal{D}}$ from the ZA is very little even just before the shell crossing. We show the time evolution of $q_{\mathcal{D}}$ for a plane-symmetric 1-dimensional model in Fig. 2. Even if a domain is extremely underdense, the domain is decelerating. This may be because our approach is still perturbative. We will discuss it further in the next section.

4 Summary

We propose new Lagrangian perturbation theory with a backreaction effect by inhomogeneity of density perturbations and present a set of basic equations. The inhomogeneity affects the expansion rate in a local domain and its own growing rate. In a one-dimensional plane-symmetric model, we have numerically analyzed our approach, and calculated the growing rate density perturbations and the PDF of several observed variables. We set our initial conditions as random Gaussian distribution. From our analysis, we show that the expansion rate of an underdense region is faster than that of the whole universe as expected.

We mention about recent observation about cosmological parameters. According to the observation of type Ia supernova, the expansion of the Universe seems to accelerate[10]. The result suggests existence of dark energy such as a cosmological constant Λ. However, this produces another difficulty, that is the so-called cosmological constant problem. To avoid such a difficulty, if we could explain the observation without cosmological constant, it would be more natural. Recently, Tomita discussed such possibility assuming we are in a large local void[11]. Globally the Universe is flat (E-dS universe), but we are sitting

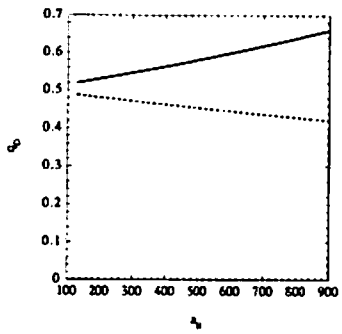

Figure 2: The evolution of a deceleration parameter $q_{\mathcal{D}}$ for l = 64-grid domain. The overdense domain shows increase of $q_{\mathcal{D}}$ (a solid line for maximum value), while the underdense domain shows decrease of $q_{\mathcal{D}}$ (a dashed line for minimum value).

near the center of a local void, which existence is observationally confirmed. Then he calculated the luminosity distance, finding that the observation can be explain by such a model. In our model, when we calculate the luminosity distance, even if we do not sit we would near the center of a local void, we may explain the observation.

References

[1] P. J. E. Peebles, *The Large Scale Structure of the Universe* (Princeton University Press, Princeton, New Jersey, 1980).

[2] Ya. B. Zel'dovich, Astron. Astrophys. **5**, 84 (1970).

[3] T. Buchert, Astron. Astrophys. **223**, 9 (1989).

[4] T. Buchert and J. Ehlers, Astron. Astrophys. **320**, 1 (1997).

[5] T. Buchert, M. Kerscher, and C. Sicka, Phys. Rev. D **62**, 043525 (2000).

[6] T. Tatekawa, M. Suda, K. Maeda, and H. Kubotani, astro-ph/0109501.

[7] X. Shi and M. Turner, Astrophys. J. **493**, 519 (1998).

[8] L. Kofman, E. Berschinger, J. M. Gelb, A. Nusser, and A. Dekel, Astrophys. J. **420**, 44 (1994).

[9] T. Padmanabhan and K. Subramanian, Astrophys. J. **410**, 482 (1993).

[10] S. Perlmutter *et al.*, Astrophys. J. **517**, 565 (1999).

[11] K. Tomita, Astrophys. J. **529**, 38 (2000).

Is dark energy the only solution to the apparent acceleration of the present universe?

Hideo Iguchi [1]

Department of Physics, Tokyo Institute of Technology Oh-Okayama, Meguro-ku, Tokyo 152-8550, Japan

Takashi Nakamura[2]

Yukawa Institute for Theoretical Physics, Kyoto University, Sakyo-ku, Kyoto 606-8502, Japan

Ken-ichi Nakao [3]

Department of Physics, Osaka City University, Osaka 558-8585, Japan

Abstract

Even for the observed luminosity distance $D_L(z)$ which suggests the existence of the dark energy, we show that the inhomogeneous dust universe solution without the dark energy is possible in general. Future observation of $D_L(z)$ for $1 \lesssim z < 1.7$ may confirm or refute this possibility.

1 Introduction

Recent measurements of the luminosity distance $D_L(z)$ using Type Ia supernovae [1, 2, 3] suggest that accurate $D_L(z)$ may be obtained in near future. Especially SNAP [4] will give us the luminosity distance of ~2000 Type Ia supernovae with an accuracy of a few % up to $z \sim 1.7$ every year. On the other hand from the observation of the first Doppler peak of the anisotropy of CMB, it is now suggested that the universe is flat [5, 6], which may be proved in future by MAP and Planck. Under the assumption of the homogeneity and the isotropy of our universe, these observations suggest that the dark energy is dominant at present. To interpret what the dark energy is [7] many arguments have been done so far. However at present we do not have a firm and reliable theoretical basis to discuss such a small amount of energy scale compared with the Planck one. In short the dark energy under the assumption of homogeneity and the isotropy of our universe is by far the great mystery.

From the observed isotropy of the CMB, if we are not in a special part of our universe, the universe should be homogeneous. However if we are in a special part, the universe might be inhomogeneous although the CMB is isotropic. Such cosmological models have been constructed using spherically symmetric models in which we are near the symmetric center. Some authors have considered such models to interpret the SNIa data for small z[8] as well as up to large z assuming a void structure[9] to avoid the dark energy. One may regard such possibilities absurd.

Recently, we have investigated to construct a possible inhomogeneous dust universe derived from the observed $D_L(z)$ without any dark energy [10].

The analysis of high redshift supernovae gives us the luminosity distance-redshift relation $D_L(z)$ along the observational past null cone up to $z \sim 1$ [1, 2, 3]. The data fit well with $D_L(z)$ in the homogeneous and the isotropic universe with $\Omega_m = 0.3$ and $\Omega_\Lambda = 0.7$ given by

$$D_L(z) = \frac{1}{H_0}(1+z)\int_0^z \frac{dz'}{\sqrt{\Omega_m(1+z')^3 + \Omega_\Lambda}}. \tag{1}$$

[1]E-mail: iguchi@th.phys.titech.ac.jp
[2]E-mail:takashi@yukawa.kyoto-u.ac.jp
[3]E-mail: knakao@sci.osaka-cu.ac.jp

Here we assume that $D_L(z)$ is given by Eq. (1) with $\Omega_m = 0.3$ and $\Omega_\Lambda = 0.7$ for $z \lesssim 1$. This is just for simplicity to make the arguments clearer. We do not claim that $D_L(z)$ with $\Omega_m = 0.3$ and $\Omega_\Lambda = 0.7$ is confirmed. While $D_L(z)$ for $1 \lesssim z < 1.7$ is not certain even at present and will be obtained in future, for example, by SNAP.

2 Formulation

Here we introduce the differential equations that we should investigate. See Ref. [10] for the derivation of them and the meanings of the variables.

The observational past null cone $t = \hat{t}(r)$ satisfies

$$\frac{d\hat{t}}{dr} = -\frac{\mathcal{R}_2(\mathcal{R}, \hat{t}, E, E', t_B, t_B', r)}{\sqrt{1+2Er^2}}. \tag{2}$$

The redshift $z(r)$ along the past null cone is given by

$$\frac{dz}{dr} = \frac{1+z}{\sqrt{1+2Er^2}}\mathcal{R}_3(\mathcal{R}, \hat{t}, E, E', t_B, t_B', r). \tag{3}$$

The total derivative of $\mathcal{R}$ on the past null cone is written as

$$\frac{d\mathcal{R}}{dr} = \left(1 - \frac{\mathcal{R}_1(\mathcal{R}, E, r)}{\sqrt{1+2Er^2}}\right)\mathcal{R}_2(\mathcal{R}, \hat{t}, E, E', t_B, t_B', r). \tag{4}$$

Our basic equations are Eqs.(2)–(4). These three equations can be regarded as a system of first order ordinary differential equations for three of the five functions $\mathcal{R}(r)$, $\hat{t}(r)$, $E(r)$, $t_B(r)$ and $z(r)$. In order to integrate these equations, we should specify two conditions on these five functions. The luminosity distance $D_L(z)$ is related to $\mathcal{R}$ [11] as

$$\mathcal{R} = \frac{D_L(z)}{(1+z)^2}. \tag{5}$$

As already mentioned, we assume that $D_L(z)$ is given by Eq.(1). Further we will specify one condition for E, t_B or the combination of them.

3 Results

At first we consider pure Big-Bang time inhomogeneity. In this case the curvature function $E(r)$ is set to be constant. From Eqs. (3) and (4), we have equations for $z(r)$ and the Big-Bang time function $t_B(r)$. The model is specified by $\Omega_0 \equiv 2M_0/H_0^2$ which is the present central density $3M_0/4\pi$ divided by the present central critical density $\rho_{\rm crit} = 3H_0^2/8\pi$, where H_0 is the present central Hubble parameter and we set it to be unity. We numerically integrate these two differential equations from $r = 0$ for ten Ω_0 from 0.1 to 1.0. The initial conditions are given by $z = 0$ and $t_B = 0$.

From Eq. (4) $R' > 0$ for positive density while from Eq. (9) $\dot{R}' > 0$ for monotonically increasing $z(r)$ so that the integration is terminated either of the following inequalities is violated,

$$R' > 0 \quad \text{or} \quad \dot{R}' > 0. \tag{6}$$

In Fig. 1 we show the relation between the parameter Ω_0 and the redshift when the integration is terminated. For low $\Omega_0 = 0.1 \quad 0.4$ (open triangles), shell-crossing singularities occur when $d\mathcal{R}/dz = 0$. For high $\Omega_0 = 0.5 \quad 1.0$ (open square), the second condition of Eq. (6) is violated first. This occurs when $\mathcal{R} = 2M$.

Fig. 2 shows the Big-Bang time functions t_B for each Ω_0. For all Ω_0 the Big-Bang time functions t_B decrease as z increases up to $z \sim 0.5$.

In Figs. 3 we plot the redshift space density

$$\hat{\rho}(z) = \rho\frac{4\pi R^2 R' dr}{4\pi z^2 dz} = \Omega_0 \frac{r^2}{z^2}\frac{dr}{dz}\rho_{\rm crit}, \tag{7}$$

along the past null cone. Observations of the mass distribution along the past null cone would give us this density profile.

Next we consider the pure curvature inhomogeneity. In this case the Big-Bang time function $t_B(r)$ is set to be zero. From Eqs. (2), (3) and (4) we obtain three differential equations for three variables $z(r)$, $E(r)$ and $\hat{t}(r)$. We numerically integrate these three differential equations from $r = 0$. The initial conditions are given by $z = 0$, $E = (1 - \Omega_0)/2$ and

$$\hat{t}(0) = \frac{\Omega_0}{2} \frac{(\sinh \eta_0 - \eta_0)}{(1 - \Omega_0)^{\frac{3}{2}}}, \tag{8}$$

where

$$\eta_0 = \ln \left(\frac{2 - \Omega_0}{\Omega_0} + \sqrt{\left(\frac{2 - \Omega_0}{\Omega_0} \right)^2 - 1} \right). \tag{9}$$

In Fig. 1 we show the relation between the parameter Ω_0 and the redshift when the integration is terminated (cross marks). For the case of curvature inhomogeneity, it was shown that the second condition of Eq. (6) is violated first [12].

Fig. 4 shows the curvature functions E for each Ω_0. We can see E decreases as z increases except for the $\Omega_0 = 1.0$ case.

The decreasing E is consistent with the apparent acceleration. E determines the specific energy of the dust elements so that the "initial" velocity is slower for more distant shells. This causes the apparent acceleration since the velocity at $r = 0$ can be the largest.

Fig. 5 shows the redshift space density $\hat{\rho}$ along the past null cone as a function of z.

4 Conclusion

We have constructed inhomogeneous dust models without the dark energy. These models can be consistent with the observed $D_L(z)$ up to $z = 1$ since from Fig. 1 we have no difficulties up to $z \sim 1$ for any parameters in both the Big-Bang time inhomogeneity and the curvature inhomogeneity cases. For $z > 1$, we have difficulties in our inhomogeneous dust models. Recently, the SNIa at the redshift of ~ 1.7 was found [13, 14] with rather large error bars. However only a single SNIa at the redshift of ~ 1.7 is not enough to construct the accurate $D_L(z)$ although it seems to rule out the 'grey-dust' hypothesis. If future observations confirm $D_L(z)$ up to $z \sim 2$ with $\Omega_m \sim 0.3$ and $\Omega_\Lambda \sim 0.7$, our inhomogeneous dust models are incompatible with the observations and some form of the dark energy will be the case. However, if future observations confirm that $D_L(z)$ for $z > 1$ does not follow Eq. (1) appreciably, the possibility of our inhomogeneous dust models remain to be studied more extensively. In such a case, the first Doppler peak as well as the higher ones will give us another constraints to the inhomogeneous universe models.

Using the cluster temperature evolution data for $0.3 < z < 0.8$, it was reported that the best-fit value of $\Omega_m = 0.45 \pm 0.1$ for open universe and $\Omega_m = 0.3 \pm 0.1$ for flat universe [15]. However recent analysis shows that the systematic error is comparable to the statistical error [16]. So we may say that $0.1 < \Omega_m < 0.5$ for $0.3 < z < 0.8$ data. It is not clear that the Press-Schechter formalism can be applied to our inhomogeneous models. One of the possible estimate would be based on the locally homogeneous approximation. As we know, the massive cluster evolution is very sensitive to the matter density. It seems that the model with local density parameter Ω_m which largely conflicts with the best-fit value would not explain the observed cluster evolutions. The pure curvature inhomogeneity case with $\Omega_0 \gtrsim 0.2$ may be difficult to survive because it is approximated by flat universe at high z. Also the Bang time inhomogeneity case with $\Omega_0 \sim 1.0$ can not survive. However, it can be expected that the pure Bang time inhomogeneity with $\Omega_0 \sim 0.5$ and the pure curvature inhomogeneity with $\Omega_0 \sim 0.1$ would predict the observed cluster abundances.

The estimate of the lensing rate and the distribution of the separation of the images depend on the model of the mass distribution of the lensing object and the luminosity function of the source objects as well as the cosmological parameters. However it has been shown that the dependence on the lens model and parameters is much larger than that on the cosmological parameters [17]. In addition, the mass distribution of the lensing objects would deeply depend on baryon density Ω_b [18]. Therefore we

conclude that the estimate of the cosmological parameters from the lensing rate and the distribution of the separation of the images is difficult at present so that we can not rule out the inhomogeneous model.

As shown in Fig. 6, the look back times along the past null cone have little difference between the inhomogeneous model and the corresponding homogeneous model with cosmological constant for $z < 0.5$. For $z \sim 1$, the difference appears, but some of the inhomogeneous models are not so different from the homogeneous model even there. The ages of stellar population would not distinguish the inhomogeneous model from the homogeneous one.

As a result, the model dependence including various undetermined parameters and the observational uncertainty are much larger than the dependence on the cosmological parameters. Therefore we think that these observations can not easily rule out the inhomogeneous model.

Here we comment on how we can be place away from the center of the symmetry. The displacement from the center would correspond to the dipole mode of CMB. Therefore we can be ~ 10 Mpc away from the center.

In conclusion, the dark energy is not the only solution to the apparent acceleration of the present universe but inhomogeneous dust models can also explain the observations.

Acknowledgements

This work was partially supported by the Grant-in-Aid for Scientific Research (No. 11217, Nos.11640274, 09NP0801) from the Japanese Ministry of Education, Science, Sports, and Culture.

References

[1] B. P. Schmidt *et al.*, Astrophys. J. **507**, 46 (1998).

[2] A. G. Riess *et al.* [Supernova Search Team Collaboration], Astron. J. **116**, 1009 (1998).

[3] S. Perlmutter *et al.* [Supernova Cosmology Project Collaboration], Astrophys. J. **517**, 565 (1999).

[4] Supernova/Acceleration Probe, http://snap.lbl.gov

[5] de Bernardis, P. *et al.*, Nature , **404**, 955 (2000).

[6] Lange, A.E. *et al.*, Phys. Rev. D **63**, 042001 (2001).

[7] S. Weinberg, in *Marina del Rey 2000, Sources and detection of dark matter and dark energy in the universe*, edited by D. B. Cline (Springer, Berlin, Germany, 2001), p.18. astro-ph/0005265.

[8] M. Celerier, Astron. Astrophys. **353**, 63 (2000).

[9] K. Tomita, Astrophys. J. **529**, 38 (2000); K. Tomita, Mon. Not. R. Astron. Soc. **326**, 287 (2001); K. Tomita, Prog. Theor. Phys. **106**, 929 (2001).

[10] H. Iguchi, T. Nakamura and K. Nakao, arXiv:astro-ph/0112419.

[11] M. H. Partovi and B. Mashhoon, Astrophys. J., **276**, 4 (1984).

[12] H. Kurki-Suonio and E. Liang, Astrophys. J., **390**, 5 (1992).

[13] R. L. Gilliland, P. E. Nugent and M. M. Phillips, Astrophys. J. **521**, 30 (1999).

[14] A. G. Riess *et al.*, astro-ph/0104455.

[15] M. Donahue and G. M. Voit, Astrophys. J.,**523**, L137 (1999).

[16] G. M. Voit, Astrophys. J., **543**, 113 (2000).

[17] R. Takahashi and T. Chiba, astro-ph/0106176; T. Chiba and R. Takahashi, astro-ph/0106273.

[18] C. S. Kochanek and M. White, Astrophys. J. **559**, 531 (2001).

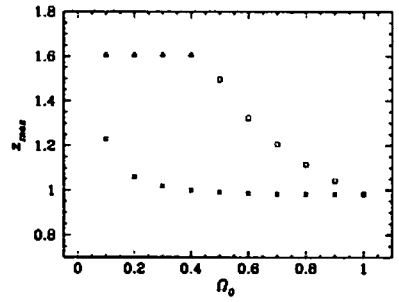

Figure 1: Plots of maximum redshifts when either of inequalities in Eq. (6) is violated as a function of the present density parameter. The open triangles and the open squares are the ones for the Big-Bang time inhomogeneity. The cross marks are the ones for the curvature inhomogeneity case.

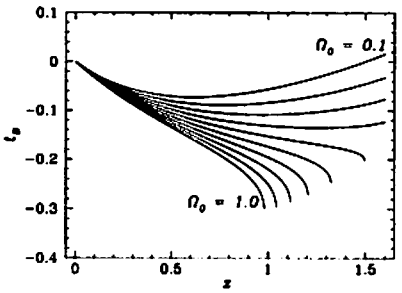

Figure 2: Plots of the Big-Bang time functions as a function of the redshift z .

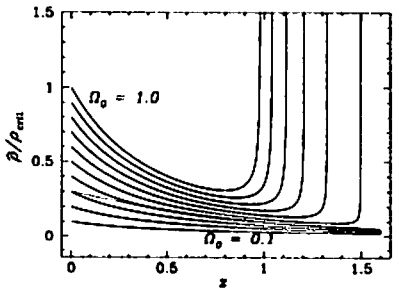

Figure 3: Plots of the redshift space density $\hat{\rho}$ divided by the central critical density. The dotted line denotes the $\Omega_m = 0.3$, $\Omega_\Lambda = 0.7$ homogeneous model.

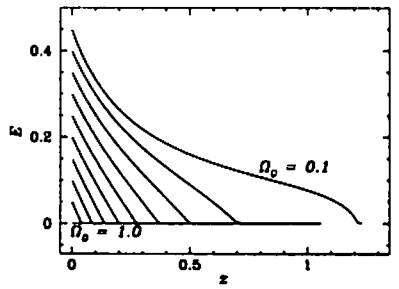

Figure 4: Plots of the curvature functions.

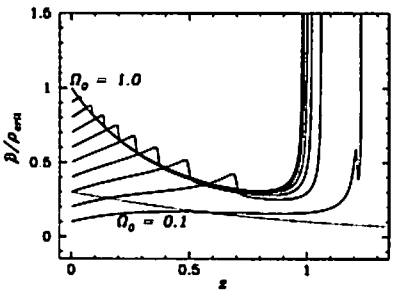

Figure 5: Plots of the redshift space density divided by the present central critical density. The dotted line denotes the $\Omega_m = 0.3$, $\Omega_\Lambda = 0.7$ homogeneous model.

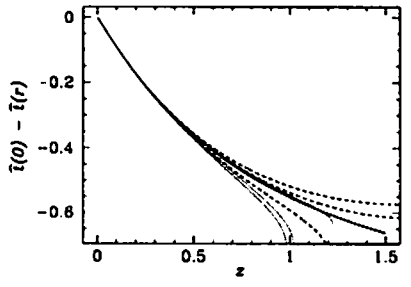

Figure 6: Plots of the look back time along the past null cone. Solid line denotes the homogeneous $\Omega_m = 0.3$ and $\Omega_\Lambda = 0.7$ case. Broken and dotted lines denote the pure Big-Bang time and the pure curvature inhomogeneity case of $\Omega_0 = 0.1, 0.3, 0.7$ in descending order, respectively.

Scalar field dark matter in supergravity [1]

Osamu Seto, [2] Kazunori Kohri [3] and Takashi Nakamura[4]

Yukawa Institute for Theoretical Physics, Kyoto University, Sakyo-ku, Kyoto 606-8502, Japan

Abstract

We show that an oscillating scalar field in supergravity of mass of the order of $\sim$ TeV with a nonzero vacuum expectation value ($\sim 10^{10}$ GeV) can be a candidate of cold dark matter (CDM). To avoid the gravitino problem, we need a low reheating temperature after the primordial inflation. Then, the energy density of the oscillating scalar field satisfies all the requirements for CDM at present in the universe.

1 Introduction

It is widely believed that a significant fraction of energy density in the universe is in the form of cold dark matter (CDM). Recently it was reported that the contribution of CDM to density parameter is approximately $\Omega \simeq 0.3$ (for a review, see Ref. [2]). It is one of the most important problems in cosmology and particle physics to clarify the nature and the origin of dark matter.

In this paper, we consider stable scalar fields with an electroweak scale mass $\sim \mathcal{O}$(TeV) and a large vacuum expectation value (VEV) $\sim \mathcal{O}(10^{10})$ GeV. These scalar fields naturally appear in supergravity. It is interesting that such a scalar filed can have a net oscillation energy after inflation because of the coupling with the inflaton field through Kähler potential and an additional SUSY breaking effect during the inflation [3, 4]. On the other hand, however, whenever we consider a model based on supergravity within the framework of inflationary cosmology, we are faced with some sticky problems. In particular, "gravitino problem" would be one of the severest problems in cosmology [5, 6]. To avoid the gravitino problem, i.e., to restrain the production of gravitinos and the photodissociation of light elements due to their late-time decays, we need a low reheating temperature after the primordial inflation [7]. In this situation, we show that the energy density of the oscillation of the scalar field satisfies the requirements for CDM at present in the universe.

2 Model

In supergravity, we know there exist a lot of scalar fields with an almost flat potential. These scalar fields are expected to acquire masses of the order of the electroweak scale from a supersymmetry breaking effect and might have a nonzero VEV.

We consider a chiral superfield Φ which is the gauge singlet and contains a scalar field ϕ. We assume that it has a minimal Kähler potential

$$K = |\Phi|^2 M_G^{-2} \tag{1}$$

and a superpotential,

$$W = \frac{\lambda}{n+3}\frac{\Phi^{n+3}}{M_G^n} + C, \tag{2}$$

where $M_G = M_{Pl}/\sqrt{8\pi} \simeq 2.4 \times 10^{18}$GeV is the reduced Planck mass, $\lambda \sim \mathcal{O}(1)$, and C is a constant.

---

[1] This talk is based on Ref. [1]

[2] E-mail:oseto@yukawa.kyoto-u.ac.jp

[3] E-mail:kohri@yukawa.kyoto-u.ac.jp

[4] E-mail:takashi@yukawa.kyoto-u.ac.jp

In addition, the scalar field acquires a soft mass ($\sim$ 1 TeV) through a SUSY breaking effect. When we assume that the cosmological constant vanishes at the VEV, it is natural to take $C \simeq m_{3/2} M_G^2$, where $m_{3/2}$ is the gravitino mass ($\sim$ 1 TeV). Then, we obtain the following low energy effective potential,

$$V(\phi) = V_0 - m_0^2 |\phi|^2 + \frac{n}{n+3} \frac{\lambda C}{M_G^2} \frac{\phi^{n+3} + \phi^{*n+3}}{M_G^n} + \lambda^2 \frac{|\phi|^{2n+4}}{M_G^{2n}}. \tag{3}$$

One finds that the VEV of the scalar field $M \equiv \langle \phi \rangle$ is given by

$$\frac{M^{n+1}}{M_G^n} = \frac{1}{2(n+2)\lambda} \left[\frac{nC}{M_G^2} + \sqrt{\left(\frac{nC}{M_G^2} \right)^2 + 4(n+2) m_0^2} \right], \tag{4}$$

and the vacuum energy at $\phi = 0$ becomes

$$V_0 = \frac{n+1}{n+2} M^2 \left[m_0^2 + \frac{nC}{2(n+2)(n+3)M_G^2} \left(\frac{nC}{M_G^2} + \sqrt{\left(\frac{nC}{M_G^2} \right)^2 + 4(n+2) m_0^2} \right) \right]. \tag{5}$$

From Eq. (4), we see that $M \sim \sqrt{m_0 M_G} \sim \mathcal{O}(10^{10})$ GeV in the case of $n = 1$.

After the primordial inflation, the inflaton field oscillates around its minimum and dominates the energy density in the universe until the reheating time $t \sim \Gamma_I^{-1}$, where Γ_I is the decay rate of the inflaton field. While the Hubble expansion rate is large $H \gg m_0$, the scalar field ϕ would be trapped dynamically at the origin by an additional SUSY breaking effect which is explained in the following reason [3, 4]. In supergravity, the scalar potential of the inflaton field I and the scalar field ϕ is expressed by

$$V(\phi, I) = e^{G(\phi, I)} \left[G_i (G_j^i)^{-1} G^j - 3 \right], \tag{6}$$

where $G = K + \ln |W|^2$ and $G_i = \partial G / \partial \phi^i, G^j = \partial G / \partial \phi_j^*$ and $G_i^j = \partial^2 G / \partial \phi^i \partial \phi_j^*$. During the oscillation of the inflaton field, the scaler potential is related to the Hubble expansion rate as $V(\phi, I) \simeq \rho_I \simeq 3 M_G^2 H^2$ through the Friedmann equation, because the energy density in the universe is dominated by the inflaton field. Then, the scalar potential is modified as

$$V(\phi) \simeq V_0 + 3H^2 |\phi|^2, \tag{7}$$

and ϕ would be trapped at $\phi = 0$.

On the other hand, when the Hubble expansion rate becomes smaller than the mass of the scalar field, i.e., $H \lesssim m_0$, the additional SUSY breaking effect disappears and the scalar field begins to roll down to its VEV while the oscillating inflaton field still dominates in the energy density in the universe because of the low reheating temperature in order to avoid the gravitino problem.

Hereafter we mainly consider the case of n = 1. The energy density of the scalar field at the reheating time ($t = t_R$) is estimated as

$$\rho_\phi(t_R) = \left. \frac{\rho_\phi}{\rho_I} \right|_{H = m_0} \rho_I(t_R), \tag{8}$$

with the energy density of the inflaton field,

$$\rho_I(t_R) = \frac{\pi^2}{30} g_* T_R^4, \tag{9}$$

where T_R is reheating temperature and g_* is the degree of freedom in the thermal bath. When the reheating process finished, the ratio of the energy density of ϕ to the entropy density s is estimated as

$$\begin{aligned} \frac{\rho_\phi}{s} &= \frac{V_0 T_R}{4 M_G^2 m_0^2}, \\ &\simeq 0.5 \times 10^{-9} \mathrm{GeV} \left(\frac{T_R}{10^7 \mathrm{GeV}} \right) \left(\frac{M}{10^{10} \mathrm{GeV}} \right)^2, \end{aligned} \tag{10}$$

where $s = 2\pi^2 g_* T_R^3/45$. Both ρ_ϕ and s decrease as $a(t)^{-3}$, so that the ratio ρ_ϕ/s is constant unless the additional entropy is produced after the reheating. If we adopt inflation models with a low reheating temperature, e.g., $T_R \lesssim 10^7$GeV, in order to avoid the gravitino problem [7], the energy density of the dark matter cannot be larger than the critical density and does not overclose the universe.

The present value of the energy density of dark matter to entropy density ratio is given by

$$\begin{aligned} \frac{\rho_{\rm DM}}{s_0} &= \frac{\Omega_{\rm DM}\rho_{cr}}{s_0} \\ &\simeq 3.6 \times 10^{-9}\Omega_{\rm DM}h^2{\rm GeV}, \end{aligned} \tag{11}$$

where ρ_{cr} is the present critical density of the universe, s_0 is the present entropy density, $\Omega_{\rm DM}$ is the density parameter of dark matter (~ 0.3) [2], and h is the present Hubble parameter normalized as $H_0 = 100h$km/sec Mpc^{-1}. From Eq. (11) we see that the energy density of the oscillating scalar field almost coincides with the energy density of dark matter. Namely the contribution of ρ_ϕ to density parameter Ω is estimated as

$$\begin{aligned} \Omega_\phi &= \frac{\rho_\phi}{\rho_{cr}} \\ &\simeq 0.28 \times \left(\frac{T_R}{10^7{\rm GeV}}\right)\left(\frac{M}{10^{10}{\rm GeV}}\right)^2\left(\frac{0.7}{h}\right)^2. \end{aligned} \tag{12}$$

From Eq. (12) we see that $\Omega_\phi \simeq 0.3$ (0.03) for $T_R \simeq 10^7$ (10^6) GeV.

3 Conclusion

In this paper, within the framework of inflationary cosmology we have shown that the stable scalar field with the electroweak scale mass and the large VEV is now oscillating, and the energy density of the oscillation significantly contributes to the density parameter Ω and satisfies the requirements for CDM at present in the universe. It is interesting that such a scalar field naturally appears in supergravity. In addition, it is also fascinating that when we require the low reheating temperature after the primordial inflation to avoid the gravitino problem ($T_R \lesssim 10^7$ GeV), it automatically ensures the appropriate energy density for CDM ($\Omega_\phi \simeq 0.3$).

acknowledgements

We would like to thank J. Yokoyama for informative comments. This work was partially supported by the Grant-in-Aid for Scientific Research (Nos.11640274, 09NP0801) from the Japanese Ministry of Education, Science, Sports, and Culture.

References

[1] O. Seto, K. Kohri and T. Nakamura, JHEP **0109**, 032 (2001).

[2] S. Schindler, astro-ph/0107028.

[3] M. Dine, W. Fischler and D. Nemeschansky, Phys. Lett. B **136** (1984) 169.

[4] O. Bertolami and G. G. Ross, Phys. Lett. B **183** (1987) 163.

[5] H. Pagels and J. R. Primack, Phys. Rev. Lett. **48** (1982) 223.

[6] S. Weinberg, Phys. Rev. Lett. **48** (1982) 1303.

[7] E. Holtmann, M. Kawasaki, K. Kohri and T. Moroi, Phys. Rev. D **60** (1999) 023506.

Gravitational Radiation Instabilities in Rotating Neutron Stars*

Lee Lindblom

Theoretical Astrophysics 130-33,
California Institute of Technology,
Pasadena, CA 91125 (USA)

Abstract

Gravitational radiation (GR) drives an instability in certain modes of rotating stars. This instability is strong enough in the case of the r-modes to cause their amplitudes to grow (in the absence of other dissipation) on a timescale of tens of seconds in rapidly rotating neutron stars. GR emitted by these modes removes angular momentum from the star at a rate which would spin it down to a relatively small angular velocity within about one year, if the dimensionless amplitude of the mode grows to order unity. A pedagogical discussion is given here of the mechanism of GR instability in rotating stars, on the relevant properties of the r-modes, and on our present understanding of the dissipation mechanisms (including interactions with the crust and hyperon bulk viscosity) that tend to suppress this instability in neutron stars. The astrophysical implications of this GR driven instability are discussed for young neutron stars, and for older systems such as low mass x-ray binaries. Recent work on the evolution and saturation of the r-modes by non-linear hydrodynamic effects is also described.

1 Introduction

The non-radial pulsations of stars couple to gravitational radiation (GR) in general relativity theory [2, 3], and the GR produced by these oscillations carries away energy and angular momentum from the star. In non-rotating stars the effect of these GR losses is dissipative, and the pulsations of the star are damped. Chandrasekhar first noted [4, 5] that in rotating stars the situation can be quite different: the emission of GR causes the amplitudes of certain modes to grow. The mechanism that drives this GR instability is fairly easy to understand: Modes that propagate in the direction opposite the star's rotation (as seen in the co-rotating frame of the fluid) have *negative* angular momentum, because these modes lower the total angular momentum of the star. In a rotating star some of these counter-rotating modes are dragged forward by the rotation of the star and appear to an inertial observer to propagate in the same direction as the star's rotation. Such modes, as illustrated in Fig. 1, emit *positive* angular momentum GR since the density and momentum perturbations appear to an observer at infinity to be rotating in the same direction as the star. The angular momentum removed by GR lowers the (already negative) angular momentum of such a mode, and therefore the amplitude of the mode grows.

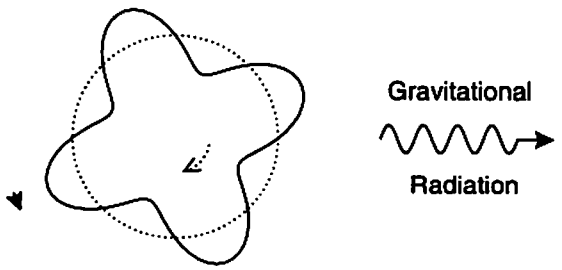

Figure 1: A counter-rotating mode (solid curve) that is dragged forward by the rotation of the background star (dashed curve) is driven unstable by the emission of gravitational radiation.

*The introductory portions of this review are based very closely on Ref. [1].

This GR driven instability was first studied extensively by Friedman and Schutz [6, 7] for the fundamental (f-) modes of rotating stars. They demonstrated that the GR instability has the remarkable property that it makes *every* rotating perfect fluid star unstable in general relativity theory. This discovery sparked an interest in the possibility that GR might play a significant role in the evolution of real neutron stars. Does the GR instability determine the maximum spin rate of pulsars? Is the GR emitted by an unstable rapidly rotating neutron star detectable? Unfortunately the generic nature of this destabilizing process does not guarantee that it plays any role at all in real neutron stars. Internal dissipation (*e.g.*, viscosity) within a star tends to damp the pulsations that are driven unstable by GR. If the internal dissipation is sufficiently strong, then the GR instability can even be suppressed completely [8, 9]. Detailed calculations of the effects of GR and internal dissipation on the f-modes of rotating stars revealed that the GR instability is effective only in very rapidly rotating stars [10, 11, 12, 13]. Stars with angular velocities smaller than some critical value, $\Omega < \Omega_c$ are stable, while those rotating more rapidly, $\Omega > \Omega_c$, are subject to the GR instability. This critical angular velocity, Ω_c, for the stability of the f-modes is depicted in Fig. 2 for realistic neutron-star models. The strength of the internal dissipation processes in neutron stars is temperature dependent, and consequently the critical angular velocity Ω_c is temperature dependent as well. Figure 2 illustrates that the GR instability is completely suppressed in the f-modes except when the temperature of the neutron star lies in the range, $10^7 < T < 10^{10}$K. Further, the internal dissipation is so strong that the f-modes are never unstable unless the angular velocity of the star exceeds $0.91\Omega_{\rm max}$. Thus the GR instability in the f-modes can not significantly reduce the spin of a neutron star below the maximum, and substantial amounts of GR can not be emitted by this process.

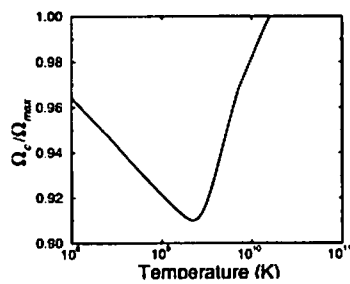

Figure 2: Temperature dependence of the critical angular velocity Ω_c in rotating neutron stars: an f-mode is driven unstable by gravitational radiation when the star's angular velocity exceeds Ω_c.

This pessimistic view of the GR instability began to change when Andersson [14] and Friedman and Morsink [15] showed that the r-modes were also subject to the GR instability. Indeed they showed that *all* the r-modes are driven unstable by GR in *all* rotating perfect fluid stars. Subsequent calculations by Lindblom, Owen and Morsink [16] showed that the GR instability in the r-modes was also strong enough to overcome the simplest internal dissipation processes in neutron-star matter, even in relatively slowly rotating stars. Thus the GR instability in the r-modes is strong enough that it might be capable of significantly reducing the angular momenta of rotating neutron stars, and the GR emitted during such spin-down events might perhaps be detectable by LIGO [17]. The remainder of this paper discusses recent developments related to the GR instability of the r-modes. Section 2 discusses the basic properties of the r-modes and their GR instability. Section 3 reviews the astrophysical scenarios in which the r-mode GR instability might play an important role. This discussion focuses on recent work that evaluates the effects of the neutron-star crust, hyperon bulk viscosity, and non-linear hydrodynamics on the r-mode instability. Taken together these various effects now make it seem rather unlikely that the r-mode instability plays an important role in any of the proposed astrophysical scenarios. Section 4 summarizes some of the open questions that prevent us at this time from knowing for certain whether the r-mode instability plays an important role in real astrophysical systems.

2 Gravitational Radiation Instability in the r-Modes

The r-modes (also called rotation dominated modes, inertial modes, or Rossby waves) are oscillations of rotating stars whose restoring force is the Coriolis force [18]. These modes are primarily velocity perturbations, which for slowly rotating barotropic stars have the simple analytical form

$$\delta\vec{v} = \alpha R\Omega \left(\frac{r}{R}\right)^m \vec{Y}^B_{mm} e^{i\omega t} + \mathcal{O}(\Omega^3), \tag{1}$$

where α is the dimensionless amplitude of the mode; R and Ω are the radius and angular velocity of the equilibrium star; $\vec{Y}^B_{lm} = \hat{r} \times r\vec{\nabla} Y_{lm}/\sqrt{l(l+1)}$ is the magnetic-type vector spherical harmonic; and ω is the frequency of the mode. The associated density perturbation, $\delta\rho = \mathcal{O}(\Omega^2)$, vanishes at lowest order. Because the Coriolis force dominates, the frequencies of the r-modes are independent of the equation of state and are proportional to the angular velocity of the star (at lowest order),

$$\omega = -\frac{(m-1)(m+2)}{m+1}\Omega + \mathcal{O}(\Omega^3). \tag{2}$$

The velocity field of the r-mode, Eq. (1), is everywhere orthogonal to the radial direction $\hat{r}$, and has an angular structure determined by Y_{mm}. Figure 3 gives equatorial and polar views of this velocity field for the $m = 2$ r-mode, which plays the dominant role in the GR instability. Figure 4 shows another view of the same field in standard polar coordinates (θ, φ). The four circulation zones propagate through the fluid with angular velocity $-\frac{1}{3}\Omega$, toward the left in Fig. 4. The fluid elements respond by moving on paths described by the Lagrangian displacement, $\vec{\xi} = -i\delta\vec{v}/(\omega + m\Omega)$. To first order these are ellipses, with θ-dependent eccentricities, as illustrated on the left side of Fig. 4.

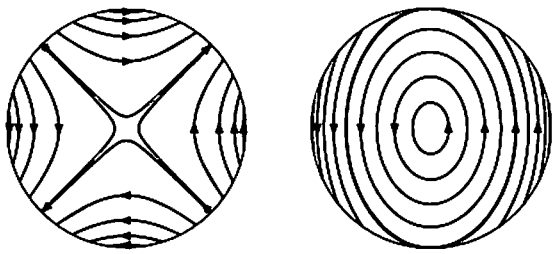

Figure 3: Polar and equatorial views of the flow pattern of the $m = 2$ r-mode. This velocity field propagates through the fluid with angular velocity $\frac{2}{3}\Omega$ relative to the inertial frame, and $-\frac{1}{3}\Omega$ relative to the fluid.

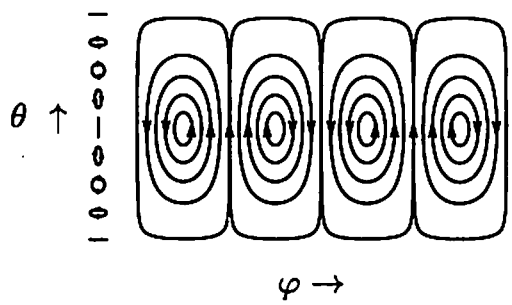

Figure 4: Polar coordinate (θ, φ) representation of the flow pattern of the $m = 2$ r-mode. The pattern moves past the individual fluid elements which respond by moving on small elliptical paths as illustrated on the left.

The effects of dissipation (*i.e.*, viscosity and GR) on the evolution of the r-mode are most easily studied by considering $\tilde{E}$, the energy of the perturbation (as measured in the co-rotating frame of the

fluid). To lowest order in Ω, $\tilde{E}$ is given by

$$\tilde{E} = \frac{1}{2}\int \rho\, \delta\vec{v}^{\,*}\cdot\delta\vec{v}\, d^3x + \mathcal{O}(\Omega^4). \tag{3}$$

This energy is conserved in the absence of dissipation, and more generally satisfies [16]

$$\frac{d\tilde{E}}{dt} = -\omega(\omega+m\Omega)\sum_{l\geq m} N_l\,\omega^{2l}\left[|\delta D_{lm}|^2 + \frac{4l|\delta J_{lm}|^2}{c^2(l+1)}\right] - \int\left(2\eta\,\delta\sigma^*_{ab}\delta\sigma^{ab} + \zeta\,\delta\sigma^*\delta\sigma\right)d^3x, \tag{4}$$

where $N_l = 4\pi G(l+1)(l+2)\{c^{2l+1}l(l-1)[(2l+1)!!]^2\}^{-1}$ are positive constants; and δD_{lm} and δJ_{lm} are the mass and current multipole moments of the perturbation,

$$\delta D_{lm} = \int \delta\rho\, r^l Y^*_{lm} d^3x, \tag{5}$$

$$\delta J_{lm} = \int r^l\,(\rho\,\delta\vec{v} + \delta\rho\,\vec{v})\cdot\vec{Y}^{B*}_{lm}\, d^3x. \tag{6}$$

The second term on the right side of Eq. (4) represents the dissipation due to the shear and bulk viscosity of the fluid: η and ζ are the viscosity coefficients, and $\delta\sigma^{ab}$ and $\delta\sigma$ are the shear and expansion of the perturbed fluid respectively. These viscosity terms in Eq. (4) always decrease the energy $\tilde{E}$ and so tend to damp the r-modes. The first term on the right side of Eq. (4) represents the effect of GR on the perturbation. The sign of this term is determined by the sign of $\omega(\omega+m\Omega)$, the product of the frequencies in the inertial and rotating frame. This product,

$$\omega(\omega+m\Omega) = -\frac{2(m-1)(m+2)}{(m+1)^2}\Omega^2 < 0, \tag{7}$$

is negative for the r-modes, thus GR tends to drive the r-modes toward instability. Further this destabilizing force is *generic* [14, 15]: GR drives all the r-modes in all rotating stars (*i.e.*, for all values of m and Ω) toward instability.

To evaluate the relative strengths of the destabilizing GR force and the dissipative viscous forces, it is convenient to define the combined dissipative timescale $1/\tau$,

$$\frac{1}{\tau} = -\frac{1}{2\tilde{E}}\frac{d\tilde{E}}{dt} = -\frac{1}{\tau_{GR}} + \frac{1}{\tau_V}, \tag{8}$$

which is just the imaginary part of the frequency of the mode. The integrals on the right sides of Eqs. (3)–(6) are easily performed to determine the GR and the viscous contributions to $1/\tau$ respectively. Using Newtonian stellar models based on fairly realistic neutron-star matter these timescales are [16, 19]:

$$\frac{1}{\tau_{GR}} = \frac{1}{38\mathrm{s}}\left(\frac{\Omega}{\Omega_{\max}}\right)^6, \tag{9}$$

$$\frac{1}{\tau_V} = \frac{1}{3\times10^8\mathrm{s}}\left(\frac{10^9\mathrm{K}}{T}\right)^2 + \frac{1}{5\times10^{11}\mathrm{s}}\left(\frac{T}{10^9\mathrm{K}}\right)^6\left(\frac{\Omega}{\Omega_{\max}}\right)^2. \tag{10}$$

For small angular velocities, $\Omega \ll \Omega_{\max}$, the GR timescale is very large so viscous dissipation always dominates, $1/\tau_{GR} \ll 1/\tau_V$. Thus neutron stars are always stable in this limit. Conversely, when Ω is sufficiently large the GR timescale is shorter than the viscous timescale and the neutron star is unstable. The critical angular velocity Ω_c,

$$\frac{1}{\tau(\Omega_c)} = 0, \tag{11}$$

marks the boundary between stability and instability. Since the viscosities are temperature dependent in neutron-star matter, so too is Ω_c. The solid curve in Fig. 5 illustrates the temperature dependence of Ω_c for the r-modes including the effects of standard microscopic shear and bulk viscosity. The minimum of

this curve occurs at $\min \Omega_c = 0.045\Omega_{max}$. For comparison Fig. 5 also illustrates Ω_c for the GR instability in the f-modes. It is obvious that GR is capable of driving the r-modes unstable over a far wider range of angular velocities than the f-modes. Thus the GR instability in the r-modes might play an interesting role in limiting the angular velocities of neutron stars, and the GR emitted during a spin-down event might be detectable. We will return to a more in depth discussion of some more realistic dissipation mechanism which may effect the r-mode instability after introducing the principal scenarios where the instability may play an interesting role in real astrophysical systems.

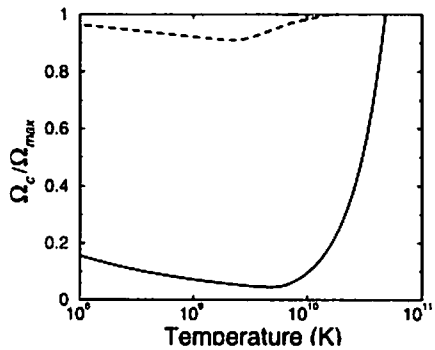

Figure 5: Temperature dependence of the critical angular velocity Ω_c for rotating neutron stars. Solid curve gives Ω_c for the instability in the $m = 2$ r-mode, while for comparison the dashed curve gives Ω_c for the f-modes.

3 Astrophysical Implications

Two astrophysical scenarios have been proposed in which the GR instability of the r-modes might play an interesting role in the evolution of real neutron stars. These are illustrated by the two evolution curves, A and B, in Fig. 6. In scenario A a rapidly rotating neutron star is formed with a very high temperature ($T \geq 10^{11}$K) as the result of the gravitational collapse of the neutron-star progenitor [16]. In this scenario the star cools within a few seconds to a point that lies above the r-mode instability curve (the dashed curve in Fig. 6). The amplitude of the r-mode then grows exponentially (with a timescale of about 40 s for a very rapidly rotating star), and becomes large within a few minutes. If the dimensionless r-mode amplitude α saturates (by some yet to be understood process) with a value of order unity, it would take about 1 y for the star to spin down to a point where stability is re-gained [17]. In this scenario a star could lose up to 95% of its angular momentum, and up to about 99% of its rotational kinetic energy by emitting GR. This scenario might provide a natural explanation for the lack of rapidly rotating neutron stars in young supernova remnants. The GR emitted in this scenario might be detectable for neutron stars as far away as the Virgo cluster [17, 20].

In scenario B an old, cold slowly rotating neutron star is spun up by accreting high angular momentum material from a companion star [21, 22]. Once the neutron star's angular velocity reaches the critical value Ω_c, the amplitude of the unstable r-mode grows exponentially. It was once thought that in this situation the amplitude of the unstable mode would grow until the rate of angular momentum lost to GR just balances the amount gained from accretion [23]. However Levin [24] has shown that viscous dissipation in the growing r-mode rapidly increases the temperature of the low specific-heat neutron-star matter. This moves the star along the horizontal section of the evolution curve B in Fig. 6. At some point the r-mode amplitude saturates (by some yet to be understood mechanism) and thermal equilibrium is established between viscous heating and neutrino cooling. The star then spins down by emitting GR until stability is regained. It has been suggested that this scenario provides an explanation for the range of rotation periods observed for the neutron stars in low mass x-ray binaries (LMXBs) [25].

These scenarios are just rough sketches and considerable work has been (and continues to be) done to fill in the details and see whether they represent realistic astrophysical possibilities. In the case of scenario B for example, it is clear that the sketch given above is too simple. The core temperatures of neutron stars in accreting systems like the LMXBs are expected to be in the range $10^8 - 10^9$K [26, 27].

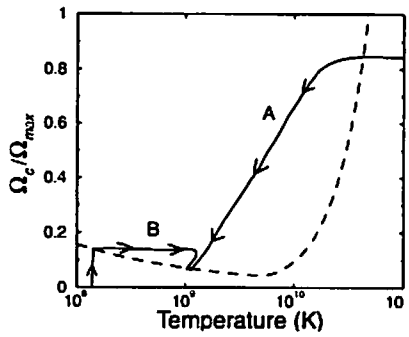

Figure 6: Rotating neutron stars may become unstable to the r-mode instability in two ways: *a)* hot young rapidly rotating stars may cool along path A, become unstable, and finally spin down to a small angular velocity; or *b)* old cold slowly rotating stars may be spun up by accretion along path B, becoming unstable, then heated by the growing r-mode, and finally spun down to a smaller angular velocity.

Simple shear viscosity gives rise to $\Omega_c \leq 0.16\Omega_{\rm max}$ in this temperature range, as seen in Fig. 5. This upper limit (of about 160 Hz) on the angular velocities of accreting systems is in conflict with the observed 300 Hz spin frequencies of the neutron stars in LMXBs, and the 600 Hz frequencies of pulsars that are believed to have been spun up in LMXB-like systems. Thus some additional dissipation mechanism must act to suppress the r-mode instability in these accreting systems. It was suggested [16] that additional dissipative effects associated with the superfluid transition in the neutron-star matter at about 10^9K might effectively suppress the r-mode instability. However, the calculations done to date indicate that the dominant superfluid dissipation mechanism (mutual friction) is generally not effective in suppressing the r-mode instability [28]. Bildsten and Ushomirsky [29] have suggested that viscous dissipation in the boundary layer between the liquid core and the solid crust of a neutron star might provide the needed stability. And Mendell [30] has shown that dissipation associated with Alfven waves (which are excited by the r-modes and then travel along magnetic field lines that are pinned to the solid crust) could in some circumstances be even stronger than the viscous boundary layer dissipation. At present it appears that some combination of these crust, magnetic field, and superfluid effects are the most likely candidates for stabilizing the r-modes in this temperature range.

At the interface between a viscous fluid and a solid (*e.g.*, the crust of a neutron star) the fluid velocity must match the velocity of the solid. Therefore viscosity significantly modifies the velocity field of an r-mode, at least in the neighborhood of the crust-core boundary. The solution of the viscous fluid equations in this boundary region [29, 33, 34] shows that the r-mode velocity field is modified significantly only in a thin layer with scale-height d,

$$d = \sqrt{\frac{\eta}{2\rho\Omega}} \approx 0.6{\rm cm}\left(\frac{10^9{\rm K}}{T}\right)\left(\frac{\Omega_{\rm max}}{\Omega}\right)^{1/2}. \qquad (12)$$

The magnitude of the shear of the fluid in this boundary layer is approximately $|\delta\sigma^{ab}| \approx |\vec{\nabla}\delta\vec{v}| \approx |\delta\vec{v}|/d$, which is larger by the factor $R/d \approx 10^6$ than the shear of the inviscid r-mode velocity field. The formation of a rigid crust therefore increases the total dissipation due to shear viscosity by approximately the factor R/d. The viscous timescale for the $m = 2$ r-mode (using a typical neutron-star model) then becomes [34],

$$\tau_V = \left(\begin{array}{ll} 280{\rm s}, & T < 10^9{\rm K} \\ 650{\rm s}, & T > 10^9{\rm K} \end{array}\right)\left(\frac{T}{10^9{\rm K}}\right)\left(\frac{\Omega_{\rm max}}{\Omega}\right)^{1/2}. \qquad (13)$$

Figure 7 illustrates the critical angular velocity Ω_c for the r-mode GR instability including the effects of this boundary-layer dissipation. The solid curves are based on neutron-star models from a number of realistic equations of state. Figure 7 illustrates that dissipation in the boundary layer significantly increases the stability of the r-modes. This suggests that rapidly rotating neutron stars, such as the 1.6 ms pulsars, are consistent with a spin-up process that operates in the $10^8 - 10^9$ K temperature range. And this suggests that the apparent clustering of spin frequencies in the LMXBs is probably not due

to the GR instability in the r-modes. However, additional work is needed to understand fully whether scenario B ever operates in real neutron stars or not. In particular the effects of a semi-rigid crust (which tend to reduce the boundary layer dissipation) [35] have not been included in Fig. 7, nor have the effects of the neutron star's magnetic field [36, 37, 30], nor have other possible effects of the superfluid core (*e.g.*, the possibility that the core vortices are pinned to the crust, or a possible dissipative interaction between neutron vortices and magnetic flux tubes).

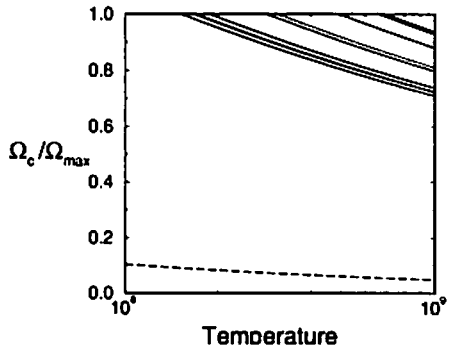

Figure 7: Solid curves represent Ω_c for neutron star models (from a variety of realistic equations of state) with rigid crust. Dashed curve represents the stability curve for a neutron star without crust.

Let us turn our attention now to astrophysical scenario A. At present it also seems unlikely that this scenario will play an interesting role in the astrophysics of real neutron stars. This pessimistic view is based on our current understanding of the effects of several complicated physical mechanisms on the r-modes. In particular the formation of a solid crust, exotic forms of microscopic dissipation in the fluid, and non-linear hydrodynamic effects are all now expected to reduce in a significant way the importance of the r-mode instability in scenario A. Here I review briefly what is known at present about how each of these processes effects the r-modes. Let us consider first the role of a solid crust. When a neutron star cools to about 10^{10}K (within about 30 s after its birth according to the standard modified URCA cooling model, or within as little as a fraction of a second according to cooling calculations that include the direct URCA process [31, 32]), a solid crust begins to form initially at densities of about $\rho_c \approx 1.5 \times 10^{14}\mathrm{gm/cm}^3$ [34]. Figure 8 shows typical values for the critical angular velocity Ω_c (the dashed curve) based on the boundary-layer dissipation from a rigid crust in the temperature range that is relevant for scenario A. If cooling proceeds by some rapid mechanism, such as direct URCA (as suggested by recent observations [38]), stars rotating slower than $\sim 0.8\Omega_{max}$ could never develop significant r-mode amplitudes: the star would cool into the stable range before the instability had time to grow. And even if the slower modified URCA cooling dominates in the portions of the star where the crust will form, only stars rotating faster than $\sim 0.5\Omega_{max}$ could develop a significant r-mode instability.

If a neutron star is born with a large angular velocity, then it may still be subject to the r-mode instability even in the presence of a rigid crust. In this case fluid flow in the boundary layer soon becomes turbulent as the amplitude of the r-mode grows. Under these conditions turbulent viscosity significantly increases the dissipation at the crust-core boundary. Wu, Matzner, and Arras [39] have shown in this case that non-linearities in the energy dissipation rate cause the amplitude of the r-mode to saturate at the value $\alpha_{sat} \approx 0.002(\Omega/\Omega_{max})^5$. In very rapidly rotating stars, $\Omega > 0.87\Omega_{max}$, this amplitude is large enough that dissipation in the boundary layer can re-melt the crust [34]. But in more slowly rotating stars the mode saturates by this turbulent viscosity mechanism before the critical melting amplitude is reached. In these cases, $\Omega < 0.87\Omega_{max}$, it appears that the crust prevents the r-mode from growing large enough to significantly change the angular momentum of the neutron star before the star cools into a region where the r-modes are no longer unstable.

Another effect that may play an important role in the r-mode stability is a form of bulk viscosity caused by hyperons in the neutron-star core [40, 41, 42]. At densities which are found in the cores of realistic neutron-star models, Σ^- and Λ hyperons probably exist in β-equilibrium with the neutrons and protons. When a fluid perturbation (such as an r-mode) changes the density of this material, weak interactions will attempt to adjust the concentrations of the hyperons to re-establish β-equilibrium. However these

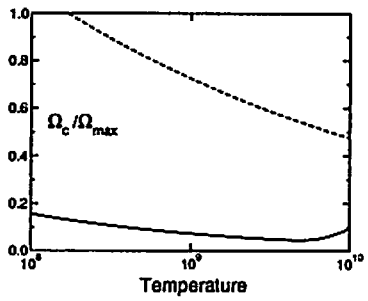

Figure 8: Curves representing the critical angular velocity Ω_c for the r-mode instability: solid curve assumes no crust has formed, dashed curve assumes standard viscous boundary layer dissipation with a rigid crust.

weak interactions are rather slow, and so equilibrium is not re-established instantaneously. There results a phase lag between the physical pressure perturbation in the material, and the appropriate equilibrium-state pressure for fluid at the density associated with the perturbation. This pressure mismatch causes dissipation, which may be characterized as a (frequency dependent) bulk viscosity. Figure 9 illustrates this bulk viscosity for a range of neutron-star matter densities, and for a range of temperatures relevant for neutron stars [42]. The effect of this type of bulk viscosity on the r-modes has been evaluated using the expressions in Eq. (4) and (8). Figure 10 illustrates the resulting neutron-star critical angular velocities for a range of neutron-star masses. We see that hyperon bulk viscosity completely suppresses the r-mode instability in 1.4 $M_\odot$ neutron stars for temperatures below a few times 10^9 K. Cooling calculations which include direct URCA reactions involving neutrons, protons and/or hyperons suggest that a neutron star will cool below this temperature within a matter of seconds: too rapidly to allow the r-mode amplitude to grow large enough to emit any significant amount of GR. Thus it appears likely that rapid cooling and the hyperon induced bulk viscosity (in addition to the dissipation from a crust discussed earlier) make it very difficult for the r-mode instability to play an interesting role in young neutron stars according to scenario A.

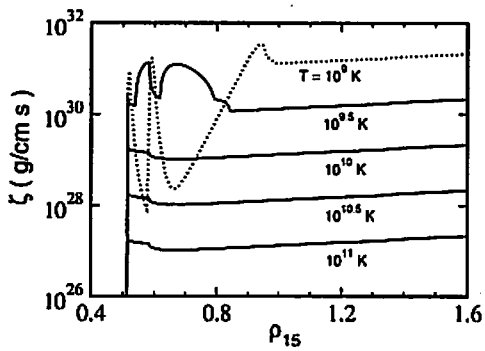

Figure 9: Density dependence (in units of 10^{15} g/cm^3) of the hyperon bulk viscosity (in units of g/cm s) for a range of temperatures.

Finally, there have been a number of recent efforts to explore the effects of non-linear hydrodynamics on the evolution of an unstable r-mode. What would happen if an r-mode in a very rapidly rotating star were somehow to escape the various dissipation mechanisms discussed above and manage (despite present expectations) to grow for several minutes so that its amplitude became large? How large could the amplitude of such an r-mode grow? What mechanism finally limits the amplitude of such a mode? There have been several large scale numerical studies, and some interesting recent analytical insights into these questions. The large-scale numerical studies consisted of putting a rapidly rotating neutron-star model

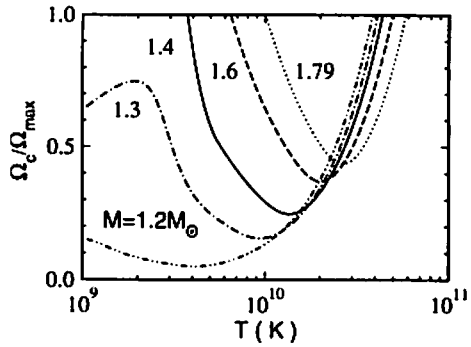

Figure 10: Critical angular velocities for neutron stars as a function of hyperon core temperature. Each curve represents a neutron star of fixed mass, ranging from $1.2M_\odot$ to the maximum mass of $1.79M_\odot$ for the equation of state used here.

with excited r-mode on a 3D numerical grid and then evolving the non-linear hydrodynamic equations to see what happens. Stergioulas and Font [43] used fully relativistic hydrodynamics in the Cowling approximation to model this system. They found that large amplitude non-linear r-modes evolve without significant dispersion in rapidly rotating fully relativistic stellar models (for tens of rotation periods). Lindblom, Tohline, and Vallisneri [44, 45] studied the growth of an unstable r-mode using Newtonian hydrodynamic equations coupled to a post-Newtonian expression for the GR reaction force. Neither study found any non-linear hydrodynamic process that prevented the amplitude of the r-mode from growing to a value of order unity. These studies however were limited by the availability of computational resources to somewhat unphysical representations of the physical system of interest: using fairly coarse spatial resolution of the fluid, lasting for only tens of rotation periods (compared to tens of thousands needed in the physical case), and using unphysical strengths for the GR reaction force (absent completely in Ref. [43], and thousands of times stronger than the physical case in Refs. [44, 45]). Recent analytical studies by Schenk, *et. al* [46], Morsink [47], and Arras, *et. al* [48] were able to overcome these limitations. They studied the non-linear hydrodynamic effects on the growth of an unstable r-mode by considering non-linear coupling between modes in the weak coupling limit. They show that an unstable r-mode couples strongly to other modes in this way. When the amplitude of an unstable r-mode reaches a certain level, α_{sat}, the energy which drives the instability is diverted by these non-linear couplings into a cascade which excites hundreds (or thousands) of other modes where the energy is ultimately converted to heat through viscous dissipation. Arras, *et. al* [48] compute the level where this saturation of the GR driven r-mode instability occurs to be

$$\alpha_{sat} \approx 0.005 \sqrt{\frac{\alpha_e}{0.1}} \sqrt{\frac{2 \times 10^5}{\tau_{GR}\Omega_{\max}}} \left(\frac{\Omega}{\Omega_{\max}}\right)^{5/2}, \tag{14}$$

where $\tau_{GR}\Omega_{\max}$ is the dimensionless product of the GR growth time and the angular velocity of the most rapidly rotating star. The "matching parameter" α_e is a measure of the strength of the mode-mode coupling, which is estimated to be in the range $4 \times 10^{-4} < \alpha_e < 0.1$. So non-linear hydrodynamic forces will limit the growth of the r-mode amplitude to values in the range: $10^{-4} < \alpha_{sat} < 5 \times 10^{-3}$. Such small amplitudes will prevent the r-modes from radiating significant amounts of GR before the neutron star becomes quite cold and consequently, according to our present understanding, quite stable. This limitation on the amplitude of the r-mode also limits the flux of GR that could be emitted during any period of instability to levels that are unlikely to be detectable.

4 Concluding Remarks

At the present time it appears that the GR instability in the r-modes may be not be strong enough to overcome the numerous dissipative processes that act to suppress it in real neutron stars. But there remain a number of important questions effecting this conclusion which have yet to be completely resolved. It is not yet completely understood (although see Refs. [36, 37, 30, 49, 50]) what role magnetic fields play in the evolution of the r-modes. Will magnetic fields suppress the instability, limit its growth, or merely change the values of the frequency and growth times? Is the formation of a solid crust delayed long enough by differential rotation or pulsations after the birth of a neutron star to allow the r-mode instability to act? Do semi-rigid crust effects move the critical angular velocity to small enough values that the GR instability can act in the LMXBs? Do superfluid effects (*e.g.*, pinning of the core vortices or vortex-fluxtube dissipation) suppress the r-mode instability completely in these stars? Does the equation of state of real neutron-star matter contain hyperons, kaons, or even free quarks which strongly increase the dissipation in the r-modes? And do rapid direct-URCA type interactions cool young stars on timescales that are short compared to the r-mode instability timescale?

Acknowledgments

It is a pleasure to thank Y. Eriguchi and M. Shibata for arranging my visit to Tokyo and for making my stay so pleasant. I also thank my collaborators N. Andersson, C. Cutler, J. Ipser, G. Mendell, S. Morsink, B. Schutz, J. Tohline, G. Ushomirsky, M. Vallisneri, A. Vecchio and especially B. Owen for their help in working out most of the material on r-modes presented in this paper. This work was supported by NASA grant NAG5-10707 and NSF grant PHY-0099568.

References

[1] L. Lindblom, in *Gravitational Waves: A challenge to Theoretical Astrophysics*, ICTP Lecture Notes Series Volume III, edited by V. Ferrari, J.C. Miller, & L. Rezzolla (2001) pp. 257–275.

[2] K.S. Thorne, and A. Campolattaro, Astrophys. J. **149**, 591 (1967); **152**, 673 (1968).

[3] K.S. Thorne, Astrophys. J. **158**, 1 (1969).

[4] S. Chandrasekhar, Phys. Rev. Letters **24**, 611 (1970).

[5] S. Chandrasekhar, Astrophys. J. **161**, 561 (1970).

[6] J.L. Friedman, and B.F. Schutz, Astrophys. J. **222**, 281 (1978).

[7] J.L. Friedman, Comm. Math. Phys. **62**, 247 (1978).

[8] L. Lindblom, and S.L. Detweiler, Astrophys. J. **211**, 565 (1977).

[9] L. Lindblom, and W.A. Hiscock, Astrophys. J. **267**, 384 (1983).

[10] C. Cutler, L. Lindblom, and R.J Splinter, Astrophys. J. **363**, 603, (1990).

[11] J.R. Ipser, and L. Lindblom, Astrophys. J. **373**, 213 (1991).

[12] C. Cutler, and L. Lindblom, Astrophys. J. **385**, 630 (1992).

[13] L. Lindblom, Astrophys. J. **438**, 265 (1995).

[14] N. Andersson, Astrophys. J. **502**, 708 (1998).

[15] J.L. Friedman, and S.M. Morsink, Astrophys. J. **502**, 714 (1998).

[16] L. Lindblom, B.J. Owen, and S.M. Morsink, Phys. Rev. Letters **80**, 4843 (1998).

[17] B.J. Owen, L. Lindblom, C. Cutler, B.F. Schutz, A. Vecchio, and N. Andersson, Phys. Rev. D **58**, 084020 (1998).

[18] J. Papaloizou, and J.E. Pringle, Mon. Not. R. Astron. Soc. **182**, 423 (1978).

[19] L. Lindblom, G. Mendell, and B.J. Owen, Phys. Rev. D **60**, 064006 (1999).

[20] B.J. Owen, and L. Lindblom, Class. Quant. Grav. **19** 1247 (2002).

[21] L. Bildsten, Astrophys. J. **501**, L89 (1998).

[22] N. Andersson, K.D. Kokkotas, and N. Stergioulas, Astrophys. J. **516**, 307 (1999).

[23] R.V. Wagoner, Astrophys. J. **278**, 345 (1984).

[24] Y. Levin, Astrophys. J. **517**, 328 (1999).

[25] N. Andersson, D.I. Jones, K.D. Kokkotas, and N. Stergioulas, Astrophys. J. **534**, L75 (2000).

[26] J.L. Zdunik, P. Haensel, B. Paczyńzki, and J. Miralda-Escudé, Astrophys. J. **384**, 129 (1992).

[27] E.F. Brown, Astrophys. J. **531**, 988 (2000).

[28] L. Lindblom, and G. Mendell, Phys. Rev. D **61**, 104003 (2000).

[29] L. Bildsten, and G. Ushomirsky, Astrophys. J. **529**, L33 (2000).

[30] G. Mendell, Phys. Rev. D **64**, 044009 (2001).

[31] C.J. Pethick, and V. Thorsson, in *Lives of the Neutron Stars*, ed. by a. Alpar, Ü. Kiziloglu, and J. van Paradijs (Kluwer, Dordrecht: 1995).

[32] D. Page, M. Prakash, J. M. Lattimer, and A. Steiner, Phys. Rev. Lett. **85**, 2048 (2000).

[33] M. Rieutord, Astrophys. J. **550** 443 (2001); Astrophys. J. **557** 493 (2001).

[34] L. Lindblom, B.J. Owen, and G. Ushomirsky, Phys. Rev. D **62**, 084030 (2000).

[35] Y. Levin, and G. Ushomirsky, Mon. Not. Roy. Astro. Soc. **324**, 917 (2001).

[36] L. Rezzolla, F. K. Lamb, and S.L. Shapiro, Astrophys. J. **531**, L139 (2000).

[37] W.C.G. Ho, and D. Lai, Astrophys. J. **543**, 386 (2000).

[38] P. Slane, D.J. Helfand, S.S.Murray, Astrophys. J. (in press) (2002); astro-ph/0204151.

[39] Y. Wu, C.D. Matzner, and P. Arras, Astrophys. J. **549**, 1011 (2001).

[40] P. Jones, Phys. Rev. Lett. **86**, 1384 (2001).

[41] P. Jones, Phys. Rev. D **64**, 084003 (2001).

[42] L. Lindblom, and B.J. Owen, Phys. Rev. D **65**, 063006 (2002).

[43] N. Stergioulas, and J.A. Font, Phys. Rev. Lett., **86** 1148 (2001).

[44] L. Lindblom, J.E. Tohline, and M. Vallisneri, Phys. Rev. Lett. **86** 1152 (2001).

[45] L. Lindblom, J.E. Tohline, and M. Vallisneri, Phys. Rev. D **65** 084039 (2002).

[46] A.K. Schenk, P. Arras, E.E. Flanagan, S.A. Teukolsky, I. Wasserman, Phys. Rev. D **65**, 024001 (2002).

[47] S.M. Morsink, astro-ph/0202051.

[48] P. Arras, E.E. Flanagan, S.M. Morsink, A.K. Schenk, S.A. Teukolsky, I. Wasserman, astro-ph/0202345.

[49] L. Rezzolla, F. L. Lamb, D. Markovic, and S. L. Shapiro, Phys. Rev. D **64**, 104013 (2001).

[50] L. Rezzolla, F. L. Lamb, D. Markovic, and S. L. Shapiro, Phys. Rev. D **64**, 104014 (2001).

Dynamical Instability in Rapidly and Differentially Rotating Self-gravitating Objects

Shigeyuki Karino[1] & Yoshiharu Eriguchi

Grad. School of Arts and Sciences, Univ. of Tokyo
Komaba 3-8-1, Meguro, Tokyo, 153-8902

Abstract

A new criteria of the dynamical instability in rapidly rotating stars is presented. It is well known that a rotating self-gravitating fluid becomes unstable under rapid rotation. Especially, simple models as like Maclaurin spheroid have been studied in detail, and it is known that in Maclaurin model bar-mode becomes dynamically unstable when the stellar $T/|W|$ is larger than 0.27. Here, T is the rotational kinetic energy, and W is the gravitational potential energy of the model. For more complicated models, however, there is no general consensus whether the result for Maclaurin model can be applied or not. Although a large number of analysis and simulations have been done, the general criterion that instabilities set in have not been given, for compressible stars or differentially rotating stars. In this paper, we have studies the limits where dynamical instabilities set in, by using linear stability analysis method for rapidly and differentially rotating compressible stellar models. As the result, when we adopt the parameter $T/|W|$ as the indicator of rotation, we find that the criteria of dynamical instabilities strongly depend on the degree of differential rotations. The critical $T/|W|$ decrease as the degree of differential rotation get stronger. If strong differential rotation is assumed, the critical value of $T/|W|$ becomes about 0.2. This value, i.e. $T/|W| \sim 0.2$ is much smaller than the critical value for Maclaurin spheroid, $T/|W| = 0.27$.

1 Introduction

It is well known that a rapidly rotating self-gravitating fluid is unstable, mainly against $m = 2$ mode. Here, m is the wave number in azimuthal direction. The $m = 2$ mode is also called as "bar-mode" according to its deformation. Also it is known that there are two types of instabilities. First one is secular instability, which grows with dissipative time scale, as like time scales of viscosities, gravitational wave radiations, and so on. On the other hand, the second type of instability, dynamical instability, grows very rapidly with dynamical time scale. In the present study, we will discuss about only dynamical instability. The physical properties of these instabilities are well known in Maclaurin spheroid, that is, rigidly rotating self-gravitational gaseous body with uniform density, and corresponding to the polytrope with $N = 0$. Dominant types of instabilities are depending on the degree of the stellar rotation [8] [12] . In order to describe the strength of rotation, we often use a parameter $T/|W|$, where T is the rotational kinetic energy, and W is the gravitational potential energy of the star. In the case of Maclaurin spheroids, very important criteria have been derived. That is, when the stellar rotation is enough large, quantitatively, when $T/|W|$ is larger than 0.14, the star is secularly unstable against bar-mode. Further more, when the stellar rotation is drastically large, that is, when $T/|W|$ is lager than 0.27, the star is also dynamically unstable against bar-mode. As mentioned before, these thresholds of instabilities have been derived from the analysis about Maclaurin spheroid. But, please notice that, also from Tensor Virial analysis about differentially rotating compressible stars, almost the same results were obtained. Hence, some authors have believed that these critical values are universal criteria, and can be expand into more general cases.

From astrophysical points of views, these instabilities may play important roles in the cases involving rapid rotations. Especially, dynamical instability is quite important since it grows much faster than secular instability. For instance, in the star forming regions, or in the collapsing massive stellar cores, dynamical instability may play a crucial role to pull out the angular momentum from the central core.

[1] e-mail:karino@valis.c.u-tokyo.ac.jp

In the past, such discussions had been made by using the stability criteria given from the case of Maclaurin spheroids. Namely, even if we adopt compressible equations of state, we had regarded the criteria to be the same as the case of rigidly rotating non-compressible cases. This expansion, however, has no guaranteed basis, because Tensor Virial method which is one of the most popular method used for stability analysis cannot be applied to differentially rotating cases, in fact.

Recently, some studies which indicate that the stability criteria in the compressible stars should be revised, have been published. Before '90s, we had believed that the stability criteria are universal values, and do not depend on the stellar parameters as like equation of states, or rotation laws. Contradictory, some authors have presented their results of numerical simulations indicating that, bar-mode grows rapidly even if $T/|W|$ is less than 0.27, in differentially rotating stars [3] [6] [7] [10]. As mentioned before, such a change of properties of the stellar stability may influence astrophysics. Therefore, it is necessary to check whether the other stability analysis give the same result with those simulated results. For such a motivation, we have tried to obtain the stability criterion of differentially and rapidly rotating self-gravitating fluid bodies, by using linear stability analysis.

2 Numerical Method

In differentially rotating polytropes, we are studying the critical values of rotation where dynamical instability sets in, by using linear stability analysis. The reason why we use linear stability analysis is following; (1)Former analytic, or semi-analytic methods as like Tensor Virial method, are very strong for simple cases as like Maclaurin spheroids. Contrary to this, for complicated models, for example models accompanied with differential rotations, those analytical methods cannot applied. (2)Non-linear simulations can not give precise limits of instability without vast computing time, although they can pursue the non-linear evolutions of unstable modes. The purpose of this paper is obtaining the criteria for several models, so non-linear analysis are not suitable for the present study. Therefore, in the present study, linear stability analysis is applied to obtain the criteria where instability sets in.

2.1 Equilibrium Models

To analyze the stability, we have to obtain the equilibrium configuration of the stellar model. We have used the SFNR (Straight Forward Newton-Raphson) method to obtain equilibrium states of differentially rotating stars [4]. Here, to compute the equilibrium state, we have assumed only polytropic equation of state,

$$p = K\rho^{1+\frac{1}{N}}, \tag{1}$$

where K and N are the polytropic constant and the polytropic index, respectively. Also, axisymmetric configurations and Newtonian gravitation are assumed. Now, since the cases accompanied with differential rotations are considered, the angular velocity is assumed to be expressed by the following formula:

$$\Omega^2 = \frac{j_0^2}{(R^2 + A^2)^2}, \tag{2}$$

where R is the distance from the rotation axis, and j_0 is a constant. The quantity A is a parameter which represents the degree of differential rotation. The rotation becomes more differentially as A becomes small, and, on the other hand, when we consider the limit of $A \to \infty$, the stellar rotation comes back to uniform rotation. As an example, when $A = 1$, the central angular velocity is as twice as the surface angular velocity on the equatorial plane. Assuming these conditions, a hydrostatic equation and a Poisson equation for gravitational potential are solved numerically by SFNR method. The solved equilibrium configurations are next used as the non-perturbed states for following stability analysis.

2.2 Perturbed States

To compute the perturbed states, perturbations are assumed to be adiabatic. The method which we use to obtain the behavior of bar-mode is advanced version of the linear stability analysis code which has been used to study f-mode secular instability [13] and r-mode instability [5].The basic concept of this

scheme is to solve the perturbed fluid equations for rotating polytropes by the Newton–Raphson iteration scheme. As solving perturbed fluid equations, the perturbed quantities (the velocity components in each directions, density perturbations) are expanded as following manner;

$$\delta f_1(r,\theta,\varphi,t) = \sum_m \exp(i(\sigma t - m\varphi)) f_m(r,\theta), \tag{3}$$

where δf means the Euler perturbation of the corresponding quantity. Here, (r,θ,φ) are the ordinary spherical coordinates, and m is the azimuthal wave number. Since we are considering bar-mode, we deal only the case with $m = 2$, in this paper. σ is corresponding to the eigenvalue of the mode. Constructing a system of perturbed fluid equations with perturbed gravitational potentials, and solving them under above conditions numerically together with boundary conditions, we can obtain the eigenfunctions and eigenvalue of the modes. Here, the point is to solve not only the real part of solved eigenvalue, σ, but also its imaginary part. Since solved quantities are expanded as eq.(3), if the eigenvalue has finite imaginary component, solved mode can be regarded to be dynamically unstable. Therefore, the critical value of instability corresponds to the first point where the imaginary part of the eigenvalue emerges when the stellar rotation getting faster.

3 Discussions

3.1 Numerical Results

By iterating computations along certain sequences with fixed the strength of differential rotation (i.e. fixing the parameter A), we can get critical points where dynamical instability sets in. Here, as the parameter describing the effect of rotation, we use a parameter, $r_p \equiv r_{axis}/r_{eq}$, called "axis ratio". r_{axis} and r_{eq} are the surface radii on the rotational axis and equatorial plane, respectively. By fixing A (and also fixing equation of state) and changing r_p, we can obtain each sequence. At present, only intermediate compressible model with $N = 1.0$ have been examined, and the parameter A have been computed in the region up to $A^{-1} = 2.0$. For the models with large As, mass shedding from equator would occur before dynamical instability sets in, hence it is not necessary to consider lager A in the present context.

In Figure 1, the absolute value of imaginary part of the eigenvalue is shown as an example. The stellar model is a polytrope with $N = 1.0$ and is under slight effect of differential rotation, where $A = 1.0$. In this case, it is clear that the absolute value of the imaginary component of eigenvalue is growing up rapidly when the stellar rotation becomes faster than $T/|W| \simeq 0.27$. Such a rapid growing of imaginary part of the eigenvalue is a typical feature of dynamical instability. Hence, in this case, it is reasonable to regard that the instability appears around the point of $T/|W| = 0.27$. When the degree of differential rotation get stronger, however, this critical value of rotation tends to decrease, as shown in Figure 2. This figure shows the critical points of $T/|W|$s, plotted against the parameter A. The horizontal axis is the reciprocal value of the parameter A, and the right-hand side is corresponding to strong differential rotations. These points in figure 2 shows that, in strong differential rotation regions, the critical point where dynamical instability sets in, becomes smaller. When we choose extremely strong differential rotation as $A^{-1} = 2.0$, the critical values of $T/|W|$ takes only about ~ 0.2. This value is much smaller than the case of rigidly rotating Maclaurin spheroid. This tendency clearly means that in strong differential rotation, bar-modes will grow rapidly and non-linearly even if the stellar rotational energy is not so large. The astrophysical implications will be discussed in following section.

3.2 Astrophysical Application

The tendency that dynamical instabilities may appear even if the rotational speed is not so fast when the strong differential rotations are considered. This result agrees with the previous results obtained by non-linear simulations about differentially rotating masses [3] [6] [7] [10]. These agreement implies that when we consider rapidly and differentially rotating astrophysical objects, we should not apply the stability criteria given from uniformly rotating fluids.

Also such a change of aspects makes us modify and reconstruct our understandings about astrophysical objects. Although there are only a few situations influenced from dynamical instability since such an

instability appears only in the cases with drastically rapid rotations, in some cases this kind of instability is so important from the astronomical point of view.

One example case being important subject of dynamical instability is nascent neutron stars. Since the radius of a neutron star is so compact, the rotational velocity is quite rapid if the angular momentum of the progenitor is conserved during neutron star formation. Additionally, it is suggested that young neutron stars made from accretion induced collapses of white dwarf - giant binary systems, and from coalescence of neutron star - neutron star binaries are differentially rotating [6] [11]. Therefore those nascent neutron stars may be suffered from dynamical instability because of their rapid and differential rotations. Hence, the decrement of the critical rotation rate where dynamical instability appears may play important roles. Neutron stars suffered from dynamical instability will be deformed due to nonlinear growth of non-axisymmetric perturbations. Then those nonlinearly deformed compact stars with rapid rotation will emit large amount of gravitational wave. Such young neutron stars with unstable modes will be important target of next generation laser interferometer [9] [10].

Another example which should be concerned with dynamical instability is star forming gas cloud. A proto-stellar object is made from widely expanded gas cloud. During contraction of a huge gas cloud into a small young stellar object (YSO), the radius of the gas cloud decreases for many orders. Throughout such a star formation, the total angular momentum must be almost preserved. Hence, the rotation rate of the final young stellar object will be extremely high, and it may be suffered from dynamical instability. What will happen if dynamical instability grows during star formation is still unclear. Several authors thought that dynamical instability during star formation is concerning with binary formation, and other some authors predicted the new systems consisted of the central young stellar object object and circum-YSO disk [1] [2]. To obtain the fact, reliable non-linear simulations and high-resolution infrared/radio observations about star forming regions.

We think that such kinds of stability analysis must be done in more detail, in near future, to discuss dynamical instability in differentially rotating compressible fluids.

We would like to thank M. Shibata for his helpful discussions and comments. We are grateful to K. Uryu and S'i. Yoshida for their discussions and useful comments.

References

[1] Bate,. M. 1998, ApJL, 508, L95

[2] Bonnell,. I. 1994, MNRAS, 269, 837

[3] Centrella, J., New, K., Lowe, L., & Brown, D. 2001, ApJ, 550, L193

[4] Eriguchi, Y., & Müller, E. 1985, A&A, 146, 260

[5] Karino, S., Yoshida, S'i., Yoshida, S'j., & Eriguchi, Y. 2000, Phys. Rev. D., 62, 084012

[6] Liu, Y. T., & Lindblom, L. 2001, MNRAS, 324, 1063

[7] Pickett, B., Durisen, R., & Davis, G. 1996, ApJ, 458, 714

[8] Shapiro, S. L., & Teukolsky, S. L. 1983, Black Holes, White Dwarfs, and Neutron Stars (New York: Wiley)

[9] Shibata, M., Baumgarte, T., & Shapiro, S. 2000, ApJ, 542, 453

[10] Shibata, M., Karino. S., & Eriguchi, Y., ApJL, submitted

[11] Shibata, M., & Uryu, K. 2000, Phys. Rev. D., 61, 064001

[12] Tassoul, J.L. 1978, Theory of Rotating Stars (Princeton: Princeton Univ. Press)

[13] Yoshida, S'i. 1995, ApJ, 830,1995

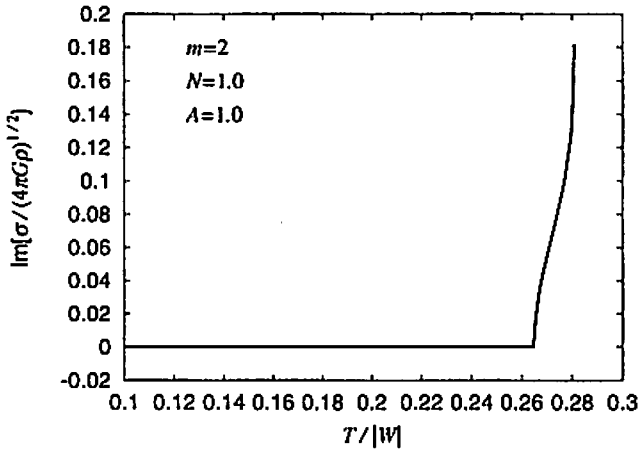

Figure 1: Imaginary part of eigenvalue of $m = 2$ mode is shown. The stellar model is $N = 1.0, A = 1.0$. In slowly rotating regions, this value is constantly zero. Contrary, once stellar rotation reaches certain point, the value grows very rapidly. This point correspond the critical limit where dynamical instability sets in.

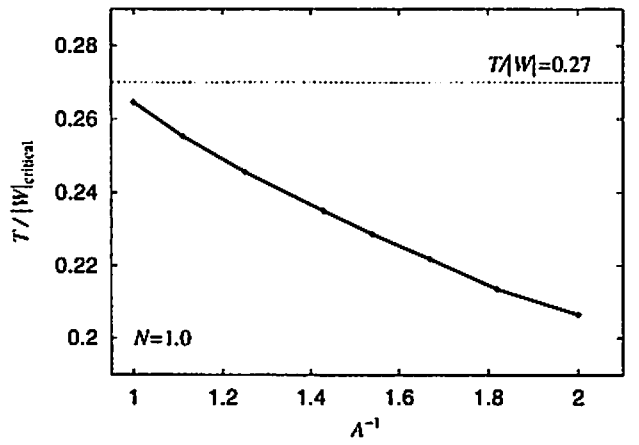

Figure 2: The behavior of critical points where dynamical instability appears. The stellar model is again $N = 1.0, A = 1.0$. When strong differential rotations are considered, the critical value of $T/|W|$ tends to decrease.

Oscillations of differentially rotating relativistic stars — f-modes and their secular stability limits

Shin'ichirou Yoshida[1] and Luciano Rezzolla

SISSA/International School for Advanced Studies,
Via Beirut 2-4, 34014 Trieste, Italy

Shigeyuki Karino and Yoshiharu Eriguchi

Department of Earth Science and Astronomy, Graduate School of Arts and Sciences,
University of Tokyo,
Komaba, Meguro-ku, Tokyo 153-8902, Japan

Abstract

We have computed the eigenfrequencies of f modes for a constant rest-mass sequences of rapidly rotating relativistic inviscid stars in differential rotation. The frequencies have been calculated neglecting the metric perturbations (the relativistic Cowling approximation) and expressed as a function of the ratio between the rotational kinetic energy and the absolute value of the gravitational energy of the stellar model $\beta \equiv T/|W|$. The zeros and the end-points of these sequences mark respectively the onset of the secular instability driven by gravitational radiation-reaction and the maximum value of β at which an equilibrium model exists. In differentially rotating stars the secular stability limits appear at a β larger than those found for uniformly rotating stars. Differential rotation, on the other hand, also allows for the existence of equilibrium models at values of β larger than those for uniformly rotating stars, moving the end-point of the sequences to larger β. As a result, for some degrees of differential rotation, the onset of the secular instability for f modes is generally favoured by the presence of differential rotation.

1 Introduction

Instabilities of rotating relativistic stars have been studied for more than three decades in relation to the emission of gravitational waves driven by radiation-reaction. Since the discovery of the so called Chandrasekhar-Friedman-Schutz (CFS) instability [4, 12], in fact, the stability properties of a number of non-axisymmetric stellar oscillations have been investigated using different techniques (see [11, 1] for recent reviews). The f (fundamental) modes were among the first modes of oscillations ever to be studied in rotating relativistic stars. These are spheroidal modes with harmonic indices $l = m$ and represent the generalization of the Kelvin modes of Newtonian Maclaurin spheroids to compressible fluid stars. Over the years, the literature on the subject has been continuously updated and the limits for the onset of the instability have been improved through different approaches. This has been done by several groups focussing on Newtonian stellar models [2, 7, 6, 9, 14, 23, 15], on post-Newtonian stellar models [8], and on rapidly rotating relativistic stars [30, 28, 25]. Part of the interest in these modes comes from the fact that they have long been regarded as the modes of oscillation most susceptible to the CFS instability. In particular, for stars rotating at a rate at which mass starts being shed at the equator (the mass-shedding limit), general relativistic calculations on the stability limit indicate that the $l = m = 2$, f-mode (also referred to as the "bar-mode") could have the shortest growth timescale. Because of this, and because of a possible weakening of the bulk viscosity at very high temperatures [19], the bar-mode may represent the most important non-axisymmetric instability in very hot and rapidly rotating newly born neutron stars.

[1] E-mail:yoshida@sissa.it

The occurrence of an f-mode instability in a newly born uniformly rotating neutron star is in general prevented by the large bulk and shear viscosities of nuclear matter in those conditions and detailed calculations have shown that the instability is suppressed except for very large rotation rates, close to the mass-shedding limit [16]; for superfluid stars an even stronger damping was calculated [20]. More recently, however, a number of new elements have improved our understanding of the instability and have again increased the expectations that the f mode instability might characterize the earliest life stages of a newly formed neutron star. The first of these new elements was provided by [8] who have shown that, within a post-Newtonian approximation, general relativistic effects tend to further destabilize the f mode, lowering the critical value of the ratio between the stellar rotational kinetic energy and the absolute value of the gravitational energy, $\beta_c \equiv (T/|W|)_c$ at which the secular f-mode instability is triggered. Analogous results have also been found by [30] within the relativistic Cowling approximation and by [28] in fully general relativistic calculations. The second new element was provided by [27], whose fully general relativistic hydrodynamical simulations have shown that the remnants of binary neutron star mergers could be, at least for polytropic equations of state, rapidly and differentially rotating stars. In addition to this, [22] have recently computed the structure of objects formed in accretion-induced collapse of rotating white dwarfs and found that these objects can rotate extremely rapidly and differentially.

Within this framework, differential rotation has two major consequences. Firstly, it allows for the existence of an equilibrium model at values of β which are considerably larger than the ones supported by the counterparts with the same rest-mass but uniform rotation [3]. Secondly, as shown by a number of authors for Newtonian stellar models [23, 14, 13] , it increases the critical value β_c for the onset of the secular instability. In this revised picture, we have computed the eigenfrequencies of f modes and determined the secular stability limits for rapidly rotating relativistic stars with differential rotation.

2 Basic equations

The equilibrium stellar models are assumed to be stationary and axisymmetric and are constructed with a numerical code based on the method of [18]. Their spacetime is therefore described by the line element

$$ds^2 = -e^{2\nu}dt^2 + e^{2\alpha}(dr^2 + r^2 d\theta^2) + e^{2\mu} r^2 \sin^2\theta (d\phi - \omega dt)^2 \ , \qquad (1)$$

where ν, α, μ, and ω are the "gravitational potentials" and are functions of the r and θ coordinates only. The stars are modeled as relativistic polytropes with the equation of state (EOS)

$$\frac{p}{\rho_c} = \kappa \left(\frac{\rho}{\rho_c}\right)^{1+1/N} \quad , \quad \epsilon = \rho + Np \ , \qquad (2)$$

where p, ρ, ϵ are the pressure, the rest-mass density and the total energy density, respectively. The subscript "c" refers to the maximum value for the equilibrium model which is used for normalization. In order to investigate how the limits for the secular instability depend on the "stiffness" of the EOS, we have performed calculations for two different polytropic models whose properties are summarized in Table I (We adopt units in which $c = G = M_\odot = 1$.). Along each sequence of rapidly rotating stellar models, the polytropic constant κ, the polytropic index N and the total rest-mass M_0 are kept constant.

	N	κ	$M_0/M_\odot$
Model (a)	0.5	6.02×10^4	1.60
Model (b)	1.0	1.00×10^2	1.52

Table 1: Properties of the polytropic equilibrium models.

The rapidly rotating stellar models are constructed after specifying a law of differential rotation $\Omega = \Omega(r, \theta)$ with a choice which is, to some extent, arbitrary. This is because there are a number of differential rotation laws that satisfy the integrability condition of the equation of hydrostatic equilibrium

as well as the Rayleigh criterion for dynamical stability [29]. All of these laws are physically consistent, cannot be excluded on physical grounds and might influence the qualitative behaviour of the results. We here follow the formulation suggested by [18] who have modeled the rotational angular velocity profile as

$$A_{\rm R}^2(\Omega_0 - \Omega) = \frac{(\Omega - \omega) r^2 \sin^2\theta e^{2(\mu-\nu)}}{1 - (\Omega - \omega) r^2 \sin^2\theta e^{2(\mu-\nu)}} \,. \tag{3}$$

Here Ω_0 is the angular velocity at the rotational axis and $A_{\rm R}$ is a dimensionless parameter accounting for the degree of differential rotation. In particular, the degree of differential rotation increases with $A_{\rm R}^{-1}$, and in the limit of $A_{\rm R}^{-1} \to 0$, the profile reduces to that of uniform rotation. In the Newtonian limit, the differential rotation law (3) reduces to the so-called "j-constant" law [5]

$$\frac{\Omega}{\Omega_0} = \frac{A_{\rm N}^2}{A_{\rm N}^2 + r^2 \sin^2\theta} \,, \tag{4}$$

and is commonly used in Newtonian calculations [10, 17, 26].

Once the rapidly and differentially rotating equilibrium stellar model has been constructed, we introduce "adiabatic" perturbations in the fluid variables so that the adiabatic index of the perturbed matter coincides with the polytropic exponent of the equilibrium configuration

$$\frac{\Delta p}{p} = \left(1 + \frac{1}{N}\right) \frac{\Delta \rho}{\rho} \,. \tag{5}$$

Here, Δ refers to a Lagrangian perturbation of a variable. Because of the stationary and axisymmetric background, the Eulerian perturbations are naturally decomposed into a harmonic component of the type $\sim \exp(-i\sigma t + im\phi)$, where σ is the mode angular frequency and m is an integer. Working within the Cowling approximation [24], we do not include Eulerian perturbations in the metric and the fluid oscillations are investigated in the fixed background spacetime of the equilibrium star (1) This simplification clearly introduces an error which is particularly large in the case of the lower order f modes. However, as discussed in previous works [21, 32, 30], the results obtained with this approximation reproduce well the qualitative behaviour of the mode eigenfrequencies with the errors being of the order of 10% for low mode-numbers and progressively less for high mode-numbers [21, 30]. Furthermore, by neglecting the contributions coming from the metric perturbations, the Cowling approximation tends, at least for the lowest mode-numbers (i.e. $m = 2, 3$), to overestimate the stability. [30]

Introducing the harmonic perturbations in the hydrodynamical equations yields a system of four partial differential equations accounting for baryon number conservation and conservation of the stress-energy tensor. These equations are then solved for the four unknown functions represented by the Eulerian perturbation of the 3-velocity $\delta v^r, \delta v^\theta, \delta v^\phi$ and the dimensionless quantity $q \equiv \delta p/(\epsilon + p)$. The partial differential equations are discretized on a two-dimensional numerical grid and are solved following the strategy discussed by [30], after imposing $\Delta p = 0$ at the surface of the unperturbed star as a boundary condition. For each degree of differential rotation $A_{\rm R}$ and for each mode-number m, the solution to the eigenvalue problem is found for increasing values of β until the limit of mass-shedding is found, which is indicated with β_s (see [18] for a definition of β).

3 Results

The results of these calculations are presented in Fig.2, where we plot the frequencies of the $m = 2$ mode as a function of the parameter β for the model (b) of Table I. Different curves refer to different degrees of differential rotation. Note that the values of β at which $\sigma = 0$ (i.e. β_c) signal the onset of the secular instability (neutral points) and that these increase as the degree of differential rotation is increased. At the same time, however, the differentially rotating models are able to support larger values of β before reaching the mass shedding limit β_s, represented by the end-points of the curves in Fig.2.

Given the results of Fig.1 it is natural to ask whether differential rotation favours or not the onset of the f-mode instability in rapidly rotating relativistic stars. The evidence that β_c increases with increasing differential rotation is not sufficient to draw a conclusion since differentially rotating models can support

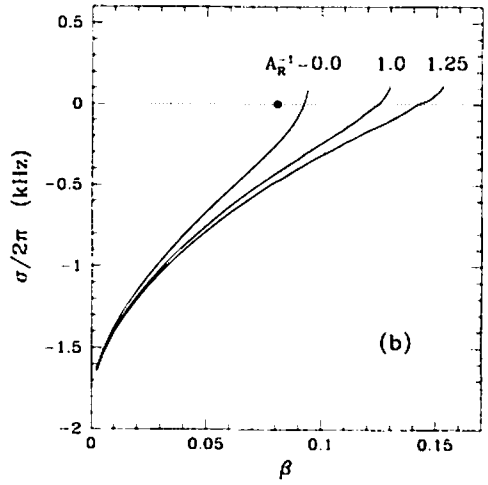

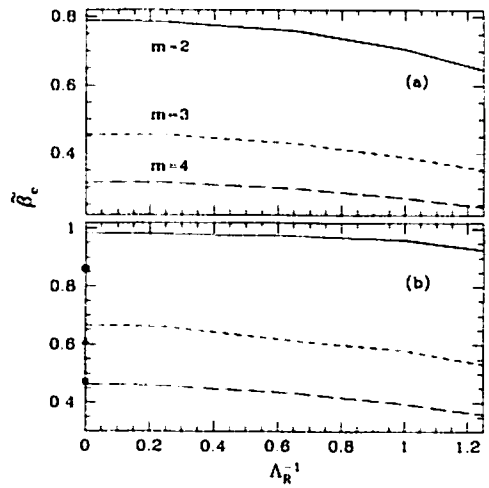

Figure 1: [Left] Eigenfrequencies of the $m = 2$ mode as a function of the parameter $\beta = T/|W|$ for the model (b) of Table I. Different curves refer to different degrees of differential rotation, with the $A_R^{-1} = 0.0$ line being the one of a uniformly rotating model. The filled dot indicates the neutral stability point of a uniformly rotating star computed in full general relativity [28].

Figure 2: [Right] $\tilde{\beta}_c$ as a function of the rate of differential rotation. The two panels refer to the two models of Table I and the different line types refer to different mode-numbers. The filled symbols show a comparison with the fully general relativistic calculations of [28].

values of β which are considerably larger than those of uniformly rotating stars before reaching the mass-shedding limit. This is simply due to the fact that in the differentially rotating model described by eq. (3) the inner regions can rotate rapidly while the outer regions rotate more slowly, preventing mass-shedding. Thus, to quantify the importance of differential rotation for the onset of the instability we need to measure not only the secular stability limit β_c, but also how close the latter is to the ultimate limit of mass-shedding β_s. A relative measure of the two quantities across sequences with different degrees of differential rotation can provide information on the likelihood of the existence of a configuration at the onset of the secular instability and clarify the role played by differential rotation. In this sense, the normalization of β_c with β_s is equivalent to the normalization, commonly used for uniformly rotating stars, of writing the stellar angular velocity in terms of the mass-shedding angular velocity.

In Fig.2 we show the behaviour of the ratio $\tilde{\beta}_c \equiv \beta_c/\beta_s$ as obtained for degrees of differential rotation ranging between $A_R^{-1} = 0$ (uniform rotation) to $A_R^{-1} = 1.25$.

The two panels of Fig.2 refer to the models (a) and (b) of Table I, respectively. In each panel, the different lines refer to the mode-numbers $m = 2, 3$ and 4. As anticipated above, the Cowling approximation overestimates the stability of the stellar models by introducing an error which is of the order of 10% for the $m = 2$ mode but is considerably smaller for higher mode-numbers. This can be appreciated by comparing with the fully general relativistic values of $\tilde{\beta}_c$ computed for uniformly rapidly rotating stellar models [28] and indicated with filled symbols in the lower panel of Fig.2. The overall decrease of $\tilde{\beta}_c$ for increasing degrees of differential rotation provides a clear indication that the onset of the secular f-mode instability is in general *favoured* by the presence of differential rotation. This is most evident in the case of a stiffer EOS [model (a) of Table I] where, for reasonable degrees of differential rotation, $\tilde{\beta}_c$ is reduced by about 17%.

A more detailed discussion of the results presented in this paper can be found in [31].

It's a pleasure to thank John Miller and Nick Stergioulas for useful discussions and comments. This research has been supported by the MIUR, EU Research Training Network Contract HPRN-CT-2000-00137 and Grant-in-Aid for Scientific Research of Japan Society for the Promotion of Science (12640255).

References

[1] N. Andersson and K.D. Kokkotas, Int. J. Mod. Phys. **D10** (2001) 381

[2] J.M. Bardeen, J.L. Friedman, B.F. Schutz and R. Sorkin, Astrophys. J. **217** (1977) L49

[3] T.W. Baumgarte, S.L. Shapiro and M. Shibata, Astrophys. J. **528** (2000) L29

[4] S. Chandrasekhar, Phys. Rev. Lett. **24** (1970) 611

[5] M.J. Clement, Astrophys. J. **222** (1978) 967

[6] M.J. Clement, Astrophys. J. **230** (1979) 230

[7] N. Comins, Mon. Not. Royal Astron. Soc. **189** (1979a) 233 ; **189** (1979b) 255

[8] C. Cutler and L. Lindblom, Astrophys. J. **385** (1992) 630

[9] R.H. Durisen and J.N. Imamura, Astrophys. J. **243** (1981), 612

[10] Y. Eriguchi and E. Müller, Astron. & Astroph. **146** (1985) 260

[11] J.L. Friedman, *Black Holes and Relativistic Stars*, R. B. Wald ed. (The Univ. of Chicago Press, Chicago, 1998)

[12] J.L. Friedman and B.F. Schutz, Astrophys. J. **222** (1978) 281

[13] J.N. Imamura and R.H. Durisen, Astrophys. J. **549** (2001) 1062

[14] J.N.Imamura, J.L.Friedman, and R.H.Durisen, Astrophys. J. **294** (1985), 474

[15] J.R. Ipser and L. Lindblom 1990, Astrophys. J. **355** (1990) 226

[16] J.R. Ipser and L. Lindblom, Astrophys. J. **373** (1991) 213

[17] S. Karino, S'i. Yoshida, and Y. Eriguchi, Phys. Rev. **D64** (2001) 024003

[18] H. Komatsu, Y. Eriguchi and I. Hachisu, Mon. Not. Royal Astron. Soc. **237** (1989a) 355 ; **239** (1989b) 153

[19] D. Lai, *Astrophysical Sources of Gravitational Radiation for Ground-Based Detectors*, J. Centrella ed. (AIP Press, 2001)

[20] L. Lindblom and G. Mendell, Astrophys. J. **444** (1995) 804

[21] L. Lindblom and R.J. Splinter, Astrophys. J. **348** (1990) 198

[22] Y.T. Liu and L. Lindblom, Mon. Not. Royal Astron. Soc. **324** (2001) 1063

[23] R.M. Managan, Astrophys. J. **294** (1985) 463

[24] P.N. McDermott, H.M. Van Horn and J.F. Scholl Astrophys. J. **268** (1983) 837

[25] S.M. Morsink, N. Stergioulas and S. Blattnig, Astrophys. J. **510** (1999) 854

[26] L. Rezzolla and S'i. Yoshida, Classical and Quantum Gravity **18** (2001) L87

[27] M. Shibata and K. Uryū, Phys. Rev. **D61** (2001) 064001

[28] N. Stergioulas and J.L. Friedman, Astrophys. J. **492** (1998) 301

[29] J-L. Tassoul, *Theory of rotating stars* (Princeton University Press, Princeton, 1978)

[30] S'i. Yoshida and Y. Eriguchi, Astrophys. J. **490** (1997) 779 ; **515** (1999) 414

[31] S'i. Yoshida, L. Rezzolla, S. Karino and Y. Eriguchi, To appear in Astrophys. J. Lett.

[32] Sj. Yoshida and Y. Kojima, Mon. Not. Royal Astron. Soc. **289** (1997) 117

r-modes of Slowly Rotating Relativistic Stars

Shijun Yoshida[1]

Astronomical Institute, Graduate School of Science, Tohoku University, Sendai 980-8578, Japan

Abstract

We investigate properties of r-mode solutions of Kojima's equation characterized by the regular eigenvalue problem in slowly rotating relativistic polytropes. Here, Kojima's equation is the master equation for pure r-modes in slowly rotating relativistic stars. Our numerical results suggest that discrete r-mode solutions of Kojima's equation for the regular eigenvalue problem exist only for restricted polytropic models. In particular, the r-mode associated with $l = m = 2$, which is considered to be the most important for gravitational radiation driven instability, does not have a discrete mode as a solution of the regular eigenvalue problem for polytropes having the polytropic index $N > 1.18$, even in the post-Newtonian order. Furthermore, for an $N = 1$ polytrope, which is employed as a typical neutron star model, discrete r-mode solutions for regular eigenvalue problem do not exist for stars whose relativistic factor M/R is larger than about 0.1, where M and R are stellar mass and stellar radius, respectively.

1 Introduction

Since the discovery of the gravitational radiation driven instability of the r-modes by Andersson [1] and Friedman and Morsink [2], a large number of studies on the properties of r-modes and inertial modes of rotating stars have been done to prove their possible importance in astrophysics (for a review, see, e.g., Lindblom's contribution of this volume or [3, 4]). Although our understandings of r-modes have been largely improved by recent energetic investigations, most studies concerning r-modes have been done in the framework of Newtonian gravity. As for r-modes in the framework of general relativity, Kojima [5] found the possible existence of a continuous spectrum for pure r-modes in relativistic stars. Here, and throughout this paper, we call the rotational mode whose eigenfunctions are composed of only one axial parity component in the non-rotating star limit a "pure r-mode". Beyer and Kokkotas [6] generally verified the existence of a continuous spectrum. Kojima's formalism was developed by Kojima and Hosonuma [7, 8] to include high order rotational effects. Recently, Lockitch, Andersson, and Friedman [9] have shown that pure r-modes in a relativistic star can exist only in non-isentropic stars, whose specific entropy distribution is not constant. They have also found that discrete r-mode solutions in Kojima's equation can exist by considering uniform density stars. It is reasonable to consider that such discrete r-mode solutions correspond to those of Newtonian r-mode. However, their study was restricted to the case of uniform density stars. As mentioned later, the frequency range for the regular eigenvalue problem is confined to the narrow region, and depends on the structure of equilibrium stars. Thus, it is interesting and important to answer the question of whether r-mode solutions of Kojima's equation for the regular eigenvalue problem exist in all non-isentropic relativistic stars. In this paper, therefore, we study discrete r-mode solutions of Kojima's equation for a large class of polytropic and non-isentropic relativistic stellar models. Throughout this paper, we will use units in which $c = G = 1$, where c and G denote the velocity of light and the gravitational constant, respectively.

2 Method of Solutions

We consider slowly rotating relativistic stars with a uniform angular velocity Ω, in which we take into account the first order rotational effect in Ω. The geometry around the equilibrium stars can be described by the line element (see, e.g., [10]):

$$ds^2 = -e^{2\nu(r)}dt^2 + e^{2\lambda(r)}dr^2 + r^2d\theta^2 + r^2\sin^2\theta d\varphi^2 - 2\omega(r)r^2\sin^2\theta dt d\varphi\,. \tag{1}$$

[1] E-mail:yoshida@astr.tohoku.ac.jp

Throughout this paper, the polytropic equation of state is assumed:

$$p = K\,\epsilon^{1+\frac{1}{N}}\,, \tag{2}$$

where N and K are constants. Here, p and ϵ stand for pressure and mass-energy density, respectively.

We consider oscillation modes in rotating relativistic stars such that the eigenfunctions are stationary and are composed of only one axial parity component in the limit $\Omega \to 0$. A subclass of those modes should be a relativistic counterpart of r-modes, which are able to oscillate in all slowly rotating Newtonian fluid stars. According to Lockitch et al. [9], such modes are allowed to exist only if the star has non-isentropic structures. Therefore, we assume stars to be non-isentropic, although the effects due to deviation from isentropic structure on oscillation modes do not appear in the first order in Ω. According to the formalism by Kojima [5] (see, also, [9]), let us write down the pulsation equation for relativistic r-modes with accuracy up to the first order in Ω. The metric perturbation, $\delta g_{\alpha\beta}$, and the Eulerian changes of the fluid velocity, δu^{α}, that do not vanish in the limit $\Omega \to 0$ are given as

$$(\delta g_{t\theta}, \delta g_{t\varphi}) = i h_{0,l}(r) \left(-\frac{\partial_\varphi Y_{lm}(\theta,\varphi)}{\sin\theta}\,, \sin\theta \partial_\theta Y_{lm}(\theta,\varphi) \right) e^{i\sigma t}\,, \tag{3}$$

$$(\delta u^{\theta}, \delta u^{\varphi}) = \frac{i U_l(r)}{r^2} \left(-\frac{\partial_\varphi Y_{lm}(\theta,\varphi)}{\sin\theta}\,, \frac{\partial_\theta Y_{lm}(\theta,\varphi)}{\sin\theta} \right) e^{i\sigma t}\,, \tag{4}$$

where $Y_{lm}(\theta,\varphi)$ are the usual spherical harmonic functions, and σ denotes the oscillation frequency measured in the inertial frame. All other perturbed quantities become higher order in Ω. The metric perturbation, $h_{0,l}$, obeys a second order ordinary differential equation,

$$\begin{aligned} & D_{lm}(r;\bar{\sigma}) \left[e^{\nu-\lambda} \frac{d}{dr} \left(e^{-\nu-\lambda} \frac{dh_{0,l}}{dr} \right) - \left(\frac{l(l+1)}{r^2} + \frac{-2+2e^{-2\lambda}}{r^2} + 8\pi(p+\epsilon) \right) h_{0,l} \right] \\ + \;& 16\pi(p+\epsilon) h_{0,l} = 0\,, \end{aligned} \tag{5}$$

where

$$D_{lm}(r;\bar{\sigma}) \equiv 1 - \frac{2m\bar{\omega}}{l(l+1)\bar{\sigma}}\,, \tag{6}$$

Here, we have introduced the effective rotation angular velocity of the fluid, $\bar{\omega} = \Omega - \omega$, and the corotating oscillation frequency, $\bar{\sigma} = \sigma + m\Omega$. The velocity perturbation of fluids U_l is determined from the function $h_{0,l}$ through the algebraic relation,

$$\left[1 - \frac{2m\bar{\omega}}{l(l+1)\bar{\sigma}} \right] U_l + h_{0,l} = 0\,. \tag{7}$$

Because equation (5) is second order ordinary differential equation, two boundary conditions are required to determine solutions uniquely. For physically acceptable solutions, the function $h_{0,l}$ must vanish both at the center and at spatial infinity. When these boundary conditions are imposed, our basic equations are solved as an eigenvalue problem, with an eigenvalue $\bar{\sigma}$. As shown by Kojima [5], when $D_{lm}(r;\bar{\sigma}) = 0$ is satisfied inside the star, the system of our basic equations becomes a singular eigenvalue problem, since the function $D_{lm}(r;\bar{\sigma})$ is proportional to the coefficient of the second derivative of function $h_{0,l}$. On the other hand, we can treat the equation as a regular eigenvalue problem if $D_{lm}(r;\bar{\sigma}) = 0$ is not satisfied inside the star, because the last term of equation (5) vanishes outside the star, as well as the function $D_{lm}(r;\bar{\sigma})$. Because of this singular property of the basic equation, Kojima also concluded that a continuous spectrum can exist in relativistic rotating stars (see, also, [6]). Recently, Lockitch et al. [9] have showed that the equality $D_{lm}(r;\bar{\sigma}) = 0$ must be satisfied at some spatial point to have non-trivial solutions $h_{0,l}$. Because $\bar{\omega}$ is a monotonically increasing positive function of r, according to the considerations of Lockitch et al. [9], in order for the equation (5) to be treated as a regular eigenvalue problem the frequency $\bar{\sigma}$ must be in the region,

$$\frac{2m\bar{\omega}(R)}{l(l+1)} < \bar{\sigma} \le \frac{2m\bar{\omega}(\infty)}{l(l+1)} = \frac{2m\Omega}{l(l+1)}\,, \tag{8}$$

where R is the stellar radius in the coordinate (1). On the other hand, when $\bar{\sigma}$ satisfies the inequality

$$\frac{2m\bar{\omega}(0)}{l(l+1)} \leq \bar{\sigma} \leq \frac{2m\bar{\omega}(R)}{l(l+1)}, \tag{9}$$

we must treat equation (5) as a singular eigenvalue problem.

3 Numerical Results

In this study, we consider only r-mode solutions of a regular eigenvalue problem, since a discrete eigenfrequency can be obtained. Therefore, we focus on eigenfrequencies in the range (8). We compute the frequencies of the r-mode for several polytropic stellar models. In the present study, only the fundamental r-modes, whose eigenfunction U_l has no node in the radial direction except at stellar center, are obtained. In Figure 1, scaled eigenfrequencies, $\kappa \equiv \bar{\sigma}/\Omega$, of discrete r-modes are given as functions of M/R for modes with $m = l$. Note that for modes associated with l, we can directly obtain the eigenfrequency of a mode with any value of m from a mode with $m = l$. Therefore, only results for modes associated with $m = l$ are shown throughout this paper. Eigenfrequencies for stars with four different polytropic indices, $N = 0$, 0.5, 0.75, and 1, are shown in the four panels of Figure 1. In each panel, frequency curves for modes with $l = 2$, 3, and 4 are depicted versus the relativistic factor M/R. From the figure, we find that the frequencies κ monotonically decrease as the relativistic factor M/R increases. This behavior is caused by the dragging of the inertial frame, due to the stellar rotation. We find that some frequency curves in Figure 1 are terminated at some value of M/R, beyond which equilibrium states can still exist. Here, the maximum values of M/R for polytropic equilibrium stars with $N = 0$, 0.5, 0.75, and 1.0 are given by 4/9, 0.385, 0.349, and 0.312, respectively. We also find that the length of those curves tends to be shorter as either the polytrope index N or the angular quantum number l increases.

Critical values of M/R are shown as functions of polytropic index N in Figure 2. Curves of critical values, $(M/R)_{crit}$, for modes with $l = 2$, 3, and 4 are given in the figure. Note that values of $(M/R)_{crit}$ shown here are numerically approximated ones. These only give the lower limit for accurate values of $(M/R)_{crit}$. In Figure 2, stars whose parameters are in regions under the curves of $(M/R)_{crit}$ have a discrete r-mode spectrum. Results of our numerical analysis also suggest that for the $N = 0$ case, the critical value of M/R is nearly equal to 4/9. Indeed, discrete r-mode solutions with frequencies in the range (8) may exist in all uniform density stars, independently of the value of M/R. This is consistent with the result by Lockitch et al. [9]. The figure also suggests that even in nearly Newtonian stars, whose value of relativistic factor M/R is sufficiently small, r-mode solutions of the regular eigenvalue problem disappear if the value of N is over some critical value, say N_{crit} (for details, see [11]).

4 Discussion and Conclusion

We have investigated the properties of r-mode solutions of Kojima's equation characterized by the regular eigenvalue problem in slowly rotating relativistic polytropes. Our numerical results suggest that discrete r-mode solutions of Kojima's equation with frequency in the range (8) disappear for some polytropic models.

As mentioned by Lockitch et al. [9], r-mode solutions with frequency in the range (8) might be considered to be counterparts of Newtonian r-modes, since the true relativistic analogue to a Newtonian r-mode should be a distinct mode with an well-defined eigenfunction. In fact, such an r-mode solution exists in all $N = 0$ polytropes, as shown numerically in Lockitch et al. [9] and in this study [11]. However, for some $N \neq 0$ polytropes, we numerically find that an r-mode solution with frequencies in the range (8) do not appear when $M/R > (M/R)_{crit}$, or $N > N_{crit}$. Although we do not have a mathematically rigorous proof for these numerical results, we can make conjectures about the relativistic r-mode as follows: for $N = 1$ polytropic models, which is employed as a typical neutron star model, discrete r-mode solutions with frequencies in the range (8) do not exist for stars whose relativistic factor M/R is larger than about 0.1. If those conjectures are true, most typical neutron stars do not have a discrete r-mode solution with frequencies in the range (8), since a typical relativistic factor for a neutron star is considered to be about 0.1–0.2. The r-modes associated with $l = m = 2$, which is considered to be the

most important for gravitational radiation driven instability, does not exist as a solution for the regular eigenvalue problem for polytropes having $N > 1.18$, even in the post-Newtonian order. As is well known, however, r-modes exist in all Newtonian stars with uniform angular velocity. Thus, it is likely that distinct r-modes can propagate in nearly Newtonian stars. Accordingly, results obtained in this study are somewhat strange. Form this consideration, some approximations used in this study might break down.

Finally, let us consider possible effects to obtain regular r-mode like solutions in relativistic stars. If the frequency has a non-zero imaginary part, a continuous part of spectrum might disappear because the singular point of our basic equation does not appears for the complex frequency. For example, the frequency should be complex when gravitational wave radiates due to r-mode oscillation. Recently, however, Yoshida and Futamase [12] and Ruoff and Kokkotas [13] have suggested that this is not the case. According to them, radiation reaction effects cannot regularize singular eigensolutions of Kojima's equation. Regrettably, we cannot still exclude this possibility because those studies employed some approximation to include radiation reaction effects. Another possibility is to include high order effects of rotation in pulsation equations. Kojima and Hosonuma [8] derived extended Kojima's equation, taking into account the rotational effects up to the third order with Ω. They found that extended Kojima's equation does not have singular properties unless the buoyant force inside the star vanishes. Although solutions of extended Kojima's equation have not been obtained yet, this equation might have regular r-mode like solutions. However, those are only speculations. In order to have a clear understanding of r-modes in relativistic stars, the further progress of studies is needed.

References

[1] N. Andersson, Astrophys. J. **502** (1998) 708.

[2] J.L. Friedman and S.M. Morsink, Astrophys. J. **502** (1998) 714.

[3] J.L. Friedman and K.H. Lockitch, Prog. Theor. Phys. Suppl. **136** (1999) 121.

[4] N. Andersson and K.D. Kokkotas, Int. J. Mod. Phys. D **10** (2001) 381.

[5] Y. Kojima, Mon. Not. R. Astron. Soc. **293** (1998) 49.

[6] H.R. Beyer and K.D. Kokkotas, Mon. Not. R. Astron. Soc. **308** (1999) 745.

[7] Y. Kojima and M. Hosonuma, Astrophys. J. **520** (1999) 788.

[8] Y. Kojima and M. Hosonuma, Phys. Rev. D **62** (2000) 044006.

[9] K.H. Lockitch, N. Andersson, and J.L. Friedman, Phys. Rev. D **63** (2001) 024019.

[10] K.S. Thorne, in *General Relativity and Cosmology*, edited by R. K. Sachs (London: Academic Press, 1971) p. 237.

[11] S. Yoshida, Astrophys. J. **558** (2001) 263.

[12] S. Yoshida and T. Futamase, Phys. Rev. D **64** (2001) 123001.

[13] J. Ruoff and K.D. Kokkotas, Mon. Not. R. Astron. Soc., in press (2001).

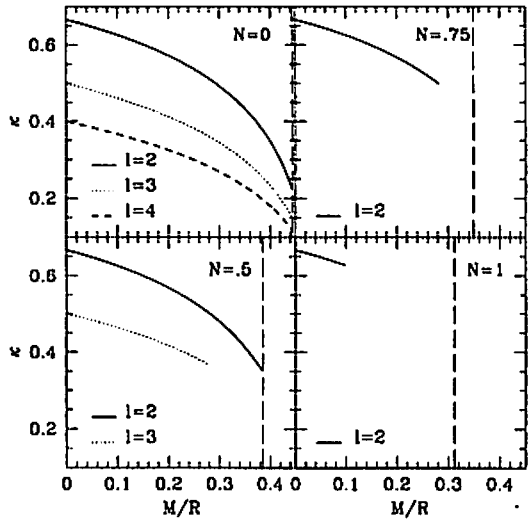

Figure 1: Scaled frequencies, $\kappa = \bar{\sigma}/\Omega$, of the r-modes in polytropic models with $N = 0$, 0.5, 0.75, and 1, plotted as functions of M/R in the four panels. In each panel, the frequencies for modes with $l = 2$, 3, and 4 are given. Labels indicating the polytropic index N are attached in the corresponding panels. The eigenvalues of the r-modes that are described above but are not given in the figure, for instance $l = 3$ mode in $N = 1$ polytrope, are not obtained by using our numerical method. Vertical dotted lines show the maximum values of M/R for equilibrium states: $M/R = 0.444$ for $N = 0$, $M/R = 0.385$ for $N = 0.5$, $M/R = 0.349$ for $N = 0.75$, and $M/R = 0.312$ for $N = 1.0$.

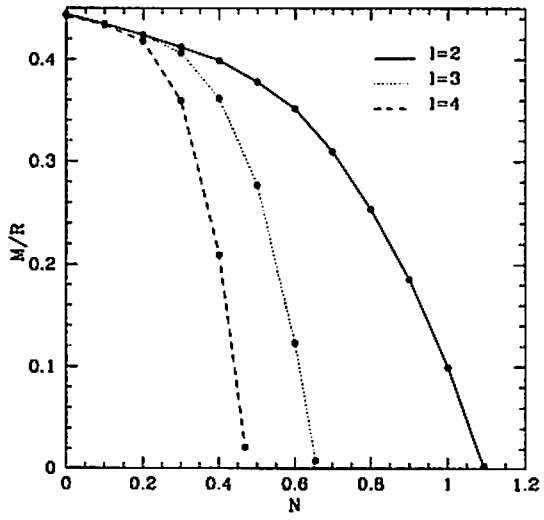

Figure 2: Critical values of the relativistic factor M/R, plotted against the polytropic index N for discrete r-modes with $l = 2$, 3, and 4. The values of $(M/R)_{crit}$ obtained from actual numerical calculations are indicated by the filled circles.

The growth of purely axial displacements by the radiation reaction in neutron stars

Masayasu Hosonuma[1] Yasufumi Kojima[2]

Department of Physics, Hiroshima University, Higashi-Hiroshima, 739-8526, Japan

Abstract

Evolution of purely axial displacement given as the initial data is calculated on slowly rotating relativistic stars. The radiation reaction effect is incorporated by the near-zone boundary condition with the out-going wave solution. We numerically evaluate the growth rate of the amplitude of the fluid oscillation due to the radiation reaction instability. The growth rate agrees with the Newtonian estimate by a factor 2 even in relativistic cases. We also discuss the secular change of the functional form in long term evolution.

1 Introduction

The axial oscillations in the rotating stars have been attractive, since the discovery of the r-mode instability [1, 2]. The radiation reaction instability may play a significant role in the spin-down of neutron stars as well as being a strong detectable gravitational wave source. Most of the studies are however limited to idealized situations. Some realistic effects such as the magnetic field and the solid crust may significantly modify the previous estimate. In this paper, we do not consider such realistic ingredients.

One important question arises. Are the estimates based on the Newtonian r-mode still good in the relativistic star? The answer is trivially no. We expect the validity breaks down in general as the relativistic factor increases. We may say that the Newtonian estimate is valid in white dwarfs, but not so good in neutron stars. One method to answer in definite way is to calculate the normal mode in lots of stellar models. We here follow a different approach. Assuming that a certain kind of displacements is dominated, the subsequent evolution is numerically calculated. The function imposed at the initial time is the axial displacement with a single spherical harmonic. This is a solution in the limit of Newtonian incompressible fluid. Since minor parts of the displacement are neglected during the early phase, the calculation is simpler. However, there is no reason that such spatial form is preserved with time. The symmetry will be broken in general, since the oscillation in the rotating star is mixed with the different spherical harmonics. The range of our approach is therefore limited by the time-scale. The time-scale is evaluated by the second order effects of rotation, and is rather long in the slow rotation case. Among the higher order effects of rotation, the radiation reaction is the most important factor, which we focus on in this paper. We calculate the evolution of purely axial displacement in the lowest-order equations, but effectively included the radiation reaction effects, which is of order Ω^{2l+2}.

Recently, some authors have published their works about numerical evolution of the r-mode oscillation. Stergioulas and Font [3] performed numerical simulation with 3-D general relativistic hydrodynamical code. They followed the time-evolution of fluids up to 20 rotations in fixed gravitational field, i.e. without the gravitational radiation. They did not consider the radiation reaction. Lindblom et al [4] studied the non-linear evolution of the Newtonian r-mode with the gravitational radiation instability. Our method is complementary to these works. We use approximate equations based on a relativistic perturbation theory with the radiation reaction.

[1] E-mail:numa@theo.phys.sci.hiroshima-u.ac.jp
[2] E-mail:kojima@theo.phys.sci.hiroshima-u.ac.jp

2 Formulation

2.1 Basic equations inside the star

We consider perturbations on the uniform rotating star with the angular velocity Ω. For the general oscillations with small amplitude, polar and axial parts are mixed in the lowest order of the rotation rate, and they form the hybrid mode. However, the classical r-mode can be described by a single purely axial spherical harmonic. The tangential components of the 3-velocity on the sphere are dominant for the mode. They can be described by the axial vector spherical harmonic. They are written in a local orthogonal frame

$$[\delta v^{\hat{\theta}}, \delta v^{\hat{\phi}}] = \Re\left(\delta v(t,r)\left[-\frac{1}{\sin\theta}\partial_\phi Y_{lm}(\theta,\phi), \sin\theta\partial_\theta Y_{lm}(\theta,\phi)\right]\right), \tag{1}$$

where the symbol $\Re$ means taking the real part, but is omitted from now on. We here restrict our calculation to the lowest order in the slow rotation formalism of the perturbation theory [5, 6]. The equations of axial oscillations depend on the time and radial coordinates,

$$(\partial_t + im(\Omega - \chi))U_{lm}(t,r) + 4\pi(p_0 + \rho_0)r^2 e^{-\nu}(\partial_t + im\Omega)\Phi_{lm}(t,r) = 0, \tag{2}$$

$$\frac{j^2r^2}{4}\left[\frac{1}{jr^4}(jr^4\Phi'_{lm}(t,r))' - (v + 16\pi(p_0 + \rho_0)e^{\lambda})\Phi_{lm}(t,r)\right] = U_{lm}(t,r), \tag{3}$$

where a prime denotes a derivation with respect to r. The function Φ_{lm} is related to components of the metric perturbations, i.e. $\delta g_{t\theta} = -r^2\Phi_{lm}/\sin\theta\partial_\phi Y_{lm}$ and $\delta g_{t\phi} = r^2\Phi_{lm}\sin\theta\partial_\theta Y_{lm}$. The fluid perturbation U_{lm} is related to the function in Eq.(1) as

$$\delta v(t,r) = \frac{U_{lm}(t,r)}{(p_0 + \rho_0)re^{-\nu}}. \tag{4}$$

Equation (2) can be formally integrated as

$$\begin{aligned} U_{lm}(t,r) &= e^{-im(\Omega-\chi)t}U_{lm}(0,r) - 4\pi(p_0 + \rho_0)r^2e^{-\nu} \\ &\times\left[\Phi_{lm}(t,r) - e^{-im(\Omega-\chi)t}\left\{\Phi_{lm}(0,r) - im\chi\int_0^t e^{im(\Omega-\chi)s}\Phi_{lm}(s,r)ds\right\}\right]. \end{aligned} \tag{5}$$

In general cases, we solve the coupled equations between $\Phi_{lm}(t,r)$ and $U_{lm}(t,r)$, Eqs.(2) and (3). The value of Φ_{lm} at t is determined by solving the second order radial differential equation, Eq.(3) with the source term U_{lm}. The right hand side of Eq.(5) is constructed by the history of the function $\Phi_{lm}(t',r)$, $0 \le t' \le t$.

2.2 Boundary conditions

We need two boundary conditions solving Eq.(3). One is imposed at the stellar center, the other is on the surface. The boundary condition at the center is regularity of the function, Φ_{lm}, i.e., $\Phi_{lm} \propto r^{l-1}$.

Outside the star, the dynamical freedom of fluid motion vanishes. As a result, the perturbation equations describe the gravitational waves only. The frequency of the gravitational wave should be connected with that of the r-mode oscillation, which is proportional to the stellar rotation. The terms with the square of frequency in the wave equation are higher order with respect to the rotation. We neglected them in the slow rotation formalism. In this way, the perturbation equation in the lowest approximation is not wave equation, but rather determines the stationary field.

It is necessary to include all kinds of more than second order corrections for the consistent calculation of radiative evolution. Such calculation would be very complicated. Among several effects, the gravitational radiation is the most important of the reaction instability. For this reason, we consider the radiation effects in the simplified situation. We approximate the exterior solution as the out-going wave in the spherical Schwarzschild space-time. That is we neglect all terms associated with the rotation except the frequency. The first order rotational effect just gives the corrections [7]. The exterior equation becomes the Regge-Wheeler equation.

As derived in Ref.[8], the metric perturbation of the out-going wave with $e^{-i\hat{\sigma}t}$ at the near zone is expressed in Fourier space by

$$\Phi_{lm}(\hat{\sigma}, r) = \frac{C}{r^{l+2}}\left[1 - i\frac{(2l+1)(l+2)\hat{\sigma}^{2l+1}}{[(2l+1)!!]^2(l-1)}r^{2l+1}\right], \tag{6}$$

where C and $\hat{\sigma}$ denote the normalization constant and the frequency of the gravitational wave, respectively. This is valid for $\hat{\sigma}r \ll 1$ (near zone) and $M/r \ll 1$ (non-relativistic), where M is the total mass of the star. We use this condition at the stellar surface $r = R$, but there is no *a priori* justice of such a usage. Lindblom et al [9] tested the same kind of boundary condition for the f-mode in several relativistic stellar models and confirmed the accuracy within 0.1%. We may follow the same approximation, but we need the boundary condition in time domain for our calculation. Such an expression can be in principle obtained by the Fourier transformation. By the direct transformation, the term with $\hat{\sigma}^{2l+1}$ becomes $(d/dt)^{2l+1}$, which is difficult to be included in the numerical calculation. Rather we adopt the following form as the exterior solution to be connected with the interior solution in real space

$$\Phi_{lm}(t, R) = (1 - i\alpha)\Phi^0_{lm}(t, R), \tag{7}$$

where $\Phi^0_{lm}(t, r)$ is a stationary solution of Eq.(3) in vacuum. In the limit of non-relativistic, $\Phi_{lm} \to C/r^{l+2}$. We have introduced the real number α in Eq.(7). The value of $\alpha = 0$ corresponds to no radiation. The boundary condition (7) is appropriate in the non-relativistic limit, when $\alpha = \alpha_0$, which is defined by

$$\alpha_0 \equiv \frac{(2l+1)(l+2)\hat{\sigma}^{2l+1}}{[(2l+1)!!]^2(l-1)}R^{2l+1}. \tag{8}$$

In this way, the value of α represents the effects of radiation in a sense. Indeed, in the normal mode calculation, α is related to the imaginary part of the frequency, i.e. the growth/decay rate. Since $|\alpha_0| \ll 1$, we extrapolate to the moderate value in the numerical calculation. We artificially change the α in Eq.(7) and examine the effect of it. As shown in the next section, the numerical solutions for several values of α grow as $\exp(\beta t)$. The true growth rate $\beta_0 \equiv \beta(\alpha_0)$ is guessed by the extrapolation with $\alpha \to \alpha_0$.

Equation (7) is employed as an exterior solution to be connected with that of interior. Then we impose the junction condition, so that Φ'_{lm}/Φ_{lm} should be continuous at the stellar surface.

3 Numerical results

We carry out the time-evolution of the perturbation on the equilibrium models, assuming that the initial function is given by Eq.(9). Our numerical calculation is limited to quadrupole, $l = m = 2$ only. The time-reversal symmetry is checked as an estimation of numerical errors of our code. That is, after the function $\Phi_{lm}(t, r)$ is calculated from the initial data $\Psi_{lm}(0, r)$, the calculation goes backward from t to 0, and the resulting function is compared with the original one. The initial data is set by

$$U_{lm}(t, r) = N(\rho_0 + p_0)r^{l+1}e^{-\nu}(\varpi e^{-\nu})^{(l-1)/2}. \tag{9}$$

This equation is reduced to the exact solution in the non-relativistic incompressible fluid. Such a solution is widely used in the estimation of the radiation reaction instability.

We begin with the analysis of the radiation effects. We have introduced a parameter α in Eq.(7), which is associated with the radiation. The time-scale would be extremely long, when we compute with the true value of $\alpha_0 \ll 1$, defined in Eq.(8). Such a numerical calculation is time-consuming. We artificially increase the strength of the radiation with increasing the value of $\alpha \sim O(1)$ to shorten the time-scale. However, as discussed later, it is possible to find out the 'true' growth rate from the calculation with an artificial parameter.

By substituting a suitable α, the amplitude of oscillation can grow manifestly. The growth rate increases with α. The time-variation of the envelope of oscillations can be fitted by the exponential curve. The ratio can be well fitted by exponential curve with a constant β, i.e., $f_\alpha(t)/f_0(t) \propto e^{\beta t}$. The ratio is much better than fitting of $f_\alpha(t)$ with the exponential curve. For several choices of α, we

Table 1: The growth rates for the numerical calculation and the multipole formula for some different values of M/R. For the relativistic case, the value of t_1 is too small and not reliable from the numerical calculation. The parameter ϵ is defined by $(R^3\Omega^2/M)^{1/2}$.

model	M/R	α_0/ϵ^5	$(\beta_0^{-1}/P)\epsilon^5$	$(t_{GW}/P)\epsilon^5$	$t_1/P/\epsilon$
1	0.0001	1.0×10^{-10}	1.0×10^{14}	1.0×10^{14}	10^4
2	0.001	3.2×10^{-8}	3.1×10^{10}	3.1×10^{10}	10^3
3	0.01	9.4×10^{-6}	1.1×10^{7}	1.1×10^{7}	10^2
4	0.10	1.8×10^{-3}	6.7×10^{3}	9.0×10^{3}	10
5	0.25	2.0×10^{-2}	2.2×10^{2}	5.0×10^{2}	–

calculate the growth rate β. Within a reasonable range of α, β can be expressed by a linear relation, $\beta = \frac{\beta_0}{\alpha_0}(\alpha - \alpha_0) + \beta_0$, where β_0 is the true growth rate.

This numerical calculation gives the growth rate around $\alpha \sim O(1)$. We now apply our result to the realistic situation, i.e., around $\alpha \sim O(\alpha_0)$. Extrapolating from numerical calculated value of α to α_0, we obtain a kind of an estimation of the growth rate β_0, which is tabulated in Table 1. For comparison, we also show the gravitational radiation time-scale by the Newtonian estimates [10]. The time-scale is given by

$$\frac{1}{t_{GW}} = \frac{32\pi G}{c^{2l+3}} \frac{(l-1)^{2l}}{[(2l+1)!!]^2} \left(\frac{l+2}{l+1}\right)^{2l+2} \Omega^{2l+2} \int_0^R \rho_0 r^{2l+2} dr, \tag{10}$$

where we have recovered the light velocity c and the gravitational constant G. In the Newtonian models, our estimate of the growth rate exactly agrees with Eq.(10). But, in the relativistic models, deviation is obvious. The origin is not clear at this stage. Our scheme is not approved, e.g., there is the ambiguity in the choice of α_0. This result however suggests a kind of estimate.

We define the time t_1 when the relative error between the fitting curve and the original envelope computed from the numerical calculation becomes more than 10%. This deviation does not arise from the radiation effect. We numerically confirmed that the functional form is almost the same even when the radiation effects are neglected, i.e., $\alpha = 0$. The functions U_{lm} and Φ_{lm} with $\alpha = 0$ are not completely periodic but have an additional secular change. This comes from the fact that Eq.(9) is not the normal mode solution but approximate form which reduces to the normal mode solution in the Newtonian incompressible limit. There are several effects involved in a relativistic system. The frame-dragging is associated with the differential rotation, which caused the functional form to be deformed. The relativistic system differs from the Newtonian one by a factor of M/R. These combined effects alter the Newtonian results. Equation (9) is no more the normal mode solution.

We investigate how good the functional form Eq.(9) evolves in almost Newtonian case. We estimate the time-scale t_1. For example, for $M/R = 10^{-3}$ and 10^{-4}, we can estimate t_1 to be $\sim 10^3$ and 10^4 period respectively. Thus these time-scales are not so much longer. The gravitational radiation time-scale is much longer as shown in Table 1. They are 10^7 and 10^{10} times longer respectively.

4 Discussion

In this paper, we have carried out the time-evolution of axial component of velocity within the first-order slow-rotation formalism. We only considered a class of the functional form that can be represented by a single magnetic-type spherical harmonic. It contains the classical r-mode solution in the limit of Newtonian incompressible fluid. In the relativistic cases, the functional form is no more exact but approximate one. We expected that the kind of form is still valid, but examined how good the approximation is. Such an axial velocity can be constrained from the relation between the density and pressure perturbations. We used the velocity perturbation as the initial data, and follow the time-evolution.

From extrapolation of large α region, we can well estimate the growth time induced by the radiation. It shows quite agreement with the results from the current multipole formula in the cases of the compactness less than 0.01. It differs by a factor 2 in a typical relativistic model. Ruoff and Kokkotas [11] studied

the time-evolution of axial oscillations with the normal mode approach. Their results show the better agreement with the Newtonian estimates. Our numerical estimate is in reasonable range as for the growth rate. In this way, the numerical method to include radiation reaction is satisfactorily tested.

The numerical results of the velocity perturbation can be described by a single frequency and the growth rate in the early stage. However such a simple treatment is broken as the system evolves in a longer time-scale. The time-scale $t_1 \sim P/(M/R)$ is numerically evaluated. This time-scale is much longer than the dynamical time-scale or oscillation period. However this is shorter than the time-scales associated with the secular effects such as the radiation reaction.

Some authors used the dynamical code to simulate the evolution [4]. They had to intensify the radiation reaction effects to save the computational time. Their calculations are limited to $10 \sim 30$ rotation period. In their models, the radiation effects are appropriately included. However, when one simulate the longer evolution to mimic a realistic situation, our results suggest that the deviation is obvious around t_1. The time-scale t_1 is much shorter than the growth time of gravitational radiation t_{GW} even in the Newtonian case. Time-scale t_1 is just one of the examples associated with the secular changes, which originate even from weak effects. In a realistic cases, there are many secular effects. Our numerical result gives a lesson that it should be careful with longer aspects as well as the short dynamical aspects for the radiation reaction instability.

Finally we comment on the validity of the numerical calculation partially including the first order rotational effects. The equations relevant to the axial oscillations are derived by expansion of rotational parameters [6]. The equations adopted here are simplified or oversimplified by neglecting the higher order terms, and hence were easily calculated. The equations are asymptotically valid as $\Omega \to 0$, but not uniformly. That is, the approximation may break down elsewhere in space-time, e.g., by increasing the significance of the neglected terms. The problem can be answered by carefully examined whole set of equations derived in Ref.[6] and others. But the method is highly cumbersome. One practical way is to calculate without any justification. We followed this method here. The secular growth of the numerical solution suggests the drawback. This property may be removed by using another appropriate gauge condition, and/or including the higher order terms in a consistent way. The drawback in the naive treatment means the unsuccessful finding, but never became clear without any actual calculation presented here.

References

[1] N. Andersson, Astrophys. J. **502** (1998), 708.

[2] J. L. Friedman and S. M. Morsink, Astrophys. J. **502** (1998), 714.

[3] N. Stergioulas and J. A. Font, Phys. Rev. Lett. **86** (2001), 1148.

[4] L. Lindblom, J. E. Tohline and M. Vallisneri, Preprint `astro-ph/0109352`.

[5] Y. Kojima, Mon. Not. R. Astron. Soc. **293** (1998), 49.

[6] Y. Kojima and M. Hosonuma, Phys. Rev. **D62** (2000), 044006.

[7] Y. Kojima, Phys. Rev. **D46** (1992), 4289.

[8] S. Yoshida and T. Futamase, Phys. Rev. **D64** (2001), 123001.

[9] L. Lindblom, G. Mendell and J. R. Ipser, Phys. Rev. **D56** (1997), 2118.

[10] L. Lindblom, B. J. Owen and S. M. Morsink, Phys. Rev. Lett. **80** (1998), 4843.

[11] J. Ruoff and K. D. Kokkotas, Preprint `gr-qc/0106073`.

The first law of binary systems

Koji Uryū[1], John L. Friedman[2]

Department of Physics, University of Wisconsin-Milwaukee, Milwaukee, WI 53201, USA

Masaru Shibata[3]

Graduate School of Arts and Sciences, University of Tokyo, Komaba, Meguro-ku, Tokyo 153-8902, Japan

Abstract

We consider compact binary systems, modeled in general relativity as vacuum or perfect-fluid spacetimes with a helical Killing vector k^a. Remarkably, there is the exact fist law relating the change in the asymptotic Noether charge Q to the changes in the entropy, baryon mass, and vorticity of the fluid and in the area of black holes, for such stationary equilibriums, although the mass and angular momentum of such a system are not defined. For asymptotic flat systems such as post-Newtonian approximation or the spatial conformal flatness formalism (Isenberg-Wilson-Mathews formalism) one can define an asymptotic mass M and angular momentum J. An equilibrium sequence of binary neutron star is constructed numerically for the same entropy, rest mass and vorticity, obey the relation $\delta M = \Omega \delta J$. For such models, a turning point theorem can be applicable, which claims that the simultaneous minima of $M(d)$ and $J(d)$ is the ISCO in this framework.

1 Introduction

Perfect fluid spacetime with a helical Killing vector k^a has been used as one of the most general model for the general relativistic compact binary in quasi circular orbit [1]. Such spacetimes have to have equal amounts of incoming and outgoing radiation to maintain circular orbit exactly. Because the radiation field of such a stationary solution has infinite energy, spacetimes that describe the corresponding general relativistic binaries are not asymptotically flat. Instead, the asymptotic mass rises linearly with a naturally defined radial coordinate.

For the exact vacuum and perfect-fluid spacetimes, the Noether current of the helical Killing vector assigns to each spacetime a charge Q [2, 3]. Despite the lack of asymptotic flatness one can choose the current to make Q finite, and it is independent of the 2-surface S on which it is evaluated, as long as S lies outside the matter and all black holes. The Noether current assigns to each black hole a charge that can be identified with its entropy (its area, in the spacetimes we consider); and we obtain a version of the first law (Eq. (6) below) that expresses the change δQ in terms of changes in the vorticity, baryon mass, and entropy of the fluid, and in the area of black holes.

In the context of the first and second post-Newtonian approximation or spacetimes with conformally flat spacelike slices which satisfies truncated set of Einstein equations, there is no radiation and one regains asymptotic flatness. In such asymptotic flat spacetimes, the helical Killing vector has the asymptotic form $k^a = t^a + \Omega \phi^a$ where t^a and ϕ^a are asymptotic Killing vectors associated with time-translations and rotations. The variation of charge Q relates to the ADM mass M and angular momentum J of the spacetime as $\delta Q = \delta M - \Omega \delta J$. Modeling the evolution of binary inspiral by a set of equilibrium solutions with fixed baryon-mass density, entropy and vorticity of fluid particles (and constant area of black hole if any), the solution sequence satisfy conditions to apply turning point theorem to determine the orbital stability of binary system, one of which is the first law in the form $\delta M = \Omega \delta J$.

[1] E-mail:uryu@uwm.edu
[2] E-mail:friedman@uwm.edu
[3] E-mail:shibata@provence.c.u-tokyo.ac.jp

In this article, we briefly introduce the generalized thermodynamic laws of perfect fluid spacetimes with a helical symmetry. It is applied to binary systems with asymptotics, especially, for the case with conformal flat 3-geometry. We compute a set of equilibrium solutions of binary neutron stars numerically, which models final inspiraling phase as a result of gravitational wave emission, and discuss that we may identify the point of orbital instability.

2 Thermodynamic laws of perfect fluid spacetimes with helical symmetry

We consider globally hyperbolic spacetime $M, g_{\alpha\beta}$. A helical vector k^α is heuristically defined by combining a timelike vector t^α and rotational vector ϕ^α with nonzero constant Ω, $k^\alpha = t^\alpha + \Omega\phi^\alpha$. Following general definition of helical vector is equivalent with the above expression when the space time admit a foliation by timelike lines. *A vector field k^α is helical if there is a smallest $T > 0$ for which $P \in M$ and $\chi_T(P)$ are timelike separated for every P outside the history $\mathcal{T}$ of a sphere $\mathcal{S}$, where χ_t is χ_t is the family of diffeos generated by k^α, and $\mathcal{T}$ is the timelike surface swept out by the action of χ_t on a spacelike sphere $\mathcal{S}$ which includes black holes: $\mathcal{T}(\mathcal{S}) = \cup_t \chi_t(\mathcal{S})$*

For a spacetime with a globally defined Killing field k^α that is transverse to Cauchy surface, event horizon is proved to be a Killing horizon. In this case, the horizon satisfy the zeroth law of black hole thermodynamics, that is, the Killing vector k^α is tangent on the event horizon to the null generators and the surface gravity κ defined by

$$k^\beta \nabla_\beta k^\alpha = \kappa k^\alpha, \tag{1}$$

is constant on the horizon. The proof follows from an analogous theorem proved by Isenberg and Moncrief, and by Friedrich, Rácz and Wald [4] (see Friedman, Uryū and Shibata [5] in detail).

As we have mentioned, spacetimes with black holes and perfect-fluid sources with a helical Killing vector will not in general be asymptotically flat. However, one can obtain a generalized first law of thermodynamics in terms of Noether charge Q associated with the Killing vector field and action of perfect-fluid spacetime.

Given a family of perfect-fluid spacetimes specified by

$$\mathcal{Q}(\lambda) := [g_{\alpha\beta}(\lambda), u^\alpha(\lambda), \rho(\lambda), s(\lambda)], \tag{2}$$

one defines the Eulerian change in each quantity by $\delta\mathcal{Q} := \frac{d}{d\lambda}\mathcal{Q}(\lambda)$. We also introduce Lagrangian perturbation associated with a displacement ξ^α as follows:

$$\Delta\mathcal{Q} := \frac{d}{d\lambda}\Psi_{-\lambda}\mathcal{Q}(\lambda)|_{\lambda=0} = (\delta + \pounds_\xi)\mathcal{Q}, \tag{3}$$

where Ψ_λ is a diffeo mapping each trajectory (worldline) of the initial fluid to a corresponding trajectory of the configuration $\mathcal{Q}(\lambda)$. Then the tangent $\xi^\alpha(P)$ to the path $\lambda \to \Psi_\lambda(P)$ can be regarded as a vector joining the fluid element at P in the configuration $\mathcal{Q}(\lambda)$ to a fluid element in a nearby configuration. The energy momentum tensor for perfect fluid is defined as $T^{\alpha\beta} = cu^\alpha u^\beta + pq^{\alpha\beta}$, where $q^{\alpha\beta} = g^{\alpha\beta} + u^\alpha u^\beta$. Here, u^α, ρ, p and c are four-velocity, the baryon-mass density, the pressure and the energy density, respectively. We assume that the fluid satisfies an equation of state of the form $p = p(\rho, s)$, $c = c(\rho, s)$. where s is the entropy per unit baryon-mass.

Our Noether charge Q is similar to that defined in [2].

$$Q = \oint_S Q^{\alpha\beta} dS_{\alpha\beta}, \quad \text{where} \quad Q^{\alpha\beta} = -\frac{1}{8\pi}\nabla^\alpha k^\beta + k^\alpha B^\beta - k^\beta B^\alpha, \tag{4}$$

and $B^\alpha(\lambda)$ is any family of vector fields that satisfies

$$\frac{1}{\sqrt{-g}}\frac{d}{d\lambda}(B^\alpha\sqrt{-g}) = \Theta^\alpha, \quad \text{where} \quad \Theta^\alpha = (c+p)q^{\alpha\beta}u\xi_\beta + \frac{1}{16\pi}(g^{\alpha\gamma}g^{\beta\delta} - g^{\alpha\beta}g^{\gamma\delta})\nabla_\beta\delta g_{\gamma\delta}. \tag{5}$$

By choosing $B^\alpha(0) = 0$ for an unperturbed spacetime, we make $Q(\lambda)$ finite ; and, Q is *independent of the sphere S*, as long as S encloses the fluid and any black holes. Note that for $\lambda = 0$, Q coincides with Komar charge $Q_K = -\frac{1}{8\pi}\oint_S \nabla^\alpha k^\beta dS_{\alpha\beta}$ with the above choice for B^α.

The first law follows from a variation of Eq.(4) :

$$\delta Q = \int_\Sigma \left[\rho\frac{T}{u^t}\Delta s u^\alpha dS_\alpha + \left(\frac{h}{u^t} + hu_\beta v^\beta\right)\Delta(\rho u^\alpha dS_\alpha) + v^\beta\Delta(hu_\beta)\rho u^\alpha dS_\alpha\right] + \sum_i \frac{1}{8\pi}\kappa_i\delta A_i$$
$$-\frac{1}{8\pi}\delta\int_\Sigma (G^\alpha{}_\beta - 8\pi T^\alpha{}_\beta)k^\beta dS_\alpha + \int_\Sigma\left[\frac{1}{16\pi}(G^{\alpha\beta} - 8\pi T^{\alpha\beta})\delta g_{\alpha\beta} + \xi^\beta\nabla_\alpha T^\alpha{}_\beta\right]k^\gamma dS_\gamma, \qquad (6)$$

where v^α is defined as $u^\alpha = u^t(k^\alpha + v^\alpha)$ where $u^\alpha\nabla_\alpha t = u^t$ and $v^\alpha\nabla_\alpha t = 0$. The change of Q relates to Δs, $\Delta(\rho u^\alpha\sqrt{-g})$, $\Delta(hu_\alpha)$, and δA_i, which are the changes in the entropy, the changes in baryon mass, a term relate to the changes in vorticity of fluid and the changes in the area of black holes, respectively.

We have mentioned that $Q(\lambda)$ is independent of the 2-surface S on which it is evaluated if S enclose the fluid and any black holes. For unperturbed spacetime with $\lambda = 0$, it follows from the fact that $Q(0) = Q_K$, and for general $Q(\lambda) = Q(0) + \delta Q$, Eq.6 shows δQ and hence $Q(\lambda)$ are independent of S.

For an isentropic fluid conservation of rest mass, entropy and vorticity have the form,

$$\pounds_u(\rho\sqrt{-g}) = 0, \quad \pounds_u s = 0, \quad \pounds_u\omega_{\alpha\beta} = 0, \qquad (7)$$

where $\omega_{\alpha\beta}$ is the relativistic vorticity, $\omega_{\alpha\beta} = q_\alpha{}^\gamma q_\beta{}^\delta\left[\nabla_\gamma(hu_\delta) - \nabla_\delta(hu_\gamma)\right] = \nabla_\alpha(hu_\beta) - \nabla_\beta(hu_\alpha)$. The perturbed conservation laws have the first integrals,

$$\Delta(\rho u^\alpha\sqrt{-g}) = 0, \quad \Delta s = 0 \quad \Delta\omega_{\alpha\beta} = 0, \qquad (8)$$

which models dynamical evolution of binary systems. It is immediate the first and second terms in Eq.(6) vanish. The third term vanishes for (i) co-rotating binary ($v^\alpha = 0$); and (ii) irrotational binary, (potential flows $hu_\alpha = \nabla_\alpha\Phi$).

In the first post-Newtonian and in the Isenberg-Wilson-Mathews (IWM) spacetimes [6, 7] that have been used to describe binary systems [8, 9, 10, 11], the 3-metric has the asymptotic form $\gamma_{ab} = f_{ab} + O(r^{-1})$. Using the 3+1 formalism, we can relate δQ to the changes of ADM mass M and the angular momentum J associated with asymptotic rotational Killing field as follows

$$\delta Q = \delta M - \Omega\delta J \qquad (9)$$

where

$$M = \frac{1}{16\pi}\int_\infty (f^{ac}f^{bd} - f^{ab}f^{cd})\partial_b\gamma_{cd}\, dS_a, \qquad J = \frac{1}{8\pi}\int_\infty K^a{}_b\,\phi^b dS_a. \qquad (10)$$

In the IWM framework, the trace part of extrinsic curvature K_{ab} is artificially omitted, and, consequently, one component of the Einstein equation is not satisfied. However, remarkably, the difference of charge Q in the Einstein spacetime and corresponding quantity in the IWM spacetime becomes a surface integral which vanish for asymptotics. As a result, for the IWM spacetime with no black hole, the first law takes a form

$$\delta M = \Omega\delta J \qquad (11)$$

for constant entropy and baryon-mass, and for co-rotating or irrotational flow in the binary systems.

3 Stability of close binary orbit

A criterion for orbital stability of binary in asymptotic flat system is derived from a turning point theorem [12] which relies on a first law in the form Eq.(11). For binary neutron stars, if one fixes the baryon number, entropy and circulation for each fluid element, the simultaneous extrema of M and J indicate an exchange of stability. We solve a set of equations for IWM spacetime and equations of fluid numerically [11] fixing the above quantities. Changing a separation, a sequence of equilibrium solutions are computed and a turning point is found for certain models depending on equations of state (the polytropic index N in our case) as well as the compactness of the neutron star.

In the left panel of Fig.1, we show such a solution sequence with a turning point. According to the turning point theorem, right (left) branch of the curve with respect to the minima corresponds to stable

(unstable) branch. Although, in general, the turning point method claims that the left branch is *secular* unstable, for irrotational

The right panel of Fig.1 shows that a set of equilibria computed numerically satisfy the first law. The size of mesh for finite difference method we adopted for numerical computation could introduce about 1% error in each solution. Also, computing a fraction $\delta M/\Omega\delta J$ for nearby equilibriums using a finite difference formula cause numerical error. The figure shows that the first law is satisfied in reasonable accuracy, despite of these possible sources of error.

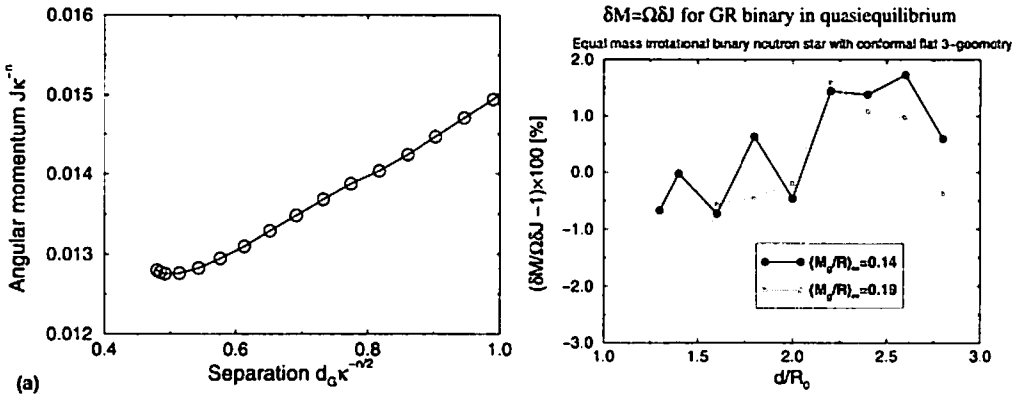

Figure 1. Left panel: The angular momentum is plotted against the binary separation for the case with the polytropic index $N = 0.5$ and the compactness $(M/R)_\infty = 0.19$. Right panel: The relation $\delta M/\Omega\delta J - 1$ is evaluated from numerical solution sequence for the case with the polytropic index $N = 1.0$ and the compactness $(M/R)_\infty = 0.14$ and 0.19.

4 Discussion

As we have discussed above, the first law provides a criterion for orbital stability for the asymptotically flat models of binary. The determination of the ISCO is crucial to develop a reliable template for matched filtering method to extract signals from data taken from ground based interferometric gravitational wave detectors. Post-Newtonian method, appropriate for binary black holes, has been successfully developed for this purpose, however it involves an indeterminate parameter which can change a location of ISCO. (See for example [13] for recent development.) This suggest that it is desirable to investigate the location of ISCO relying on a turning point of a solution sequence of equilibriums as an alternative method [14]. For a neutron star binary, the location of ISCO systematically changes with the compactness of the neutron star and a typical value of $M\Omega$ at the ISCO can be $\sim 50\%$ smaller than that predicted by post-Newtonian method when the compactness of neutron star is in a realistic range $0.14 \lesssim (M/R)_\infty \lesssim 0.20$ [11]. This implies that the method using equilibrium sequence which solve internal structure of a star numerically, is a promising way to determine the ISCO for binary neutron stars and probably for stellar mass neutron star-black hole binaries.

References

[1] J. K. Blackburn and S. Detweiler, Phys. Rev. D **46**, 2318 (1992); S. Detweiler, Phys. Rev. D **50**, 4929 (1994).

[2] R. M. Wald, Phys. Rev. D. **48**, R3427 (1993); V. Iyer and R. M. Wald, Phys. Rev. D. **52**, 4430 (1995); V. Iyer, Phys. Rev. D. **55**, 3411 (1997);

[3] B. F. Schutz and R.D. Sorkin, Annals of Phys., **107**,1 (1977); R.D. Sorkin, *Proceedings of the Royal Society London A* **435**: 635-644 (1991); J. D. Brown, Class. Quant. Grav. **10**, 1579 (1993).

[4] V. Moncrief and J. Isenberg, Comm. Math. Phys. 89, 387 (1983); J. Isenberg and V. Moncrief, J. Math. Phys. 26, 1024 (1985); H. Friedrich, I. Rácz, and R. M. Wald, Comm. Math. Phys. 204, 691 (1999).

[5] J. L. Friedman, K. Uryū, and Masaru Shibata, Phys. Rev. D in press, (gr-qc/0108070)

[6] J. Isenberg and J. Nester, in *General Relativity and Gravitation* Vol.1, edited by A. Held, (Plenum Press, New York 1980); Waveless Approximation Theories of Gravity, preprint (1978), University of Maryland.

[7] J. R. Wilson and G. J. Mathews, Phys. Rev. Lett. 75, 4161 (1995); J. R. Wilson, G. J. Mathews and P. Marronetti, Phys. Rev. D 54, 1317 (1996).

[8] T. W. Baumgarte, G. B. Cook, M. A. Scheel, S. L. Shapiro and S. A. Teukolsky, Phys. Rev. D 57, 6181 (1998); *ibid* 57, 7299 (1998).

[9] S. Bonazzola, E. Gourgoulhon and J.-A. Marck, in the proceedings of 19th Texas Symposium on Relativistic Astrophysics: Texas in Paris, Paris, France (1998); S. Bonazzola, E. Gourgoulhon and J.-A. Marck, Phys. Rev. Lett. 82, 892 (1999); E. Gourgoulhon, P. Grandclement, K. Taniguchi, J.-A. Marck, S. Bonazzola, Phys. Rev. D63 (2001) 064029.

[10] P. Marronetti, G. J. Mathews and J. R. Wilson, in the proceedings of 19th Texas Symposium on Relativistic Astrophysics: Texas in Paris, Paris, France (1998); P. Marronetti, G. J. Mathews and J. R. Wilson, Phys. Rev. D 60, 087301 (1999).

[11] K. Uryū and Y. Eriguchi, Phys. Rev. D. 61, 124023 (2000); K. Uryū, M. Shibata and Y. Eriguchi, Phys. Rev. D. 62, 104015 (2000).

[12] R. Sorkin, Astrophys. J. 249, 254 (1981).

[13] L. Blanchet, Phys. Rev. D. in press (gr-qc/0112056).

[14] E. Gourgoulhon, P. Grandclement, S. Bonazzola Phys. Rev. D 65, 044020 (2002); *ibid.*, 044021 (2002).

Quasi-equilibrium sequences of binary neutron stars

Keisuke Taniguchi[1]

Max-Planck-Institut für Gravitationsphysik, Albert-Einstein-Institut
Am Mühlenberg 1, D-14476 Golm, Germany

Eric Gourgoulhon[2]

Laboratoire de l'Univers et de ses THeories (LUTH), CNRS/Observatoire de Paris
F-92195 Meudon Cedex, France

Abstract

Quasi-equilibrium sequences of binary neutron stars are numerically obtained in both cases of synchronized and irrotational rotation states. In the present article, we use the spectral method and adopt the conformally flat spatial metric in the general relativistic framework. We will show the numerical results of binary systems composed of both identical and different mass stars with the polytropic index $\gamma = 2$. The stellar mass combination in a binary system is parametrized by its compactness $(M/R)_{\infty}$ instead of mass itself, where M and R denote the gravitational mass and radius of a spherical star with the same baryon mass, respectively. The computations are performed for the cases $(M/R)_{\infty,\mathrm{star\ 1}}$ vs. $(M/R)_{\infty,\mathrm{star\ 2}} = 0.12$vs.0.12 and 0.12vs.0.14. We will discuss the difference between identical and different mass stars.

1 Introduction

Coalescing binary neutron stars are expected to be one of the most promising sources of gravitational waves that could be detected by the ground based, kilometer size laser interferometers such as LIGO, VIRGO, GEO600, and TAMA300[3], and also are considered as one of candidates of gamma-ray burst sources[2].

Due to the emission of gravitational radiation, binary neutron stars decrease their orbital separations and finally merge. When we consider such an evolutionary sequence, it is convenient to separate it into three phases. The first one is the *inspiraling phase* in which the orbital separation is much larger than the radius of a neutron star, and the post-Newtonian expansion constitutes an excellent approximation. (For a recent review, see [3]). The second one is the *intermediate phase* in which the orbital separation becomes only a few times larger than the radius of a neutron star, so that hydrodynamics as well as general relativity play an important role. In this phase, since the shrinking time of the orbital radius due to the emission of gravitational waves is still larger than the orbital period, it is possible to approximate the state as quasi-equilibrium[4, 5, 6, 7]. The final one is the *merging phase* in which the two stars coalesce dynamically. As in the intermediate phase, since hydrodynamics as well as general relativity play an important role, fully relativistic hydrodynamical treatments are required in this phase which results in the field of numerical simulation. The first stable computation of binary neutron star merger from their innermost stable circular orbits to black hole or massive neutron star formations has been succeeded in by Shibata[8, 9]

In the series of our research[5, 10, 11], we have paid particular attention to the intermediate phase. This stage is important because we may get informations about equation of state of neutron stars through the gravitational wave signal. Furthermore, the initial data for the merging phase is obtained. Until now, several groups produce initial data for binary neutron stars. There are results of both synchronized[12, 13, 14] and irrotational rotation states[4, 5, 6, 7] in general relativistic framework for identical star binaries,

[1]E-mail:keisuke@aei-potsdam.mpg.de
[2]E-mail:Eric.Gourgoulhon@obspm.fr
[3]TAMA300 has already started data taking, and the recent result of the data analysis was published[1].

and those in Newtonian gravity for both identical[15, 10] and different mass star binaries[11]. However, the calculations for different mass star binaries in general relativity have not been performed yet. In the present article, we will show the numerical results of binary systems composed of not only identical stars but also different mass stars, even though we restrict our computations in the case of polytropic index $\gamma = 2$.

Throughout this article, we adopt the units $G = c = 1$ where G and c denote the gravitational constant and speed of light, respectively.

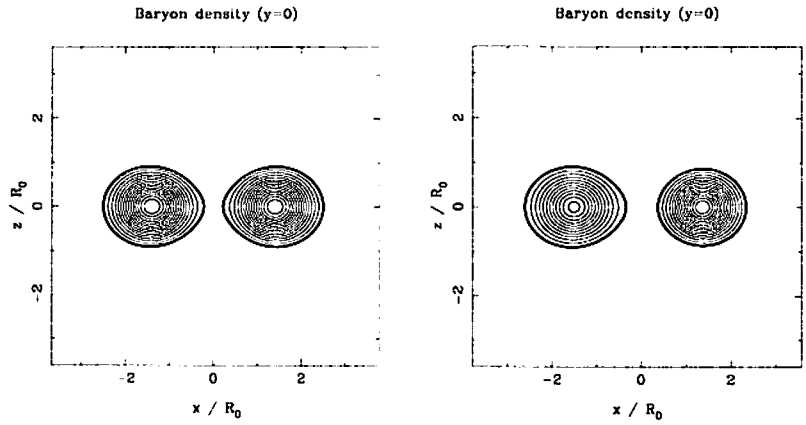

(a) Synchronized, 0.12vs.0.12

(b) Synchronized, 0.12vs.0.14

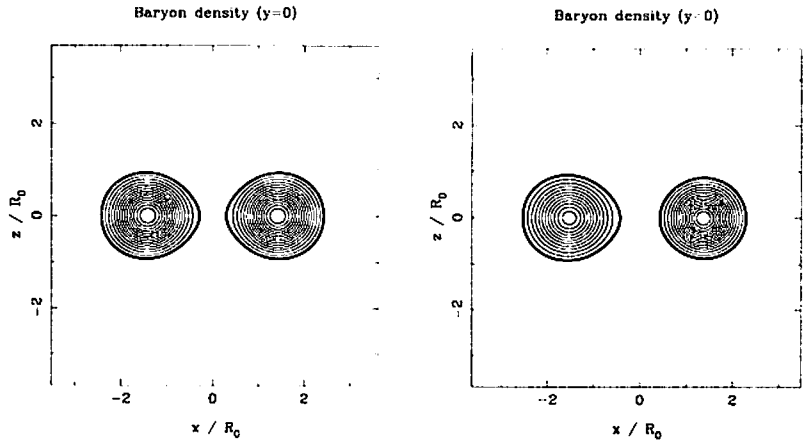

(c) Irrotational, 0.12vs.0.12

(d) Irrotational, 0.12vs.0.14

Figure 1: Isocontours of the baryon density of synchronized and irrotational binaries with $\gamma = 2$ and $(M/R)_{\infty,\text{star 1}}$ vs. $(M/R)_{\infty,\text{star 2}} = 0.12$vs.0.12 and 0.12vs.0.14 just before contact or appearance of cusp. The plots are cross sections of $Y = 0$ planes. The thick solid lines denote the stellar surface.

2 Formulation

The basic equations, the numerical method, and the solving procedure which we use in this article are explained in detail in Paper I[5]. Then, we briefly summarize the formulation here.

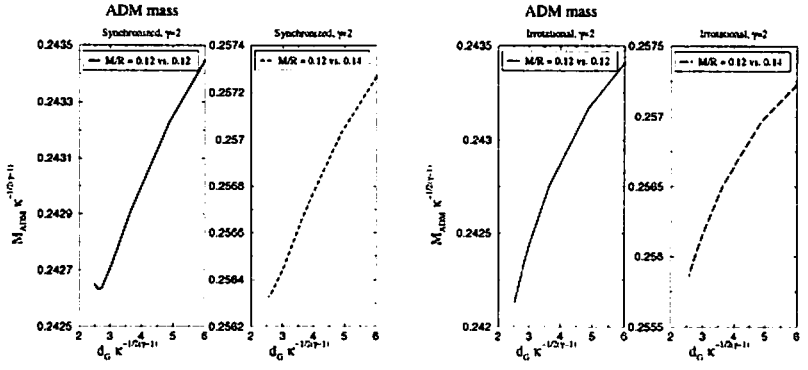

(a) Synchronized (b) Irrotational

Figure 2: ADM mass along a constant baryon mass sequence. Here d_G denotes the separation between the centers of mass of two stars.

2.1 Basic assumptions

- Quasi-equilibrium:
  Since the time scale of the orbital shrinking is larger than that of the orbital revolution, we assume that there exists a Killing vector: $l = \dfrac{\partial}{\partial t} + \Omega \dfrac{\partial}{\partial \varphi}$.
- Perfect fluid:
  The matter stress-energy tensor: $T_{\mu\nu} = (e + p)u_\mu u_\nu + p g_{\mu\nu}$
- Synchronized or irrotational flow:
  Although the realistic rotation state will be irrotational one[16, 17], we calculate both cases in order to compare their differences.
- Polytropic equation of state: $p = \kappa n^\gamma$
- Conformally flat spatial metric:
  Then the full spacetime metric takes the form: $ds^2 = -(N^2 - B_i B^i)dt^2 - 2B_i dt dx^i + A^2 f_{ij} dx^i dx^j$

Here e denotes the fluid proper energy density, p the fluid pressure, u_μ the fluid 4-velocity, $g_{\mu\nu}$ the spacetime metric, n the fluid baryon number density, κ and γ some constants, N the lapse function, B^i the shift vector, and A the conformal factor.

2.2 Basic equations

1. Fluid equations
   - First integral of fluid motion: $H + \nu - \ln \Gamma_0 + \ln \Gamma = \text{constant}$
   - Differential equation for the velocity potential of irrotational flow:
     $$\zeta H \underline{\Delta} \Psi_0 + \left[(1 - \zeta H)\bar{\nabla}^i H + \zeta H \bar{\nabla}^i \beta\right] \bar{\nabla}_i \Psi_0 = (W^i - W_0^i)\bar{\nabla}_i H + \zeta H \left(W_0^i \bar{\nabla}_i (H - \beta) + \frac{W^i}{\Gamma_n} \bar{\nabla}_i \Gamma_n\right)$$
2. Gravitational field equations
   - The trace of the spatial part of the Einstein equation combined with the Hamiltonian constraint equation:
     $$\underline{\Delta}\nu = 4\pi A^2 (E + S) + A^2 K_{ij} K^{ij} - \bar{\nabla}_i \nu \bar{\nabla}^i \beta$$
     $$\underline{\Delta}\beta = 4\pi A^2 S + \frac{3}{4} A^2 K_{ij} K^{ij} - \frac{1}{2}(\bar{\nabla}_i \nu \bar{\nabla}^i \nu + \bar{\nabla}_i \beta \bar{\nabla}^i \beta)$$

- Momentum constraint equation:

$$\bar{\Delta}N^i + \frac{1}{3}\bar{\nabla}^i(\bar{\nabla}_j N^j) = -16\pi NA^2(E+p)U^i + 2NA^2K^{ij}\bar{\nabla}_j(3\beta - 4\nu)$$

Here $H := \ln h$ denotes the logarithm of the fluid specific enthalpy, $\nu := \ln N$, $\beta := \ln(AN)$, K_{ij} the extrinsic curvature tensor, and $N = B + \Omega\dfrac{\partial}{\partial\varphi}$. Since there are some terms which we do not define here, please read Paper I in detail.

3 Numerical results

In Figs.1 - 4, we present the isocontours of the baryon density, the ADM mass along a constant baryon mass sequence, the relative change in central energy density, and the equatorial to polar ratio of the radial derivative of enthalpy. One can see from Fig.2 that there is no turning point for the cases of irrotational binary systems with $\gamma = 2$. On the other hand, the turning point appears clearly for the synchronized case of identical mass stars. It is marginal for the synchronized case of different mass stars with compactness 0.12vs.0.14. This is because the tidal force from massive star is larger than that of identical mass star and it becomes easier for the less massive star to reach its mass-shedding limit before the turning point.

One of important results in the present work is that there is no increase of central energy density. The results are shown in Fig.3. The reason why the relative change is about 10% for synchronized cases while only a few % for irrotational ones is that there exists an intrinsic spin for the former case which contributes the decrease of central energy density.

Finally we discuss the end points of sequences. A good indicator of the appearance of a cusp at the stellar surface is the quantity χ which is defined as

$$\chi := \frac{(\partial H/\partial r)_{\rm eq,comp}}{(\partial H/\partial r)_{\rm pole}},$$

where $(\partial H/\partial r)_{\rm eq,comp}[(\partial H/\partial r)_{\rm pole}]$ stands for the radial derivative of the enthalpy at the point on the stellar surface located in the orbital plane and looking toward the companion star [at the intersection between the surface and the axis perpendicular to the orbital plane and going through the stellar center (z axis)]. The mass-shedding limit corresponds to $\chi = 0$. Comparing χ with $d/(a_1 + a_1')$ which becomes unity for a contact configuration, we can determine whether a quasi-equilibrium sequence will end by a mass-shedding configuration or by a contact one. Here d and a_1 denote the coordinate orbital separation and the radius of a star towards its companion, respectively. The prime ($'$) means the value concerning with the companion star. It is found from Fig.4 that the two stars contact with each other in the synchronized case for identical mass binaries, while the synchronized sequences for different mass binaries and the irrotational ones terminate by a cusp point, if we extrapolate the curves up to $\chi = 0$.

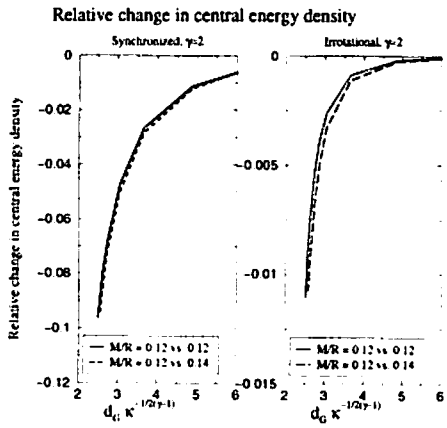

Figure 3: Relative change in central energy density. The curves for different mass cases are those of less massive stars.

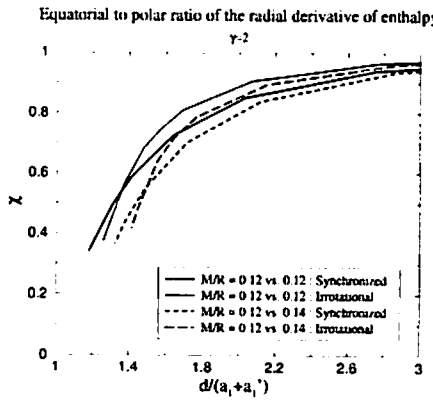

Figure 4: Equatorial to polar ratio of the radial derivative of enthalpy.

4 Summary

We have calculated quasi-equilibrium sequences of binary neutron stars with synchronized and irrotational rotation states in general relativity. Although we have shown only the case of $\gamma = 2$ in this article, we have preliminary results of other polytropic indices. The summary including such results is as follows:

1. End points of sequences
   - Irrotational sequences terminate by a cusp point (mass-shedding point).
   - The two stars contact with each other in the synchronized case for equal mass binaries.
   - For different mass binaries, sequences terminate by a cusp point.
2. Turning points of ADM mass
   - They appear in the case of $\gamma \geq 2.5$ in the irrotational case for equal mass binaries.
   - They appear in the case of $\gamma \geq 1.8$ in the synchronized case for equal mass binaries.
   - For different mass binaries, the critical γ becomes larger in both cases.

Acknowledgments

The code development and the numerical computations have been performed on SGI workstations purchased thanks to a special grant from the C.N.R.S.

References

[1] H. Tagoshi et al, Phys. Rev. **D63** (2001) 062001.

[2] R. Narayan, B. Paczynski, and T. Piran, Astrophys. J. Lett. **395** (1992) L83.

[3] L. Blanchet, submitted to Living Review in. Relativity, preprint gr-qc/0202016.

[4] S. Bonazzola, E. Gourgoulhon, and J.-A. Marck, Phys. Rev. Lett. **82** (1999) 892.

[5] E. Gourgoulhon, P. Grandclément, K. Taniguchi, J.-A. Marck, and S. Bonazzola, Phys. Rev. **D63** (2001) 064029: Paper I.

[6] K. Uryu and Y. Eriguchi, Phys. Rev. **D61** (2000) 124023.

[7] K. Uryu, M. Shibata, and Y. Eriguchi, Phys. Rev. **D62** (2000) 104015.

[8] M. Shibata, Phys. Rev. **D60** (1999) 104052.

[9] M. Shibata and K. Uryu, Phys. Rev. **D61** (2000) 064001.

[10] K. Taniguchi, E. Gourgoulhon, and S. Bonazzola, Phys. Rev. **D64** (2001) 064012.

[11] K. Taniguchi and E. Gourgoulhon, Phys. Rev. **D65** (2002) 044027.

[12] T. W. Baumgarte, G. B. Cook, M. A. Scheel, S. L. Shapiro, and S. A. Teukolsky, Phys. Rev. Lett. **79** (1997) 1182; Phys. Rev. **D57** (1998) 7299.

[13] F. Usui, K. Uryu, and Y. Eriguchi, Phys. Rev. **D61** (2000) 024039.

[14] F. Usui and Y. Eriguchi, Phys. Rev. **D65** (2002) in press.

[15] K. Uryu and Y. Eriguchi, Astrophys. J. Suppl. **118** (1998) 563.

[16] C. S. Kochaneck, Astrophys. J. **398** (1992) 234.

[17] L. Bildsten and C. Cutler, Astrophys. J. **400** (1992) 175.

Effects of the equations of state on the evolutions of binary neutron stars

Fumihiko Usui[1] and Yoshiharu Eriguchi[2]

Department of Earth Science and Astronomy, Graduate School of Arts and Sciences, University of Tokyo, Komaba 3-8-1, Meguro, Tokyo 153-8902, Japan

Abstract

We compute configurations and evolutional sequences of binary neutron stars for several realistic equations of state by assuming that neutron stars are in quasiequilibrium states and synchronously rotating. We find that for typical neutron stars, there appear minimum angular momentum states along the evolutional sequences for constant rest mass binaries prior to contact phases, i.e., the binary system would suffer from secular instability against excitation of internal motion and that behavior of the system cannot be described by a single polytrope during its evolution.

1 Introduction

One of the most important problems for theorists of relativistic astrophysics is constructing reliable models for quasiequilibrium configurations of binary neutron star systems. This is because such systems are the most promising sources of gravitational waves which will be observed by the gravitational wave detectors under construction.

It is, however, still difficult to deal with three-dimensional configurations such as binary neutron star systems in general relativity. This difficulty is mainly due to the non-linearity of the Einstein equations and the boundary conditions at infinity, and practically due to the requirement of a large amount of computational resources.

Since the timescale of the orbital change due to gravitational wave emission is rather long compared with the orbital period except for the final stage of coalescence, we can neglect gravitational wave emission for the most stages of evolution. In other words, we can treat the systems in "quasiequilibrium". Even if we assume the quasiequilibrium condition, we further need to consider many other physical situations or conditions such as effects of viscosity, the form of the rotation law, and so on. In particular, we have to be careful about the equation of state (EOS), although, in all the previous works, the EOS has been assumed to be polytropic. There is no assurance that neutron stars can be approximated by polytropes all through their evolutions of binary systems.

In this work, taking several realistic EOS into account, we construct quasiequilibrium sequences with constant rest mass which can be considered to approximate evolutionary tracks, and compare the results with those of polytropic binary systems. Hereafter, we use the units of $c = G = 1$.

2 Models of binary neutron star systems in quasiequilibrium

2.1 Equations of state

We make use of three kinds of realistic EOS: (1) Bethe & Johnson's [1] model (I), (2) Bethe & Johnson's [1] model (V), which are referred to as models C and D by Arnett & Bowers [2], respectively, and (3) Wiringa et al.'s [3], joined to the more modern EOS by Lorenz et al. [4], which is cited as a model FPS by Cook et al. [5].

The EOS C and D include the effects of hyperons together with the modified Reid soft core potential and the difference between them is the implementation of hyperonization. The characteristic feature of the EOS C is "stiff" and the maximum gravitational mass of a spherical star for this EOS is $1.85M_{\odot}$, while

[1] E-mail:usui@provenco.c.u-tokyo.ac.jp
[2] E-mail:eriguchi@valis.c.u-tokyo.ac.jp

the feature of the EOS D is "soft" and the maximum gravitational mass is $1.65M_\odot$. The EOS FPS is one of the best candidates for the very high density region and include a two-body Urbana UV_{14} potential as a model of nucleon-nucleon interaction and the phenomenological three-nucleon TNI interaction. The feature of FPS is "intermediately stiff" and the maximum gravitational mass is $1.84M_\odot$.

Since the realistic EOS are given in the form of table, values of the pressure and the density at the intermediate points are interpolated by using the polytropic relation. We adopt the piecewise polytropic approximation (PPA) method proposed by Müller and Eriguchi [7] for interpolation.

2.2 Numerical computations

We make the following assumptions (see, Usui, Uryū, and Eriguchi [6] for a more detail):

1. We deal with a binary system which consists of two stars of equal masses in a circular orbit.
2. The binary system is in a stationary state in the rotating frame with the orbital angular velocity Ω.
3. Axes of spins of two stars and that of the orbital motion are parallel to one another.
4. Spins of two stars are synchronized to the orbital motion. Each star is rigidly rotating with the angular velocity Ω if seen from a distant place.
5. We assume the following form for the metric in the spherical coordinates (r, θ, φ) :

$$ds^2 = -e^{2\nu}dt^2 + r^2\sin^2\theta e^{2\beta}(d\varphi - \omega dt)^2 + e^{2\alpha}dr^2 + r^2e^{2\alpha}d\theta^2 \ , \qquad (1)$$

where ν, β, ω, and α are the metric potentials which are functions of r, θ, and φ. Although this form of the metric becomes exact for stationary axisymmetric configurations, it is not exact for nonaxisymmetric configurations.

Under these assumptions, the Einstein equations are written down explicitly and transformed into integral form by taking the boundary conditions at infinity into account. These integral equations and the hydrostatic equation are solved iteratively (see, [6]).

Using this numerical scheme, we have obtained several quasiequilibrium configuration. In order to apply our results to realistic evolutions of binary neutron stars, we construct quasiequilibrium sequences by keeping the baryon number of the system constant because neither mass accretion nor mass loss are assumed. These sequences of a constant rest mass (baryon mass) can be considered to provide realistic evolutionary tracks (see, Usui and Eriguchi [8]). For simplicity, the rotation law is fixed to synchronous rotation, although it is not realistic assumption for binary neutron star evolution. One evolutionary sequence is parameterized by the strength of gravity, such as $(M/R)_\infty$. Here M_∞ and R_∞ are the gravitational mass and the radius of a spherical star.

3 Results

3.1 Sequences with constant rest mass for realistic equations of state

In Fig. 1, the dimensional angular velocity is plotted against the dimensional angular momentum, J, along the evolutionary sequences of constant rest mass configurations for the EOS FPS with various strength of gravity. From this figure, we can see that turning points appear before contact phases for $(M/R)_\infty > 0.15$, while there are no turning points for weaker strength of gravity ($(M/R)_\infty \leq 0.15$). If there exist turning points along the the curves of sequences, secular instability against excitation of internal motion sets in at those points.

Hereafter we consider evolutionary sequences of constant rest mass configurations for three kinds of EOS for the strength of gravity which results in $1.4M_\odot$ gravitational mass at the contact phases. The value of the strength gravity for such configurations is about $(M/R)_\infty > 0.15$. The feature of sequences does not change drastically for the range of the strength of gravity which can be regarded as those of typical neutron stars.

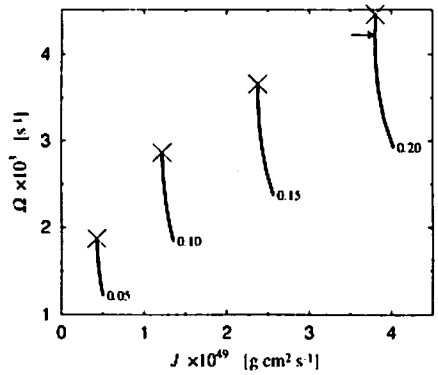

Figure 1: Dimensional angular velocity Ω in units of 10^3 [s^{-1}] is plotted against dimensional angular momentum J in units of 10^{49} [g cm^2 s^{-1}] for the sequences of constant rest mass with the EOS FPS. Curves are labeled by the strength of gravity $(M/R)_\infty$. Crosses denote configurations at the contact phases, and arrows denote the turning points, i.e., the minima of angular momentum.

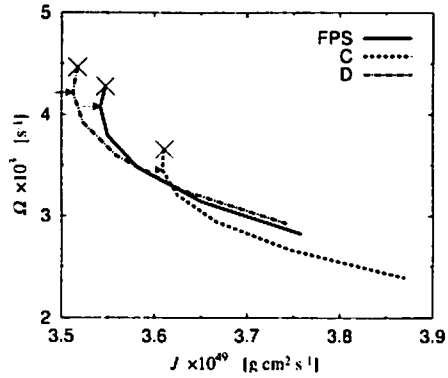

Figure 2: Same as Fig. 1 but for realistic EOS: C, D, and FPS.

In Fig. 2, the dimensional angular velocity is plotted against the dimensional angular momentum for three kinds of realistic EOS. From this figure, it is clear that the turning points appear before the contact phases, i.e. the systems would suffer from secular instability, although the values of the angular momentum and the angular velocity at the turning points are different among three EOS. Consequently, it is highly likely that for the realistic EOS the binary systems would become "unstable" against excitation of internal motion.

3.2 Comparison with polytropic binary stars

In all the previous works, (e.g., [9], [8]), EOS is assumed to be polytropic:

$$p = K\rho^{1+1/N}, \tag{2}$$

$$\varepsilon = \rho + Np, \tag{3}$$

where p, ε, ρ, K and N are the pressure, the energy density, the rest mass density, a polytropic constant and the polytropic index, respectively and assumed that N and K are fixed during binary evolutions [9]. Concerning the value of K, it might be a reasonable assumption because K means the entropy in the Newtonian limit and the evolution can be treated as an almost adiabatic processes, i.e., the timescale of viscous heating is much longer than evolutionary timescale due to the back reaction of gravitational wave emission.

In realistic evolutions of binary neutron star systems, however, the matter could not be represented by a single polytrope and micro physics of neutron stars might change during evolution. Consequently it is very difficult to apply polytropic stars directly to neutron stars because it is very uncertain which kinds of polytropic sequences correspond to real evolution. When we employ realistic EOS, there remains little uncertainty except for the uncertainty of the matter at very high density region. Therefore, it is important to know how differently the quasiequilibrium sequences behave if we choose different EOS.

To compare the realistic sequences with the polytropic sequences, we need to choose the value of the polytropic constant K , in addition to N. This is because the physical quantities for polytropes vary according to the following formula:

$$M = K^{N/2}\bar{M} , \tag{4}$$

$$\varepsilon = K^{-N}\bar{\varepsilon} , \tag{5}$$

$$\Omega = K^{-N/2}\bar{\Omega} , \tag{6}$$

$$J = K^{N}\bar{J} , \tag{7}$$

where quantities with "bar" mean nondimensional ones.

For polytropes, in order to get dimensional quantities, we make the following two choices: (1) fixing the gravitational mass at the contact phase to $1.4M_\odot$ and (2) fixing the angular momentum at turning points to the same value by taking appropriate values of $(M/R)_\infty$. The values of K and other quantities are shown in Table 1.

Table 1: Physical quantities of binary polytropes

(1) $1.4M_\odot$ gravitational mass models at contact phase

N	K	M_G	M_0
0.5	1.73×10^{-10}	$1.40M_\odot$	$1.59M_\odot$
0.7	4.79×10^{-2}	1.40	1.58
1.0	1.13×10^{5}	1.40	1.54

(2) Equal angular momentum models at turning points

N	K	M_G	M_0
0.5	1.69×10^{-10}	$1.39M_\odot$	$1.58M_\odot$
0.7	4.75×10^{-2}	1.40	1.57
1.0	1.12×10^{5}	1.40	1.54

Comparison between realistic sequences and polytropic sequences are shown in Fig. 3. Using the choice (1), the sequences for the EOS FPS and $N = 0.5$ or 0.7 polytropes behave similar at larger separation. However disagreements appear for closer separations. For choice (2), the sequences for polytropes almost coincide each other, although sequences for the EOS FPS is clearly different from them.

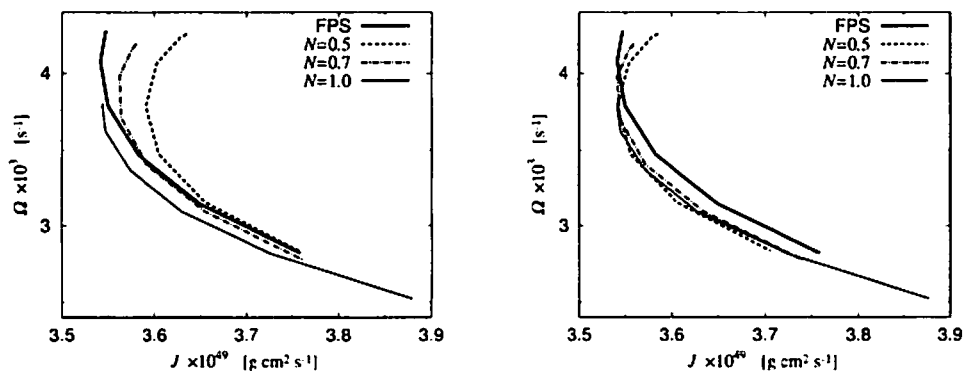

Figure 3: Same as Fig. 1 but for the EOS FPS and polytropes, $N = 0.5$, 0.7, and 1.0. Physical quantities for polytropes are dimensionalized according to Table 1.

Since we can choose many kinds of dimensionalization for polytropes, it is difficult (or impossible) to make meaningful comparison between the realistic sequences and polytropic sequences. It is not so curious because the behavior of the realistic EOS itself cannot be described by a single polytrope as shown in Fig. 4.

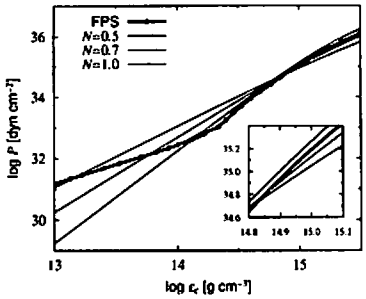

Figure 4: Detailed features of the EOS FPS and polytropes. Polytropes are dimensionalized according to Table 1(1).

4 Summary and Discussion

In this paper, we have calculated quasiequilibrium structures of synchronously rotating binary neutron star systems for several realistic EOS and compared them with the results for polytropes. For typical neutron stars, there appear turning points along their sequences, i.e., system would suffer from the secular instability against excitation of internal motion.

Although we have used the term "realistic" EOS, they have not been definitely determined yet but contain some uncertainties which originate from difficulty to know the feature of the matter beyond the nuclear density experimentally and the theory of the neutron star matter is not fully developed yet. Consequently, many kinds of realistic EOS have been proposed by considering different kinds of particle interactions into account at high density regions, say, $\varepsilon \gtrsim 2.7 \times 10^{14}$ g cm^{-3}. In this work, we adopt three kinds of EOS for the high density region, while there is no assurance that our choice is appropriate for the binary evolution. However, it is important to know what differences arise for realistic EOS and polytropes which contain arbitrary parameters K and N.

Although we have fixed the rotation law as synchronous rotation, we need to extend our formulation to treat irrotational binary neutron star systems because for neutron stars the viscosity does not work enough and synchronous rotation cannot be maintained.

References

[1] H.A. Bethe and M.B. Johnson, Nucl. Phys. **A230**, 1 (1974).

[2] W.D. Arnett and R.L. Bowers, Astrophys. J. Suppl. **33**, 415 (1977).

[3] R.B. Wiringa, V. Fiks, and A. Fabrocini, Phys. Rev. C **38**, 1010 (1988).

[4] C.P. Lorenz, D.G. Ravenhall, and C.J. Pethick, Phys. Rev. Lett. **70**, 379 (1993).

[5] G.B. Cook, S.L. Shapiro, and S.A. Teukolsky, Astrophys. J. **424**, 823 (1994).

[6] F. Usui, K. Uryū, and Y. Eriguchi, Phys. Rev. D. **61**, 24039 (2000).

[7] E. Müller and Y. Eriguchi, Astron. Astrophys. **152**, 325 (1985).

[8] F. Usui, and Y. Eriguchi, Phys. Rev. D. to be published (astro-ph/0112571).

[9] T.W. Baumgarte, G.B. Cook, M.A. Scheel, S.L. Shapiro, and S.A. Teukolsky, Phys. Rev. D **57**, 7299 (1998).

Gravitational Radiation from Coalescence of Binary Neutron Stars — Gauge-Invariant Wave Extraction —

Mari Kawamura,[1] Makoto Nozawa

Graduate School of Science and Technology, Niigata University
Niigata, 950-2181, Japan

Ken-ichi Oohara[2]

Department of Physics, Niigata University
Niigata, 950-2181, Japan

Takashi Nakamura[3]

Yukawa Institute for Theoretical Physics, Kyoto University,
Sakyo-ku, Kyoto 606-8502, Japan

Abstract

We are developing 3 dimensional simulation codes for coalescing binary neutron stars. A stable code using maximal slicing condition is obtained. To evaluate the gravitational radiation, we implemented a gauge-invariant wave extraction and compared the wave forms with a simple estimate of waves with a previous code. The energy spectrum of the waves was also evaluated to investigate the possibility that the excitation of the quasi-normal modes of black hole, which may be formed after merger of two stars, can be caught.

1 Introduction

The main targets of an interferometric detector of gravitational waves such as LIGO[1], VERGO[2], GEO600[3] and TAMA[4] are the waves from compact star binary. We are constructing 3D, fully relativistic computer codes for coalescing binary neutron stars. In a previous code we used a conformal slicing condition and we were faced with instability that is contained in this slicing. Then we choose maximal slicing instead. Disadvantage to maximal slicing is that as extraction of gravitational waves is not straightforward as well as that more CPU hours are required since an elliptic partial differential equation should be solved for the lapse function α.

Abrahams et.al.[5] gave the gauge-invariant wave extraction technique for axially symmetric, even-parity perturbations of a Schwarzschild metric. We extend it to non-axially symmetric perturbations both with even- and odd-parities. In this article, we present summary of it and some numerical results. The details will be given elsewhere[6].

2 Gauge Invariant Wave Extraction

In the (3+1)-formalism, the spacetime metric is given by

$$ds^2 = -\alpha^2 dt^2 + \gamma_{ij}(dx^i + \beta^i dt)(dx^j + \beta^j dt), \tag{1}$$

[1] E-mail:mari@astro.sc.niigata-u.ac.jp
[2] E-mail:oohara@astro.sc.niigata-u.ac.jp
[3] E-mail:takashi@yukawa.kyoto-u.ac.jp

where α, β^i and γ_{ij} are the lapse function, the shift vector and the intrinsic metric on 3-dimensional spacelike hypersurface, respectively. The details on formulation of our code are described in Oohara and Nakamura [7]. As for the coordinate conditions, we adopt the maximal slicing and the pseudo-minimal distortion conditions in the present code. In this coordinate conditions, non-wave parts of the perturbations decrease as $O(r^{-1})$ for large r and therefore h_{ij} defined by

$$\gamma_{ij} = \phi^4(\delta_{ij} + h_{ij}), \quad \phi = \det(\gamma_{ij})^{1/12} \tag{2}$$

cannot be considered as the gravitational waves [8], but it includes gauge dependent modes. Then it is necessary to perform a gauge-invariant wave form extraction. Here we apply a gauge-invariant wave form extraction technique suggested by Abrahams et.al. [5], which is based on Moncrief's formalism [9].

On the outside of the star, we can consider the total spacetime metric $g_{\mu\nu}$ which is generated numerically as a sum of a Schwarzschild spacetime and non-spherical perturbation parts:

$$g_{\mu\nu} = g^{(B)}_{\mu\nu} + h^{(e)}_{\mu\nu} + h^{(o)}_{\mu\nu}, \tag{3}$$

where $g^{(B)}_{\mu\nu}$ is a spherically symmetric metric given by

$$g^{(B)}_{\mu\nu} = \begin{pmatrix} -N^2 & 0 & 0 & 0 \\ 0 & A^2 & 0 & 0 \\ 0 & 0 & R^2 & 0 \\ 0 & 0 & 0 & R^2\sin^2\theta \end{pmatrix} \tag{4}$$

and $h^{(e)}_{\mu\nu}$, $h^{(o)}_{\mu\nu}$ are even-parity and odd-parity metric perturbations, respectively, given by

$$h^{(e)}_{\mu\nu} = \sum_{lm} \begin{pmatrix} N^2 H_{0lm} Y_{lm} & H_{1lm} Y_{lm} & h^{(e)}_{0lm} Y_{lm,\theta} & h^{(e)}_{0lm} Y_{lm,\phi} \\ * & A^2 H_{2lm} Y_{lm} & h^{(e)}_{1lm} Y_{lm,\theta} & h^{(e)}_{1lm} Y_{lm,\phi} \\ * & * & r^2[K_{lm} + G_{lm}\frac{\partial^2}{\partial\theta^2}]Y_{lm} & r^2 G_{lm} X_{lm} \\ * & * & * & h^{(e)}_{33} \end{pmatrix}, \tag{5}$$

$$h^{(e)}_{33} = r^2\sin^2\theta\left[K_{lm}Y_{lm} + G_{lm}\left(\frac{\partial^2}{\partial\theta^2}Y_{lm} - W_{lm}\right)\right] \tag{6}$$

$$h^{(o)}_{\mu\nu} = \sum_{lm} \begin{pmatrix} 0 & 0 & -h^{(o)}_{0lm}\frac{1}{\sin\theta}Y_{lm,\phi} & h^{(o)}_{0lm}\sin\theta Y_{lm,\theta} \\ 0 & 0 & -h^{(o)}_{1lm}\sin\theta Y_{lm,\phi} & h^{(o)}_{1lm}\sin\theta Y_{lm,\theta} \\ * & * & \frac{1}{2}h^{(o)}_{2lm}\frac{1}{\sin\theta}X_{lm} & -\frac{1}{2}h^{(o)}_{2lm}\sin\theta W_{lm} \\ * & * & * & -\frac{1}{2}h^{(o)}_{2lm}\sin\theta X_{lm} \end{pmatrix}, \tag{7}$$

where N^2, A^2, R^2, H_{1lm}, $h^{(e)}_{0lm}$, $h^{(e)}_{1lm}$, K_{lm}, G_{km}, $h^{(o)}_{0lm}$, $h^{(o)}_{1lm}$, and $h^{(o)}_{2lm}$ are the functions of t and r; Y_{lm} is the spherical harmonics and

$$X_{lm} = 2\left(\frac{\partial^2}{\partial\phi\partial\theta} - \cot\theta\frac{\partial}{\partial\phi}\right)Y_{lm}, \tag{8}$$

$$W_{lm} = \left(\frac{\partial^2}{\partial\theta^2} - \cot\theta\frac{\partial}{\partial\theta} - \frac{1}{\sin^2\theta}\frac{\partial^2}{\partial\phi^2}\right)Y_{lm}. \tag{9}$$

The symbol $*$ in Eqs.(5) and (7) indicates the symmetric components. From the linearized theory about perturbations of the Schwarzschild spacetime, the gauge invariant quantities $\Psi^{(o)}$ and $\Psi^{(e)}$ are given by

$$\Psi^{(o)}_{lm}(t,r) = \sqrt{2l(l+1)(l-1)(l+2)}N^2\frac{1}{r}\left(h^{(o)}_{1lm} + \frac{r^2}{2}\frac{\partial}{\partial r}\left(\frac{h^{(o)}_{2lm}}{r^2}\right)\right), \tag{10}$$

$$\Psi^{(e)}_{lm}(t,r) = -\sqrt{\frac{2(l-1)(l+2)}{l(l+1)}}\frac{4rN^2k_{2lm} + l(l+1)rk_{1lm}}{(l(l+1)+1-3N^2)}, \tag{11}$$

for the odd and even parity modes, respectively, where

$$k_{1lm} = K_{lm} + N^2 r G_{lm,r} - 2\frac{N^2}{r} h^{(o)}_{1lm}, \tag{12}$$

$$k_{2lm} = \frac{H_{2lm}}{2N^2} - \frac{1}{\sqrt{N^2}}\frac{\partial}{\partial r}\left(\frac{r}{N^2}K_{lm}\right). \tag{13}$$

The quantities $\Psi^{(o)}$ and $\Psi^{(e)}$ satisfy the Regge-Wheeler and the Zerilli equations, respectively,

$$\left[\frac{\partial^2}{\partial t^2} - \frac{\partial^2}{\partial r_*^2} + V^{(I)}\right]\Psi^{(I)}_{lm} = 0, \quad (I = \mathrm{e}, \mathrm{o}), \tag{14}$$

where $V^{(o)}$ and $V^{(e)}$ are the Regge-Wheeler and the Zerilli potential[10], respectively. The symbol r_* is the tortoise coordinate defined by $r_* = r + 2M\ln(r/2M - 1)$. Two independent polarizations of gravitational waves h_+ and $h_\times$ are given by

$$h_+ - ih_\times = \frac{1}{\sqrt{2}r}\sum_{l,m}(\Psi^{(e)}_{lm}(t,r) + \Psi^{(o)}_{lm}(t,r))_{-2}Y_{lm}, \tag{15}$$

where

$$_{-2}Y_{lm} = \frac{1}{\sqrt{l(l+1)(l-1)(l+2)}}\left(W_{lm} - \frac{i}{\sin\theta}X_{lm}\right) \tag{16}$$

In numerical calculation, the functions $N^2(t,r)$, $A^2(t,r)$ and $R^2(t,r)$ of the background metric are calculated by performing the following integration over a two-sphere of radius r:

$$N^2(t,r) = -\frac{1}{4\pi}\int g_{tt}d\Omega, \tag{17}$$

$$A^2(t,r) = \frac{1}{4\pi}\int g_{rr}d\Omega, \tag{18}$$

$$R^2(t,r) = \frac{1}{8\pi}\int (g_{\theta\theta} + \frac{g_{\phi\phi}}{\sin^2\theta})d\Omega. \tag{19}$$

The components of the even parity metric perturbations are

$$H_{2lm}(t,r) = \frac{1}{A^2}\int g_{rr}Y^*_{lm}d\Omega, \tag{20}$$

$$G_{lm}(t,r) = \frac{1}{l(l-1)(l+1)(l+2)}\frac{1}{R^2}\int\left[\left(g_{\theta\theta} - \frac{g_{\phi\phi}}{\sin^2\theta}\right)W^*_{lm} + \frac{2g_{\theta\phi}}{\sin\theta}\frac{X^*_{lm}}{\sin\theta}\right]d\Omega, \tag{21}$$

$$K_{lm}(t,r) = \frac{1}{2}l(l+1)G_{lm} + \frac{1}{2R^2}\int\left(g_{\theta\theta} + \frac{g_{\phi\phi}}{\sin^2\theta}\right)Y^*_{lm})d\Omega, \tag{22}$$

$$h^{(e)}_{1lm}(t,r) = \frac{1}{l(l+1)}\int\left(g_{r\theta}Y^*_{lm,\theta} + \frac{g_{r\phi}}{\sin\theta}\frac{Y^*_{lm,\phi}}{\sin\theta}\right)d\Omega, \tag{23}$$

where $*$ denotes the complex conjugate. The components of odd parity metric perturbations are

$$h^{(o)}_{1lm}(t,r) = -\frac{1}{l(l+1)}\int\left(g_{r\theta}\frac{Y^*_{lm,\phi}}{\sin\theta} - \frac{g_{r\phi}}{\sin\theta}Y^*_{lm,\theta}\right)d\Omega, \tag{24}$$

$$h^{(o)}_{2lm}(t,r) = \frac{1}{l(l-1)(l+1)(l+2)}\int\left[\left(g_{\theta\theta} - \frac{g_{\phi\phi}}{\sin^2\theta}\right)\frac{X^*_{lm}}{\sin\theta} - \frac{2g_{\theta\phi}}{\sin\phi}W^*_{lm}\right]d\Omega. \tag{25}$$

3 Numerical results

We performed numerical simulation for coalescing binary neutron stars and evaluated the gravitational waves. We used 251 × 251 × 126 Cartesian grid assuming the symmetry with respect to the equatorial

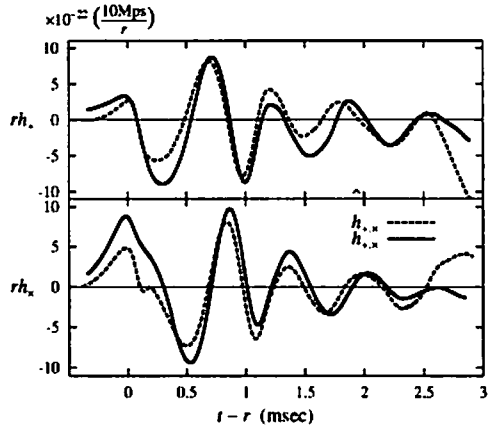

Figure 1: Comparison of 'wave forms' $h_{+,\times}$ and $\widehat{h}_{+,\times}$ along z-axis at $r = 100M_\odot$.

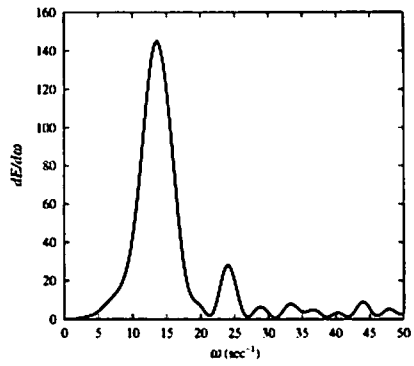

Figure 2: The energy spectrum of the gravitational waves.

plane. As the initial condition, we put two spherical stars of rest mass $1.5M_\odot$ and radius $7.7M_\odot = 11.6$km. The separation between the center of each mass is $30.2M_\odot = 46.2$km. As for an equation of state, we use the $\gamma = 2$ polytropic equation of state. The initial rotational velocity is given so that the circulation of the system vanishes;

$$\vec{V}_a(\vec{r}) = \vec{\Omega} \times \vec{r} - \vec{\Omega} \times (\vec{r} - \vec{r}_a), \tag{26}$$

where $\vec{\Omega}$ is the orbital angular velocity and $\vec{r}_a$ $(a = 1, 2)$ is the location of the center of each star. Now we set $\Omega = 0.010/M_\odot$, then the angular momentum J becomes $6.7M_\odot^2$. The total gravitational mass M_g of the system is $2.76M_\odot$ and $q \equiv J/M_g^2 = 0.89$.

The metric tensor g_{rr}, $g_{\theta\theta}$ etc. on the spherical coordinate system appearing in Eqs.(18)–(25) are calculated from g_{xx}, g_{yy} etc. on the Cartesian coordinate system, such as

$$\begin{aligned} g_{rr} &= \sin^2\theta\,(g_{xx}\cos^2\phi + 2g_{xy}\sin\phi\cos\phi + g_{yy}\sin^2\phi) \\ &\quad + g_{zz}\cos^2\theta + 2\sin\theta\cos\theta\,(g_{yz}\sin\phi + g_{zx}\cos\phi). \end{aligned} \tag{27}$$

Figure 1 shows the gravitational wave forms rh_+ and $rh_\times$ on the z-axis evaluated at $r = 100M_\odot$ as functions of the retarded time $t - r$. The metric perturbations $\widehat{h}_+$ and $\widehat{h}_\times$ defined by

$$\widehat{h}_+ = \frac{1}{2}(h_{xx} - h_{yy}), \tag{28}$$

$$\widehat{h}_\times = h_{xy}, \tag{29}$$

where h_{ij} is defined by Eq.(2), are also plotted for comparison. Although $\widehat{h}_+$ and $\widehat{h}_\times$ includes gauge dependent mode, they are quantitatively coincide with the gauge independent waves h_+ and $h_\times$.

If a black hole is formed after merger of two neutron stars, quasi-normal modes of the black hole are excited. To investigate the possibility that the excitation of the quasi-normal modes can be caught by the numerically calculated waves, we evaluated the energy spectrum of the gravitational waves, which is given by

$$\frac{dE_{GW}}{d\omega} = \frac{1}{16}\sum_{l,m}\omega^2\left(\left|\Psi^{(e)}_{lm\omega}(r)\right|^2 + \left|\Psi^{(o)}_{lm\omega}(r)\right|^2\right), \tag{30}$$

where

$$\Psi^{(I)}_{lm\omega}(r) = \frac{1}{2\pi}\int \Psi^{(I)}_{lm}(t,r)\,e^{-i\omega t}\,dt \tag{31}$$

is the Fourier transformation of $\Psi^{(I)}_{lm}(t,r)$, and show in Fig. 2. The frequencies of the quasi-normal modes depend on the angular momentum of the black hole, but the fundamental frequency of $l = 2$ for

a Schwarzschild black hole of mass $2.8M_\odot$ is $\omega = 25$ msec^{-1}. A peak near this frequency appears in Fig. 2. Unfortunately, however, rotating angular frequency just when the merger of the stars finishes is $12 \sim 15$ msec^{-1} and thus they will radiate the waves of frequency near $\omega = 25$ msec^{-1}. So it is not clear whether the star become a black hole or not.

4 Conclusion

We were able to extract the gauge-invariant gravitational waves with maximal slicing and pseudo-minimal distortion conditions. The calculation presented here used very coarse grid and only 6 or 7 grid points are included from the center through the surface of the central star at the final stage of our calculation. Then it is difficult to follow the black hole formation. The second peak of the energy spectrum at $\omega = 25$ msec^{-1} may not be from the quasi-normal mode of the black hole. We should perform simulation using finer grid to study the final destiny of the coalescing binary neutron stars.

Acknowledgment

Numerical computations were carried out on SR8000/F1 at Hight Energy Accelerator Research Organization(KEK) as the Supercomputer Project and on VPP5000 at the Astronomical Data Analysis Center of the National Astronomical Observatory Japan(NAO). This work was in part supported by Grand-in-Aid 13640271 for Scientific Research from the Ministry of Education, Science and Culture of Japan.

References

[1] A. Abramovici, et.al., Science **256** (1992), 325.

[2] B. Caron, et.al., in *Gravitational Wave Experiments*, eds. E. Coccia, G. Pizzela and F. Ronga, (World Scientific, Singapore, 1995).

[3] K. Danzmann, et.al., in *Gravitational Wave Experiments*, eds. E. Coccia, G. Pizzela and F. Ronga, (World Scientific, Singapore, 1995).

[4] K. Tsubono, in *Gravitational Wave Detection* eds, K. Tsubono, M.-K. Fujimoto and K. Kuroda, Universal Academic Press, INC.-TOKYO (November 12-14 1996 Saitama, Japan), 183-192.

[5] A. Abrahams, D. Dernstein, D. Hobill and E. Seidel, Phys. Rev. **D45** (1992), 3544.

[6] K. Oohara, M. Kawamura, M. Nozawa and T. Nakamura, in preparation.

[7] K. Oohara and T. Nakamura, in *Proceedings of the Ninth Marcel Grossmann Meeting on General Relativity*, (2002), 2273-2276.

[8] K. Oohara, T. Nakamura and M. Shibata, Prog. Theor. Phys. Suppl. **128** (1997), 183.

[9] V. Moncrief, Ann. Phys. (N.Y.) **88** (1974), 322.

[10] F. J. Zerilli, Phys. Rev. lett. **24** (1970), 737.

A Class of Rigidly Rotating Ellipsoidal Perfect-Fluid Spacetimes

József Zsigrai[1]

Department of Physics, Hiroshima University,
Higashi-Hiroshima, 739-8526, Japan
and
Institute for Isotope- and Surface Chemistry of the Hungarian Academy of Science
H-1525 P.O. Box 77, Budapest 114, Hungary

Abstract

Stationary axisymmetric perfect-fluid spacetimes with a so-called inside ellipsoidal symmetry are considered in the framework of general relativity under the assumption that the four-velocity of the fluid is parallel to a time-like Killing vector field. The notion of ellipsoidal spacetimes is shortly reviewed and the conditions for the existence of rigidly rotating perfect-fluid solutions of Einstein's equations are examined for a particular case of ellipsoidal spacetimes in which the gradient of the norm of the time-like Killing vector field and its twist are linearly dependent. Furthermore, some previously known rigidly rotating, perfect-fluid solutions are shown to belong to the class of metrics studied in the present work.

Although exact solutions of Einstein's equations are available to describe in general relativity the gravitational field outside of an isolated rapidly rotating source, no exact solution giving a satisfactory description of the field inside the source has been found yet. An exact solution of the vacuum Einstein equations, which is believed to represent appropriately the exterior field at some distance from a rotating source, has been first obtained by Kerr in 1963 [1]. Since then much effort has been made to find an exact solution representing the gravitational field inside a compact rapidly rotating object, which might be the source of the external field, but without much success. In particular, a great deal of work has been done concerning stationary, axially symmetric, perfect fluid configurations as possible candidates for modeling the interior of rapidly rotating bodies. In the present work we examine this problem by using an approach based on simple geometrical considerations.

In Newtonian gravity extensive work has been done concerning the equilibrium configurations of rotating fluids and numerous results have been obtained for the case in which the fluid has an ellipsoidal shape [2]. Furthermore, in the theory of slowly rotating stars in general relativity [3] it is implicitly assumed that the surface of the star is an ellipsoid. In the present work we will constrain our attention to those rapidly rotating configurations in general relativity, for which there is a natural way for imposing the restriction that the surface of the fluid is ellipsoidal. As a starting point, in the following we will consider rotationally invariant ellipsoidal shapes in stationary, axially symmetric curved spacetimes. We wish to emphasize, however, that other shapes for a rotating fluid might also be possible in both general relativity and Newtonian theory as well.

This paper is organized as follows. First the definition of inside ellipsoidal symmetry is recalled and the basic notions pertaining to rigidly rotating fluids are reviewed. It has been shown [4] that rigidly rotating perfect fluids can be considered to be the equilibrium configurations of relativistic dissipative fluids so they are of obvious astrophysical interest. Next the considerations are specialized to the case in which the gradient of the norm of the time-like Killing vector field and its twist are linearly dependent and the integrability conditions of the field equations are examined. Using the obtained conditions the general form of the metric for the selected configurations is determined and it is demonstrated that the resulting metric can be joined smoothly to the Taub-NUT solution. Finally, some previously known exact solutions are shown to belong to the class of ellipsoidal spacetimes studied here.

In order to carry out a general-relativistic analysis of the fluids having an ellipsoidal shape, it is necessary to define first what an ellipsoid in curved spacetime is. As it has been proposed in [5], we

[1] E-mail:zsigrai@theo.phys.sci.hiroshima-u.ac.jp

consider a three-dimensional, axially symmetric Riemannian space to be ellipsoidal if there exists a coordinate system in which the line element ${}^{(3)}ds^2$ of the three-dimensional space can be written as

$$ {}^{(3)}ds^2 = z^2(\rho,\theta)d\rho^2 + (\rho^2 + a^2cos^2\theta)d\theta^2 + (\rho^2 + a^2)sin^2\theta d\Phi^2, \tag{1} $$

where a is a constant. In such spaces the coordinate surfaces $\rho = const$ give a one-parameter congruence of confocal ellipsoids of revolution. Note that a more general, coordinate-free definition of ellipsoidal (not necessarily axially symmetric) Riemannian spaces is also available [6], however, for the purposes of the present work we will content ourselves with the definition given by equation (1).

Following [6] we will consider stationary axially symmetric spacetimes for which the Riemannian space of time-like Killing trajectories is ellipsoidal and we will refer to such spacetimes as having an "inside ellipsoidal symmetry" or simply "ellipsoidal spacetimes"[2]. More precisely, we will require the line element of the three-dimensional Riemannian metric

$$ h_{ab} := -vg_{ab} + \xi_a\xi_b, \tag{2} $$

to be of the form given by (1), where g_{ab} is the spacetime metric and $v = \xi_a\xi^a$ is the norm of the time-like Killing vector field ξ^a. Then the line element of a stationary, axially symmetric ellipsoidal spacetime can be given in the form

$$ ds^2 = v(\rho,\theta)\left(dt^2 + A(\rho,\theta)d\phi^2\right) - \frac{1}{v(\rho,\theta)}\left(\frac{\rho^2 + a^2cos^2\theta}{\rho^2 + a^2}u(\rho,\theta)d\rho^2 + (\rho^2 + a^2cos^2\theta)d\theta^2 + (\rho^2 + a^2)sin^2\theta d\phi^2\right) \tag{3} $$

where $A(\rho,\theta)$ and $u(\rho,\theta) := z^2(\rho,\theta)(\rho^2 + a^2)/(\rho^2 + a^2cos^2\theta)$ are the remaining unknown metric functions.

In [7] stationary axially symmetric empty spacetimes with inside ellipsoidal symmetry have been considered. By examining the integrability conditions of the field equations it has been demonstrated that the full set of solutions to the vacuum Einstein equations satisfying the above conditions coincides with the family of the Kerr-NUT solutions with vanishing electric and magnetic charges. In the following we use a method analogous to that of [7] to study ellipsoidal perfect-fluid configurations having the four-velocity parallell to a timelike Killing vector field.

We will restrict our attention to perfect-fluid spacetimes for which the four-velocity of the fluid is a unit vector field u^a aligned with a timelike Killing field ξ^a, so that $u^a = (-v)^{-1/2}\xi^a$. Such fluids are "rigid" in the sense that they are expansion- and shear-free. Moreover, for the selected configurations the twist of the Killing field, defined by $\omega_a := \varepsilon_{abcd}\xi^b\nabla^c\xi^d$, can be given as a gradient of a function, that is $\omega_a = \nabla_a\omega$ where ω is called the twist potential. The existence of the Killing field allows one to use the projection formalism of general relativity [1, 8, 9] and to write the field equations for the selected perfect-fluid configurations in the form

$$ H_{ab} := R_{ab} - 16\pi v^{-1}Ph_{ab} = \frac{1}{2}v^{-2}\left[(D_av)(D_bv) + (D_a\omega)(D_b\omega)\right], \tag{4} $$

$$ D_mD^mv = v^{-1}\left[(D_mv)(D^mv) - (D_m\omega)(D^m\omega)\right] - 8\pi(\mu + 3P), \tag{5} $$

$$ D_mD^m\omega = 2v^{-1}(D_m\omega)(D^mv), \tag{6} $$

where μ is the mass-density and P is the pressure of the fluid, while R_{ab} and D_a are the Ricci-tensor and covariant derivative associated with the three-dimensional Riemannian metric h_{ab}. In addition to the above equations the Euler-Lagrange equation

$$ \partial_aP + \frac{1}{2}(\mu + P)\frac{\partial_av}{v} = 0 \tag{7} $$

which follows from the above ones, has to be satisfied.

[2]Note, however, that the definition of ellipsoidal spacetimes given in [5] is essentially different from the one given in [6] and which is used here. Namely, according to [5] in a spacetime filled with matter the Riemannian space which is required to be ellipsoidal is the union of the rest spaces of observers co-moving with matter. Furthermore, in [5] an empty spacetime is considered to be ellipsoidal if there exist *any* congruence of observes for which the union of their local rest spaces can be written in the form given by (1).

In studying the above field equations it is convenient to consider separately two cases: one in which the twist, ω_a, and the gradient of the norm of the Killing field, $D_a v$, are linearly independent, and the other in which they are linearly dependent. The linearly independent case is the subject of ongoing research, while in the present article we concentrate on the results obtained for the linearly dependent case.

If $D_a v$ and $D_a \omega$ are linearly dependent, then the functions v and ω are functionally related, so that one can write $\omega = \omega(v)$. Then using the field equation (4) one obtains

$$H_{AB} = \frac{1}{2} D_A V D_B V, \tag{8}$$

where $A, B = 1, 2$ and we have introduced the function V by

$$D_A V := v^{-1} \sqrt{1 + (d\omega/dv)^2} D_A v. \tag{9}$$

From equation (8) then it follows that in any local coordinate system

$$H_{11} H_{22} - H_{12}^2 = 0. \tag{10}$$

Furthermore, the integrability condition for the existence of a function V satisfying (8) can be written as

$$H_{11} \partial_1 H_{22} - H_{12} \partial_2 H_{11} = 0. \tag{11}$$

Suppose now that the surfaces of constant pressure are given by the coordinate ellipsoids $\rho = const$, that is $P = P(\rho)$. Because of the Euler-Lagrange equation, this implies $v = v(\rho)$, which, in turn, implies $\omega = \omega(\rho)$. With this result, in an ellipsoidal spacetime the (ρ, θ) component of the field equation (4) yields $u(\rho, \theta) = u(\rho)$. Now using the metric corresponding to the examined case of ellipsoidal spacetimes, we obtain that the necessary and sufficient condition for equation (8) to be satisfied is $a = 0$ (where we have excluded the case $u = 1$, which recovers Minkowski spacetime, and the case $u = 0$). With this condition equation (11) is also identically satisfied. On the other hand, the equation for recovering the metric function A from the quantities used in the projection formalism (see e.g. [1, 9]) now reads

$$\frac{1}{sin\theta} \frac{dA}{d\theta} = -v^{-2} \rho^2 u^{-1/2} \frac{d\omega}{d\rho} =: 2R \tag{12}$$

where we could introduce the constant R because the left-hand side of (12) depends merely on the variable θ, while the right-hand side depends merely on ρ, so both sides should be equal to a constant. Then it follows that $A = 2Rcos\theta$. Therefore the line element of all stationary, axially symmetric, rigidly rotating perfect-fluid configurations with inside ellipsoidal symmetry for which the gradient of the norm of the timelike Killing vector field and its twist are linearly dependent can be written in the form

$$ds^2 = v(\rho)(dt + 2Rcos\theta d\phi)^2 - \frac{1}{v(\rho)} \left(u(\rho) d\rho^2 + \rho^2 (d\theta^2 + sin^2\theta d\phi^2) \right) \tag{13}$$

provided that the surfaces of constant pressure are given by the $\rho = const$ ellipsoids. Equivalently, by performing the coordinate transformation $-v(\rho)^{-1} \rho^2 \rightarrow \rho^2$ and introducing the function $f(\rho) := -u(\rho)/v(\rho)$ one may write the metric also as

$$ds^2 = v(\rho)(dt + 2Rcos\theta d\phi)^2 + f(\rho) d\rho^2 + \rho^2 (d\theta^2 + sin^2\theta d\phi^2) \tag{14}$$

It can be easily checked, that the metric corresponding to the line element (13) or (14) is of Petrov type D. Furthemore it can be shown that these perfect-fluid spacetimes can be matched to an external Taub-NUT solution, provided that there exists a $P = 0$ surface. The line-element of the Taub-NUT metric is

$$ds^2 = -F(r)(d\tau + 2lcos\theta d\phi)^2 + F^{-1}(r) dr^2 + (r^2 + l^2)(d\theta^2 + sin^2\theta d\phi^2) \tag{15}$$

$$F(r) = \frac{r^2 - 2mr - l^2}{r^2 + l^2} \tag{16}$$

where l and m are constants [1]. For the purpose of the matching we assume that there exists a ρ_s for which $P(\rho_s) = 0$ and that on the $\rho = \rho_s$ surface the relationships $\tau = \alpha t$ ($\alpha = const$) and $r = r(\rho)$ hold. Then, using the Darmois-Israel junction conditions, one can express the parameters m and l of the Taub-NUT metric, as well as the junction parameter α, in terms of the functions of the interior spacetime evaluated on the surface $P = 0$. This way one arrives at:

$$\alpha^2 = \frac{\rho_s^2 v_s f_s}{R^2 v_s f_s - \rho_s^2} \tag{17}$$

$$l = \alpha R \tag{18}$$

$$m = \frac{1}{2\sqrt{\rho_s^2 - \alpha^2 R^2}}\left(\rho_s^2 - 2\alpha^2 R^2 + \frac{v_s \rho_s^2}{\alpha^2}\right) \tag{19}$$

where $v_s = v(\rho_s)$ and $f_s = f(\rho_s)$.

In the following we list some examples of ellipsoidal perfect-fluid spacetimes having the gradient of the norm of the Killing vector field $D_a v$ and its twist ω_a linearly dependent. In [10, 11] a spacetime originally given by Ferwagner [12] and later rediscovered by Marklund [13] is extensively studied. This spacetime represents an incompressible, rigidly rotating Petrov type D perfect-fluid configuration and it can be joined to the Taub-NUT spacetime. By performing the coordinate transformation $Rsin\chi \to \rho$, $dt \to dt + \frac{R^2}{\rho^2}\frac{d\rho}{\sqrt{1-\rho^2/R^2}}$ on the metric given in [10], we arrive at

$$ds^2 = -\frac{\rho^4}{R^4}(dt + 2Rcos\theta d\phi)^2 + \frac{1}{1 - \frac{\rho^2}{R^2}}d\rho^2 + \rho^2(d\theta^2 + sin^2\theta d\phi^2), \tag{20}$$

where R is a constant. The above line element is exactly in the form given by (14). The density and pressure of the fluid are

$$\mu = \frac{6}{R^2}, \; P = \frac{4}{\rho^2} - \frac{6}{R^2}. \tag{21}$$

Next, it has been shown in [14] that if $\omega = \omega(v)$ and $\mu + 3P \neq 0$, there exist such a coordinate system (t, x^1, x^2, ϕ) in which the line element of all stationary, axisymmetric, rigidly rotating perfect-fluid spacetimes can be written as

$$ds^2 = v(x^1)(dt^2 + A(x^2)d\phi^2) + \frac{1}{v(x^1)}(h_{11}(x^1)(dx^1)^2 + h_{22}(x^1)((dx^2)^2 + e^2(x^2)d\phi^2), \tag{22}$$

where all possible forms of the functions $e(x^2)$ and $A(x^2)$ are listed in [14]. By setting $x^1 = \rho$, $x^2 = \theta$, $h_{22} = \rho^2$ and with the allowed choice $e^2 = sin^2\theta$, which implies $A = 2Rcos\theta$ one recovers the general form (13) of the studied ellipsoidal spacetimes. An exact solution of this type was also given in [14], which, because of its complexity, we do not list here but rather refer the reader to equations (49)-(53) in the original article [14]. Finally, in [15], by using the three-dimensional spin coefficient method the authors have arrived to a line element which has, up to a coordinate transformation, the same general form as that given by equation (13), but they could obtain exact non-vacuum solutions only for the dust case. We wish to emphasize, however, that the list of known ellipsoidal perfect-fluid solutions presented here is by no means meant to be complete, there might as well exist other solutions in the literature, also belonging to the examined class, but at the moment we are not aware of any other such solutions.

An immediate step forward along the line of research presented here is to examine the integrability conditions of the field equations by dropping the assumption that the surfaces of constant pressure are given by the $\rho = const$ surfaces and to assume merely that the surface $P = 0$ is given by a coordinate ellipsoid. Furthermore, it would be instructive to check whether the results obtained here still remain valid if one alters the choice of the Riemannian space which is expected to be ellipsoidal, and requires e.g. the local rest space of matter to be ellipsoidal, as is the case in [5]. Also an open issue is to examine whether the Ferwagner-Marklund solution is the only incompressible fluid solution of the described kind. However, from the metric (14) it can be seen that the corresponding perfect-fluid configuration does not have a regular axis of rotation, so it should not be expected to represent the gravitational field of a rotating body, but rather, as it has been shown, an interior NUT solution. Nevertheless, it is expected

that in the case in which ω_a and $D_a v$ are linearly independent, which is complementary to the case studied here, one could obtain ellipsoidal perfect-fluid solutions appropriate for describing the interior of rapidly rotating objects. This case is the subject of ongoing work.

Acknowledgment

The author has been supported by a fellowship from the Japan Society for the Promotion of Science under fellowship number P 00787.

References

[1] Kramer D., Stephani H., MacCallum M. and Herlt E.: *Exact solutions of Einstein's field equations* (Cambridge; Cambridge University Press, 1980)

[2] S. Chandrasekhar: *Ellipsoidal Figures of Equilibrium* (New York, Dover Publications Inc, 1987)

[3] J. B. Hartle, Ap. J. **150**, p1005 (1967)

[4] R. Geroch and L. Lindblom, Ann. Phys. **207** p394 (1991)

[5] A. Krasiński, Ann. Phys. **112**, p22 (1978)

[6] I. Rácz, Class. Quantum Grav. **9**, pL93 (1992)

[7] I. Rácz, M. Süveges, Mod. Phys. Lett. A, **13**, No. 14, p1101 (1998)

[8] R. Geroch, J. Math. Phys. **12**, p918 (1972)

[9] J. Zsigrai, Prog. Theor. Phys. **104**, No. 2, p359 (2000)

[10] L. Á. Gergely, Z. Perjés, Gy. Fodor, Rotating Incompressible Perfect Fluid Source of the NUT Metric, gr-qc/9811056 (1998)

[11] Z. Perjés, Gy. Fodor, L. Á. Gergely, M. Marklund, A Rotating Incompressible Perfect Fluid Spacetime, gr-qc/9806095 (1998)

[12] R. Ferwagner, in *Relativity Today*, ed. Z. Perjés, p133 (Nova Sci., 1992)

[13] M. Marklund, Class. Quantum Grav. **14**, p1267 (1997)

[14] E. Herlt, Gen. Rel. Grav. **20**, No. 7. p635 (1988)

[15] B. Lukács, E.T. Newman, G.Sparling, J. Winicour, Gen. Rel. Grav, **15** p567 (1983)

Reconstructing the equation of state for cold nuclear matter

Hajime Sotani[1] and Tomohiro Harada[2]

Department of Physics, Waseda University, Shinjuku, Tokyo, 169-8555, Japan

Abstract

We examine the numerical stability and the feasivility of a direct method to reconstruct the equation of state for supranuclear density matter from the relationship between any two properties of neutron stars, which was proposed by T. Harada [7].

1 Introduction

For supranuclear-density matter, it is thought that there may generate Kaon condensation, pion condensation, hyeronic matter, strange quark matter, and so on. However, it is extremely difficult that these sort of peculiar conditions for cold high density nuclear matter is predicted theoretically by accelerator-experimental test on the ground. On the other hand, neutron stars are constructed by the equation of state (EOS) for such high-density matter with zero temperature. Therefore, neutron stars are very unique laboratories for supraunclear-density matter. Through some observation, the properties of neutron stars such as mass, radius, moment of inertia, and so on, can be determined or restricted [1] - [5]. It is expected that we will have a good amount of data on the properties of neutron stars in the near future. Then, if we get the data set of neutron stars, is it possible to reconstruct the EOS for high density matter with the aid of these data set, and if it is possible to reconstruct the EOS, can we discriminate the difference between the EOS with phase transition and the one without phase transition? Against these problem, the direct method to reconstruct the EOS was proposed by L. Lindblom [6] and recently by T. Harada [7]. The method that L. Lindblom proposed is the way to reconstruct the EOS from the observed masses and radii of neutron stars. This method is the way which is used only the relationship between masses and radii, but numerical simulation is roughly successful for the realistic EOS. The method proposed by T. Harada is the way to reconstruct the EOS from the relationship between any two properties of neutron stars. This is a big merit of this method, but his paper states only how to reconstruct, and do not say its numerical stability and how feasible it is in practice. It is important that the method by T. Harada is how useful, because this method is a more practical use than the one by L. Lindblom. In this report, we examine the numerical stability and the feasibility of the algorithm by T. Harada proposed.

2 Algorithm

First, we state the algorithm proposed by T. Harada. The problem is how to reconstruct the EOS from a complete observed data set; i.e. how to determine the EOS $\rho = \rho(P)$ on the region $P_0 \leq P \leq P_U$, where P_U is some cutoff pressure. This algorithm is assumed that neutron stars are static and spherically symmetric, and that we have a complete relationship $f(Q^{(1)}, Q^{(2)}) = 0$ between the properties of neutron stars $Q^{(1)}$ and $Q^{(2)}$ by some observation. And it is also assumed that there exist the correct EOS for $P \leq P_0$. First step is a preparation of N grid points in the domain $[P_i, P_{i+1}]$ as $P_0 < P_1 < \cdots < P_i < P_{i+1} < \cdots < P_N = P_U$. This algorithm adopts the grid points as

$$\log P_i = \log P_0 + \frac{1}{N} (\log P_N - \log P_0) . \tag{1}$$

Second step is an interpolation of the EOS in the interval $[P_i, P_{i+1}]$, when we have the EOS for $P \leq P_i$. Here, this algorithm is supposed that the EOS in this interval is locally polytropic, that is, the EOS is

[1] E-mail:sotani@gravity.phys.waseda.ac.jp
[2] E-mail:harada@gravity.phys.waseda.ac.jp

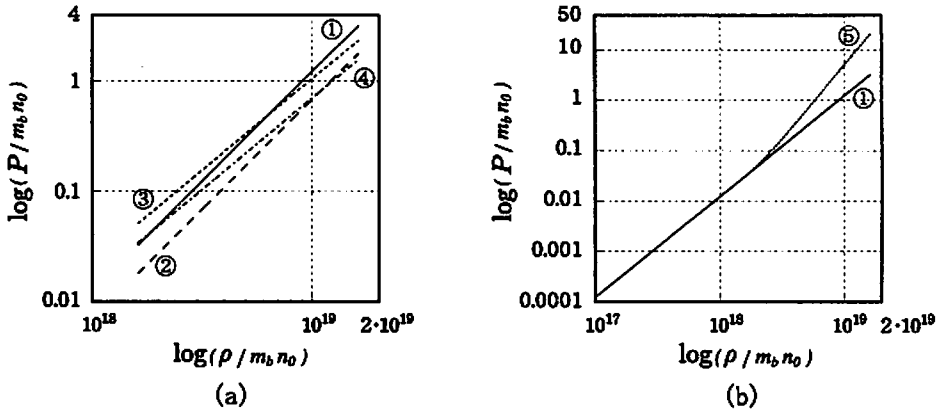

Figure 1: The given EOS to test the algorithm proposed by T. Harada. (a) Polytropic type. The polytropic coefficient K and polytropic index n is (K, n) = (180 km^2, 1.0), (100 km^2, 1.0), (15 km$^{4/3}$, 1.5), (10 km$^{4/3}$, 1.5) from label 1 to label 4 respectively. (b) Smooth continuous type. This panel also shows the EOS of label 1 to compare.

produced by the logarithmically linear interpolation. So, the pressre P ,"local adiabatic index" Γ_i and "local polytropic coefficent" K_i are given as

$$\log P = \log P_i + \Gamma_i (\log \rho - \log \rho_i), \tag{2}$$

$$\Gamma_i \equiv \log\left(\frac{P_{i+1}}{P_i}\right) / \log\left(\frac{\rho_{i+1}}{\rho_i}\right), \tag{3}$$

$$K_i \equiv P_i / {\rho_i}^{\Gamma_i}. \tag{4}$$

Third step is a construction of the neutron star by integrating the TOV equations with the boundary conditions $P(0) = P_{i+1}$, $\rho(0) = \rho_{i+1}$ and $m(0) = 0$ at the center of neutron star. By this step, we get the value of properties $Q^{(1)}_{i+1}$, $Q^{(2)}_{i+1}$, which are the function of ρ_{i+1}, and we obtain the value of function $f(Q^{(1)}_{i+1}(\rho_{i+1}), Q^{(2)}_{i+1}(\rho_{i+1}))$. Therefore, the EOS in the interval $[P_i, P_{i+1}]$ is only one parameter of ρ_{i+1}. Then, forth step is a search of root ρ_{i+1} $(> \rho_i)$ numerically, which gives $f(Q^{(1)}_{i+1}(\rho_{i+1}), Q^{(2)}_{i+1}(\rho_{i+1})) = 0$. Now, the EOS in the interval $[P_i, P_{i+1}]$ is decided. Finally, by repeating these processes from second step to forth step, the EOS for $P \leq P_N$ is reconstructed. Moreover, the algorithm proposed by T. Harada notes the way how to reconstruct the EOS by using a finite data sets of the properties of neutron stars. However, in this time, we explore the former algorithm.

3 Feasibility

To test this algorithm, we explore as follows. First, we give the appropriate EOS to calculate sets of some properties of neutron stars $Q^{(1)}$ and $Q^{(2)}$, which ought to be obtained by some observation originally. Next, we reconstruct the EOS by using this algorithm described above with the data sets $Q^{(1)}$ and $Q^{(2)}$. And finally, the new reconstructed EOS is compared with the original given EOS. Figure 1 shows the given EOS in this time, where the density corresponding to P_0 and P_N are $\rho_0 = 2.0 \times 10^{14}$ g/cm^3 and $\rho_N = 2.0 \times 10^{15}$ g/cm^3 respectively. The EOS from label 1 to label 4 are polytropic one ($P = K\rho^\Gamma$), and the EOS of label 5 is the smooth continuous one ($P = b\rho^3 + a\rho^2 + c$), where we select $b = 1.0$ and other constants a and c is decided by conecting the lower EOS smoothly. This lower EOS is chosen to be the polytropic one. Figure 2 shows the relationship between radii and masses of the constructed neutron stars. It should be possible that this algorithm is applide except for the relationship beween radii and masses, but we use only this relation for simplicity in this time. In Figure, broken lines and solid lines

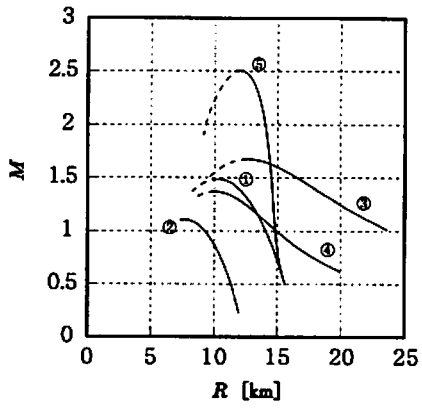

Figure 2: The constructed radius and mass relation by using the EOS of Figure 1.

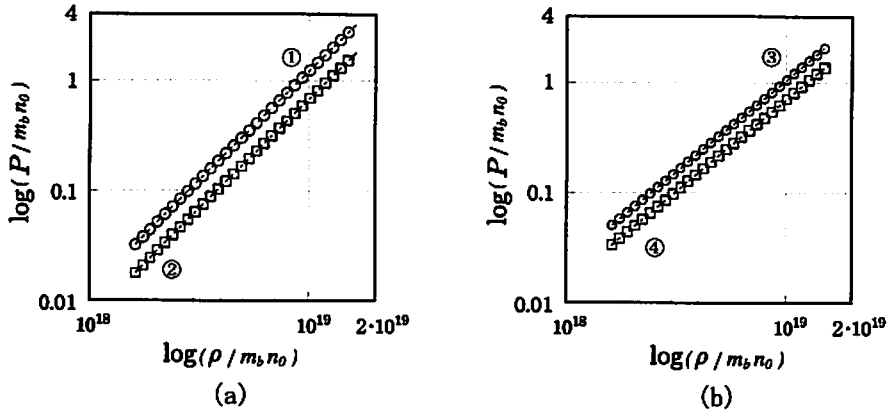

Figure 3: Reconstructed EOS for the case of polytrope.

are corresponding to unstable and stable neutron stars respectively. We can only use the properties of neutron stars on solid lines, because the neutron stars on broken lines don't exist.

We try to reconstruct with 30 grid points, and this numerical result for the polytropic case is showed on Figure 3. In Figure, a broken line is the original EOS, and signs of circle or square are the datas which are reconstructed EOS. From this Figure, this reconstruction of EOS seems be successful. For this algorithm bases on the interpolation of locally polytropic, in the case that the original EOS is polytrope should go well. However, see Figuer 4. This Figure is the relationship between times of reconstruction N and adiabatic index Γ for the case of EOS 1. The adiabatic index of this given EOS is constant 2.0. However, this Figure shows that even for the polytropic EOS, if the number of grid point N is increased, the numerical instability arises. The reason of numerical instability is that the numerical error is accumlated each grid. Moreover, for the EOS 5 which isn't polytrope, the reconstruction is unsuccessful in the case of $N = 30$. However, in this case the number of grid, $N = 30$, may be not enough to reconstruct the EOS, even though the numerical error isn't accumlated.

4 Discussion

We can reconstruct the polytropic EOS almost exactly, but we can't reconstruct the EOS except for polytrope. This algorithm to reconstruct the unknown EOS may have a fundamental problem. This

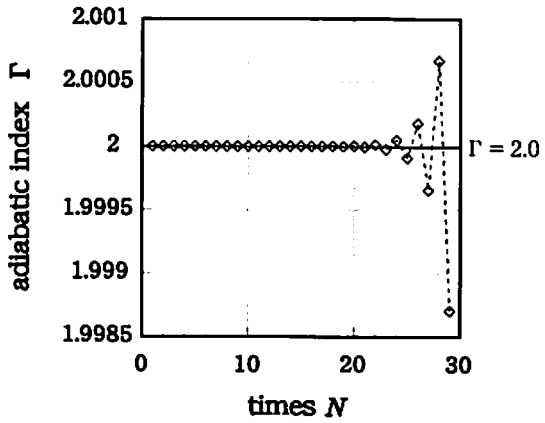

Figure 4: Relationship times of reconstruction N and adiabatic index Γ for the case of EOS 1. The signs of diamond are result of reconstructed adiabatic index.

problem is that the numerical error is accumulated each iteration, so that if the number of grid point N is increased then the numerical instability arises. However, if the number of grid point N is a few, the reconstructed EOS is not exact or it is impossible to reconstruct the EOS except for the polytropic one. For the avoidance from the problem mentioned above, we must improve this algorithm to work for the various EOS. And we confirm the possibility to reconstruct the EOS by using the sets of properties except for the relationship between radii and masses, for example the relationship bewteen masses and moments of inertia relation. Furthermore we try to reconstruct the EOS from a finite data sets by using the method that proposed by T. Harada [7]. This case must determine two parameter P_{i+1} and ρ_{i+1}, but basical plan of reconstruction is similar to the case by using a complete data set.

References

[1] S.E. Thorsett and D. Chakrabarty, Astrophys. J. bf 512, 288 (1999).

[2] R.E. Rutledge, L. Bildsten, E.F. Brown, G.C. Pavlov, and V.E. Zavlin, Astrophys. J. **551**, 921 (2001).

[3] M. Vallisneri, Phys. Rev. Lett. **84**, 3519 (2000).

[4] M. Saijo and T. Nakamura, Phys. Rev. Lett. **85**, 2665 (2000); Phys. Rev. D **63**, 064004 (2001).

[5] L. Stella and M. Vietri, Astrophys. J. **492**, L59 (1999).

[6] L. Lindblom, Astrophys. J. **398**, 569 (1992).

[7] T. Harada, Phys. Rev. C **64**, 048801 (2001).

Ultra-high Energy Cosmic Rays

Shigeru Yoshida[1]

Institute for Cosmic Ray Research, University of Tokyo,
5-1-5 Kashiwa-no-Ha, Kashiwa City, Chiba 277-8582, Japan

Abstract

Physics and astrophysics of cosmic rays with energies above 1 EeV (10^{18} eV) are reviewed. The existence of Ultra-high Energy (UHE) cosmic rays beyond the expected GZK cutoff (5×10^{19} eV) have been established to challenge our understanding of the high energy particle emissions in extragalactic space.

1 Introduction

Many kinds of radiation exist in the universe, including photons and particles with a wide range of energies. Some of the radiation is produced in stars and galaxies, and some is cosmological background radiation, a relic from the history of cosmic evolution. Among all this radiation, the most energetic are cosmic ray particles: nucleons, nuclei, and even extremely energetic gamma rays. Their energies appear to reach beyond 10^{20} eV. Cosmic rays with energies above 10^{19} eV were first detected by the Volcano Ranch group led by John Linsley of the University of New Mexico more than 30 years ago. Since then, where and how these particles are produced and how they propagate in space have been puzzles. Their extremely high energies, seven orders of magnitude greater than those of any nucleons that humans are able to accelerate on earth, suggest that unbelievably energetic phenomena have occurred somewhere in the universe.

There are some observational facts about cosmic rays to give suggestions on their origin. The most important one among them is that the energy spectrum of high energy cosmic rays above 10 GeV (where the magnetic field of the sun is no longer a concern) is well represented by a power law form. This indicates cosmic ray particles are products of non-thermal processes. Figure 1 is a drawing of the measured energy spectrum. Their energy extends over more than 13 decades from 10^7 eV up to 10^{20} eV. In terms of its structure, the spectrum can be divided into three regions: two "knees" and one "ankle". The first "knee" appears around 3×10^{15} eV where the spectral power law index changes from -2.7 to -3.0. The second "knee" is somewhere between 10^{17} eV and 10^{18} eV where the spectral slope changes from -3.0 to around -3.3. The "ankle" is seen at or after 3×10^{18} eV. Above that energy the spectral slope is around -2.7, but with a large uncertainty because of poor statistics and resolution. Our interest is this final and most energetic population, the Ultra High Energy Cosmic Rays (UHECRs).

[1] E-mail:syoshida@icrr.u-tokyo.ac.jp

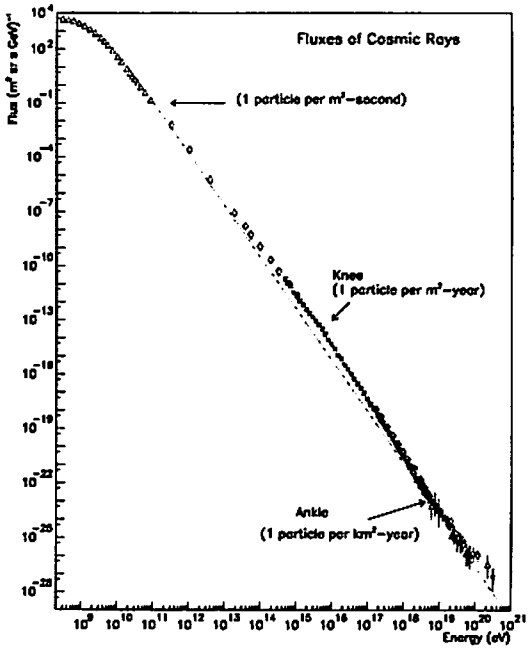

Figure 1: The energy spectrum of cosmic ray. Compiled by Simon Swady of University of Chicago.

The first two population of cosmic rays with energies up to ankle is considered to be galactic in origin. The ankle is interpreted as the cross over energy from a galactic cosmic ray spectrum to an extragalactic one. One would think their origin would be easily resolved by looking at directions where they came from. Unfortunately, things are not so straightforward. The galactic magnetic field ($\sim 3\mu$ Gauss) strongly modulate the trajectories of cosmic rays because they are charged particles. We cannot trace back their arrival directions to identify cosmic ray emitters, which makes it extremely difficult to search for origin of cosmic rays. The observed anisotropy of cosmic ray arrival directions is indeed quite isotropic and gives very few hints on cosmic ray production sites. Nevertheless, the cosmic ray populations below ankle is considered to be originated in our Galaxy because the energies where the cosmic ray energy spectrum has a structure can be related to typical dimension of our Galaxy and its magnetic structure by estimating the Larmor radius of particle motion in the Galaxy. For the first knee energies ($\sim 10^{16}$ eV) the Larmor radius is expected to be $\sim 3(1/Z)$ pc for the particle with charge Z. The scale $\sim$ 1 pc corresponds to the typical size of a magnetic field turbulence in the disk of our Galaxy. In the energy region where the angle appears, The gyro radius of cosmic rays is calculated to be $\sim$ 3 kpc $(E/10^{19}$ eV$)(1/Z)$, which is comparable to radius of galactic disc. Consequently these cosmic rays propagate more freely than at lower energy suggesting that the galactic population of cosmic rays makes less contribution above the angle energy.

As energies of comic rays becomes higher, their trajectories are less deflected by the galactic magnetic field. The deflection angle in the propagation of these particles is less

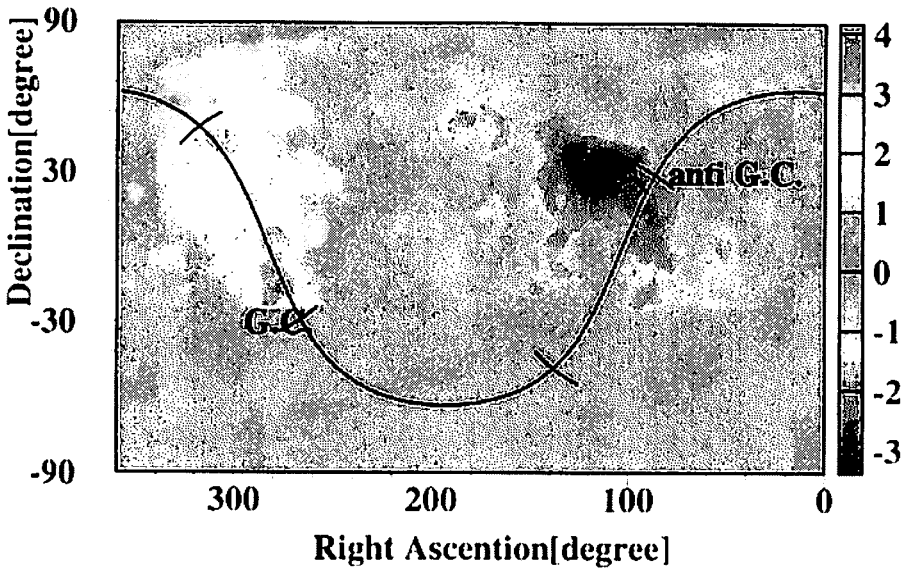

Figure 2: Significance map of excess or deficit events with energies of 10^{18} eV detected by the Akeno Giant Air Showers Array. Events within radius of 20° are summed up in each bin.

than a radian for particles with energies above 10^{19} eV. Therefore, arrival directions of cosmic rays may point back the region of their origin. This has first been realized for cosmic rays with energies of 10^{18} eV. Figure 2 shows the arrival direction distribution in equatorial coordinates for events with energies of $10^{18.0} \sim 10^{18.5}$ eV[1]. 4σ and 3σ excess can be seen while there is a deficit in the cosmic ray intensity near the direction of anti-Galactic Center. This is the first clear experimental evidence that a bulk of high energy cosmic rays originated in our galaxy indeed exists.

When energies become further higher entering into the third and most energetic population of cosmic rays, the particle trajectories would not be bent by galactic magnetic field at all, which may provide opportunities to open the new astronomy – Hadron particle astronomy – because arrival directions of UHE cosmic rays could directly point back individual emitters of cosmic rays. One problem is that the extremely low flux at these energies (the typical rate of cosmic rays above 10^{20} eV is one event/km^2/century!) requires detectors with huge acceptance which have always been challenging to build because of technological and economical difficulties. The recent experiments have improved in terms of both statistics and data quality, however. Throughout these years of continuous effort, signatures concerning the origin of these Ultra High Energy Cosmic Rays (UHECRs) have started to emerge. This is the main subjects of this article: Astrophysics and astronomy of UHECRs as a new window to study very high energy phenomena in the Universe. This is a good example of intersections of particle physics, astronomy, and cosmology. UHE particle radiation and propagation always involve elementary processes of high energy

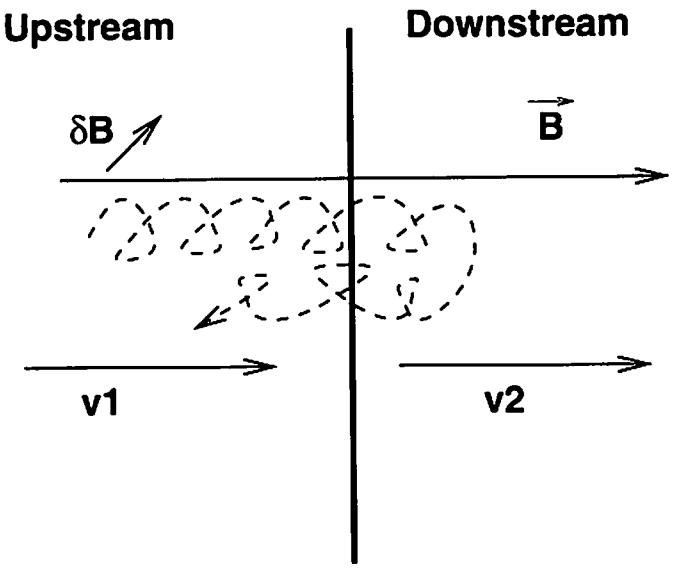

Figure 3: Conceptual illustration of the diffusive shock acceleration. A charged particle diffuse to pass the boundary of upstream and downstream shock back and forth.

particle interactions. Their ultra high energies may require consideration of new physics beyond the standard model of particle physics. If UHECRs are indeed arriving from extragalactic space, their interactions with the 3k cosmic microwave background involves issues of cosmology. Ultra-high energy astro-particles provides an unique opportunity to explore the cosmos and the physics that governs high energy Universe.

2 Origin of the UHE Cosmic Rays : Overview

Production mechanism of high energy cosmic rays has been a main topic of astrophysics. The most representative one among the various proposal is the acceleration of charged particles by "shock-waves" in violent environment of the Universe. The technical issues in the cosmic acceleration have been discussed in the literature and it is not necessary to describe them in detail here. We rather focus on the problem of UHECR production: What environment could possibly realize such extreme acceleration? Where the possible site exist to radiate UHE particles? We will see many of the cosmic accelerators, even if they exist, may not be powerful enough to accelerate particles to energies beyond 10^{20} eV.

2.1 The Shock Acceleration Mechanism for UHECRs

The existence of high energy cosmic rays implies that our Universe must have a function of "cosmic accelerators" to channel tremendous energies to microscopic particles. The most famous and solid example is supernovae in the Galaxy. The explosion of a star in its last moment of life produces a turbulent shock wave in the surrounding plasma

and many kinds of nuclei blown out of the explosion are "shock-accelerated" to ultra-high energies, which ends up with high energy cosmic rays we are observing now. Once the shock waves are generated in the cosmic environment, the so-called diffusive shock acceleration mechanism could accelerate charged particles: they are scattered by magnetic field turbulence and accelerated by the first-order Fermi acceleration. Now let us consider a particle cycling back and forth between two sides of the shock with upstream velocity v_1 and downstream velocity v_2 as illustrated in Figure 3. When the particle crosses the boarder, it gains the energy of

$$\frac{\Delta E}{E} = \frac{4}{3}\frac{v_1 - v_2}{c}, \tag{1}$$

where c is the speed of light. The time scale of this energy gain cycle is

$$\tau_{cyc} = \frac{4}{c}\left(\frac{D_1(E)}{v_1} + \frac{D_2(E)}{v_2}\right). \tag{2}$$

Here $D(E)$ is the diffusion coefficient on either side of the shock. Then the acceleration time scale is given by

$$\tau_A = \int dE \frac{\tau_{cyc}}{\Delta E} = \frac{3c}{v_1 - v_2}\int \frac{dE}{E}\left(\frac{D_1(E)}{v_1} + \frac{D_2(E)}{v_2}\right). \tag{3}$$

In the Bohm diffusion limit, $D(E) = (1/3)r_g$ where r_g is the Larmor radius of the particle motion. Using the relation $v_1 = 4v_2$ assuming the compression ratio of 4, we find

$$\tau_A = \frac{20}{3}\frac{E}{ZeB_{rms}}\frac{c}{V_1^2} \tag{4}$$

where Z is the charge of the accelerating particle and B_{rms} is the averaged strength of turbulent magnetic field in the shock plasma. Equation 4 shows the acceleration efficiency in this mechanism: The faster acceleration time leads to more efficient particle acceleration. Putting the typical numbers into Equation 4 gives the time scale to accelerate particles to 10^{20} eV;

$$\tau_A = 2.6 \times 10^6 Z \left(\frac{B_{rms}}{10\mu\mathrm{G}}\right)^{-1}\left(\frac{\beta_1}{0.3}\right)^{-2} \quad \mathrm{yr}, \tag{5}$$

where $\beta_1 \equiv v_1/c$. It implies that the system with time scale of $\sim 10^6$ year would be favored as a site for accelerating particles to UHE range. Next we will see that there would be very few sites to allow this scale, however.

2.2 The Possible Sites for UHECR acceleration

We have seen that the typical diffusive shock acceleration time is $\sim 10^6(B_{rms}/10\mu\mathrm{G})^{-1}$ year. During this time, the particles must be confined within the diffusive shock region. Consequently size of the site must be sufficiently large for particles not to escape before gaining enough energy. For the shock region scale of D, the escape time from the acceleration site is $t_E = D/v_1$ which must be longer than the acceleration time t_A. From Equation 4, we obtain

$$E_{max} \leq 4 \times 10^{20} Z \left(\frac{B_{rms}}{100\mu\mathrm{G}}\right)\left(\frac{\beta_1}{0.3}\right)\left(\frac{D}{100\mathrm{kpc}}\right) \quad \mathrm{eV}. \tag{6}$$

Table 1: Examples of physical dimensions of extended radio sources

Radio sources	Dimension
Virgo A	3 kpc
Cygnus A	80 kpc
3C236	5.6 Mpc

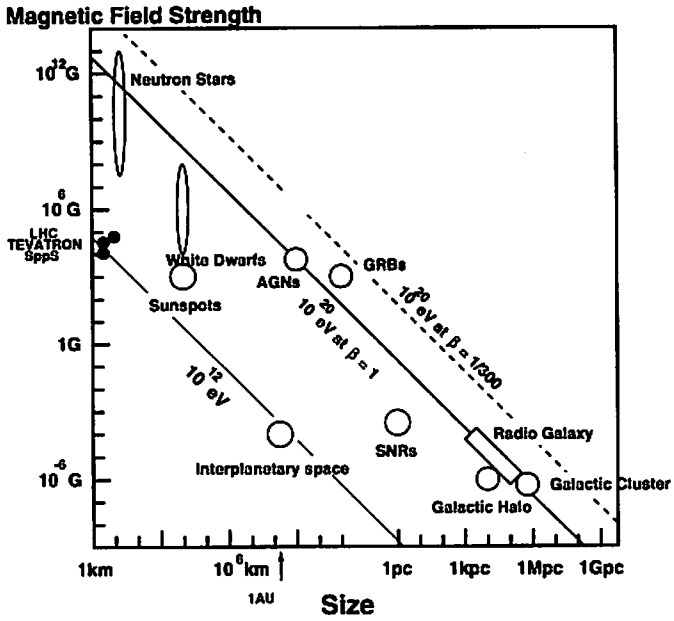

Figure 4: The astronomical objects as cosmic ray sources. They are plotted on size and magnetic field strength map.

This simple requirement known as the Hillas relation[2] already rules out most of the astronomical objects in the universe. Figure 4 shows which objects satisfy this dimensional requirement. Most of the galactic objects are excluded simply because they are too small with magnetic fields that are too weak. Only a few extragalactic objects such as Active Galactic Nuclei (AGNs), radio galaxies, and Gamma Ray Bursts (GRBs) remain as possible candidates. Not all the AGNs/radio galaxies are capable of accelerating particles to UHE range, however. As shown in Table 1, the strong nearby radio galaxy Virgo A ($\sim$ 16Mpc away) may be too small for the UHECR acceleration. Only largely extended AGN jets or hot spots of radio galaxies could be the site where UHECR acceleration takes place. Origin of UHECRs is likely to be extragalactic in terms of the acceleration efficiency, but number of the possible sources is actually limited.

Sites with sufficiently strong magnetic field such as neutron stars ($B \sim 10^{12}$G) may appear to be good sites as shown in Figure 4, because the stronger magnetic field leads to higher acceleration efficiency as represented in Equations 4 and 6. In any actual acceleration site, however, energy loss mechanisms always compete with the processes of energy gain. Too strong a magnetic field would be negative for particle acceleration

because it can cause charged particles to lose energy via the synchrotron process. The synchrotron loss time for a cosmic ray particle with energy E and mass M_{CR} is given by

$$\tau_{sync}^{-1} = \frac{4}{3} U_{mag} \frac{\sigma_t}{Z^4} \frac{m_e^2}{M_{CR}^4} E, \tag{7}$$

where $U_{mag} \equiv B_{rms}^2/8\pi$ is energy density of the magnetic field, $\sigma_t = 6.7 \times 10^{-25}$ cm^2 is the Thompson scattering cross section, $m_e = 511$ keV is electron's mass. Requiring $\tau_A \leq \tau_{sync}$ gives the upper bound of energy of accelerated particles balancing to the synchrotron cooling. We find

$$\begin{aligned} E &\leq \left[\frac{9}{80} \frac{eB_{rms}}{U_{mag}\sigma_t}\right]^{\frac{1}{2}} \beta_1 \left(\frac{M_{CR}}{m_e}\right) M_{CR}c^2 \\ &\leq 8.8 \times 10^{21} \left(\frac{B_{rms}}{100\mu\mathrm{G}}\right)^{-\frac{1}{2}} \left(\frac{\beta_1}{0.3}\right) \quad \mathrm{eV} \end{aligned} \tag{8}$$

for cosmic ray protons. One can find that a typical neutron star with $B_{rms} \sim 10^{12}$ G can only accelerate protons to $\sim 10^{14}$ eV at most.

If an acceleration site such as the AGN core region has a dense photon field, another significant energy loss process compete with the particle acceleration: The photopion production ($\gamma p \to \pi p/n$). This process puts another sever limitation for UHECR production, since many powerful astronomical objects which appears sufficiently sizable to accelerate UHECR particles are luminous in radio band, which suggests that they have dense target photons to initiate the photopion production. The cross section of this reaction has a resonance behavior at $s_{res} = 1.47$ GeV^2 where s is the Lorentz invariant center of mass (CM) energy squared and the typical time scale of the energy loss can be approximately written in rather simple form as

$$\tau_{p\gamma}^{-1} = \frac{8}{3} \frac{U_\gamma}{\log \frac{k_\gamma^{max}}{k_\gamma^{min}}} \frac{\Delta s_{res}}{(s_{res} - M_{CR}^2)^2} \sigma_{p\gamma}^{res} K_{p\gamma} E, \tag{9}$$

where U_γ is the energy density of the photon field, $\Delta s_{res} \simeq 0.6$ GeV^2 is the width of the resonance, $\sigma_{p\gamma}^{res} \simeq 5 \times 10^{-28}$ cm^2 is the photopion cross section at its resonance, $K_{p\gamma} \simeq 0.3$ is the averaged inelacity. Here the photon field is assumed to have the energy spectrum of $\sim k_\gamma^{-2}$ between k_γ^{min} and k_γ^{max}. Comparing it with the synchrotron cooling time Eq. 7, we get

$$\tau_{p\gamma}^{-1} = a\tau_{sync}^{-1} \tag{10}$$

$$\begin{aligned} a &= 2\frac{U_\gamma}{U_{mag}} \left[\log \frac{k_\gamma^{max}}{k_\gamma^{min}}\right]^{-1} \frac{\sigma_{p\gamma}^{res}}{\sigma_t} K_{p\gamma} \left(\frac{M_{CR}^4}{m_e^2}\right) \frac{\Delta s_{res}}{(s_{res} - M_{CR}^2)^2} \\ &= 3.6 \times 10^3 \xi \left[\log \frac{k_\gamma^{max}}{k_\gamma^{min}}\right]^{-1}, \end{aligned} \tag{11}$$

where $\xi \equiv U_\gamma/U_{mag} \sim 1$ implies the equipartition of the photon field and the magnetic field. Thus the energy loss by the photopion production dominates the synchrotron cooling

if the photon field is comparable to the magnetic field. Requiring $\tau_A \leq \tau_{p\gamma}$ gives the maximum acceleration energy which is similar to the expression of Eq. 8:

$$E \leq \left[\frac{9}{80}\frac{eB_{rms}}{U_{mag}a\sigma_t}\right]^{\frac{1}{2}} \beta_1 \left(\frac{M_{CR}}{m_e}\right) M_{CR}c^2$$
$$\leq 5.7 \times 10^{20}\xi^{\frac{1}{2}} \left(\frac{B_{rms}}{100\mu\mathrm{G}}\right)^{-\frac{1}{2}} \left(\frac{\beta_1}{0.3}\right) \quad \mathrm{eV} \qquad (12)$$

under assumption that $k_\gamma^{min} \sim 10^{-3}$ eV and $k_\gamma^{max} \sim 10$ keV. If $\xi \geq 30$, it would be difficult to produce 10^{20} eV cosmic rays.

We should remark here that the arguments we have made here assumes that the diffusive shock acceleration takes place in very efficient manner. This is not very likely. The diffusive shock may be likely to be terminated by any instability of the plasma system for example. The values of the relevant parameters are somewhat in the side of extreme. Only a limited number of extragalactic radio galaxies or GRBs seems to meet the requirements of the energetics. The theories of origin of UHECRs are far from solid.

3 The Standard Scenario : The GZK Mechanism

Although the theoretical understanding of UHECR production mechanism is rather poor, there exists a fact concerning UHE particles that is well known and accurately predictable, which is cosmic ray physics version of the "Standard Model". When UHE nucleons are traveling in space, they interact with the Cosmic Microwave Background (CMB) photons that results in significant energy loss. If UHECRs are extragalactic in origin, the collisions in the CMB field provides many interesting and observable features whose detection would lead to solid signatures indicating that the UHE particles are indeed coming from extragalactic space.

This effect was firstly realized by Ken Greisen in 1967 who published a paper[3] in which he predicted, that if cosmic ray sources were uniformly distributed throughout the universe and if their flux extended past $10^{20}eV$, then they would interact inelastically with the black body radiation. This interaction has a threshold given by the threshold for single photopion production. He predicted that a smooth power law spectrum of cosmic rays would be cut off by this onset of inelastic interactions near $5.0\text{x}10^{19}$ eV. This effect was independently predicted by Zatsepin and Kuzmin[4]. The search for this so-called Greisen-Zatsepin-Kuzmin cut-off has been the holy grail of UHE cosmic ray physicists ever since. Let us examine here how much fraction of the energies are lost via these inelastic interactions in *average*.

The attenuation length, $\lambda_{att}(E)$, is plotted in Fig. 5[5]. It exhibits that the attenuation length above the photopion production threshold is contracted by rapid energy losses. This feature leads to certain constraint on any UHECR sources: no UHECRs sources can be very distant from earth. We can limit the source distances because UHECRs collide with cosmological backgrounds and lose energy during their propagation. This is

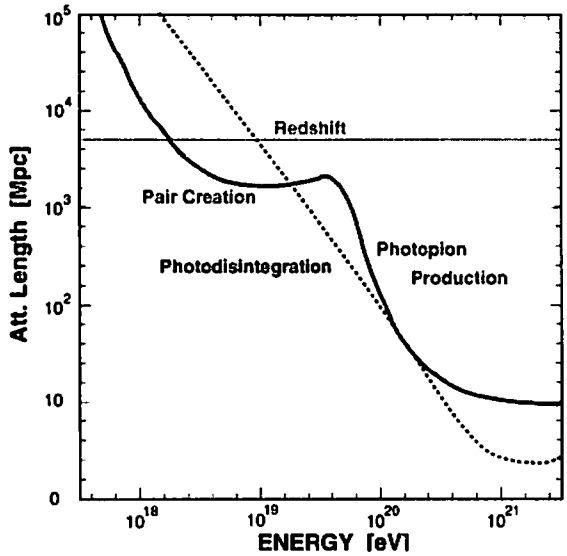

Figure 5: The attenuation length of cosmic rays as a function of energy. The thick solid curve shows the case for UHECR nucleons. The dashed curve shows the case for iron interacting with CMB photons through photodisintegration. The bound given by redshift (adiabatic energy loss) are applicable to all primaries.

the most important effect on the propagation of UHECRs. For example the attenuation length for protons with energies higher than 7×10^{19} eV (the threshold energy of photopion production) is shorter than 500 Mpc. Any sources contributing to the bulk of UHECRs above this energy should be within 500 Mpc of earth. The higher the energy, the shorter the upper bound on the distance. A 3×10^{20} eV proton would require sources within only $\sim$ 50 Mpc. Nearby sources would make dominant contributions at the high energy end.

Although the constraint mentioned above universally valid in spite of the fact that the average behavior of UHECR propagation we have seen in Fig. 5 is not necessarily precise because of the stochastic nature of the photopion production. The upperbound of source distances based on the energy attenuation length is substantially lowerestimated because of the sizable chance of UHECRs penetration that some particles happens not to interact with CMB photons via photopion production. We need to resolve the transport equation and examine the behavior of UHECR energy transfers in detail during the propagation. The effects appear in form of modification of the UHECR energy spectral *shape* by the GZK mechanism. Let us see the resultant energy spectra and their implications next.

First let us show the energy spectrum of UHECRs emitted from a *single* source located at a given distance. Fig. 6 shows the energy spectra numerically calculated by the transport equation[5]. The label along each curve gives the red shift value of the source. The "distance" of a source is related to the redshift. The differential energy spectrum at the source is assumed to follow a power law with the power of -2 up to 10^{22} eV. The fluxes are normalized so that they have the same value at 10^{17} eV. The energy loss by photopion production creates the cut off, and the recoiling UHECRs pile up just below the threshold energy of photopion production, forming a bump structure in the spectrum. For the case

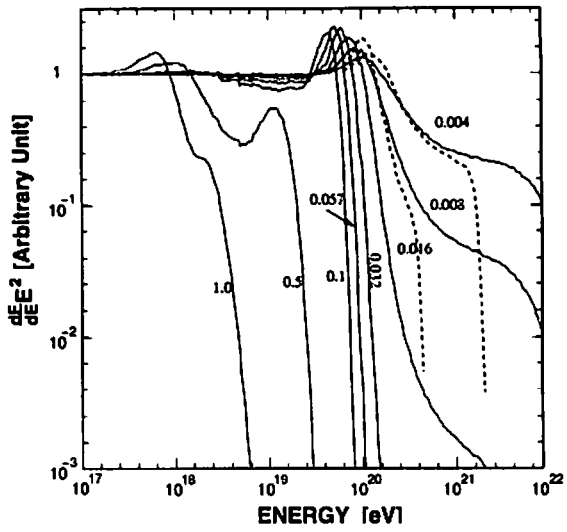

Figure 6: The spectra of a single source of UHECR nucleons for a various red shift are shown. The primary spectra are assumed to have a power law behavior with a spectral index of 2.0. The spectra calculated analytically by the CEL approximation are also shown for the cases of $z = 0.004$(16 Mpc) and $z = 0.008$(32 Mpc) (the dashed lines).

of $z = 0.057(\sim 1.3$ Gpc), the cut off is found at about 6×10^{19} eV and the bump is created at around 5×10^{19} eV. This cutoff is known as Greisen-Zatsepin-Kuzmin cutoff (GZK cutoff), and is the centerpiece of the UHECRs physics. A detection of this effect proves the extragalactic origin of UHECRs and limits the distance to possible sources to less than $\simeq 100$ Mpc for particles above 10^{20} eV.

One of the important results appeared in Fig. 6 is that energies at which the cut off and the bump appear decrease as the red shift of the sources increases. This is mainly due to the evolution of the CMB photons. The interaction probability is scaled as $E(1+z)$ concerning its energy dependence, which results in the strong redshift dependence of the spectral structure. Consequently it implies that the measurement of the spectrum leads to estimation of the typical source distance. Observation of UHECRs with energies beyond 10^{20} eV would require at least substantial emission of UHE particles within ~ 60 Mpc, for example. This is the key to search for UHECR emitters that can be responsible for observed superhigh energetic particles.

In Fig. 6, the spectra calculated analytically using the CEL approximation are also shown for the cases of $z = 0.004$ and $z = 0.008$. We should remark here that the structures of the bump and cut off obtained by this analytical method are more prominent than those obtained by the full numerical calculation. The stochastic nature of the photopion production that results in a spread in collision times and the energy loss makes the differences. Let us consider the case when the propagation length is ~ 30 Mpc ($z = 0.008$) for example. Although this is substantially longer than the energy attenuation length of 10^{21} eV nucleons(~ 10 Mpc), $\sim 5\%$ of UHECRs with energies higher than $\sim 10^{21}$ eV survive to arrive at the earth without losing their energies. However, in the analytical

calculation, all UHECRs are forced to lose the energies by the same fraction given by averaged energy loss rate dE/dt to form the pronounced cut-off structure. The sizable probability of survival of UHE particles after propagation over $\sim$ 20 Mpc and large spread in the energy loss rate might be crucial to interpretate the observed data.

4 The Observational Results

We have seen that cosmic ray particles with energies reaching to 10^{20} eV or above are likely to be originated in extragalactic objects because accelerating particles to such ultra-high energies requires physically huge sites to confine the particles in acceleration. If they are indeed extragalactic in origin, the GZK mechanism limits distances to their sources and their energy spectrum has a cut off structure at around 6×10^{19} eV no matter how they are produced.

The standard GZK scenario predicts two main observable signatures. One is the cut-off structure of the energy spectrum below 10^{20} eV. Another is existence of cosmic ray emitters inside the GZK horizon where the particles survive as UHECRs in their arrival after their propagation in the CMB field. For example from Figure 6, one can see that existence of particles above 10^{20} eV requires their radiators with redshift 0.016 ($\sim$ 60 Mpc) or below. Because Ultra-high energies of the particles would prevent the particle trajectories from being largely bent by the magnetic field in extragalactic and/or galactic space, study of their arrival direction may identify the primary emitters within the GZK horizon. In this section we show the several observational results to see if the standard GZK picture for extragalactic particles can explain the UHECR data.

4.1 Energy Spectrum

Figure 7 shows the energy spectrum measured by AGASA[6]. Surprisingly, it exhibits no cut-off structure expected by the GZK scenario. The dotted curve in the figure indicates the spectrum in the case when the UHECR sources are distributed uniformly in the Universe that shows the GZK cut-off. 10 events have been observed above 10^{20} eV while 1.2 events are expected if the spectrum has the GZK cutoff taking into account the experimental energy resolution ($\sim$ 30 %). The energy spectrum extends well beyond the energies where the GZK mechanism should have formed a strong attenuation. The intensity of the flux above 10^{19} eV was obtained to be

$$J(E) = 2.3 \times 10^{-14} \left(\frac{E}{10^{19}\mathrm{eV}}\right)^{-\gamma} \mathrm{m}^{-2}\mathrm{sec}^{-1}\mathrm{sr}^{-1}\mathrm{eV}^{-1}, \qquad (13)$$

where $\gamma = 2.78^{+0.22}_{-0.33}$ is the spectral power index.

Super-energetic events well beyond the GZK energy has muddied the simple GZK picture. Figure 8 shows the AGASA event whose energy has been estimated to be $2.1^{+0.5}_{-0.4} \times 10^{20}$ eV, the highest record in their data set[7]. This event hit the array almost at its center, and 23 detectors surrounding the shower core measured local electron densities and the time of arrival of the shower front. Even detectors more than 2 km away from

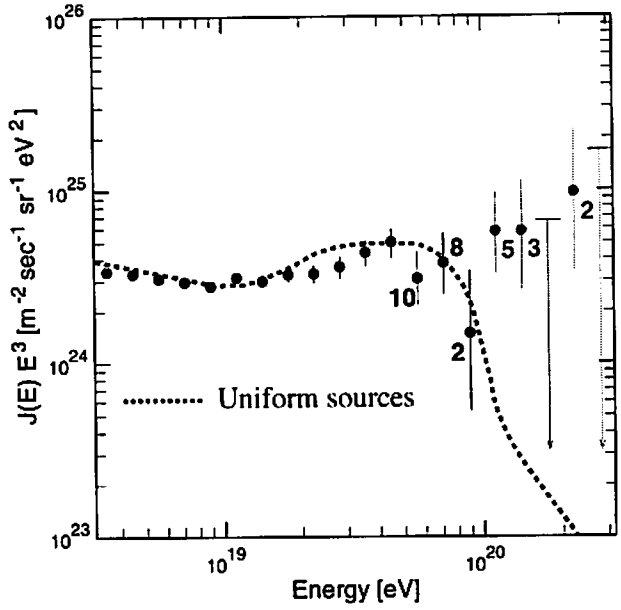

Figure 7: The AGASA energy spectrum.

the core were triggered. Thus the reconstruction of the lateral distribution of electrons for this event was excellent. The functional fit of the electron density distribution agreed well with all the measured densities, which led to an error in the estimation of the charged particle density at 600 meters (S(600)), of +21 % and -6.6 %. Since the location of the shower core is well inside the array, it is very difficult to push down the estimated energy towards the range below the expected GZK cut-off without substantially increasing χ^2 value as illustrated in Figure 9. The largest uncertainty in the energy estimation arises from the fact that the attenuation length of S(600) as a function of the atmospheric depth is not well known. The zenith angle of this event was 23°. A correction must be made to convert the observed S(600) to what would be expected for a vertical shower. The Monte Carlo prediction suggests that the attenuation effect on S(600) is rather moderate and exhibits excellent agreement with the measurement. The correction factor for this event cannot be measured, however, because number of events detected clearly above 10^{20} eV is too small to carry out the experimental study of the attenuation effect in the highest energy regime, and we cannot fully exclude the possibility that this event happened to be observed at the maximum of S(600) development. It implies that the density at 600 m may not be attenuated at all. Nevertheless, assuming no attenuation gives a lower bound on the primary energy of 1.7×10^{20} eV, which is still well beyond the GZK cutoff. We should also remark that taking into account the possible systematic differences due to introducing the modern interaction code leads to even higher energy estimation than the presently determined energy.

If our understanding of the energy estimation on these events is correct, we have another mystery. How could these UHECRs reach earth with such enormous energies? It

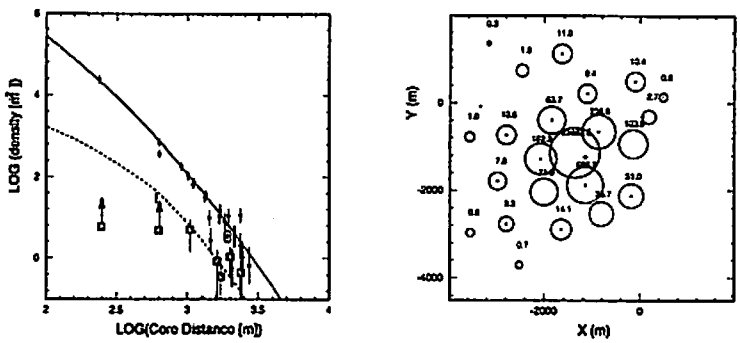

Figure 8: Left:The lateral distribution of charged particles (closed circles) and muons (squares) of the super energetic event recorded by AGASA. The large open circle is the density measured by a detector designed to study the arrival time distribution of particles in air showers. The signals in the muon detector are also shown by the shaded squares. Right: Map of the density distribution of the event. A cross shows the estimated location of the shower core.

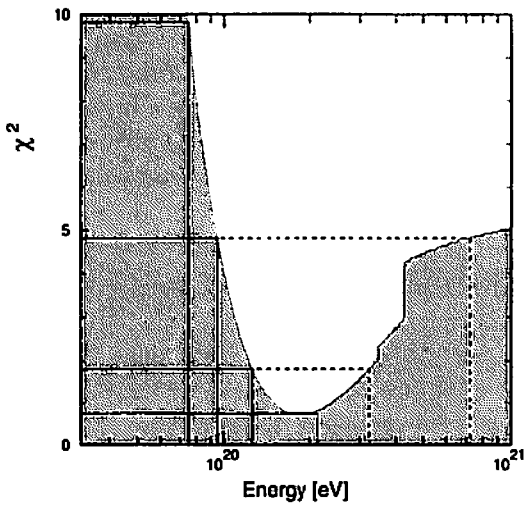

Figure 9: The χ^2 in the fitting of the AGASA's highest energy event as a function of energy.

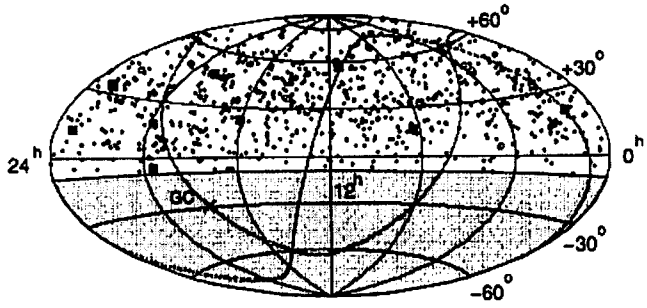

Figure 10: Arrival directions of cosmic rays with energies above 10^{19}eV in Equatorial coordinates. Dots, circles, and squares represent cosmic rays with energies of (1–4) $\times$ 10^{19}eV, (4–10) $\times$ 10^{19}eV, and $\geq$ 10^{20}eV, respectively. The shaded regions indicate the celestial regions excluded in this plot due to the zenith angle cut of $\leq 45°$. The Galactic and supergalactic planes are drawn by the dashed curves.

requires their sources to be remarkably close - less than 50 Mpc to prevent the expected significant energy loss by the GZK mechanism. Their super-high energies allow the arrival directions to point back to the source locations because the extragalactic magnetic field could not bend their trajectories too much. The upper bound of the deflection angle of a $\sim 10^{20}$ eV is only $\sim 1.7°$ for a source distance of 50 Mpc, provided that larger inter-cluster magnetic fields do not actually exist along the propagation path. This is comparable to or smaller than the angular resolutions of the experiments. Many searches for possible astronomical sources have been conducted but nothing interesting has been found in the arrival directions of the highest energy particles.

4.2 The Arrival Directions

The arrival directions of the UHECR events are very important to examine their origins. Because the gyro radius of 10^{19} eV protons in the galactic magnetic field is ~ 3 kpc, which is substantially thicker than the thickness of the galactic disk, the arrival directions should be correlated with the galactic plane if any galactic sources are responsible for the main observed bulk. Figure 10 shows the directions of the UHECRs with energies above 10^{19} eV detected by the AGASA experiment[8]. There found no correlations with the galactic plane suggesting that they came from extragalactic space. Also the data indicated no large-scale anisotropy in this energy range.

The higher the energy range we see becomes, the smaller the deflection angle by the magnetic field during the propagation is. Consequently the arrival direction is more likely to point back to its original emission region and we can expect some anisotropy depending on the source distribution in extragalactic space. In the high energy end regime with energies greater than 4×10^{19} eV, some of the events have been observed to form clustering, although there found no global scale anisotropy. There are one triplet and 5 doublets within a separation angle of 2.5° which is consistent with the experimental angular resolution. The chance probability that these clusters happened to be observed

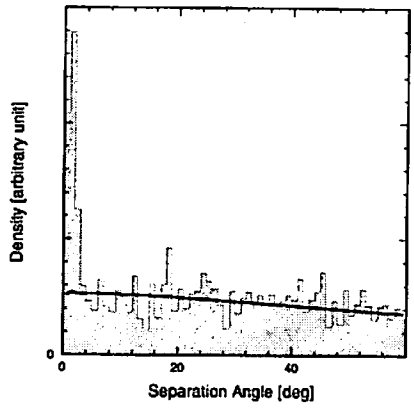

Figure 11: Self-Correlation analysis for the events with energies greater than 4×10^{19} eV.

from the isotropic distribution of the events is 5×10^{-4}[8]. The significance is even more clear when the self-correlation analysis, the separation angle distribution between an event and all the others, is made. Figure 11 shows the results and the clear peak appears in the region of the small separation angles. This peak width is well consistent with the point spread function of the experiment. The small-scale anisotropy has indicated that the UHECRs forming the clusters may be neutral particles such as γ-rays. Also the fact that none of the clusters lies on the galactic plane suggested that compact sources emitting UHECRs indeed exist in extragalactic space.

It should be remarked that one of the observed doublets are associated with the highest energy event described in detail in the previous subsection. The arrival timing and the energy of the events contributed in the clusters were examined and there is no clear correlation between them.

The observed doublets and triplets imply that either there are neutral particle population or the extragalactic magnetic field is rather small so that the particle trajectories are not substantially bent. The standard GZK mechanism would then require the UHECR sources in the directions of the event pairs at distances short enough to prevent the significant energy loss during the propagation. Serious searches have been made to identify the remarkable astronomical objects but nothing encouraging has been found in the directions of the pairs. For example, the doublet containing the highest energy event appears to arrive from the direction of the radio galaxy Mrk 359 that may be powerful enough to accelerate protons to well beyond 10^{20} eV. The distance to Mrk 359 is, however, 65 Mpc which is obviously too far away to have the 2×10^{20} eV particle arrive at earth. The only candidate which may be responsible for the event clusters is an interacting galaxy Mrk 40 at redshift of 0.02 that lies in the direction of the AGASA triplet. Further improvement of the statistics is needed to see if this type of sources is an origin of UHECRs.

4.3 The GZK crisis

The arrival direction distribution including the apparent small-scale anisotropy strongly indicates that UHECRs are indeed extragalactic in origin. A change from a heavy to a light component deduced from the X_{max} distribution observed by the Fly's Eye and the HiRes/MIA[9] also suggested a changing origin towards the extragalactic population. Nevertheless, the observational facts that there are no obvious astronomical sources within $\simeq$ 100 Mpc in the directions of the event clusters and that the energy spectrum extends well beyond 10^{20} eV have challenged the standard GZK scenario.

One of the economical and easiest way possibly to evade the GZK mechanism is to introduce the 0.1μ G scale extragalactic magnetic field (EGMF) which is associated with the structure of galaxies , galaxy clusters, and superclusters. This localized EGMFs influence the propagation of charged cosmic rays by deflecting and delaying them relative to straight line propagation with the speed of light. The diffusion motion in local EGMFs generally enhances the cosmic ray flux below 10^{20} eV, which leads to less prominent cut-off structure at 10^{20} eV. Moreover, the deflection angle of trajectories of the UHECR propagating in localized stronger EGMF can be reached beyond 10 degree or so even in 10^{20} eV range and may be able to fit the observed features such as the large-scale distribution of arrival directions of the UHECRS which is quite isotropic.

The local strong EGMF would not resolve all the issues in straightforward manner, however. Since the local EGMF is not likely to be in an infinite medium, but to be associated with local galaxy clusters which has a local boundary, the structure of the EGMF influences the energy spectrum of UHECRs. Furthermore, the strength of EGMF is also very sensitive to the spectral shape because too strong EGMF would cause particles with energies even higher than the GZK cutoff to diffuse, which results in prominent cutoff even when a source distance is well shorter than the energy attenuation length. It implies that we have faced the "fine tuning" problem: The location of the earth in the super cluster space, the strength of EGMF and its structure which determines the diffusion constant, and the spectral power law index must be carefully chosen to reconstruct the observed energy spectrum[10]. It implies that our local neighborhood including the earth *happens* to be in the special environment to accommodate both the spectrum extending beyond 10^{20} eV *and* the large scale isotropy.

In order to resolve the GZK paradox without relying on finely tuned parameters, one can consider the other extreme: a possibility that ALL galaxies not only in the local Supercluster, but outside the cluster are responsible for UHECR emission, although it seems difficult to accelerate particles to such ultra-high energies at these sites. It has been realized that we do not live in a space where galaxies are completely isotropically distributed. There are more number of galaxies within a sphere of $\sim$ 500 Mpc. Therefore if the density of unknown sources of UHECRs follows the luminous matter density in the Universe, there are more contributions from nearby sources than one expect in case of the isotropic source distribution, which leads to less pronounced cut-off structure even if it exists[11]. It has been argued, however, that the overdensity of the galaxies in our local space is just a factor of two according to the galaxy survey such as CfA1 and PSCz when

the survey bias is properly taken into account. Then contributions of localized nearby sources would not be enough to prevent the cut-off[12].

No matter how the sources of UHECRs are distributed in the Universe, the observational fact that all the events above 10^{20} eV detected by the AGASA has arrived isotropically without forming clusters by themselves gives a rough estimate of the source density. No clusters observed above 10^{20} eV implies that we have rather many but dim sources to emit 10^{20} eV particles in the GZK sphere if bending of the particle trajectories by the EGMF is negligible. Otherwise a nearby bright source would have formed event clusters. The source density is estimated to be

$$\rho_{\rm AGASA} \sim 1 \times 10^{-2} \left(\frac{R_{GZK}}{50{\rm Mpc}} \right)^{-3} {\rm Mpc}^{-3}. \tag{14}$$

It should be remarked that this value is much larger than most of the estimated density of the astronomical candidates of UHECR sources. The number density of AGNs are $\leq 5 \times 10^{-4}$ Mpc^{-3}. The rate of GRB is $\sim 10^{-9}$ Mpc^{-3} yr^{-1} and delay time is obtained to be $\sim 1.5 \times 10^5 (B_{rms}/{\rm nG})$ yr. Thus the effective density of GRB emission is $\sim 10^{-4}$ Mpc^{-3}. The AGNs and GRBs would be unlikely to match up the density numbers based on the AGASA observation without finely tuning the unknown parameters such as the EGMF strength. Only the normal galaxies seems naturally to be consistent with the observational estimate. Then it would be difficult to explain why we have not observed the GZK cutoff.

Another possible but also economical solution to resolve the GZK paradox, although there is no observational evidence, is to consider the emission of UHE heavy nuclei such as iron at nearby sources. Then even the conservative 1 nG order of EGMF would be able to bend their trajectories and the large-scale isotropy of UHECRs could easily be explained. Moreover, our discussion about the source density would not be valid here because events with different arrival directions may not be independent because of the magnetic bending. The source density can be much lower than our estimate above. In terms of the acceleration efficiency, the high charge of the heavy nuclei is a benefit also. It has been argued that even galactic objects such as young neutron starts may be able to drive plasma wind strong enough to accelerate irons up to 8×10^{20} eV. Whether the primary emission of heavy nuclei would not create the GZK cut-off structure is questionable, however. The photodisintegration in the radiation field is a crucial energy loss process of UHECR heavy nuclei. Their energy attenuation length depends on the poorly known infrared-optical (IR-O) backgrounds, but the CMB photons would still make dominant contributions to the overall energy loss process above $\sim 10^{20}$ eV and the situation may not be so different from the case of protons. Existence of UHE heavy nuclei is an open issue both observationally and theoretically.

Acknowledgments

The author wishes to thank the workshop organizers for their warm hospitality at this meeting. He also wishes to acknowledge very valuable discussions with members in the

AGASA collaboration and the HiRes collaboration. He is grateful to his collaborators to work on the UHE astrophysics, especially Günter Sigl and and Pijushpani Bhattacharjee.

References

[1] N. Hayashida *et al*, Astroparticle Physics **10** (1999) 303.

[2] A.M. Hillas, Ann. Rev. Astron. Astrophys. **22** (1984) 425.

[3] K. Greisen, Phys. Rev. Lett. **16** (1966) 748.

[4] G. T. Zatsepin and V. A. Kuzmin, JETP Lett. **4** (1966) 178.

[5] S. Yoshida and M. Teshima Prog. Theor. Phys. **89** (1993) 833.

[6] S. Yoshida *et al*, Astroparticle Physics **3** (1995) 105.; M. Takeda *et al*, Phys. Rev. Lett. **81** (1998) 1163.; See also **http://www-akeno.icrr.u-tokyo.ac.jp/AGASA/**

[7] N. Hayashida *et al*, Phys. Rev. Lett. **73** (1994) 3491.

[8] M. Takeda *et al*, Astrophys. Journal **522** (1999) 225.

[9] T. Abu-Zayyad *et al*, Phys. Rev. Lett. **84** (2000) 4276.

[10] G. Sigl, M. Lemoine, and P. Biermann, Astroparticle Physics **10** (1999) 141.

[11] G.A. Medina-Tanco, Astrophys. Journal **510** (1999) 91.

[12] M. Blanton, P. Blasi, and A.V. Olinto, Astroparticle Physics **15** (2001) 275.

Have we already detected astrophysical symptoms of space-time noncommutativity ?

Takashi Tamaki[1] , Tomohiro Harada[2] , Umpei Miyamoto[3]

Department of Physics, Waseda University, Shinjuku, Tokyo, 169-8555, Japan

and Takashi Torii[4]

Research Center for the Early Universe, University of Tokyo, Hongo, Bunkyo, Tokyo 113-0033, Japan

Abstract

We discuss astrophysical implications of κ-Minkowski space-time, in which there appears space-time noncommutativity. We first derive a velocity formula for particles based on the motion of a wave packet. The result is that a massless particle moves at a constant speed as in the usual Minkowski space-time, which implies that an arrival time analysis by γ-rays from Markarian (Mk) 421 *does not* exclude space-time noncommutativity. Based on this observation, we analyze reaction processes in κ-Minkowski space-time which are related to the super Greisen-Zatsepin-Kuzmin (GZK) events and the high-energy ($\sim$20 TeV) γ-rays from Mk 501.

1 Introduction and outline

Recently, much attention has been paid to extremely high-energy cosmic rays (EHECRs)[1] because some of these detections seem to be inconsistent with existing physics[2]. That is, if we consider the interaction between EHECRs and CMB photons, particles with energy $\gtrsim 7 \times 10^{19}$ eV from distant sources cannot reach the Earth. Detections of γ-rays above $\sim$ 20 TeV from distant sources ($\gtrsim$ 100 Mpc) reported in Refs. [3] are similar to this. These γ-rays are expected to interact with infrared background (IRBG) photons and not to reach the Earth in a LI scenario.

Some authors argue that violation of Lorentz invariance (LI) might solve them[4, 5, 6, 7]. One of the ways to introduce LI violation is to consider space-time noncommutativity with deformed LI[8, 9]. Amelino-Camelia et al.[10, 11, 12] considered an interesting model called κ-Minkowski space-time[13, 14]. They obtained a severe constraint on this model through an arrival time analysis of signals from γ-rays[10, 11]. If we accept this scenario, there is no room to explain EHECRs[12].

In these papers, the velocity of particles was evaluated using a group velocity formula in the usual Minkowski space-time. Here, we derive a more realistic velocity formula based on the motion of a wave packet in κ-Minkowski space-time and find that the space-time noncommutativity does not affect the velocity of massless particles. Motivated by this observation, we analyze reaction processes which are related to both detections of super GZK events and of $\sim$20 TeV photons. Though our approach is purely kinematical, our result will provide a strong motivation to consider realistic model of space-time noncommutativity. Throughout this paper, we use the units in which $c = \hbar = 1$.

2 κ-Minkowski space-time

The basic commutation relations are $[x^i, t] = i\lambda x^i$, $[x^i, x^j] = 0$, where the indices i, j run $1, 2, 3$. In order to define Fourier transformation consistently, the energy E and the momentum $\boldsymbol{p} = (p_1, p_2, p_3)$ of

[1] E-mail:tamaki@gravity.phys.waseda.ac.jp
[2] E-mail:harada@gravity.phys.waseda.ac.jp
[3] E-mail:umpei@gravity.phys.waseda.ac.jp
[4] E-mail:torii@resceu.s.u-tokyo.ac.jp

a particle form a non-Abelian group G which can be written as [13],

$$(E,\boldsymbol{p}) := \begin{pmatrix} e^{\lambda E} & p_1 & p_2 & p_3 \\ 0 & 1 & 0 & 0 \\ 0 & 0 & 1 & 0 \\ 0 & 0 & 0 & 1 \end{pmatrix} . \tag{1}$$

Thus, if we denote the additive operator in this space-time by $\hat{+}$ to distinguish from the conventional one, we can write as $(E_1 \hat{+} E_2, \boldsymbol{p}_1 \hat{+} \boldsymbol{p}_2) := (E_1,\boldsymbol{p}_1)(E_2,\boldsymbol{p}_2) = (E_1 + E_2, \boldsymbol{p}_1 + e^{\lambda E_1}\boldsymbol{p}_2)$.

Following Ref.[11], we describe a plane wave as $\psi_{(E,\boldsymbol{p})} = e^{i\boldsymbol{p}\cdot\boldsymbol{x}}e^{iEt}$, and place the t generator to the right of x generator, i.e., $\psi_{(E,\boldsymbol{p})} \neq e^{iEt}e^{i\boldsymbol{p}\cdot\boldsymbol{x}}$. Then, the following property holds.

$$\psi_{(E_1,\boldsymbol{p}_1)(E_2,\boldsymbol{p}_2)} = \psi_{\boldsymbol{p}_1,E_1}\psi_{\boldsymbol{p}_2,E_2} . \tag{2}$$

We can also define the wave in the reverse direction as $\psi_{(E,\boldsymbol{p})^{-1}} := e^{-i\boldsymbol{p}e^{-\lambda E}\cdot\boldsymbol{x}}e^{-iEt} = e^{-iEt}e^{-i\boldsymbol{p}\cdot\boldsymbol{x}}$, which implies that $(E,\boldsymbol{p})^{-1}$ is an inversion of $(E,\boldsymbol{p})$.

The rotation and boost generators can be written as[14]

$$M_i = -\epsilon_{imn}p_m\frac{\partial}{\partial p_n}, \quad N_i = p_i\frac{\partial}{\partial E} - \left(\frac{\lambda}{2}\boldsymbol{p}^2 + \frac{1-e^{2\lambda E}}{2\lambda}\right)\frac{\partial}{\partial p_i} + \lambda p_i p_j\frac{\partial}{\partial p_j} . \tag{3}$$

Using (3), a finite boost transformation for the $i = 1$ direction can be obtained as[15]

$$p_1 = \frac{\tanh(\lambda m)\sinh\xi}{\lambda[1-\tanh(\lambda m)\cosh\xi]}, \quad p_2 = p_3 = 0, \quad E = m + \frac{1}{\lambda}\ln\left[\frac{1-\tanh(\lambda m)}{1-\tanh(\lambda m)\cosh\xi}\right], \tag{4}$$

where ξ is a boost parameter and we choose $\boldsymbol{p} = 0$ and $E = m$, i.e., m is a rest mass of the particle, for $\xi = 0$. Because of (3), the dispersion relation is altered as

$$\lambda^{-2}(e^{\lambda E} + e^{-\lambda E} - 2) - \boldsymbol{p}^2 e^{-\lambda E} = \lambda^{-2}(e^{\lambda m} + e^{-\lambda m} - 2). \tag{5}$$

3 The velocity formula

The velocity of the particle in the usual Minkowski space-time is $\boldsymbol{v} = dE/d\boldsymbol{p}$. If we apply this in κ-Minkowski space-time, $|\boldsymbol{v}| = e^{-\lambda E}$ for a massless particle, where we used Eq. (5). This formula, together with the data on γ-rays from Mk 421 in Ref. [16] leads to the constraint $|\lambda| \lesssim 10^{-33}$ meter [10, 11, 16]. Since this discussion depends crucially on the form of velocity, we reexamine the group velocity formula by forming a wave packet in κ-Minkowski space-time. For this purpose, we consider infinitesimal changes ΔE and $\Delta\boldsymbol{p}$ in E and $\boldsymbol{p}$, respectively, as a result of adding $(\Delta E', \Delta\boldsymbol{p}')$ as

$$(E \hat{+} \Delta E', \boldsymbol{p} \hat{+} \Delta\boldsymbol{p}') = (E + \Delta E, \boldsymbol{p} + \Delta\boldsymbol{p}). \tag{6}$$

In this case, we can express $(\Delta E', \Delta\boldsymbol{p}') \cong (\Delta E, \frac{\Delta\boldsymbol{p}}{e^{\lambda E}})$, where we keep only terms in first order in ΔE and $\Delta\boldsymbol{p}$. By using this and Eq. (2), we make a wave packet as follows[17]

$$\begin{aligned} I &:= \psi_{(E-\Delta E,\boldsymbol{p}-\Delta\boldsymbol{p})} + \psi_{(E+\Delta E,\boldsymbol{p}+\Delta\boldsymbol{p})} = \psi_{(E,\boldsymbol{p})(-\Delta E',-\Delta\boldsymbol{p}')} + \psi_{(E,\boldsymbol{p})(\Delta E',\Delta\boldsymbol{p}')} \\ &= \psi_{(E,\boldsymbol{p})}\psi_{(-\Delta E',-\Delta\boldsymbol{p}')} + \psi_{(E,\boldsymbol{p})}\psi_{(\Delta E',\Delta\boldsymbol{p}')} = \psi_{(E,\boldsymbol{p})}[e^{-i\Delta\boldsymbol{p}'\cdot\boldsymbol{x}}e^{-i\Delta E't} + e^{i\Delta\boldsymbol{p}'\cdot\boldsymbol{x}}e^{i\Delta E't}] \\ &\cong 2e^{i\boldsymbol{p}\cdot\boldsymbol{x}}e^{iEt}\cos\left[\frac{\Delta\boldsymbol{p}}{e^{\lambda E}}\cdot\left(\boldsymbol{x} + \frac{e^{\lambda E}\Delta Et}{\Delta\boldsymbol{p}}\right)\right]. \end{aligned} \tag{7}$$

By considering $|I|^2$, the group velocity $\boldsymbol{v}_I$ can be written as $\boldsymbol{v}_I := e^{\lambda E}dE/d\boldsymbol{p}$.

We also consider a similar relation $(\Delta E' \hat{+} E, \Delta\boldsymbol{p}' \hat{+} \boldsymbol{p}) = (E + \Delta E, \boldsymbol{p} + \Delta\boldsymbol{p})$, which is different from Eq. (6). In this case, the corresponding group velocity $\boldsymbol{v}_r$ is $\boldsymbol{v}_r := \frac{dE}{d\boldsymbol{p}}\left(1 - \lambda\boldsymbol{p}\cdot\frac{dE}{d\boldsymbol{p}}\right)^{-1}$.

Using (5), we obtain the important conclusion that *massless particles move in a constant speed* $|\boldsymbol{v}_I| = |\boldsymbol{v}_r| = 1$ *as in the usual Minkowski space-time.* Therefore, the argument in Ref.[10, 11, 16] does not apply. We emphasis on the importance of the result *not* because κ-Minkowski space-time can avoid the constraint *but* because our result provides an opportunity to reconsider LI deformation models in general.

4 Threshold anomaly

We first consider the two-body head-on collision of particles and subsequent creation of two particles $1+2 \to 3+4$. We define the energy E_i and momentum $\boldsymbol{p}_i$ of the i-th particle as those in the laboratory frame. We denote the rest mass of the i-th particle as m_i. We also assume that $m_2 = 0$, $m_3 \neq 0$, $m_4 \neq 0$ and $\boldsymbol{p}_i = (p_i, 0, 0)$. In the usual Minkowski space-time, we use the dispersion relation $E_i^2 - p_i^2 = m_i^2$, and the energy momentum conservation law, $p_1 + p_2 = p_3 + p_4$, $E_1 + E_2 = E_3 + E_4$, to obtain the threshold value of E_1, which we denote by $E_{th,0}$. We assume that the resultant particles are at rest in the center-of-mass frame in the threshold reaction. In the laboratory frame, this means that the resultant particles move in the same speed, that is $p_3/m_3 = p_4/m_4$. We also assume that p_2 has an opposite sign against that of p_1. If we neglect higher order terms in E_2, then

$$E_{th,0} = \frac{(m_3+m_4)^2 - m_1^2}{4E_2}. \tag{8}$$

Next, we consider the same reaction in κ-Minkowski space-time. The dispersion relation is

$$\lambda^{-2}(e^{\lambda E_i} + e^{-\lambda E_i} - 2) - (p_i)^2 e^{-\lambda E_i} = \lambda^{-2}(e^{\lambda m_i} + e^{-\lambda m_i} - 2). \tag{9}$$

If we interpret the algebra in κ-Minkowski space-time faithfully, the energy momentum conservation law is expressed as $(E_1, p_1)(E_2, p_2) = (E_3, p_3)(E_4, p_4)$. Even if it holds, one should note that we need a rule to distinguish two particles. If we consider the collision of two particles with A, $B \in G$, respectively, does it correspond to AB, BA or anything else ? At present, we have no way to determine it. Here, we introduce a phenomenological parameter a, which controls the form of conservation law as follows:

$$a(E_1,p_1)(E_2,p_2) + (1-a)(E_2,p_2)(E_1,p_1) = a(E_3,p_3)(E_4,p_4) + (1-a)(E_4,p_4)(E_3,p_3). \tag{10}$$

As regards plausible values for a, care must be taken. If we consider two particles of the same species, $a = 1/2$ would be physically reasonable value, since if they have same energy and move opposite direction each other, they have zero total momentum only for this choice. In fact, the parameter a may be a function of physical quantities of two particles such as mass, charge and/or spin for two different species. Here, we use the same value of a on the left and the right hand sides of (10) for convenience. Moreover, we restrict our attention to $0 \leq a \leq 1$ for clarity.

We also need to impose the condition that the resultant particles are at rest in the center-of-mass frame. To obtain a relation between momenta p_3 and p_4, we use the boost transformation (4). For the same value of ξ, we obtain

$$\frac{p_3}{\tanh(\lambda m_3)} = \frac{p_4}{\tanh(\lambda m_4)}. \tag{11}$$

We can solve E_1 as a function of a, λ, m_1, m_3, m_4 and E_2 by using (9), (10) and (11). We apply this result to two astrophysical cases.

4.1 Threshold anomaly for TeV γ-rays

Here, we consider the process $\gamma + \gamma \to e^+ + e^-$, which may occur when a γ-ray travels in the IRBG. In this case, $m_1 = 0$ and $m_3 = m_4 = m_e$, where m_e is the electron mass. We summarize the equation for the threshold in κ-Minkowski space-time which is derived from (9), (10) and (11) as

$$AB = yx(yx+1)^2 \sinh^2 \frac{\lambda m_e}{2}, \tag{12}$$

where $A := (1-a)y^4 - (1-2a)y^2 - a$, $B := ax^4 + (1-2a)x^2 + a - 1$, and $x := e^{\lambda E_1/2}$, $y := e^{\lambda E_2/2}$.

We should recall that, to estimate the energy of primary particles, we calculate the sum of energy of all secondary particles. Since energy is conserved in the usual sense even in this case, the observation of $\sim$20 TeV photons in usual Minkowski space-time has the same meaning also in κ-Minkowski space-time.

We show the dependence of E_{th} on $\lambda > 0$ in Fig. 1 (a). For simplicity, E_2 is chosen as $E_2 = 1$ eV. For $a = 0$, E_{th} increases with λ, compared with the same quantities in Minkowski space-time. In

particular, E_{th} diverges for $\lambda := \lambda_c \sim 4$ TeV^{-1}. That is, the universe is entirely tranparent for $\lambda > \lambda_c$. For $a = 1/2$ and 1, E_{th} decreases. If we expand E_{th} as $E_{th} = \sum_{k=0}^{\infty} \frac{E_{th,k}}{k!}\lambda^k$, the first-order coefficient $E_{th,1}$ is $E_{th,1} = E_{th,0}(E_{th,0} - E_2)\left(\frac{1}{2} - a\right)$. The reason why E_{th} disappears for $a = 0$ above $\lambda_c \sim 4$ TeV^{-1} can be understood as follows. For $\lambda E_{th} \gg 1$, and λm_e, $\lambda E_2 \ll 1$, we can approximate eq. (12) as

$$(1 + \lambda E_2)x \approx \lambda E_2 - \frac{\lambda^2 m_e^2}{2} \quad \text{for } a = 0, \quad aE_2 x \approx \frac{\lambda m_e^2}{4} \quad \text{for } a \neq 0. \tag{13}$$

In this range of approximation, since $\lambda E_{th,0} = \lambda m_e^2/E_2$ is larger than 1, eq.(13) has no real solution E_{th} while it has for $a \neq 0$. This means that λ_c for $a = 0$ is characterized by $1/E_{th,0} \sim 1$ TeV^{-1}. To investigate properties for $\lambda < 0$, we replace λ with $-\lambda$. In eq. (12), this corresponds to the replacement $x \to 1/x$ and $y \to 1/y$. Eq. (12) becomes invariant if a is also replaced by $(1 - a)$.

4.2 Threshold anomaly for GZK cutoff

We consider the interaction of ultra high energy protons with CMB photons which results in $p+\gamma \to p+\pi_0$. In this case, $m_1 = m_3 = m_p$ and $m_4 = m_\pi$, where m_p and m_π are the proton mass and the pion mass, respectively. We solve (9), (10) and (11) numerically. We show the dependence of E_{th} for $\lambda > 0$, in Fig. 1 (b). E_2 is chosen as $E_2 = 10^{-3}$ eV. Compared with Fig. 1 (a), we find that the qualitative features for small λ are quite similar, i.e., $E_{th}/E_{th,0} > 1$ for $a = 0$ and $E_{th}/E_{th,0} < 1$ for $a = 1$.

However, we find qualitative differences from Fig. 1 (a) for $\lambda \gtrsim 10^{-8}$ TeV^{-1}. The threshold disappears for $\lambda > \lambda_c \sim 2 \times 10^{-8}$ TeV^{-1} in the $a = 0$ case, which can be explained as in the γ-ray case since λ_c coincides approximately with $1/E_{th,0}$. For the case $a = 1/2$ and 1, $E_{th}/E_{th,0}$ increases with $\lambda(\gtrsim 3 \times 10^{-8}$ TeV$^{-1})$ and disappears for $\lambda \gtrsim 5 \times 10^{-8}$ TeV^{-1}, unlike the γ-ray case. In this case, there is no simple symmetry about $\lambda \to -\lambda$, as found in the previous case. We omit this case here.

5 Conclusion and discussion

We have first considered a velocity formula to describe the particle motion based on the motion of a wave packet in κ-Minkowski space-time and showed that an arrival time analysis of γ-ray bursts in Refs. [10, 11, 16] does not exclude space-time noncommutativity. Since this feature had not been discussed so far, it should be stressed and is one of our main conclusions here.

Based on this consideration, we have obtained threshold values for reactions $\gamma + \gamma \to e^+ + e^-$ and $p + \gamma \to p + \pi_0$ in κ-Minkowski space-time and analyzed their relavance to the puzzling observations of $\sim$20 TeV photons and super GZK events, introducing a parameter a.

In the TeV γ-ray case, only $a \ll 1$ for $\lambda \gtrsim 4$ TeV^{-1} appears able to explain the detections of γ-rays above $\sim$20 TeV. In the EHECR case, the possibilities $a \ll 1$ and $\lambda \gtrsim 2 \times 10^{-8}$ TeV^{-1}, or $a = O(1)$ and $\lambda \gtrsim 5 \times 10^{-8}$ TeV^{-1} remain viable. Thus, $a \ll 1$ for $\lambda \gtrsim 4$ TeV^{-1} appears able to explain both phenomena. Our results are important because they suggest that extremely high-energy particles might be expected in realistic models with space-time noncommutativity. If this is the case, then we might have already detected symptoms of the space-time noncommutativity.

Acknowledgments

Special thanks to Kei-ichi Maeda for continuous encouragement. This work was supported partly by the Grant-in-Aid (No.05540) from the Japanese Ministry of Education, Culture, Sports, Science and Technology, and partly by the Waseda University Grant for Special Research Projects.

References

[1] D. J. Bird et al., Astrophys. J. **441**, 144 (1995); M. Takeda et al., Phys. Rev. Lett. **81**, 1163 (1998).

[2] K. Greisen, Phys. Rev. Lett. **16**, 748 (1966); G. T. Zatsepin and V. A. Kuzmin, Sov. Phys. JETP Lett. **4**, 78 (1966).

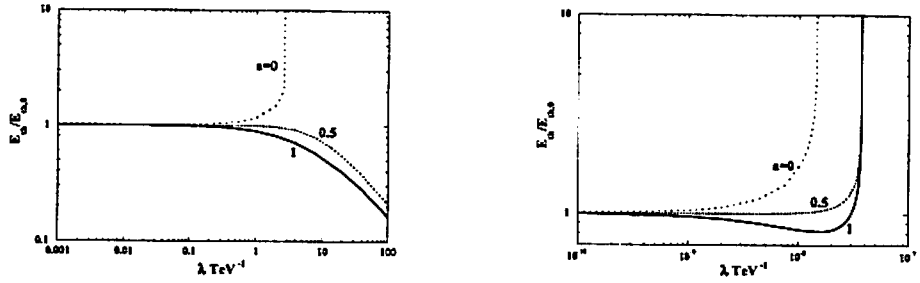

(a) (b)

Figure 1: Threshold anomaly for (a) TeV-γ rays and (b) GZK cutoff for $\lambda > 0$.

[3] F. A. Aharonian et al., Astron. Astrophys. **349**, 11A (1999).

[4] S. Coleman and S. L. Glashow, Phys. Rev. D **59**, 116008 (1999).

[5] H. Sato and T. Tati, Prog. Theor. Phys. **47**, 1788 (1972); H. Sato, *Proc. of the International Workshop: Space Factory on JEM/ISS* (1999), astro-ph/0005218.

[6] T. Kifune, Astrophys. J. Lett. **518**, L21 (1999).

[7] G. Amelino-Camelia and T. Piran, Phys. Rev. D **64**, 036005 (2001).

[8] A. Connes, M. R. Douglas and A. Schwarz, JHEP **02**, 3 (1998).

[9] M. Jimbo, Lett. Math. Phys. **10**, 63 (1985).

[10] G. Amelino-Camelia et al., Nature **393**, 763 (1998); L. J. Garay, Phys. Rev. Lett. **80**, 2508 (1998); R. Gambini and G. Pullin, Phys. Rev. D **59**, 124021 (1999).

[11] G. Amelino-Camelia, J. Lukierski and A. Nowicki, Int. J. Mod. Phys. A **14**, 4575 (1999); G. Amelino-Camelia and S. Majid, Int. J. Mod. Phys. A **15**, 4301 (2000).

[12] G. Amelino-Camelia and T. Piran, Phys. Lett. B **497**, 265 (2001); G. Amelino-Camelia, J. Lukierski and A. Nowicki, hep-th/0103227.

[13] S. Majid and R. Oeckl, Commun. Math. Phys. **205**, 617 (1999).

[14] J. Lukierski, A. Nowicki, H. Ruegg and V. N. Tolstoy, Phys. Lett. B **264**, 331 (1991); S. Majid and H. Ruegg, Phys. Lett. B **334**, 348 (1994).

[15] N. R. Bruno, G. Amelino-Camelia and J. Kowalski-Glikman, hep-th/0107039.

[16] Biller et al., Phys. Rev. Lett. **83**, 2108 (1999).

[17] Strictly speaking, this is not a Gaussian wave packet. However, it is sufficient to obtain a group velocity.

Adjusted ADM systems and their expected stability properties

Hisa-aki Shinkai[1] and Gen Yoneda[2]

shinkai@atlas.riken.go.jp, yoneda@mn.waseda.ac.jp
[1] *Computational Science Division, Institute of Physical & Chemical Research (RIKEN), Hirosawa 2-1, Wako, Saitama, 351-0198 Japan*
[2] *Department of Mathematical Sciences, Waseda University, Shinjuku, Tokyo, 169-8555, Japan*

Abstract

In order to find a way to have a better formulation for numerical evolution of the Einstein equations, we study the propagation equations of the constraints based on the Arnowitt-Deser-Misner formulation. By adjusting constraint terms in the evolution equations, we try to construct an "asymptotically constrained system" which is expected to be robust against violation of the constraints, and to enable a long-term stable and accurate numerical simulation. We first provide useful expressions for analyzing constraint propagation in a general spacetime, then apply it to Schwarzschild spacetime. We search when and where the negative real or non-zero imaginary eigenvalues of the homogenized constraint propagation matrix appear, and how they depend on the choice of coordinate system and adjustments. The predictions here may help the community to make further improvements. [a]

[a] The full version of the article is available as [1]

1 Introduction

Computing the Einstein equations numerically is a necessary direction for general relativity research. This approach, so-called numerical relativity, already gives us much feedback to help understand the nature of strong gravity, such as singularity formations, critical behavior of gravitational collapses, cosmology, and so on [2].

There are several different approaches to simulate the Einstein equations, among them the most robust is to apply 3+1 (space + time) decomposition of spacetime, which was first formulated by Arnowitt, Deser and Misner (ADM) [3] (we refer to this as the "original ADM" system). A current important issue in the 3+1 approach is to control long-term stability of time integrations in simulating black hole or neutron star binary coalescences. So far, the use of fundamental variables (γ_{ij}, K_{ij}), the internal 3-metric and extrinsic curvature, has been the most popular approach [4] (we refer to this as the "standard ADM" system). In recent years, however, many groups report that another re-formulation of the Einstein equations provides more stable and accurate simulations. We try here to understand these efforts through "adjusting" procedures to the evolution equations (that we explain later) using eigenvalue analysis of the constraint propagation equations.

At this moment, there may be three major directions to obtain longer time evolutions.

1. The first is to use a modification of the ADM system that was developed by Japanese group, which is now often abbreviated as BSSN (Baumgarte-Shapiro-Shibata-Nakamura) fromulation [5]. This is a combination of the introduction of new variables, conformal decompositions, rescaling the conformal factor, and the replacement of terms in the evolution equation using momentum constraints. Although there are many studies to show why this re-formulation is better than the standard ADM, as far as we know, there is no definite conclusion yet. One observation [6] pointed out that to replace terms using momentum constraints appears to change the stability properties.

2. The second is to re-formulate the Einstein equations in a first-order hyperbolic form [7]. This is motivated from the expectation that the symmetric hyperbolic system has well-posed properties in its Cauchy treatment in many systems and also that the boundary treatment can be improved if we know the characteristic speed of the system. We note that, in constructing hyperbolic systems,

the essential procedures are to adjust equations using constraints and to introduce new variables, normally the spatially derivatived metric. Several groups report that the hyperbolic formulation actually has advantages over the direct use of ADM formulation [8, 9, 10]. However it is also reported that there are no drastic changes in the evolution properties *between* hyperbolic systems (weakly/strongly and symmetric hyperbolicity) by systematic numerical studies by Hern [11] based on Frittelli-Reula formulation [12], and by the authors [13] based on Ashtekar's formulation [16, 14, 15]. Therefore we may say that the mathematical notion of "hyperbolicity" is not always applicable for predicting the stability of numerical integration of the Einstein equations (See also §4.4.2 in [2]). It will be useful if we have an alternative procedure to predict stability including the effects of the non-principal parts of the equation, which are neglected in the discussion of hyperbolicity.

3. The third is to construct a robust system against the violation of the constraints, such that the constraint surface is the attractor. The idea was first proposed as "λ-system" by Brodbeck et al [18] in which they introduce artificial flow to the constraint surface using a new variable based on the symmetric hyperbolic system. This idea was tested and confirmed to work as expected in some test simulations by the authors[19] (based on the formulation developed by [20]). Although it is questionable whether the recovered solution is true evolution or not [21], we think that to enforce the decay of errors in its initial perturbative stage is the key to the next improvements. Actually, by studying the evolution equations of the constraints (hereafter we call them constraint propagation) and by evaluating eigenvalues (amplification factors, AFs) of constraint propagation in its homogenized form, we found that a similar "asymptotically constrained system" can be obtained by simply adjusting constraints to the evolution equations, even for the ADM equations [22].

The purpose of this report is to extend our previous study [22] in more general expressions and also to apply the systems to spacetime which has non trivial curvature, Schwarzschild black hole spacetime. The actual numerical simulations require many ingredients to be considered such as the choice of integration schemes, boundary treatments, grid structures and so on. However, we think that our approach to the stability problem through an *implementation to the equations* is definitely one of the aspects that should be improved.

Adjusting evolution equations is not a new idea. Actually the standard ADM system for numerical relativists [4] is adjusted from the original one [3] using the Hamiltonian constraint (See Frittelli's analysis on constraint propagation between the original and standard ADM formulations [23]). Detweiler [24] proposed a system using adjustments so that the L2 norm of constraints may not blow up. Several numerical relativity groups recently report the advantages of the adjusting procedure with a successful example [9]. We try here to understand the background mathematical features systematically by using AFs of constraint propagation.

2 Adjusted systems

2.1 Procedure and background – general discussion –

We begin with an overview of the adjusting procedure and the idea of background structure, which were described in our previous work [19, 22].

Suppose we have a set of dynamical variables $u^a(x^i, t)$, and their evolution equations

$$\partial_t u^a = f(u^a, \partial_i u^a, \cdots), \tag{1}$$

and the (first class) constraints

$$C^\alpha(u^a, \partial_i u^a, \cdots) \approx 0. \tag{2}$$

For monitoring the violation of constraints, we propose to investigate the evolution equation of C^α (constraint propagation),

$$\partial_t C^\alpha = g(C^\alpha, \partial_i C^\alpha, \cdots). \tag{3}$$

(We do not mean to integrate (3) numerically, but to evaluate them analytically in advance.)

We propose to homogenize (3) by a Fourier transformation, e.g.

$$\partial_t \hat{C}^\alpha = \hat{g}(\hat{C}^\alpha) = M^\alpha{}_\beta \hat{C}^\beta, \quad \text{where } C(x,t)^\rho = \int \hat{C}(k,t)^\rho \exp(ik\cdot x) d^3k, \tag{4}$$

then to analyze the set of eigenvalues, say As, of the coefficient matrix, $M^\alpha{}_\beta$, in (4). We call As the amplification factors (AFs) of (3). As we have proposed and confirmed in [19]:

Conjecture:

(a) If the amplification factors have a *negative real-part* (the constraints are forced to be diminished), then we see more stable evolutions than a system which has positive amplification factors.

(b) If the amplification factors have a *non-zero imaginary-part* (the constraints are propagating away), then we see more stable evolutions than a system which has zero amplification factors.

We found heuristically that the system becomes more stable when more As satisfy the above criteria [13, 19]. We remark that this eigenvalue analysis requires the fixing of a particular background spacetime, since the AFs depend on the dynamical variables, u^a.

The above features of the constraint propagation, (3), will differ when we modify the original evolution equations. Suppose we add (adjust) the evolution equations using constraints

$$\partial_t u^a = f(u^a, \partial_i u^a, \cdots) + F(C^\alpha, \partial_i C^\alpha, \cdots), \tag{5}$$

then (3) will also be modified as

$$\partial_t C^\alpha = g(C^\alpha, \partial_i C^\alpha, \cdots) + G(C^\alpha, \partial_i C^\alpha, \cdots). \tag{6}$$

Therefore, the problem is how to adjust the evolution equations so that their constraint propagations satisfy the above criteria as much as possible.

2.2 Standard ADM system and its constraint propagation

We start by analyzing the standard ADM system. By "standard ADM" we mean here the most widely adopted system, due to York [4], with the evolution equations,

$$\partial_t \gamma_{ij} = -2\alpha K_{ij} + \nabla_i \beta_j + \nabla_j \beta_i, \tag{7}$$

$$\partial_t K_{ij} = \alpha R^{(3)}_{ij} + \alpha K K_{ij} - 2\alpha K_{ik} K^k{}_j - \nabla_i \nabla_j \alpha + (\nabla_i \beta^k) K_{kj} + (\nabla_j \beta^k) K_{ki} + \beta^k \nabla_k K_{ij}, \tag{8}$$

and the constraint equations,

$$\mathcal{H} := R^{(3)} + K^2 - K_{ij} K^{ij}, \tag{9}$$

$$\mathcal{M}_i := \nabla_j K^j{}_i - \nabla_i K, \tag{10}$$

where (γ_{ij}, K_{ij}) are the induced three-metric and the extrinsic curvature, (α, β_i) are the lapse function and the shift covector, ∇_i is the covariant derivative adapted to γ_{ij}, and $R^{(3)}_{ij}$ is the three-Ricci tensor.

The constraint propagation equations, which are the time evolution equations of the Hamiltonian constraint (9) and the momentum constraints (10), can be written as

$$\partial_t \mathcal{H} = \beta^j (\partial_j \mathcal{H}) + 2\alpha K \mathcal{H} - 2\alpha \gamma^{ij} (\partial_i \mathcal{M}_j) + \alpha (\partial_l \gamma_{mk})(2\gamma^{ml}\gamma^{kj} - \gamma^{mk}\gamma^{lj}) \mathcal{M}_j - 4\gamma^{ij} (\partial_j \alpha) \mathcal{M}_i, \tag{11}$$

$$\partial_t \mathcal{M}_i = -(1/2)\alpha (\partial_i \mathcal{H}) - (\partial_i \alpha)\mathcal{H} + \beta^j (\partial_j \mathcal{M}_i) + \alpha K \mathcal{M}_i - \beta^k \gamma^{jl} (\partial_i \gamma_{lk}) \mathcal{M}_j + (\partial_i \beta_k) \gamma^{kj} \mathcal{M}_j. \tag{12}$$

Further expressions of these constraint propagations are introduced in Appendix A of [1].

2.3 Adjustment to ADM evolution equations and its effects on constraint propagations

Generally, we can write the adjustment terms to (7) and (8) using (9) and (10) by the following combinations (using up to the first derivatives of constraints for simplicity in order to include Detweiler's case, see the next subsection),

$$\text{adjustment term of } \partial_t\gamma_{ij}: \quad +P_{ij}\mathcal{H} + Q^k{}_{ij}\mathcal{M}_k + p^k{}_{ij}(\nabla_k\mathcal{H}) + q^{kl}{}_{ij}(\nabla_k\mathcal{M}_l), \tag{13}$$

$$\text{adjustment term of } \partial_t K_{ij}: \quad +R_{ij}\mathcal{H} + S^k{}_{ij}\mathcal{M}_k + r^k{}_{ij}(\nabla_k\mathcal{H}) + s^{kl}{}_{ij}(\nabla_k\mathcal{M}_l), \tag{14}$$

where P, Q, R, S and p, q, r, s are multipliers.

According to this adjustment, the constraint propagation equations are also modified as

$$\partial_t\mathcal{H} = (11) + H_1^{mn}(13) + H_2^{imn}\partial_i(13) + H_3^{ijmn}\partial_i\partial_j(13) + H_4^{mn}(14), \tag{15}$$

$$\partial_t\mathcal{M}_i = (12) + M_{1i}{}^{mn}(13) + M_{2i}{}^{jmn}\partial_j(13) + M_{3i}{}^{mn}(14) + M_{4i}{}^{jmn}\partial_j(14). \tag{16}$$

with appropriate changes in indices. (See detail in Appendix A in [1]. The definitions of $H_1, \cdots, M_1, \cdots$ are also there.)

3 Eigenvalue analysis of constraint propagation equations

We proposed several examples of adjustments (ways to fix above multipliers), and showed their resultant AFs in graphs [1, 22]. (We have to omit the details due to the space limitation. Please refer our articles.) In conclusion, we found that it is possible to obtain an asymptotically constrained system in ADM formulation by adjusting a particular combination of the multipliers. In our studies, Detweiler's proposal (1987) is still the best one according to our conjecture but has a growing mode of error near the horizon if we apply the system to the Schwarzschild spacetime.

The reader might ask why we can break the time-reversal invariant feature of the evolution equations by a particular choice of adjusting multipliers against the fact that the "Einstein equations" are time-reversal invariant. This question can be answered by the following. If we take a time-reversal transformation ($\partial_t \to -\partial_t$), the Hamiltonian constraint and the evolution equations of K_{ij} keep their signatures, while the momentum constraints and the evolution equations of γ_{ij} change their signatures. Therefore if we adjust γ_{ij}-equations using Hamiltonian constraint and/or K_{ij}-equations using momentum constraints (supposing the multiplier has +-parity), then we can break the time-reversal invariant feature of the "ADM equations". In fact, the examples we obtained all obey this rule.

4 Concluding Remarks

Motivated by performing a long-term stable and accurate numerical simulation of the Einstein equation, we proposed to adjust evolution equations by adding constraint terms by analyzing the constraint propagation equations in advance. The idea is to construct an asymptotically constrained evolution system, which is robust against violation of the constraint. This method works even for the ADM formulation (which is not a hyperbolic system) against flat background spacetime [22], and here we applied the analyses to a curved spacetime, a spherically symmetric black hole spacetime.

Recently, several numerical relativity groups report the effects of adjustments. They are mostly searching for a suitable combination of multipliers through trial and error. We hope our discussion here helps to understand the background mathematics systematically, though it may not be the perfect explanation. The main difference between our analysis and actual numerical studies is that this is a local analysis only on the evolution equations. The actual numerical results are obtained under a certain treatment of the boundary conditions, the choice of numerical integration schemes and grid structures, and also depend on the accuracy of the initial data. We think, however, that our proposal is an alternative to the hyperbolicity classification in that it includes the non-principal part of the evolution equations, and we expect that the discussion here will provide fundamental information on the stable formulation of the Einstein equations to the community.

We observed that the effects of adjustments depend on the choice of coordinate, gauge conditions, and also on its time evolution. Therefore our basic assumption of the constancy of the multipliers may be better to be replaced with more general procedures in our future treatment.

References

[1] H. Shinkai and G. Yoneda, gr-qc/0110008, to be published in Class. Quantum Grav. (2002).

[2] For a recent review, see e.g. L. Lehner, Class. Quantum Grav. **18**, R25 (2001).

[3] R. Arnowitt, S. Deser and C. W. Misner,"The Dynamics of General Relativity", in *Gravitation: An Introduction to Current Research*, ed. by L.Witten, (Wiley, New York, 1962).

[4] J. W. York, Jr., "Kinematics and Dynamics of General Relativity", in *Sources of Gravitational Radiation*, ed. by L.Smarr, (Cambridge, 1979) ; L. Smarr, J.W. York,Jr., Phys. Rev. D **17**, 2529 (1978).

[5] T. Nakamura and K. Oohara, in *Frontiers in Numerical Relativity* edited by C.R. Evans, L.S. Finn, and D.W. Hobill (Cambridge Univ. Press, Cambridge, England, 1989). M. Shibata and T. Nakamura, Phys. Rev. D **52**, 5428 (1995). T. W. Baumgarte and S. L. Shapiro, Phys. Rev. D **59**, 024007 (1999).

[6] M. Alcubierre, G. Allen, B. Brügmann, E. Seidel, and W.M. Suen, Phys. Rev. D **62**, 124011 (2000).

[7] *e.g.*, O. A. Reula, Livng Rev. Relativ. **1998-3** at `http://www.livingreviews.org/`; H. Friedrich and A. Rendall, in *Einstein's field equations and their physical interpretation*, ed. by B.G.Schmidt (Springer, Berlin 2000), available as gr-qc/0002074. See other references in [13], and the most recent study [10].

[8] C. Bona, J. Massó, E. Seidel and J. Stela, Phys. Rev. Lett. **75**, 600 (1995); Phys. Rev. D **56**, 3405 (1997).

[9] B. Kelly, P. Laguna, K. Lockitch, J. Pullin, E. Schnetter, D. Shoemaker, and M. Tiglio, Phys. Rev. D **64**, 084013 (2001).

[10] L. E. Kidder, M. A. Scheel and S. A. Teukolsky, Phys. Rev. D **64**, 064017 (2001).

[11] S. D. Hern, PhD thesis, gr-qc/0004036.

[12] S. Frittelli and O. A. Reula, Phys. Rev. Lett. **76**, 4667 (1996). See also J. M. Stewart, Class. Quantum Grav. **15**, 2865 (1998).

[13] H. Shinkai and G. Yoneda, Class. Quantum Grav. **17**, 4799 (2000).

[14] G. Yoneda and H. Shinkai, Phys. Rev. Lett. **82**, 263 (1999).

[15] G. Yoneda and H. Shinkai, Int. J. Mod. Phys. D **9**, 13 (2000).

[16] A. Ashtekar, Phys. Rev. Lett. **57**, 2244 (1986); Phys. Rev. D **36**, 1587 (1987); *Lectures on Non-Perturbative Canonical Gravity* (World Scientific, Singapore, 1991).

[17] A. Anderson and J. W. York, Jr, Phys. Rev. Lett. **82**, 4384 (1999).

[18] O. Brodbeck, S. Frittelli, P. Hübner and O.A. Reula, J. Math. Phys. **40**, 909 (1999).

[19] G. Yoneda and H. Shinkai, Class. Quantum Grav. **18**, 441 (2001).

[20] H. Shinkai and G. Yoneda, Phys. Rev. D **60**, 101502 (1999).

[21] F. Siebel and P. Hübner, Phys. Rev. D **64**, 024021 (2001).

[22] G. Yoneda and H. Shinkai, Phys. Rev. D **63**, 120419 (2001).

[23] S. Frittelli, Phys. Rev. D **55**, 5992 (1997).

[24] S. Detweiler, Phys. Rev. D **35**, 1095 (1987).

Astrometric Weak Microlensing due to an Extrasolar Planet

Hideki Asada[1]

Faculty of Science and Technology, Hirosaki University, Hirosaki 036-8561, Japan

Abstract

We have developed a perturbative approach to microlensing due to an extrasolar planetary lens. In particular, we have found analytic formulae for triple images. We have used the formulae to investigate the astrometric microlensing due to the extrasolar planetary lens, in expectation of dramatic improvements in the precision of the future astrometric measurements. For a weak lensing case, we have shown how the maximum angular size and the typical time scale of the anomalous shift of the light centroid are dependent on the mass ratio and angular separation between the star and the planet.

1 Introduction

Extrasolar planets searches are successfully going on [1] By the Doppler method, the number of candidates for the planets have reached about 70. In spite of the success, this technique has some drawbacks: The inferred mass is the lower bound, since the inclination angle of the orbital plane is not determined except for the eclipse case. In addition, the radial velocity of a star becomes too small to detect its Doppler effect when separation between the star and the planet is of the order of AU. Hence, it seems quite difficult to discover earth-type planets by this method. Astrometry is considered as a supplementary method to find out planets by measuring the transverse motion of a star. Indeed, we can expect dramatic improvements in the precision of the future astrometric measurements by FAME, SIM, DIVA and GAIA. Their precision will achieve a few micro arcseconds.

Also by these future astrometry missions, the astrometric microlensing will become the third method for searching extrasolar planets: The typical scale in the gravitational lensing is the Einstein ring radius, which is of the order of AU for a lensing star within our galaxy. Hence, the microlensing is quite effective even for earth-type planets [2, 3] In the planetary lens case, we can determine its true mass through observation of spikes in the light curve, which are produced by the magnification effect of the gravitational lensing. On the other hand, the astrometric microlensing is a consequence of a combination of the magnification and the position shift of the image. The numerical results [4, 5] have shown that the photo centroid shifts provide us a clue for extrasolar planets. However, the parameter dependence is not clear in the numerical approach. The purpose of my talk is to present the analytic formulae and clarify the parameter dependence [6].

2 Microlensing due to a single lens

A single lens is located at the distance D_L from the observer, and a source at D_S. The distance between the lens and the source is denoted by D_{LS}. Then, under the thin lens approximation, the lens equation for the single lens is written as

$$\beta = \theta - \frac{D_{LS}}{D_S}\alpha, \tag{1}$$

where β and θ are the angular positions of the source and the image, respectively, and α is the deflection angle. For a spherical lens with mass M, at least axisymmetric along the line of sight, the deflection angle is

$$|\alpha| = \frac{4GM}{c^2 b}, \tag{2}$$

[1] E-mail:asada@phys.hirosaki-u.ac.jp

where G is the gravitational constant and b is the impact parameter of the light ray. It is convenient to normalize our equations by the angular radius of the Einstein ring

$$\theta_E = \sqrt{\frac{4GMD_{LS}}{c^2 D_L D_S}}, \tag{3}$$

which is of the order of a milli arcsecond (mas) for a solar mass lens within our galaxy. In units of the Einstein ring radius, the lens equation is rewritten as

$$\boldsymbol{\beta} = \boldsymbol{\theta} - \frac{\boldsymbol{\theta}}{\theta^2}, \tag{4}$$

where θ denotes $|\boldsymbol{\theta}|$ and similar notations are taken below. We find out the two solutions

$$\boldsymbol{\theta}^{(\pm)} = k^{(\pm)}\boldsymbol{\beta}, \tag{5}$$

where we defined

$$k^{(\pm)} = \frac{1}{2}\Big(1 \pm \sqrt{1 + \frac{4}{\beta^2}}\Big). \tag{6}$$

The amplification for each image is respectively

$$A^{(\pm)} = \frac{1}{2}\Big(\frac{\beta^2 + 2}{\beta\sqrt{\beta^2 + 4}} \pm 1\Big). \tag{7}$$

Following the definition of the center of mass, we define the photo center as [7]

$$\boldsymbol{\theta}_C = \frac{A^{(+)}\boldsymbol{\theta}^{(+)} + A^{(-)}\boldsymbol{\theta}^{(-)}}{A^{(+)} + A^{(-)}}. \tag{8}$$

With respect to the unlensed position, the location of the photo center is

$$\Delta\boldsymbol{\theta}_C = \boldsymbol{\theta}_C - \boldsymbol{\beta}, \tag{9}$$

which expresses the deviation due to the lensing. For a single lens, it becomes simply

$$\Delta\boldsymbol{\theta}_C = \frac{\boldsymbol{\beta}}{\beta^2 + 2}, \tag{10}$$

where we used Eq. (7). We can assume that the stellar motion in our galaxy is approximated over several decades by a straight line, since the curvature of the orbit in our galaxy is negligible. For the later convenience, we decompose $\boldsymbol{\beta}$ into the orthogonal vectors as

$$\boldsymbol{\beta} = \boldsymbol{b} + \boldsymbol{V}, \tag{11}$$

where $\boldsymbol{b}$ is the vector for the impact parameter from the lens to the stellar orbit, and

$$\boldsymbol{V} = t\boldsymbol{v}_\perp, \tag{12}$$

for $\boldsymbol{v}_\perp$, the transverse angular velocity of the source to the lens. Here, we have chosen $t = 0$ as the time when the star is closest to the lens. We introduce ξ as

$$V = \sqrt{\beta^2 + 2}\tan\xi, \tag{13}$$

so that the photo center can be rewritten as

$$\Delta\boldsymbol{\theta}_C - \frac{\boldsymbol{b}}{2(b^2 + 2)} = \frac{\boldsymbol{b}\cos 2\xi}{2(b^2 + 2)} + \frac{\boldsymbol{V}\sin 2\xi}{2V\sqrt{b^2 + 2}}, \tag{14}$$

which is an ellipse [7, 8] Its size is of the order of mas for stellar cases in our galaxy. The center of the ellipse is at $\frac{\boldsymbol{b}}{2(b^2+2)}$, and the length of the semimajor and semiminor axes are $\frac{1}{2\sqrt{b^2+2}}$ and $\frac{b}{2(b^2+2)}$, respectively. The photo center passes the two points on the semiminor axes at $t = 0$ $(\xi = 0)$ and $t = \pm\infty$ $(\xi = \pm\frac{\pi}{2})$.

3 Microlensing due to a planetary lens

3.1 Perturbative Formulae

Let us consider the astrometric microlensing due to the planetary system, where the mass of the star and the planet are M_1 and M_2 respectively. Let us consider the separation vector from the star to the planet. Its projection onto the lens plane is denoted by $\boldsymbol{s}$. We adopt the frame of center of mass. Then, in the unit of the Einstein ring radius angle due to the total mass $M_1 + M_2$, the lens equation is written as

$$\boldsymbol{\beta} = \boldsymbol{\theta} - \Big(\mu_1 \frac{\boldsymbol{\theta} + \mu_2 \boldsymbol{\epsilon}}{|\boldsymbol{\theta} + \mu_2 \boldsymbol{\epsilon}|^2} + \mu_2 \frac{\boldsymbol{\theta} - \mu_1 \boldsymbol{\epsilon}}{|\boldsymbol{\theta} - \mu_1 \boldsymbol{\epsilon}|^2}\Big), \tag{15}$$

where we defined

$$\mu_1 = \frac{M_1}{M_1 + M_2}, \tag{16}$$

$$\mu_2 = \frac{M_2}{M_1 + M_2}, \tag{17}$$

$$\boldsymbol{\epsilon} = \frac{\boldsymbol{s}}{D_L}. \tag{18}$$

In the planetary case, M_2 is much smaller than M_1. For instance, the Jupiter mass is about 10^{-3} of the solar mass. Hence, we introduce an expansion parameter as $\mu = \mu_2$ in our perturbation approach. Since we wish to consider the microlensing as a method supplementary to the Doppler technique, we concentrate ourselves on a large separation case $\epsilon > 1$, which is beyond the reach of the Doppler method. It is straightforward to extend our investigation to the case of $\epsilon < 1$. In addition, we consider a case of a large impact parameter $\beta \gg 1$, which is most probable because of the large cross section. In total, we consider the case of $\beta \gg \epsilon > 1$. Let us look for the solutions of the lens equation by taking a form of

$$\boldsymbol{\theta} = \boldsymbol{\theta}_0 + \delta\boldsymbol{\theta}, \tag{19}$$

where $\boldsymbol{\theta}_0$ and $\delta\boldsymbol{\theta}$ are the solutions at the zeroth and first order, respectively.

It is interesting that we find the three solutions at the first order as

$$\delta\boldsymbol{\theta}^{(+)} = \frac{\mu}{\beta^6}\Big(-2\boldsymbol{\epsilon}(\boldsymbol{\beta}\cdot\boldsymbol{\epsilon})\beta^2 - \beta\epsilon^2\beta^2 + 4\boldsymbol{\beta}(\boldsymbol{\beta}\cdot\boldsymbol{\epsilon})^2 + O(\epsilon^3\beta^2)\Big), \tag{20}$$

$$\delta\boldsymbol{\theta}^{(-)} = \mu\Big(-\boldsymbol{\epsilon} + \frac{\boldsymbol{\beta}}{\beta^2} + O(\frac{1}{\epsilon\beta^2})\Big), \tag{21}$$

$$\boldsymbol{\theta}^{(3)} = \boldsymbol{\epsilon} - \mu\Big(\boldsymbol{\epsilon} + \frac{\boldsymbol{\beta} + (\frac{1}{\epsilon^2} - 1)\boldsymbol{\epsilon}}{|\boldsymbol{\beta} + (\frac{1}{\epsilon^2} - 1)\boldsymbol{\epsilon}|^2}\Big), \tag{22}$$

where the first and second solutions are perturbations around the zeroth-order solutions, and the third solution does not appear until at the linear order of μ. Actually, for $\mu = 0$, the third image is located at the direction to the planet. As for the number of the images, see also Witt [9].

Hence, we obtain the Jacobian of the mapping between the source and the lens planes,

$$\Big|\frac{\partial\boldsymbol{\theta}^{(+)}}{\partial\boldsymbol{\beta}}\Big| = 1 + O(\frac{\mu\epsilon^4}{\beta^6}, \mu^2), \tag{23}$$

$$\Big|\frac{\partial\boldsymbol{\theta}^{(-)}}{\partial\boldsymbol{\beta}}\Big| = -\frac{1 - 2\mu}{\beta^4} + O(\mu^2), \tag{24}$$

$$\Big|\frac{\partial\boldsymbol{\theta}^{(3)}}{\partial\boldsymbol{\beta}}\Big| = O(\mu^2). \tag{25}$$

The contribution of the third solution to the photo center is negligible for the large impact parameter.

3.2 Distortion of an ellipse for light centroid shifts

By the use of the preceding subsection, we find a correction to the photo centroid as

$$\delta\theta_C = \frac{\mu}{\beta^6}\Big(-2\epsilon(\beta\cdot\epsilon)\beta^2 - \beta\epsilon^2\beta^2 + 4\beta(\beta\cdot\epsilon)^2 + O(\beta^3)\Big) + O(\mu^2). \tag{26}$$

This is due to a primary effect caused by a position shift given by Eq. (20), since Eq. (23) shows that the correction to amplification appears only at higher orders.

Let us investigate in detail the photo center shift. We consider the expansion of the following superposition of two ellipses

$$\begin{aligned}&(1-\mu)\frac{\beta+\mu\epsilon}{|\beta+\mu\epsilon|^2+2} + \mu\frac{\beta-\epsilon}{|\beta-\epsilon|^2+2}\\ =\ & \frac{\beta}{\beta^2+2} + \frac{\mu}{\beta^6}\Big(-2\epsilon(\beta\cdot\epsilon)\beta^2 - \beta\epsilon^2\beta^2 + 4\beta(\beta\cdot\epsilon)^2 + O(\epsilon^3\beta^2)\Big) + O(\mu^2),\end{aligned} \tag{27}$$

where the first term of the left hand side is considered as the primary ellipse and the second as the perturbation around the primary. The position of the first ellipse is shifted by $\mu\epsilon$ in comparison with Eq. (10), and its size changes by factor $1-\mu$. Next, let us take a closer look at the secondary ellipse. The orthogonal decomposition by Eq. (11) is modified as

$$\beta - \epsilon = (b - \epsilon_\perp) + (t - t_C)v_\perp, \tag{28}$$

where we defined

$$\epsilon_\parallel = \frac{(\epsilon\cdot v_\perp)v_\perp}{v_\perp^2}, \tag{29}$$

$$\epsilon_\perp = \epsilon - \epsilon_\parallel, \tag{30}$$

$$t_C = \frac{\epsilon_\parallel}{v_\perp}. \tag{31}$$

For stellar cases in our galaxy, the maximum angular size of the distortion is estimated as

$$\frac{\mu\theta_E}{\beta}\Big(\frac{\epsilon}{\beta}\Big)^2 \sim \text{micro arcsec.}\Big(\frac{\mu}{10^{-3}}\Big)\Big(\frac{1}{\beta}\Big)\Big(\frac{\theta_E}{\text{mas}}\Big), \tag{32}$$

where we assumed that β is comparable to ϵ. The maximal distortion occurs at

$$t_C \sim 10^6\text{s}\Big(\frac{\epsilon_\parallel}{\text{AU}}\Big)\Big(\frac{100\text{km/s}}{v_\perp}\Big), \tag{33}$$

about a few months before/after, depending on a location of the planet, the source passes the point closest to the lensing star.

3.3 Discussion

In a small impact parameter case, the caustic crossing produces sufficiently large magnification of the images, so that we might be able to detect it much more easily by the astrometric microlensing as well as photometric microlensing [4]. Because of the nonlinear behavior, such an investigation needs numerical implementations. In order to evaluate feasibility in the future mission, we must take account of the brightness of the lensing star. It might be important to pay attention also to fluctuation of extragalactic reference frame due to gravitational lensing of black holes [10] and MACHOs [11] in our galaxy. Finally, the Keplerian motion might cause an appreciable effect on the distortion of the photo center ellipse, since the orbital period of the planet ranges from months to more than years, presumably comparable to t_C. Therefore, it would be an important subject to study these effects in detail.

4 Conclusion

In expectation of dramatic improvements in the precision of the future astrometric measurements, we have developed a perturbative approach to microlensing due to an extrasolar planetary lens. Formulae for triple images due to the planetary lens are given perturbatively by Eqs. (20) – (22). In particular, we have shown by Eqs. (32) and (33), how the light centroid shifts are dependent on the mass ratio and separation between the star and the planet. The typical time scale is of the order of months, depending strongly on $\epsilon_{\|}$, a projection of the separation vector onto the source motion.

Acknowledgment

The author would like to thank M. Bartelmann, L. Blanchet, G. Boerner, C. Cutler, N. Gouda, M. Kasai and B. Schutz for fruitful conversation and encouragements. This work was supported in part by a Japanese Grant-in-Aid for Scientific Research from the Ministry of Education.

References

[1] Marcy, G. W. and Butler, R. P. 1998, ARA&A, 36, 57

[2] Mao, S. and Paczynski, B. 1991, ApJ, 374, 37L ApJ, 522, 512

[3] Gould, A. and Loeb, A. 1992, ApJ, 396, 104

[4] Safizadeh, N., Dalal N. and Griest, K. 1999,

[5] Han, C. and Lee, C. 2001, MNRAS, *in press.* (astro-ph/0108157)

[6] Asada, H. 2002, submitted to ApJ

[7] Walker, M. A. 1995, ApJ, 453, 37

[8] Jeong, Y., Han, C. and Park, S. 1999, ApJ, 511, 569

[9] Witt, H. J. 1993, ApJ, 403, 530

[10] Schutz, B. F. 1982, in Proc. of an International Colloquium on The Scientific Aspects of the Hipparcos Mission (ESA SP-177), 181

[11] Hosokawa, M., Ohnishi, K. and Fukushima, T. 1997, AJ, 114, 1508

Black holes and traversible wormholes: a synthesis

Sean A. Hayward[1]

Department of Science Education, Ewha Womans University, Seoul 120-750, Korea

Abstract

A unified framework for black holes and traversible wormholes is described, where both are locally defined by outer trapping horizons, two-way traversible for wormholes and one-way traversible for black or white holes. In a two-dimensional dilaton gravity model, examples are given of: construction of wormholes from black holes; operation of wormholes for transport, including back-reaction; maintenance of an operating wormhole; and collapse of wormholes to black holes. In spherically symmetric Einstein gravity, several exotic matter models supporting wormhole solutions are proposed: ghost scalar fields, exotic fluids and pure ghost radiation.

1 Introduction

Space-time wormholes, short cuts between otherwise distant or even unconnected regions of the universe, are now a familiar plot device in science fiction. As a theoretical possibility in General Relativity, they gained some scientific respectability after the article of Morris & Thorne [1]. Apart from attracting public interest and young people to the field, one serious motivation is that wormholes can increase our understanding of gravity when the usual energy conditions are not satisfied, due to quantum effects such as the Casimir effect or Hawking radiation, or in alternative gravitational theories, such as the recently fashionable brane-world models.

2 Wormholes and black holes

The author's interest in wormholes originated with the realization that they are very similar to black holes, if one thinks of local properties, rather than the global properties which are usually used to define them. Global traversibility is incompatible with event horizons, leading to the widespread view, even among proponents [1], that wormholes are quite distinct from black holes. However, in terms of local properties, both are characterized by the presence of marginal (marginally trapped) surfaces, and indeed may be defined by outer trapping horizons, types of hypersurface foliated by marginal surfaces [2, 3, 4]. For a static black hole, the event horizons or Killing horizons are examples of outer trapping horizons, and for a static wormhole, the wormhole throat is an example of a double outer trapping horizon, composed of doubly marginal surfaces (Fig.1). The spatial topology of standard black-hole solutions and Morris-Thorne (static, spherically symmetric) wormholes is the same, $R \times S^2$, and the spatial geometry can be identical, as for the Schwarzschild black hole and the spatially Schwarzschild wormhole [1]. In each case, a minimal surface connects two asymptotically flat regions.

The key difference is the causal nature of the trapping horizons. This, however, is locally determined by the field equations and so may change with time. Summarizing an earlier proposal [4], black holes and wormholes may be locally defined by outer trapping horizons which are respectively achronal (space-like or null) and temporal (time-like). This means that they are respectively one-way and two-way traversible, as desired in each case. The Einstein equation then shows that they occur respectively under positive and negative energy density, specifically referring to the null energy condition. This means that they are supported respectively by normal matter or vacuum, and what has been dubbed exotic matter [1]. Given the preponderance of normal matter in the universe, this means that they respectively occur naturally and are unlikely to occur naturally, according to present knowledge. However, the possibility of constructing wormholes seems to be open, given the widespread appearance of negative energy densities in quantum

[1] E-mail: hayward@mm.ewha.ac.kr

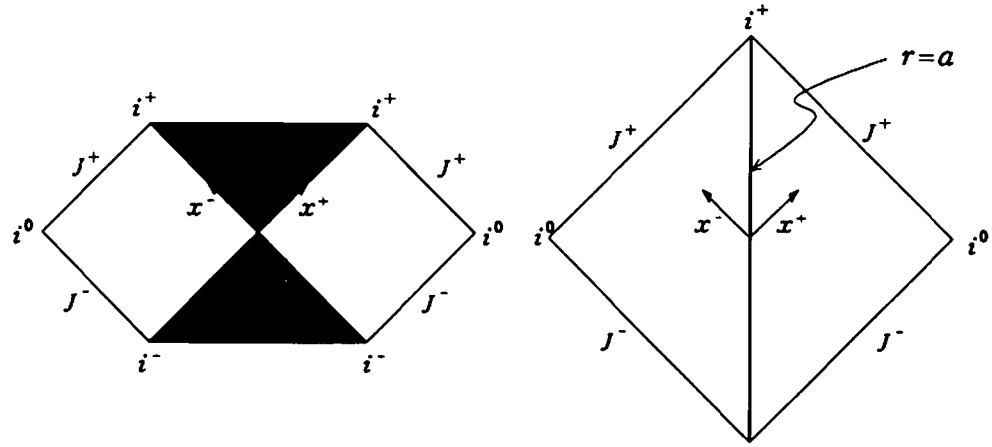

Figure 1: Penrose diagrams of (i) the Schwarzschild black-hole space-time, (ii) a Morris-Thorne wormhole space-time. The black-hole horizons and the wormhole throat are outer trapping horizons, respectively null and time-like.

field theory. Theoretically, if exotic matter can exist in sufficient concentrations, wormholes are as much a prediction of General Relativity as black holes.

A consequence of this synthesis is that black holes and wormholes are interconvertible. The trapping horizons evolve under positive or negative energy density, changing their causal type to locally characterize black holes or wormholes. A wormhole could be converted to a black hole if the supporting exotic matter disperses, or if normal matter is added. Looking at the geometry, the double trapping horizon constituting a static wormhole throat will bifurcate under generic perturbations, forming a trapped region. If the two horizons eventually become null, enclosing a future trapped region, this would be a black hole (Fig.2(i)). Conversely, a black hole could be converted to a wormhole by addition of exotic matter, which causes the two black-hole horizons to become time-like and, if circumstances allow, merge to form a wormhole throat (Fig.2(ii)). In fact, if one considers a Schwarzschild black hole evaporating semi-classically by Hawking radiation, the trapping horizons do indeed become time-like, due to negative-energy radiation absorbed by the black hole, created by pair production with the escaping radiation. The evaporating object is a traversible wormhole by any reasonable definition. This also suggests a wormhole as the endpoint of Hawking evaporation [4, 5].

Finding concrete examples of wormhole and black-hole interconversion requires a specific exotic matter model, so that there are field equations to determine the evolution. Four such models are described below, beginning with a simple model in which analysis is complete, then more realistic models which are under development.

3 Two-dimensional dilaton gravity

The CGHS two-dimensional dilaton gravity model [6] was known to contain black-hole solutions analogous to Schwarzschild ones, and to share similar properties such as cosmic censorship [7]. Generalizing the model to include a ghost massless Klein-Gordon field, i.e. with the gravitational coupling taking the opposite sign to normal, leads to static wormhole solutions analogous to Morris-Thorne ones [8]. Moreover, the field equations are explicitly integrable, so it is possible to set initial data corresponding to dynamical perturbations of black holes or wormholes, then analytically find the evolved space-time. Four types of processes have been considered in detail [8], summarized as follows.

i. Wormhole collapse to a black hole. Initial data is set so that there is initially a static wormhole, with the supporting ghost radiation then switched off from both sides of the wormhole. The double trapping horizon bifurcates and each section becomes null, forming a black hole. Solutions were found for both sudden and gradual collapse (Fig.2(i)).

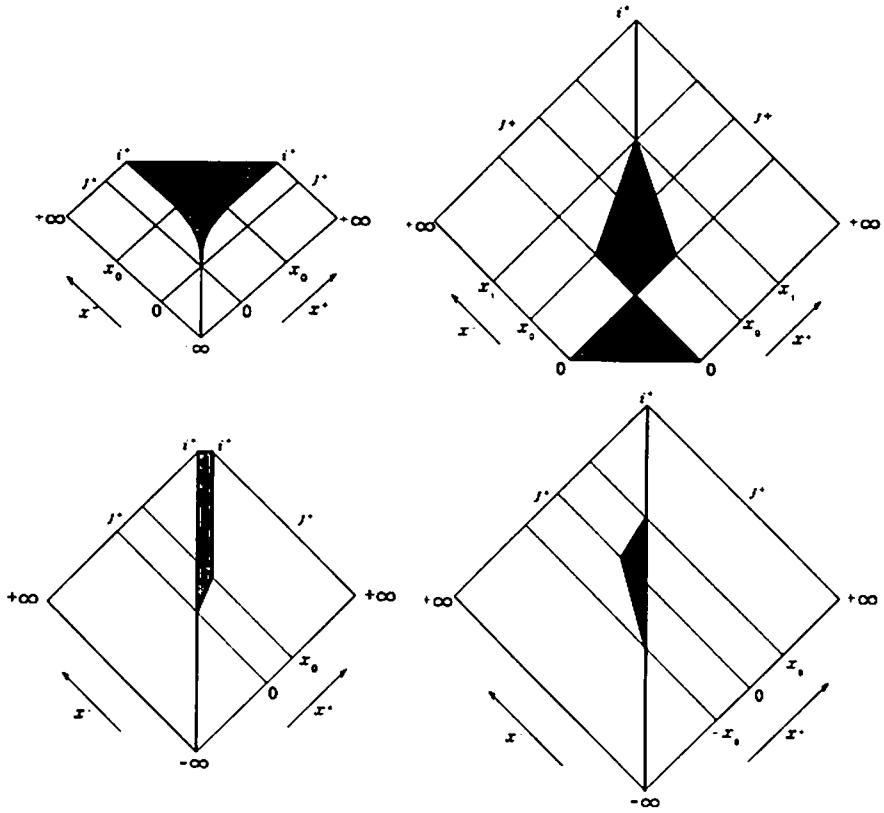

Figure 2: Penrose diagrams of wormhole (i) collapse to a black hole, (ii) construction from a black hole, (iii) operation for transport and (iv) maintenance of a static state, as described in the text. Shading indicates trapped regions. The trapping horizons evolve under positive or negative energy density, changing their causal type accordingly.

ii. Wormhole construction from a black hole. Initial data is set so that there is initially a static black hole, which is then irradiated from both sides with the ghost field. The two null trapping horizons of the black hole become time-like and, for appropriate radiation profiles, merge to form the throat of a static wormhole (Fig.2(ii)).

iii. Wormhole operation for transport or signalling, including the back-reaction on the wormhole. Initial data is set so that there is initially a static wormhole, with a pulse of normal Klein-Gordon radiation then sent through it. The double trapping horizon again bifurcates, but if the pulse energy is small, the wormhole remains traversible for a long time (Fig.2(iii)). This demonstrates the dynamic stability of the static wormhole.

iv. Wormhole maintenance of a static state. As above, but the pulse of normal radiation is preceded by an extra pulse of ghost radiation with equal and opposite energy. The double trapping horizon bifurcates and then merges again, returning the wormhole to its original static state (Fig.2(iv)).

4 Exotic matter models

An important shift from the Morris-Thorne approach [1] is to first specify an exotic matter model, then discover (suspiciously often) that wormhole solutions arise naturally. The following exotic matter models are under study in spherically symmetric Einstein gravity.

i. Ghost scalar fields. For the massless ghost Klein-Gordon field, there is a classic Morris-Thorne wormhole which was actually found previously by Ellis [9] and several other authors. It has recently been

argued to be stable [10]. A numerical code for spherically symmetric Einstein gravity with a massless ghost Klein-Gordon field has been written and used to study dynamical perturbations of the wormhole [11]. Preliminary results suggest that the Ellis wormhole is unstable, with a weakening ghost field causing collapse to a black hole, and a strengthening ghost field causing an explosion to an inflating universe.

ii. Exotic fluids, i.e. fluids not obeying the usual energy conditions. In particular, the spatially Schwarzschild wormhole [1] is a solution for an anisotropic fluid with density zero, radial pressure $-\tau$ and tangential pressure $\tau/2$, where the tension τ is positive. This model has vanishing energy trace, like the Maxwell electromagnetic field. Similar models have recently been proposed elsewhere [12].

iii. Pure ghost radiation, i.e. pure radiation (or null dust) with negative energy density. With both ingoing and outgoing radiation, static wormhole solutions were conjectured in the conference presentation and found shortly afterwards [13].

5 Conclusion

A unified theory of black holes and traversible wormholes has been proposed. Its development includes definitions of mass and surface gravity, and zeroth, first and second laws of black-hole dynamics and wormhole dynamics [2, 3, 4]. This synthesis is useful even for existing problems such as black-hole evaporation, where the Hawking radiation converts a Schwarzschild black hole, at least semi-classically, into a traversible wormhole. It also raises the largely unexplored issue of wormhole thermodynamics.

Black holes are now generally accepted as astrophysical realities, whereas traversible wormholes are often regarded as unphysical theoretical curiosities, outside mainstream scientific research, just as black holes once were. The dual nature of black holes and wormholes, in particular their dynamic interconvertibility, forces new viewpoints. Wormholes are just black holes under negative energy density.

Research supported by Korea Research Foundation grant KRF-2001-015-DP0095. Thanks to the conference organizers for support and Hyunjoo Lee for preparing the figures.

References

[1] M S Morris & K S Thorne, Am. J. Phys. **56**, 395 (1988).

[2] S A Hayward, Phys. Rev. **D49**, 6467 (1994).

[3] S A Hayward, Class. Quantum Grav. **15**, 3147 (1998).

[4] S A Hayward, Int. J. Mod. Phys. **D8**, 373 (1999).

[5] D Hochberg, A Popov & S V Sushkov, Phys. Rev. Lett. **78**, 2050 (1997).

[6] C Callan, S Giddings, J Harvey, and A Strominger, Phys. Rev. D **45**, R1005 (1992).

[7] S A Hayward, Class. Quantum Grav. **10**, 985 (1993).

[8] S A Hayward, S-W Kim & H Lee, Phys. Rev. **D65**, 064003 (2002).

[9] H G Ellis, J. Math. Phys. **14**, 395 (1973).

[10] C Armendariz-Picon, gr-qc/0201027.

[11] H Shinkai & S A Hayward, in preparation.

[12] N Dadhich, S Kar, S Mukherji & M Visser, Phys. Rev. **D65**, 064004 (2002).

[13] S A Hayward, gr-qc/0202059.

Quantum Entropy Bound by Information in Black Hole Spacetime

A. Hosoya and A. Carlini

Department of Physics, Tokyo Institute of Technology, Oh-Okayama, Meguro-ku, Tokyo 152, Japan

Abstract

We show that the increase of the generalized entropy by quantum process outside the horizon of a black hole is more than the Holevo bound of classical information lost into the black hole .

1 Introduction

In the black hole thermodynamics the total entropy is the sum of the black hole entropy $S_{BH} = A/4$ $(= 4\pi M^2)$ and of the ordinary matter entropy S_{matter}, i.e. $S_{tot} = S_{BH} + S_{matter}$, where A is the area of the horizon of the black hole of mass M. The generalized second law is motivated by the paradox of Wheeler's demon: although the entropy S_{matter} of the matter outside the black hole decreases by disposing it to the black hole, the total entropy ΔS_{tot} increases. [1, 2]

In the present work we will show further that the increase of the generalized entropy is bounded below by the Holevo bound [3, 4], which in turn is the upper bound of the classical information lost into the black hole which could be obtained by quantum measurements. Before showing the inequality, let us clarify the concept of information from our point of view. Information can be processed (sent, received, disposed of etc.) only by performing physical measurements. We say, for example, that the information prepared by an agent outside a black hole is retrieved by another agent at infinity if the two experimental outcomes are correlated. A quantification of the correlation is the mutual information defined below.

The quantum state of the matter in the black hole spacetime is the Hartle-Hawking state[5],

$$|\psi>_{HH} \equiv \sum_n \sqrt{c_n}|n>_B |n>_A, \tag{1}$$

where $c_n \equiv \exp[-\omega n/T_{BH}]/Z$ is the Boltzmann factor, $Z \equiv \sum_n \exp[-\omega n/T_{BH}]$ and $T_{BH} \equiv (8\pi M)^{-1}$ is the Hawking temperature. The state (1) is an entangled state [8] of the particles inside ($|n>_B$) and outside ($|n>_A$) of the black hole just like the Einstein-Podolsky-Rosen pair, a key concept in quantum information theory [6]. The state inside the black hole is not accessible from the outside so that we trace over the B-state to obtain a mixed state for the observer outside, i.e. $\rho_A = \mathrm{Tr}_B(|\psi>_{HH}<\psi|) = \sum_n c_n |n>_A < n|$, which is nothing but the canonical density operator [5].

2 Quantum measurement in black hole spacetime

Imagine a detector of zero mass in the pure state $|\Phi_0>$, initially located far away from the black hole horizon, which is slowly lowered by a string up to a point near the horizon, and then a quantum experiment outside of the black hole is performed. [7, 9, 10, 11] When the agent outside the black hole switches on his experimental apparatus, the system will undergo a unitary transformation U for the compound state of A and the detector as

$$|\Psi> \rightarrow |\Psi>', \tag{2}$$

where

$$\begin{aligned} |\Psi> &\equiv \sum_n \sqrt{c_n}|n>_B |n>_A \otimes |\Phi_0(x_0)> \\ |\Psi>' &\equiv \sum_n \sqrt{c_n}|n>_B U(|n>_A \otimes |\Phi_0(x_0)>| \\ &= \sum_{\alpha,n} \sqrt{c_n}|n>_B \sum_m U^{\alpha}_{nm}|m>_A \otimes |\Phi_\alpha(x_0)>, \end{aligned} \tag{3}$$

and where x_0 is the spacetime point of the detector, which is initially located outside the horizon. We assume that by the measurement the state decoheres (on a proper timescale which ensures that the process is quasi-static, and which is smaller than the dynamical timescale of the process itself) to a diagonal form with respect to the detector states $|\Phi_\alpha(x_0)>$. The resultant mixed state ρ' is then

$$\begin{aligned}\rho' &= \sum_\alpha \left(\sum_n \sqrt{c_n} |n>_B \sum_m U^\alpha_{nm} |m>_A \right) \\ &\otimes \left(\sum_{n'} \sqrt{c_{n'}}_B < n'| \sum_{m'} U^{*\alpha}_{n'm'A} < m'| \right) \\ &\otimes |\Phi_\alpha(x_0)><\Phi_\alpha(x_0)|. \end{aligned} \tag{4}$$

Now let us consider the most general case in which the observer disposes of the detector in a gedanken experiment a lá Geroch-Bekenstein. Suppose that the observer conditionally drops the detector into the black hole if the experiment outcome is $\alpha \in D$, while keeping it outside the black hole if $\alpha \notin D$. In other words, the detector might alter the state inside the black hole if the measurement outcome $\alpha \in D$. In general the state (4) will change further to

$$\begin{aligned}\rho'' &= \sum_\alpha \left(\sum_n \sqrt{c_n} V_\alpha |n>_B \sum_m U^\alpha_{nm} |m>_A \right) \\ &\otimes \left(\sum_{n'} \sqrt{c_{n'}}_B < n'| V^\dagger_\alpha \sum_{m'} U^{*\alpha}_{n'm'A} < m'| \right) \\ &\otimes |\Phi_\alpha(x_\alpha)><\Phi_\alpha(x_\alpha)|, \end{aligned} \tag{5}$$

where V_α is a nontrivial unitary transformation if the experimental outcome is $\alpha \in D$ and $V_\alpha = 1$ if $\alpha \notin D$. Moreover, x_α is the spacetime point of the detector sufficiently after the measurement: x_α is inside the black hole if $\alpha \in D$ and it is outside otherwise. This corresponds to the "classical communication from Alice to Bob" in the standard quantum communication set-up, except that in the present case it is an inherently one-way communication.

The trace over the B states washes out the V_α dependence altogether and we obtain the reduced density matrix for the compound state of A and Φ,$\rho''_{A\Phi}$ as

$$\rho''_{A\Phi} = \sum_{\alpha \in D} p_\alpha \rho'_\alpha E_D + \sum_{\alpha \notin D} p_\alpha \rho'_\alpha |\Phi_\alpha(x_\alpha)><\Phi_\alpha(x_\alpha)|, \tag{6}$$

where $p_\alpha = Tr_A(U_\alpha \rho U^\dagger_\alpha)$ and $\rho'_\alpha = \frac{1}{p_\alpha} U_\alpha \rho U^\dagger_\alpha)$.We have also defined the reduced density operator $E_D = \sum_{\alpha \in D} p_\alpha |\Phi_\alpha(x_\alpha)><\Phi_\alpha(x_\alpha)|/P_D$ with $P_D = \sum_{\alpha \in D} p_\alpha$ is the total probability for the detector to drop into the black hole.

3 Quantum entropy bound

Now, the experiment is a local and isothermal process due to the Unruh effect of the accelerated system with the temperature $\tilde{T}(r) \equiv T_{BH}/\chi(r)$, the blue shifted temperature from the Hawking temperature T_{BH} of the cavity surrounding the black hole at infinity. The first law of black hole physics is

$$\Delta S_{BH} = \frac{\Delta M}{T_{BH}} = \frac{\Delta W}{T_{BH}}, \tag{7}$$

where ΔW is the work needed for the quantum experiment. In the semi-classical gedanken experiment, this corresponds to the work to push down the box towards the black hole against the buoyancy force by the Hawking radiation [9, 10].

Ordinary thermodynamics tells us that the work ΔW needed in the isothermal process is more than or equal to the variation of the free energy:

$$\Delta W \geq \Delta F \tag{8}$$

(with the equality in (8) holding for a quasi-static process), where

$$\begin{aligned}\Delta F &\equiv \sum_\alpha p_\alpha [E_\alpha - \tilde{T}(S'_\alpha - \log p_\alpha)]\chi - (E_0 - \tilde{T}S_M)\chi \\ &= \left[S_M - \left(\sum_\alpha p_\alpha S'_\alpha - \sum_\alpha p_\alpha \log p_\alpha\right)\right] T_{BH}, \end{aligned} \tag{9}$$

and we have used the conservation of the internal energy $E_0 = \sum_\alpha p_\alpha E_\alpha$, which holds in the isothermal system (E_0 and E_α are the energies of the Hawking state before and after the experiment, respectively). Furthermore, S_M and S'_α are defined by $S_M \equiv S(\rho_A)$ (the initial matter entropy) and $S'_\alpha \equiv S(\rho'_\alpha)$, where $S(\rho) \equiv -\mathrm{Tr}\,(\rho \log \rho)$ is the von Neumann entropy for a general state ρ. The last term on the r.h.s. of eq. (9) represents the final entropy of the detector, which reflects our ignorance about the actual outcome of the measurement. Combining the first law of black hole physics and the second law of thermodynamics given above, we then easily obtain $\Delta S_{BH} = S'_{BH} - S_{BH} \geq S_M - (\sum_\alpha p_\alpha S'_\alpha - \sum_\alpha p_\alpha \log p_\alpha)$ or, in a more illuminating way,

$$(S'_{BH} + S'_M) - (S_{BH} + S_M) \geq S'_M - \sum_\alpha p_\alpha S'_\alpha + \sum_\alpha p_\alpha log p_\alpha. \tag{10}$$

Substituting $S'_M = S(\rho''_{A\Phi})$ into eq.(10), we obtain

$$\Delta S_{tot} \equiv (S'_{BH} + S'_M) - (S_{BH} + S_M) \geq P_D [S\left(\sum_{\alpha \in D} p_\alpha \rho'_\alpha\right) - \sum_{\alpha \in D} p_\alpha S(\rho'_\alpha)] \tag{11}$$

The quantity inside the bracket on the right hand side of eq. (11) appears in the famous Holevo bound [3, 4]:

$$H_D \equiv S\left(\sum_{\alpha \in D} \tilde{p}_\alpha \rho'_\alpha\right) - \sum_{\alpha \in D} \tilde{p}_\alpha S(\rho'_\alpha) \geq I'_D, \tag{12}$$

with $\tilde{p}_\alpha = p_\alpha / P_D$. The right hand side I'_D is the mutual information lost into the black hole of the components $\alpha \in D$ which would be obtained if one performed a further observation.

4 Summary

To summarize, we have obtained an inequality:

$$\Delta S_{tot} \geq P_D I'_D. \tag{13}$$

The classical information lost into the black hole which could be obtained by further observations is bounded above by the change of the generalized entropy.

References

[1] J.D. Bekenstein, *Phys. Rev.* **D7**, 2333 (1973); *ibid.* **D9**, 3292 (1974); *ibid.* **D12**, 3077 (1975).

[2] S.W. Hawking, *Commun. Math. Phys.* **43**, 199 (1975).

[3] A.S. Holevo, *Probl. Peredachi Inform.* **9**, 177 (1973).

[4] A. Peres, *Quantum Theory: Concepts and Methods*, (Kluwer Academic Publishers, New York, 1995).

[5] R.M. Wald, *Quantum Field Theory in Curved Spacetime and Black Hole Thermodynamics* (Chicago University Press, Chicago, 1994).

[6] e.g.,V. Vedral, e-print quant-ph/0102094.

[7] J.D. Bekenstein, *Phys. Rev.* **D23**, 287 (1981).

[8] V.P. Frolov and D. Page, *Phys. Rev. Lett.* **71**, 3902 (1993).

[9] W.G. Unruh and R.M. Wald, *Phys. Rev.* **D25**, 942 (1982).

[10] W.G. Unruh and R.M. Wald, *Phys. Rev.* **D27**, 2271 (1983).

[11] A. Hosoya, A. Carlini and T. Shimomura, *Phys. Rev.* **D63**, 104008 (2001).

Topological derivation of Black Hole entropy by analogy with a chain polymer

Masaru Siino[1]

Department of Physics, Tokyo Institute of Technology,
Oh-Okayama, Megro-ku, Tokyo 152-, Japan

1 Introduction: A topological viewpoint of Event Horizon

When we concentrate on the topological feature of an event horizon, it can be reduced to the structure of the crease set of the event horizon[7]. On the crease set, two or more generators of the event horizon cross and the event horizon is not smooth[8]. Furthermore the catastrophe theory[9][10][11] tells that the generic structure of the crease set is composed of not a point related to a spherical black hole but two-dimensional sets and their bifurcations. By an appropriate timeslice, this two-dimensional crease set provides a toroidal event horizon. Hence, in this sense, the spherical topology of event horizon is structurally unstable.

Here it should be noted that these facts do not mean that a black hole and its crease set are always highly anisotropic. Since the catastrophe theory implies that the spherical topology changes under the small perturbation in a corresponding microscopic scale, the anisotropicity would be very small in some cases. For example, when almost spherically symmetric matter collapses to an almost spherical black hole, in microscopic scale its crease set will be highly distorted and bifurcated, and its event horizon will be with very complicated topology, while in a macroscopic scale the crease set can be treated as a point and the event horizon is with a spherical topology.

These aspects make us expect that the crease set possesses a micro-canonical entropy. In the present article, we estimate the entropy of the crease set by analogy with a chain polymer, since the one-dimensional crease set possesses similar structure to the chain polymer (and two-dimensional one will be similar in statistics). Assuming that a multiply folded crease set changes its form like the chain polymer, we can estimate the entropy of the crease set. Then we are going to interpret this entropy as the entropy of falling matters. We will have gotten an entropy coincident with the Bekenstein-Hawking entropy.

In the next section, we recall the way to calculate the entropy of a chain polymer in a simple Ising model. The third section shows how to estimate the entropy associated with a considering black hole from such a topological view point. The final section is devoted to summary, discussions and speculations.

2 Entropy of Chain Polymer

In this section, we recall a simple Ising model of elasticity of a chain polymer[12]. Suppose a large number N of monomers with a length a form a chain polymer with a total length Na. Nevertheless, this polymer would be folded into an appropriate length $l < Na$. To give a simple model of folding it, we suppose that each element of the monomers can be directed only to the right or the left in equal probabilities.

In micro-canonical statistics, the length l should be a parameter describing a state of the system. The number of allowed configurations $W(l)$ is given by

$$W = \frac{2N!}{N_+!N_-!} = \frac{2N!}{(\frac{1}{2}N - l/a)!(\frac{1}{2}N + l/a)!}, \tag{1}$$

where N_+ and N_- are the number of right- and left-directed elements, respectively. Then, using the Stirling formula $\log N! \simeq N \log N - N$, the entropy of this polymer becomes

$$S = \log W \simeq N \log N - (\frac{1}{2}N - l/a)\log(\frac{1}{2}N - l/a) - (\frac{1}{2}N + l/a)\log(\frac{1}{2}N + l/a). \tag{2}$$

[1] E-mail:msiino@th.phys.titech.ac.jp

Under the assumption that the length l is much smaller than Na, this is approximated as

$$S(l) = N\log 2 - \frac{l^2}{2Na^2} + O(N\cdot(l/Na)^4) \quad (3)$$

$$= S(l=0) - \frac{l^2}{2Na^2} + O(N\cdot(l/Na)^4), \quad (4)$$

where we use $\log(1+x) = x - x^2/2+,,,(x \sim l/Na \ll 1)$.

This gives a simple model of elasticity. Indeed, from the first low of thermodynamics $TdS = dU - fdl$, an elastic force f obeys well known Hooke's low in the leading order as

$$f = T\left(\frac{\partial S}{\partial l}\right)_U = -\frac{Tl}{Na^2}, \quad (5)$$

where T and U are the temperature and the internal energy. The force is proportional to the temperature T. Actually, a rubber band contracts when it is wormed up, while an iron wire expands.

3 Black Hole Entropy

Now we will estimate an entropy associated with the crease set of an event horizon. On the crease set, two or more generators of the event horizon cross. The closure of the crease set is the set of the endpoint of the event horizon generators, and the event horizon is indifferentiable there[7][8]. From Ref.[7], the spatial topology of an event horizon in a timeslicing is determined only by the timeslicing of the crease set. This implies that the crease set possesses all of the topological information of the black hole. In other words, an event horizon is completely determined if once we know the crease set and all of the light rays starting from the crease set, since the event horizon should be their envelope. Hence we expect that the crease set gives all of the global information about the event horizon while the light rays can be determined only by a local geometry. In this section, we try to estimate the entropy associated with that global information carried by the crease set of the event horizon.

In our point of view, the entropy of the crease set is brought by falling bodies when they fall beyond the event horizon of a black hole. Since the crease set is the multiple point of the generator of the event horizon, its own structure will be changed provided that a falling body affects a congruence of the generators of the event horizon when the falling body crosses it. Then both of the topology of the event horizon and the structure of the crease set reflect some information included in the configuration of matter outside of the black hole. If we suppose that the topology of a black hole finally settles to a single spherical one after all outside matter has fallen into the black hole, this information of the topology of the event horizon turns out to be absorbed into the black hole. Therefore we expect this information corresponds to the black hole entropy and try to estimate the entropy of the crease set.

To consider the degeneracy of the crease set, one might assign the degrees of freedom to each Planckian scale segment of the crease set as the simplest model. The crease set, however, can be two-, one- or zero-dimensional. Each fundamental element becomes Planckian area or length or vanishes, respectively. For example, the entropy of a one-dimensional crease set with a length L will intuitively estimated as $S = \log W = \log(C^{L/l_{Pl}})$, where C is the number of possible states for each fundamental element. This is not what we have expected since L could not be proportional to the area of the event horizon in the case of the one-dimensional crease set.

On the contrary, on the analogy of a chain polymer, we will derive an entropy of the crease set proportional to the area of the event horizon in the following. To determine an entropy, we count the logarithm of the micro-state degeneracy. Though there may be various model of the micro-state, in the present article we apply following very simple Ising model similar to the chain polymer.

First, we consider only the case of one-dimensional crease set for simplicity since the case of two-dimensional crease set will be different only by a factor in their entropy. On the other hand, from the catastrophe theory it is concluded that the point-wise crease set is not generic[9][10][11]. This implies that even for an almost spherically symmetric collapsing of matter, the matter and spacetime are not rigorously spherically symmetric 'in a microscopic scale' because of an anisotropic small perturbation.

This will cause a highly folded crease set, which is confined within a very small region. Then it is not point-wise in a microscopic scale but in a macroscopic scale.

There should be many ways to fold and confine the crease set. Considering a number of ideal small fundamental elements of the crease set to fold, this situation is very similar to the chain polymer discussed in the previous section. Then we will count the number of them and estimate a related entropy, by the analogy with the chain polymer.

In the case of the chain polymer, its entropy S_{CP} is given by (4) and we think that the entropy of the crease set S_C is same as S_{CP};

$$S_C(l) = S_{CP}(l) = S_{CP}(0) - \frac{l^2}{2Na^2}, \tag{6}$$

where l is the length of the crease set. N and a are the number and length of the ideal fundamental element, respectively.

In our discussion, the state with $l = 0$ is regarded as an almost spherically symmetric black hole, since this state is macroscopically similar to a spherical black hole with a zero-dimensional (point-wise) crease set. On the other hand, to make the black hole most anisotropic, collapsing matter must be most tilted in a special direction and this configuration will not allow the degeneration of the micro-state. Nevertheless, the black hole would not be allowed to take such an arbitrary tilted configurations; rather, it is natural that there is an upper bound l_{max} for l since a black hole with infinitely large l seems to be unphysical. Then if we have an upper bound l_{max}, it will be valid to regard $S(l_{max})$ as the zero-point of the entropy of the black hole. Therefore the entropy of an almost spherical black hole is given by

$$S_{BH}(l = 0) \equiv S_C(l = 0) - S_C(l_{max}) = \frac{l_{max}^2}{2Na^2} \ . \tag{7}$$

We may expect that the upper bound l_{max} is about a final black hole mass M, since it is the only reasonable scale in a gravitational dust collapse. Furthermore, the hoop conjecture[13] requires the length of the crease set should be bounded by $2\pi M$[14]. Hence we assume $l_{max} \simeq 2\pi M$. In addition to it, we should assume $l_{max}/a \ll N$ in order to derive eqn.(4) in the previous section. The consistency and validity of this condition will be discussed later. Hence we observe that this entropy proportional to the area of the event horizon $\mathcal{A} \propto \mathcal{M}^{\epsilon}$.

By the way, eqn.(7) has an unpreferable factor a^2/N. Expecting that this entropy coincides to the Bekenstein-Hawking entropy, Na^2 should be on a scale of l_{pl}^2. This turns out that a is $\frac{l_{pl}}{\sqrt{N}} \ll l_{pl}$ as N is a very large number. Since it is unreasonable to give a much smaller structure than Planckian length to quantum spacetime, we cannot accept such a small a.

This problem of the scale of a small segment is resolved by considering the branches of the crease set. As pointed out in [9][11], there are possibilities that the crease set is branched at a hinge where the crease set can angle. We assume that a new branch (child chain) with a length αl ($\alpha < 1$, since a child should be smaller than its mother by definition) comes up at some hinges in a probability β and is composed of N elements, which will be justified later. The number of such a branch is given by the probability and the number of mother's hinges as βN.

Moreover there are also grandchildren and further descendants. Naively, the number of n-th descendants might be considered to be $(\beta N)^n$ in geometrical progression. However this is not realistic because we require infinite volume to embed all the family of geometrical progression $\Sigma_i^{\infty}(\beta N)^i$. Since the territory of a child and his all descendants would be limited around each of N hinges of the mother chain, we assume that the number of n-th descendants is $\beta^n N$ rather than $(\beta N)^n$. By this assumption, the total length of the family becomes $N\Sigma_i^{\infty}\alpha^i\beta^i l$ and will converge so as to be embedded, as the n-th descendant is with a length $\alpha^n l$. Then the total number of degenerated micro-states is given by

$$W_{tot} = W(l) \cdot W(\alpha l)^{N\beta} \cdot W(\alpha^2 l)^{N\beta^2} ..., \tag{8}$$

where n-th factor is the contribution of all $(n-1)$-th descendants. The entropy of a crease set (7) is changed by a factor and now we are not worried about the factor $1/N$ any more: the total entropy is

$$S_{Ctot} = \log W_{tot} \quad = \quad S_0 - \frac{l^2}{2Na^2} - \frac{(\alpha l)^2}{2Na^2}N\beta - \frac{(\alpha^2 l)^2}{2Na^2}N\beta^2 - \ ... \ + O(l^4)$$

$$
\begin{aligned}
&= S_0 - \frac{l^2}{2a^2}\left(\frac{1}{N} + \alpha^2\beta + \alpha^4\beta^2 + ... + \alpha^{2n}\beta^n + ...\right) + O(l^4) \\
&\sim S_0 - \frac{\alpha^2\beta}{1-\alpha^2\beta}\frac{l^2}{2a^2}, \\
S_{BH} &= \frac{\alpha^2\beta}{1-\alpha^2\beta}\frac{l_{max}^2}{2a^2}
\end{aligned}
$$

where S_0 is the sum of all l-independent terms. On the third line, it is supposed that N is sufficiently large. Though the infinite sum might have any cut off, it would change the result only by a numerical factor of the order of magnitude of one.

If we rigorously require $S = \mathcal{A}/4l_{pl}^2 = \pi M^2/l_{pl}^2$, the relation

$$
\begin{aligned}
\frac{4\pi^2 M^2}{2l_{pl}^2}\frac{\alpha^2\beta}{1-\alpha^2\beta} &= \frac{\pi M^2}{l_{pl}^2} \\
\frac{\alpha^2\beta}{1-\alpha^2\beta} &= \frac{1}{2\pi},
\end{aligned}
$$

will determine $\alpha^2\beta$, since hoop conjecture say $l_{max} \sim 2\pi M$ and a should naturally be l_{pl}.

Now we must discuss the case of a non-chain-like crease set. Indeed, Refs [10][9][11][15] tell us that it is important to consider a crease set with two dimensions. The discussion of a two-dimensional crease set can be proceeded with, as following. Intuitively, the two-dimensional crease set has two independent degrees of freedom to fold. This will cause the state counting to become the square of that of an one-dimensional crease set and its entropy to be two times. For further accurate estimation, it might be valid to discuss in the theory of random surface. In the case of the random surface, the regular term of its entropy around $l = 0$ is also proportional to l^2[16]. Then the elastic force is always proportional to the amount of its deformation (see eqn.(5)) independently of its form, size and dimensions. This is consistent with the general Hooke's law, i.e. a stress tensor is proportional to a distortion tensor.

So we summary the estimation as

$$
S_{BH} = F(n)G(\alpha^2\beta)\frac{\mathcal{A}}{4l_{pl}^2}, \tag{9}
$$

where $F(n)$ and $G(\alpha^2\beta)$ are numerical factors of the order of magnitude of one related to the dimensions and branching of the crease set, respectively.

Finally, we discuss the assumptions we have made above. Here we should discuss the meaning of N and the validity of the assumptions about the amount of it. In the present estimation we have supposed that the number of mother's elements N is a fixed large number when the collapsing changes l between extremely anisotropic collapse $l = l_{max}$ and almost spherical collapse $l = 0$, and $0 < l/a < l_{max}/a$ is much less than N.

One may be doubtful that these assumption is consistent to physical situation. To make clear this point, we consider the relation between N and the falling bodies as following. We think an ideal process in which some small elements with a volume l_{pl}^3 and a mass m fall into a black hole. It is considered that a falling body gravitationally deforms a generator of the event horizon, and consequently the crease set will form a hinge and be angled there. If many bodies randomly fall into the black hole, the crease set will be repeatedly angled in various directions and finally confined into a small region. Therefore we guess that almost spherical collapse can occur through such a random falling process of a large number of small bodies. On the other hand, if the small bodies are not random but ordered to be anisotropic in a special direction, the crease set will be more spread and the anisotropic black hole is once formed. Then the entropy of the crease set is related to that randomness of falling bodies. To determine N, it will be valid to relate the number of the hinges of the crease set and the falling ideal volume elements with a volume l_{pl}^3, into which the collapsing matter could be decomposed.

In a simple-mind, we regard the number of the collapsing ideal volume elements as the number of the hinges of the mother chain N. The consistent interpretation of the child and descendant chain is following. The mother chain is angled by a falling body directly when the body crosses event horizon generators and there comes up a child chain (dotted arrows) in a probability β. Besides, this child chain

is also affected by another falling volume element through three point interaction (one body making the child chain, another body and one event horizon generator) since gravitation is long range force. Therefore we consider that the hinges of the child chain are formed by this three point interaction. Then the hinges of the child chain are assigned to the two falling volume elements, one of which have made the child chain. Hence the child chain possesses N hinges. Similarly, a n-th descendant chain also forms $\sim N$ hinges under the influences of $(n+1)$ different elements. This consistently gives an explanation to the formation and number of the hinges of the descendant chain.

Now we consider the number of elements $N \sim M/m$, inheriting the number of falling volume elements l_{pl}^3 with a mass m. The mass m of the volume element should be much smaller than Planckian mass so that it will not be a black hole but an ordinary matter. Then we have following inequalities,

$$N \sim \frac{M}{m} \gg \frac{M}{l_{pl}} \sim \frac{l_{max}}{l_{pl}=a} > \frac{l}{a}. \tag{10}$$

Therefore we have confirmed all parameters are in a realistic range and the assumptions are consistent.

The picture considered here might be something kinematical while the process we think of is dynamical. Nevertheless, this will put an interpretation that this black hole entropy reflects the number of the ways to form an almost spherical black hole.

References

[1] J. D. Bekenstein, *Lett. Nuovo Cimento* 11467 (1974)

[2] I. B. Khriplovich, K. Krasnov *Phys. Rev.* **D** 3505 (1997), A. Ashtekar, J. Baez, A. Corichi and K. Krasnov, *Phys. Rev. Lett.* **80** 904 (1998)

[3] A. Strominger *JETP* **9802** 009 (1998), S. Carlip Class. Quant. Grav. **16** 3327 (1999)

[4] L. Bombelli, R. K. Koul, J. Lee and R. D. Sorkin *Phys. Rev.* **D34** 373 (1986), M. Srednicki *Phys. Rev. Lett.* **71** 666 (1993), S. Mukohyama, M. Seriu and H. Kodama *Phys. Rev.* **D58** 064001 (1998)

[5] G. Horowitz, S. Hawking and S. Ross *Phys. Rev.* **D51** 4302 (1995)

[6] A. Strominger and C. Vafa *Phys. Lett.* **B379** 99 (1996)

[7] M. Siino *Phys. Rev.* **D58** 104016 (1998)

[8] Beem and Królak, gr-qc/9709046

[9] T. Koike and M. Siino, in preparation

[10] M. Siino *Phys. Rev.* **D59** 064006 (1999)

[11] V.I. Arnold in *Dynamical systems VIII, Encycropedia of Mathematical Science Vol. 39* Springer-Verlag, Chap 2, Sec. 3

[12] H. M. Japmes and E. Guth, *J. Chem. Phys.* **11** 455 (1943), *J. Polymer Sci.* **iv** 153 (1949)
R. Kubo, *J. Phys. Soc. Japan* **2** 47-,51-,84- (1947)

[13] K. Thorne in *Magic Without Magic : John Archibald Wheeler* edited by J. Klauder (Freeman, San Francisco 1972) p231

[14] D. Ida, K. Nakao, M. Siino and S. Hayward *Phys. Rev.* **D58** 121501 (1998)

[15] S. L. Shapiro, S. A. Teukolsky and J. Winicour *Phys. Rev.* **D52** 6982 (1995)

[16] A. B. Zamolodchikov *Phys. Lett.* **117B** 87 (1982)

Stable structure of the event horizon

Tatsuhiko Koike[1]

Department of Physics, Keio University,
Hiyoshi, Kohoku, Yokohama 223-8522

Masaru Siino[2]

Graduate school of Science and Engineering, Tokyo Institute of Technology,
Oh-okayama, Meguro, Tokyo 152-8551

Abstract

Different levels of stability of the event horizon against small perturbations of light cones are defined and causal assumptions for the space-time to gurantee them are found.

1 Introduction

In the real world we only find generic black holes. For example, one does not find a perfect Schwarzschild black hole for many reasons. Nevertheless, the Schwarzschild black hole is important because many real black holes are approximately Schwarzschild. The approach via genericity which we are going to take in this talk is complementary to the approach via exact solutions. The results obtained in the context are equally true for space-times which are close to an exact solution and for those which are not. One can find the qualitative features of generic black holes first and then pursue quantitative ones for thus obtained generic blak holes.

Here we will define genericity as follows, though it could be defined in many other ways. A property of a space-time is generic if it is invariant under small changes of the metric at each point of the space-time. The origin of the small changes may be one of the following. (1) There is limitation of our ability to feel or measure the curvature of the space-time. (2) We apply a theoretical model, for example, an equation of state of the matter, to analyze the universe, and the model is usually not completely true. (3) The space-time itself may be a classical approximation of something which have small quantum fluctuations.

In this talk we will focus on small changes of causal structure and will not treat differentiability which will be treated elsewhere. We begin by the definition of future null infinity and the event horizon (Sec. 2). Then we will define stability of an event horizon when we slightly widen or narrow the light cone (Sec. 3). The aim of the talk is to clarify the notion of stability of the event horizon against small perturbation of the light cones (Sec.4) and the relationship of the stability and causality conditions (Sec. 5). There we will establish stability of the event horizon on the assumption of a certain causality condition. Sec. 6 is for summary and discussion. We will not give explicit proofs for the theorems.

2 Infinity

A space-time (M, g) is a pair of a differentiable manifold M and a Lorentian metric g on M. We assume that (M, g) is time-oriented. For simplicity we also assume that (M, g) is smooth. The space of such metrics on M is denoted by $\mathrm{Lor}(M)$. We mainly follow the notation of [1] but we explicitly include the metric g with which the causality is defined. For example, for a subset A of M, $I^+(A, U; g)$ denotes the chronological future of A within U with respect to the metric g. We usually omit U above if $U = M$.

We assume that (M, g) has a *conformal completion* $(\overline{M}, \bar{g})$ defined as follows. $\overline{M}$ is a manifold with boundary whose interior is M. The boundary $\overline{M} \setminus M$ will be denoted by $\mathcal{I}$. There is a smooth function

[1]E-mail: koike@phys.keio.ac.jp
[2]E-mail: msiino@th.phys.titech.ac.jp

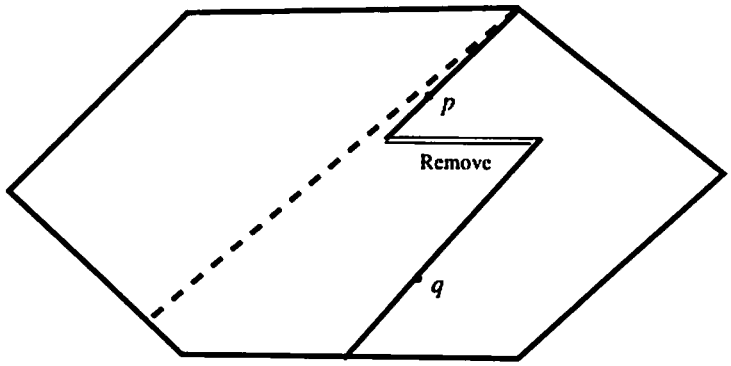

Figure 1: A space-time whose event horizon is stable but not stable.

Ω on $\overline{M}$ which is positive on M and vanishes on $\mathcal{I}$ and $d\Omega$ is nowhere vanishing on $\mathcal{I}$. The metric $\overline{g}$ is continuous on $\overline{M}$ and $\overline{g} = \Omega^2 g$ on M. We do not make causal assumptions on $\mathcal{I}$ so that the definition includes asymptotically flat or asymptotically de Sitter space-times as special cases.

The future [past] null infinity $\mathcal{I}^+$ [$\mathcal{I}^-$] is defined by

$$\mathcal{I}^{\pm} := \{p \in \mathcal{I}; I^{\mp}(p, \overline{M}; \overline{g}) \cap M \neq \emptyset\}. \tag{1}$$

The future event horizon of the space-time (M, g) is defined by $\dot{J}^-(\mathcal{I}^+, \overline{M})$, the boundary of the causal past of $\mathcal{I}^+$. All the results on the future event horizon shown below is valid for the past event horizon $\dot{J}^+(\mathcal{I}^-, \overline{M})$, which can be shown by reversing the direction of time. Hereafter we shall simply refer to future event horizons as event horizons, and we shall often denote $\dot{J}^-(\mathcal{I}^+, \overline{M}; g)$ by $EH^+(g)$.

3 Topology on the space of metrics

We define a topology on $\mathrm{Lor}(M)$ to express "small difference" of the metric precisely. We adopt C^r-(fine, or equivalently, open) topology on metrics defined as follows. Fix a locally finite atlas on M. An open set of $\mathrm{Lor}(M)$ is defined as a union of finite intersections of the sets

$$\begin{aligned} \mathcal{U}^r_{g,\delta} := \{g' \in \mathrm{Lor}(M);\ & \sup_{\beta,\gamma,|\alpha|\le r} |D_\alpha g'_{\beta\gamma}(x) - D_\alpha g_{\beta\gamma}(x)| < \delta(x) \\ & \text{for each } x \in M \text{ and for each chart at } x\}, \end{aligned} \tag{2}$$

where all Greek indices denote components with respect to the coodinate basis, α is a collective index $(\alpha_1, ..., \alpha_{|\alpha|})$, $D_\alpha := \partial_{\alpha_1} ... \partial_{\alpha_{|\alpha|}}$, $g \in \mathrm{Lor}(M)$, and δ is a positive continuous function on M. When $r = \infty$, $|\alpha| \le r$ in the definition (2) is replaced by $|\alpha| < \infty$. The topology does not depend on the choice of the atlas. The C^r-topology is strong in the sense that one can impose arbitrarily fast fall-off condition for the difference of two metrics at infinity by choise of the function δ.

A property P which depends on the metric is called *C^r-stable* if $P(g)$ implies that there is an C^r-neighbourhood $\mathcal{U}$ of g such that $P(g')$ is true for all $g' \in \mathcal{U}$. Obviously, if P is C^r-stable it is C^s-stable for all $s \ge r$. It can be shown that asymptotic flatness (which requires control over curvature) is C^r-stable if r is sufficiently large, say, $r \ge 3$. Existence of conformal completion and causal structure at infinity $\mathcal{I}$ defined in Sec. 2 is C^0-stable hence C^r-stable for any $r \ge 0$. In this talk we will consider C^0-stability. Whenever the property is only concerned with causal structure, the C^0-open set such as $\mathcal{U}$ can always be chosen as $(g_1, g_2) := \{g \in \mathrm{Lor}(M);\ g_1 < g < g_2\}$. Hereafter $g_1 > g_2$ mean that the light cone of g_1 is strictly wider than that of g_2 everywhere, *i.e.*, $g_2(X, X) \le 0$ implies $g_1(X, X) < 0$.

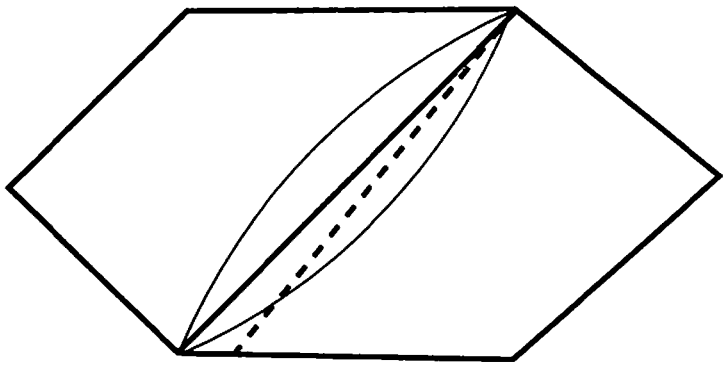

Figure 2: The Schwarzschild space-time as an example of space-time whose event horizon is stable but not uniformly stable. The space-time is globally hyperbolic.

4 Definitions of stability

Let us say that $EH^+(g)$ is *inner* [*outer*] *stable* if for each compact set K of $I^-(\mathcal{I}^+, \overline{M})$ [$M \setminus \overline{I^-}(\mathcal{I}^+, \overline{M})$] there is a C^0-neighbourhood $\mathcal{U}$ of g such that $K \subset I^-(\mathcal{I}^+, \overline{M})$ [$K \subset M \setminus \overline{I^-}(\mathcal{I}^+, \overline{M})$] for each $g' \in \mathcal{U}$. $EH^+(g)$ is *stable* if it is both inner and outer stable. Fig. 1 shows an example of space-time whose event horizon is not stable. It is the two-dimensional Schwarzchild space-time with a spacelike line segment removed. If one choose K slightly inside the horizon at q, K is not seen from $\mathcal{I}^+$ with respect to g but would be so with respect to any $g' > g$.

We can define even stronger notion of stability which we call uniform stability. The event horizon $EH^+(g)$ is *uniformly stable* if for each neighbourhood U of $EH^+(g)$ there is a C^0-neighbourhood $\mathcal{U}$ of g such that for each $g' \in \mathcal{U}$, $EH^+(g') \subset U$. Note that the definition of uniform stability is equivalent to that of stability with "compact set" replaced by "closed set."

Stability does not necessarily imply *topological stability* of the event horizon, *i.e.*, that $EH^+(g)$ and $EH^+(g')$ are not homeomorphic in general. Uniform stability, however, implies the topological stability:

Proposition 1. *Let λ be timelike fibration of M (or its suitable subset) such that λ_q denotes If $EH^+(g)$ is uniformly stable then for each neighbourhood U of $EH^+(g)$ there is a C^0-neighbourhood $\mathcal{U}$ of g such that for each $g' \in \mathcal{U}$ the map $\phi_{\lambda,g'} : q \mapsto \lambda_q \cap EH^+(g')$ is a Lipshitz homeomorphism from $EH^+(g)$ onto $EH^+(g')$.*

5 Stability and causality: results

In this section we state the relationship of the stability and the causal conditions. First, the event horizon has a good property against narrowing perturbation without any causal assumption:

Theorem 1. *The event horizon is inner stable.*

Stable causality does not guarantee stability of the event horizon. In fact, the space-time shown in Fig. 1, which has an unstable event horizon, is stably causal. One needs a stronger causal condition, and can show the following:

Theorem 2. *If the space-time is causally continuous the event horizon is stable.*

A space-time (M, g) is called causally continuous [2] if the causal past I^- is outer continuous at all points. I^- is outer continuous at p if for each compact subset K of $\mathrm{int}\,(M \setminus I^-(p))$ there is a neighbourhood U of p such that for each $q \in U$, K is also contained in $\mathrm{int}\,(M \setminus I^-(q))$. Though this definition does not involve widening or narrowing of light cones, there is a result connecting them [2], which is essential for the proof of the theorem:

Lemma 1. *If (M,g) is causally continuous,* $\bigcap_{g'>g} J^-(p,\overline{M};g') = \overline{J^-}(p,\overline{M};g)$.

The event horizon is not uniformly stable in general even when the space-time is globally hyperbolic. The space-time in Fig. 2 is such an example. Nevertheless, it can be shown that a class of space-times of interest has stable event horizons. Though the assumptions below could be relaxed significantly, they are satisfied by most cases of gravitational collapse.

Theorem 3. *Let* (M,g) *be a space-time which satisfies the following.*
(a) (M,g) *is asymptotically flat.*
(b) (M,g) *is globally hyperbolic from a Cauchy surface* Σ,
(c) Σ *is homeomorphic to* $\mathbb{R}^3$.
(d) The event horizon of (M,g) *is in the future of* Σ, *i.e.,* $\Sigma \subset J^-(\mathcal{I}^+,\overline{M};g)$.
Then the event horizon of (M,g) *is uniformly stable.*

Note that condition (b) can be replaced by the following: (M,g) is strongly future asymptotically predictable from a partial Cauchy surface Σ. In fact, one can always remove a certain region inside the event horizon from such a space-time to obtain a globally hyperbolic space-time. Note also that in the theorem the components of $J^-(\mathcal{I}^+,\overline{M};g)$ can be more than one.

6 Summary and discussion

We have defined two levels of stability of the event horizon and found suitable causal assumptions to guarantee them. Since one would not find unstable event horizons in nature, it turns out that causal continuity seems a good and realistic assumption in the theoretic investigation of the event horizon. On the other hand, event horizons which appear in usual gravitational collapse are shown to be sound and topologically stable.

In Theorem 2 we needed much stronger causal assumptions than the Cauchy horizon case where strong causality gurantees stability in a similar sense [3]. The reason may be the following. For narrowing perturbations the causal structure is fairly well controled because the set of g'-timelike curves is a proper subset of the set of g-timelike curves if $g' < g$. In the event horizon case there was no need of any causal condition (Theorem 1). In the Cauchy horizon case strong causality was enough. For widening perturbations there appear new timelike curves which may behave badly. In the event horizon case one needed causal continuity of the original space-time to control them. In the Cauchy horizon case, the new domain of dependence of a partial Cauchy surface will be inside the original one which is globally hyperbolic. In other words, a very strong causality condition, global hyperbolicity, is satisfied *a priori*.

Our original motivation was to classify the stable structure of the non-differentiable subset of the event horizon whose physical significance was discussed in [4, 5, 6]. Stability of the non-differentiable subset is meaningful only when the event horizon horizon itself is topologically stable. Our Theorem 3 states that a wide class of space-time representing gravitational collapse are guaranteed to have topologically stable event horizons. Thus it provides a good setting to discuss non-differentiable subset of the event horizon. The classification will be carried out elsewhere.

References

[1] S. W. Hawing and G. F. R. Ellis, *Large scale structure of the spacetime*, Cambridge, 1973.

[2] S. W. Hawking and R. K. Sachs, *Commun. Math. Phys.* **35** (1974) 287.

[3] J. K. Beem, *Gen. Rel. Grav.* **27** (1995) 93.

[4] M. Siino, *Phys. Rev.* **D58** (1998) 064006.

[5] M. Siino, *Phys. Rev.* **D59** (1999) 064006.

[6] S. Husa and J. Winicour, *Phys. Rev.* **D60** (1999) 084019.

Characterization of curved spacetimes by means of a classical field

Masafumi Seriu[1]

Department of Physics, Faculty of Engineering,
Fukui University, Fukui, 910-8507, Japan

Abstract

We present a framework which describes the curvature information of a spacetime by means of a classical field. The central ingredient of this framework is a procedure of comparing Σ^+ (a future spatial surface) and Σ^- (a past spatial surface). For comparison, the information on Σ^- should be transmitted to Σ^+, where a classical field ϕ plays the role of a "messenger". Due to the curvature between Σ^+ and Σ^-, the information coded in ϕ is distorted, thereby the discrepancy between Σ^+ and Σ^- indirectly describes the curvature information in between. We introduce a natural measure of comparison, $d_N(\Sigma^+, \Sigma^-)$, which efficiently characterizes the curvature of the spacetime.

We then study a relation between the present framework and the standard field theoretical treatment. Quite surprisingly, it is possible to interpret our measure of comparison ($d_N(\Sigma^+, \Sigma^-)$) as the net particle creation between Σ^+ and Σ^-, if the curvature is not very large (compared to the cut-off scale). It suggests that a large portion of the black-hole thermodynamics could be described purely in classical terms, which is reasonable since black holes are essentially classical, geometrical objects. The present framework extracts purely geometrical features of a spacetime; it might be useful to clarify the origin of the black-hole thermodynamics by separating its purely classical, geometrical features from the quantum ones.

1 Introduction

It is well-known that black holes behave just like a thermodynamical system, when parameters are sutably identified with thermodynamical variables, such as mass $M \sim$ internal energy E, area of horizon $A \sim$ entropy S, surface gravity $\kappa \sim$ temperature T. It is also known that part of such thermodynamical behavior of black holes are *compatible* with the behavior the quantum field on a blsck-hole spacetime.[2] Namely, the discrepancy between the in- and the out- vacuums causes the particle-creation, which follows the Planckian-spectrum with the temperature T given by the surface gravity κ, as $k_B T = \kappa/2\pi$. However, the origin of the black-hole thermodynamics still remains an unresolved issue. Considering that a black hole is a purely classical, geometrical object, it is meaninful to make it clear to what extent *quantum* field is essential in these arguments. It is possible that the *field* property of a quantum field is playing a more important role than its *quantum* property. Therefore, let us try to characterize a black hole in purely geometrical terms, using a *classical* field as a probe of spacetime structures.

Instead of considering a black-hole spacetime itself, here we focus on a more well-defined situation: Suppose a curvature region C is compact and it is sandwitched by the in- and out- spatial surfaces, Σ^+ and Σ^-, that are both spatially flat. (Here Σ^+ and Σ^- are located in the future and the past of the region C, respectively.) For simplicity, we assume that Σ^+ and Σ^- are congruent to each other throughout this paper.

Now our basic procedure is to compare these two spatial surfaces Σ^+ and Σ^- using a *classical* field ϕ. For comparing Σ^+ and Σ^- to each other, we need some "messenger" who carries the information on Σ^- all the way up to Σ^+. Here the classical field ϕ plays the role of the messenger. On its way up to Σ^+, the field ϕ feels the curvature in the region C, so that its "message" is distorted influenced by the curvature. In this way, by comparing Σ^+ and Σ^-, we can indirectly measure the curvature information on C, using the classical field as a probe.

[1] E-mail:mseriu@edu00.f-edu.fukui-u.ac.jp

[2] *Compatibility* between A and B does not necessarily imply one among them being the origin of the other. Regarding the black-hole thermodynamics, we should always keep this point in mind.

2 General comparison procedure

There is a convenient general procedure for comparing two objects, when they are not easy to compare with each other directly. Suppose we want to compare two objects a and a'. We introduce a normalized, positive-definite function $p_a(\cdot)$ corresponding to the object a;

$$p_a(x) \geq 0 \quad , \quad \int_\Omega d\mu(x)\, p_a(x) \;= 1 \quad , \tag{1}$$

where Ω is a suitable integral region for the variable x. Here the shape of the function p_a is so chosen as to reflect a particular property of a in concern. A function $p_{a'}(\cdot)$ is chosen corresponding to a' in the same manner. (A simple example is the comparison of two positive numbers σ and σ'; it is achieved by comparing two Gaussian functions $p_\sigma(\cdot)$ and $p_{\sigma'}(\cdot)$ with the dispersion σ and σ', respectively.)

Now the overlapping-integral between $p_a(\cdot)$ and $p_{a'}(\cdot)$ reflects the similarity of the shapes of p_a and $p_{a'}$, so that it indirectly compares a and a';

$$\xi_\Omega(a,a') := \int_\Omega d\mu(x)\, (p_a(x)p_{a'}(x))^{1/2} \quad . \tag{2}$$

This ξ has nice properties as

(i) $\xi_\Omega(a,a') = \xi_\Omega(a',a)$,

(ii) $0 \leq \xi_\Omega(a,a') \leq 1$;
where $\xi_\Omega(a,a') = 1 \iff p_a(\cdot) \equiv p_{a'}(\cdot) \iff a = a'$, and $\xi_\Omega(a,a') = 0 \iff p_a(\cdot)p_{a'}(\cdot) \equiv 0$.

Thus, we can introduce a measure of comparison between a and a';

$$d_\Omega(a,a') := -\ln \xi_\Omega(a,a') \quad . \tag{3}$$

Corresponding to the above properties for $\xi(a,a')$, $d_\Omega(a,a')$ satisfies

(i) $d_\Omega(a,a') = d_\Omega(a',a)$,

(ii) $d_\Omega(a,a') \geq 0$ where $d_\Omega(a,a') = 0 \iff a = a'$.

3 Curvature information detected by the comparison procedure

Now we consider the spacetime introduced in Sec. 1. We take a classical massless Klein-Gordon field ϕ. The dynamical equation for ϕ, $\Box\phi = 0$, induces the eigenvalue problem of the form $\Delta f = -\omega^2 f$ on Σ^+ and Σ^- (Here f denotes a function induced from ϕ on Σ^+ or Σ^-). Then we get the set of basic modes $\{f_i,\ \omega_i\}$ on Σ^+, and the same on Σ^-, $\{\bar{f}_k, \bar{\omega}_k\}$.

Now two spatial surfaces Σ^+ and Σ^- correspond to the two objects to be compared, a and a', in the previous section. Then we choose a suitable functional $P_\Sigma(f)$ which plays the role of the previous function $p_a(x)$. To take the over-lapping functional integral between $P_{\Sigma^+}(\cdot)$ and $P_{\Sigma^-}(\cdot)$, we need to assign how to identify a function defined on Σ^+ with another function defined on Σ^-. In this case, this identification is carried out by means of the dynamical equation $\Box f = 0$; the dynamical equation defines a S-matrix which carries the modes $\bar{f}_i$'s defined on Σ^- onto Σ^+.

In this manner, the overlapping-integral can be evaluated on Σ^+, which naturally picks up the information of the curvature though S-matrix.

The basic modes f_i's and $\bar{f}_i$'s are normalized on each slice,

$$\langle f_i, f_j \rangle_{\Sigma^+} = \delta_{ij} \quad , \quad \langle \bar{f}_i, \bar{f}_j \rangle_{\Sigma^-} = \delta_{ij} \quad , \tag{4}$$

where $\langle f, g \rangle_\Sigma := \int_\Sigma f\, g$.

The basic modes $\bar{f}_i$'s defined on Σ^- evolve onto Σ^+, where it is expanded in terms of the mode f. This evolutional effect is described by a matrix γ, which is essentially an orthogonal matrix;

$$\bar{f}_j = \gamma_{ji} f_i \quad . \tag{5}$$

For taking the overlapping functional-integral, we identify a function on Σ^+ and a function on Σ^- when the expantion coefficients are identical. Then, $\bar{f}$'s are developed onto the surface Σ^+ by means of the matrix γ;

$$f = \sum_i c_i f_i \quad , \quad \bar{f} = \sum_j c_j \bar{f}_j = \sum_j c_j \gamma_{ji} f_i \quad . \tag{6}$$

Now we need to choose the functional $P_\Sigma[\cdot]$. As one natural choice, we choose $P_\Sigma[f] := \exp -\langle \partial f \, , \partial f \rangle_{\Sigma^+}$, where $\langle \partial f \, , \partial f \rangle := \int_\Sigma \partial^a f \; h_{ab} \; \partial^b f \sqrt{h}$.

Due to Eqs.(6) and (4), this functional is evalueted on Σ^+ and Σ^- as

$$\begin{aligned} P_{\Sigma^+}[f] &= \exp(-\langle \partial f \, , \partial f \rangle_{\Sigma^+}) = \exp(-\frac{1}{2} c^T \Lambda c), \\ P_{\Sigma^-}[f] &= \exp(-\langle \partial \, Sf \, , \partial \, Sf \rangle_{\Sigma^+}) = \exp(-\frac{1}{2} c^T \gamma \Lambda \gamma^T c) \quad , \end{aligned} \tag{7}$$

where $\Lambda := diag(\omega_1^2, \omega_2^2, \cdots, \omega_N)$. By taking the overlapping-integral between P_{Σ^+} and P_{Σ^-} (see Eq.(2)), we get the formula,

$$\xi_N(\Sigma^+, \Sigma^-) = \int [df]_N (P_{\Sigma^+}[f] P_{\Sigma^-}[f])^{1/2} = \left\{ \frac{\det \Lambda}{\det \frac{1}{2}(\Lambda + \gamma \Lambda \gamma^T)} \right\}^{1/2} \quad . \tag{8}$$

Here $\int [df]_N$ corresponds to $\int_\Omega d\mu(x)$ in Eq.(1), and the suffix N indicates that the fonctional integral is evaluated only up to the N-th eigenmode component. When f is expanded as $f = \sum_k c_k f_k$, we evaluate the integral by replacing f with $\sum_{k=1}^N c_k f_k$. (This correponds to restricting the integral region to Ω in Eq.(1).) Due to this cut-off, scale-dependent features of the spacetime structure are described. This is the advantage of the present framework, since spacetime physics requires scale-dependent treatment.

One can show the matrix version of the well-known inequality, $\frac{a+b}{2} \geq \sqrt{ab}$ for $a, b > 0$.

Theorem

For any positive-definite, real symmetric matrices A and B it follows that

$$\det \frac{1}{2}(A + B) \geq (\det AB)^{1/2}$$

where $=$ holds when and only when $A = B$.

Thus, the quantity ξ in Eq.(8) manifestly satisfies,

(i) $\xi_N(\Sigma^+, \Sigma^-) = \xi_N(\Sigma^-, \Sigma^+)$,

(ii) $0 \leq \xi_N(\Sigma^+, \Sigma^-) \leq 1$.

Following the general comparison procedure in Sec.2, we get the measure of comparison between Σ^+ and Σ^-.

$$d_N(\Sigma^+, \Sigma^-) := -\ln \xi_N(\Sigma^+, \Sigma^-) = \frac{1}{2} \ln \det \frac{1}{2}(1 + \Lambda^{-1/2} \gamma \Lambda \gamma^T \Lambda^{-1/2}) \quad . \tag{9}$$

Here we note that when the spacetime is flat, the matrix γ becomes trivial, then this measure d_N becomes zero. Therefore, d_N *reflects the curvature information between Σ^+ and Σ^- detected by a classical field.*

4 Relation to the particle creation picture

Though our analysis so far has been done purely in classical terms, it is meaningful to clarify its relation to the standard particle-creation picture.

Usually a scalar field is expanded in terms of complex-valued modes u_i's normalized by the Klein-Gordon inner-product, while in our framework, the field is expanded in terms of the real-valued modes;

$$f = \sum_i (a_i u_i + a_i^\dagger u_i^*) = \sum_i (c_i^{(1)} f_i^{(1)} + c_i^{(2)} f_i^{(2)}) \quad .$$

Here the fuffices (1) and (2) in $f_i^{(1)}$ and $f_i^{(2)}$ describe the degeneracy of the mode. [3] There is a relation between two frameworks, and one can find the relation of our expansion coefficients $c_i^{(1)}$ and $c_i^{(2)}$ with the creation and annihilation operators, a_i and $a_i^\dagger$ that would arise *if the classical field we use were qunatized*;

$$\begin{aligned} a_i &= \sqrt{\omega_i}(c_i^{(1)} - ic_i^{(2)}) \ , \ a_i^\dagger = \sqrt{\omega_i}(c_i^{(1)} + ic_i^{(2)}) \\ c_i^{(1)} &= \frac{1}{2\sqrt{\omega_i}}(a_i + a_i^\dagger) \ , \ c_i^{(2)} = \frac{i}{2\sqrt{\omega_i}}(a_i - a_i^\dagger) \ . \end{aligned}$$

Accordingly the matrix γ is related to the Bogolubov coefficients;

$$\begin{aligned} |\alpha_{ji}|^2 &= \frac{1}{4}\frac{\omega_i}{\bar{\omega}_j}\left\{(\gamma_{ji}^{(11)} + \gamma_{ji}^{(22)})^2 + (\gamma_{ji}^{(21)} - \gamma_{ji}^{(12)})^2\right\} \\ |\beta_{ji}|^2 &= \frac{1}{4}\frac{\omega_i}{\bar{\omega}_j}\left\{(\gamma_{ji}^{(11)} - \gamma_{ji}^{(22)})^2 + (\gamma_{ji}^{(21)} + \gamma_{ji}^{(12)})^2\right\} \ . \end{aligned}$$

With these relations, one can give an interpretation in terms of the standard particle creation picture to our comparison measure, d_N;

$$\begin{aligned} d_N(\Sigma^+, \Sigma^-) : &= \frac{1}{2}\ln\det\frac{1}{2}(1 + \Lambda^{-1/2}\gamma\Lambda\gamma^T\Lambda^{-1/2}) \simeq \frac{1}{4}\mathrm{Tr}\left(\Lambda^{-1/2}\gamma\Lambda\gamma^T\Lambda^{-1/2} - I_{2N}\right) \\ &\simeq \frac{1}{2}\mathrm{Tr}\left(\alpha\alpha^\dagger + \beta\beta^\dagger\right) - \frac{N}{2} \\ &\simeq \mathrm{Tr}\ \beta\beta^\dagger = \sum_{i=1}^{N}\langle 0|\tilde{N}_i|0\rangle \end{aligned}$$

Thus, one finds that *the comparison measure d_N approximately reduces to the amount of the particle creation between Σ^+ and Σ^-*, when the spacetime curvature is not large compared with the cut-off frequency, ω_N^2.

5 Discussion

We have presented a framework which describes geometrical structures of a spacetime through the comparison between Σ^+ and Σ^- using a classical field as a medium. We should keep in mind that black holes are essentially classical, geometrical objects, and at least portion of their thermodynamical behavior should be attributed to purely geometrical aspects of black holes. The standard field theoretical approach to the black-hole thermodynamics is, though its attractive outlook, prone to miss the essence of the mechanism since it additionally introduces new elemets-quantum aspects- which may not be necessarily essential in the arguments. Cosidering this point, the present framework is expected to be quite useful for clarifying the origin of the black-hole thermodynamics.

References

[1] For instance, G.F.R. Ellis, in *"Proceedings of the Tenth International Conference on General Relativity and Gravitation"*, edited by B. Bertotti, F. De Felice and A. Pascolini (Reidel, Dordrecht, 1984). See also, A. Krasiński, *Inhomogeneous Cosmological Models* (Cambridge University Press, Cambridge, 1997), Chapter 8, and the references therein.

[2] M. Kac, Am. Math. Mon. **73**(4) (1966), 1.

[3] M. Seriu, Physical Review **D53** (1996) 6902.

[3] Roughly speaking, their typical functional forms are $u_i \sim \exp ikx$, $f_i^{(1)} \sim \cos kx$ and $f_i^{(2)} \sim \sin kx$.

[4] M. Seriu, in *"Proceedings of the 8th Workshop on General Relativity and Gravitation"* (K.Oohara et. al. (eds.), Niigata University, 1999).

[5] M. Seriu, Communications in Mathematical Physics **209** (2000) 393.

[6] M. Seriu, Physical Review **D62** (2000) #023516.

[7] M. Seriu, General Relativity and Gravitation **32** (2000) 1473.

[8] See e.g., I. Chavel, *Eigenvalues in Riemannian Geometry* (Academic Press, Orland, 1984).

[9] M. Visser, Physical Review D41 (1990) 1116.

[10] M. Seriu, Physics Letters **B319** (1993) 74.

[11] M. Seriu, "Evolution of the discrepancy between the real Universe and its model", submitted for publication.

Hawking radiation in an expanding universe

Hiromi Saida[1]

Department of Natural Environment,
Graduate School of Human and Environmental Studies,
Kyoto University, [2]
Sakyo-ku, Kyoto 606-8247, Japan

Abstract

The Hawking radiation forms the essential basis of the black hole thermodynamics. The black hole thermodynamics denotes a nice correspondence between black hole kinematics and the laws of ordinary thermodynamics, but has been so far considered only in an asymptotically flat case. *Does such the correspondence rely strongly on the vanishing feature of the gravity at the infinity?* In order to resolve this question, it should be considered for the first to extend the Hawking radiation to a case with a dynamical boundary condition. Therefore the Hawking radiation in an expanding universe is discussed in this talk. As a concrete model of a black hole in an expanding universe, we use the swiss cheese universe which is the spacetime including a Schwarzshild black hole in the Friedmann-Robertson-Walker universe. Further for simplicity, our calculation is performed in two dimension. The resultant spectrum of the Hawking radiation measured by a comoving observer is totally different from a thermal one, and it seems that its intensity is enhanced by the presence of a cosmological expansion. It is appropriate to say that *a black hole with an asymptotically flat boundary condition stays in a lowest energy thermal equilibrium state, and that, once a black hole is put into an expanding universe, it is excited to a non-equilibrium state and emits its mass energy faster than a thermal one.* But we cannot search which non-equilibrium state the black hole in an expanding universe is excited to.

1 Introduction

So far various properties of black hole spacetimes have been revealed. Among so many well-known properties of the black hole, one of the most remarkable ones is the black hole thermodynamics. This tells us a nice correspondence between the classical properties of a black hole spacetime and the laws of ordinary thermodynamics [2]. The black hole thermodynamics is one of the most important stages for understanding the nature of a strong gravity. However this nice correspondence has been considered only in an asymptotically flat case. *Does such the correspondence rely strongly on the vanishing feature of the gravity at the infinity?* It has not been clarified if such the correspondence is true of the case with a dynamical boundary condition. [3] My general purpose is to *extend the black hole thermodynamics to a dynamical situation, and hopefully find a non-gravitational system which corresponds to a black hole with a dynamical boundary condition like an expanding universe.* By the way, the Hawking radiation plays the essential role in the black hole thermodynamics to determine precisely the temperature of a black hole with asymptotically flatness [3]. Hence, as the first step for my purpose, this talk is designed for the Hawking radiation in an expanding universe.

A black hole cannot be defined unless the asymptotic structure of the spacetime is known [4]. However, under a dynamical boundary condition, it is generally quite difficult to extract the asymptotic structure of the spacetime directly from the Einstein equation. Then, in order to avoid the problem of defining the black hole, we make use of the *swiss cheese universe* (SCU) [5]. The SCU is the spacetime including a Schwarzschild black hole in a Friedmann-Robertson-Walker (FRW) universe. It is not the solution obtained by solving directly the Einstein equation, but the solution constructed by connecting

[1] E-mail: saida@phys.h.kyoto-u.ac.jp

[2] From Apr.2002 attached to: Dpt. of Math. and Phys., Grad. Sch. of Science, Osaka city university

[3] It is not too much to say that only a few studies have been done on the issue of a black hole in some dynamical background [1].

the Schwarzschild spacetime with the FRW universe at a given spherically symmetric timelike hypersurface Σ by the Israel junction condition [6] with requiring no surface energy density confined on Σ. In considering a spatial slice of Σ which is the two dimensional sphere, it is expanding as seen from the black hole side with respect to the Schwarzschild coordinate. So once the two sphere (on Σ) was placed outside the gravitational radius $R_g = 2GM$ at a given time, the event horizon should last to exist after that time. That is, the existence of a black hole is guaranteed in the SCU.

Though the SCU allows us to define a black hole, another technical problem is still left. Even if with the asymptotic flatness, it is very difficult to obtain a complete form of the Hawking spectrum for four dimensional case because of the curvature scattering. Indeed, the curvature scattering is ignored in the statement that an asymptotically flat black hole is in a thermal equilibrium state. However due to the conformal flatness of general two dimensional spacetimes, we can neglect the curvature scattering in two dimensional case for a minimal coupling massless scalar field. Therefore in this talk, we treat the SCU in two dimension for simplicity, and introduce the minimal coupling massless scalar field for calculating the Hawking radiation.

In section 2, we explain the two dimensional "eternal" SCU and show the strategy to obtain the Hawking radiation. The behavior of a minimal coupling massless scalar field on the eternal SCU is analyzed in section 3. Section 4 is devoted to computing the Hawking radiation. Summary and discussions are given in section 5. The unit throughout is $c = \hbar = k_B = 1$. The metric signature is $(-,+,+,+)$ for four dimension and similarly for two dimension.

2 "Eternal" swiss cheese universe and the strategy

2.1 Two dimensional "eternal" SCU

The two dimensional SCU is constructed by connecting a Schwarzschild black hole with a FRW universe at a given timelike surface (curve) Σ. The metrics are given by these forms,

$$\begin{aligned} \textit{BH-side} \quad &: \quad ds^2 = -\left(1-\frac{R_g}{R}\right)dT^2 + \left(1-\frac{R_g}{R}\right)^{-1} dR^2 \\ \textit{FRW-side} \quad &: \quad ds^2 = -dt^2 + a^2\,\frac{dr^2}{1-kr^2}\,, \end{aligned}$$

where $R_g = 2GM$, M is the mass of the black hole and k is the spatial curvature of the universe outside the black hole. The junction surface Σ is set to be expanding in the BH-side and comoving with the FRW-side, $R(t) = a(t)\,r_0$, where $R(t)$ denotes the radial coordinate of Σ measured in the BH-side and r_0(=constant) is the comoving radius of Σ measured in the FRW-side.

If one consider the four dimensional case, the relation of temporal coordinates T and t on Σ can be obtained via the Israel junction condition without requiring any matter density confined on Σ [5], where the equation of state of the matter on the FRW-side should also be used. However for our two dimensional case, because no matter can exist on any two dimensional spacetimes, the matter equation does not exist, and consequently the relation between T and t is left arbitrary. By the way, the requirment of absence of any matter on Σ is automatically satisfied for two dimensional case. Therefore we assume that the temporal coordinates T and t on Σ are related by the same equation as for four dimensional case,

$$\frac{dT(t)}{dt} = \frac{\sqrt{1-kr_0^2}}{1-R_g/R(t)}\,.$$

Further, due to the absence of any matter on two dimensional SCU, the scale factor $a(t)$ is left undetermined. Hereafter we require that Σ stays outside the gravitational radius for infinite temporal interval, $R(t) > R_g$ for $-\infty < t < \infty$. That is, our background spacetime is the "eternal" SCU. The conformal diagram is given at the figure 1, where the two exterior regions of the eternal SCU are distinguished by "R-region" and "L-region".

2.2 Strategy for the Hawking radiation

We aim to compute the Hawking radiation received by the observer comoving in the FRW-side.

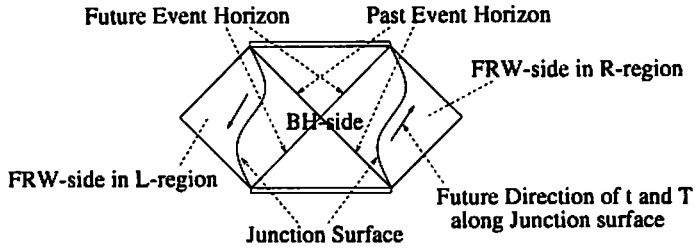

Figure 1: Two dimensional eternal swiss cheese universe.

For the first, we should quantize the massless sclar field Φ, and prepare the following three vacuum states,

$$\begin{aligned} |0\rangle_{KS} &= \text{Vacuum state w.r.t. Kruskal-Szekeres system of BH-side} \\ |0\rangle_{Sch} &= \text{Vacuum state w.r.t. Schwarzschild system of BH-side} \\ |0\rangle_{Cmv} &= \text{Vacuum state w.r.t. Comoving system of FRW-side.} \end{aligned}$$

That is, for example, $|0\rangle_{KS}$ is the vacuum state obtained by quantizing Φ with respect to the positive and negative frequency modes of the Kruskal-Szekeres coordinate system of the BH-side.

Next, we construct the initial vacuum state $|0\rangle_{in}$ in a similar way to the Unruh vacuum state [7],

$$|0\rangle_{in} = \begin{cases} |0\rangle_{KS} & \text{on the past event horizon} \\ |0\rangle_{Cmv} & \text{on the past null infinity} \end{cases} .$$

And because the observer is in the FRW-side and comoving with the cosmological expansion, the vacuum state corresponding to the observer is $|0\rangle_{Cmv}$ on the future null infinity.

Finally, we can calculate the spectrum of the Hawking radiation as $I_{HR}(\omega) = {}_{in}\langle 0| N_\omega |0\rangle_{in}$, where N_ω is the number operator of the "comoving" particle and ω is the frequency of the radiation received by the comoving observer. Since ${}_{Cmv}\langle 0| N_\omega |0\rangle_{Cmv} = 0$, I_{HR} is simplified to be

$$I_{HR} = {}_{KS}\langle 0| N_\omega |0\rangle_{KS} .$$

This expectation value is calculated by the successive Bogoljubov transformations: first transformation is from $|0\rangle_{KS}$ to $|0\rangle_{Sch}$ and second one is from $|0\rangle_{Sch}$ to $|0\rangle_{Cmv}$. The first transformation has to create the thermal spectrum [7]. The second one should raise the effects of the cosmological expansion onto the thermal spectrum.

3 Massless scalar field in the eternal SCU

In order to carry out the strategy, the positive frequency mode is needed. The positive frequency mode of positive (or negative) wave number is the out-going (or in-going) mode. Therefore the central task for our strategy is to solve the Klein-Gordon equation $\Box\Phi = 0$ on the SCU and find the out-going mode. The mode solution on the SCU is obtained by connecting the ordinary mode solution on the Schwarzschild spacetime and that on the FRW spacetime. To do so, the junction condition of Φ at Σ should be specified. As the junction condition, we require that no potential of Φ is confined at Σ,

$$\Phi_{BH}|_\Sigma = \Phi_{FRW}|_\Sigma \quad \text{and} \quad \partial_n\Phi_{BH}|_\Sigma = \partial_n\Phi_{FRW}|_\Sigma , \tag{1}$$

where Φ_{BH} and Φ_{FRW} are the scalar field evaluated in the BH-side and FRW-side respectively and $\mathbf{n}$ is the unit normal vector to Σ. [4]

[4] If a potential of Φ is confined on Σ, the derivative $\partial_n\Phi$ is not continuous through Σ.

Then due to the absence of the potential at Σ, no reflection of Φ takes place at Σ. That is, for example, the monochromatic out-going mode of frequency Ω in the BH-side with respect to the Schwarzschild system connects to a superposition of out-going modes in the FRW-side. This mode looks like,

$$\Phi_{Sch,\Omega} = \begin{cases} \phi_{Sch,\Omega} & \text{in BH-side} \\ \int d\omega A_{\Omega,\omega}\, \phi_{Cmv,\omega} & \text{in FRW-side} \end{cases}, \tag{2}$$

where $\phi_{Sch,\Omega}$ and $\phi_{Cmv,\omega}$ are respectively the out-going solution of $\Box\phi = 0$ on the Schwarzchild spacetime and that on the FRW spacetime. The junction coefficient $A_{\Omega,\omega}$ is determined by the conditions (1) to be

$$A_{\Omega,\omega} = \frac{e^{-i\omega r_0^*}}{2\pi}\sqrt{\left|\frac{\omega}{\Omega}\right|}\int_{-\infty}^{\infty} d\eta\, \exp\left(i\omega\eta - i\Omega\left[T(\eta) - R^*(\eta)\right]\right) \tag{3}$$

where η is the conformal time of the FRW-side and $R^*(\eta)$ and r_0^* are the radial coordinates at Σ. By quantizing Φ with respect to this mode, we can construct the vacuum state $|0\rangle_{Sch}$. The other vacuum states, $|0\rangle_{KS}$ and $|0\rangle_{Cmv}$, can also be constructed by the similar way.

4 Hawking radiation in the SCU

By the successive Bogoljubov transformation, we find the Hawking spectrum,

$$I_{HR}(\omega) = {}_{KS}\langle 0|\, N_\omega\, |0\rangle_{KS} = \int_0^\infty d\Omega\, \frac{1}{e^{2\pi\Omega/\kappa} - 1}\, D_H(\Omega,\omega),$$

where the *deviation factor* D_H is

$$D_H(\Omega,\omega) = |A_{\Omega,\omega}|^2 + e^{2\pi\Omega/\kappa}\, |A_{\Omega,-\omega}|^2 + 2\, e^{\pi\Omega/\kappa}\, \Re\left(A^{(1)}_{\Omega,\omega}\, A^{(1)}_{\Omega,-\omega}\right),$$

where $\Re$ denotes the real part, and $\kappa = 1/2R_g$. The factor $e^{\pi\Omega/\kappa}$ is the effect of the first Bogoljubov transformation, $|0\rangle_{KS} \to |0\rangle_{Sch}$. The junction coefficient $A_{\Omega,\omega}$ comes from the second transformation, $|0\rangle_{Sch} \to |0\rangle_{Cmv}$. In order to see some concrete forms of I_{HR}, we should specify the form of $a(t)$ which is included in the equation (3).

For the case $a(t) =$ const., the resultant spectrum is $I_{HR}(\omega) = b_c\,(e^{2\pi/b_c\kappa} - 1)^{-1}\,\delta(0)$, where $b_c = dT/dt$ =constant. The divergence of $\delta(0)$ comes from the infinite interval of integral in (3).

When $T(\eta) - R^*(\eta) = c\eta^2 + b\eta + p$, it is found that $a(t) \propto t$, which corresponds to the open FRW universe at remote future $t \to \infty$. The equation (3) can be calculated exaclty, and gives the spectrum,

$$I_{HR}(\omega) = \omega \int_0^\infty d\Omega\, \frac{1}{4\pi c\,\Omega^2}\left[\frac{e^{2\pi\Omega/\kappa} + 1}{e^{2\pi\Omega/\kappa} - 1} + \frac{2\, e^{\pi\Omega/\kappa}}{e^{2\pi\Omega/\kappa} - 1}\cos\left(\frac{b^2\Omega^2 + \omega^2}{2c\,\Omega} - 2\Omega p - \frac{\pi}{2}\right)\right]. \tag{4}$$

Finally consider the case $a(\eta) = b\arctan(\eta/\sigma) + c$, for which $A_{\Omega,\omega}$is not exactly computable. We assume $\sigma \gg R_g$ and $c \gg b \gg 1$, and further approximate $T(\eta) - R^*(\eta)$ up to the leading term of b/c and $O(\eta/\sigma)^3$. Then the spectrum contributed from the cosmological expansion era, $-\sigma < \eta < \sigma$, is evaluated to be

$$\begin{aligned} D_H(\Omega,\omega) \;\sim\; & \frac{\omega}{27\Omega^2 H_3}\Big[\, |\omega - \Omega H_1|\, F^2_{\Omega,\omega} + e^{2\pi\Omega/\kappa}\,(\omega - \Omega H_1)\, F^2_{\Omega,-\omega} \\ & + 2\, e^{\pi\Omega/\kappa}\sqrt{|\omega^2 - \Omega^2 H_1{}^2|}\,\cos(2\,\Omega H_c)\; F_{\Omega,\omega}\, F_{\Omega,-\omega}\,\Big], \end{aligned} \tag{5}$$

where $H_3 = b r_0/3\sigma^3$, $H_1 = c\sqrt{1 - k r_0^2}$, $H_c =$ an integration constant, and $F_{\Omega,\omega}$ is given using the Bessel functions $J_{\pm 3/2}$,

$$F_{\Omega,\omega} = J_{-1/3}\left[2\left(\frac{|\omega - \Omega H_1|}{3(\Omega H_3)^{1/3}}\right)^{3/2}\right] - \mathrm{sgn}(\omega - \Omega H_1)\, J_{1/3}\left[2\left(\frac{|\omega - \Omega H_1|}{3(\Omega H_3)^{1/3}}\right)^{3/2}\right].$$

The amplitude for this case behaves like $I_{HR}(\omega) \sim \sqrt{\omega}$ as $\omega \to \infty$.

5 Summary and discussion

We have calculated the Hawking spectrum I_{HR} on the eternal SCU. Our two dimensional analysis does not include the cosmological particle creation, since the minimal coupling massless scalar field in two dimension cannot cause particle creation as explained in [8]. So the deviation factor D_H expresses purely the effects of the cosmological expansion onto the Hawking radiation.

The resulant spectrum I_{HR} differs totally from the thermal one. The naive reason for the non-thermality is that, as denoted at (2), a monochromatic mode of Φ connects to a superposition of monochromatic modes through Σ, that is, the doppler effect by the conditions (1) creates a non-thermal distribution of the particle.

The divergence of $\delta(0)$ for the case a = constant may be normalized by considering the radiation during a finite time interval, that is, by restricting the integration interval of η in (3) to a finite one. By the similar way, the high frequency divergence of I_{HR} for (4) and (5) may also be noramlized. If the intensity of the radiation is stronger than the thermal spectrum after normalizing I_{HR}, it is probable that *a black hole with an asymptotically flat boundary condition stays in a lowest energy thermal equilibrium state, and that, once a black hole is put into an expanding universe, it is excited to a non-equilibrium state and emits its mass energy faster than a thermal one.*

At present, due to the high frequency divergence of I_{HR}, the physical interpretaions of the form of I_{HR} for the cases (4) and (5) are not clear. Therefore for future, firstly, we should develop the analysis given here to make I_{HR} be finite. Then we should search the non-gravitational and non-equilibrium system to which the black hole in an expanding universe would correspond.

References

[1] Barrow J.D., 1992 *Phys.Rev.*D46 R3227; Barrow J.D. and Carr B.J., 1996 *Phys.Rev.*D54 3920; Shibata M. and Sasaki M., 1999 *Phys.Rev.*D60 084002; Jacobson T., 1999 *Phys.Rev.Lett.*83 2699; Saida H. and Soda J., 2000 *Class.Quant.Grav.*17 4967; Harada T., Carr B.J. and Goymer C.A., 2001 *Preprint* astro-ph/0102058 (submitted to *Phys.Rev.*D); Sakai N. and Barrow J.D., 2001 *Class.Quant.Grav.*18 4717

[2] See for example and the references therein, Wald R.M., 1994 *"Quantum Field Theory in Curved Spacetime and Black Hole Thermodynamics"*, the University of Chicago Press

[3] Hawking S.W., 1975 *Commun.Math.Phys.*43 199

[4] Hawking S.W. and Ellis G.F.R., 1973 *"The large scale structure of space-time"*, Cambridge University Press

[5] Dyer C.C. and Oliwa C., 2000 *Preprint* astro-ph/0004090

[6] Israel W., 1966 *Nuovo Cim.*44B 1, 1967 *Nuovo Cim.*48B 463

[7] Unruh W.G., 1976 *Phys.Rev.*D14 870

[8] See for expample the section 3.4: Birrell N.D. and Davies P.C.W., 1982 *"Quantum fields in curved space"*, Cambridge University Press

Gravitation and cosmology in a brane-universe

David Langlois[1]

Institut d'Astrophysique de Paris,
98bis Boulevard Arago, 75014 Paris, France

Abstract

Recent theoretical developments have generated a strong interest in the "brane-world" picture, which assumes that ordinary matter is trapped in a three-dimensional submanifold, usually called brane, embedded in a higher dimensional space. The purpose of this review is to introduce some basic results concerning gravity in these models and then to present various aspects of the cosmology in a brane-universe.

1 Introduction

The idea that our world may contain hidden extra dimensions is rather old since one can trace this idea, in the modern context of general relativity, back to the beginning of the twentieth century, with the pioneering works of Kaluza and Klein, trying to reinterpret electromagnetism as a geometrical effect from a fifth dimension. The idea of extra-dimensions was revived more recently with the advent of string theory as the most promising avenue for conciling gravitation and quantum field theory. In order to get a consistent theory at the quantum level, ten spacetime dimensions are needed in superstring theories, which means that six dimensions must be somehow hidden to four-dimensional observers such as us.

The simplest way to hide extra dimensions is to assume that they are flat, compact with a radius sufficiently small to be unobservable. Consider for example the case of one extra-dimension described by the coordinate y and compactified via the identification

$$y \to y + 2\pi R,$$

R being the "radius" of the extra-dimension. Any matter field, for example a scalar field, depends on both the ordinary spacetime coordinates x^μ and the extra-coordinate y. It can be Fourier expanded along the extra-dimension so that

$$\phi(x^\mu, y) = \sum_{p=-\infty}^{\infty} e^{ipy/R} \phi_p(x^\mu). \tag{1}$$

The corresponding Fourier modes ϕ_p are designated as Kaluza-Klein modes, and each of them can be seen as a four-dimensional scalar field satisfying the four-dimensional Klein-Gordon equation with the effective squared mass

$$M_p^2 = m^2 + \frac{p^2}{R^2}. \tag{2}$$

A simple way to identify an extra-dimension would thus be to detect the characteristic spectrum of the Kaluza-Klein modes. To do this one needs enough energy to excite a least the first Kaluza-Klein modes and the non observation of Kaluza-Klein modes can be interpreted as meaning that the size of the extra-dimension is smaller than the inverse energy scale probed by the experiment. Present constraints from colliders thus imply

$$R \lesssim 1 \text{ (TeV)}^{-1}.$$

Let us now turn to gravity. The natural way to extend Einstein gravity to higher dimensions is to start from the Einstein-Hilbert action defined in a generalized spacetime with, say, n extra-dimensions:

$$S_{grav} = \int d^4x d^n y \frac{R}{2\kappa^2}, \tag{3}$$

[1] E-mail:langlois@iap.fr

where R is the scalar curvature in the $(4+n)$-dimensional spacetime. Variation of the action including the matter part leads to the generalized Einstein equations which read

$$G_{AB} \equiv R_{AB} - \frac{1}{2} R\, g_{AB} = \kappa^2 T_{AB}. \tag{4}$$

This equation has exactly the same form as the familiar one, with the difference that all tensors are now $(4+n)$-dimensional tensors.

In the static weak field regime (in a flat $(4+n)$-dimensional spacetime) Einstein equations imply as usual the Poisson equation. However, the solution of Poisson's equation depends on the number of space dimensions, and the general form of the Newtonian potential is

$$\phi_N(r) \propto \frac{G_{(4+n)}}{r^{(n+1)}}, \tag{5}$$

where the generalized Newton's constant $G_{(4+n)}$ is proportional to the gravitational coupling κ^2 introduced above in the Einstein equations (4).

This means that, a priori, the presence of extra-dimensions implies that gravity is modified. The simplest way to recover the familiar gravity law is once more to compactify the extra-dimensions. The resulting gravity is

- the $(4+n)$ dimensional gravity on scales smaller than the radius R of compactification (assumed to be the same in all extra-dimensions for simplicity)
- the usual 4-dimensional gravity on scales much larger than R, with the Newton's constant given by

$$G_{(4)} \sim G_{(4+n)}/R^n, \tag{6}$$

or, equivalently, expressed in terms of the Planck mass,

$$M_{(4)}^2 \sim M_{(4+n)}^{2+n} R^n. \tag{7}$$

This result can be understood is the following way. In a compactified space, the gravitational field induced by a point mass m can be computed by unwrapping the extra-space and by summing the contributions of all the images of the true mass m. At small distances with respect to R, the influence of the image masses can be ignored and one gets $(4+n)$ dimensional gravity. By contrast, on scales much larger than R, all image masses contribute to the gravitational field and they can be assimilated to a continuous massive line (for one extra-dimension) with constant linear mass density. Applying then Gauss' law to a cylinder surrounding the massive line yields the usual gravitational force with the above gravitational coupling.

As a consequence, like in particle physics, an upper constraint on the compactification radius can be deduced from the absence of any observed deviation from ordinary Newton's law. The present experimental constraints yield (see e.g. [1])

$$R \lesssim 0.2\,\mathrm{mm}. \tag{8}$$

The latest developments in the models with extra-dimensions come from the realization that the observational constraint on the size of extra-dimensions from gravity experiments is much weaker than that from accelerator experiments. This suggests the idea to decouple the extra-dimensions "felt" by ordinary particles from the extra-dimensions "felt" by gravity. Concretely, this can be realized by invoking a mechanism that confines fields of the particle physics Standard Model to a subspace with three spatial dimensions, called three-brane, within a higher dimensional space where gravity lives.

The purpose of this review, far from being exhaustive, is to present the basic results concerning gravity and cosmology in the brane scenarios where the self-gravity of the brane is taken into account, and to illustrate some more advanced aspects like cosmological perturbations or brane collisions. Complementary information can be found in two recent reviews, one by R. Maartens [2] and the other by V. Rubakov [3], the latter more focused on the particle physics aspects.

2 Braneworld models

The braneworld scenarios have attracted much attention only recently but one can find in the literature a few precursor works [4] considering our four-dimensional universe as a subspace of a larger spacetime. A wider interest in braneworlds has developed when this idea has emerged in the context of superstring theories and M-theory. An important step is the Horava-Witten supergravity [5], which is supposed to describe the effective low energy theory in the strong coupling limit of heterotic $E_8 \times E_8$ superstrings. This theory is based on an eleven-dimensional spacetime with an orbifold S_1/Z_2 eleventh dimension, with 11-dimensional supergravity in the bulk and a gauge group E_8 on each of the 10-dimensional boundaries corresponding to the worldsheets of 9-branes located at the two fixed points along the eleventh dimension. After compactification of six dimensions, one finds a five-dimensional spacetime with two four-dimensional boundaries where matter is supposed to be localized.

At the phenomenological level, Arkani-Hamed, Dimopoulos and Dvali (ADD) [6] then suggested the more radical step to assume that the fundamental Planck mass is of the order of the TeV so as to solve the famous hierarchy problem in particle physics, i.e. why there are so many orders of magnitude between the electroweak scale and the Planck scale. In these models the observed Planck scale seems huge simply because the volume of the extra dimensions is large, according to the formula (7). The ADD proposal has had a tremendous impact, especially in the particle physics community.

In the general relativity and cosmology communities, more interest was suscitated by the later proposal of Randall and Sundrum [7, 8]. By contrast with the ADD models, their specificities are the following:

- there is only one single extra-dimension
- the bulk spacetime is not flat but curved: it is a portion of Anti-de Sitter (AdS) with a negative cosmological constant
$$\Lambda \equiv -\frac{1}{\ell^2} \equiv -\mu^2 \tag{9}$$
where ℓ has the dimension of length, and μ the dimension of mass.
- there is a tension, σ, in the brane(s), which is (are) supposed to be Z_2-symmetric like in the Horava-Witten model.

The metric can then be written in the form

$$ds^2 = a^2(y)\eta_{\mu\nu}dx^\mu dx^\nu + dy^2, \tag{10}$$

where $\eta_{\mu\nu}$ is the usual Minkowski metric and the warping factor is given by

$$a(y) = e^{-|y|/\ell}. \tag{11}$$

There are in fact two models due to Randall and Sundrum, with essentially the same framework but which differ in the rôle assigned to the positive tension brane:

- RS1: two branes are bounding the AdS portion, one positive tension brane at $y = 0$ and one negative tension brane, the latter corresponding to our accessible world [7]. This model suggests a solution to the hierarchy problem, by showing that TeV energy scales on the hidden brane (the TeV brane) correspond to M_P energy scales in our brane (the Planck brane), due to the exponential warping factor.
- RS2: in this model [8], our world corresponds to the positive tension brane which is located at $y = 0$. The negative tension brane is now facultative. The goal of this model is not to solve the hierarchy problem, but to show that an infinite extra dimension can lead to usual four-dimensional gravity, as explained below.

The tension of the branes is not a free parameter for the above setup to be valid. They must be fine-tuned with the AdS cosmological constant so as to satisfy the condition

$$\frac{\kappa}{6}|\sigma| = \frac{1}{\ell}. \tag{12}$$

From now on, I will consider only the second model RS2 and show how ordinary gravity is approximately recovered. In order to study weak gravity, the usual method is to consider tensor-like linear perturbations of the metric. Denoting these fluctuations h_{AB} so that

$$g_{AB} = \bar{g}_{AB} + h_{AB}, \tag{13}$$

and imposing the gauge requirements $h_{Ay} = 0$, $h^{\nu}_{\mu\ ,\nu} = 0$ and $h^{\mu}_{\mu} = 0$, the linearized Einstein equations yield the following wave equation for the gravitons

$$\left[a^{-2}\Box^{(4)} + \partial_y^2 - \frac{4}{\ell^2} + \frac{4}{\ell}\delta(y)\right] h_{\mu\nu} = 0, \tag{14}$$

where the delta function takes into account the presence of the brane. This equation is separable and the general solution can be written as the superposition of solutions of the form

$$h_{\mu\nu}(x^{\lambda}, y) = u_m(y) e^{ik_{\lambda}x^{\lambda}} \epsilon_{\mu\nu}, \tag{15}$$

where m (satisfying $k_{\lambda}k^{\lambda} = -m^2$) can be interpreted as the four-dimensional mass and $u_m(y)$ satisfies an ordinary differential equation, which is deduced from (14) by replacing the d'Alembertian operator with m^2. Following Randall and Sundrum, it is convenient to rewrite this equation in a Schrödinger-like form,

$$-\frac{d^2\psi_m}{dz^2} + V(z)\,\psi_m = m^2\psi_m \tag{16}$$

where $\psi_m = a^{-1/2}u_m$ and $z = sgn(y)\ell(\exp(|y|/\ell) - 1)$. The potential $V(z)$ is "volcano"-shaped, its expression being given by

$$V(z) = \frac{15}{4(|z| + \ell)^2} - \frac{3}{\ell}\delta(z). \tag{17}$$

The delta function part of the potential leads to the existence of a zero mode, with the functional dependence

$$u_m \propto a^2,$$

which is (exponentionally) localized near the brane and which reproduces the usual four-dimensional graviton, the four-dimensional gravitational coupling being given by

$$8\pi G_{(4)} = \kappa^2/\ell. \tag{18}$$

In addition to this zero mode, there is a whole continuum of massive graviton modes, which induce some corrections to the usual gravitational law, although significant only on scales of the order of the AdS lengthscale ℓ and below. The resulting gravitational potential is of the form

$$V(r) = \frac{G_{(4)}}{r}\left(1 + \alpha\frac{\ell^2}{r^2}\right). \tag{19}$$

The coefficient $\alpha = 1$, given initially by RS, was corrected to $\alpha = 2/3$ by a more detailed analysis [9], which considered explicitely the coupling of graviton to matter in the brane.

Finally, let us mention that a rewriting of the Einstein equations, in the Randall-Sundrum type models, leads to effective four-dimensional Einstein equations, which can be written in the form [10]

$${}^{(4)}G_{\mu\nu} = 8\pi G_{(4)}\tau_{\mu\nu} + \kappa^4\Pi_{\mu\nu} - E_{\mu\nu}. \tag{20}$$

where $\tau_{\mu\nu}$ is the brane energy-momentum tensor (not including the tension σ), $\Pi_{\mu\nu}$ is quadratic in the brane energy momentum tensor,

$$\Pi_{\mu\nu} = -\frac{1}{4}\tau_{\mu\sigma}\tau^{\sigma}_{\nu} + \frac{1}{12}\tau\tau_{\mu\nu} + \frac{1}{8}g_{\mu\nu}\left(\tau_{\sigma\rho}\tau^{\sigma\rho} - \frac{1}{3}\tau^2\right). \tag{21}$$

and $E_{\mu\nu}$ is the projection of the five-dimensional Weyl tensor

$$E_{\mu\nu} = {}^{(5)}C^{A}{}_{BCD}n_A n^C g_{\mu}^{B} g_{\nu}^{D}. \tag{22}$$

n^A being the unit vector normal to the brane. Although very nice, one must be aware that the above equation is only a rewriting of the five-dimensional Einstein's equations using the junction conditions, and in practical problems, the full system remains to be solved. In particular one must be careful with the interpretation of the gravitational coupling to brane matter, even in the linear case, because $E_{\mu\nu}$ will in general depend on the matter $\tau_{\mu\nu}$.

In a two-brane model, in contrast with the single brane model, what is obtained is Brans-Dicke type gravity with the radion, i.e. the interbrane separation playing the rôle of the Brans-Dicke scalar field [9]. The model RS1 leads to a Brans-Dicke gravity which is incompatible with observations: this model can be saved only by introducing a more complicated setting, for example a scalar field in the bulk with a potential and couplings to the branes, which provides an stabilization mechanism for the radion [11].

3 Homogeneous cosmology in a brane-universe

Let us now turn to cosmology. The main motivation for exploring cosmology in models with extra-dimensions is that the potentially new effects could arise significantly only at very high energies, i.e. in the very early universe, and leave some relic imprints which could be tested today via cosmological observations. Before discussing the potentially rich but very difficult question of cosmological perturbations in the next section, one must first describe homogeneous cosmology, following [12] and [13].

Let us thus consider a five-dimensional spacetime with three-dimensional isotropy and homogeneity, which contains a three-brane representing our universe. It is convenient, but not necessary, to work in a Gaussian normal coordinate system based on our brane-universe. Due to the spacetime symmetries, the metric is then of the form

$$ds^2 = -n(t,y)^2 dt^2 + a(t,y)^2 \delta_{ij} dx^i dx^j + dy^2. \tag{23}$$

where we have assumed that our brane-universe is spatially flat (but this can be generalized very easily to hyperbolic or elliptic spaces). In these coordinates, our brane-universe is always located at $y = 0$.

The energy-momentum tensor can be decomposed into a bulk energy-momentum tensor and a brane energy-momentum tensor, the latter being of the form

$$T^A_B = S^A_B \delta(y) = \{\rho_b, p_b, p_b, p_b, 0\}\delta(y), \tag{24}$$

where the delta function expresses the confinement of matter in the brane. ρ_b and P_b are respectively the total energy density and pressure in the brane and depend only on time. For simplicity, we neglect the bulk energy-momentum tensor but allow for the presence of a cosmological constant in the bulk, Λ, so that the five-dimensional Einstein equations read

$$G_{AB} + \Lambda g_{AB} = \kappa^2 T_{AB}. \tag{25}$$

Because of the distributional nature of the energy-momentum tensor, one way to solve the Einstein equations is to solve them first in the bulk and then apply the junction conditions [14] for the metric at $y = 0$. According to the junction conditions, the metric must be continuous and the jump of the extrinsic curvature tensor K_{AB} (related to the derivatives of the metric with respect to y) depends on the distributional energy-momentum tensor,

$$\left[K^A_B - K\delta^A_B\right] = \kappa^2 S^A_B, \tag{26}$$

where the brackets here denote the jump at the brane, i.e. $[Q] = Q_{\{y=0^+\}} - Q_{\{y=0^-\}}$, and the extrinsic curvature tensor is defined by

$$K_{AB} = h^C_A \nabla_C n_B, \tag{27}$$

n^A being the unit vector normal to the brane. As before, one can add the extra assumption that the brane is mirror symmetric so that the jump in the extrinsic curvature is twice its value on one side (see [15] for references where this is not assumed). Substituting the ansatz metric (23) in (26), one ends up with the two junction conditions:

$$\left(\frac{n'}{n}\right)_{0^+} = \frac{\kappa^2}{6}\left(3p_b + 2\rho_b\right), \qquad \left(\frac{a'}{a}\right)_{0^+} = -\frac{\kappa^2}{6}\rho_b. \tag{28}$$

Going back to the bulk Einstein equations (their explicit form can be found in e.g. [13]), one can solve the $(t-y)$ component to get

$$\dot{a}(t,y) = \alpha(t) n(t,y), \tag{29}$$

and the integration of the component $(t-t)$ with respect to y and of the component $(y-y)$ with respect to time, yields the first integral

$$(aa')^2 - \alpha^2 a^2 + \frac{\Lambda}{6} a^4 + \mathcal{C} = 0, \tag{30}$$

where $\mathcal{C}$ is an integration constant. When one evaluates this first integral at $y = 0$, i.e. in our brane-universe, substituting the junction conditions given above in (28), one ends up with the following equation

$$H_0^2 \equiv \frac{\dot{a}_0^2}{a_0^2} = \frac{\kappa^4}{36}\rho_b^2 + \frac{\Lambda}{6} + \frac{\mathcal{C}}{a^4}. \tag{31}$$

where the subscript '0' means evaluation at $y = 0$. This equation is analogous to the (first) Friedmann equation, since it relates the Hubble parameter to the energy density, but it is different from the usual Friedmann equation $[H^2 = (8\pi G/3)\rho]$. Its most remarkable feature is that the energy density of the brane enters quadratically on the right hand side in contrast with the standard four-dimensional Friedmann equation where the energy density enters linearly. As for the energy conservation equation it is unchanged in this five-dimensional setup and still reads

$$\dot{\rho}_b + 3H(\rho_b + p_b) = 0. \tag{32}$$

In the simplest case where $\Lambda = 0$ and $\mathcal{C} = 0$, one can easily solve the above cosmological equations for a perfect fluid with an equation of state $p_b = w\rho_b$ and w constant. One finds that the evolution of the scale factor is given by

$$a_0(t) \propto t^{\frac{1}{3(1+w)}}. \tag{33}$$

In the most interesting cases for cosmology, radiation and pressureless matter, one finds respectively $a \sim t^{1/4}$ (instead of the usual $a \sim t^{1/2}$) and $a \sim t^{1/3}$ (instead of $a \sim t^{2/3}$). Such behaviour is problematic because it cannot be reconciled with nucleosynthesis. Indeed, the nucleosynthesis scenario depends crucially on both the microphysical reaction rates and the expansion rate of the universe. And changing in a drastic way the evolution of the scale factor between nucleosynthesis and now modifies dramatically the predictions for the light element abundances.

The above Friedmann law with the ρ_b^2 term, but without the bulk cosmological constant (and without the $\mathcal{C}$ term) was first derived in [12], just before Randall and Sundrum proposed their models. In fact, the unusual Friedmann law can be related to a gravity which should be five-dimensional rather than four-dimensional. With the obtention in RS2 of a five-dimensional model yielding a four-dimensional gravity, one could expect that the corresponding cosmology should be compatible with the usual cosmology [16]. In fact, it is clear from (31) that a Minkowski brane with a tension, as in the RS2 model, requires the presence of a negative cosmological constant in the bulk to compensate the squared tension term and get $H = 0$.

If one wants to go beyond a Minkowski geometry and consider non trivial cosmology in the brane, one must then assume that the total energy density in the brane, ρ_b, consists of two parts,

$$\rho_b = \sigma + \rho, \tag{34}$$

the tension σ, constant in time, and the usual cosmological energy density ρ. Substituting this decomposition into (31), one obtains

$$H^2 = \left(\frac{\kappa^4}{36}\sigma^2 - \mu^2\right) + \frac{\kappa^4}{18}\sigma\rho + \frac{\kappa^4}{36}\rho^2 + \frac{\mathcal{C}}{a^4}. \tag{35}$$

If one fine-tunes the brane tension and the bulk cosmological cosmological constant as in (12), the first term on the right hand side vanishes. The second term then becomes the dominant term if ρ is small enough and *one thus recovers the usual Friedmann equation at low energy*, with the identification

$$8\pi G = \frac{\kappa^4}{6}\sigma, \tag{36}$$

which is exactly the relation obtained in RS2 by combining (12) and (18).

The third term on the right hand side, quadratic in the energy density, provides a *high-energy correction* to the Friedmann equation which becomes significant when the value of the energy density approaches the value of the tension σ and dominates at higher energy densities. In the very high energy regime, $\rho \gg \sigma$, one thus recovers the unconventional behaviour analysed before since the bulk cosmological constant becomes negligible. It is in fact not difficult to obtain explicit solutions for the scale factor, which interpolate between the low energy regime and the high energy regime.

Finally, the last term on the right hand side behaves like radiation and arises from the integration constant $\mathcal{C}$. This constant $\mathcal{C}$ is quite analogous to the Schwarzschild mass and it is related to the bulk Weyl tensor, which vanishes when $\mathcal{C} = 0$. In a cosmological context, this term is constrained to be small enough at the time of nucleosynthesis in order to satisfy the constraints on the number of extra light degrees of freedom. In the matter era, this term then redshifts quickly and would be in principle negligible today.

In the present section, we have so far considered only the metric in the brane. The metric outside the brane can be also determined explictly [13]. In the special case $\mathcal{C} = 0$, the metric has a much simpler form and its components are given by

$$a(t,y) = a_0(t)\,(\cosh\mu y - \eta \sinh\mu|y|) \tag{37}$$

$$n(t,y) = \cosh\mu y - \tilde{\eta}\sinh\mu|y| \tag{38}$$

where

$$\eta = 1 + \frac{\rho}{\sigma}, \qquad \tilde{\eta} = \eta + \frac{\dot{\eta}}{H_0} \tag{39}$$

and we have chosen the time t corresponding to the cosmic time in the brane. In the RS2 limit, $\rho = 0$, i.e. $\rho_b = \sigma$, which implies $\eta = \tilde{\eta} = 1$ and one recovers $a(t,y) = a_0 \exp(-\mu|y|)$.

In summary, we have obtained a cosmological model, based on a braneworld scenario, which appears to be compatible with current observations a low enough energies. Let us now quantify the constraints on the parameters of the model in order to ensure this compatibility with observations. As mentioned above an essential constraint comes from nucleosynthesis: the evolution of the universe since nucleosynthesis must be approximately the same as in usual cosmology. This is the case if the energy scale associated with the tension is higher than the nucleosynthesis energy scale, i.e.

$$M_c \equiv \sigma^{1/4} \gtrsim 1 \text{ MeV}. \tag{40}$$

Combining this with (36) this implies for the fundamental mass scale (defined by $\kappa^2 = M^{-3}$)

$$M \gtrsim 10^4 \text{ GeV}. \tag{41}$$

There is however another constraint, which is not of cosmological nature: the requirement to recover ordinary gravity down to scales of the submillimeter order. This implies

$$\ell \lesssim 10^{-1} \text{ mm}, \tag{42}$$

which yields the constraint

$$M \gtrsim 10^8 \text{ GeV}. \tag{43}$$

Therefore the most stringent constraint comes, not from cosmology, but from gravity experiments in this particular model. So far, we have thus been able to build a model, which reproduces all qualitative and quantitative features of ordinary cosmology in the domains that have been tested by observations. The obvious next question is whether this will still hold for a more realistic cosmology that includes perturbations from homogeneity, and more interestingly, whether brane cosmology is capable of providing predictions that deviate from usual cosmology and which might tested in the future. This is still an open question today.

4 Brane cosmological perturbations

Endowed with a viable homogeneous scenario, one would like to explore the much richer domain of cosmological perturbations and investigate whether brane cosmology leads to new effects that could be tested in the forthcoming cosmological observations, in particular of the anisotropies of the Cosmic Microwave Background.

Brane cosmological perturbations is a difficult subject and although there are now many published works on this question (see e.g. [17, 18, 19, 20, 21, 22, 23, 24, 25]), no observational signature has yet been predicted. Below I will summarize some results concerning two differents aspects of perturbations. The first aspect deals with the evolution of scalar type perturbations on the brane, the second aspect with the production of gravitational waves from quantum fluctuations during a de Sitter phase in the brane.

Let us first discuss scalar type cosmological perturbations in brane cosmology. Choosing a GN coordinate system the "scalarly" perturbed metric can be written

$$ds^2 = -n^2(1+2A)dt^2 + 2n^2\partial_i B dt dx^i + a^2\left[(1+2C)\delta_{ij} + 2\partial_i\partial_j E\right]dx^i dx^j + dy^2, \tag{44}$$

where the perturbations turn out to coincide exactly with the standard scalar cosmological perturbations since we are in the GN gauge. One can find other gauge choices in the literature. Using the compact notation $h_\alpha = \{A, B, C, E\}$ $(\alpha = 1, \ldots, 4)$, the linearized Einstein equations

$$\delta G_{AB} + \Lambda \delta g_{AB} = \kappa^2 \delta T_{AB} \tag{45}$$

yield, *in the bulk*, expressions of the form

$$\delta G^{(5)}_{00} = \delta G^{st}_{00} + [h_\alpha, h'_\alpha, h''_\alpha] = -\Lambda \delta g_{00} \tag{46}$$

$$\delta G^{(5)}_{ij} = \delta G^{st}_{ij} + [h_\alpha, h'_\alpha, h''_\alpha] = -\Lambda \delta g_{ij} \tag{47}$$

$$\delta G^{(5)}_{0i} = \delta G^{st}_{0i} + [h_\alpha, h'_\alpha, h''_\alpha] = -\Lambda \delta g_{0i} \tag{48}$$

$$\delta G^{(5)}_{05} = [h_\alpha, h'_\alpha] = 0 \tag{49}$$

$$\delta G^{(5)}_{5i} = [h_\alpha, h'_\alpha] = 0 \tag{50}$$

$$\delta G^{(5)}_{55} = [h'_\alpha, h''_\alpha] = 0 \tag{51}$$

where the brackets represent linear combinations of the perturbations and their derivatives. Brane matter enters only in the junction conditions, which at the linear level relate the first derivatives (with respect to y) of the metric perturbations h'_α to brane matter perturbations $\delta\rho$, δP, v, π. One can then substitute these relations back into the perturbed Einstein equations. $\delta G^{(5)}_{05} = 0$ then yields the usual perturbed energy conservation equation, whereas $\delta G^{(5)}_{i5} = 0$ yields the perturbed Euler equation. The other equations yield equations of motion for the perturbations where one recognizes the usual equations of motion in ordinary cosmology, but with two types of corrections:

- modification of the homogeneous background coefficients due to the additional terms in the Friedmann equation. These corrections are negligible in the low energy regime $\rho \ll \sigma$. For long wavelength (larger than the Hubble scale) perturbations, one can thus obtain a transfer coefficient, $T = 5/6$, characterizing the high/low energy transition, i.e.

$$\Phi_{\rho \ll \sigma} = \frac{5}{6}\Phi_{\rho \gg \sigma}. \tag{52}$$

- presence of source terms in the equations. These terms come from the bulk perturbations and cannot be determined solely from the evolution inside the brane. To determine them, one must solve the full problem in the bulk (which also means to specify some initial conditions in the bulk). From the four-dimensial point of view, these terms from the fifth dimension appear like external source terms and their impact is formally similar to that of "active seeds", which have been studied in the context of topological defects.

Let us turn now to another facet of the brane cosmological perturbations: their origin. In standard cosmology, the main mechanism for producing the cosmological perturbations is inflation. One can thus try to generalize this mechanim to the context of brane cosmology. Brane inflation generated by a scalar field confined to the brane has been investigated in [26]. The spectrum of gravitational waves generated in such a scenario is however more subtle to compute because gravitational waves have an extension in the fifth dimension. It has been first computed in [27] and confirmed (and extended) in a different approach [28].

To compute the production of gravitational waves, one can approximate slow-roll brane inflation by a succession of de Sitter phases. The metric for a de Sitter brane (see also [29]) corresponds to a particular case of (38) with $\eta = \tilde{\eta}$ and can be written as

$$a(t,y) = a_0(t)\mathcal{A}(y), \quad n = \mathcal{A}(y), \tag{53}$$

with

$$\mathcal{A}(y) = \cosh \mu y - \left(1 + \frac{\rho}{\sigma}\right) \sinh \mu |y|. \tag{54}$$

The gravitational waves appear in a perturbed metric of the form

$$ds^2 = -n^2 dt^2 + a^2 \left[\delta_{ij} + E_{ij}^{TT}\right] dx^i dx^j + dy^2, \tag{55}$$

where the 'TT' stands for transverse traceless. Decomposing E_{ij}^{TT} in Fourier modes of the form

$$E_{ij} = E\, e^{i\vec{k}.\vec{x}}\, e_{ij}, \tag{56}$$

one gets a wave equation, which reads

$$\ddot{E} + 3H_0\dot{E} + \frac{k^2}{a_o^2}E = \mathcal{A}^2 E'' + 4\mathcal{A}\mathcal{A}' E' . \tag{57}$$

This equation is separable, and one can look for solutions $E = \varphi_m(t)\mathcal{E}_m(y)$, where the time-dependent part must satisfy

$$\ddot{\varphi}_m + 3H_0\dot{\varphi}_m + \left[m^2 + \frac{k^2}{a_0^2}\right]\varphi_m = 0\,, \tag{58}$$

and the y-dependent part satisfies

$$\mathcal{E}_m'' + 4\frac{\mathcal{A}'}{\mathcal{A}}\mathcal{E}_m' + \frac{m^2}{\mathcal{A}^2}\mathcal{E}_m = 0\,. \tag{59}$$

Like in the Minkowski case, the latter equation can be reformulated as a Schroedinger type equation,

$$\frac{d^2\Psi_m}{dz^2} - V(z)\Psi_m = -m^2\Psi_m\,, \tag{60}$$

after introducing the conformal coordinate $z = \int dy/\mathcal{A}(y)$ and defining $\Psi_m \equiv \mathcal{A}^{3/2}\mathcal{E}_m$. The potential is given by

$$V(z) = \frac{15H_0^2}{4\sinh^2(H_0 z)} + \tfrac{9}{4}H_0^2 - 3\mu\left[1 + \frac{\rho}{\sigma}\right]\delta(z - z_b)\,. \tag{61}$$

The non-zero value of the Hubble parameter signals the presence of a gap between the zero mode and the continuum of Kaluza-Klein modes, as noticed earlier by [30].

The zero mode corresponds simply to

$$\mathcal{E}_0 = C_1 \equiv \sqrt{\mu}\; F(H_0/\mu)\,, \tag{62}$$

where, imposing the normalization $2\int_{z_b}^{\infty} |\Psi_0^2| dz = 1$, the constant C_1 has been expressed in terms of H_0 via the function

$$F(x) = \left\{\sqrt{1+x^2} - x^2 \ln\left[\frac{1}{x} + \sqrt{1 + \frac{1}{x^2}}\right]\right\}^{-1/2}. \tag{63}$$

Asymptotically, $F \simeq 1$ at low energies, i.e. $H_0 \ll \mu$, and $F \simeq \sqrt{3H_0/(2\mu)}$ at high energies, i.e. $H_0 \gg \mu$. One can then evaluate the vacuum quantum fluctuations of the zero mode by using the standard canonical quantization. To do this explicitly, one writes the five-dimensional action for gravity at second order in the perturbations. Keeping only the zero mode and integrating over the fifth dimension, one obtains

$$S_g = \frac{1}{8\kappa^2} \sum_{+,\times} \int d\eta d^3\vec{k} a_o^2 \left[\left(\frac{d\varphi_o}{d\eta} \right)^2 + k^2 {\varphi_o}^2 \right], \tag{64}$$

This has the standard form for a massless graviton in four-dimensional cosmology, apart from the overall factor $1/8\kappa^2$ instead of $1/8\kappa_4^2$. It follows that quantum fluctuations in each polarization, φ_o, have an amplitude of $2\kappa(H_o/2\pi)$ on super-horizon scales. Quantum fluctuations on the brane at $y = 0$, where $E_o = C_1\varphi_0$, thus have the typical amplitude

$$\frac{1}{2\kappa_4}\delta E_{\rm brane} = \left(\frac{H_0}{2\pi} \right) F(H_0/\mu) \tag{65}$$

At low energies, $F = 1$ and one recovers exactly the usual four-dimensional result but at higher energies the multiplicative factor F provides an *enhancement of the gravitational wave spectrum amplitude with respect to the four-dimensional result.* However, comparing this with the amplitude for the scalar spectrum obtained in [26], one finds that, at high energies ($\rho \gg \sigma$), the *tensor over scalar ratio is in fact suppressed with respect to the four-dimensional ratio.* An open question is how the gravitational waves will evolve during the subsequent cosmological phases, the radiation and matter eras.

5 Collisions of branes

The last topic I would like to discuss is of interest for scenarios with several branes which are allowed to collide. So far, I have focused on cosmology for a single brane embedded in a five-dimensional AdS spacetime. For homogeneous cosmology, if one assumes the bulk to be empty, then the derivation summarized above proves that the bulk and the other branes it might contain can affect our brane-universe only *via the constant C of the Weyl radiation term*, where C is a constant in time. This property can be understood, more formally, as a generalized Birkhoff theorem [31].

Another brane can however have a dramatic influence when it collides with the initial brane. This possibility, which could provide a new interpretation of the Big-Bang in our brane-universe, has raised some interest recently, in particular the ekpyrotic scenario [32] based on the five-dimensional reduction of Horava-Witten model [33], but other, simpler, models have also been proposed [34].

With K. Maeda and D. Wands [35], I have recently given a general analysis of the collision of n-branes in a $(2 + n)$-dimensional empty spacetime with n-dimensional isotropy and homogeneity, i.e. branes separated by patches of Sch-AdS spacetimes (allowing for different Schwarschild-type mass and cosmological constant in each region), with the metric

$$ds^2 = -f(R)dT^2 + \frac{dR^2}{f(R)} + R^2 d\Omega_n^2, \tag{66}$$

where the 'orthogonal' metric $d\Omega_n^2$ does not depend on either T or R. The well-known case of a Schwarzschild-(anti)-de Sitter spacetime corresponds to $f(R) = k - (\mathcal{C}/R^{n-1}) \mp (R/\ell)^2$.

Contrarily to the coordinates of the previous section, a brane is no longer at rest in this coordinate system. It can be described by its trajectory $(T(\tau), R(\tau))$, where τ is the proper time. An alternative way [36] to obtain the generalized Friedmann equation (31) is simply to write the junction conditions at the location of the moving brane, with the Z_2 symmetry assumption, by noting that the brane coordinate R can be reinterpreted as the scale factor of the induced metric, as is clear from the metric (66). It can also been shown explicitly that the expression for the metric (23) given above in GN coordinates can indeed be deduced from (66) by an appropriate change of coordinates [37].

To analyse the collision, it is very convenient to introduce an angle α, which characterizes the motion of the brane with respect to the coordinate system (23), defined by

$$\alpha = \sinh^{-1}(\epsilon \dot{R}/\sqrt{f}). \tag{67}$$

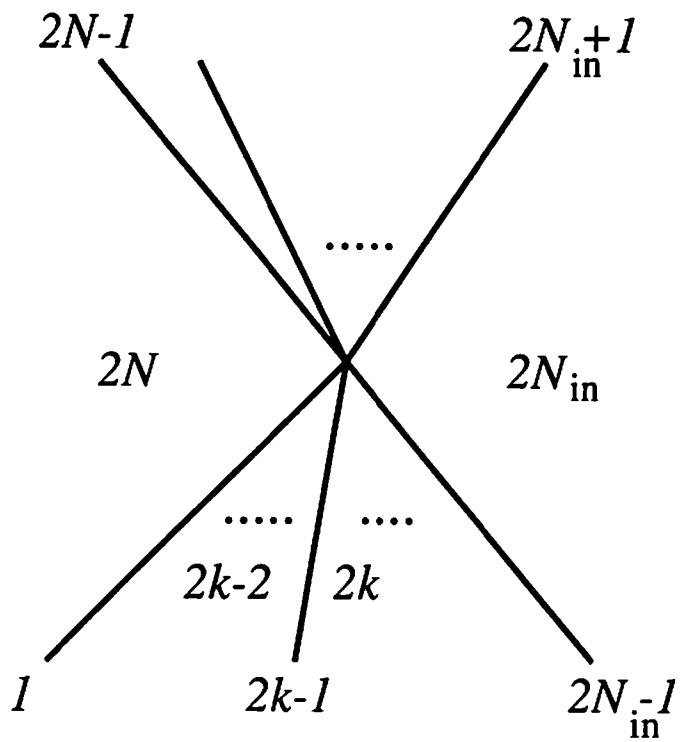

Figure 1: Collision of $N_{\rm in}$ ingoing branes, yielding $N_{\rm out} = N - N_{\rm in}$ outgoing branes. Odd integers denote branes and even integers denote regions in between.

where $\epsilon = +1$ if R decreases from "left" to "right", $\epsilon = -1$ otherwise. Considering a collision involving a total number of N branes, both ingoing and outgoing, thus separated by N spacetime regions one can label alternately branes and regions by integers, starting from the leftmost ingoing brane and going anticlockwise around the point of collision (see Figure). The branes will thus be denoted by odd integers, $2k-1$ ($1 \leq k \leq N$), and the regions by even integers, $2k$ ($1 \leq k \leq N$). Let us introduce, as before, the angle $\alpha_{2k-1|2k}$ which characterizes the motion of the brane $\mathcal{B}_{2k-1}$ with respect to the region $\mathcal{R}_{2k}$, and which is defined by

$$\sinh \alpha_{2k-1|2k} = \frac{\epsilon_{2k} \dot{R}_{2k-1}}{\sqrt{f_{2k}}}. \tag{68}$$

Conversely, the motion of the region $\mathcal{R}_{2k}$ with respect to the brane by the Lorentz angle $\alpha_{2k|2k-1} = -\alpha_{2k-1|2k}$. It can be shown that the junction conditions for the branes can be written in the form

$$\tilde{\rho}_{2k-1} \equiv \pm \frac{\kappa^2}{n} \rho_{2k-1} R = \epsilon_{2k} \sqrt{f_{2k}} \exp\left(\pm \alpha_{2k-1|2k}\right) - \epsilon_{2k-2} \sqrt{f_{2k-2}} \exp\left(\mp \alpha_{2k-2|2k-1}\right), \tag{69}$$

with the plus sign for ingoing branes ($1 \leq k \leq N_{\rm in}$), the minus sign for outgoing branes ($N_{\rm in}+1 \leq k \leq N$). An outgoing positive energy density brane thus has the same sign as an ingoing negative energy density brane.

The advantage of this formalism becomes obvious when one writes the *geometrical consistency relation* that expresses the matching of all branes and spacetime regions around the collision point. In terms of the angles defined above, it reads simply

$$\sum_{i=1}^{2N} \alpha_{i|i+1} = 0. \tag{70}$$

Moreover, introducing the generalized angles

$$\alpha_{j|j'} = \sum_{i=j}^{j'-1} \alpha_{i|i+1}, \tag{71}$$

if $j < j'$, and $\alpha_{j'|j} = -\alpha_{j|j'}$, the sum rule for angles (70) combined with the junction conditions (69) leads to the laws of energy conservation and momentum conservation. The energy conservation law reads

$$\sum_{k=1}^{N} \tilde{\rho}_{2k-1} \gamma_{j|2k-1} = 0, \tag{72}$$

where $\gamma_{j|j'} \equiv \cosh \alpha_{j|j'}$ corresponds to the Lorentz factor between the brane/region j and the brane/region j' and can be obtained, if j and j' are not adjacent, by combining all intermediary Lorentz factors (this is simply using the velocity addition rule of special relativity), or the relative angle formula (71). The index j corresponds to the reference frame with respect to which the conservation rule is written. Similarly, the *momentum conservation law* in the j-th reference frame can be expressed in the form

$$\sum_{k=1}^{N} \tilde{\rho}_{2k-1} \gamma_{2k-1|j} \beta_{2k-1|j} = 0, \tag{73}$$

with $\gamma_{j|j'} \beta_{j|j'} \equiv \sinh \alpha_{j|j'}$. One thus obtains, just from geometrical considerations, conservation laws relating the brane energies densities and velocities before and after the collision point. Our results apply to any collision of branes in vacuum, with the appropriate symmetries of homogeneity and isotropy. An interesting development would be to extend the analysis to branes with small perturbations and investigate whether one can find scenarios which can produce quasi-scale invariant adiabatic spectra, as seems required by current observations.

Acknowledgements

I would like to thank the organizers of the 11th Workshop on General Relativity and Gravitation (Waseda University, Tokyo, Japan) for a very interesting meeting. I would also like to acknowledge the financial support of the Yamada Science Foundation for my visit to Japan.

References

[1] C. D. Hoyle, U. Schmidt, B. R. Heckel, E. G. Adelberger, J. H. Gundlach, D. J. Kapner and H. E. Swanson, Phys. Rev. Lett. **86**, 1418 (2001) [arXiv:hep-ph/0011014].

[2] R. Maartens, arXiv:gr-qc/0101059.

[3] V. A. Rubakov, Phys. Usp. **44**, 871 (2001) [Usp. Fiz. Nauk **171**, 913 (2001)] [arXiv:hep-ph/0104152].

[4] V.A. Rubakov, M.E. Shaposhnikov, Phys. Lett. B **125**, 139 (1983); M. Visser, Phys. Lett. B **159**, 22 (1985); E.J. Squires, Phys. Lett. B **167**, 286 (1986); G.W. Gibbons, D.L. Wiltshire, Nucl. Phys. B **287**, 717 (1987); K. Akama, Lect. Notes Phys. **176**, 267 (1982) [arXiv:hep-th/0001113].

[5] P. Horava and E. Witten, Nucl. Phys. B **460**, 506 (1996) [arXiv:hep-th/9510209]; Nucl. Phys. B **475**, 94 (1996) [arXiv:hep-th/9603142].

[6] N. Arkani-Hamed, S. Dimopoulos, G. Dvali, Phys.Lett. B429, (1998) 263; I. Antoniadis, N. Arkani-Hamed, S. Dimopoulos, G. Dvali, Phys. Lett. **B436**, 257 (1998); N. Arkani-Hamed, S. Dimopoulos and G. Dvali, Phys. Rev. **D59** (1999) 086004.

[7] L. Randall and R. Sundrum, Phys. Rev. Lett. **83** (1999) 3370 [arXiv:hep-ph/9905221].

[8] L. Randall and R. Sundrum, Phys. Rev. Lett. **83** (1999) 4690 [arXiv:hep-th/9906064].

[9] J. Garriga and T. Tanaka, Phys. Rev. Lett. **84** (2000) 2778 [arXiv:hep-th/9911055].

[10] T. Shiromizu, K. i. Maeda and M. Sasaki, Phys. Rev. D **62**, 024012 (2000) [arXiv:gr-qc/9910076].

[11] W. D. Goldberger and M. B. Wise, Phys. Rev. Lett. **83** (1999) 4922 [arXiv:hep-ph/9907447].

[12] P. Binétruy, C. Deffayet and D. Langlois, Nucl. Phys. B **565** (2000) 269 [arXiv:hep-th/9905012].

[13] P. Binétruy, C. Deffayet, U. Ellwanger and D. Langlois, Phys. Lett. B **477** (2000) 285 [arXiv:hep-th/9910219].

[14] W. Israel, Nuovo Cim. B **44S10**, 1 (1966) [Erratum-ibid. B **48**, 463 (1966)].

[15] R. A. Battye, B. Carter, A. Mennim and J. P. Uzan, Phys. Rev. D **64**, 124007 (2001) [arXiv:hep-th/0105091].

[16] C. Csáki, M. Graesser, C. Kolda, J. Terning, Phys. Lett. **B462**, 34 (1999); J.M. Cline, C.Grosjean, G.Servant, *Phys. Rev. Lett.* **83**, 4245 (1999).

[17] S. Mukohyama, Phys. Rev. D **62**, 084015 (2000) [arXiv:hep-th/0004067]; S. Mukohyama, Class. Quant. Grav. **17**, 4777 (2000) [arXiv:hep-th/0006146].

[18] H. Kodama, A. Ishibashi and O. Seto, Phys. Rev. D **62**, 064022 (2000) [arXiv:hep-th/0004160].

[19] R. Maartens, Phys. Rev. D **62**, 084023 (2000) [arXiv:hep-th/0004166]; C. Gordon and R. Maartens, Phys. Rev. D **63**, 044022 (2001) [arXiv:hep-th/0009010].

[20] D. Langlois, Phys. Rev. D **62**, 126012 (2000) [arXiv:hep-th/0005025].

[21] C. van de Bruck, M. Dorca, R. H. Brandenberger and A. Lukas, Phys. Rev. D **62**, 123515 (2000) [arXiv:hep-th/0005032].

[22] K. Koyama and J. Soda, Phys. Rev. D **62**, 123502 (2000) [arXiv:hep-th/0005239].

[23] D. Langlois, Phys. Rev. Lett. **86**, 2212 (2001) [arXiv:hep-th/0010063].

[24] N. Deruelle, T. Dolezel and J. Katz, Phys. Rev. D **63**, 083513 (2001) [arXiv:hep-th/0010215].

[25] D. Langlois, R. Maartens, M. Sasaki and D. Wands, Phys. Rev. D **63**, 084009 (2001) [arXiv:hep-th/0012044].

[26] R. Maartens, D. Wands, B. A. Bassett and I. Heard, Phys. Rev. D **62**, 041301 (2000) [arXiv:hep-ph/9912464].

[27] D. Langlois, R. Maartens and D. Wands, Phys. Lett. B **489**, 259 (2000) [arXiv:hep-th/0006007].

[28] D. S. Gorbunov, V. A. Rubakov and S. M. Sibiryakov, JHEP **0110**, 015 (2001) [arXiv:hep-th/0108017].

[29] N. Kaloper, Phys. Rev. D **60**, 123506 (1999) [arXiv:hep-th/9905210].

[30] J. Garriga and M. Sasaki, Phys. Rev. D **62**, 043523 (2000) [arXiv:hep-th/9912118].

[31] P. Bowcock, C. Charmousis and R. Gregory, Class. Quant. Grav. **17**, 4745 (2000) [arXiv:hep-th/0007177].

[32] J. Khoury, B. A. Ovrut, P. J. Steinhardt and N. Turok, Phys. Rev. D **64** 123522 (2001) [arXiv:hep-th/0103239]; R. Kallosh, L. Kofman and A. D. Linde, Phys. Rev. D **64**, 123523 (2001) [arXiv:hep-th/0104073].

[33] A. Lukas, B. A. Ovrut, K. S. Stelle and D. Waldram Phys. Rev. D **59**, 086001 (1999) [arXiv:hep-th/9803235]; Nucl. Phys. B **552**, 246 (1999) [arXiv:hep-th/9806051].

[34] M. Bucher, arXiv:hep-th/0107148; U. Gen, A. Ishibashi and T. Tanaka, arXiv:hep-th/0110286.

[35] D. Langlois, K. Maeda and D. Wands, "Conservation laws for collisions of branes (or shells) in general relativity," arXiv:gr-qc/0111013.

[36] P. Kraus, JHEP **9912** (1999) 011 [arXiv:hep-th/9910149].

[37] S. Mukohyama, T. Shiromizu and K. i. Maeda, Phys. Rev. D **62**, 024028 (2000) [Erratum-ibid. D **63**, 029901 (2000)] [arXiv:hep-th/9912287].

Present Status of Experimental Tests of Newtonian Gravity

Kazuaki Kuroda‡

Institute of Cosmic Ray Research, The University of Tokyo,
5-1-5, Kashiwanoha, Kashiwa, Chiba, 177-8582, Japan

Abstract

This paper reviews precise measurements for testing the foundation of gravitation theories. Testing the equivalence principle is the most fundamental experiment, and no contradiction to the equivalence principle has been reported. The time variation of the gravitational constant (G) is inferred by much indirect evidence without any indication of a change. Testing the inverse square law of Newtonian gravitation is the most popular experiment in this field, but no sign of a cntradiction has appeared. Recent reports on sub-millimeter scale tests of Newtonian gravity are introduced.

1. Introduction

The equivalence principle in gravity is the basis of metric theories of gravitation and the starting point of modern gravitational experiments. Although this principle has been confirmed to be correct to an accuracy of 5×10^{-13} [1][2][3][4], much more accurate new experiments are being considered and planed [5][6][7]. Owing to this principle, the effect of gravity can be locally replaced by an accelerated frame, which allows a geometry of spacetime to represent the physics of gravitation. As far as we know, any theory of gravitation should not break this equivalence principle. An apparent break of the principle was suggested by the fifth force presented by a re-analysis of the Eötvös experiment conducted in the 1980's [8] and many experiments to find this rather short-range force were conducted, but in vain [10][11][12][13][14][15].

A large number hypotheses by Dirac [16] lets us consider the time change of the Newtonian gravitational constant. The gravitational constant may decrease with time according to the evolution of the universe. Theoretical suggestions about a change of the gravitational constant have been summarized[17].

The inverse square law of gravitation was deduced by Newton analyzing the motions of planets and it has been accurately confirmed by observing the solar system to a scale of 10^8 km. However, the scalar-tensor theory by Fujii suggested a failure of the inverse-square law on the km-scale [18]. A original experiment showing a failure of the inverse-square law [19] triggered several succeeding tests. [20][21][22][23][24][25][26][27][28][29][30]. No evidence of a break has been confirmed so far.

Above all, the experimental attempts to find an anomaly of the law or the principle of gravitation adopted macroscopic force measurements with precise accuracy, where the measured force range toward small scale is limited due to a rapid decrease of the gravity. Therefore, a test of Newtonian gravity on the sub-millimeter scale, suggested by an extra-dimension theory [32], may require other new methods than the above macroscopic measurements in order to be completely tested. Reported results are introduced [33][34] along with some planned experiments [35][36].

2. Tests of Equivalence principle

It is difficult to answer the question why the ratio of the gravitational mass to the inertial mass of a particle is the same for all bodies, independent of their composition. This principle underlies the theory of gravitation. Historically, Newton measured its proportionality using a pendulum to an accuracy of 10^{-3}. After Newton, several measurements were made, as listed in Table 1.

Eötvös tried to measure a pair of possible torque forces produced by unbalanced composite forces of the Earth's gravitation and the centrifugal force produced by the rotation of the Earth for two suspended objects [1] using the apparatus shown in Fig 1. He adopted a platinum standard and measured 8 kinds of

‡ E-mail:kuroda@icrr.u-tokyo.ac.jp

Table 1. Historical list of tests of the equivalence principle.

Author	Method	Accuracy
Newton	pendulum	10^{-3}
Bessel	pendulum	10^{-6}
Eötvös	torsion balance	10^{-8}
Dicke	torsion balance	10^{-11}
Braginskii	torsion balance	10^{-12}
JPL	lunar ranging	5×10^{-13}

material, such as copper, water solutions, and wood. When the torsion beam was placed in the east-west direction, the centrifugal forces pointed towards the sky orthogonal to the beam of the balance, whereas the gravitational force pointed towards the center of the Earth. Each composite force might point toward the center of the Earth in a way slightly different from the gravity force because the centrifugal force is not large enough to deflect the composite force much from the gravity force. If the proportionality of the inertial mass to the gravitational mass differs for each object, the composite force would not lie in the same plane, which produces a torque force around the torsion fiber suspending the beam. Since the torsion fiber had a nature of drift, and tending to twist to one direction, the effect was removed by a measurement procedure in which the apparatus was rotated by 180 degrees after recording the measurement and the same measurement was repeated. The result was drawn by subtracting the recorded angle from the other. This process cancelled the drift effect. The result was summarized by a parameter (η), which is

$$\eta = \left| 2 \frac{\left(\frac{m_I}{m_G}\right)_1 - \left(\frac{m_I}{m_G}\right)_2}{\left(\frac{m_I}{m_G}\right)_1 + \left(\frac{m_I}{m_G}\right)_2} \right| \approx \left| \left(\frac{m_I}{m_G}\right)_1 - \left(\frac{m_I}{m_G}\right)_2 \right|, \quad (1)$$

where m_I, m_G are the inertial mass and its gravitational mass, respectively, and the suffix specifies the pair of compared objects for torsion-balance measurements. Eötvös reported that he could not find any anomaly exceeding $\eta > 10^{-8}$.

The experiment of Eötvös was greatly improved by Dicke *et al.* using solar gravitation with the Earth's orbital centrifugal force [2]. Although Eötvös needed to rotate the apparatus artificially, the Earth's rotation automatically rotated the apparatus of Dicke *et al.* Test masses were made of aluminum and gold. The effect of the gravity gradient by the surrounding mass distribution was coped with by symmetrical configuration of the suspended masses. A new electric device was introduced, which was later named a lock-in-amplifier. An accuracy of 10^{-11} was achieved. A Moscow group made a further improvement of the accuracy by one order ten years later after Dicke *et al* [3].

After a test of the equivalence principle in Moscow, a more precise laboratory measurement was not attempted for a long time until the appearance of a paper suggesting a fifth force [8], which revived experiments of gravitation in the 1980's. This suggestion came from a theory of particle physics which advocated a hypercharge field that produces a composition-dependent force on a short range, which apparently contradicts the equivalence principle. Since composition-independence had been widely believed due to precise tests [1][2][3], a possible force that had the dependence of both force range and composition attracted many experimentalists.

The result given in the lowest column of the Table 1 came from a lunar ranging of the Apollo program [4]. The equivalence principle had not been tested for bodies large enough to have a significant fraction of their mass coming from gravitational self-energy. The fraction of self-energy of the Earth is 4.6×10^{-10} of the Earth mass and that of the moon is 1.9×10^{-11} of the moon mass. If this self-energy does not behave as a part of its inertial mass, the equivalence principle may break and the orbit of the moon would slightly shift towards the sun, which gives an observable departure from the measurement [9]. However, no shift has been found within the observational accuracy. The equivalence principle has been confirmed to be correct to an accuracy of 5×10^{-13}.

As Dicke stated in his paper[2], no one knows how much accuracy is sufficient to prove the correctness of the equivalence principle. Therefore, much more accurate tests are still considered and planed to be conducted. The STEP:Satellite Test of the Equivalence Principle is one of them. Masses of different

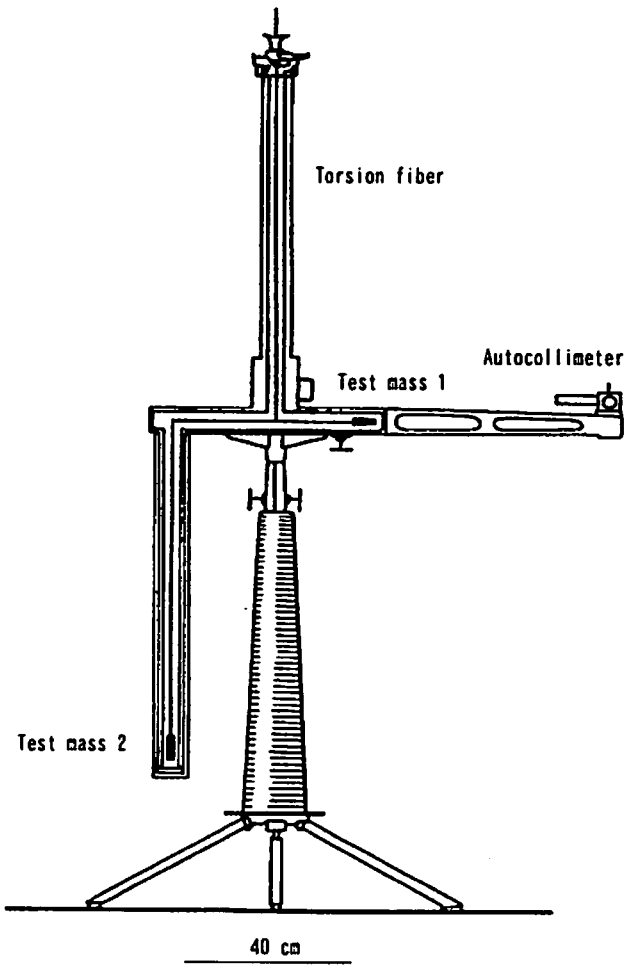

Figure 1. Torsion balance used by Eötvös for testing the equivalence principle. It was a device used to search Earth minerals by measuring the gravitational gradient field. This is why one of the suspended masses was placed lower than the other.

composition are placed inside a satellite orbiting the Earth to obtain a long duration of free fall. A very high positional sensor is made by adopting a cryogenic temperature of 1.8 K and using SQUIDs. Micro-Newton thrusters are used to cancel the small accelerations of the satellite due to residual air drag, radiation pressure and the solar wind which could couple to masses. STEP aims to measure the equivalence principle at the level of 1 part in 10^{18} [5]. Since STEP is a big project that needs a huge amount of money and much manpower, some alternative experiments are planed. A drop-tower experiment is a modern version of Galileo's Pisa tower experiment that uses a 100 m tall dropping tower in Bremen, Germany [6]. Another idea is planed by the GiZero project, which adopts a free-fall capsule from a balloon [7].

3. Time variation of the Newtonian gravitational constant

A concise short summary can be found in the introductory phrases of Ref. [17] about the time variation of the Newtonian gravitational constant (G). Briefly, they are introduced here. The time variation of G

Table 2. Time-variation limit on G.

method	limit
Lunar	$0 \pm 11 \times 10^{-12}$ yr^{-1}
Mar	$2 \pm 4 \times 10^{-12}$ yr^{-1}
Pulsar-White-dwarf	$-9 \pm 18 \times 10^{-12}$ yr^{-1}
PSR 1913+16	$4 \pm 5 \times 10^{-12}$ yr^{-1}
^{4}He abundance	$\leq 0.9 \times 10^{-12}$ yr^{-1}
Long term stability of clusters	$\leq 4 - 6 \times 10^{-11}$ yr^{-1}
Initial luminosity of Sun	$\leq 1 \times 10^{-10}$ yr^{-1}
Chandrasekhar limit	$-0.6 \pm 2 \times 10^{-12}$ yr^{-1}

can be known by observing the change in the orbit of a planet or satellite according to the equation

$$\frac{\dot{G}}{G} = -\frac{\dot{a}}{a}, \tag{2}$$

where a is the semi-major axis of the orbit. Direct length measurements to astrophysical objects gave a rather tight limit on the change of G. From a precise observation of pulsar timing, the orbital change of compact binary stars can be measured. Indirectly, the past values of G can be inferred by comparing big-bang nucleosynthesis models with the observed ^{4}He abundance. From the point of the long-term stability of Galaxies or globular clusters, the change of G can be estimated. Since the luminosity of the sun or stars is proportional to the 7th power of G, its evolution gives a limit on the change of G. This does not necessarily give a tight limit due to poor memory of the evolution of the Sun from the Earth preservation. On the other hand, the galactic population of neutron stars gives a more precise record of early stellar evolution from the Chandrasekhar limit on the mass of a neutron star. The above all estimations are summarized in Table 2.

4. Experiments concerning the inverse square law of Newtonian gravitation

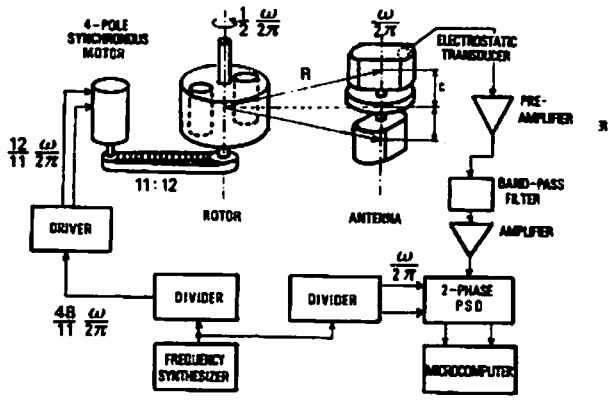

Figure 2. Dynamic Newton method to test the inverse-square law of Newtonian gravitation[27]

Although long-term observations of astronomical objects give a reliable and highly accurate test of the inverse-square law of Newtonian gravitation at the astronomical scale, 10^4 km $\geq r \geq 10^{10}$ km, the dependence on the laboratory scale had not been well-studied until the appearance of Long's anomaly of

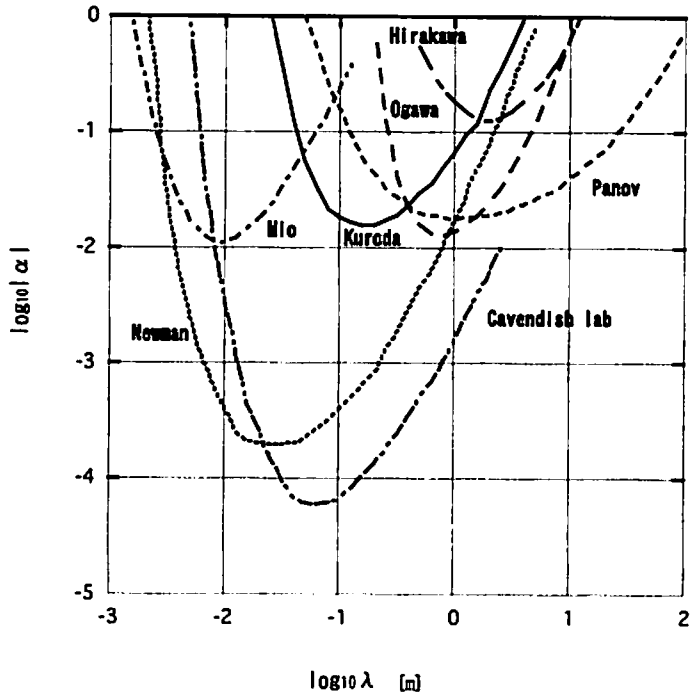

Figure 3. Constrain on $\alpha - \lambda$ representing the deviation from Newtonian gravity by laboratory experiments.

gravitation [19]. He compared the gravitational constant at a mass separation of 29.9 cm with the value at a separation of 4.48 cm using a torsion balance, and gave a discrepancy of 0.37% of G. The larger was the separation, the greater was the constant. This result was denied by several successive experiments. Panov and Frontov made measurements using a torsion balance the difference of the constant G at three different distance points(0.4 m, 3 m and 10 m). They could not find the anomaly published by Long [21]. Newman conducted a quite elegant null-experiment, where the scale dependence over a range of 2 cm to 5 cm by a test mass suspended from a torsion balance was used to probe the gravitational field inside a mass tube. Neglecting an end effect of the hollow cylinder, no torque would be observed if the inverse square law is correct. The result supported the inverse-square law within the experimental error [20]. Much more stringent limits were obtained using a torsion balance after these tests[24][25]. A different technique to test the dependence was devised by Hirakawa[22] and improved[26][27][28]. Figure 2 shows a schematic diagram of one of them using dynamic modulation of the gravitational field[27]. The modulator was put in a vacuum. The antenna developed as a resonant gravitational wave antenna was also suspended through an anti-vibration system in a vacuum chamber surrounded by a magnetic shield. The measurement was done over a range of from 8 cm to 20 cm, and its signal was limited by the thermal vibration noise of the antenna. These experiments could not find any anomaly of the Newtonian gravitation.

A devitation from Newtonian gravity is generally expressed by the following formula as a replacement of the Newtonian gravitational potential:

$$V(r) = -G\frac{m_1 m_2}{r}\left(1 + \alpha e^{-r/\lambda}\right), \tag{3}$$

where α and λ are the coupling strength and the force range parameter, respectively. The limit on the scale dependence of G by these laboratory experiments is given in Fig. 3.

Since the gravitational force decreases at larger distances in the laboratory, the maximum distance tested by a torsion balance or the dynamic Newton method with finite masses has remained within 10 m. To conduct a test at distances larger than 10 m, geophysical measurements were used. The first example is to measure the difference in the gravity acceleration due to a layer of mass distribution such as water, using a mass balance. If Newtonian gravity is correct, the difference in the gravity accelerations (Δg) is given assuming on infinite two-dimensional spread of the layer by

$$\Delta g = 4\pi\rho G h, \tag{4}$$

where h is the thickness of the water layer and ρ is the density of the water. A regular change of water height is used for modulating the measured magnitude with time, which can improve the signal-to-noise ratio. The most recent result using this kind of geophysical measurement has given a limit at a scale of 100 m [29]. In order to extend a much larger scale, a geophysical survey of gravity acceleration (g) on a terrain is conducted using a gravity meter, such as the Lacoste-Romberg type. By supposing a spherical surface of the Earth with a homogeneous mass distribution inside, one can easily calculate the upward continuation of g, which is compared with the observation made at elevating points along a tower [30]. Although one of tower measurements gave an anomaly of Newtonian gravity, many other tower measurements obtained no evidence of a deviation from the Newtonian law.

5. Sub-millimeter scale tests of Newtonian gravity

As described in the previous section, there is little experimental knowledge concerning gravity in the scale range under 1 cm. Tests of Newtonian gravity in this region is becoming important because of recent theoretical predictions of new forces that come from modern theories, which attempt to unify gravity with the strong and electroweak interactions [31].

In an attempt to describe gravitation and the other fundamental interactions within a single framework, the mass of the light boson is typically given by

$$m \approx M_P\left(\frac{M}{M_P}\right)^n, \tag{5}$$

where $M_P \approx 10^{19}$GeV is the Planck mass, M a mass scale associated with the known elementary particles, and n a small integer. In superstring theory, supersymmetry breaking occurs at low energy, 10-100 TeV, which corresponds to a force range of up to 20 μm for $n = 2$. A related theory predicts lower energy of supersymmetry breaking, such as $M = 1$ TeV (moduli) which produces a longer force range on the millimeter scale. Another theoretical possibility is the dilaton of string theory, which gives a stronger coupling of light scalars. The axion is a light pseudoscalar boson motivated by the strong CP problem of the standard model. The cosmological constant implies the existence of new quanta, the range of which can be adjusted to be 100 μm. Apart from these bosons born in supersymmetry breaking, new compact dimensions arising from the consideration of a fundamental short scale in nature may solve the hierarchy problem, where gravitons propagate freely, but the standard model fields do not. Since the smallest number of new dimensions has not been ruled out by an experiment ($n = 2$), yet, the size of the new dimensions is in the millimeter region. Gravitational measurements in this regime would be sensitive to potentials dictated by Gauss's law in $(4 + n)$ dimensions, which means that the gravitational forces vary as r^{-4} in the case of $n = 2$. Extra spatial dimensions are curled up in very small regions (scale R_P) in this theory (brane world).

In Eq.(3) r is assumed to be fairly greater than the curled-up scale (R_P). The simplest scenario predicts $\lambda = R_c$ and $\alpha = 3$ for compactification on a 2-sphere, where R_c is the Compton wavelength corresponding to mass M in Eq.(5). On the other hand, dilaton and moduli exchange could produce forces with $\alpha \sim 10^5$ for the Yukawa ranges, $\lambda \sim 0.1$ mm.

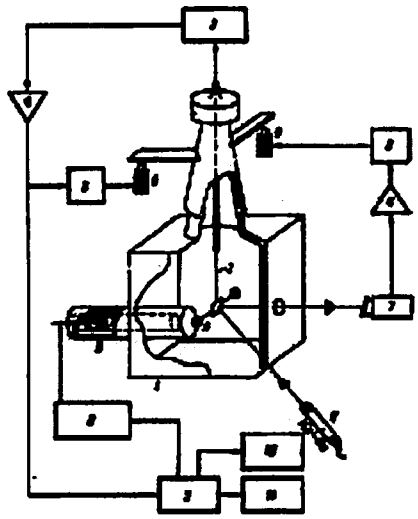

Figure 4. Block diagram of the experimental arrangement. 1, Vaccum chamber; 2, torsion balance; 3, capacitive displacement transducer; 4, amplifier; 5, filter; 6, electromagnet; 7, photodetector; 8, displacement control system for mass; 9, laser source; 10, recorder; 11, voltmeter. This figure was taken from [33].

Since the gravitational force decreases along with a reduction of the mass scale towards small scales, precise measurements become difficult to test any breakage of the Newtonian law of gravitation in the millimeter region. First, a general difficulty comes from the small-sized source and the test mass. This reduces the gravitational force, itself, and relatively increases the noise forces of the background. However, two direct measurements in this region have been made so far. One of them was done for finding a possible fifth force [8] by a Moscow group [33]. Figure 4 shows a block diagram of the experimental arrangement to measure the gravitational force between two spherical masses. Two spheres were fixed to both ends of a torsion beam that was suspended in a vacuum chamber by a quartz fiber 5 μm in diameter and 14 mm long. The spheres were made of platinum weighing 60 mg. An attracting force was produced by a slowly oscillating sphere of mass 706 mg in coincidence with a torsion oscillation period of 42 s. The source mass could be approached to the one of test mass as close as the order of 0.5 mm through inside a cylindrical insert invading into the vacuum. The angular displacement was detected by a capacitive transducer formed by the insert and the test mass. An important device to accomplish this measurement was an active anti-vibration system to stabilize the pendulum motion of the fiber using an optical lever system. The force measurement was made by knowing the response of the test mass with time. The analyzed force ratio at two different points gave no evidence of the expected anomaly, which is summarized in Fig. 7.

The second test was made by a Eöt-Wash group, lead by Adelberger [34]. A test mass with 10-fold rotational symmetry was suspended by an 82 cm-long, 20 μm-diameter wire above a rotating attractor with the same rotational symmetry as given in Fig. 5. The test mass was a 2.002 mm-thick aluminum annulus containing ten equally spaced 9.528 mm-diamter holes, centered on a 55.33 mm-diameter large circle. The active component of the attractor consisted of two coaxial copper disks. The 1.846 mm-thick upper disk had ten 9.535 mm-diameter holes centered on a 55.31 mm-diameter circle, while the 7.825 mm-thick lower disk had ten 12.690 mm-diameter holes centered on a 55.33 mm-diameter circle. The lower disk holes were rotated azimuthally by 18 ° compared to the upper holes. This configuration reduced the signal from Newtonian gravity without reducing the effect of a possible short-range force. The separation (ς) between the test mass and the attractor upper disk was changed from 218 μm to 10.78 mm. The measured torque varied with the rotation at 10 times the attractor rotation frequency, and was measured by an autocollimeter. The data was decomposed into three Fourier components(T_{10}, T_{20}, T_{30}), which may

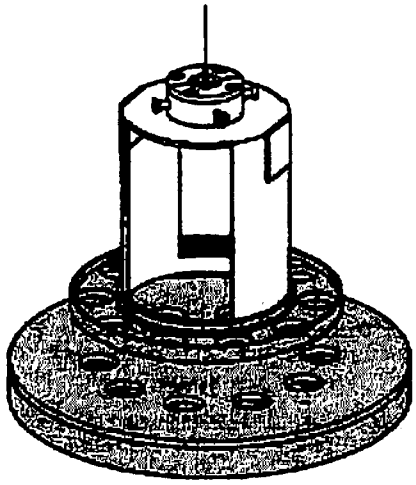

Figure 5. Suspended test mass with 10-fold symmetry used in the Eöt-Wash experiment. The figure was copied from [34].

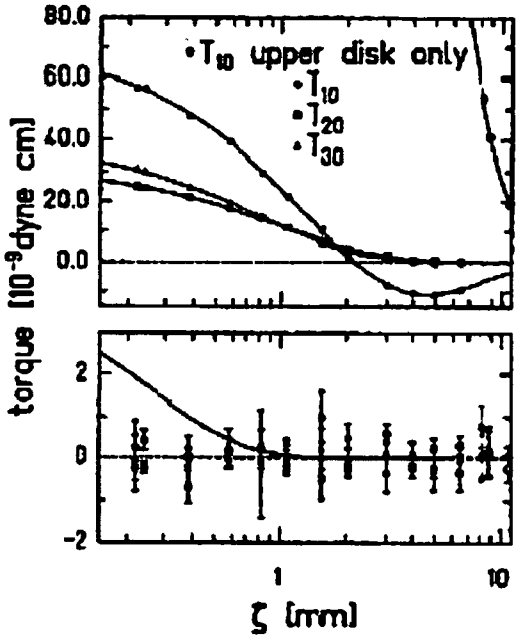

Figure 6. Harmonical torques(T_{10}, T_{20}, T_{30}) obtained by the Eöt-Wash experiment plotted with a fitted curve to the Newtonian gravity. The lower panel displays the Newtonian fit residuals; the solid curve shows the effect on T_{10} of an interaction with $\alpha = 3$ and $\lambda = 250$ μm. This graph was taken from reference [34]

reflect higher haromonics of Newtonian gravity.

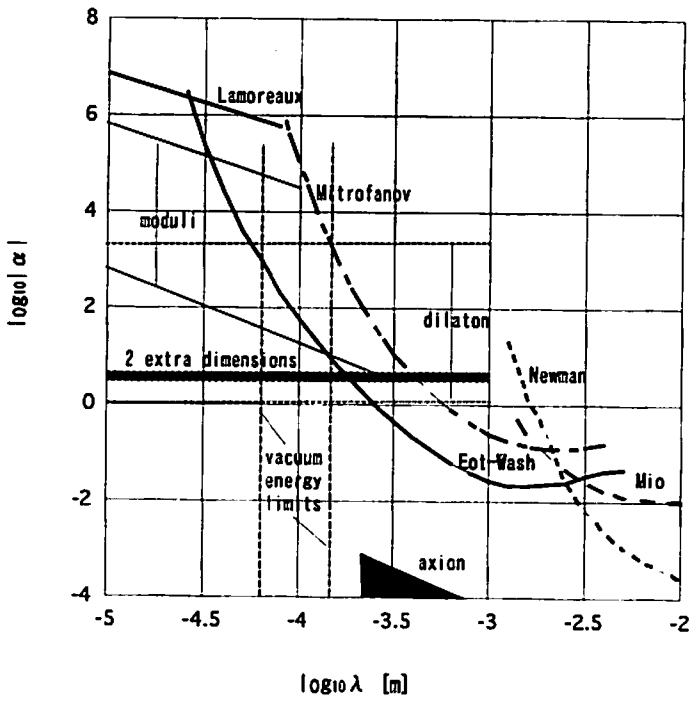

Figure 7. Experimental results summarized using the parameters in Eq.(3). The scenario of 2 extra dimensions is excluded at 95% confidence for $\lambda \geq 190$ μm. The estimation curves were referenced from [34].

Figure 6 represents the torques of these components and the departure curve from the Newtonian gravity against ζ [34]. Without the set of two disks reducing Newtonian gravity, T_{10} would be fairly larger than the recorded one. The data was well described by the Newtonian gravity with a χ^2 per degree of freedom of 1.03 and a probability of 41%. The parameters of new physics of the form given in Eq.(3) are allowed as long as the estimated torques remain within the obtained error ranges. They are plotted in Fig. 7 along with results of other experiments. Scenarios with $\alpha \geq 3$ are excluded at the 95% confidence for $\lambda \geq 190$ μm. The author emphasized in the paper that the test can be improved by more than one order of magnitude in the future.

Other than the above experiments, new projects are being considered using new tools [35][36][31]. One of them adopts a device developed for studies on the microscopic scale, such as a scanning tunneling microscope. Another effort to enhance the signal uses a resonant amplification technique. Since new tools require extensive R&D, physical results may not be obtained very soon. However, efforts to apply techniques developed in precise measurements to this new frontier are significantly important.

6. Conclusion

Testing the equivalence principle for the foundation of gravitation physics has been reviewed and experimental tests of the empirical law of gravitation have been introduced to find possible time change and a distance dependence. No evidence of a deviation from either the equivalence principle or Newtonian gravity has been reported. A new force born in relation to the unification theory opens a frontier of gravity experiments. In order to explorer new forces on fairly small spatial scale, revolutionary ideas are certainly needed along with the establised techniques. This may be a big challenge for experimentalists.

References

[1] R.v.Eötvös, D.Pekar and E.Fekete, Ann. Phys. (Leipzig) **68** (1922) 11; R.v.Eötvös, D.Pekar and E.Fekete, in *Roland Eötvös Gesammelte Arbeiten*, Edited by P. Selenyi (Akademiai Kiado, Budapest, 1953) pp.307-372, which was translated to English by E. Fischbach *et al*, University of Washington preprint 40048-13-N6.
[2] P.G.Roll, R.V.Krotkov, R.H.Dicke, Ann. Physics (New York) **26** (1964) 442.
[3] V.B.Braginskii, V.I.Panov, Soviet Physics JETP **34** (1972) 463.
[4] J.O.Dickey, *et al.*, Science **265** (1994) 482.
[5] *http://www.ssd.rl.ac.uk/fundphys/step/*
[6] *http://www.zarm.uni-bremen.de/index.htm*
[7] V.Iafolla, S.Nozzoli, E.C.Lorenzini, V.Milyukov, Rev. Sci. Instr. **69** (1998) 4145.
[8] E.Fischbach, *et al.*, Phys. Rev. Lett. **56** (1986) 3.
[9] K.Nordtvedt, Phys. Rev. **170** (1968) 1186.
[10] C.W.Stubbs, *et al.*, Phys. Rev. Lett. **58** (1987) 1070.
[11] T.M.Niebauer, M.P.McHugh, J.E.Faller, Phys. Rev. Lett. **59** (1987) 609.
[12] P.G.Nelson, D.M.Graham, R.D.Newman, Phys. Rev. D**42** (1990) 963.
[13] K.Kuroda, N.Mio, Phys. Rev. D **42** (1990) 3903.
[14] R.Cowsik, *et al.*, Phys. Rev. Lett. **61** (1988) 2179.
[15] C.C.Speake, T.J.Quinn, Phys. Rev. Lett. **61** (1988) 1340.
[16] P.A.M.Dirac, Nature (London) **139** (1937) 323.
[17] S.E.Thorsett, Phys. Rev. Lett. **77** (1996) 1432.
[18] Y. Fujii, GRG J. **13** (1981) 1147.
[19] D.R.Long, Nature **260** (1976) 417.
[20] R.Spero, *et al.*, Phys. Rev. Lett. **44** (1980) 1645.
[21] V.I.Panov, V.N.Frontov, Sov. Phys. JETP **50** (1979) 852.
[22] H.Hirakawa, K.Tsubono, K.Oide, Nature **283** (1980) 184.
[23] H.-T.Yu, W.-T.Ni, Phys. Rev. D **20** (1979) 1813.
[24] Y.T.Chen, A.H.Cook, A.J.F.Metherell, Proc. R. Soc. Lond. A**394** (1984) 47.
[25] J.K.Hoskins, *et al.*, Phys. Rev. D **32** (1985) 3084.
[26] Y.Ogawa, K.Tsubono, H.Hirakawa, Phys. Rev. D **26** (1982) 729.
[27] K.Kuroda, H.Hirakawa, Phys. Rev. D **32** (1985) 342.
[28] N.Mio, K.Tsubono, H.Hirakawa, Phys. Rev. D **36** (1987) 2321.
[29] A. Cornaz, B.Hubler, W. Kündig, Phys. Rev. Lett. **72** (1994) 1152.
[30] C.C.Speake, *et al.*, Phys. Rev. Lett. **65** (1990) 1967.
[31] J.C.Long, H.W.Chan, J.C.Price, Nucl. Phys. B **539** (1999) 23.
[32] L.Randall, R.Sundrum, Phys. Rev. Lett. **83** (1999) 4690.
[33] V.P.Mitrofanov, O.I.Ponomareva, Sov. Phys. JETP **67** (1988) 1963.
[34] C.D.Hoyle, *et al.*, Phys. Rev. Lett. **86** (2001) 1418.
[35] G.Carugno, *et al*, Phys. Rev. D **55** (1997) 6591.
[36] G.L.Klimchitskaya, *et al*, Int. J. Mod. Phys. A**12** (1997) 1465.

Scalar Field Cosmology With Negative Potentials

Gary N. Felder[1], Andrei Frolov[2], Lev Kofman[3]

CITA, University of Toronto
60 St. George Street, Toronto, ON M5S 3H8, Canada

Andrei Linde[4]

Department of Physics, Stanford University
Stanford, CA 94305, USA

Abstract

We investigate cosmological evolution in models where the effective potential $V(\phi)$ may become negative for some values of the field ϕ. Phase portraits of such theories in space of variables $(\phi, \dot{\phi}, H)$ have several qualitatively new features as compared with phase portraits in the theories with $V(\phi) > 0$. Cosmological evolution in models with potentials with a "stable" minimum at $V(\phi) < 0$ is similar in some respects to the evolution in models with potentials unbounded from below. Instead of reaching an AdS regime dominated by the negative vacuum energy, the universe reaches a turning point where its energy density vanishes, and then it contracts to a singularity with properties that are practically independent of $V(\phi)$.

1 Introduction

Since the invention of inflationary cosmology [1], the theory of the evolution of scalar fields in an expanding universe has been investigated quite extensively, both at the classical and the quantum level. While many features of scalar field cosmology are well understood, the overall picture remains somewhat incomplete. In this paper we will extend the investigation of scalar field cosmology to models with negative effective potentials.

There are several reasons to study cosmology with negative potentials. The first one is related to the cosmological constant problem. The simplest potential used in inflationary cosmology is $V(\phi) = \frac{1}{2}m^2\phi^2$. One can add to this potential a small cosmological constant V_0 without changing any features of inflation. A small positive $V_0 \sim 10^{-120}$ (in Planck units) would be sufficient to describe the present acceleration of the universe in a de Sitter-like state. But why should V_0 be so small and positive? What would happen for $V_0 < 0$? Does the post-inflationary universe with $V_0 < 0$ behave like anti-de Sitter space, which is so popular in M-theory?

Rather unexpectedly, the answer to this question appears to be negative: After a long stage of inflation the universe with $V_0 < 0$ cannot approach an AdS regime; instead of that it collapses [3]. In this paper we will study cosmological behavior in a large class of theories with negative potentials and explain why the universe in these theories stops expanding and eventually collapses.

Another reason to study theories with negative potentials is provided by the investigation of cosmology in N=2,4,8 gauged supergravity. Recently it was found that in all known versions of these theories potentials with extrema at $V(\phi) > 0$ are unbounded from below. Despite this fact, such models can, under certain conditions, describe the present stage of acceleration of the universe [3].

One more reason is related to a formal connection with warp factor/bulk scalar dynamics in brane cosmology. It has recently been shown that the equations for the warp factor and scalar field in brane

[1]Email: folder@cita.utoronto.ca
[2]Email: frolov@cita.utoronto.ca
[3]Email: kofman@cita.utoronto.ca
[4]Email: linde@physics.stanford.edu

cosmology with a scalar field potential $V(\phi)$ are similar to the equations for the scale factor and scalar field in 4D cosmology with the opposite potential $-V(\phi)$ [4]. This reveals an interesting relation of cosmology with negative potentials and warp geometry with positive potentials.

We are going to use a general approach based on the investigation of 3D phase portraits that show the behavior of the scalar field ϕ, its velocity $\dot{\phi}$, and the Hubble constant $H = \frac{\dot{a}}{a}$ as trajectories in a phase space. We will describe several basic regimes that are possible in scalar field cosmology, and apply phase diagram methods to models with positive definite as well as negative scalar field potentials. We will see that the phase portraits of models with $V(\phi) > 0$ and with $V(\phi) < 0$ are qualitatively different and the models with negative potential generically enter a stage of contraction. This makes potentials having a global minimum with $V(\phi) < 0$ as dangerous as potentials unbounded from below.

Although we are going to focus on the simplest model $V(\phi) = m^2\phi^2/2 + V_0$ in this presentation, many of the features of scalar field cosmology that we are going to discuss are model-independent. More extensive analysis, including the effects of matter and radiation, can be found in Ref. [5].

2 Four Basic Regimes in Scalar Field Cosmology

We will study the behavior of a homogeneous scalar field in a Friedmann universe with the metric

$$ds^2 = -dt^2 + a^2(t)ds_3^2 \,, \tag{1}$$

where $ds_3^2 = \gamma_{ij}dx^i dx^j$ is the metric of a 3D space with constant curvature, $k = 0, \pm 1$. Adopting a system of units in which $M_p = 1$, where $M_p = (8\pi G)^{-1/2} \sim 2 \times 10^{18}$ GeV, the Friedmann equation for a scalar field with potential energy density $V(\phi)$ is written as

$$H^2 = \left(\frac{\dot{a}}{a}\right)^2 = \frac{1}{3}\rho - \frac{k}{a^2} = \frac{1}{3}\left(\frac{1}{2}\dot{\phi}^2 + V(\phi) + \rho_\alpha\right) - \frac{k}{a^2} \,. \tag{2}$$

Here ρ is the total energy density and ρ_α is the density of matter with equation of state $p_\alpha = \alpha\rho_\alpha$. For non-relativistic matter $\alpha = 0$, while for radiation $\alpha = 1/3$. The evolution of H is given by a combination of the Einstein equations

$$\dot{H} = -\frac{1}{2}(\rho + p) + \frac{k}{a^2} = -\frac{1}{2}(\dot{\phi}^2 + \rho_\alpha(1 + \alpha)) + \frac{k}{a^2} \,, \tag{3}$$

while the evolution of the scalar field ϕ follows from the Einstein equations,

$$\ddot{\phi} + 3H\dot{\phi} + V_{,\phi} = 0 \,. \tag{4}$$

We shall study the basic properties of scalar field cosmology using as an example the simplest harmonic oscillator potential

$$V(\phi) = \frac{1}{2}m^2\phi^2 + V_0 \,. \tag{5}$$

There are four basic regimes that we may encounter: the universe can be dominated by the potential energy density $V(\phi)$, by the kinetic energy density $\dot{\phi}^2/2$, by the energy density of an oscillating scalar field, in which case $V(\phi) \sim \dot{\phi}^2/2$, or by matter/radiation ρ_α. In this presentation, we discuss the first three regimes in the case of spatially flat universe ($k = 0$), while the effects of matter and curvature are analyzed in Ref. [5].

2.1 The inflationary regime: Energy density dominated by $V(\phi)$

Inflation occurs when the energy density is dominated by $V(\phi)$. In this case $\dot{\phi}^2/2, \rho_\alpha \ll V(\phi)$ and $|\ddot{\phi}| \ll |3H\dot{\phi}|$. This corresponds to the vacuum-like equation of state $p = -\rho$. The equations for a and ϕ in this regime have the following form:

$$H^2 = \frac{m^2\phi^2}{6} + \frac{V_0}{3} \,, \qquad 3H\dot{\phi} + m^2\phi = 0 \,. \tag{6}$$

The solutions of the equations for $\phi(t)$ and $a(t)$ for the most interesting case $\frac{m^2\phi^2}{2} \gg |V_0|$ are given by

$$\phi(t) = \phi_0 - \sqrt{\frac{2}{3}}mt\,, \qquad a(t) = a_0 \exp\left(\frac{\phi_0^2 - \phi^2(t)}{4}\right)\,. \tag{7}$$

These solutions, which describe inflationary expansion, are valid only for $\dot\phi^2/2 \ll V(\phi)$, which implies that inflation ends at $|\phi_e| \sim 1$. In this paper we will assume that $m^2 \gg |V_0|$, in which case $\frac{m^2\phi^2}{2} \gg |V_0|$ is always satisfied during inflation.

2.2 The kinetic regime: Energy density dominated by $\dot\phi^2/2$

Another important regime occurs when the energy density is dominated by $\dot\phi^2/2$. In this case $V(\phi), \rho_a \ll \dot\phi^2/2$ and $|\ddot\phi|, |3H\dot\phi| \gg m^2\phi$. This corresponds to the "stiff" equation of state $p = \rho$. The equations for a and ϕ are:

$$H^2 = \frac{\dot\phi^2}{6}\,, \qquad \ddot\phi + 3H\dot\phi = 0\,. \tag{8}$$

The solutions can be written as follows:

$$a(t) = t^{1/3}\,, \qquad \phi = \phi_0 \pm \sqrt{\frac{2}{3}}\,\ln\frac{t_0}{t}\,, \qquad \frac{\dot\phi^2}{2} = \frac{1}{3t^2}\,. \tag{9}$$

These solutions can describe an expanding universe or a universe collapsing towards a singularity.

During the expansion of the universe, the inflationary regime $V(\phi) \gg \dot\phi^2/2$ represents a stable intermediate asymptotic attractor. Even if a flat universe begins in a state with $\dot\phi^2/2 \gg V(\phi)$, it typically rapidly switches to an inflationary regime with $V(\phi) \gg \dot\phi^2/2$ [2]. This occurs because during the expansion of the universe with $\dot\phi^2/2 \gg V(\phi)$, the value of the kinetic energy drops down like t^{-2}, whereas the field changes only logarithmically. Therefore for all power-law potentials, the value of $V(\phi)$ decreases much more slowly than $\dot\phi^2/2$. When it becomes greater than $\dot\phi^2/2$, inflation begins.

During the collapse of the universe, the opposite occurs. $V(\phi)$ grows only logarithmically, whereas $\dot\phi^2/2$ diverges as t^{-2}, where t is the time remaining before the big crunch singularity. This means that the regime $\dot\phi^2/2 \gg V(\phi)$ generically occurs at the stage of collapse. In this regime one can neglect $V(\phi)$ in the investigation of the singularity at $t \to 0$.

2.3 The oscillatory regime

Now let us assume that the field ϕ oscillates near $\phi = 0$ with frequency much greater than H, and that the average value of $V(\phi)$ during these oscillations is much greater than $V_0 = V(0)$. In this case one can neglect the term $3H\dot\phi$ in Eq. (4), so that in the first approximation one simply has

$$\ddot\phi + m^2\phi = 0 \tag{10}$$

and $\phi = \Phi \sin mt$. Here Φ is the amplitude of the oscillation. As the pressure $p = \dot\phi^2/2 - V(\phi) = \frac{m^2}{2}\Phi^2 \cos 2mt$ produced by these oscillations vanishes on average, the universe in this regime expands as $a \sim t^{2/3}$, and the amplitude of the oscillations decreases as $\Phi(t) \sim a^{-3/2} \sim t^{-1}$.

The regime of oscillations usually begins after the end of inflation, at $\phi \lesssim 1$. As long as one can neglect V_0, the field oscillations after inflation approach the following asymptotic regime:

$$\phi(t) \approx \frac{2\sqrt{2}}{\sqrt{3}\,mt}\,\sin mt \;\approx\; \frac{\sqrt{2}}{\pi\sqrt{3}\,N}\,\sin mt\,. \tag{11}$$

Here t is the time after the end of inflation and N is the number of oscillations.

When the amplitude becomes very small the term V_0 will become important. If $V_0 > 0$, the universe enters a second stage of inflation with $H^2 = V_0/3$. The amplitude of oscillations of the field ϕ in this regime falls down exponentially as $e^{-3Ht/2}$. However, if $V_0 < 0$, a dramatic change in behavior occurs when the energy density of oscillations (and matter) gradually decreases and becomes comparable to $-V_0$, as the expansion of the universe slows down at that time, and eventually the universe begins collapsing. When the universe contracts, the amplitude of oscillations grows as $a^{-3/2}$ until the stage of oscillations ends and the regime dominated by kinetic energy begins at $|\phi_b| \sim 1$.

3 Phase Portraits and Cosmological Evolution

Having discussed some important limiting regimes in scalar field cosmology, we are now ready to investigate the complete evolution of a Friedmann universe with a scalar field. To study this system we find it most convenient to rewrite the evolution equations for a and ϕ as a set of three coupled, first-order, differential equations:

$$\frac{d\phi}{dt} = \dot{\phi}, \qquad \frac{d\dot{\phi}}{dt} = -3H\dot{\phi} - V_{,\phi}, \qquad \frac{dH}{dt} = -\frac{1}{3}\left(\dot{\phi}^2 - V\right) - H^2 \tag{12}$$

plus the constraint equation

$$H^2 - \frac{1}{6}\dot{\phi}^2 - \frac{1}{3}V = -\frac{k}{a^2}. \tag{13}$$

All solutions to these three equations can be represented as trajectories in the 3D phase space of ϕ, $\dot{\phi}$, and H, with trajectories never intersecting each other. Every trajectory must begin and end at critical points, i.e. the points for which the derivatives of all three phase variables vanish. There are finite and infinite critical points.

To find infinite critical points and visualize the flow of trajectories at infinity, it is useful to do a Poincaré mapping $x_P \equiv \frac{x}{1+r}$ where x is any of $(\phi, \dot{\phi}, H)$ and $r^2 = \phi^2 + \dot{\phi}^2 + H^2$. The interior of the unit sphere $\phi_P^2 + \dot{\phi}_P^2 + H_P^2 = 1$ maps to the infinite phase space of ϕ, $\dot{\phi}$, and H, so by plotting trajectories in these new coordinates the entire phase space can be easily visualized. Infinite critical points, which represent the possible starting and ending points for all trajectories that go off to infinity in the usual coordinates, occur on the boundary of Poincaré sphere $\phi_P^2 + \dot{\phi}_P^2 + H_P^2 = 1$. For 2D projection of phase portraits, e.g. in the variables ϕ and $\dot{\phi}$, we use a 2D Poincaré mapping where $r^2 = \phi^2 + \dot{\phi}^2$.

Trajectories for the flat universe are located on a 2D surface defined by constraint equation (13) with $k = 0$, i.e. the phase portrait for the flat universe is two dimensional. This surface divides the phase space into three separate regions (including the surface itself) representing the possible types of curvature. No trajectory can pass from one of these regions to another. Although the location of the finite critical points for a given model depends strongly on V, the structure of the infinite critical points is very similar across a wide range of potentials. See Ref. [4] for recent discussion.

4 Cosmology with a Non-Negative Potential

As a simple example we consider the model $V(\phi) = \frac{1}{2}m^2\phi^2 + V_0$ discussed in Section 2. By rescaling the field and time variables the mass m can be eliminated from the equations, so for simplicity we set $m = 1$ in what follows. The hypersurface representing a flat universe is given by

$$6H^2 - \dot{\phi}^2 - \phi^2 = 2V_0. \tag{14}$$

The surface defined by this equation is a hyperboloid. For positive definite potentials $V_0 > 0$ it is a hyperboloid of two sheets, meaning the two branches at $H > 0$ and $H < 0$ are disconnected. For $V_0 = 0$ this hyperboloid reduces to a double cone. For an open or closed universe the trajectories would lie in the interior or exterior of the hyperboloid, respectively [2].

There are two finite critical points for this system at $\phi = \dot{\phi} = 0$, $H = \pm\sqrt{V_0/3}$. For $V_0 = 0$ these two points reduce to a single finite critical point at the origin. There are also eight infinite critical points.

Figure 1 shows the phase space for this model with $V_0 > 0$ along with a sample of trajectories for $k = 0$. The hyperboloid along which all of these trajectories lie represents a flat universe. The upper branch corresponds to expansion and the lower one to contraction. The fact that the two branches are disconnected means that in a flat universe in this model expansion can never reverse and become contraction. (Note that this conclusion is unchanged for the case $V_0 = 0$, as no trajectory can pass through a critical point that connects two branches of a double cone.) Figure 1 also shows the 2D Poincaré projection of upper branch of the flat universe hyperboloid. This plot is very similar to the one shown in [2] for this model with $V_0 = 0$.

For an expanding universe there are four infinite critical points, two repulsors labeled R_1 and R_2 and two saddle points labeled S_1 and S_2. All trajectories begin at R_1, R_2 and wind towards the focus at the

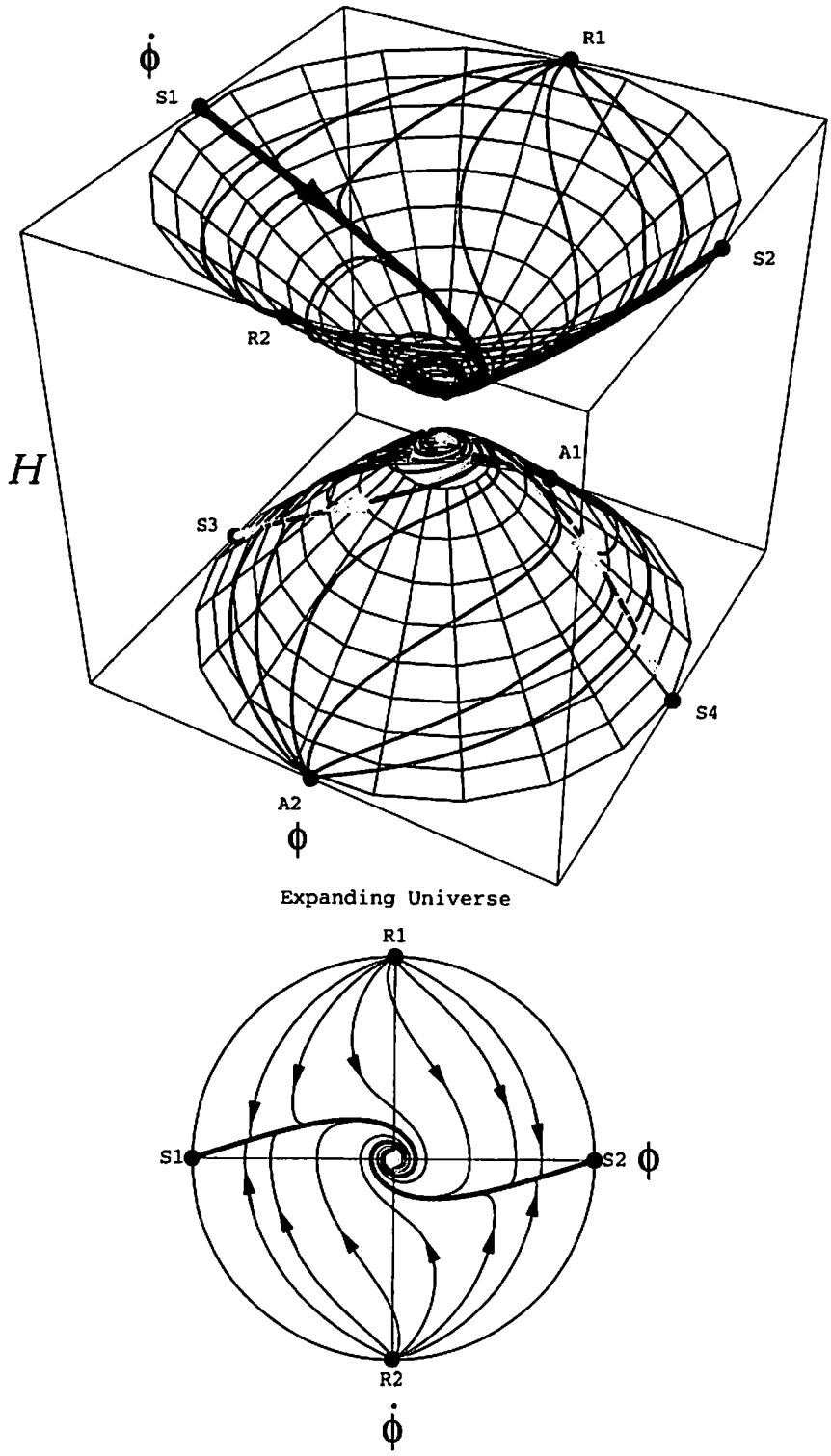

Figure 1: Phase portrait for the theory $V(\phi) = \frac{1}{2}m^2\phi^2 + V_0$ with $V_0 > 0$ in rescaled coordinates $(\phi, \dot{\phi}, H)$. The branches describing stages of expansion and contraction (upper and lower parts of the hyperboloid) are disconnected. Bottom: Projection of the upper ($H > 0$) branch of the full phase portrait onto $(\varphi, \dot{\varphi})$ plane.

center. The separatrices emanating from S_1 and S_2 represent attractor trajectories (not to be confused with attractor critical points). Along these trajectories the universe experiences inflation ($\phi^2 \gg \dot{\phi}^2$) until it nears the center and begins winding around it, corresponding to field oscillations near the potential minimum. These separatrices represent a set of measure zero in the space of trajectories; the two shown are the only trajectories that begin at the saddle points. Nonetheless they are important because most of the trajectories emanating from the repulsor points asymptotically approach the separatrices. This is why inflation is a generic feature of models such as this one, and also why inflation erases all information about the initial conditions that preceded it.

Thus a typical trajectory passes through three of the four regimes described in Section 2. Near the repulsors the kinetic energy dominates and the equation of state is stiff, $p \approx \rho$. Near the main part of the separatrices the equation of state is inflationary, $p \approx -\rho$. Finally near the center the scalar field oscillates with decreasing amplitude (11) and the equation of state is that of non-relativistic matter, $p \ll \rho$. Although particle production is not included in these phase portraits, this evolution will typically end with the scalar field decaying into other forms of matter, thus finishing the evolution in the fourth regime, matter and/or radiation domination. The contracting branch is a mirror image of the expanding one, with the same three regimes occurring in the opposite order, finally ending with a big crunch singularity at the attractor points A_1 and A_2.

5 Cosmology with a Negative Potential

Now we turn to the investigation of cosmological models with scalar field potentials that may become negative. We will continue using the simple example $V(\phi) = \frac{1}{2}m^2\phi^2 + V_0$, but now we will consider $V_0 < 0$. The hypersurface representing a flat universe is still defined by

$$6H^2 - \dot{\phi}^2 - \phi^2 = 2V_0, \tag{15}$$

but with V_0 negative, this surface is a hyperboloid of one sheet.

Figure 2 shows the phase space for this model and sample trajectories for a flat universe. The phase space is two dimensional, but its topology is very different from that for non-negative potentials. The infinite critical points are unchanged because the finite term V_0 has no effect at infinity, but there are no finite critical points. Thus all trajectories begin at infinity with $H > 0$ and end at infinity with $H < 0$. This is possible because the regions corresponding to expansion and contraction are now connected. This property is valid for all types of curvature k, i.e. for open, flat or closed universes.

To show a 2D projection of the flat universe hypersurface for this model, we have to plot both the expanding and contracting branches, as depicted on the bottom part of Figure 2. Trajectories in the expanding universe region spiral in towards the center. When they touch the inner circle, the "throat" of the hyperboloid, they pass into the contracting universe region. There they spiral back out to infinity, i.e. the big crunch. Thus typical trajectories in this scenario pass through the three regimes described above, kinetic energy domination, potential energy domination, and oscillations, and then pass back through them in reverse order. As before, including particle production will typically introduce a matter/radiation dominated regime after the first stage of oscillations. Eventually, however, the matter and radiation will redshift away and the universe will begin contracting.

Aside from this "wormhole" connecting the expanding and contracting branches this phase portrait looks a lot like the one for $V_0 > 0$ shown in Figure 1. Note, however, that in this case the separatrices emanating from the saddle points S_1 and S_2 no longer spiral in to the center, but rather end up reaching the points A_1 and A_2. Likewise there are separatrices that begin at R_1 and R_2 and end on S_3 and S_4. In the expanding phase their segments and segments of nearby trajectories represent the rare cases that manage to avoid inflation. In the contracting phase they become the marginal trajectories separating those that end at positive and negative ϕ. The number of windings (i.e. field oscillations) can be estimated by setting $m^2\phi^2/2 = |V_0|$ and using (11) to give $N \approx \frac{m}{6}|V_0|^{-1/2}$.

The phase portraits in Figure 2 were constructed in a way symmetric with respect to time reversal $t \to -t$. However, if one considers trajectories originating at $H > 0$ and homogeneously distributed with respect to the field ϕ at the Planck density, they tend to merge with the attractor trajectories going from $S1$ to $A2$ and from $S2$ to $A1$, and to be repelled from the trajectories going from $R1$ to $S3$ and from $R2$

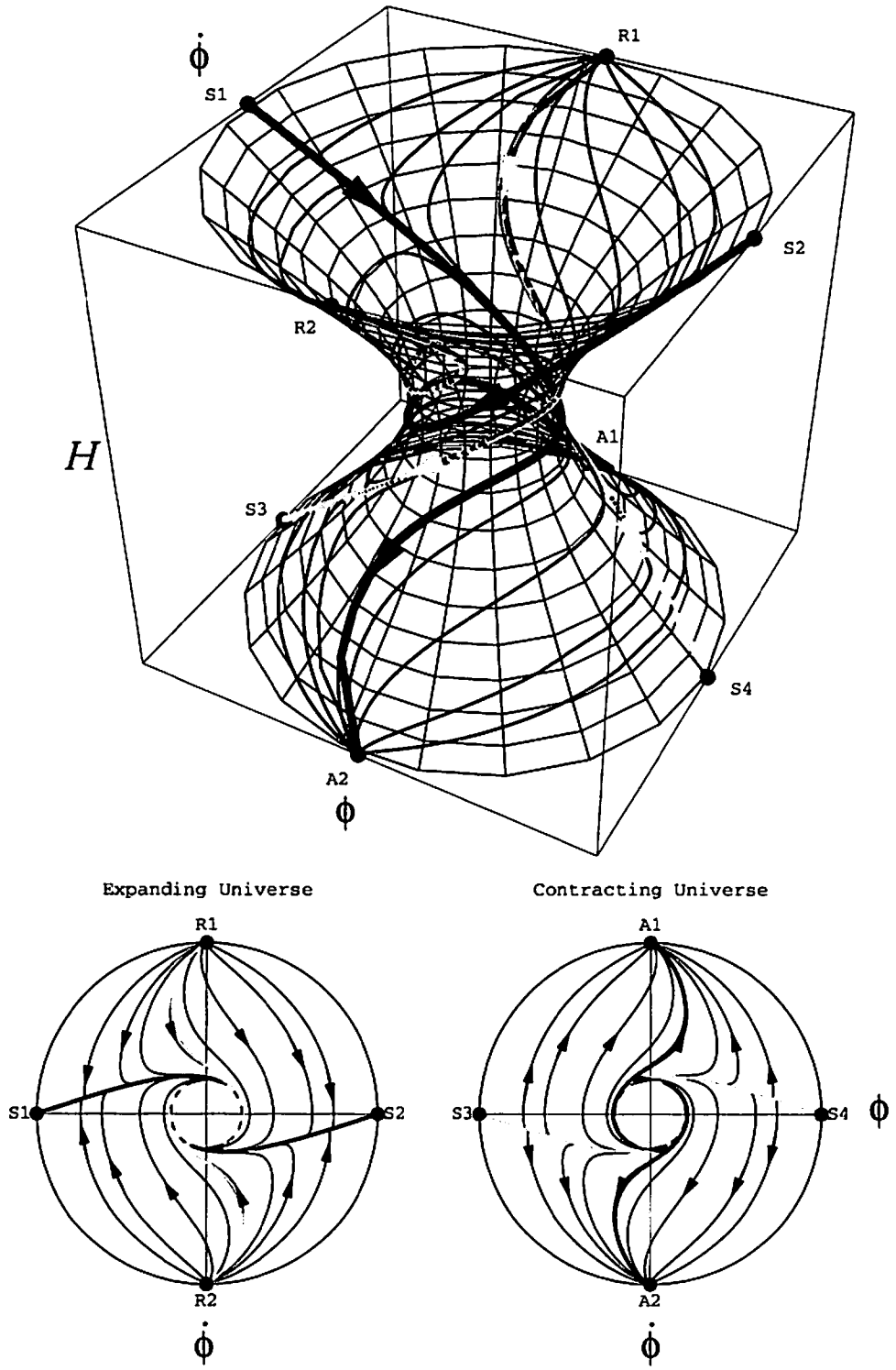

Figure 2: Phase portrait for the theory $V(\phi) = \frac{1}{2}m^2\phi^2 + V_0$ for $V_0 < 0$. The branches describing stages of expansion and contraction (upper and lower parts of the hyperboloid) are connected by a throat. Bottom left: $(\phi, \dot{\phi})$ projection of the $H > 0$ branch. Bottom right: $(\phi, \dot{\phi})$ projection of the $H < 0$ branch. Trajectories from the left panel continue on the right panel.

to $S4$. Therefore, if one traces their evolution into the lower part of hyperboloid ($H < 0$), the distribution of trajectories is not homogeneous anymore, and most trajectories closely follow lines to $A1$ and $A2$.

It is instructive to estimate the time that the universe may spend in its post-inflationary expanding phase before it begins to contract. The energy density of the oscillations of the scalar field decreases as $\rho \sim \frac{4}{3}t^{-2}$. The universe begins to collapse when $\rho + V_0 = 0$, which happens at $t \sim 2(3|V_0|)^{-1/2}$. As one could expect, this time can be greater than the present age of the universe only if $|V_0| \lesssim 10^{-120}$. However, in the theories where $V(\phi)$ has a very flat plateau or a local minimum, the universe may spend a very long time before the field ϕ falls down to the minimum with $V(\phi) < 0$ [3]. Therefore in general, the life-time of the universe may be very large even in theories with a very deep minimum of $V(\phi)$.

6 Conclusions

The main goal of our work was to perform a general investigation of scalar field cosmology in theories with negative potentials. We have found that the phase portraits of such theories in the 3D space $(\phi, \dot{\phi}, H)$ have different geometry as compared with phase portraits in theories with $V(\phi) \geq 0$. In theories with $V(\phi) > 0$ the phase portraits for flat universes are divided into two disconnected parts describing expanding and contracting universes ($H > 0$ and $H < 0$). Meanwhile in theories with $V(\phi) < 0$ these two parts become connected. The trajectories moving towards $V(\phi) < 0$ simultaneously move from the parts of the phase portrait with $H > 0$ towards the parts with $H < 0$. Once the universe begins to contract, it never returns to the stage of expansion until it reaches the singularity.

This does not mean that theories with negative potentials should be banned from consideration. In some cases the scalar field may be trapped in a metastable minimum, or it may roll towards $V(\phi) < 0$ extremely slowly. However, it is quite interesting that with an account taken of general relativity potentials that have minima at $V(\phi) < 0$ can be as dangerous as potentials unbounded from below.

A general feature of all trajectories bringing the universe towards the singularity is that in all theories with power-law potentials the kinetic energy $\dot{\phi}^2/2$ becomes much greater than $V(\phi)$ near the singularity. This means that the description of the singularity is nearly model-independent, at least at the classical level. In particular, the equation of state of the universe approaching the singularity typically is $p = \rho$.

Acknowledgements

The authors are grateful to R. Brandenberger, R. Kallosh, A. Maroto, S. Rasanen, A. Starobinsky, and N. Turok for many interesting discussions. The work by G.F., A.F. and L.K. was supported by PREA of Ontario, NSERC and CIAR. The work by A.L. was supported by NSF grant PHY-9870115, by the Templeton Foundation grant No. 938-COS273. G.F., L.K. and A.L. were also supported by NATO Linkage Grant 975389.

References

[1] A. A. Starobinsky, *Phys. Lett. B* **91**, 99 (1980); A. H. Guth, *Phys. Rev. D* **23**, 347 (1981); A. D. Linde, *Phys. Lett. B* **108**, 389 (1982); A. Albrecht and P. J. Steinhardt, *Phys. Rev. Lett.* **48**, 1220 (1982); A.D. Linde, *Phys. Lett. B* **129**, 177 (1983); A. D. Linde, *Phys. Lett. B* **259**, 38 (1991); A. D. Linde, *Phys. Rev. D* **49**, 748 (1994) [astro-ph/9307002].

[2] V. A. Belinsky, I. M. Khalatnikov, L. P. Grishchuk and Y. B. Zeldovich, *Phys. Lett. B* **155**, 232 (1985); V. A. Belinsky and I. M. Khalatnikov, *Sov. Phys. JETP* **66**, 441 (1987); V. A. Belinsky, H. Ishihara, I. M. Khalatnikov and H. Sato, *Prog. Theor. Phys.* **79**, 676 (1988).

[3] R. Kallosh, A. D. Linde, S. Prokushkin and M. Shmakova, [hep-th/0110089]; A. Linde, JHEP **0111**, 052 (2001) [hep-th/0110195].

[4] G. Felder, A. Frolov and L. Kofman, [hep-th/0112165].

[5] G. Felder, A. Frolov, L. Kofman and A. Linde, [hep-th/0202017].

On the origin of the cosmological constant

Jun'ichi Yokoyama

Department of Earth and Space Science, Graduate School of Science, Osaka University, Toyonaka 560-0043, Japan

Abstract

Under the assumption that the cosmological constant vanishes in the true ground state with lowest possible energy density, we argue that the observed small but finite vacuum-like energy density can be explained if we consider a theory with two or more degenerate perturbative vacua, which are unstable due to quantum tunneling, and if we still live in one of such states. An example is given making use of the topological vacua in non-Abelian gauge theories.

There are *two* cosmological constant (Λ) problems today. One is the older problem why the vacuum energy density is vanishingly small, or why the intrinsic cosmological term cancels with accumulation of zero-point energy in quantum field theory almost exactly. Observationally, the vacuum energy density $\rho_v = 3M_G^2\Lambda$ is no larger than the critical density $\rho_{cr0} = 4 \times 10^{-47}\mathrm{GeV}^4 = (3\mathrm{meV})^4$ today, where $M_G = M_{Pl}/\sqrt{8\pi} = 2.4 \times 10^{18}$ GeV is the reduced Planck scale. On the other hand, since a natural cutoff scale of zero-point fluctuations of each quantum field is the Planck scale, we would expect $\langle\rho_v\rangle \simeq M_G^4$ from them, which is larger than the observational constraint by a factor of 10^{120} [1].

The second, newer problem is that the above miraculous cancellation does not seem to work in a perfect manner, that is, there is increasing evidence that a finite positive component still remains in the vacuum-like energy density and that our Universe is in a stage of accelerated expansion now. For example, the analysis of SNIa data shows that the probability that we live in a universe with $\Lambda = 0$ is less than one percent [2].

Historically, a number of solutions have been proposed about the first problem [1, 3]. Among them, the quantum cosmological approach is based on the Euclidean path integral of the wave function of the universe [4]. It has been claimed that such a path integral is dominated by the de Sitter instanton solution proportional to $\exp(\frac{3\pi}{G\Lambda})$ and hence it is likely that the cosmological constant vanishes [5]. Coleman further incorporated fluctuations of the spacetime topology in terms of the "wormhole" configurations and found a double exponential dependence [6]. One should note, however, that the expectation values obtained in these approaches should be regarded as giving an average over the time in the history of the universe [1]. So they may not necessarily be related with the values we observe today. We may rather interpret it as predicting a vanishing cosmological constant in some ground state where the universe spends most of the time in history. [1] More recently, a number of higher dimensional models have been proposed in which the maximally symmetric solution of the three-brane must have a vanishing four-dimensional cosmological constant [9]. Since our Universe has not settled in a maximally symmetric state, it is difficult to understand implications of these results on current values of cosmological parameters in our Universe, but we are tempted to interpret them as predicting a vanishing cosmological constant again in some ultimate ground state.

Here we argue the possible origin of the small but finite cosmological constant without introducing any small numbers. We solve the second problem under the assumption that the first one is solved in the true ground state by arguing that we have not fallen into that state. Other proposed solutions to the second problem, such as quintessence [10] (see also [11] for earlier work) or meV-scale false vacuum energy [12], are also based on such a hypothesis.

Our starting point is that the energy eigenvalue of the true ground state of a theory with two or more degenerate perturbative vacua, which cannot be transformed from one another without costing energy, is smaller than that of a quasi-ground state localized around one of these states in field space by an

[1] We must also point out problems with Euclidean formulation of quantum gravity, namely, positive-nondefiniteness of the Euclidean action, the ambiguity of the signature of rotation [7], and the negativity of the phase of the saddle point solution [8].

exponentially small amount. Here, by perturbative vacua we mean a state with the lowest energy density without taking possible tunneling effect to another perturbative vacuum into account. Our hypothesis is that the cosmological constant vanishes *not* in these degenerate perturbative vacua but in the absolute ground state with quantum tunneling effects taken into account, because there are both classical and quantum contributions to the cosmological constant and what we observe is their sum.

For illustration let us first consider an abstract field theory model whose perturbative vacuum states are classified into two distinct categories labeled by $|+\rangle$ and $|-\rangle$ with $\langle +|-\rangle = 0$ at the lowest order. We also assume that, although the transition from $|+\rangle$ to $|-\rangle$ is classically forbidden, there is an instanton solution which describes quantum tunneling from $|+\rangle$ to $|-\rangle$ and vice versa. By nature the instanton is localized in space and (Euclidean) time with a finite Euclidean action S_0. Then the true ground state, $|S\rangle$, with this tunneling effect taken into account, is given by the symmetric superposition of $|+\rangle$ and $|-\rangle$, namely,

$$|S\rangle = \frac{|+\rangle + |-\rangle}{\sqrt{2}}, \tag{1}$$

where we have assumed that $|+\rangle$ and $|-\rangle$ are normalized.

Now we evolve $|S\rangle$ with Euclidean time T to calculate $\langle S|e^{-\mathcal{H}T}|S\rangle$ by summing up contributions of instantons and anti-instantons as

$$\begin{aligned}
\langle S|e^{-\mathcal{H}T}|S\rangle &= \frac{1}{2}\left(\langle +|e^{-\mathcal{H}T}|+\rangle + \langle -|e^{-\mathcal{H}T}|-\rangle + \langle +|e^{-\mathcal{H}T}|-\rangle + \langle -|e^{-\mathcal{H}T}|+\rangle\right) \\
&= e^{-\rho_0 VT}\sum_{j=0}^{\infty}\frac{1}{(2j)!}\left(kVTe^{-S_0}\right)^{2j} + e^{-\rho_0 VT}\sum_{j=0}^{\infty}\frac{1}{(2j+1)!}\left(kVTe^{-S_0}\right)^{2j+1} \\
&= \exp\left(-\rho_0 VT + kVTe^{-S_0}\right),
\end{aligned} \tag{2}$$

where $\mathcal{H}$ is the Hamiltonian, $k \equiv m^4$ is a positive constant and V represents spatial volume [13]. Here ρ_0 is the energy density of the perturbative vacua, $|+\rangle$ and $|-\rangle$, which are presumably translationally invariant. Thus the energy density of the true ground state $|S\rangle$ is given by

$$\rho_S = \rho_0 - m^4 e^{-S_0}. \tag{3}$$

It is this energy density that vanishes under our hypothesis. This in turn implies that we find a nonvanishing vacuum energy density

$$\rho_0 = m^4 e^{-S_0} \tag{4}$$

in either of the perturbative vacuum states, $|+\rangle$ or $|-\rangle$.

Thus if our Universe is in one of the perturbative vacuum states because it is too young to be relaxed into the true ground state $|S\rangle$, we observe a nonvanishing vacuum energy density (4) today. Since the tunneling rate per unit volume per unit time is given by $\Gamma \simeq m^4 e^{-2S_0}$ apart from a prefactor of order unity [14], the requirement that there should be no transition in the horizon volume in the cosmic age reads

$$\Gamma H_0^{-4} \simeq 9M_G^4/m^4 \lesssim 1, \tag{5}$$

where $H_0^2 \cong \rho_0/(3M_G^2)$ is the current Hubble parameter squared. We therefore find that, if the parameters satisfy $m \gtrsim M_G$ and $S_0 = 120\ln 10 + 4\ln(m/M_G)$, we can account for the observed small value of the cosmological constant without introducing any small numbers.

So far is a generic study to generate an exponentially small difference in energy density using a theory with degenerate perturbative vacua whose real ground state is given by their superposition. Next in order to see how this mechanism may be implemented in a more specific theory with this property, let us consider a famous example of an SU(N) ($N \geq 2$) gauge theory whose perturbative vacuum states are classified in terms of the winding number n and denoted by $|n\rangle$ [15, 16]. States with different winding numbers cannot be transformed from each other by a continuous gauge transformation [16] and there is an energy barrier between them. Let us concentrate on the simplest case with $N = 2$ hereafter. An instanton solution [17], which describes quantum tunneling from one perturbative vacuum to another with the change of the winding number $\Delta n = 1$, can be expressed as

$$A_\mu(x) = \frac{2R^2\eta_{a\mu\nu}(x_\nu - y_\nu)\sigma^a}{(x-y)^2\left[(x-y)^2 + R^2\right]}, \tag{6}$$

where $\eta_{a\mu\nu}$ is the 't Hooft symbol [18], σ^a is the Pauli matrix and R is the size of the instanton. Here y_ν represents spacetime coordinates at its center. Thanks to the translational and the scale invariance, the Euclidean action does not depend on these quantities, namely,

$$S_0 = \frac{1}{4g^2}\int d^4x F^a_{\mu\nu}F^{a\mu\nu} = \frac{8\pi^2}{g^2}, \tag{7}$$

where $F^a_{\mu\nu} = \partial_\mu A^a_\nu - \partial_\nu A^a_\mu + g\varepsilon^{abc}A^b_\mu A^c_\nu$ is the field strength and g is the gauge coupling constant.

The true ground state in the presence of quantum tunneling is given by an infinite sum of these $|n\rangle$ states as

$$|\theta\rangle = \sum_{n=-\infty}^{\infty} e^{in\theta}|n\rangle, \tag{8}$$

where θ is a real parameter [15, 16]. One can easily find that this state is a real eigenstate of the Hamiltonian $\mathcal{H}$ in terms of the following calculation based on the dilute instanton approximation [15].

$$\langle\theta'|\, e^{-\mathcal{H}T}\,|\theta\rangle = \exp\left(2KVTe^{-S_0}\cos\theta\right)\delta\left(\theta-\theta'\right), \tag{9}$$

where $KVTe^{-S_0}$ represents contribution of a single instanton or anti-instanton. Here K is a positive constant and VT again represents spacetime volume.

Then the above equality (9) clearly shows that each θ-vacuum $|\theta\rangle$ has a different energy density than the perturbative vacuum $|n\rangle$ by

$$\Delta\rho = -2Ke^{-S_0}\cos\theta. \tag{10}$$

Apparently the $\theta = 0$ vacuum has the lowest energy (and no CP violation), but one cannot conclude that this is the only vacuum state, because other θ-vacua are also stable against gauge-invariant perturbations [15, 16] and transition between different θ-vacua is impossible even when instantons are incorporated into calculation as is seen in (9). Since different θ-vacua have different energy density they behave differently in the presence of gravity, and we must choose some particular value of θ where we assume the cosmological vanishes. This choice should ultimately be made together with the solution of the older cosmological constant problem. At present, however, since there is no completely satisfactory solution to this problem, we simply normalize the vacuum energy density to vanish in the most natural CP-symmetric $\theta = 0$ vacuum state here. We point out that the wormhole mechanism [6] is an example of proposed solutions to the older cosmological constant problem which selects $\theta = 0$ vacuum as the "ground" state with $\Lambda = 0$ where the universe presumably spends most of the time [19]. With this normalization of Λ, the vacuum energy density in each perturbative vacua is found to be

$$\langle n|\rho_v|n\rangle = 2Ke^{-S_0}. \tag{11}$$

In fact, the factor K, which is expressed as

$$K = \frac{\pi^2}{4}\left(\frac{8\pi}{g^2(\mu)}\right)^4\int\frac{dR}{R^5}\exp\left(-\frac{8\pi^2}{g^2(\mu)}+\frac{22}{3}\ln(\mu R)+6.998435\right), \tag{12}$$

in the case of the pure SU(2) gauge theory [20], is divergent due to the contribution of arbitrary large instantons. Here μ is a renormalization scale. In order to obtain a physical cutoff scale let us introduce an SU(2) doublet scalar field Φ with a potential $V[\Phi] = \lambda(|\Phi|^2 - M^2/2)^2/2$, following 't Hooft [20]. For $M \neq 0$, the solution (6) is no longer an exact one, but one could find an approximate solution, a constrained instanton [21], with the following properties.

(i) For $RM \lesssim 1$, the solution is given by (6) and

$$|\Phi(x)| = \left(\frac{(x-y)^2}{(x-y)^2+R^2}\right)^{1/2}\frac{M}{\sqrt{2}}, \tag{13}$$

for $(x-y)^2 \lesssim M^{-2}$.

(ii) For larger $(x-y)^2$, the solution rapidly approaches to the vacuum values with

$$|\Phi(x)| - \frac{M}{\sqrt{2}} \sim e^{-\sqrt{\lambda}M|x-y|}, \qquad A_\mu(x) \sim e^{-gM|x-y|}. \tag{14}$$

(iii) The Euclidean action is finite and approximately given by

$$S = \frac{8\pi^2}{g^2} + \pi^2 R^2 M^2. \tag{15}$$

Using (15) in (12), the integral is now given by

$$K = \frac{\pi^2}{4}\left(\frac{8\pi}{g^2}\right)^4 \int \frac{dR}{R^5} \exp\left[-\frac{8\pi^2}{g^2} - \pi^2 R^2 M^2 + \frac{43}{6}\ln\left(\frac{RM}{\sqrt{2}}\right) + 6.759189\right], \tag{16}$$

and we find,

$$\rho_v \cong M^4 \left(\frac{8\pi}{g^2}\right)^4 e^{-\frac{8\pi^2}{g^2}}, \tag{17}$$

$$\Gamma \simeq M^4 \left(\frac{8\pi}{g^2}\right)^4 e^{-\frac{16\pi^2}{g^2}}. \tag{18}$$

Demanding that $\rho_v = 10^{-120} M_G^4$ and that the tunneling rate in the current horizon should be smaller than unity in the cosmic age, $\Gamma H_0^{-4} \lesssim 1$, we find

$$\frac{\pi}{\alpha} + 2\ln\alpha = 60\ln 10 + 2\ln\left(\frac{M}{M_G}\right), \tag{19}$$

$$M \gtrsim \alpha M_G, \tag{20}$$

where $\alpha \equiv g^2/(4\pi)$ is the coupling strength at the energy scale $M/\sqrt{2}$. If the inequality (20) is marginally satisfied, we find $\alpha = 1/44.4$ and $M = 5 \times 10^{16}$GeV. If, on the other hand, we take $M = M_G$ so that the cutoff scale of instanton is identical to the presumed field-theory cutoff, we find $\alpha = 1/47$.

Thus if our Universe happened to be created in a state with some specific winding number and remains there up until now, we would observe a nonvanishing vacuum energy density (17). Although θ-vacuum is the real ground state of the theory, there is no *a priori* reason that the Universe is created in this state. In fact, in the possibly chaotic initial state of the early universe [22], there may well be a small domain where the scalar field has a nonvanishing expectation value with a constant SU(2) phase and A_μ^a vanishes. If such a region is exponentially stretched by cosmological inflation [23] and our Universe is contained in it, the state of our Universe would be more like the perturbative vacuum $|n = 0\rangle$ than some θ-vacuum. Then it is not surprising that we observe a nonvanishing vacuum energy density (17) today. Thus our mechanism can be naturally implemented in the chaotic inflation scenario [22].

Note that the Hubble parameter in the observable regime of inflation, H, is constrained as $H/(2\pi) \lesssim 4 \times 10^{13}$GeV so that the tensor-induced anisotropy of cosmic microwave background radiation [24] satisfies $\delta T/T \lesssim 10^{-5}$ [25]. Hence the amplitude of quantum fluctuations generated along the phase direction of the fields during inflation is much smaller than M, and it does not affect the realization of the state $|n = 0\rangle$. Furthermore gravitational effects are negligibly small for the instanton configuration even during inflation because $H \ll M$. We also note that thermal transition to a state with a different winding number is suppressed since the reheat temperature after inflation, T_R, is typically much smaller than M [23]. In fact, to avoid overproduction of gravitinos, it should satisfy $T_R < 10^{12}$GeV [26]. Hence we have only to worry about quantum transition (18) as we have already done.

In summary, we have pointed out that in a field theory with two (or more) degenerate perturbative vacua, the vacuum energy density of the true ground state is smaller than that in a perturbative vacua by an exponentially small amount if quantum tunneling between degenerate vacua is possible, and that this may be utilized to explain the observed small value of the cosmological constant without introducing any small quantities.

References

[1] S. Weinberg, Rev. Mod. Phys. **61**, 1 (1988).

[2] S. Perlimutter et al., Astrophys. J. **517**, 565 (1999); B.P. Schmidt et al., Astrophys. J. **507**, 46 (1998);A.G. Riess et al., Astron. J. **116**, 1009 (1998).

[3] A. Vilenkin, hep-th/0106083.

[4] J.B. Hartle and S.W. Hawking, Phys. Rev. **D28**, 2960 (1983).

[5] E. Baum, Phys. Lett. B **133**, 185 (1983); S.W. Hawking, Phys. Lett. B **134**, 403 (1984)

[6] S.R. Coleman, Nucl. Phys. B **310**, 643 (1988).

[7] A.D. Linde, Sov. Phys. JETP **60**, 211 (1984); A. Vilenkin, Phys. Rev. **D30**, 509 (1984).

[8] J. Polchinski, Phys. Lett. B **219**, 251 (1989).

[9] S. Kachru, M. Schulz, and E. Silverstein, Phyr. Rev. **D62**, 045021 (2000); N. Arkani-Hamed, S. Dimopoulos, N. Kaloper, and R. Sundrum, Phys. Lett. B **480**, 193 (2000); S.-H. Henry Tye and I. Wasserman, Phys. Rev. Lett. **86**, 1682 (2001).

[10] I. Zlatev, L. Wang and P.J. Steinhardt, Phys. Rev. Lett. **82**, 896 (1999); P.J. Steinhardt, L. Wang and I. Zlatev, Phys. Rev. D **59**, 123504 (1999)

[11] Y. Fujii, Phys. Rev. **D26**, 2580 (1982); L.H. Ford, Phys. Rev. **D35**, 2339 (1987); P.J. Peebles and B. Ratra, Astrophys. J. **325**, L17 (1988); Y. Fujii and T. Nishioka, Phys. Rev. **D42**, 361 (1990); K. Sato, N. Terasawa, and J. Yokoyama, in Proc. XXIVth Recontre de Moriond, "The Quest for the Fundamental Constants in Cosmology," eds. J. Audouze and J. Tran Thanh Van. (Editions Frontières, France 1990) 193; T. Nishioka and S. Wada, Int. J. Mod. Phys. **A8**, 3933 (1993).

[12] N. Arkani-Hamed, L.J. Hall, C. Kolda, H. Murayama, Phys. Rev. Lett. **85**, 4434 (2000); S.M. Barr and D. Seckel, hep-ph/0106239;

[13] S. Coleman, Aspects of symmetry, (Cambridge, UK 1985).

[14] A. Lapedes and E. Mottola, Nucl. Phys. B **203**, 58 (1982).

[15] C.G. Callan Jr, R.F. Dashen, and D.J. Gross, Phys. Lett. **63B**, 334 (1976).

[16] R. Jackiw and C. Rebbi, Phys. Rev. Lett. **37**, 172 (1976).

[17] A.M. Polyakov, Phys. Lett. **59B**, 82 (1975); A.A. Belavin, A.M. Polyakov, A.S. Schvartz, and Yu.S. Tyupkin, Phys. Lett. **59B**, 85 (1975).

[18] G. 't Hooft, Phys. Rev. Lett. **37**, 8 (1976).

[19] H.B. Nielsen and M. Ninomiya, Phys. Rev. Lett. **62**, 1429 (1989).

[20] G. 't Hooft, Phys. Rev. **D14**, 3432 (1976); **D18**, 2199 (1978) (E).

[21] I. Affleck, Nucl. Phys. B **191**, 429 (1981); M. Nielsen and N.K. Nielsen, Phys. Rev. **D61**, 105020 (2000).

[22] A.D. Linde, Phys. Lett. **129B**, 177(1983).

[23] For a review of inflation, see, e.g. A.D. Linde, Particle Physics and Inflationary Cosmology (Harwood, Chur, Switzerland, 1990); K.A. Olive, Phys. Rep. **190**,181(1990); A.R. Liddle and D.H. Lyth, Cosmological inflation and large-scale structure (Cambridge, UK, 2000).

[24] V.A. Rubakov, M.V. Sazin, and A.V. Veryaskin, Phys. Lett. **115B**, 189(1982); L.F. Abbott and M.B. Wise, Nucl. Phys. B **244**, 541 (1984).

[25] C.L. Bennet *etal.*, Astrophys. J. Lett. **464**, L1(1996).

[26] M. Kawasaki and T. Moroi, Prog Theor. Phys. **93**, 879 (1995).

Observational Constraints on Decaying-Λ Models

James Overduin[1]

Department of Physics, Waseda University,
Shinjuku, Tokyo, 169-8555, Japan

Abstract

Strict bounds are placed on theories in which the vacuum energy has a time-varying component that can exchange energy with radiation. Under the conservative assumption that this process does not distort the shape of the cosmic microwave background spectrum, the latter's absolute intensity alone is enough to require that the present energy density of the decaying-vacuum component be no higher than 0.06 times that of radiation. This is consistent with other limits.

1 Variable-Λ Cosmology

It is now routine to treat Einstein's cosmological "constant" Λ as a dynamical quantity related to the energy density of the vacuum. This may decay from the very large primordial values expected on the basis of quantum field theory to the small but nonzero present values now implied by observational cosmology. Mechanisms such as quintessence [1], Brans-Dicke-type scalar fields [2] and quantum effects during inflation [3] can produce an effective Λ-term with the desired behaviour, although fine-tuning remains an issue in some cases [4].

There are several ways to constrain theories of this kind using observational data. Among the most important are early-time bounds on the vacuum energy density $\rho_\Lambda c^2 = \Lambda c^4/8\pi G$. The success of standard nucleosynthesis theory implies that ρ_Λ was smaller than ρ_r and ρ_m during the radiation-dominated era, and large-scale structure formation could not have proceeded in the conventional way unless $\rho_\Lambda < \rho_m$ during the early matter-dominated era. Since $\rho_r \propto R^{-4}$ and $\rho_m \propto R^{-3}$ in standard cosmology, these requirements mean in practice that a vacuum energy density which climbs more steeply than R^{-3} in the past direction must be smaller than that of radiation at present.

The variable-Λ term must also satisfy late-time bounds like those which have been placed on the cosmological constant using data from number counts of faint galaxies, gravitational lens statistics, Type Ia supernovae and the power spectra of galaxies and anisotropies in the spectrum of the cosmic microwave background radiation (CMB). Some of these tests are less restrictive in the case of a variable Λ-term than they are for $\Lambda = \text{const}$, and this can open up new regions of parameter space, including the possibility of nonsingular "big bounce" models [5].

A third group of limits comes from the products of vacuum decay. In quintessence theories, vacuum energy is transferred to the kinetic energy of a scalar field as it "rolls" down a gradient toward the minimum of its potential. This may have observable consequences if the scalar field is coupled strongly to ordinary matter, but is hard to constrain in general. A simpler situation is that in which the vacuum decays into known particles such as baryons, neutrinos or photons. The baryonic decay channel is disfavoured since it should produce equal numbers of baryons and antibaryons, whose subsequent annhilation would have been seen in the γ-ray background [6]. We will focus here on the second possibility, that of decay into photons and massless neutrinos.

2 Dynamics

We adopt a phenomenological approach with the field equations and their covariant derivatives as follows:

$$\mathcal{R}_{\mu\nu} - \frac{1}{2}\mathcal{R}\,g_{\mu\nu} = -\frac{8\pi G}{c^4}\left(\mathcal{T}_{\mu\nu} - \rho_\Lambda c^2\, g_{\mu\nu}\right), \qquad 0 = \nabla^\nu\left(\mathcal{T}_{\mu\nu} - \rho_\Lambda c^2\, g_{\mu\nu}\right), \tag{1}$$

[1] E-mail:overduin@gravity.phys.waseda.ac.jp

with matter fields described by a perfect fluid of the usual form $\mathcal{T}_{\mu\nu} = (\rho + p/c^2)U_\mu U_\nu + p\,g_{\mu\nu}$. The vacuum energy density $\rho_\Lambda c^2$ can in principle vary as it likes, subject to the conservation equation in (1). For a homogeneous and isotropic Universe the latter reduces to

$$\frac{1}{R^3}\frac{d}{dt}\left[R^3\left(\rho c^2 + p\right)\right] = \frac{d}{dt}\left(p - \rho_\Lambda c^2\right) . \tag{2}$$

We assume that the vacuum energy density ρ_Λ consists of both a time-varying component $\rho_v(t)$ and a constant-density component ρ_c so that $\rho_\Lambda = \rho_v(t) + \rho_c$. We also assume that the matter in the theory can be modelled as a mixture of dustlike matter and radiation, so that $\rho = \rho_m + \rho_r$ and $p = \frac{1}{3}\rho_r c^2$. Under these conditions eq. (2) takes the form

$$\frac{1}{R^4}\frac{d}{dt}\left(R^4\rho_r\right) + \frac{1}{R^3}\frac{d}{dt}\left(R^3\rho_m\right) + \frac{d\rho_v}{dt} = 0 . \tag{3}$$

To solve this we make several assumptions. First, conservation of particle number:

$$R^3\rho_m = \text{ const} . \tag{4}$$

Second, we assume that the energy density ρ_v of the decaying vacuum component is proportional to that of radiation, $\rho_v \propto \rho_r$. This idea goes back to Pollock in 1980 [7]. If the proportionality factor is taken as $x/(1-x) =$ constant following Freese et al. [6], then we may set

$$x \equiv \frac{\rho_v}{\rho_r + \rho_v} = \begin{cases} x_r & (t < t_{eq}) \\ x_m & (t \geq t_{eq}) , \end{cases} \tag{5}$$

where x_r and x_m are two (possibly different) constants and t_{eq} is the time of equality between matter and radiation. Standard cosmology is recovered as $x \to 0$. With eqs. (4) and (5), eq. (3) is solved to give

$$R^{4(1-x)}\rho_v = \text{ const} . \tag{6}$$

The cosmological term in this theory therefore goes as $\Lambda \propto R^{-4(1-x)}$. Λ-decay laws of this form have been reviewed in [5]. From eq. (5) it follows that $\rho_r \propto R^{-4(1-x)}$ as well. We thus require $x < \frac{1}{4}$ if there is to be a dynamical distinction between matter and radiation. This in (5) implies that $\rho_v < \frac{1}{3}\rho_r$ at present, consistent with the fact that ρ_v rises more steeply than R^{-3} in the past direction (§ 1).

To solve for the scale factor R we make use of the field equations in (1). These reduce to the following form, where we have assumed spatial flatness ($k = 0$) as justified by CMB data:

$$\left(\frac{\dot{R}}{R}\right)^2 = \frac{8\pi G}{3c^2}(\rho_m + \rho_r + \rho_v + \rho_c) . \tag{7}$$

Eq. (7) can be solved in two limiting cases: (a) the radiation-dominated era ($t < t_{eq}$) for which $\rho_m + \rho_c \ll \rho_r + \rho_v$; and (b) the matter-dominated era ($t \geq t_{eq}$) for which $\rho_m + \rho_c \gg \rho_r + \rho_v$. We subdivide case (b) further into two subcases where $\rho_c = 0$ (no cosmological constant) and $\rho_c \neq 0$. The former can be used to describe Einstein-de Sitter-like models in which $\Omega_{m,0} \equiv \rho_{m,0}/\rho_{crit,0} = 1$, while the latter will be necessary to describe vacuum-dominated models such as the Λ+ Cold Dark Matter (ΛCDM) model in which $\Omega_{m,0} = 0.3$. Solving eqs. (4-7), we find for the vacuum and radiation densities:

$$\rho_v(t) = \begin{cases} \dfrac{\alpha x_r}{(1-x_r)^2}\,t^{-2} \\ \left(\dfrac{x_m}{1-x_m}\right)\rho_r(t) \end{cases} , \qquad \rho_r(t) = \begin{cases} \left(\dfrac{1-x_r}{x_r}\right)\rho_v(t) & (t < t_{eq}) \\ \rho_{r,0}\left[\dfrac{S(t)}{S(t_0)}\right]^{-8(1-x_m)/3} & (t \geq t_{eq}) , \end{cases} \tag{8}$$

with $\alpha = 3/(32\pi G)$. The matter density and scale factor are similarly obtained as:

$$\rho_m(t) = \rho_{m,0} \times \begin{cases} \left[\dfrac{S(t_{eq})}{S(t_0)}\right]^{-2}\left(\dfrac{t}{t_{eq}}\right)^{-3/[2(1-x_r)]} \\ \left[\dfrac{S(t)}{S(t_0)}\right]^{-2} \end{cases} , \qquad R(t) = R_0 \times \begin{cases} \left(\dfrac{t}{t_0}\right)^{1/[2(1-x_r)]} & (t < t_{eq}) \\ \left[\dfrac{S(t)}{S(t_0)}\right]^{2/3} & (t \geq t_{eq}) . \end{cases} \tag{9}$$

The function $\mathcal{S}(t)$ in these equations is defined as $\mathcal{S}(t) \equiv t$ for models with $\Omega_{m,0} = 1$ or $\sinh(t/\tau_0)$ for models with $0 < \Omega_{m,0} < 1$, where $\tau_0 \equiv 2/(3\sqrt{1-\Omega_{m,0}}H_0)$ and H_0 is Hubble's constant. The age of the Universe is $t_0 = 2/(3H_0)$ for models with $\Omega_{m,0} = 1$ as usual, while $t_0 = \tau_0 \sinh^{-1}\sqrt{(1-\Omega_{m,0})/\Omega_{m,0}}$ for $0 < \Omega_{m,0} < 1$. The epoch of equality may be found by equating $\rho_r(t_{eq}) = \rho_m(t_{eq})$, giving

$$t_{eq} = \begin{cases} t_0\,\Omega_{r,0}^{3/[2(1-4x_m)]} & (\Omega_{m,0} = 1) \\ \tau_0 \sinh^{-1}\left[\sqrt{\dfrac{1-\Omega_{m,0}}{\Omega_{m,0}}}\left(\dfrac{\Omega_{r,0}}{\Omega_{m,0}}\right)^{3/[2(1-4x_m)]}\right] & (0 < \Omega_{m,0} < 1)\,. \end{cases} \tag{10}$$

Values of t_{eq} in decaying-vacuum theories can be up to several hundred times smaller than those in standard cosmology, depending on the values of $x_m, \Omega_{r,0}$ and $\Omega_{m,0}$.

3 Background Radiation from Vacuum Decay

To constrain the theory outlined above, we wish to calculate the intensity of background radiation that would be produced by the decay of the vacuum. For this purpose we consider spherically-symmetric regions of arbitrary comoving volume V_0. The rate of change of mass-energy in such regions is given as a function of the surface pressure p by solving Einstein's equations [8], giving $\dot{M}c^2 = -4\pi r^2 p\dot{r}$ where $r(t) = [R(t)/R_0]r_0$ is the physical radius and $V_0 = \frac{4}{3}\pi r_0^3$. We will assume that some fraction (β) of this energy flux goes into photons and may hence be interpreted as the "luminosity of the vacuum:"

$$L_v(t) = \beta \dot{M}c^2 = \beta\, c^2 \rho_v(t)\, \dot{V}(t)\,, \tag{11}$$

where $V(t) = [R(t)/R_0]^3 V_0$ is the region's physical volume and we have used the equation of state $p = p_v = -\rho_v c^2$. With the help of eq. (9) this expression is evaluated as

$$L_v(t) = \mathcal{L}_{v,0} V_0 \times \begin{cases} \left(\dfrac{t}{t_0}\right)^{-(5-8x_m)/3} \\ \left[\dfrac{\cosh(t/\tau_0)}{\cosh(t_0/\tau_0)}\right]\left[\dfrac{\sinh(t/\tau_0)}{\sinh(t_0/\tau_0)}\right]^{-(5-8x_m)/3} \end{cases}, \tag{12}$$

where the comoving vacuum luminosity density is:

$$\mathcal{L}_{v,0} = \frac{9c^2 H_0^3\, \Omega_{r,0}\beta\, x_m}{8\pi G(1-x_m)} = 6.8 \times 10^{-30} h_0 \text{ erg s}^{-1} \text{ cm}^{-3} \left(\frac{\beta\, x_m}{1-x_m}\right)\,. \tag{13}$$

Here we have taken $\Omega_{r,0} = 4.2 \times 10^{-5} h_0^{-2}$ with $h_0 = H_0/(100 \text{ km s}^{-1} \text{ Mpc}^{-1})$. A reasonable guess for the value of β might be the ratio of energy density in CMB photons to that in photons and neutrinos combined, $\beta = 1/1.68$ [9]. Letting $x_m \to \frac{1}{4}$ and $t \to t_0$, we then find from (13) that the comoving luminosity density of the vacuum could in principle reach 50 times that of galaxies ($\mathcal{L}_* = 2.6 \times 10^{-32} h_0$ erg s^{-1} cm^{-3}).

The integrated bolometric intensity of vacuum decay over the matter-dominated era is [10]:

$$Q_v = c\int_{t_{eq}}^{t_0} n_v(t) L_v(t) \frac{R(t)}{R_0} dt\,, \tag{14}$$

where $n_v(t)$ is the comoving number density of vacuum decay regions, $n_v(t) = V_0^{-1} = \text{const}$. Putting eqs. (9) and (12) into this integral, we find that

$$Q_v = Q_{v,0}\left[1 - \left(\frac{\Omega_{r,0}}{\Omega_{m,0}}\right)^{4x_m/(1-4x_m)}\right] \qquad \text{(all models)}\,. \tag{15}$$

where

$$Q_{v,0} \equiv \frac{c\mathcal{L}_{v,0}}{4H_0\, x_m} = \frac{9c^3 H_0^2 \Omega_{r,0}\beta}{32\pi G(1-x_m)} = \frac{0.0094 \text{ erg cm}^{-2} \text{ s}^{-1}}{(1-x_m)}\,. \tag{16}$$

This reaches 0.013 erg cm^{-2} s^2 in the limit $x_m \to \frac{1}{4}$, some 50 times the bolometric intensity of the night sky due to galaxies. The primary reason for this high background is the assumption that 60% of the

energy created by vacuum decay goes into photons. By comparison, less than 1% of the mass of ordinary matter has been converted into light so far in the history of the Universe.

To set firm upper limits on x_m we calculate the spectral intensity of background radiation due to vacuum decay. This is given by [10]

$$I_\lambda(\lambda_0) = \frac{c}{4\pi}\int_{t_{eq}}^{t_0} n_v(t) F_v\left[\frac{R(t)\lambda_0}{R_0}, t\right]\left[\frac{R(t)}{R_0}\right]^2 (t)\,dt\,, \tag{17}$$

where $F_v(\lambda, t)$ is the spectral energy distribution of the decay photons. If this is nonthermal, it will be severely constrained by COBE data on the shape of the CMB [6]. In order to obtain the most conservative limits on the theory, we therefore concentrate on the blackbody case, although such a scenario is disfavoured thermodynamically [11]. This means:

$$F_v(\lambda, t) = \frac{C(t)/\lambda^5}{\exp\left[hc/kT(t)\lambda\right] - 1}\,. \tag{18}$$

where the function $C(t)$ is fixed by setting $\int_0^\infty F_v(\lambda, t)\,d\lambda = L_v(t)$ and temperature $T(t)$ can be obtained from Stefan's law $\rho_r \propto T^4$ under the assumption that vacuum decay photons reach thermal equilibrium with those already present. With the help of eqs. (8) and (12), we find in this way that

$$C(t) = \frac{15\lambda_v^4 \mathcal{L}_{v,0} V_0}{\pi^4} \times \begin{cases} \left(\dfrac{t}{t_0}\right) & (\Omega_{m,0} = 1) \\ \left[\dfrac{\cosh(t/\tau_0)}{\cosh(t_0/\tau_0)}\right]\left[\dfrac{\sinh(t/\tau_0)}{\sinh(t_0/\tau_0)}\right] & (0 < \Omega_{m,0} < 1) \end{cases} \tag{19}$$

$$\frac{hc}{kT(t)} = \lambda_v \times \begin{cases} \left(\dfrac{t}{t_0}\right)^{2(1-x_m)/3} & (\Omega_{m,0} = 1) \\ \left[\dfrac{\sinh(t/\tau_0)}{\sinh(t_0/\tau_0)}\right]^{2(1-x_m)/3} & (0 < \Omega_{m,0} < 1)\,, \end{cases} \tag{20}$$

where

$$\lambda_v \equiv \left(\frac{8\pi^5 hc}{15\rho_{r,0}c^2}\right)^{1/4} = 0.46\ \text{cm}\left(\frac{\Omega_{r,0}h_0^2}{4.17\times 10^{-5}}\right)^{-1/4}\,. \tag{21}$$

Putting these expressions into eq. (17), we obtain

$$I_\lambda(\lambda_0) = I_v(\lambda_0) \times \begin{cases} \displaystyle\int_{\frac{t_{eq}}{t_0}}^{1} \frac{\tau^{-1}\,d\tau}{\exp\left[\left(\dfrac{\lambda_v}{\lambda_0}\right)\tau^{-\frac{2}{3}x_m}\right] - 1} & (\Omega_{m,0} = 1) \\ \displaystyle\int_{\frac{t_{eq}}{\tau_0}}^{\frac{t_0}{\tau_0}} \frac{\coth\tau\,d\tau}{\exp\left[\dfrac{\lambda_v}{\lambda_0}\left(\dfrac{\sqrt{\Omega_{m,0}}\sinh\tau}{\sqrt{1-\Omega_{m,0}}}\right)^{-\frac{2}{3}x_m}\right] - 1} & (0 < \Omega_{m,0} < 1)\,, \end{cases} \tag{22}$$

where

$$I_v(\lambda_0) \equiv \frac{5\mathcal{L}_{v,0}}{2\pi^5 h H_0}\left(\frac{\lambda_v}{\lambda_0}\right)^4 = 26{,}000\ \text{CUs}\left(\frac{\beta x_m}{1-x_m}\right)\left(\frac{\lambda_v}{\lambda_0}\right)^4\,. \tag{23}$$

Here 1 CU $\equiv$ 1 photon s^{-1} cm^{-2} Å^{-1} ster^{-1}. Eq. (22) gives the combined intensity of the decaying vacuum out to a distance corresponding to the look-back time $t_0 - t_{eq}$. The parameter V_0 has dropped out of the integral as expected, and eq. (22) is also independent of the uncertainty h_0 in Hubble's constant, since there is a factor of h_0 in both $\mathcal{L}_{v,0}$ and H_0. The vacuum decay photons making up the quantity $I_\lambda(\lambda_0)$ have been emitted at many wavelengths and redshifted by various amounts, but reach us in a waveband centered on λ_0. Results are shown in Figure 1. The intensity of background radiation produced by vacuum decay during the matter-dominated era exceeds that of the CMB unless $x_m \leq 0.06$. This is consistent with a limit of 0.07 based on entropy conservation [6], and could be tightened significantly if the vacuum is assumed to decay only into photons (and not massless neutrinos) as advocated by Birkel

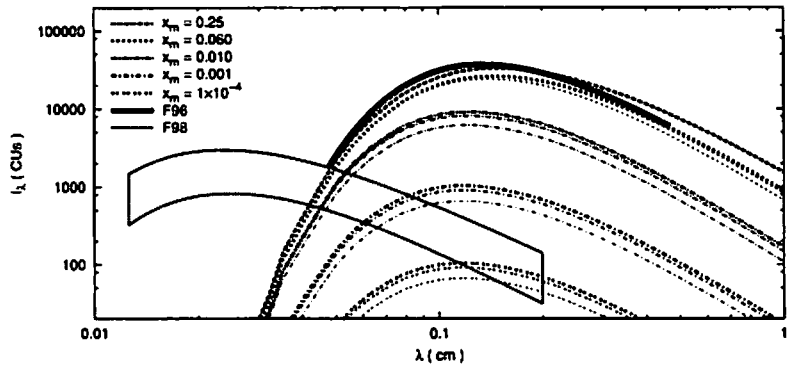

Figure 1: The spectral intensity of background radiation due to the decaying vacuum for various values of x_m, compared with COBE data in the microwave (F96 [12]) and far infrared regions (F98 [13]). For each value of x_m there are three curves representing cosmologies with $\Omega_{m,0} = 1$ (heaviest lines), $\Omega_{m,0} = 0.3$ (medium-weight lines) and $\Omega_{m,0} = 0.03$ (lightest lines).

and Sarkar [14]. It is interesting that these results are almost independent of the value of $\Omega_{m,0}$ — a situation very different from that in the optical background where lower values of $\Omega_{m,0}$ lead to higher intensities because the Universe is older [15]. The same effect is present here, but it is cancelled out by the fact that smaller values of $\Omega_{m,0}$ also raise the value of t_{eq}.

Acknowledgment:

The author is supported by a JSPS postdoctoral fellowship.

References

[1] L. Wang et al., Astrophysical Journal **530** (2000) 17

[2] T. Fukui and J. M. Overduin, International Journal of Modern Physics D, in press (2002)

[3] R. H. Brandenberger, *COSMO-99 proceedings*, hep-th/0004016 (2000)

[4] S. Weinberg, *Dark Matter 2000 proceedings*, astro-ph/0005265 (2000)

[5] J. M. Overduin and F. I. Cooperstock, Physical Review **D58** (1998) 043506

[6] K. Freese et al., Nuclear Physics **B287** (1987) 797

[7] M. D. Pollock, Monthly Notices of the Royal Astronomical Society **193** (1980) 825

[8] C. W. Misner, K. S. Thorne and J. A. Wheeler, *Gravitation* (W. H. Freeman, New York, 1973), p.858

[9] P. J. E. Peebles, *Principles of Physical Cosmology* (Princeton University Press, Princeton, 1993), p.164

[10] J. M. Overduin and P. S. Wesson, Vistas in Astronomy **35** (1992) 439

[11] W. Hu and J. Silk, Physical Review **D48** (1993) 485

[12] D. J. Fixsen et al., Astrophysical Journal **473** (1996) 576

[13] D. J. Fixsen et al., Astrophysical Journal **508** 1998 128

[14] M. Birkel and S. Sarkar, Astroparticle Physics **6** (1997) 197

[15] J. M. Overduin, *5th RESCEU Symposium proceedings* (Universal Academy Press, Tokyo, 2002)

Cosmological evolution of global monopoles : scaling property and peculiar velocity

Masahide Yamaguchi[1]

Research Center for the Early Universe, University of Tokyo, Hongo, Tokyo, 113-0033, Japan

Abstract

We investigate the scaling property of global monopoles in the expanding universe. By directly solving the equations of motion for scalar fields, we follow the time development of the number density of global monopoles in the radiation dominated (RD) universe and the matter dominated (MD) universe. It is confirmed that the global monopole network relaxes into the scaling regime and the number per the hubble volume is a constant irrespective of the cosmic time. The number density $n(t)$ of global monopoles is given by $n(t) \simeq (0.43 \pm 0.07)/t^3$ during the RD era and $n(t) \simeq (0.25 \pm 0.05)/t^3$ during the MD era. We also examine the peculiar velocity v of global monopoles. For the purpose, we establish the method to measure the peculiar velocity by use of only the local quantities of the scalar fields. It is found that $v \sim (1.0 \pm 0.3)$ during the RD era and $v \sim (0.8 \pm 0.3)$ during the MD era. By use of it, a more accurate analytic estimate for the number density of global monopoles is obtained.

1 Introduction

Global monopoles may be favorable for the cosmic history because they may produce primordial density fluctuations responsible for the large scale structure formation and the anisotropy of the cosmic microwave background radiation (CMB) [1, 2, 3, 4, 5]. Recent observations of the CMB by the Boomerang [6] and the MAXIMA [7] experiments found the first acoustic peak with spherical harmonic multipole $l \sim 200$ predicted by the standard inflationary scenario. But, they also found the relatively low second peak, which may suggest the contribution of topological defects [8]. Moreover, deviations from Gaussianity in CMB are reported in [9]. Thus, though it is improbable for topological defects to become the primary source of primordial density fluctuations, a hybrid model is still attractive, where primordial density fluctuations are comprised of adiabatic fluctuations induced by inflation and isocurvature ones induced by topological defects. In fact, topological defects can be easily compatible with inflation [10, 11, 12].

The key property of global monopoles to contribute primordial density fluctuations properly is scaling, where the typical scale of the global monopole network grows in proportion to the horizon scale. Then the number density of global monopoles is proportional to t^{-3} (t : the cosmic time). Here we define the scaling parameter ξ as

$$\xi \equiv n(t)t^3, \tag{1}$$

where $n(t)$ is the number density of global monopoles. If ξ becomes a constant irrespective of the cosmic time, we can conclude that the global monopole network goes into the scaling regime.

In this talk, we give the formulation and the results of our numerical simulations [13, 14]. First of all, we will confirm scaling property of global monopoles. Later we will also investigate the peculiar velocity of global monopoles. Finally, we give an analytic estimate for the number density of global monopoles by use of the peculiar velocity obtained from numerical simulations.

2 Numerical Simulations

First of all, we give the formalism of our numerical simulations to follow the evolution of the global monopole. Later we discuss whether the global monopole network goes into the scaling regime. Furthermore, the peculiar velocity of global monopoles is investigated.

[1] E-mail:gucci@resceu.s.u-tokyo.ac.jp

We directly solve the equations of motion for scalar fields in the expanding universe, which have the $O(3)$ symmetry at high temperature and later break to generate global monopoles. We consider the following Lagrangian density for scalar fields $\phi^a(x)(a = 1, 2, 3)$,

$$\mathcal{L}[\phi^a] = \frac{1}{2} g_{\mu\nu} \partial^\mu \phi^a \partial^\nu \phi^a - V_{\rm eff}[\phi^a, T]. \tag{2}$$

Here $g_{\mu\nu}$ is the flat Robertson-Walker metric and the effective potential $V_{\rm eff}[\phi^a, T]$, which represents the typical second order phase transition, is given by

$$\begin{aligned} V_{\rm eff}[\phi^a, T] &= \frac{\lambda}{4}(\phi^2 - \sigma^2)^2 + \frac{5}{24}\lambda T^2 \phi^2, \\ &= \frac{\lambda}{4}(\phi^2 - \eta^2)^2 + \frac{\lambda}{4}(\sigma^4 - \eta^4), \end{aligned} \tag{3}$$

where $\phi \equiv \sqrt{\phi^a \phi^a}$, $\eta \equiv \sigma\sqrt{1 - (T/T_c)^2}$ and $T_c \equiv \frac{2}{5}\sqrt{15}\sigma$ is the critical temperature. For $T > T_c$, the potential $V_{\rm eff}[\phi^a, T]$ has a minimum at the origin and the $O(3)$ symmetry is restored. On the other hand, for $T < T_c$, new minima $\phi = \eta$ appear and the symmetry is broken, which leads to the formation of global monopoles.

The equations of motion for the scalar fields ϕ^a in the expanding universe are given by

$$\ddot{\phi^a}(x) + 3H\dot{\phi^a}(x) - \frac{1}{R(t)^2}\nabla^2 \phi^a(x) + \lambda(\phi^2(x) - \eta^2)\phi^a(x) = 0, \tag{4}$$

where the dot represents the time derivative and $R(t)$ is the cosmic scale factor. The Hubble parameter $H = \dot{R}(t)/R(t)$ and the cosmic time t are given by

$$\begin{aligned} H^2 &= \frac{4\pi^3}{45 m_{\rm pl}^2} g_* T^4, \quad t = \frac{1}{2H} \equiv \frac{\epsilon_{RD}}{T^2} \qquad \text{(for RD)}, \\ H^2 &= \alpha(T)\frac{4\pi^3}{45 m_{\rm pl}^2} g_* T^4, \quad t = \frac{2}{3H} \equiv \frac{\epsilon_{MD}}{T^{3/2}} \quad \text{(for MD)}, \end{aligned} \tag{5}$$

with g_* to be the total number of degrees of freedom for the relativistic particles. For the MD case, we have defined $\alpha(T)$ $[\alpha(T) > 1]$ as $\alpha(T) \equiv \rho_{\rm mat}(T)/\rho_{\rm rad}(T) = \alpha_c(T_c/T)$, where $\rho_{\rm mat}(T)$ is the contribution to the energy density from non-relativistic particles, $\rho_{\rm rad}(T)$ is the contribution from relativistic particles at the temperature T, and $\alpha_c \equiv \rho_{\rm mat}(T_c)/\rho_{\rm rad}(T_c)$. We also define the dimensionless parameter ζ as

$$\begin{aligned} \zeta_{RD} &\equiv \frac{\epsilon_{RD}}{\sigma} = \left(\frac{45}{16\pi^3 g_*}\right)^{1/2} \frac{m_{\rm pl}}{\sigma} \qquad \text{(for RD)}, \\ \zeta_{MD} &\equiv \frac{\epsilon_{MD}}{\sigma^{1/2}} = \left(\frac{5\sqrt{15}}{6\alpha_c \pi^3 g_*}\right)^{1/2} \frac{m_{\rm pl}}{\sigma} \quad \text{(for MD)}. \end{aligned} \tag{6}$$

In our simulation, we take $\zeta_{RD,MD} = 10$ and 5 to investigate the ζ dependence on the result.

We start the numerical simulations from the $O(3)$ symmetric phase with the temperature $T_i = 2T_c$, which corresponds to $t_i = t_c/4$(RD) and $t_i = t_c/(2\sqrt{2})$(MD). At the initial time ($t_i < t_c$), we adopt as the initial condition the thermal equilibrium state with the mass

$$m = \sqrt{\frac{5}{12}\lambda(T_i^2 - T_c^2)}, \tag{7}$$

which is the inverse curvature of the potential at the origin at $t = t_i$.

We perform numerical simulations in seven different sets of lattice sizes and lattice spacings in the RD universe and the MD universe. In all cases, the time step is taken to be $\delta t = 0.01$. In the typical case, the box size is nearly equal to the horizon volume $(H^{-1})^3$ and the lattice spacing to the typical core size of a monopole $\delta x \sim 1.0/(\sqrt{\lambda}\sigma)$ at the final time t_f. Also, in order to investigate the effect of the boundary condition (BC), we adopt both the periodic BC and the reflective BC ($\nabla^2 \phi^a(x) = 0$ on the boundary).

2.1 Number Density

In order to judge whether the global monopole network relaxes into the scaling regime, we follow the time development of ξ. If ξ becomes a constant irrespective of the cosmic time, we can conclude that the global monopole network goes into the scaling regime.

First of all, we discuss the evolution of global monopoles in the RD universe. We find that after some relaxation period, ξ_{RD} becomes a constant irrespective of time for all cases. In particular, it is found that ξ_{RD} converges to a constant $\xi_{RD} \simeq (0.43 \pm 0.07)$. For the MD case, we also find that after some relaxation period, the number of global monopoles per the horizon volume becomes a constant irrespective of the cosmic time and ξ_{MD} converges to a constant $\xi_{MD} \simeq (0.25 \pm 0.05)$. Thus, we have completely confirmed that the global monopole network goes into the scaling regime in both the RD universe and MD universe.

2.2 Peculiar Velocity

In this subsection, we investigate the peculiar velocity of global monopoles in the expanding universe. In order to measure the peculiar velocity, we need to know where a monopole moves at the next step. For the purpose, we need to find the method to look on the monopole found at each time as the same. But, generally speaking, it is very difficult in case there are a lot of monopoles in the simulation box.

Then, looking at the matter from another angle, we make best use of the information of scalar fields. Since the values and the time derivatives of scalar fields include all informations about monopoles, the velocity of a monopole can be represented by only the information of scalar fields, that is, local quantities. In fact, it is possible as shown below. First of all, we expand scalar fields $\phi^a(\boldsymbol{x}, t)$ around $\phi^a(\boldsymbol{x}_0, t_0)$ up to the first order,

$$\phi^a(\boldsymbol{x}, t) \simeq \phi^a(\boldsymbol{x}_0, t_0) + \nabla\phi^a(\boldsymbol{x}_0, t_0) \cdot (\boldsymbol{x} - \boldsymbol{x}_0) + \dot{\phi}^a(\boldsymbol{x}_0, t_0)(t - t_0) \qquad (a = 1, 2, 3). \tag{8}$$

The monopole core is identified with the zero of all scalar fields ϕ^a. Assuming a monopole lies at $\boldsymbol{x}_0$ at the time t_0, the position $\boldsymbol{x}$ of the monopole core at the sufficiently near time t is obtained as the intersection of the following three planes,

$$\boldsymbol{A}^a \cdot (\boldsymbol{x} - \boldsymbol{x}_0) + B^a(t - t_0) = 0, \tag{9}$$

where $\boldsymbol{A}^a \equiv \nabla\phi^a(\boldsymbol{x}_0, t_0)$ and $B^a \equiv \dot{\phi}^a(\boldsymbol{x}_0, t_0)$. These equations are easily solved by the Cramer's formula,

$$\frac{(\boldsymbol{x} - \boldsymbol{x}_0)_j}{t - t_o} = -\frac{\begin{vmatrix} A^1_x & B^1 & A^1_z \\ A^2_x & B^2 & A^2_z \\ A^3_x & B^3 & A^3_z \end{vmatrix}}{\begin{vmatrix} A^1_x & A^1_y & A^1_z \\ A^2_x & A^2_y & A^2_z \\ A^3_x & A^3_y & A^3_z \end{vmatrix}} \qquad (j) \tag{10}$$

Thus, the peculiar velocity of a global monopole v can be estimated as

$$v = \frac{|\boldsymbol{x} - \boldsymbol{x}_0|}{t - t_o}. \tag{11}$$

Though there is still large uncertainty, it is found that the peculiar velocity v takes almost the same constant asymptotically and is given by $v_{RD} \sim (1.0 \pm 0.3)$. On the other hand, the peculiar velocity v is given by $v_{MD} \sim (0.8 \pm 0.3)$ during the MD era.

The obtained values of the peculiar velocity are roughly understood as follows. A constant long-range attractive force works between a monopole and an anti-monopole due to the gradient energy of the scalar fields. Then, the monopole is accelerated very much and the relative velocity rapidly gets to the order of unity. In the RD universe, the cosmic expansion is not so rapid that the redshift of the velocity due to the cosmic expansion becomes negligible and the velocity reaches almost the unity. On the other hand, in the MD era, the universe expands so rapid that the velocity is redshifted and it takes a value smaller than the unity.

3 Analytic Estimate

In this section, we give a simple analytic estimate for the scaling parameter ξ.

The evolution for the number density of global monopoles $n(t)$ can be described by the following Boltzmann equation,[2]

$$\begin{aligned}\frac{dn(t)}{dt} &= -P(t)n(t) - 3H(t)n(t), \\ &= -\frac{n(t)}{T(t)} - \frac{3mn(t)}{t},\end{aligned} \tag{12}$$

where $R(t) \propto t^m$, $P(t)$ is the probability per unit time that a monopole annihilates with an anti-monopole, and $T(t)$ is the period it takes for a pair of monopoles at rest with the mean separation $l(t)$ to pair-annihilate. The mean separation $l(t)$ is given by $l(t) \equiv R(t)r_s = n(t)^{-1/3}$, where r_s is the mean comoving separation. In the previous publication [13], we assumed that the relative velocity between them reaches the order of unity at once because a constant attractive force works between a pair of monopoles irrespective of the separation length. In the previous section, we have confirmed that the above assumption is basically correct but the peculiar velocity is smaller than unity in the MD universe. Then, assuming that the relative velocity is given by the peculiar velocity obtained in the previous section and a pair of monopoles does not spiral around each other for a long time, we give a more accurate analytic estimate for the number density of global monopoles. The period $T(t)$ is given by the following relation,

$$v \int_{t_0}^{T+t_0} \frac{dt}{R(t)} = \int_0^{r_s} dr, \tag{13}$$

where t_0 is the initial time where a pair of monopoles are at rest. Then, the period $T(t)$ reads

$$T(t) \simeq \left(\frac{1-m}{v\, t^m n(t)^{1/3}} \right)^{\frac{1}{1-m}} \qquad (\text{for } t_0 \ll T). \tag{14}$$

Inserting this result into the Boltzmann equation (12), the number density $n(t)$ takes a following asymptotic value,

$$n(t) \simeq \frac{3^{3(1-m)}\,(1-m)^{3(2-m)}}{v^3 t^3} \propto t^{-3}. \tag{15}$$

From the above asymptotic form, first of all, we find that the number density $n(t)$ is proportional to the inverse of the cosmic time cubed, t^{-3}, which implies that ξ becomes a constant irrespective of the cosmic time. ξ is also estimated as

$$\xi = \frac{3^{3(1-m)}\,(1-m)^{3(2-m)}}{v^3}. \tag{16}$$

Inserting $m = 1/2$ and $v_{RD} \sim (1.0 \pm 0.3)$, $\xi_{RD} \sim (0.45 \pm 0.22)$. On the other hand, inserting $m = 2/3$ and $v_{MD} \sim (0.8 \pm 0.3)$, $\xi_{MD} \sim (0.17 \pm 0.13)$. Thus, ξ obtained by the analytic estimates can well reproduce that obtained from the numerical simulations both in the RD universe and the MD universe.

4 Summary

In this talk, we have discussed the evolution of the global monopole network in the expanding universe. We have completely confirmed that the global monopole network relaxes into the scaling regime, where the number of global monopoles per the horizon volume is a constant. The scaling parameter ξ is given by $\xi_{RD} \simeq (0.43 \pm 0.07)$ in the RD universe and $\xi_{MD} \simeq (0.25 \pm 0.05)$ in the MD universe. We also investigated the peculiar velocity of global monopoles. First of all, we established the method to measure the peculiar velocity by using only the local quantities of the scalar fields. This method compensates the weak point of the Eulerian view which our numerical simulations are based on. that is, we cannot follow the motion of each monopole in detail. We find that the peculiar velocity also becomes a constant

[2] A similar discussion was done in [15, 16]

irrespective of the cosmic time and is given by $v_{RD} \sim (1.0 \pm 0.3)$ and $v_{MD} \sim (0.8 \pm 0.3)$ though there is still large uncertainty. By use of the Boltzmann equation for the time development of the number density and the peculiar velocity obtained from numerical simulations, we give a simple analytic estimate for the number density, which can well reproduce the results from the numerical simulations up to the proportional coefficient ξ.

Acknowledgments

The author is grateful to J. Yokoyama for useful comments. This work was partially supported by the Japanese Grant-in-Aid for Scientific Research from the Ministry of Education, Culture, Sports, Science, and Technology.

References

[1] M. Barriola and A. Vilenkin, Phys. Rev. Lett. **63**, 341 (1989).

[2] D. P. Bennett and S. H. Rhie, Phys. Rev. Lett. **65**, 1709 (1990).

[3] D. P. Bennett and S. H. Rhie, Astrophys. J. Lett. **406**, L7 (1993).

[4] U. Pen, D. N. Spergel, and N. Turok, Phys. Rev. D **49**, 692 (1994); Phys. Rev. Lett. **79**, 1611 (1997).

[5] M. Kunz and R. Durrer, Phys. Rev. D **55**, R4516 (1997);
R. Durrer, M. Kunz, and A. Melchiorri, *ibid.* **59**, 123005 (1999).

[6] P. de Bernardis *et al.*, Nature (London) **404**, 955 (2000);
A. E. Lange *et al.*, Phys. Rev. D **63**, 042001 (2001).

[7] S. Hanany *et al.*, Astrophys. J. Lett. **545**, L5 (2000);
A. Balbi *et al.*, *ibid.* **545**, 1 (2000).

[8] F. R. Bouchet, P. Peter, A. Riazuelo, and M. Sakellariadou, Phys. Rev. D **65**, 021301 (2002);
C. R. Contaldi, astro-ph/0005115.

[9] P .G. Ferreira, J. Magueijo, and K. M. Gorski, Astrophys. J. Lett. **503**, L1 (1998);
J. Pando, D. Valls-Gabaud, and L. Fang, Phys. Rev. Lett. **81**, 4568 (1998);
D. Novikov, H. Feldman, and S. Shandarin, Int. J. Mod. Phys. **D8**, 291 (1999).

[10] A. D. Linde, Phys. Lett. B **259**, 38 (1991); Phys. Rev. D **49**, 748 (1994).

[11] J. Yokoyama, Phys. Lett. B **212**, 273 (1988); Phys. Rev. Lett. **63**, 712 (1989).

[12] L. Kofman, A. Linde, and A. A. Starobinsky, Phys. Rev. Lett. **76**, 1011 (1996).

[13] M. Yamaguchi, Phys. Rev. D **64**, 081301 (2001).

[14] M. Yamaguchi, hep-ph/0107230, Phys. Rev. D in press.

[15] J. Preskill, Phys. Rev. Lett. **43**, 1365 (1979).

[16] M. Yamaguchi, J. Yokoyama, and M. Kawasaki, Prog. Theor. Phys. **100**, 535 (1998).

Gravitational particle production from metric perturbations

Shinji Tsujikawa [1]

Research Center for the Early Universe, University of Tokyo, Hongo, Bunkyo-ku, Tokyo 113-0033, Japan

Bruce A. Bassett

Relativity and Cosmology Group (RCG), University of Portsmouth, Mercantile House, Portsmouth, PO1 2EG, England

Marco Peloso

Physikalisches Institut, Universität Bonn Nussallee 12, D-53115 Bonn, Germany

Lorenzo Sorbo

SISSA/ISAS, via Beirut 2-4, I-34013 Trieste, Italy, and INFN, Sezione di Trieste, via Valerio 2, I-34127 Trieste, Italy

Abstract

We study gravitational creation of light fermions in the presence of classical scalar metric perturbations about a flat Friedmann-Lemaitre- Robertson-Walker (FLRW) background. These perturbations can be large during preheating, breaking the conformal flatness of the background spacetime. We compute numerically the total number of particles generated by the modes of the metric perturbations which have grown sufficiently to become classical. In the absence of inhomogeneities massless fermions are not gravitationally produced, and then this effect may be relevant for abundance estimates of light gravitational relics.

1 Introduction

It is well known that particles are created in an expanding Universe. Pioneering work by Parker [1] highlighted the creation of nonconformally-invariant particles even in flat Friedmann-Lemaitre-Robertson-Walker (FLRW) Universes. The extension to anisotropic Bianchi cosmologies by Zel'dovich and Starobinsky [2], showed that massless, conformally coupled, scalar particles are created due to the breaking of conformal invariance which, in four dimensions, is signaled by a non-vanishing Weyl tensor. In the presence of small, inhomogeneous metric perturbations, Horowitz and Wald [3] obtained the vacuum expectation value of the stress tensor for a conformally invariant field and showed that particle production only occurs if $\langle T_{\mu\nu}(x)\rangle$ is non-local (i.e., has non-zero contributions with support on the past-null cone of the event x).

The number of particles created by inhomogeneities can be computed by a perturbative evaluation of the S-matrix [4, 5, 6]. In the inhomogeneous case, the occupation number of produced particles is composed by three parts, *viz.* the zeroth-order contribution due to the homogeneous expansion, a first-order (in the perturbation amplitude) part arising from the interference between 0- and 2- particle states, and a second-order contribution which comes from the interaction between nonzero particle states. In the case of massive or nonconformally coupled scalar fields, the last two terms (respectively linear and

[1] E-mail:shinji@resceu.s.u-tokyo.ac.jp

quadratic in the metric perturbations) typically give a contribution small compared with the first one. However, in the massless and conformally coupled cases, the first two terms vanish in rigid, exactly FLRW backgrounds, and only inhomogeneity contributes to the gravitational particle production.

Nonperturbative production during the coherent oscillation of the inflaton fields [7, 8], dubbed preheating, can alter the simple picture of small amplitude metric perturbations. Hence on certain scales the Weyl tensor can actually be quite large. This means that there can be significant particle production even if the field is governed by a conformally invariant equation of motion, the classic examples being photons, massless fermions and conformally coupled scalars. Hereafter we shall analyze gravitational production of fermions due to the growth of metric perturbations in preheating.

2 Formalism for production of fermions

Let us consider metric perturbations in the longitudinal gauge $h_{\mu\nu} = 2\,\Phi\,\delta_{\mu\nu}$, *viz*:

$$ds^2 = a^2(1+2\Phi)d\eta^2 - a^2(1-2\Phi)\delta_{ij}dx^i dx^j \ . \tag{1}$$

The action of a fermionic field ψ with mass m in the background is, to first order in Φ,

$$\begin{aligned} \mathcal{S} &= \int d^4x\, a^3\,(1-2\,\Phi)\,\bar{\psi}\left\{ i\left[(1-\Phi)\,\gamma^0\,\partial_\eta + \frac{3}{2a}\frac{da}{d\eta}\,(1-\Phi)\,\gamma^0 - \frac{3}{2}\frac{d\Phi}{d\eta}\,\gamma^0 \right.\right. \\ &\quad \left.\left. + (1+\Phi)\,\gamma^i\,\partial_i - \frac{3}{2}\,\gamma^i\,\partial_i\,\Phi\right] - a\,m\right\}\psi \\ &= \int d^4x\,\tilde{\bar{\psi}}\left[\left(i\gamma^0\,\partial_\eta + i\gamma^i\,\partial_i - a\,m\right) - 3\,\Phi\,\gamma^0\,\partial_\eta - \Phi\,\gamma^i\,\partial_i - \frac{3}{2}\frac{d\Phi}{d\eta}\,\gamma^0 - \frac{3}{2}\,\gamma^i\,\partial_i\Phi\right]\tilde{\psi} \\ &\equiv \int d^4x\,\left[\mathcal{L}_0 + \mathcal{L}_I\,(\Phi)\right], \end{aligned} \tag{2}$$

where we have defined $\tilde{\psi} \equiv a^{3/2}\,\psi$ and $\mathcal{L}_0$, $\mathcal{L}_I$ denote the homogeneous and interaction Lagrangians.

The number density of produced particles is easily computed in the interaction picture, where the evolution of the operators is just determined by the homogeneous expansion of the Universe, and the states evolve according to the small inhomogeneities in the metric. In the interaction picture, the evolution of the initial vacuum (zero particle) state $|0\rangle$ is determined by the interaction Lagrangian $\mathcal{L}_I(\Phi)$. At first order in Φ we have

$$|\psi\rangle = |0\rangle + \frac{1}{2}\int d^3k\,d^3k'\,|k,r\,;\,k',s\rangle\,\langle k,r\,;\,k',s|S|0\rangle \ , \tag{3}$$

with the S-matrix element (T stands for time ordering)

$$\langle k,r\,;\,k',s|S|0\rangle \equiv i\,T\,\langle k,r\,;\,k',s|\mathcal{L}_I\,(\Phi)\,|0\rangle \ . \tag{4}$$

The expectation value of the number operator $\hat{N} \equiv (2\,\pi\,a)^{-3}\int d^3p\,\hat{a}_r^\dagger\,(p,\eta_f)\,\hat{a}_r\,(p,\eta_f)$ in the state $|\psi\rangle$ is given by the sum of three terms, $N_0 + N_1 + N_2$, which are of zeroth, first, and second order in Φ, respectively [4, 5, 6],

$$N_0 = \frac{V}{(2\pi a)^3}\int d^3k\,\langle 0|\,\hat{a}_r^\dagger(k)\,\hat{a}_r(k)\,|0\rangle = \frac{V}{(2\pi a)^3}\int d^3k\,|\beta_k|^2 \ , \tag{5}$$

$$N_1 = -\frac{1}{(2\pi a)^3}\int d^3k\,\mathrm{Re}\,\left[\alpha_r\,(k)\,\beta_r\,(k)\,\langle k,r\,;\,-k,r|S|0\rangle\right], \tag{6}$$

$$N_2 = \frac{1}{4\,(2\pi a)^3}\int d^3k\,d^3k'\,|\langle 0|S|k,r\,;\,k',s\rangle|^2\,\left[|\alpha_r\,(k)|^2 + |\beta_s\,(-k')|^2 + 1\right] \ , \tag{7}$$

where the Bogolyubov coefficients α_r and β_r satisfy $|\alpha_r|^2 + |\beta_r|^2 = 1$, which holds in the fermionic case. The zeroth-order term (5) is the well known expression arising from the homogeneous expansion of the Universe. V denotes the volume of the Universe at late times, when the perturbations can be neglected. The first-order contribution (6) comes from the combined effect of expansion and inhomogeneities. These

two terms vanish for massless fermions, which are conformally coupled to the FLRW background (more explicitly, we notice that $\beta_r(k,\eta) = 0$ in this case).

In the massless case, only the last term (7) contributes to the particle production. For the metric (1), one finds

$$N_2 = \frac{1}{15\,(2\pi)^2\,a^3}\int_0^\infty dp_0 \int_{|\mathbf{p}|<p_0} d^3\mathbf{p}\,|\mathbf{p}|^4 \left|\int_{\eta_i}^{\eta_f} d\eta\, e^{i\,p_0\,\eta}\,\tilde{\Phi}\,(\mathbf{p},\eta)\right|^2 , \tag{8}$$

where $\tilde{\Phi}$ is defined by

$$\Phi\,(\eta\,,\mathbf{x}) \equiv \int \frac{d^3\mathbf{p}}{(2\pi)^{3/2}}\,\tilde{\Phi}\,(\mathbf{p},\,\eta)\;e^{i\,\mathbf{p}\cdot\mathbf{x}} \quad . \tag{9}$$

In these expressions, Φ should be regarded as a purely classical perturbation. The normalization as well as the classicality condition for Φ will be discussed in the subsequent sections.

3 Numerical results for the production of fermions

Hereafter we assume the metric perturbations to be statistically isotropic and homogeneous, so that $\Phi_{\mathbf{k}} = \Phi_{|\mathbf{k}|}$. In this case, the final particle density is given by

$$N_\psi \equiv \frac{N_2}{V} = \frac{1}{15\,(2\pi)^4\,a^3}\int_0^\infty dp_0 \int_0^{p_0} dp\,p^6 \left|\int_{\eta_i}^{\eta_f} d\eta\, e^{ip_0\eta}\,\Phi_p\,(\eta)\right|^2 . \tag{10}$$

In the numerical calculations we take as the upper limit η_f of the time integral the moment in which backreaction effects start to shut off the resonance.

Before presenting the numerical results, we briefly consider the occupation number of massive fermions produced by the homogeneous FLRW expansion, eq. (5). For sufficiently small masses, the final occupation number is still (approximately) given by (10), since the Bogolyubov coefficient β is very close to zero in this limit. The term (5), although quadratic in β, is not suppressed by the small perturbations. Thus, by solving the equation

$$N_0\,(m_\psi) = N_2\,(m_\psi = 0) \tag{11}$$

we can estimate up to which mass m_ψ the productions by the inhomogeneities is comparable with that from the homogeneous expansion.

The calculation of N_0 has been performed numerically in [9]. For low fermionic masses, the gravitational production from the homogeneous expansion mainly occurs when the Hubble expansion rate equals m_ψ. After this time, the comoving fermion number density is given by [9]

$$n_\psi^{\rm hom} \equiv a^3\,N_0/V \simeq C_\alpha\,m_\psi^3\left(\frac{H_0}{m_\psi}\right)^{3\alpha} . \tag{12}$$

In this expression, H_0 denotes the value of the Hubble rate at the initial time t_0, where the scale factor $a\,(t_0)$ is normalized to unity. The parameter α is instead the exponent appearing in the expansion law $a\,(t) \propto t^\alpha$ when $H\,(t) = m_\psi$ (as is well known, the coherent inflaton oscillations give effective matter domination, $\alpha = 2/3$, in the $V = m^2\phi^2/2$ case, and effective radiation domination, $\alpha = 1/2$, for $V = \lambda\phi^4/4$). For the first coefficient of eq. (12), the two values $C_{2/3} \simeq 3\times10^{-3}$ and $C_{1/2} \simeq 10^{-2}$ have been numerically found [9].

3.0.1 $V = \frac{1}{4}\lambda\phi^4$

In the single field self-coupling potential $V = \frac{1}{4}\lambda\phi^4$, the sub-Hubble modes which lie in the range $3/2 < \kappa^2 < \sqrt{3}$ are enhanced by parametric resonance. In calculating the total number densities of produced fermions due to inhomogeneities, we take the cut-off value in momentum space at $p_c = 3$, over which Δ_k^2 approaches unity. Then the final particle density reached at the end of preheating is numerically found to be

$$n_\psi \equiv \frac{N_\psi}{s} \simeq 1\times10^{-13}\,(\sqrt{\lambda}\phi_0)^3. \tag{13}$$

where $\phi_0 \simeq 0.1 M_{\rm pl}$ is the value of inflaton at the beginnig of preheating.

Proceeding as in the previous subsection we find that the production from metric perturbations dominates over that from the homogeneous expansion as long as the fermions have masses smaller than

$$m_\psi = \frac{1}{H_0}\left(\frac{n_\psi}{C_{1/2}}\right)^{2/3} \simeq 10^5 \text{ GeV} . \tag{14}$$

By assuming an instantaneous inflaton decay into a thermal bath characterized by the reheat temperature $T_{\rm rh}$, the particle density divided by the entropy density, s, is given by

$$Y_\psi(T_{\rm rh}) \simeq 10^{-22} . \tag{15}$$

In the case of other light gravitational relics, such as gravitini or modulini, the primordial abundance is severely constrained by the successful predictions of Big Bang nucleosynthesis. For masses of order the electroweak breaking scale, the limit is about $Y \lesssim 10^{-13} - 10^{-12}$ [10]. In the present case, eq. (15) gives a much smaller abundance.

3.0.2 $V = \frac{1}{4}\lambda\phi^4 + \frac{1}{2}g^2\phi^2\chi^2$

Since the presence of the coupling $\frac{1}{2}g^2\phi^2\chi^2$ leads to an infinite number of resonance bands whose center are $R \equiv g^2/\lambda = 2n^2$ (n is integer) [11], it is the case of most interest. By comparison with the single field case ($g = 0$, here reproduced by the choice $R = 3$) the two equations (14) and (15) are generalized to

$$m_\psi \simeq 5 \times 10^{13}\, \tilde{n}_\psi^{2/3} \text{ GeV} \quad , \quad Y_\psi(T_{\rm rh}) \simeq 10^{-9}\, \tilde{n}_\psi , \tag{16}$$

where $\tilde{n}_\psi \equiv n_\psi/(\sqrt{\lambda}\phi_0)^3$. When $R < 10$ we have maximal production when R is in the center of the first resonance band ($R = 2$), in which case n_ψ is found to be $\tilde{n}_\psi \simeq 5 \times 10^{-10}$, which is about 5000 times larger than in the single-field case. In the second resonance band, particle production is slightly smaller than in the $R = 2$ case (see ref. [12] for details).

As R increases, the inflationary suppression of χ [13] becomes important, and particle production from first order perturbations is consequently reduced. Nevertheless, the second order effect of field perturbationscan lead to the excitation of metric perturbations on sub-Hubble scales [14]. Just for indicative purposes, we report a couple of our numerical results in this range. For large R, the resonance bands cover only modes up to [11]

$$\kappa \lesssim \left(\frac{R}{2\pi^2}\right)^{1/4} . \tag{17}$$

In the center of the 10-th instability band, $R = 200$, one finds resonant amplification up to $\kappa \lesssim 1.78$, in which case one has $\tilde{n}_\psi \simeq 6 \times 10^{-11}$. As R increases, higher momentum modes contribute to the growth of metric perturbations. As a consequence, this enhances fermionic production. The comoving occupation number in the $R = 5000$ case is found to be $\tilde{n}_\psi \simeq 1 \times 10^{-7}$, $Y_\psi(T_{\rm rh}) \simeq 10^{-16}$.

It is however important to mention that for $R \gg 1$ the whole analysis becomes very delicate. For large coupling g, the backreaction effect of produced particles ends resonant amplification of field perturbations earlier. In addition, it was found in Ref. [15] that the final field variances get smaller if rescattering of the $\delta\chi$ fluctuations is taken into account in the rigid FLRW spacetime ($\Phi = 0$). On the contrary, the effect of rescattering can lead to the excitation of inflaton fluctuations through the amplification of $\delta\chi$ fluctuations. The study of these effects is certainly worth separate detailed investigation.

4 Conclusions

We have discussed gravitational creation of fermions by inhomogeneous scalar perturbations of a Friedmann-Lemaitre-Robertson-Walker (FLRW) Universe. Massless fermions are conformally coupled to this background, and thus are not generated by the homogeneous gravitational field. As a consequence, gravitational production of light particles is solely induced by metric perturbations which break the conformal flatness of the background.

This is particularly true in scenarios in which metric perturbations undergo parametric amplification during preheating at the end of inflation. We studied the massless self-coupled inflaton field ($V = \lambda\phi^4/4$) case, in which parametric resonance occurs for modes in a small band in momentum space near the Hubble scale. As a consequence, particle production is enhanced. However, the final result for the production is still well below the limit from nucleosynthesis.

More efficient production is expected when more fields are present, such as the model characterized by the potential $V = \lambda\phi^4/4 + g^2\phi^2\chi^2/2$. In this case, the crucial parameter which determines the resonance bands is $R \equiv g^2/\lambda$. In particular, the longwavelength modes of the second field χ are parametrically amplified whenever $R \simeq 2n^2$ with integer n. At linear order in field perturbations, these modes are coupled to metric perturbations through a term proportional to $\dot{\chi}\delta\chi_k$. For relatively small R, metric perturbations are amplified by this term, and particle production is strongly enhanced.

For $R > 10$ the large χ effective mass ($m_\chi = g\langle\phi\rangle \propto R^{1/2}$) causes the χ field to be exponentialy suppressed during inflation. As a consequence, for large R metric perturbations mainly increase due to second order field fluctuations. Particle production may be expected to become more significant at very large R. This is indeed suggested by our numerical results, although in the cases considered the final abundance is still below the nucleosynthesis bounds.

References

[1] L. Parker, Phys. Rev. Lett. **21**, 562 (1968); Phys. Rev. **183**, 1057 (1969).

[2] Ya. B. Zel'dovich and A. A. Starobinsky, Sov. Phys. JETP **34**, 1159 (1972).

[3] G. T. Horowitz and R. M. Wald, Phys. Rev. D **21**, 1462 (1980)

[4] J. A. Frieman, Phys. Rev. D **39**, 389 (1989).

[5] A. Campos and E. Verdaguer, Phys. Rev. D **45**, 4428 (1992).

[6] J. Cespedes and E. Verdaguer, Phys. Rev. D **41**, 1022 (1990).

[7] J. Traschen and R. H. Brandenberger, Phys. Rev. D **42**, 2491 (1990); Y. Shatanov, J. Trashen, and R. H. Brandenberger, Phys. Rev. D **51**, 5438 (1995).

[8] L. Kofman, A. Linde, and A. A. Starobinsky, Phys. Rev. Lett. **73**, 3195 (1994); Phys. Rev. D **56**, 3258 (1997).

[9] V. Kuzmin and I. Tkachev, Phys. Rev. D **59**, 123006 (1999).

[10] M. Kawasaki and T. Moroi, Astrophys. J. **452**, 506 (1995).

[11] P.B. Greene, L. Kofman, A. Linde, and A. A. Starobinsky, Phys. Rev. D **56**, 6175 (1997).

[12] B. A. Bassett, M. Peloso, L. Sorbo, and S. Tsujikawa, Nucl. Phys. B 622, 393 (2002).

[13] K. Jedamzik and G. Sigl, Phys. Rev. D **61**, 023519 (2000); P. Ivanov, Phys. Rev. D **61**, 023505 (2000).

[14] A. R. Liddle, D. H. Lyth, K. A. Malik, and D. Wands, Phys. Rev. D **61**, 103509 (2000).

[15] S. Khlebnikov and I. I. Tkachev, Phys. Rev. Lett. **77**, 219 (1996); Phys. Lett. **390**, 80 (1997); Phys. Rev. Lett. **79**, 1607 (1997).

The Two Dimensional String Effective Action, Duality and Monodromy Matrix

Ashok Das and A. Melikyan

Department of Physics of Physics and Astronomy, University of Rochester, NY 14627-0171, USA

J. Maharana,

Theory Division, KEK, Tsukuba, Japan
Institute of Physics, Bhubaneswar, India

Abstract

We present a prescription for constructing the monodromy matrix, $\widehat{\mathcal{M}}(\omega)$, for $O(d,d)$ invariant string effective actions and derive its transformation properties under the T-duality group. This allows us to construct $\widehat{\mathcal{M}}(\omega)$ for new backgrounds, starting from known ones, which are related by T-duality. As an application, we derive the monodromy matrix for the exactly solvable Nappi-Witten model, both when $B = 0$ and $B \neq 0$.

The symmetries of string theory such as, dualites, have been crucial in our understanding of string dynamics [1, 2, 3]. The tree level string effective action, compactified on a d-dimensional torus, T^d, is known to be invariant under the noncompact global symmetry group $O(d,d)$. The dimensionally reduced string effective action, in two space-time dimensions, is known to possess enlarged symmetries, which has been explored by several authors [4, 5, 6, 7]. The effective action is described by a nonlinear σ-model, defined over a coset, which is coupled to gravity. In the past, two dimensional models, derived from dimensional reduction of higher dimensional Einstein gravity as well as supergravity theories, have been studied to bring out their integrability properties [8, 9, 10]. In this context, one may recall that the construction of the monodromy matrix turns out to be one of the principal objectives in the study of integrable systems [11, 12]. Recently, we have investigated the scattering of plane fronted waves, in four dimensions, which correspond to massless states of closed strings [13]. The scattering process is described by an effective two dimensional action due to the presence of isometries along the directions transverse to the axis of collision. Therefore, the reduced action is endowed with an $O(2,2)$ symmetry, as is obvious from the preceding discussion. We were able to derive the monodromy matrix for such a scattering process for the specific background configurations involved and had established an intimate connection between the integrability properties of the model and the underlying $O(2,2)$ symmetry.

The central result of our work [14] is to derive the monodromy matrix, $\widehat{\mathcal{M}}(\omega)$, for a 2-dimensional string effective action, obtained from a D-dimensional effective action, which is compactified on T^d and thus enjoys isometries along $d = D - 2$ spatial directions. We provide the prescription for the construction of the monodromy matrix, in this case, and derive the transformation property of $\widehat{\mathcal{M}}(\omega)$ under $O(d,d)$ transformations. In this process, we are able to synthesize the classical integrability properties and the duality symmetry of string theory in a novel way. Furthermore, as an illustrative example, we construct the monodromy matrix for the well known Nappi-Witten model [15], both for $B = 0$ and $B \neq 0$, and demonstrate explicitly the transformation of $\widehat{\mathcal{M}}(\omega)$ under T-duality. Namely, as is well known, one can start from background configurations where the NS-NS field $B_{ij} = 0$ and generate new backgrounds with $B_{ij} \neq 0$ through a T-duality rotation. Correspondingly, we can construct $\widehat{\mathcal{M}}^{(B=0)}(\omega)$ explicitly and generate $\widehat{\mathcal{M}}^{(B)}(\omega)$ through a T-duality rotation. Alternatively, we can also construct the $\widehat{\mathcal{M}}^{(B)}(\omega)$ directly and demonstrate that the two methods indeed lead to identical results.

Our starting point is the D-dimensional tree level string effective action

$$\hat{S} = \int d^D x \sqrt{-\widehat{G}} \left(R_{\widehat{G}} + (\hat{\partial}\hat{\phi})^2 - \frac{1}{12}\widehat{H}^2 \right) \tag{1}$$

where $\widehat{G}_{\hat{\mu}\hat{\nu}}$ is the metric in D-dimensions in the string frame, $\widehat{G}$ its determinant, $R_{\widehat{G}}$ the corresponding scalar curvature, $\hat{\phi}$ is the dilaton and $\widehat{H} = d\widehat{B}$. When compactified on T^d, the reduced action takes the following form [16]:

$$S = \int dx^0 dx^1 \sqrt{-g} e^{-\bar{\phi}} \left(R + (\partial\bar{\phi})^2 + \frac{1}{8}\mathrm{Tr}(\partial_\alpha M^{-1}\partial^\alpha M) \right) \tag{2}$$

where $g_{\alpha\beta}$ with $\alpha, \beta = 0, 1$ is the two dimensional space-time metric, and R is the corresponding scalar curvature. The shifted dilaton is $\bar{\phi} = \phi - \frac{1}{2}\log\det G$, with G_{ij} the metric corresponding to the transverse coordinates $x^i, i = 2, 3.., D-1$. M is a $2d \times 2d$ symmetric matrix belonging to $O(d,d)$,

$$M = \begin{pmatrix} G^{-1} & -G^{-1}B \\ BG^{-1} & G - BG^{-1}B \end{pmatrix} \tag{3}$$

where B represents the moduli coming from the reduction of the B-field in D space-time dimensions. The symmetric nature of M is evident since G is symmetric and B is anti-symmetric. In general, there will be additional terms in (2) corresponding to d Abelian gauge fields coming from the original metric and another set of d gauge fields coming from the anti-symmetric tensor $B_{\hat{\mu}\hat{\nu}}$ as a result of dimensional reduction [16] ($d = D - 2$). Furthermore, there would also have been the field strength of the two dimensional tensor field $B_{\alpha\beta}$. Since we are effectively in two space-time dimensions, we have dropped the gauge field terms and, in the same spirit, have not kept the field strength of $B_{\alpha\beta}$, which can be removed if it depends only on the coordinates x^0 and x^1.

The action (2) is invariant under the global $O(d,d)$ transformations,

$$g_{\alpha\beta} \to g_{\alpha\beta}, \quad \bar{\phi} \to \bar{\phi}, \qquad M \to \Omega^T M \Omega \tag{4}$$

where $\Omega \in O(d,d)$ is the transformation matrix, which leaves the $O(d,d)$ metric, $\eta = \begin{pmatrix} 0 & 1 \\ 1 & 0 \end{pmatrix}$, invariant ($1$ is the d-dimensional unit matrix). It is convenient to introduce the lower triangular matrix

$$V = \begin{pmatrix} E^{-1} & 0 \\ BE^{-1} & E^T \end{pmatrix} \tag{5}$$

where E is the vielbein with $(EE^T)_{ij} = G_{ij}$. It is easy to check that $V \in O(d,d)$ and that $M = VV^T$ so that under $O(d,d)$ transformations, $V \to \Omega^T V$. In fact, V belongs to the coset $\frac{O(d,d)}{O(d)\times O(d)}$.

We may decompose the current as

$$V^{-1}\partial_\alpha V = P_\alpha + Q_\alpha \tag{6}$$

where $Q_\alpha \in O(d) \times O(d)$, the Lie algebra for the maximally compact subgroup and P_α belongs to the complement. It follows from the property of the coset under study that $P_\alpha^T = P_\alpha$ and $Q_\alpha^T = -Q_\alpha$ and it is straightforward to check that the last term of (2) can be expressed as

$$\mathrm{Tr}\ (\partial_\alpha M \partial^\alpha M^{-1}) = -4\mathrm{Tr}\ g^{\alpha\beta} P_\alpha P_\beta \tag{7}$$

Let us note that, under a global $O(d,d)$ rotation $V \to \Omega^T V$, the current in (6) is invariant, while under a local $O(d) \times O(d)$ transformation $V \to Vh(x)$, P_α and Q_α transform as

$$P_\alpha \to h^{-1}(x) P_\alpha h(x), \quad Q_\alpha \to h^{-1}(x) Q_\alpha h(x) + h^{-1}(x)\partial_\alpha h(x) \tag{8}$$

which leaves (7) invariant.

A few comments are in order at this stage. We are dealing with a 2-dimensional σ-model [4, 6, 7] coupled to gravity and, in addition, the action (2) contains a shifted dilaton field, $\bar{\phi}$. We may rescale the metric $g_{\alpha\beta} \to e^{\bar{\phi}} g_{\alpha\beta}$, which will eliminate the kinetic energy term of $\bar{\phi}$. Recall that in a curved space, the spectral parameter becomes space-time dependent in the zero curvature formulation of the sigma model, unlike in flat space, where the spectral parameter is a constant. Let $\widehat{V}(x,t)$, where t is the space-time

dependent spectral parameter, be the one parameter family of matrices such that $\widehat{V}(x,t=0)=V(x)$ and

$$\widehat{V}^{-1}(x,t)\partial_\alpha\widehat{V}(x,t)=Q_\alpha+\frac{1+t^2}{1-t^2}P_\alpha+\frac{2t}{1-t^2}\epsilon_{\alpha\beta}P^\beta \tag{9}$$

Then, it is easy to check that the integrability condition

$$\partial_\alpha(\widehat{V}^{-1}\partial_\beta\widehat{V})-\partial_\beta(\widehat{V}^{-1}\partial_\alpha\widehat{V})+[\widehat{V}^{-1}\partial_\alpha\widehat{V},\widehat{V}^{-1}\partial_\beta\widehat{V}]=0 \tag{10}$$

leads to the dynamical equations of the theory, provided the spectral parameter is related to the shifted dilaton through the equation

$$\partial_\alpha t=-\frac{1}{2}\epsilon_{\alpha\beta}\partial^\beta\left(e^{-\bar{\phi}}(t+\frac{1}{t})\right) \tag{11}$$

The solution to this equation has the form

$$t(x)=\frac{\sqrt{\omega+\rho_+(x^+)}-\sqrt{\omega-\rho_-(x^-)}}{\sqrt{\omega+\rho_+(x^+)}+\sqrt{\omega-\rho_-(x^-)}} \tag{12}$$

where we have defined $\rho=e^{-\bar{\phi}}=\rho_+(x^+)+\rho_-(x^-)$ for later use and ω is the constant of integration (which can be thought of as a global, constant spectral parameter). The light cone coordinates are defined to be $x^+=\frac{1}{\sqrt{2}}(x^0+x^1)$ and $x^-=\frac{1}{\sqrt{2}}(x^0-x^1)$.

The next important step is to solve for the monodromy matrix, $\widehat{\mathcal{M}}(\omega)$. The linear system (9) is known to be invariant under a generalization of the symmetric space automorphism, τ^∞, defined through

$$\tau^\infty\widehat{V}(x,t)=\left(\widehat{V}^{-1}\right)^T(x,\frac{1}{t}) \tag{13}$$

This relation has the following action on the elements of the Lie algebra, $Q_\alpha\rightarrow Q_\alpha$, $P_\alpha\rightarrow -P_\alpha$ and $t\rightarrow\frac{1}{t}$. The monodromy matrix, defined as,

$$\widehat{\mathcal{M}}(\omega)=\widehat{V}(x,t)\tau^\infty\widehat{V}^{-1}(x,t)=\widehat{V}(x,t)\widehat{V}^T(x,\frac{1}{t}) \tag{14}$$

is space-time independent and plays a cardinal role in the study of integrable models. The reconstruction of solutions and properties of integrability are all deeply encoded in $\widehat{\mathcal{M}}(\omega)$. For example, if we were to use a solution of the $\bar{\phi}$ equation as input, then we can determine t from its relation with the dilaton and eventually obtain $\widehat{V}(x,t)$.

Now we want to present a crucial observation which enables us to derive the transformation property of $\widehat{\mathcal{M}}(\omega)$ under T-duality. Note that the one parameter family of matrices $\widehat{V}(x,t)\in\frac{O(d,d)}{O(d)\times O(d)}$ much like $V(x)=\widehat{V}(x,t=0)$. Therefore, under a global $O(d,d)$ rotation, $\widehat{V}(x,t)\rightarrow\Omega^T\widehat{V}(x,t)$ and the monodromy matrix transforms as

$$\widehat{\mathcal{M}}(w)\rightarrow\Omega^T\widehat{\mathcal{M}}(w)\Omega \tag{15}$$

Furthermore, although under a local $O(d)\times O(d)$ transformation $\widehat{V}(x,t)\rightarrow\widehat{V}(x,t)h(x)$, the only local transformations, which will preserve the global nature of the monodromy matrix are the ones which do not depend on the spectral parameter explicitly. This is very much like what we already know for the case $t=0$, namely, although $V\rightarrow\Omega^T V h(x)$ under combined $O(d,d)$ and $O(d)\times O(d)$ transformations, $M=VV^T$ undergoes only a global $O(d,d)$ rotation. In other words, the monodromy matrix, $\widehat{\mathcal{M}}(\omega)$, is only affected by the global $O(d,d)$ rotation, as is the case with the M-matrix. Thus, we are able to synthesize the integrability properties of the two dimensional string effective action with its T-duality properties. Indeed, this relation can be explicitly checked in specific examples (as we will show shortly) and can be used as a specific examples (as we will show shortly) and can be used as a powerful tool in determining solutions. Let us derive the transformation properties of $\widehat{\mathcal{M}}$ under infinitesimal $O(d,d)$ transformations. We may express $\widehat{\mathcal{M}}$ as

$$\widehat{\mathcal{M}}=\begin{pmatrix}\widehat{\mathcal{M}}_{11} & \widehat{\mathcal{M}}_{12}\\ \widehat{\mathcal{M}}_{21} & \widehat{\mathcal{M}}_{22}\end{pmatrix} \tag{16}$$

where each element is a $d \times d$ matrix. The matrix Ω assumes the following form

$$\Omega = \begin{pmatrix} 1+X & Y \\ Z & 1+W \end{pmatrix} \tag{17}$$

where the infinitesimal parameters of the transformation are required to satisfy, $Y^T = -Y, Z^T = -Z$ and $W = -X^T$. Under (17), the elements of (16) transform as

$$\begin{aligned} \delta\widehat{\mathcal{M}}_{11} &= \widehat{\mathcal{M}}_{11}X + X^T\widehat{\mathcal{M}}_{11} - Z\widehat{\mathcal{M}}_{12} + \widehat{\mathcal{M}}_{12}Z \\ \delta\widehat{\mathcal{M}}_{12} &= \widehat{\mathcal{M}}_{11}Y + X^T\widehat{\mathcal{M}}_{12} - Z\widehat{\mathcal{M}}_{22} - \widehat{\mathcal{M}}_{12}X^T \\ \delta\widehat{\mathcal{M}}_{21} &= -Y\widehat{\mathcal{M}}_{11} - X\widehat{\mathcal{M}}_{21} + \mathcal{M}_{21}X + \widehat{\mathcal{M}}_{22}Z \\ \delta\widehat{\mathcal{M}}_{22} &= \widehat{\mathcal{M}}_{21}Y - Y\mathcal{M}_{12} - X\widehat{\mathcal{M}}_{22} - \widehat{\mathcal{M}}_{22}X^T \end{aligned} \tag{18}$$

Since, we can obtain $\widehat{\mathcal{M}}(\omega)$ for the case when $B \neq 0$ starting from a vanishing B configuration, let us derive $\widehat{\mathcal{M}}(\omega)$ for the case when $B = 0$, E is diagonal so that G_{ij} is also diagonal. It is easy to check that $Q_\alpha = 0$ for this choice of backgrounds and the relevant equation for determining $\widehat{V}^{(B=0)}$ are given by

$$(\widehat{V}^{(B=0)})^{-1}\partial_+\widehat{V}^{(B=0)} = \frac{1-t}{1+t}P_+ \quad \text{and} \quad (\widehat{V}^{(B=0)})^{-1}\partial_-\widehat{V}^{(B=0)} = \frac{1+t}{1-t}P_- \tag{19}$$

and t satisfies (12).

The factorizability property of $\widehat{\mathcal{M}}(\omega)$, namely (14), together with the assumption that it has only isolated single poles determines that the monodromy matrix (as well as the $\widehat{V}^{(B=0)}(x,t)$ matrix) will have $2d$ poles in the spectral parameter. We can check this in the following manner. Let us assume that G_{ij} has the diagonal structure

$$G = \mathrm{diag}\,(e^{\lambda+\psi_1}, e^{\lambda+\psi_2}, \cdots, e^{\lambda+\psi_d}) \tag{20}$$

with $\sum\psi_i = 0$, so that $\lambda = \frac{1}{d}\log\det G$ as adopted in [19]. The E-matrix is also diagonal and has the form

$$E = \mathrm{diag}\,(e^{\frac{1}{2}(\lambda+\psi_1)}, e^{\frac{1}{2}(\lambda+\psi_2)}, \cdots, e^{\frac{1}{2}(\lambda+\psi_d)}) \tag{21}$$

Correspondingly, the $\widehat{V}^{(B=0)}$ matrix is diagonal as well and has the form

$$\widehat{V}^{(B=0)}(x,t) = \begin{pmatrix} \overline{V}^{(B=0)}(x,t) & 0 \\ 0 & (\overline{V}^{(B=0)})^{-1}(x,t) \end{pmatrix} \tag{22}$$

Let us assume the following form for the diagonal matrix $\overline{V}^{(B=0)}(x,t) = (\overline{V}_1, \overline{V}_2, \cdots, \overline{V}_d$ with

$$\overline{V}_i = \frac{t_{d+i}}{t_i}\frac{t-t_i}{t-t_{d+i}}E_i^{-1} \tag{23}$$

which explicitly brings out the $2d$ pole structures in $\widehat{V}^{(B=0)}(x,t)$. The spectral parameters satisfy

$$\partial_\pm t = \frac{1\mp t}{1\pm t}\partial_\pm \ln\rho, \qquad \partial_\pm t_i = \frac{1\mp t_i}{1\pm t_i}\partial_\pm \ln\rho \tag{24}$$

Using this, it is easy to verify that (t_{d+i} and t_i have opposite signatures, following from the double valued nature of the solutions in Eq. (12))

$$\overline{V}_i^{-1}\partial_\pm\overline{V}_i = \partial_\pm \ln E_i^{-1} \mp \frac{t}{1\pm t}\partial_\pm \ln\left(-\frac{t_i}{t_{d+i}}\right) = \frac{1\mp t}{1\pm t}\partial_\pm \ln E_i^{-1} \tag{25}$$

provided we identify $-\frac{t_i}{t_{d+i}} = E_i^{-2}$. In such a case, we can write

$$(\widehat{V}^{(B=0)})^{-1}(x,t)\partial_\pm\widehat{V}^{(B=0)}(x,t) = \frac{1\mp t}{1\pm t}\begin{pmatrix} -E^{-1}\partial_\pm E & 0 \\ 0 & E^{-1}\partial_\pm E \end{pmatrix} = \frac{1\mp t}{1\pm t}P_\pm \tag{26}$$

Thus, we see that, for the case at hand, we have to introduce $2d$ poles, a pair for every diagonal element E_i. Furthermore, the diagonal elements of $\overline{V}^{(B=0)}(x,t)$, in this case, are determined to be

$$\overline{V}_i(x,t) = \frac{t_{d+i}}{t_i}\,\frac{t-t_i}{t-t_{d+i}}\,E_i^{-1} = \sqrt{-\frac{t_{d+i}}{t_i}}\,\frac{t-t_i}{t-t_{d+i}} \tag{27}$$

It is easy to check that the global (constant) spectral parameters satisfy

$$\frac{\omega-\omega_i}{\omega-\omega_{d+i}} = \frac{t_{d+i}}{t_i}\,\frac{t-t_i}{t-t_{d+i}}\,\frac{\frac{1}{t}-t_i}{\frac{1}{t}-t_{d+i}} \tag{28}$$

Using this relation as well as the definition of the monodromy matrix, we note that we can write

$$\widehat{\mathcal{M}}^{(B=0)}(\omega) = \widehat{V}^{(B=0)}(x,t)(\widehat{V}^{(B=0)})^T(x,\frac{1}{t}) = \begin{pmatrix} \mathcal{M}(\omega) & 0 \\ 0 & \mathcal{M}^{-1}(\omega) \end{pmatrix} \tag{29}$$

where $\mathcal{M}(\omega)$ is diagonal with

$$\mathcal{M}_i(\omega) = \overline{V}_i(x,t)\overline{V}_i(x,\frac{1}{t}) = -\frac{\omega-\omega_i}{\omega-\omega_{d+i}} \tag{30}$$

The double valued relation between the global and the local spectral parameters allows us to choose $\omega_{d+i} = -\omega_i$, which leads to

$$\mathcal{M}_i(\omega) = \frac{\omega_i-\omega}{\omega_i+\omega} \tag{31}$$

This determines the monodromy matrix for a pure G background and starting from this, we can determine the monodromy matrix for a background with a non-vanishing G and B generated through an $O(d,d)$ transformation.

We shall adopt the Nappi-Witten model to illustrate these points explicitly. The Nappi-Witten model is described by the following $\frac{SU(2)}{U(1)} \times \frac{SL(2,R)}{SO(1,1)}$ gauged WZW model [15]. The worldsheet action, in terms of holomorphic and anti-holomorphic coordinates, is:

In summary, we have unravelled a deep connection between duality symmetry of two dimensional string effective action and its integrability properties. This is established by constructing the monodromy matrix in a general setting We showed that $\widehat{\mathcal{M}}(\omega)$ transforms nontrivially under the $O(d,d)$ transformations. It is evident that our results will have applications in a variety of problems in string theory which are described by an effective two dimensional action. As an illustration we examined an exactly solvable WZW model [15], which revealed some of the fascinating aspects of our investigation.

Acknowledgment: One of us (JM) acknowledges the warm hospitality of Prof. Y. Kitazawa and KEK. This work is supported in part by US DOE Grant No. DE-FG 02-91ER40685.

References

[1] A. Giveon, M. Porrati and E. Rabinovici, Phys. Rep. **C244** (1994) 77.

[2] A. Sen, Developments in Superstring Theory, hep-th/9810044.

[3] J. Maharana, Recent Developments in String Theory, hep-th/9911200

[4] I. Bakas, Nucl. Phys. **B428** (1994) 374.

[5] J. Maharana, Phys. Rev. Lett. **75** (1995) 205; Mod. Phys. Lett. **A11** (1996).

[6] J. H. Schwarz, Nucl. Phys. **B447** (1995) 137, Classical Duality Symmetries in Two Dimensions, hep-th/9505170.

[7] A. Sen Nucl. Phys. **B447** (1995) 62 .

[8] P. Breitenlohner and D. Maison, Inst. H. Poincare, **46** (1987) 215; F. J. Ernst, A. Garcia and I. Hauser, J. Math. Phys. **28** (1987) 2155.

[9] H. Nicolai, Phys. Lett. **B235** (1990) 195.

[10] V. Belinskii and V. Zakharov, Sov. Phys. JETP, **48** (1978) 985; H. Nicolai, Schladming Lectures, Springer-Verlag, Berlin (1991) eds. H. Mitter and H. Gausterer.

[11] H. Nicolai, D. Korotkin and H. Samtleben, Integrable Classical and quantum Gravity, NATO Advanced Study Institute on quantum Fields and quantum spacetime, Cargese, 1996; hep-th/9612065.

[12] A. Das, "Integrable Models", World Scientific, Singapore (1989).

[13] A. Das, J. Maharana and A. Melikyan, Phys. Lett. **B518** (2001) 306, hep-th/0107229.

[14] A. Das, J. Maharana and A. Melikyan, hep-th/ 0111158.

[15] C. Nappi and E. Witten, Phys. Lett. **B293** (1992) 309, hep-th/9206078.

[16] J. Maharana and J. H. Schwarz, Nucl. Phys. **B390**, hep-th/9207016.

[17] S. Mizoguchi, Nucl. Phys. **B461** (1996), A. Biswas, A. Kumar and K. Ray, Nucl. Phys. **B453** (1995) 181, A. A. Kehagias, Phys. Lett. **B360** (1995) 19, E. Abdalla and M. C. B. Abdalla, Phys. Lett. **B365** (1996) 41.

[18] M. Gasperini, J. Maharana and G. Veneziano, Phys. Lett. **B296** (1993) 51, hep-th/9209052.

[19] V. Bozza and G. Veneziano, JHEP **0010** (2000) 035, hep-th/0007159.

Gravitational Waves in Brane World
— A Midi-superspace Approach —

Jiro Soda,[1]

Department of Fundamental Sciences, FIHS, Kyoto University, Sakyo-ku, Kyoto 606-8501, Japan

Abstract

It is important to reveal the brane-bulk correspondence for understanding the brane world cosmology. When gravitational waves exist in the bulk, however, it is difficult to make the analysis of the interrelationship between the brane and the bulk. Hence, the minimal model which allows gravitational waves in the bulk would be useful. As for such models, we adopt the Bianchi type midi-superspace models. In particular, the effects of gravitational waves in the bulk on the brane cosmology is examined using the midi-superspace approach.

1 Introduction

The idea of the brane world has provided an active area in the field of cosmology. The main attractive point of this idea is its testability. However, to make a definite prediction, we need to understand the role of the bulk on the brane world cosmology. Before considering the complicated cosmological perturbation theory, we would like to try to understand the essence of the problem in the simple models. The aim of this paper is to study some aspects of the brane-bulk correspondence in the Bianchi Type I midi-superspace model.

Let us start to describe the Z_2 symmetric brane world model which we want to analyze from now on. The action for it is given by [1, 2]

$$S = \frac{1}{2\kappa^2}\int d^5x\sqrt{-g}\left(\mathcal{R}^5 + \frac{12}{l^2}\right) - \sigma\int d^4x\sqrt{-g_{brane}} + \int d^4x\sqrt{-g_{brane}}\mathcal{L}_{matter} \tag{1}$$

where l denotes the curvature radius of the AdS spacetime, κ^2 is the gravitational constant in the 5 dimensional spacetime, and σ and g_{brane} represnt the brane tension and the induced metric on the brane respectively. Here we assume the relation $\kappa^2\sigma = 6/l$ which is necessary to have the Minkowski vacuum.

From the above action, we obtain the 5-dimensional Einstein equations;

$$G^M_N = \frac{6}{l^2}\delta^M_N + \kappa^2\frac{\sqrt{-g_{brane}}}{\sqrt{-g}}T^M_N,\ (M,N = y,t,x^i)\ . \tag{2}$$

As for the matter confined to the brane, we consider the perfect fluid

$$T^M_N = diag(0,-\rho,p,p,p)\delta(y)\ . \tag{3}$$

First, let us consider the FRW cosmology. The cosmological principle restricts the bulk metric in the following form:

$$ds^2 = e^{2\beta(y,t)}(-dt^2+dy^2) + e^{2\alpha(y,t)}\delta_{ij}dx^idx^j\ . \tag{4}$$

Then, the induced metric on the brane becomes

$$ds^2 = -dt^2 + e^{2\alpha_0(t)}\delta_{ij}dx^idx^j\ . \tag{5}$$

Due to the generalized Birkoff's theorem, only AdS-Schwarzschild black hole solutions are allowed. Correspondingly, the cosmology on the brane is also simple. Putting $8\pi G_4 = \kappa^2/l$, we get the effective Friedmann equation as

$$\dot{\alpha}_0^2 = \frac{8\pi G_4}{3}\rho + \frac{\kappa^4\rho^2}{36} + e^{-4\alpha_0}C_0\ , \tag{6}$$

[1] E-mail:jiro@phys.h.kyoto-u.ac.jp

where the parameter C_0 corresponds to the mass of the black hole. It should be noted that there exists no gravitational waves in this back ground. This makes the understanding of brane-bulk correspondence easier.

To proceed to the cosmological perturbation theory is a natural next step for understanding cosmology. [3, 4, 5, 6, 7] To reveal the nature of the cosmological perturbation, we need to consider the bulk spacetime with gravitational waves. However, it is too complicated to analyze in detail.

In this circumstances, we take the midi-superspace approach to attack the issue. Namely, we consider the minimal model which can allow the bulk gravitational waves. We shall consider the Bianchi type midi-superspace models:

$$ds^2 = e^{2\beta(y,t)}(-dt^2 + dy^2) + e^{2\alpha(y,t)} g_{ij}(y,t)\omega^i\omega^j \ . \tag{7}$$

Apparently, there can exist (nonlinear) gravitational waves in this bulk spacetime. The induced cosmology on the brane is nothing but the anisotropic bianchi type cosmology;

$$ds^2 = -dt^2 + e^{2\alpha_0(t)} g_{ij0}(t)\omega^i\omega^j \ . \tag{8}$$

It includes FRW model as a special case. Hence, it should have implications into the cosmological perturbations. For simplicity, we will consider only the Bianchi type I model in this paper, althogh the generalization is straightforward.

2 Anisotropic Cosmology

Bianchi Type I midi-superspace metric is given by

$$ds^2 = e^{2\beta(y,t)}(-dt^2+dy^2)+e^{2\alpha(y,t)}\left(e^{2(\chi_+(y,t)+\sqrt{3}\chi_-(y,t))}dx_1^2 + e^{2(\chi_+(y,t)-\sqrt{3}\chi_-(y,t))}dx_2^2 + e^{-4\chi_+(y,t)}dx_3^2\right) . \tag{9}$$

As is mentioned previously, gravitational waves can propagate in the bulk. From the above metric, it is easy to calculate the components of the Einstein tensor relevant to the junction conditions as

$$\begin{aligned}
G^0_0 &= -3e^{-2\beta}(\dot\alpha^2 + \dot\alpha\dot\beta - \alpha'' - 2\alpha'^2 + \alpha'\beta' - \dot\chi_+^2 - \dot\chi_-^2 - \chi_+'^2 - \chi_-'^2) && (10)\\
G^1_1 &= e^{-2\beta}(-2\ddot\alpha - 3\dot\alpha^2 - \ddot\beta + 2\alpha'' + 3\alpha'^2 + \beta'' + \ddot\chi_+ + \sqrt{3}\ddot\chi_- - \chi_+'' - \sqrt{3}\chi_-'' \\
&\quad -3\dot\chi_+^2 + 3\chi_+'^2 - 3\dot\chi_-^2 + 3\chi_-'^2 + 3\dot\alpha\dot\chi_+ - 3\alpha'\chi_+' + 3\sqrt{3}\dot\alpha\dot\chi_- - 3\sqrt{3}\alpha'\chi_-') && (11)\\
G^2_2 &= e^{-2\beta}(-2\ddot\alpha - 3\dot\alpha^2 - \ddot\beta + 2\alpha'' + 3\alpha'^2 + \beta'' + \ddot\chi_+ - \sqrt{3}\ddot\chi_- - \chi_+'' + \sqrt{3}\chi_-'' \\
&\quad -3\dot\chi_+^2 + 3\chi_+'^2 - 3\dot\chi_-^2 + 3\chi_-'^2 + 3\dot\alpha\dot\chi_+ - 3\alpha'\chi_+' - 3\sqrt{3}\dot\alpha\dot\chi_- + 3\sqrt{3}\alpha'\chi_-') && (12)\\
G^3_3 &= e^{-2\beta}(-2\ddot\alpha - 3\dot\alpha^2 - \ddot\beta + 2\alpha'' + 3\alpha'^2 + \beta'' - 2\ddot\chi_+ + 2\chi_+'' \\
&\quad -3\dot\chi_+^2 + 3\chi_+'^2 - 3\dot\chi_-^2 + 3\chi_-'^2 - 6\dot\alpha\dot\chi_+ + 6\alpha'\chi_+') \ . && (13)
\end{aligned}$$

The power series expansion near the brane

$$\alpha(y,t) = \alpha_0(t) + \alpha_1(t)|y| + \frac{\alpha_2(t)}{2}y^2 + \cdots \tag{14}$$

defines our notations. From the Einstein equation, we get the junction conditions

$$\begin{aligned}
\alpha_1(t) &= -\frac{1}{l} - \frac{\kappa^2\rho(t)}{6} \ , \\
\beta_1(t) &= -\frac{1}{l} + \frac{\kappa^2\rho(t)}{3} + \frac{\kappa^2 p(t)}{2} \ , \\
\chi_{+1} &= 0 \ , \\
\chi_{-1} &= 0 \ , && (15)
\end{aligned}$$

where we set $e^{\beta_0(t)} = 1$.

2 The Hilbert space approach to bulk field dynamics

Anti-de Sitter space has a timelike Killing vector, hence equation of motion for bulk fields can be written in the form:

$$\frac{\partial^2}{\partial\tau^2}\phi = -A\phi\,, \tag{1}$$

where τ is the Killing parameter and A is an elliptic operator defined on τ = constant hypersurfaces Σ_τ. In the regular boundary case, one could determine the evolution of fields in the entire spacetime by imposing suitable boundary conditions, if needed, on the bulk fields at the conformal boundary. Alternatively, identifying the elliptic differential operator A with a symmetric (Hermitian) operator in a Hilbert space suitably chosen, one can define the dynamics everywhere in the bulk by using self-adjoint extensions of the symmetric operator A. In most of interesting cases, however, the conformal boundary of anti-de Sitter space appears singular for bulk fields, except for the conformally invariant fields. Then, effects of such a singular boundary on the bulk field dynamics should be argued in terms of self-adjoint extensions rather than in terms of ordinary boundary conditions. Actually, this prescription by means of self-adjoint extensions works even when spacetime admits curvature singularities consistent with staticity [13].

In the Hilbert space approach to the study of bulk field dynamics, the uniqueness and positivity of the self-adjoint operator are essential issues, which we are concerned with in the present work. The uniqueness yields that dynamical evolution is deterministic from initial data, without any requirements for nature of the boundary, or no need of any additional boundary conditions [14, 15], and the positivity implies the stability [16, 17].

We address these issues focusing on bulk scalar fields and gravitational waves on the universal covering space of $(d+1)$-dimensional anti-de Sitter space. In the horospherical coordinates, we can find that, after suitable field redefinition, the field equations reduce to the form (1) with the operator

$$A = -\frac{d^2}{d\rho^2} + \frac{d^2 - 1 + 4\mu^2\ell^2}{4\rho^2}\,. \tag{2}$$

where $\rho \in [0,\infty)$ with the conformal boundary located at $\rho = 0$. Here μ^2 is the mass squared which appears in the Klein-Gordon equation, ℓ denotes the curvature radius of the spacetime, and c^2 is the wave number squared in the $(d-1)$-dimensional spatial section. The gravitational wave corresponds to the $\mu^2 = 0$ case. It is worth noting that since μ^2 involves the coupling to the scalar curvature of anti-de Sitter space, which is constant and negative, μ^2 can be negative. It turns out that whenever $d^2 - 1 + 4\mu^2\ell^2 = 0$, the field ϕ is conformally invariant.

Now we can identify the differential operator A on Σ with an operator on the Hilbert space $\mathcal{H} = L^2(0,\infty)$, and the function ϕ in the spacetime with a vector $\phi(\tau) \in \mathcal{H}$. Thence, the problem looks just like a quantum mechanical problem of particle motion on a half-line $\rho \in [0,\infty)$ with an inverse square potential. If one chooses the initial domain of A to be $C_0^\infty(\Sigma)$, a set of smooth functions with compact support, the operator is said to be *symmetric*. To find the one-parameter family $\phi(\tau)$ in the Hilbert space $\mathcal{H}$, one must extend the domain of A so that A becomes a self-adjoint operator A_E. There is a systematic way to carry out the self-adjoint extensions [18]. Note first that the simplest extension of a symmetric operator A with domain $C_0^\infty(\Sigma)$ is obtained by taking its closure. Further closed symmetric extensions of a closed symmetric operator A with domain $\mathcal{D}(A)$ can be made by considering the sets of vectors $\mathcal{K}_\pm := \{\phi_\pm \in \mathcal{H} | A^*\phi_\pm = \pm i\phi_\pm\}$, which are called the *deficiency subspaces* of A. If $\dim\mathcal{K}_+ = \dim\mathcal{K}_-$, then there are partial isometries $U : \mathcal{K}_+ \to \mathcal{K}_-$ and self-adjoint extensions A_E can be obtained by taking its domain as

$$\mathcal{D}(A_E) = \{\phi_0 + \phi_+ + U\phi_+ \,|\, \phi_0 \in \mathcal{D}(A),\, \phi_+ \in \mathcal{K}_+\}\,. \tag{3}$$

Therefore A_E's are in one-to-one correspondence with the set of partial isometries U. If $\dim\mathcal{K}_\pm = 0$, then $(A, \mathcal{D}(A))$ is already self-adjoint. It is worth noting that if symmetric operator A is semi-bounded, there is a distinguished self-adjoint extension, called the *Friedrichs extension*, A_F, whose domain is given by the Cauchy completion with respect to the norm defined by $\|f\|^2 + (f, Af)$. This extension A_F has the same lower bound as A. It provides the generalized notion of the Dirichlet boundary conditions.

Given self-adjoint extension A_E, the dynamics of the vector $\phi(\tau)$ for an initial data $(\phi(0), \dot\phi(0)) \in \mathcal{D}(A_E) \times \mathcal{D}(A_E)$ can be described as

$$\phi(\tau) = \cos({A_E}^{1/2}\,\tau)\,\phi(0) + A_E^{-1/2}\sin(A_E^{1/2}\,\tau)\,\dot\phi(0)\,. \tag{4}$$

The point of this prescription for dynamics [13] is that, once self-adjoint extension is determined, the vector $\phi(\tau)$ is defined not only inside the domain of dependence $D^+(\Sigma_0)$ of the initial hypersurface Σ_0 but even outside $D^+(\Sigma_0)$.

In general, self-adjoint extension are not necessarily unique. In particular, anti-de Sitter space is non-globally hyperbolic, it is non-trivial whether or not self-adjoint extension is unique. If it is not the case, there are infinitely many different self-adjoint extensions, and we have to choose one of them. If a symmetric operator A has a unique self-adjoint extension, then the initial operator A is said to be *essentially self-adjoint*. In this case, bulk field dynamics is unambiguously defined for all time without any additional conditions at the boundary [14, 15].

Essential self-adjointness of the symmetric operator has been studied in literature (see e.g. [18]). We can show that $(A, C_0^\infty(0,\infty))$ in (2) is essentially self-adjoint if and only if

$$\nu^2 := \frac{d^2}{4} + \mu^2\ell^2 \geqslant 1\,. \tag{5}$$

Thus, dynamics of bulk fields satisfying this inequality is uniquely determined from initial data.

We omit any arguments on the positivity issues for want of space, but show our results below together with the uniqueness issue.

3 Summary

In the Hilbert space approach to bulk field dynamics, the problem of defining dynamics in the entire spacetime becomes that of finding a suitable self-adjoint extension A_E of A. For scalar fields and gravitational waves, the operator A can be written as (2). The bulk fields are characterized by ν defined by (5). Then, we can observe the following.

(i) $\nu^2 \in [1,\infty)$: There is a unique self-adjoint extension, which is non-negative, i.e., the Friedrichs extension A_F. For example, the gravitational waves and the minimally coupled scalar, i.e., $\mu^2 = 0$, are in the case, provided the spacetime dimension is larger than three ($d \geqslant 2$). The positivity of A_E yields the stability of anti-de Sitter space against linear perturbations.

(ii) $0 < \nu^2 < 1$: In this case, self-adjoint extensions are in one-to-one correspondence with the $U(1)$ parameter $\alpha \in [0, 2\pi)$. One obtains infinitely many different non-negative self-adjoint extensions as well as infinitely many negative ones. We can show that, self-adjoint extensions A_E are non-negative, if and only if α takes a value satisfying

$$\sin\left(\frac{\alpha}{2} + \frac{1}{4}\pi\nu\right)\sin\left(\frac{\alpha}{2} + \frac{3}{4}\pi\nu\right) \leqslant 0\,. \tag{6}$$

For example, the conformally invariant fields, that is the case $\nu = 1/2$, are in this case, for which the problem looks like a problem of free particle motion on a half-line, and the boundary $\rho = 0$ is a regular point on $\mathbb{R}$. It is worth to note how self-adjoint extensions A_E are related to the boundary conditions, in such a regular boundary case. We can see that the parameter α appears in the Robin boundary condition as

$$a^{-1} = \frac{\phi'}{\phi}\Big|_{x=0} = -\frac{\sin\left(\frac{\alpha}{2} + \frac{3\pi}{8}\right)}{\sin\left(\frac{\alpha}{2} + \frac{\pi}{8}\right)}\,, \tag{7}$$

with $a \in \mathbb{R}\cup\{\infty\}$. The Dirichlet and the Neumann boundary conditions correspond to $a = 0\,(\alpha = 7\pi/4)$ and $a = \infty\,(\alpha = 5\pi/4)$, respectively.

(iii) $\nu^2 = 0$: One can obtain infinitely many negative extensions, but only one positive self-adjoint extension, which is the Friedrichs extension A_F.

(iv) $\nu^2 \in (-\infty, 0)$: Note first that since μ^2 involves the scalar curvature of anti-de Sitter space, ν^2 actually can take a negative value. In the case, there are infinitely many self-adjoint extensions parameterized

by α, all of which are negative, unbounded from below.

We should comment that the uniqueness and the positivity of self-adjoint extension depend on the choice of our Hilbert space. In the present work, we take $\mathcal{H} = L^2(0, \infty)$ of square integrable functions on Σ as our Hilbert space. For example, if we choose a Sobolev space instead of L^2-space, the results will change [15].

We might give some physical interpretation of the self-adjoint extensions. When $\nu^2 \geqslant 1$, for which A is essentially self-adjoint, the inverse square potential in A is repulsive enough so that the boundary bounces bulk fields off. This means that the bulk fields cannot reach the boundary, and thus it is needless to care for the boundary effects on the bulk field dynamics. On the other hand, when $\nu^2 < 1$, the potential is not repulsive enough, or even attractive. Thus bulk fields can reach and interact with the boundary. In this sense, one may say that self-adjoint extensions define the nature of bulk-boundary interactions. In other words, self-adjoint extensions provide generalized notion of boundary conditions, which are characterized by the $U(1)$ parameter α in the present case, and there are infinitely many self-adjoint extensions. Different self-adjoint extension defines different bulk dynamics for the same initial data. Thence, we have to choose one which is appropriate for the physics of the situation. For example, when we are interested in some aspects of anti-de Sitter space as a ground state of supergravity, as discussed in [2, 3, 4], the compatibility with supersymmetry would be important for the choice of physically sensible self-adjoint extension. In the context of the AdS/CFT correspondence, according to the works [11, 12], one can think that choice of self-adjoint extensions determines the type of the interactions in the corresponding boundary quantum field theory.

Acknowledgments

A.I. would like to thank Prof. H. Kodama for discussions. This work is supported in part by Japan Society for the Promotion of Science.

References

[1] S.J. Avis, C.J. Isham, and D. Storey, *Quantum field theory in anti-de Sitter space-time*, Phys. Rev. **D18**, 3565 (1978).

[2] P. Breitenlohner and D.Z. Freedman, *Stability in Gauged Extended Supergravity*, Ann. Phys. **144**, 249-281 (1982).

[3] C.J.C. Burges, D.Z. Freedman, S. Davis, and G.W. Gibbons, *Supersymmetry in Anti-de Sitter Space*, Ann. Phys. **167**, 285-316 (1986).

[4] S.W. Hawking, *The boundary conditions for gauged supergravity*, Phys. Lett. **126B**, 175 (1983).

[5] L. Randall and R. Sundrum, *Large Mass Hierarchy from a Small Extra Dimension*, Phys. Rev. Lett. **83**, 3370 (1999).

[6] L. Randall and R. Sundrum, *An Alternative to Compactification*, Phys. Rev. Lett. **83**, 4690 (1999).

[7] J. Maldacena, *The Large N Limit of Superconformal field theories and supergravity*, Adv. Theor. Math. Phys. **2**, 231-252 (1998).

[8] S.S. Gubser, I.R. Klebanov, and A.M. Polyakov, *Gauge theory correlators from non-critical string theory*, Phys. Lett. **B428**, 105 (1998).

[9] E. Witten, *Anti de Sitter space and Holography*, Adv. Theor. Math. Phys. **2**, 253-291 (1998).

[10] E. D'Hoker and D.Z. Freedman, *Supersymmetric Gauge Theories and the AdS/CFT Correspondence*, hep-th/0201253.

[11] E. Witten, *Multi-Trace Operators, Bondary Conditions, And AdS/CFT Correspondence*, hep-th/0112258.

[12] M. Berkooz, A. Sever, and A. Shomer, *"Double-trace" Deformations, Boundary Conditions and Spacetime Singularities*, hep-th/0112264.

[13] R.M. Wald, *Dynamics in nonglobally hyperbolic, static space-times*, J. Math. Phys. **21**, 2802 (1980).

[14] G. Horowitz and D. Marolf, *Quantum probes of spacetime singularities*, Phys. Rev. D **52**, 5670 (1995).

[15] A. Ishibashi and A. Hosoya, *Who's afraid of naked singularities? Probing timelike singularities with finite energy waves*, Phys. Rev. D **60**, 104028 (1999).

[16] R.M. Wald, *Note on the stability of the Schwarzschild metric*, J. Math. Phys. **21**, 2802 (1980); errata J. Math. Phys. **21**, 218 (1980).

[17] R.M. Wald, *On the instability of the $n = 1$ Einstein-Yang-Mills black holes and mathematically related systems*, J. Math. Phys. **33**, 248 (1992).

[18] M. Reed and B. Simon, *Fourier Analysis, Self-Adjointness*, (Academic Press, New York, 1975).

[19] A. Ishibashi and R.M. Wald, in preparation.

On the Stability of Black Strings/Branes

Gungwon Kang[1]

Theory Group, KEK, Tsukuba, Ibaraki 305-0801, Japan

Abstract

Some issues on the stability of black string or brane solutions are summarized briefly. The stability of dS/AdS-Schwarzschild black strings has been investigated. Interestingly, the AdS-Schwarzschild black strings turn out to be stable as the horizon size becomes larger than the AdS scale. It is also shown that BTZ black strings in four dimensions are stable regardless of the horizon size. Such stable feature seems to be common for several known black strings in dimensions lower than five. Some implications of our results on the role of non-uniformity in stable black string configurations are also discussed.

1 Introduction

Black holes are solutions of Einstein gravity, which possess usually a compact null hypersurface with topology of sphere. Black strings or branes are a sort of higher dimensional generalizations of black holes. The simplest black strings or branes are the product of Schwarzschild black holes and an infinite line or a p-dimensional plane. The extra dimensions can also be compactified. Black string/brane solutions arise naturally in string theory as well. One of the most important reasons that one considers black hole solutions seriously, inspite of their odd causal structure, is that they are stable. The stability of black strings/branes was studied by Gregory and Laflamme [1]. They showed that black strings/branes are generically unstable to linearized perturbations with a large wavelength along the string. For example, the four-dimensional Schwarzschild black hole cross a circle of length L becomes unstable under linearized perturbations as L becomes larger than the order of the Schwarzschild radius r_h.

One naive explanation for this instability is the entropy comparison with that of a black hole with the same mass. Namely, a black hole configuration is entropically preferable as the size of the black string L increases. However, the idea of assigning entropy to black holes or strings is based on the quantum behavior of such black objects which is not neccessarily related to the classical stability behavior of the black string. Moreover, this argument of entropy comparison is global in nature. Recently, Gubser and Mitra have refined this global thermodynamic analysis by considering the local thermodynamic properties of the black object [2]. They conjectured that a black string/brane with noncompact translational symmetry is classically stable if, and only if, it is locally thermodynamically stable. A slightly modified version of this conjecture applicable even for compact cases is recently stated by Hubeny and Rangamani [3]. The proof of this Gubser-Mitra (GM) conjecture is sketched by Reall [4], and a more complete illustration in the simplest case of Schwarzschild black strings/branes is given by Gregory and Ross [5]. The GM conjecture practically provides a very powerful and easy way to check whether given black string/brane solutions are stable or not, compared to the usually complicated numerical analysis of classical linearized perturbations.

The black string instability found at the linear level was believed to indicate that the full nonlinear evolution of the instability would result in the fragmentation of the black string. In order to be consistent with the classical theorem of no bifurcation of the event horizon, presumably quantum effects will play some important role when the shrinkage of the string horizon reached to the stage of large enough curvature. This widely accepted idea of black string fragmentations has been used in many discussions in the literature, involving black string/brane configurations. Recently, however, Horowitz and Maeda have shown that black strings do not break up within a finite affine time in their full classical nonlinear evolution [6]. Thus, unstable black strings are likely to evolve into black string-like configurations which are probably non-uniform and stable even under linearized perturbations. In addition, the recent numerical

[1] E-mail address: gwkang@post.kek.jp

study about approximate non-uniform black string solutions by Gubser [7] indicates that such transition is not continuous, but the first order in thermodynamic nature.

In order to understand the black string instability better, it will be of interest to see whether or not stable black string/brane solutions exist, and, if it does so, to understand what makes them stable. The only known black string/brane solutions even when $L \geq r_h$ are the extremal black p-branes carrying certain charges [8]. In this talk, I present some black string/brane solutions that reveal stable behavior under linearized perturbations. One type of them is AdS-Schwarzschild black strings in anti-de Sitter space with/without a uniform tension brane [9]. These black strings/branes become stable as the horizon radius becomes larger than the order of the AdS radius of the background geometry perpendicular to black strings/branes. The other type is black string/brane solutions in the spacetime dimensions lower than five [10]. In particular, the BTZ black strings in four dimensions turn out to be stable *always*, regardless of the transverse horizon size. Some physical implications of our results and some open issues are also discussed.

2 Stable Black Strings in Anti-de Sitter Space

In this section, I briefly summarise the results in Ref. [9] and give some further results obtained. In the five-dimensional Einstein gravity with negative cosmological constant $\Lambda_5 = -6/l_5^2$, one can have black string solutions whose metrics are given by

$$ds^2 = H^{-2}(z)(\gamma_{\mu\nu}dx^\mu dx^\nu + dz^2), \tag{1}$$

$$= H^{-2}(z)\Big[-f(r)dt^2 + \frac{1}{f(r)}dr^2 + r^2 d\Omega_2^2 + dz^2\Big], \tag{2}$$

where the warping factors are

$$H(z) = \begin{cases} l_4/l_5 \sinh z/l_4, & dS_4(\Lambda_4 > 0) \\ z/l_5, & M_4(\Lambda_4 = 0) \\ l_4/l_5 \sin z/l_4, & AdS_4(\Lambda_4 < 0), \end{cases} \tag{3}$$

and $f(r) = 1 - r_0/r - \Lambda_4 r^2/3$. Here the four-dimensional cosmological constant $\Lambda_4 = \pm 3/l_4^2$ is arbitrary. When $r_0 = 0$, these metrics actually describe the same five-dimensional pure anti-de Sitter spacetime (AdS_5), and simply correspond to different ways of slicing it, e.g., de Sitter, flat, and anti-de Sitter slicings. If a 3-brane with uniform tension is introduced at $z = 0$, the resulting geometries are still described by the metrics above with replacing $z \to |z| + c$ and now Λ_4 is determined by the location and the tension of the 3-brane accordingly. The stability for the flat case (i.e., $\Lambda_4 = 0$) has been already studied in Refs. [11, 12].

In order to check the linearized stability, let us consider small metric perturbations, $g_{MN}(x) \to g_{MN}(x) + h_{MN}(x, z)$, about these black string background spacetimes, and see whether or not there exists any mode which is regular spatially, but grows exponentially in time. As in the usual Kaluza-Klein reduction, the massive scalar (h_{zz}) and vector ($h_{\mu z}$) fluctuations can always be set to be zero by using the five-dimensional diffeomorphism symmetry, leaving only four-dimensional *massive* spin-2 gravity fluctuations. Moreover, the scalar and vector components of the five-dimensional linearized perturbation equations reduce to the four-dimensional transverse traceless gauge conditions for the massive spin-2 fluctuations $h_{\mu\nu}$ [13, 4]. By putting $h_{\mu\nu}(x, z) = H^{3/2}(z)\xi(z)h_{\mu\nu}(x)$, the linearized equations turn out to be

$$\Delta_L h_{\mu\nu}(x) \equiv \Box h_{\mu\nu}(x) + 2R_{\mu\rho\nu\tau}h^{\rho\tau}(x) = m^2 h_{\mu\nu}(x), \tag{4}$$

$$\nabla^\mu h_{\mu\nu} = 0, \quad h = \gamma^{\mu\nu}h_{\mu\nu} = 0, \tag{5}$$

$$\big[-\partial_z^2 + V(z)\big]\xi(z) = m^2\xi(z), \quad V(z) = -\frac{3}{2}\frac{H''}{H} + \frac{15}{4}\Big(\frac{H'}{H}\Big)^2. \tag{6}$$

Notice first that, even if the black strings we are considering are not uniform due to the warping factors along the string, the perturbation equations above become separable as in the case of translationally invariant black strings. The only difference is the spectrum of the Kaluza-Klein (KK) mass with the

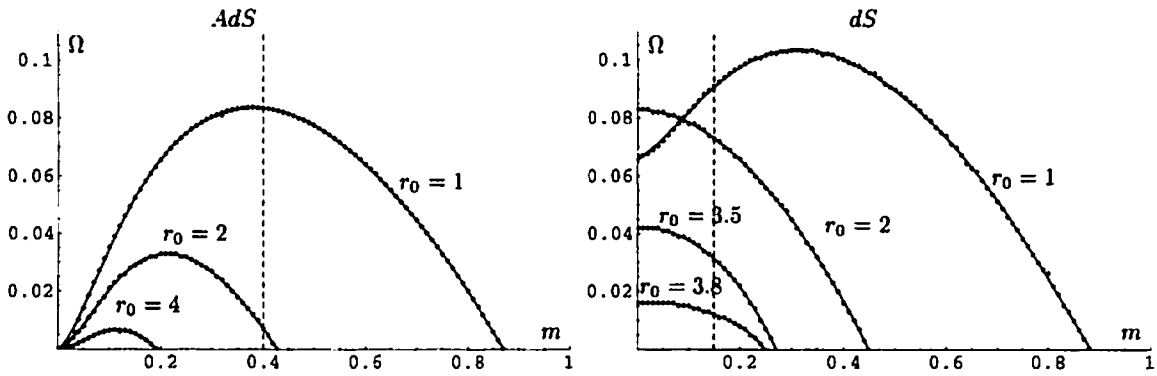

Figure 1: The left figure is for the *AdS* case with $r_0 = 1, 2$ and 4. The right figure is for the dS case with $r_0 = 1, 2, 3.5$, and 3.8. The Nariai solution corresponds to $r_0 \simeq 3.85$. The fixed AdS and dS radius is $l_4 = 10$. The straight vertical lines denote the lowest KK masses, 0.4 for AdS and 0.15 for dS.

non-vanishing effective potential $V(z)$ in Eq. (6). When $m^2 = 0$, as is pointed out in Ref. [1], Eqs. (4) and (5) are exactly same as those for perturbations about four-dimensional black hole spacetimes, which are known to be stable. Since adding a mass term usually increases stability, it had been believed for some time that black strings are stable. However, it turns out that the extra degrees of freedom coming from the massiveness could give unstable solutions [1, 13].

The strongest instability is expected for the s-wave fluctuations. General, spherically symmetric perturbations can be written in canonical form as [14, 1]

$$h_{\mu\nu}(x) = e^{\Omega t} \begin{pmatrix} H_{tt}(r) & H_{tr}(r) & 0 & 0 \\ H_{tr}(r) & H_{rr}(r) & 0 & 0 \\ 0 & 0 & K(r) & 0 \\ 0 & 0 & 0 & K(r)\sin^2\theta \end{pmatrix}, \tag{7}$$

with $\Omega > 0$. From the coupled equations in Eqs. (4) and (5), we can eliminate all but one variable, say H_{tr}, obtaining a second order ordinary differential equation in the following form:

$$A(r; r_0, \Lambda_4, \Omega^2, m^2) H''_{tr} + B H'_{tr} + C H_{tr} = 0. \tag{8}$$

With suitable boundary conditions (see the details in Ref. [9]), one can solve this equation numerically, and unstable solutions for the *massive* spin-2 fluctuations in Eq. (4) are shown in Fig. 1 for given dS/AdS-Schwarzschild black hole background spacetimes.

As shown in Ref. [9] explicitly, the most important observation is that adding a negative cosmological constant Λ_4 has a stabilization effect. As the horizon size increases, the instability becomes weak as in the case of Schwarzschild black holes [11]. For the AdS case, however, the threshold mass $m_* \equiv m(r_0, \Lambda_4, \Omega = 0)$ vanishes even at a finite r_0, not as $r_0 \to \infty$. The numerical search shows that this termination of unstable solutions occurs approximately at $r_0 \simeq 0.77 l_4$ (i.e., $r_+ \simeq 0.58 l_4$). In addition to it, the KK mass spectrum determined by Eq. (6) has a finite mass gap as indicated by the vertical line in Fig. 1. Therefore, it turns out that AdS_4-Schwarzschild black strings in AdS_5 space become stable when the horizon size is $r_+ > r_+^{cr} \simeq 0.20 l_4$. The presence of a 3-brane as in the brane world model [15] simply increases this critical value. For the dS case, on the other hand, the threshold masses remain larger than the lowest KK mass for all horizon radii bounded by the cosmological horizon. In addition, since the KK mass spectrum is continuous, all dS_4-Schwarzschild black strings in AdS_5 space are unstable.

The local thermodynamic stability of a segment of AdS/dS black string will be determined by the sign of the heat capacity given by $dM/dT \sim -2\pi r_+^2 (1 - \Lambda_4 r_+^2)/(1 + \Lambda_4 r_+^2)$. For the AdS case, one can easily see that the heat capacity becomes positive for $r_+ > l_4/\sqrt{3}$. Thus, we expect AdS black strings become stable classically when $r_+ > l_4/\sqrt{3} \simeq 0.58 l_4$ according to the GM conjecture. The slight difference in the critical values is expected because of the non-uniformity of the AdS black string due to the warping

factor [9]. On the other hand, dS black strings are expected to be unstable classically since the heat capacity is always negative for all $r_+ < l_4/\sqrt{3}$ within the cosmological horizon.

3 Lower Dimensional Black Strings/Branes

It was argued in Ref. [16] that the instability of BTZ black strings in the four-dimensional brane worlds sets in when the transverse size of the black string reaches the AdS scale. Here we show that this naive expectation, which is based on the entropy comparison with a localized black hole around a 2-brane with same mass, is not true. Surprisingly, they turn out to be stable always. The metric of rotating BTZ black strings in four dimensions can be written by

$$ds^2 = H^{-2}(z)\left[-f dt^2 + \frac{dr^2}{f} + r^2(d\varphi - \frac{J}{2r^2}dt)^2 + dz^2\right], \tag{9}$$

where $f(r) = -M + r^2/l_3^2 + J^2/4r^2$ and $H(z) = l_3/l_4 \sin z/l_3$. The first evidence for the stable behavior can easily be obtained by applying the GM conjecture. The local thermodynamic stability of a segment of this black string is governed by that of the three-dimensional BTZ black hole. The heat capacities are given by

$$C_J \equiv T(\partial S/\partial T)_J = 4\pi r_+(r_+^2 - r_-^2)/(r_+^2 + 3r_-^2), \tag{10}$$

$$C_M \equiv T(\partial S/\partial T)_M = 4\pi r_+(r_+^2 - r_-^2)/(3r_+^2 + r_-^2), \tag{11}$$

both of which are always positive since the inner horizon radius is $r_- \leq r_+$. If a thermal system has rotations, the thermodynamic stability requires $(\partial\Omega_H/\partial J)_T \geq 0$ additionally since adding angular momentum is expected to increase the angular velocity of the system in average. For the rotating BTZ black hole, it turns out that

$$\left(\frac{\partial\Omega_H}{\partial J}\right)_T = \frac{\Omega_H}{J}\frac{r_+^2 - r_-^2}{r_+^2 + 3r_-^2} \tag{12}$$

which is also positive always. According to the GM conjecture, therefore, we expect that the rotating BTZ black string in four dimensions is stable under linearized perturbations, regardless of the horizon size.

Now for the linearized perturbation analysis, the equations can be separated as before, and the most general form of the three-dimensional metric fluctuations is given by [10]

$$h_{\mu\nu}(x) = e^{\Omega t + in\varphi}\begin{pmatrix} H_{tt}(r) & H_{tr}(r) & inH_{t\varphi}(r) \\ H_{tr}(r) & H_{rr}(r) & 0 \\ inH_{t\varphi}(r) & 0 & r^2K(r) \end{pmatrix}. \tag{13}$$

The decoupled equation is in the same form as Eq. (8), but it becomes much complicated and a complex equation due to the rotation parameter $J \neq 0$. For static BTZ black holes (i.e., $J = 0$), however, one can set $H_{t\varphi} = 0$ by using the gauge freedom and easily solve the equation numerically. We could not find any unstable mode for various values of M and l_3 [10]. That is, *massive* spin-2 fluctuations do not seem to possess any instability for the *three-dimensional* BTZ black hole background. Therefore, we expect that the static BTZ black strings in four-dimensions are always stable under linearized perturbations. This result agrees well with the local thermodynamic stability through the GM conjecture.

4 Discussion

We have shown briefly that the AdS-Schwarzschild black strings in five dimensions become stable under linearized perturbations as the horizon size parameter (i.e., r_+) becomes larger than the order of the AdS_4 radius l_4. The higher dimensional extension of this result is straightforward. The AdS black strings in $(4+n)$-dimensions can be obtained simply by replacing $f(r) \to 1 - (r_0/r)^n + r^2/l_{3+n}^2$ and $d\Omega_2^2 \to d\Omega_{1+n}^2$ in Eq. (2). One can easily see that the sign of the heat capacity for such systems also becomes positive as

the horizon size increases. For black p-branes (i.e., $dz^2 \to \delta_{ij}dz^i dz^j$ for $i,j = 1,\cdots,p$), the basic feature of the stability is also same.

It should be pointed out that the essential reason for having stable AdS black strings is that AdS_4-Schwarzschild black hole bacgrounds do not allow unstable massive spin-2 fluctuations as the horizon size increases. Furthermore, a sort of effective compactification due to the warping geometry along the string increases its stability in addition. Namely, the warping factor for the AdS case rises up as one approaches to the AdS_5 horizon whereas those for flat and dS cases go down to zero. Consequently, the potential in Eq. (6) for the AdS case becomes box-like with a finite mass gap, giving a confining effect for waves along the string. Notice that the proper lengths of black strings in the extra direction are infinite for all three cases. It is interesting to see that the scale of this effective compactification of AdS black strings is governed by the AdS_4 scale l_4, instead of l_5, because the AdS_5 scale does not enter in Eq. (6) at all. However, note that, when the instability sets in, the *minimum* horizon size of the AdS black string in *proper length* is indeed of order the AdS_5 scale, i.e., $r_+^{\rm PL} = r_+^{\rm cr} H_{\rm min.}^{-1} = r_+^{\rm cr} l_5/l_4 \simeq 0.20 l_5$, which is consistent with the instability mechanism argued in Ref. [12].

As mentioned above, it is suggested by Horowitz and Maeda [6] that, even in the case that a black string is unstable under linearized perturbations, its full non-linear evolution presumably ends up with a sort of non-uniform black string configuration, instead of fragmentations of the string horizon. This final state must be stationary and stable. Then it will be interesting to see what makes this configuration stable even under linearized perturbations. In other words, what is the role of the "non-uniformity"? The perturbation equations will in general consist of two parts; that is, fluctuations for black holes on "transverse" slicings of the black string and that along the string. Of course, they become separable perhaps only for special cases such as uniform black strings and those ones with overal warping factors. Now our study above seems to indicate that the stability of spin-2 fields with *"bigger" degrees of freedom* on black hole backgrounds of slicings is crucial generically for the stability of a non-uniform black string. However, even if such fields have "instability", some effective compactification due to the curvature or periodicity along the black string could also make the black string stable.

For the BTZ black strings in four dimensions, we have shown that they are stable *independent of the transverse horizon size* since the massive spin-2 fluctuation equation itself does not possess unstable modes at all. It seems that this stable behavior for black strings/branes in dimensions lower than five is common. The thermodynamic analysis for several such solutions [17, 18, 19] shows that all of them are locally thermodynamically stable [10]. Consequently, the GM conjecture implies that they are classically stable under linearized perturbations. This special property might be related to the fact that gravitational waves in lower dimensions than four do not have enough degrees of freedom for propagations. However, we point out that the *massive* spin-2 fluctuations in lower dimensions must have the same number of degrees of freedom as that of the four-dimensional massless gravitational waves. Further study is required concerning this issue.

Since the discovery of the Gregory-Laflamme instability in 1993, it is somewhat surprising that no specific work has been done for the stability of Kerr black strings. This is probably because the wide belief was that such rotating black string is also unstable. However, a naive application of the GM conjecture shows that this may not be the case. For instance, the heat capacity of the Kerr black hole is negative, but becomes positive as the angular momentum parameter increases towards the extremal value. Thus, the Kerr black string with large angular momentum parameter might be stable under linearized perturbations possibly due to the "centrifugal" effect of rotations in the background geometry. On the other hand, however, another thermodynamic quantity (e.g., $(\partial\Omega_H/\partial J)_T$ as in Eq. (12)) becomes negative exactly for the values of angular momentum where the heat capacity is positive. The direct analysis of linearized fluctuations in Eqs. (4)-(6) with $H(z) = 1$ is not available at the present since the equations are not easily decoupled in this Kerr background geometry. We expect that a partial application of the four-dimensional Newman-Penrose formalism to this five-dimensional system may decouple the set of equations, resulting in a sort of "Teukolsky equations" [20]. The detailed analysis of this decoupled equation will reveal all non-trivial behaviors for the stability of Kerr balck strings in the parameter space of mass and angular momentum. Consequently, it will also hint at how to extend Reall's proof of the GM conjecture to a system with *rotation*.

Finally, it is also very interesting to extend the proof in Ref. [6] to the cases of Schwarzschild or dS-Schwarzschild black strings in AdS_5. It is because such spacetimes have naked singularities at the

AdS_5 horizon outside the event horizon.

Acknowledgments

The author would like to thank T. Hirayama, K. Lee, Y. Lee, R. Myers, and P. Yi for useful discussions. This work was supported by JSPS (Japanese Society for Promotion of Sciences) Postdoctoral Fellowships.

References

[1] R. Gregory and R. Laflamme; *"Black Strings and p-Branes are Unstable,"* Phys. Rev. Lett. **70**, 2837 (1993), hep-th/9301052.

[2] S. S. Gubser and I. Mitra; *"Instability of charged black holes in anti-de Sitter space,"* hep-th/0009126; JHEP **0108**, 018 (2001), hep-th/0011127.

[3] V. E. Hubeny and M. Rangamani; *"Unstable Horizons,"* hep-th/0202189.

[4] H. S. Reall; *"Classical and Thermodynamic Stability of Black Branes,"* Phys. Rev. **D64**, 044005 (2001), hep-th/0104071.

[5] J. P. Gregory and S. F. Ross; *"Stability and the negative mode for Schwarzschild in a finite cavity,"* Phys. Rev. **D64**, 124006 (2001), hep-th/0106220.

[6] G.T. Horowitz and K. Maeda; *"Fate of the Black String Instability,"* Phys. Rev. Lett. **87**, 131301 (2001), hep-th/0105111.

[7] S.S. Gubser; *"On non-uniform black branes,"* hep-th/0110193.

[8] R. Gregory and R. Laflamme; *"The Instability of Charged Black Strings and p-Branes,"* Nucl. Phys. **B428**, 399 (1994), hep-th/9404071.

[9] T. Hirayama and G. Kang; *"Stable black strings in anti-de Sitter space,"* Phys. Rev. **D64**, 064010 (2001), hep-th/0104092.

[10] T. Hirayama, G. Kang, and Y. Lee; *"Lower Dimensional Black Strings/Branes Are Stable,"* in preparation.

[11] R. Gregory; *"Black string instabilities in anti-de Sitter space,"* Class. Quantum Grav. **17**, L125 (2000), hep-th/0004101.

[12] A. Chamblin, S. W. Hawking and H. S. Reall; *"Brane-World Black Holes,"* Phys. Rev. D **61**, 065007 (2000), hep-th/9909205.

[13] G. Kang; *"What makes black strings unstable?,"* work in progress.

[14] C. V. Vishveshiwara, Phys. Rev. D 1, 2870 (1970); T. Regge and J. A. Wheeler, Phys. Rev. **108**, 1063 (1957).

[15] L. Randall and R. Sundrum, Phys. Rev. Lett. **83**, 4690 (1999), hep-th/9906064.

[16] R. Emparan, G. T. Horowitz and R. C. Myers, JHEP **0001**, 021 (2000), hep-th/9912135.

[17] J. H. Horne and G. T. Horowitz, Nucl. Phys. **B368**, 444 (1992).

[18] J. P. S. Lemos and V. T. Zanchin, Phys. Rev. D **54**, 3840 (1996); R. Cai and Y. Zhang, Phys. Rev. D **54**, 4891 (1996), gr-qc/9609065.

[19] N. Kaloper, Phys. Rev. D **48**, 4658 (1993).

[20] G. Kang; "Stabilty of Kerr Black Strings," work in progress.

Natural Quintessence Scenario in a Brane World

Shuntaro Mizuno[1] and Kei-ichi Maeda,[2]

Department of Physics, Waseda University, Shinjuku, Tokyo, 169 8555, Japan

Abstract

We study a new quintessence scenario based on the brane cosmology. We show that in the quadratic dominant stage, which generically appears in brane world cosmology, the density parameter of a scalar field Ω_ϕ decreases regardless of the potential-term contribution. This feature enables us to take natural initial condition. We also discuss the constraints on parameters for the natural and successful quintessence scenario. (This talk is based on our articles [1].)

1 Introduction

Recent several observations suggest that the universe is dominated by a cosmological constant, or dark energy, whose value is comparable to the present mass of the universe. From the viewpoint of particle physics, however, it is quite difficult to explain such a tiny value. (Cosmological Constant Problem[2]) It may be more plausible that such a value is achieved through the dynamics of a fundamental field. Among such models, the so-called quintessence seems to be more promising i.e. a quintessence field follows a common evolutionary track just as an attractor in a wide range of the initial conditions [3],[4],[5]. According to a successful quintessence scenario, the energy of a scalar field tracks the radiation energy (or matter energy) for a rather long time in order not to affect the successful points of the standard Big-Bang cosmology, and then becomes dominant just before the present time.

There seems to be, however, still a kind of fine-tuning problem for these models. Although the initial energy of a scalar field could be the same as that of radiation fluid, most contribution is from its kinetic energy. Its energy density drops as a^{-6} which is much faster than the radiation energy. Then it drops in the radiation dominant universe until a tracking solution is found. This is why the density parameter of a scalar field decreases before reaching a tracking solution. Hence, an equipartition condition, which may be expected in the early stage of the universe, is impossible in such models.

As for the early stage of the universe, recently we have a new interesting idea, that is, brane cosmology. In a brane world scenario, our universe is embedded in higher dimensions and standard-model particles are confined to four-dimensional hypersurfaces (3-branes), while gravity is propagating in higher-dimensions (a bulk) [6] -[8]. The main modified point from conventional cosmology is the appearance of the quadratic term of energy-momentum and dark radiation[9]. Among them, since the former changes the cosmology in its early stage, we expect some improvement for a quintessence scenario.

2 Basic Equations and models

We start with the Randall-Sundrum type II brane scenario[8], because the model is simple and concrete. It is, however, worthwhile noting that the present mechanism may also work in other types of brane world models, in which a quadratic term of energy-momentum tensor generically appears. In the Randall-Sundrum type II model, even though the extra-dimension is not compactified, gravity is confined in the brane, showing the Newtonian gravity in our world. Since the gravity is confined in the brane, it can be described by the intrinsic metric of the brane spacetime. Assuming the flat Friedmann-Robertson-Walker spacetime and ${}^{(4)}\Lambda$ vanishes in our brane world, we find the Friedmann equation as

$$H^2 = \frac{1}{3m_4^2}\rho + \frac{1}{36m_5^6}\rho^2 + \frac{\mathcal{C}}{a^4} \tag{1}$$

[1] E-mail:shuntaro@gravity.phys.waseda.ac.jp
[2] E-mail:maeda@gravity.phys.waseda.ac.jp

where a is a scale factor of the Universe, $H = \dot{a}/a$ is its Hubble parameter, P and ρ are the total pressure and the total energy density of matter fields. We use the 4-dimensional Planck mass $m_4 = (2.4 \times 10^{18}\mathrm{GeV})$ and the 5-dimensional Planck mass m_5, which could be much smaller than m_4. C is a constant, which describes "dark" radiation coming from the information of a bulk [9], [10].

As for matter fields on the brane, we consider a scalar field ϕ as well as the conventional radiation and matter fluids, i.e. $\rho = \rho_\phi + \rho_\mathrm{r} + \rho_\mathrm{m}$, where $\rho_\phi, \rho_\mathrm{r}$ and ρ_m are the energy densities of scalar field ϕ, radiation and matter, respectively.

Since the energy of each field on the brane is conserved in the present model, we can use the conventional energy conservation equation, i.e. for the scalar field,

$$\ddot{\phi} + 3H\dot{\phi} + \frac{dV}{d\phi} = 0, \tag{2}$$

where V is a potential of the scalar field, and for the radiation and matter fluids, we have

$$\dot{\rho_{\mathrm{r,m}}} + 3H(\rho_{\mathrm{r,m}} + P_{\mathrm{r,m}}) = 0, \tag{3}$$

The quadratic term was very important in the early stage of the Universe. We find that the quadratic term dominates when

$$\rho > \rho_\mathrm{c} \equiv 12 m_5^6/m_4^2. \tag{4}$$

When the quadratic term is dominant, the expansion law of the Universe is modified. In this talk, we investigate a model with an inverse power law potential [3],[4], i.e. $V(\phi) = \mu^{\alpha+4}\phi^{-\alpha}$, where μ is a typical mass scale of the potential, which is not fixed here. Although this potential is not renormalizable, it may appear as an effective potential for a kind of fermion condensation in a supersymmetric QCD model [11]. The $SU(N_c)$ gauge symmetry is broken by a pair condensation of N_f-flavor quarks, and the effective potential for a fermion condensate field ϕ is this type with $\alpha = 2(N_c+N_f)/(N_c-N_f)$. In such a situation, it seems to be natural for the scalar field to be confined on the brane.

3 Quintessence Scenario

Because the quintessence scenario with this potential has been well studied in the conventional universe[5], we first turn our attention to the quadratic term (ρ^2) dominant stage. If radiation dominates the universe in this situation, the scale factor expands as $a \propto t^{1/4}$. For the dynamics of the scalar field, we find an analytic solution for $\alpha < 6$, that is

$$\phi = \phi_0 \left(\frac{t}{t_0}\right)^{\frac{2}{\alpha+2}}, \tag{5}$$

with $\phi_0^{\alpha+2} = \frac{2\alpha(\alpha+2)^2}{6-\alpha}\mu^{\alpha+4}t_0^2$, where t_0 and ϕ_0 are integration constants. And because $\rho_\mathrm{r} \propto a^{-4}$

$$\Omega_\phi = \frac{\rho_\phi}{\rho_\mathrm{r}+\rho_\phi} \approx \frac{\rho_\phi}{\rho_\mathrm{r}} = \Omega_\phi^{(0)} \left(\frac{a}{a(t_0)}\right)^{\frac{4(2-\alpha)}{\alpha+2}}, \tag{6}$$

where $\Omega_\phi^{(0)} = \frac{3\alpha(\alpha+2)}{6-\alpha}V(\phi_0)/\rho_\mathrm{r}(t_0)$. From Eq.(6), if $6 > \alpha > 2$, just contrary to the tracking solution, the scalar field energy decreases faster than that of the radiation. We can show that this solution is the attractor solution of this system. Since the quintessence solution in the conventional universe model is an attractor, our solution should also recover the same trajectory after the quadratic term decreases to be very small. After that, it is known that for the attractor solution in conventional cosmology, Ω_ϕ, changes as

$$\begin{aligned} \Omega_\phi &\propto t^{4/(2+\alpha)} \sim a^{8/(2+\alpha)} \quad \text{(radiation dominant)} \\ &\propto t^{4/(2+\alpha)} \sim a^{6/(2+\alpha)} \quad \text{(matter dominant)} \end{aligned} \tag{7}$$

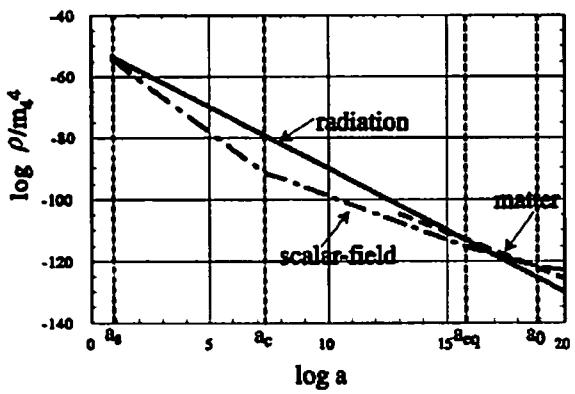

Figure 1: The evolution of the energy densities in terms of a scale factor. We set $\mu = 6.0 \times 10^{-14} m_4$, and $m_5 = 6.0 \times 10^{-14} m_4$. As for the initial conditions, we set $\rho_\varphi^{(K)} = 3.82 \times 10^{-55} m_4^4$, $\rho_\phi^{(P)} = 2.50 \times 10^{-56} m_4^4$, and $\rho_r = 3.78 \times 10^{-54} m_4^4$. The matter fluid is also included to find the present matter dominant universe as $\rho_m = 5.43 \times 10^{-69} m_4^4$. The amount of matter fluid is chosen in order to find the present universe.

Now we are ready to discuss a quintessence scenario in the brane world. We introduce t_s (the cosmic time when the attractor solution in ρ^2 dominant stage is reached), t_c (when $\rho(t_c) = \rho_c$), $t_{\rm NS}$(nucleosynthesis), $t_{\rm eq}$ (when $\rho_r = \rho_m$), $t_{\rm dec}$(the decoupling time) and t_0 (the present time). Since the radiation energy must be continuous, we can naively evaluate the present density parameter $\Omega_\phi^{(0)}$ as

$$\Omega_\phi^{(0)} = \Omega_\phi^{(s)} \times \left(\frac{a_c}{a_s}\right)^{\frac{-(4\alpha-2)}{\alpha+2}} \times \left(\frac{a_{\rm eq}}{a_c}\right)^{\frac{6}{\alpha+2}} \times \left(\frac{a_0}{a_{\rm eq}}\right)^{\frac{6}{\alpha+2}}, \tag{8}$$

where $\Omega_\phi^{(s)}$ is the density parameter when the attractor solution is reached. For a successful quintessence scenario, we require that the present value of the density parameter of the scalar field is $\Omega_\phi^{(0)} \sim 0.7$.

It may be useful to confirm the above analysis by numerical study. This is because with the above analytic attractor solutions, we cannot properly treat the transition between ρ^2-dominant stage and the conventional universe. In Fig.1, we show one numerical result and confirm that the conventional quintessence scenario (a tracking solution) is really recovered when the quadratic energy density becomes small enough for $\alpha = 5$. We set $\mu = 6.0 \times 10^{-14} m_4$, $m_5 = 6.0 \times 10^{-14} m_4$ for a successful quintessence. As initial conditions at $a_s = 1$, we have chosen the attractor solution in the ρ^2-dominant stage, and solve the basic equations (1),(2) and (3) including radiation and matter fluids. We depict the energy densities of a scalar field, radiation and matter in terms of a scale factor a in Fig.1.

4 Constraints

We discuss constraints for a natural and successful quintessence. We consider three constraints: nucleosynthesis, matter dominance at decoupling time, and natural initial conditions, in order. Since we do not know the value of μ from the viewpoint of particle physics, we shall let its value be free.

(a) nucleosynthesis

During nucleosynthesis (NS), the universe must expand as conventional radiation dominant. Therefore the transition from ρ^2-dominant stage to the conventional universe must take place before NS. This constraint gives a lower bound for the value of m_5. Introducing two temperatures, T_c and $T_{\rm NS}$, we describe this constraint as $T_c > T_{\rm NS}$, which implies $\rho_c > \rho_r(t_c) = (\pi^2/30) g_{\rm NS} T_{\rm NS}^4$, where $g_{\rm NS}$ is the degree of freedom of particles at NS. In the Planck unit, this constraint can be expressed as $m_5 > 10^{-14} m_4$. If the Randall-Sundrum II model is a fundamental theory, in order to recover the Newtonian force above 1mm scale in the brane word, the 5-dimensional Planck mass is constrained as $m_5 \geq 10^8$ GeV $\sim 4 \times 10^{-11} m_4$[8].

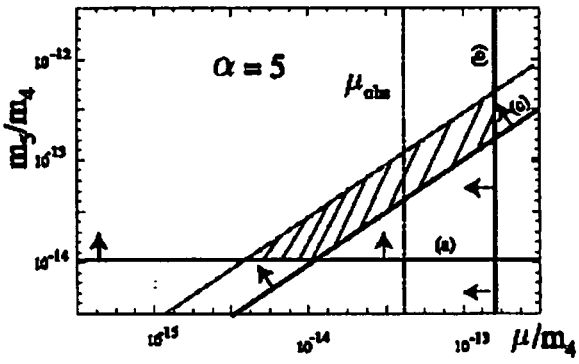

Figure 2: Constraints in the μ-m_5 parameter space. Three solid lines are from (a) nucleosynthesis, (b) matter dominance at the decoupling time, and (c) the energy scale smaller than the 5-D Planck mass. The observation ($\Omega_\phi^{(0)} \sim 0.7$) fixes the value of μ ($\mu_{obs} \sim 4.06 \times 10^{-14} m_4$), which is given by the vertical dot-dashed lines. If we assume that the potential energy of a scalar field is initially not very small compared with its kinetic energy, a successful quintessence is possible for a narrow range of parameters, which is shown by the shaded region.

which would be a stronger constraint. However, the Randall-Sundrum II model could be an effective theory, derived from more fundamental higher-dimensional theories such as Hořava and Witten theory[7]. Thus, we do not adopt this constraint here.

(*b*) The decoupling

In order to form some structure from the decoupling time to the present, the energy density of matter fluid should be larger than that of a scalar field by a few orders of magnitude at the decoupling time. The energy density of matter fluid at decoupling time is given as $\rho_m(t_{dec}) = (\pi^2/30) g_{eq} T_{eq}^4 \times (T_{dec})^3/(T_{eq})^3$. As for a scalar field, assuming that the attractor is reached , we can estimate $\rho_\phi(t_{dec})$ in terms of μ, T_{eq} and T_{dec}. In order to impose the stringent constraint, we adopt $T_{eq} = 10^4$ K here. Setting $T_{dec} = 4000$ K, from the constraint of $\rho_m(t_{dec}) > \rho_\phi(t_{dec})$, we find the upper bound for the value of μ, i.e. $\mu < 2.40 \times 10^{-13} m_4$ for $\alpha = 5$. In Fig. 2, we depict these constraints (a) and (b) by solid lines in the m_5 -μ parameter space for $\alpha = 5$.

(*c*) Initial condition

About initial conditions, since a quintessence solution is an attractor, we may not need to worry. In fact, the conventional quintessence will be recovered even in the present model. Nevertheless, here we will study about natural initial conditions in the present scenario. Here we invoke a further constraint which could be derived from natural initial conditions. Since we assume that a quintessence field ϕ is confined on the brane, the maximally possible energy density of radiation is also about m_5^4.

Furthermore, one plausible condition is an equipartition of each energy density. In this case, the radiation energy is larger than that of the scalar field because the degree of freedom of all particles g is larger than that of the scalar field. How about the ratio of the kinetic energy to total one of the scalar field ? In the conventional quintessence scenario, the potential energy should be initially much smaller than the kinetic one. In the present model, it is not the case. This is because the attractor solution in the ρ^2-dominant stage reduces the density parameter of the scalar field. Therefore, we may impose natural initial conditions for a scalar field. To be more concrete, we focus on the potential by fermion condensation. After our 3-dimensional brane world is created, a fermion pair is condensed by a symmetry breaking mechanism and it behaves as a scalar filed with a potential $V(\phi)$. In this case, we expect that the potential term should play an important role from the initial stage.

If the kinetic and potential energy of a scalar field are the same order of magnitude, the attractor solution is reached soon, and then we expect $\Omega_\phi^{(s)} \sim O(g_s^{-1})$, where g_s is a degree of freedom of particles at a_s. If the potential energy is dominant, it will not change so much before reaching the attractor solution, and then we expect that $\Omega_\phi^{(s)} \geq O(g_s^{-1})$. If the kinetic energy is larger than the potential one, which

we do not want to assume here, it will decay soon, finding an attractor solution, then $\Omega_\phi^{(s)} \leq O(g_s{}^{-1})$. Therefore, a natural initial condition predicts $\Omega_\phi^{(s)} \geq O(g_s{}^{-1})$

We find

$$\Omega_\phi^{(s)} = G(\alpha) \left(\frac{\mu}{m_5}\right)^{\frac{2(\alpha+4)}{(\alpha+2)}} (m_5 t_s)^{-\frac{2\alpha}{\alpha+2}}, \tag{9}$$

where $G(\alpha) = 2^{\frac{\alpha+4}{\alpha+2}} \alpha^{-\frac{\alpha}{\alpha+2}} (\alpha+2)^{-\frac{\alpha-2}{\alpha+2}} (6-\alpha)^{-\frac{2}{\alpha+2}}/3$. We find that for $4 < \alpha \leq 6$, this constraint is satisfied. For $\alpha = 5$, $\rho_r(t_s) \sim m_5^4$, $\Omega_\phi^{(s)} \sim O(g_s{}^{-1})$ and $g_s \sim 10^3$ gives the lower bound for μ/m_5 as $\mu \sim 0.146 m_5$. Then, we find a narrow strip, which is shown by a shaded region in Fig.2. If we adopt the value $\mu_{\rm obs} \sim 4.06 \times 10^{-14} m_4$, we find $4.06 \times 10^{-14} m_4 \leq m_5 \leq 2.78 \times 10^{-13} m_4$.

5 Summary

In this paper, we have discussed a quintessence model in the context of a brane world scenario. We show that the energy density of the scalar field decreases faster than the radiation when the quadratic energy density is dominant. As a result, when we recover conventional cosmology, the density parameter of the scalar field is small enough for the scalar field to dominate just at the present epoch. $\alpha \geq 4$ may provide a natural quintessence scenario.We should add that even though our model prefers a rather large value of α ($\alpha \geq 4$), recent observation may force the constraint of $\alpha \leq 2$. If this is really the case, we have to look for another model.

References

[1] S. Mizuno, and K. Maeda, Phys. Rev. D **64**, 123521 (2001); K. Maeda, *ibid* **64**, 123525 (2001).

[2] Weinberg, Rev. Mod. Phys. **61**, 1 (1989); V. Sahni and A. Starobinsky, Int. J. Mod. Phys. D **9**, 373 (2000) ; S. Weinberg, astro-ph/0005265.

[3] R. R. Caldwell, R. Dave and P. J. Steinhardt, Phys. Rev. Lett. **80**, 1582 (1998); L. Wang, R. R. Caldwell, J. P. Ostriker and P. J. Steinhardt, Astrophys. J. **530**,17 (2000).

[4] B. Ratra and P. J. E. Peebles, Phys. Rev. D **37**, 3406 (1988) ; A.R. Liddle and R. J. Scherrer *ibid* **59**, 023509 (1998).

[5] I. Zlatev, L. Wang and P. J. Steinhardt, Phys. Rev. Lett. **82**, 896 (1999); P. J. Steinhardt, L. Wang and I. Zlatev, Phys. Rev. D **59**, 123504 (1999).

[6] N. Arkani-Hamed, S. Dimopoulos and G. Dvali, Phys. Lett. B **429**, 263 (1998); I. Antoniadis, N. Arkani-Hamed, S. Dimopoulos and G. Dvali, *ibid* **436**, 257 (1998).

[7] P. Hořava and E. Witten, Nucl. Phys. B **460**, 506 (1996); *ibid* B **475**, 94 (1996).

[8] L. Randall and R. Sundrum, Phys. Rev. Lett. **83**, 4690 (1999); **83**, 3370 (1999).

[9] T. Shiromizu, K. Maeda, and M. Sasaki, Phys. Rev. D **62**, 024012 (2000).

[10] P. Binétruy, C. Deffayet and D. Langlois, Nucl. Phys. B **565**, 269 (2000); N. Kaloper, Phys. Rev. D **60**, 123506 (1999) ; C. Csaki, M. Graesser, C. Kolda and J. Terning Phys. Lett. B **462**, 34 (1999) ; T. Nihei, Phys. Lett. B **465**, 81 (1999) ; P. Kanti, I. I. Kogan, K. A. Olive and M. Prospelov, Phys. Lett. B **468**, 31 (1999); J. M. Cline, C. Grojean and G. Servant, Phys. Rev. Lett. **83**, 4245 (1999); P. Binétruy, C. Deffayet, U. Ellwanger and D. Langlois, Phys. Lett. B **477**, 285 (2000) ; S. Mukohyama, T. Shiromizu and K. Maeda, Phys. Rev. D **62**, 024028 (2000).

[11] P. Binétruy, Phys. Rev. D **60**, 063502 (1999); P. Brax and J. Martin, Phys. Rev. D **61**, 103502 (2000); T. R. Taylor, G. Veneziano and S. Yankielowicz, Nucl. Phys. B **218**, 493 (1983); I. Affleck, M. Dine and N. Seiberg, Nucl. Phys. B **256**, 557 (1985).

Dynamics of a bulk scalar field on the inflating braneworld

— A bulk scalar in the braneworld can mimic the 4d inflaton dynamics —

Yoshiaki Himemoto,[1] Misao Sasaki[2]

Department of Earth and Space Science, Graduate School of Science, Osaka University, Toyonaka 560-0043, Japan

Takahiro Tanaka,[3]

Yukawa Institute for Theoretical Physics, Kyoto University, Sakyo-ku, Kyoto 606-8502, Japan

Abstract

Based on the recently proposed scenario of inflation driven by a bulk scalar field in the braneworld of the Randall-Sundrum (RS) type, we investigate the dynamics of a bulk scalar field on the inflating braneworld. We derive the late time behavior of the bulk scalar field by analyzing the property of the retarded Green function. The mapping to the 4-dimensional effective theory is given by a simple scaling of the potential with a redefinition of the field. Our result supports the picture that the scenario of inflation driven by a bulk scalar field works in a quite similar way to that in the standard 4-dimensional cosmology.

1 Introduction

It is very likely that our 4-dimensional universe is a subspace in a higher dimensional spacetime. In fact, sting theory, which is a candidate for the unified theory, is a higher dimensional theory. As a realization of such a higher dimensional theory, the braneworld scenario has attracted a lot of attention recently. In particular, the second Randall-Sundrum (RS) braneworld scenario [1] has attracted much attention from the relativity or cosmology community because of its attractive feature.

It is natural that the 5-dimensional action includes some scalar fields of gravitational origin from the viewpoint of unified theories in a yet higher dimensional spacetime. Then one can consider a scenario in which inflation on the brane is driven by a scalar field living in the bulk in place of an inflaton field confined on the brane [2]. Provided there is a bulk scalar field with a suitable potential, it was shown in Ref. [2] that there exists a field configuration in the bulk that indeed realizes inflation on the brane. Subsequently the quantum fluctuations in this scenario of brane inflation were investigated [3, 4]. In particular it was shown that the correction due to the 5-dimensional nature of the inflaton field is small, as long as $|m^2|\ell^2 \ll 1$ and $H^2\ell^2 \ll 1$ are satisfied, where ℓ is the curvature radius of AdS_5, m is the mass of the bulk scalar field, and H is the Hubble parameter on the brane [4]. Furthermore, the reheating after inflation based on this scenario has been discussed by Yokoyama and Himemoto[5], and they found that the standard inflationary cosmology is reproduced under the same conditions.

However, these results for this new scenario are more or less based on a particular scalar field configuration discussed in [2], the detail of which will be explained in the succeeding section. Therefore, strictly speaking, the viability and generality of this scenario should be more carefully examined. To overcome the limitations of the previous analyses, in this proceeding, we develop a method to discuss the dynamics of a bulk scalar field in more general situations which is applicable to most of the stages of inflation including the reheating era.

[1] E-mail:himemoto@vega.ess.sci.osaka-u.ac.jp
[2] E-mail:misao@vega.ess.sci.osaka-u.ac.jp
[3] E-mail:tanaka@yukawa.kyoto-u.ac.jp

2 Brane-world inflation without inflaton on the brane

Under the second RS scenario, we assume that the 5-dimensional bulk gravitational equation takes the form

$$R_{ab} - \frac{1}{2}g_{ab}R + \Lambda_5 g_{ab} = \kappa_5^2 \left(T_{ab} + S_{ab}\delta(r - r_0)\right) . \tag{1}$$

As for the forms S_{ab} and T_{ab}, we neglect the contribution to S_{ab} from the matter fields confined on the brane at $r = r_0$, and consider a minimally coupled bulk scalar field with the potential $V(\phi)$. Thus we have

$$\begin{aligned} S_{ab} &= -\sigma q_{ab}, \\ T_{ab} &= \phi_{,a}\phi_{,b} - g_{ab}\left(\frac{1}{2}g^{cd}\phi_{,c}\phi_{,d} + V(\phi)\right), \end{aligned} \tag{2}$$

where σ is the tension of the brane.

In order to recover the Randall-Sundrum flat braneworld when T_{ab} vanishes, we choose Λ_5 as $\Lambda_5 = -\kappa_5^4\sigma^2/6$. Then, the effective 4-dimensional Einstein equations on the brane become [6, 2]

$$G_{\mu\nu} = \kappa_4^2 T^{(s)}_{\mu\nu} - E_{\mu\nu}, \tag{3}$$

where

$$\kappa_4^2 = \frac{\kappa_5^4\sigma}{6}, \tag{4}$$

$$T^{(s)}_{\mu\nu} = \frac{1}{\kappa_5^2\sigma}\left(4\phi_{,\mu}\phi_{,\nu} + \left(\frac{3}{2}(\phi_{,r})^2 - \frac{5}{2}q^{\alpha\beta}\phi_{,\alpha}\phi_{,\beta} - 3V(\phi)\right)q_{\mu\nu}\right), \tag{5}$$

$$E_{\mu\nu} = {}^{(5)}C_{rbrd}\, q^b_\mu\, q^d_\nu . \tag{6}$$

Here, $q_{\mu\nu}$ is the induced metric on the brane and ${}^{(5)}C_{rbrd}$ is the 5-dimensional Weyl tensor with its two indices projected in the r-direction.

Focusing on the zeroth order description of the cosmological model, we consider the case in which the metric induced on the brane is isotropic and homogeneous. Because of the assumed Z_2 symmetry, the boundary condition for the bulk scalar field at the position of the brane is given by

$$\partial_r\phi|_{r=r_0} = 0. \tag{7}$$

Here we have further assumed that the bulk scalar does not couple to the metric on the brane. Then, the 4-dimensional effective Friedmann equation is given by

$$3\left[\left(\frac{\dot{a}}{a}\right)^2 + \frac{K}{a^2}\right] \equiv 3H^2 = \kappa_4^2\rho_{\rm eff} , \tag{8}$$

with

$$\rho_{\rm eff} = \frac{3}{\kappa_5^2\sigma}\left(\frac{\dot{\phi}^2}{2} + V(\phi)\right) - \frac{E_{tt}}{\kappa_4^2}, \tag{9}$$

where $a(t)$ is a scale factor and K is the constant curvature. The equations for ϕ and E_{tt}, are basically 5-dimensional. However, in the present spatially homogeneous case, the Bianchi identities supply the evolution equation of E_{tt} on the brane as[2]

$$E_{tt} = \frac{\kappa_5^2}{2a^4}\int^t a^4\dot{\phi}(\partial_r^2\phi + \frac{\dot{a}}{a}\dot{\phi})\, dt. \tag{10}$$

We then see that E_{tt} can be neglected if both $\dot{\phi}$ and $\partial_r^2\phi$ are sufficiently small on the brane. Thus a sufficient condition for inflation to occur on the brane is that ϕ is a slowly varying function with respect to both t and r in the vicinity of the brane.

In the previous work[2], assuming that the potential of the form

$$V(\phi) = V_0 + \frac{1}{2}m^2\phi^2 \quad \text{for} \quad \frac{|m^2|\phi^2}{2} \ll V_0, \tag{11}$$

we considered the effecitve 5-dimensional AdS spacetime,

$$ds^2 = dr^2 + (H\ell)^2 \sinh^2(r/\ell)(-dt^2 + a^2(t)\gamma_{ij}dx^i dx^j), \tag{12}$$

with

$$\ell^2 = \frac{6}{|\Lambda_5 + \kappa_5^2 V_0|}, \quad H^2 = \frac{\kappa_5^2 V_0}{6}, \tag{13}$$

and found the unique solution of a bulk scalar field in the separable form that induces slow-roll inflation on the brane. In particular, when $|m^2\ell^2| \ll 1$ and $H^2\ell^2 \ll 1$, using this solution, it is shown that the dynamics of this system may be well described by the effective 4-dimensional scalar field and the standard slow-roll inflation is realized by the bulk scalar field.

However, since the above solution is obtained by imposing the constraint of separability, it is not clear to what extent we can trust the speculations based on this specific solution. Moreover, the analysis in Ref. [2] was restricted to the case with $m^2 < 0$ to avoid the singular behavior of the solution at $r = 0$. In next section, we give a rigorous foundation of the arguments given in the previous papers, and show that the scenario is valid for a much more general class of initial conditions for which there is no need to assume the separable form (??) nor the case $m^2 < 0$.

3 Bulk scalar dynamics

We consider the evolution of a bulk scalar field on the background spacetime which consists of the AdS_5 bulk and the boundary de Sitter brane. We consider arbitrary, regular initial data for this scalar field and investigate the generic behavior of the scalar field at sufficiently late times by analyzing the properties of the retarded Green function.

The bulk geometry is given by Eq. (12) with $a(t)$ of the de Sitter space. For simplicity, we take the spatially flat chart of the de Sitter space. Then, the field equation for ϕ is

$$(-\Box_5 + m^2)\phi = \left[-\hat{L}_r + \frac{1}{(H\ell)^2\sinh^2(r/\ell)}\left(\hat{L}_t - H^2 e^{-2Ht}\partial_{\mathbf{x}}^2\right)\right]\phi = 0, \tag{14}$$

where

$$\hat{L}_t = \frac{\partial^2}{\partial t^2} + 3H\frac{\partial}{\partial t} \quad \text{and} \quad \hat{L}_r = \frac{1}{\sinh^4(r/\ell)}\frac{\partial}{\partial r}\sinh^4(r/\ell)\frac{\partial}{\partial r} - m^2. \tag{15}$$

The retarded Green function satisfies

$$(-\Box_5 + m^2)G(x, x') = \frac{\delta^5(x - x')}{\sqrt{-g}}. \tag{16}$$

with the causal condition that $G(x, x') = 0$ for x' not in the causal past of x. For given initial data on the hypersurface $t = t_i$, the time evolution of a scalar field is given by

$$\phi(x) = \int_{t'=t_i} [(n^a\partial'_a G(x, x'))\phi(x') - G(x, x')n^a\partial'_a\phi(x')]\sqrt{\gamma(x')}\, d^4x'. \tag{17}$$

where n^a is the time-like unit vector normal to the initial hypersurface, and γ is the determinant of the metric induced on this initial hypersurface. Once the retarded boundary condition is satisfied, the Green function vanishes for spatially separated (t, r) and (t', r'). In particular, it vanishes in the limit $r \to 0$ for fixed values of t and t'. This guarantees the regularity at $r = 0$ of the scalar field for arbitrary, regular initial data. From the expression of ϕ (17), we find that the asymptotic behavior of the bulk scalar field can be understood by the behavior $G(x, x')$ at the large $t - t'$.

According to Ref.[7], when $H^2\ell^2 \ll 1$ and $m^2\ell^2 \ll 1$, we then find the late time behavior of the Green function as

$$\mathcal{G}(x,x') \propto \begin{cases} e^{(\sqrt{(9/4)H^2-m_{\rm eff}^2}-(3/2)H)t} & \text{for} \quad m_{\rm eff}^2/H^2 < 9/4\,, \\ e^{-(3/2)Ht}\cos\left(\left[m_{\rm eff}^2-\frac{9}{4}H^2\right]^{1/2}t+\eta\right) & \text{for} \quad m_{\rm eff}^2/H^2 > 9/4\,, \end{cases} \tag{18}$$

where $m_{\rm eff}^2$ is $m^2/2$ and η is a real constant phase. Since we are interested in the spatially homogeneous brane, we focus on the x-independent scalar field configurations. Namely, we considered the spatially averaged Green function defined by

$$\mathcal{G}(t,r;t',r') := \int dx'\, G(x,x'). \tag{19}$$

4 Effective 4-dimensional scalar field

From the asymptotic behavior obtained in Eq. (18), we can conclude that the bulk scalar field evaluated on the brane behaves as an effective 4-dimensional field with the mass squared $m_{\rm eff}^2$ after a sufficiently long period of de Sitter expansion. Our present analysis proves that this simple correspondence continues to hold in more general cases, irrespective of initial field configurations and of the value of m^2/H^2.

This is not the whole story of the correspondence. From Eq. (8), we see that the back-reaction to the geometry starts with the second order in the amplitude of ϕ. Thus, it is justified to evaluate the effective energy density $\rho_{\rm eff}$ defined in (9) by substituting the leading order evolution of the scalar field on the fixed background. It is then important to check if thus evaluated $\rho_{\rm eff}$, which describes the effect of the back-reaction to the geometry, coincides with the energy density of the effective 4-dimensional field with $m_{\rm eff}^2 = m^2/2$. Here we shall show that this correspondence also continues to hold in general, irrespective of the form of the scalar field configuration and of the ratio m^2/H^2.

For this purpose, we first note that from the asymptotic behavior of the Green function (18), the bulk scalar field satisfies the equation,

$$\ddot{\phi} + 3H\dot{\phi} + \frac{1}{2}V' = 0, \tag{20}$$

on the brane at late times. On the other hand, the 5-dimensional field equation (14) implies

$$\ddot{\phi} + 3H\dot{\phi} - \partial_r^2\phi + V' = 0, \tag{21}$$

on the brane. Thus we have

$$\partial_r^2\phi = \frac{1}{2}V' = -\ddot{\phi} - 3H\dot{\phi}\,. \tag{22}$$

Inserting this to the integrand of Eq. (10), we obtain

$$E_{tt} = -\frac{\kappa_5^2}{2a^4}\int^t a^4\dot{\phi}(\ddot{\phi}+2H\dot{\phi})\,dt = -\frac{\kappa_5^2}{4a^4}\int^t \frac{d}{dt}\left(a^4\dot{\phi}^2\right)\,dt = -\frac{\kappa_5^2}{4}\dot{\phi}^2, \tag{23}$$

where we have neglected the integration constant term ($\propto a^{-4}$) that vanishes rapidly as time goes on. Thus we find $\rho_{\rm eff}$ is given by

$$\rho_{\rm eff} = \frac{3}{\kappa_5^2\sigma}\left(\frac{\dot{\phi}^2}{2}+V(\phi)\right) - \frac{E_{tt}}{\kappa_4^2} = \frac{1}{2}\dot{\Phi}^2 + V_{\rm eff}(\Phi), \tag{24}$$

where

$$\Phi = \sqrt{\ell_0}\,\phi\,; \quad \ell_0 = \frac{6}{\kappa_5^2\sigma}\,, \tag{25}$$

and

$$V_{\rm eff}(\Phi) = \frac{\ell_0}{2} V(\Phi/\sqrt{\ell_0}). \tag{26}$$

It should be noted that not only the mass term but also the constant vacuum energy term is included in this scaling relation of the potentials.

This result is quite suggestive. Although our analysis is done for the specific form of the potential (11) on the fixed AdS bulk plus de Sitter brane background, it is tempting to conjecture that the relations (25) and (26) continue to hold in more general situations, as far as the dynamics in the zeroth order of $H^2\ell^2$ and $m^2\ell^2$ is concerned. The crucial point in the above arguments was the equality,

$$\partial_r^2 \phi = \frac{1}{2} V'(\phi), \tag{27}$$

on the brane. In other words, if this equality holds at the zeroth order of $H^2\ell^2$ and $m^2\ell^2$, the effective dynamics of the Einstein-scalar system on the brane will be almost identical to the corresponding system in the standard 4-dimensional theory.

5 Summary

We have analyzed the late time behavior of a bulk scalar field in the inflating braneworld of the Randall-Sundrum type. We have considered a simple model, in which the background spacetime is given by the 5-dimensional anti-de Sitter space, and the brane is expanding with constant Hubble rate H. Assuming the spatial homogeneity of the brane, we have formally solved the field equation of the bulk scalar field as an initial value problem by using the Green function. To conclude, irrespective of the ratio m^2/H^2, the bulk scalar field seen on the brane behaves as a 4-dimensional effective scalar field with mass $m_{\rm eff} = m/\sqrt{2}$.

Using the late time behavior of the bulk scalar field ϕ as described above, we have examined the lowest order back-reaction to the geometry which starts at the quadratic order in the amplitude of ϕ. We have found that the leading order back-reaction to the geometry is equivalently represented by a 4-dimensional effective scalar field Φ with the effective 4-dimensional mass $m_{\rm eff}$ mentioned above, where Φ is related to ϕ by a simple scaling (25).

Although we have studied only the case with a quadratic potential (11), we have described this correspondence in a more suggestive manner, $V_{\rm eff}(\Phi) = \ell_0 V(\Phi/\sqrt{\ell_0})/2$. Note that this relation holds not only for the mass term but also for the vacuum energy term. We have conjectured that this correspondence may hold in more general cases. If this is indeed the case, apart from small corrections of $O(H^2\ell^2, m^2\ell^2)$, **'A bulk scalar in the braneworld can mimic the 4d inflaton dynamics'**.

References

[1] L. Randall and R. Sundrum, Phys. Rev. Lett. **83**, 4690 (1999) [hep-th/9906064].

[2] Y. Himemoto and M. Sasaki, Phys. Rev. D **63**, 044015 (2001) [gr-qc/0010035].

[3] S. Kobayashi, K. Koyama and J. Soda, Phys. Lett. B **501**, 157 (2001) [hep-th/0009160].

[4] N. Sago, Y. Himemoto and M. Sasaki, Phys. Rev. D **65**, 024014 (2002) [gr-qc/0104033].

[5] J. Yokoyama and Y. Himemoto, Phys. Rev. D **64**, 083511 (2001) [hep-ph/0103115].

[6] T. Shiromizu, K. Maeda and M. Sasaki, Phys. Rev. D **62**, 024012 (2000) [gr-qc/9910076].

[7] Y. Himemoto, T. Tanaka and M. Sasaki, [gr-qc/0112027].

Scattering in Two Black Hole Moduli Space

Kenji Sakamoto[1] and Kiyoshi Shiraishi[2]

Faculty of Science, Yamaguchi University
Yoshida, Yamaguchi-shi, Yamaguchi 753-8512, Japan

Abstract

In this work, we discuss the quantum mechanics on the moduli space consisting of two maximally charged dilaton black holes. We study the quantum effects resulting from the different structure of the moduli space geometry in the scattering process.

1 Introduction

Recently the study of black hole moduli space has attracted much attention. Quantum black holes have been studied by means of quantum fields or strings interacting with a single black hole. In the past few years the new quantum mechanics of an arbitrary number N of supersymmetric black holes has been focused. Configurations of N static black holes parametrize a moduli space. The low-lying quantum states of the system are governed by quantum mechanics on the moduli space. The effective theories of quantum mechanics on a moduli space of Reissner-Nordström multi-black holes were constructed in [1]. Recently, (super)conformal quantum mechanics are constructed on a moduli spaces of five-dimensional multi-black holes in the near-horizon limit in [2].

The motivation behind these works is the hope that information of these quantum states will lead to the black hole entropy. The quantum states supported in the near-horizon region can be interpreted as internal states of black holes, and the number of such states is related to the black hole entropy. The other motivation is the expectation that investigation of these moduli spaces will lead to the understanding of AdS_2/CFT_1 correspondence and unravel some novel features behind the quantum states in multi-black hole mechanics.

The geometry of black hole moduli spaces was first discussed by Ferrell and Eardley in four dimensions [3]. Further the black hole moduli spaces geometry with dilaton coupling in $N+1$ dimensions was discussed by Shiraishi [4]. In these works the structure of the moduli space geometry is different according to dimensions and values of dilaton coupling.

In this work, we discuss quantum mechanics on the moduli space consisting of two maximally charged dilaton black holes. We study the quantum effect resulting from the different structure of the moduli space geometry in the scattering process. In the section 2, we discuss the moduli space structure of two black hole system with dilaton coupling in any dimensions. In the section 3, we study the quantum mechanics on this moduli space and the general view of potential in the (3+1) dimensions. In the section 4, we consider the scattering process on the moduli space. Then we discuss the quantum effects from the different structures of the moduli space geometry. In the section 5, we will give the conclusion and the discussion.

2 The Moduli Space Metric for the System Consisting of Maximally Charged Dilaton Black Holes

The Einstein-Maxwell-dilaton system contains a dilaton field ϕ coupled to a $U(1)$ gauge field A_μ beside the Einstein-Hilbert gravity. In the $N+1$ dimensions ($N \geq 3$), the action for the fields with particle sources is

$$S = \int d^{N+1}x \frac{\sqrt{-g}}{16\pi}\left[R - \frac{4}{N-1}(\nabla\phi)^2 - e^{-\{4a/(N-1)\}\phi}F^2\right]$$

[1] E-mail:b1795@sty.cc.yamaguchi-u.ac.jp
[2] E-mail:shiraish@sci.yamaguchi-u.ac.jp

$$-\sum_{i=1}^{n}\int ds_i\left(m_i e^{-\{4a/(N-1)\}\phi}+Q_iA_\mu\frac{dx_i^\mu}{ds_i}\right), \tag{1}$$

where R is the scalar curvature and $F_{\mu\nu}=\partial_\mu A_\nu-\partial_\nu A_\mu$. We set the Newton constant $G=1$. The dilaton coupling constant a can be assumed to be a positive value.

The metric for the N-body system of maximally-charged dilaton black holes has been known as [4]

$$ds^2=-U^{-2}(\mathbf{x})dt^2+U^{2/(N-2)}(\mathbf{x})d\mathbf{x}^2, \tag{2}$$

where

$$U(\mathbf{x}) = (F(\mathbf{x}))^{(N-2)/(N-2+a^2)}, \tag{3}$$

$$F(\mathbf{x}) = 1+\sum_{i=1}^{n}\frac{\mu_i}{(N-1)|\mathbf{x}-\mathbf{x}_i|^{N-2}}. \tag{4}$$

Using these expressions, the vector one form and dilaton configuration are written as

$$A=\sqrt{\frac{N-1}{2(N-2+a^2)}}\,(F(\mathbf{x}))^{-1}\,dt, \tag{5}$$

$$e^{-4a\phi/(N-1)}=(F(\mathbf{x}))^{2a^2/(N-2+a^2)}. \tag{6}$$

In this solution, the asymptotic value of ϕ is fixed to be zero.

The electric charge Q_i of each black hole are associated with the corresponding mass m_i by

$$m_i = \frac{A_{N-1}(N-1)}{8\pi(N-2+a^2)}\mu_i, \tag{7}$$

$$|Q_i| = \sqrt{\frac{N-1}{2(N-2+a^2)}}\mu_i, \tag{8}$$

where $A_{N-1}=2\pi^{n/2}/\Gamma(\frac{1}{2}N)$.

The perturbed metric and potential can be written in the form

$$ds^2=-U^{-2}(\mathbf{x})dt^2+2\mathbf{N}d\mathbf{x}dt+U^{2/(N-2)}(\mathbf{x})d\mathbf{x}^2, \tag{9}$$

$$A=\sqrt{\frac{N-1}{2(N-2+a^2)}}(F(\mathbf{x}))^{-1}dt+\mathbf{A}d\mathbf{x}, \tag{10}$$

where $U(\mathbf{x})$ and $F(\mathbf{x})$ are defined by (3) and (4). We have only to solve linearized equations with perturbed sources up to $O(v)$ for N_i and A_i. (Here v represents the velocity of the black hole as a point source.) We should note that each source plays the role of a maximally charged dilaton black hole.

Solving the Einstein-Maxwell equations and substituting the solutions, the perturbed dilaton field and sources to the action (1) with proper boundary terms, we get the effective Lagrangian up to $O(v^2)$ for N-maximally charged dilaton black hole system

$$\begin{aligned} L &= -\sum_{i=1}^{n}m_i+\sum_{i=1}^{n}\frac{1}{2}m_i(\mathbf{v}_i)^2 \\ &\quad+\frac{(N-1)(N-a^2)}{16\pi(N-2+a^2)^2}\int d^Nx(F(\mathbf{x}))^{2(1-a^2)/(N-2+a^2)}\sum_{i,j}^{n}\frac{(\mathbf{n}_i\cdot\mathbf{n}_j)|\mathbf{v}_i-\mathbf{v}_j|^2\mu_i\mu_j}{2|\mathbf{r}_i|^{N-1}|\mathbf{r}_j|^{N-1}}, \end{aligned} \tag{11}$$

where $\mathbf{r}_i=\mathbf{x}-\mathbf{x}_i$ and $\mathbf{n}_i=\mathbf{r}_i/|\mathbf{r}_i|$. $F(\mathbf{x})$ is defined by (4). In general, a naive integration in equation (11) diverges. Therefore, we regularize that divergent terms proportional to $\int d^Nx\delta^n(x)/|x|^p(p>0)$ which

appear when the integrand is expanded must be regularized [5]. We set them to zero. The prescription is equivalent to carrying out the following replacement in equation (11)

$$(F(x))^{\frac{2(1-a^2)}{(N-2+a^2)}} \to -1 + \left[1 + \frac{8\pi(N-2+a^2)}{A_{N-1}(N-2)(N-1)} \frac{m_a}{|\mathbf{r}_a|^{N-2}}\right]^{\frac{2(1-a^2)}{N-2+a^2}} + \left[1 + \frac{8\pi(N-2+a^2)}{A_{N-1}(N-2)(N-1)} \frac{m_b}{|\mathbf{r}_b|^{N-2}}\right]^{\frac{2(1-a^2)}{N-2+a^2}}. \tag{12}$$

After regularization, the effective Lagrangian for two body system (consisting of black hole labeled with a and b) can be rewritten. From this rewriting effective Lagrangian, we obtain the metric of the $N+1$ dimensional moduli space for two-body system as

$$g_{ab} = \gamma(r)\delta_{ab}, \tag{13}$$

with

$$\begin{aligned}\gamma(r) = 1 \quad &- \quad \frac{M}{\mu} - \frac{8\pi(N-a^2)}{A_{N-1}(N-2)(N-1)} \frac{M}{r_{ab}^{N-2}} \\ &+ \quad \frac{M}{m_a}\left(1 + \frac{8\pi(N-2+a^2)}{A_{N-1}(N-2)(N-1)} \frac{m_a}{r_{ab}^{N-2}}\right)^{(N-a^2)/(N-2+a^2)} \\ &+ \quad \frac{M}{m_b}\left(1 + \frac{8\pi(N-2+a^2)}{A_{N-1}(N-2)(N-1)} \frac{m_b}{r_{ab}^{N-2}}\right)^{(N-a^2)/(N-2+a^2)},\end{aligned} \tag{14}$$

where $M = m_a + m_b$, $\mu = m_a m_b/M$, and $r_{ab} = |\mathbf{x}_a - \mathbf{x}_b|$.

3 Quantum mechanics in two-black hole moduli space

We consider the quantum mechanics on moduli space. The quantization of moduli parameters has been discussed in [6].

Let us introduce a wave function Ψ on the moduli space, which obeys the Schrödinger equation

$$i\hbar\frac{d\Psi}{dt} = \left(-\frac{\hbar^2}{2\mu}\nabla^2 + \hbar^2\xi R_{(MS)}\right)\Psi, \tag{15}$$

where ∇^2 is the covariant Laplacian constructed from the moduli space metric and $R_{(MS)}$ is the scalar curvature of the moduli space. We assume $\xi = 0$ in this paper though this term may be present in most general case.

To simplify, we fix the case of the (3+1) dimensional case. The partial wave in a stationary state is

$$\Psi = \psi_{ql}(r)Y_{lm}(\theta,\phi)\exp(-iEt/\hbar), \tag{16}$$

where $Y_{lm}(\theta,\phi)$ is the spherical harmonic function and $E = \hbar^2 q^2/(2\mu)$. We redefine the variables as

$$R = \int\sqrt{\gamma}dr, \tag{17}$$

$$\psi = \frac{\chi}{r\sqrt{\gamma}}. \tag{18}$$

The Schrödinger equation (15) is rewritten as

$$\frac{d^2\chi}{dR^2} + (q^2 - V)\chi = 0, \tag{19}$$

where the potential V is

$$V = \frac{\gamma(r\gamma')' - r(\gamma')^2}{2r\gamma^3} + \frac{l(l+1)}{r^2\gamma}. \tag{20}$$

Here $'$ stands for $\frac{d}{dr}$.
To study the scattering process, we find the general view of potential on the moduli space. The potential for dilaton coupling $a^2 = 0$, $1/3$ and 1 are plotted in Fig.1.

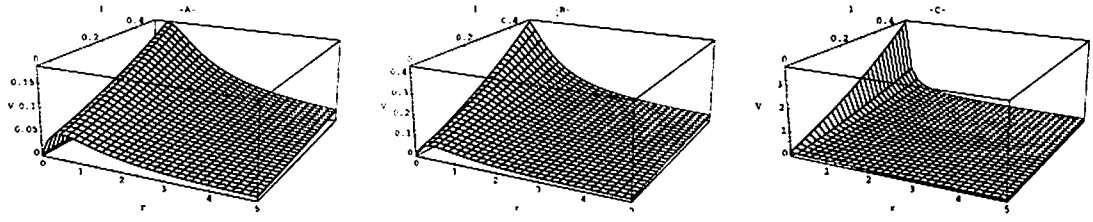

Figure 1: The potential V as the function of r and angular momentum l, A for $a^2 = 0$, B for $a^2 = 1/3$ and C for $a^2 = 1$.

In the case of $a^2 = 0$ for all values of l and $a^2 = 1/3$ for $l = 0$, the potential has a maximal value. Then the incoming particle into two black hole moduli space are scattered or coalesced in the scattering process. On the other hand, in the case of $a^2 = 1/3$ for all values of $l \neq 1$ and $a^2 = 1$ all values of l, the incoming particle are always scattered away. We notice that the value of $a^2 = 1/3$ is the critical point of moduli structures [4]. For simplicity, we will study the scattering-away processes in the case of $a^2 = 1/3$ and $a^2 = 1$.

4 Scattering on two-black hole moduli space

We consider the case of $a^2 = 1/3$ and $a^2 = 1$. As the first study of quantum effects, we discuss the scattering process in the WKB approximation. For the WKB approximation, the phase shift in the scattering process are

$$\delta_l = -qR_0 + \int_{R_0}^{\infty} dR \left(\sqrt{q^2 - V(R) - \frac{1}{4R^2}} - q \right) + \frac{2l+1}{4}\pi, \tag{21}$$

where R_0 is the solution of $V(R_0) = q^2 - \frac{1}{4R_0^2}$.
The partial cross section are

$$\sigma_l = \frac{4\pi}{q^2}(2l+1)\sin^2\delta_l. \tag{22}$$

The deflection angle are

$$\Theta = \pi + \int_{R_0}^{\infty} dR \frac{\partial}{\partial l}\sqrt{q^2 - V(R) - \frac{1}{4R^2}}. \tag{23}$$

The phase shift δ_l and the deflection angle Θ for $q = 0.1$ and 0.2 are plotted in Fig.2. The solid line in Fig.2 A2, B2 represents the classical deflection angle which are obtained from the impact parameter. For $a^2 = 1$, the effects for the different value of q are not found, and the deflection angle are almost correspond to the classical deflection angle. Although, for $a^2 = 1/3$, we can find that the behaviours of the phase shift and the deflection angle depend on the incoming particle energy q. Then the deflection angle are different from the classical deflection angle at the small value of l/q. These effects are interpreted as the quantum effects arisen by the difference of the moduli space structures in the scattering process. Although we used the WKB semi-classical approximation in this analysis, the quantum effects can be obtained sufficiently.

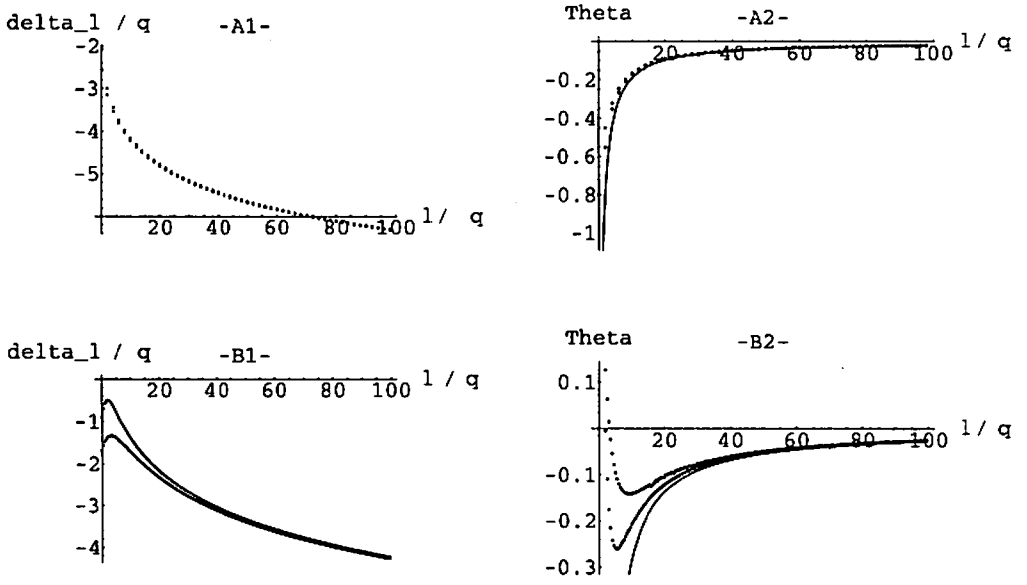

Figure 2: The phase shift and the deflection angle. A1 is a phase shift for $a^2 = 1$, A2 is a deflection angle for $a^2 = 1$, B1 and B2 are phase shift and deflection angle for $a^2 = 1/3$.

5 Conclusion

In this work, we studied the quantum effects on the different moduli structure. We obtained the black hole moduli space metrics in any dimensions. In the (3+1) dimensions, we considered the quantum mechanics on the moduli space, and investigated the potential for $a^2 = 0$, $1/3$ and 1. For the process in which the incoming particle are always scattered away, $a^2 = 1/3$ and 1, we obtained the phase shift and the deflection angle in the WKB approximation. Then we revealed the quantum effects in scattering process for $a^2 = 1/3$. We considered that these effects due to the difference in the moduli space structure. So, the moduli space structure affect to the quantum scattering process.
In the further study, we will consider the behavior in the different dimensions and for the other values of dilaton coupling a^2. The moduli space structures are different in the other dimensions and at the other values of dilaton coupling a^2. In (4+1) dimensions for $a^2 = 1$, the moduli space structure are resemble the structure in (3+1) dimensions for $a^2 = 1/3$ [4]. Then we expect that the similar quantum effects are also arisen. In this work, we consider the quantum effects in the WKB approximation. So, we will more precisely study in quantum mechanically analysis in further study.

References

[1] G. W. Gibbons and P. J. Ruback, *Phys. Rev. Lett.* **57**, 1492 (1986).

[2] J. Michelson, and A. Strominger, *JHEP* **09**, 005 (1999).

[3] F. Ferrell, and D. Eardley, *Phys. Rev. Lett.* **59**, 1617 (1987).

[4] K. Shiraishi, *Nucl. Phys.* **B402**, 399 (1993).

[5] L. Infeld and J. Plebański, *Motion and Relativity* (Pergamon Press, 1960).

[6] J. Traschen and R. Ferrell, Phys. Rev. **D45**, 2628 (1992).

Equation of state for a classical gas of BPS black holes [1]

Nahomi Kan[2], Kiyoshi Shiraishi[3]

Graduate School of Science and Engineering, Yamaguchi University, Yoshida, Yamaguchi-shi, Yamaguchi 753-8512, Japan

Takuya Maki[4]

Japan Woman's College of Physical Education, Kita-karasuyama, Setagaya, Tokyo 157, Japan

Abstract

A point-particle treatment for the statistical mechanics of Bogomol'nyi-Prasad-Sommerfield (BPS) black holes in Einstein-Maxwell-dilaton theory is developed. Because of the absence of the static potential, the canonical partition function for N BPS black holes can be expressed by the volume of the moduli space for them. We estimate the equation of state for a classical gas of BPS black holes by the Padé approximation and find that the result agrees with the one obtained by the mean-field approximation.

1 Introduction

The thermodynamics of a self-gravitating system has some importance in the context of cosmology. The long-range nature of gravity gives rise to the breakdown of the conventional description statistical properties, such as the additivity of the free energy or other "extensive" thermodynamical quantities. While a statistical treatment of nonequilibrium systems has recently been developed, the existence of the long-range force seems essential for explaining the formation of the peculiar local structure in the system.

Recently, de Vega and Sánchez studied the statistical mechanics of a self-gravitating particle gas [2]. They showed that the "thermodynamic limit" must be taken as $N \to \infty$ with $N/\mathcal{V}^{1/3}$ fixed in three dimensions, where N is the number of particles and $\mathcal{V}$ is the volume of the system. This treatment is required by the long-range nature of gravity, because there is no *ad hoc* cutoff scale. [5]

On the other hand, two of the present authors have studied the statistical mechanics of well-separated charged particles in Einstein-Maxwell-scalar theory [3]. The system was found to be unstable in general, although there exists a critical case in which the static forces cansel each other.

In general relativity, the critical case was investigated and exact static solutions which describe multi-black hole systems have been obtained [4, 5]. In such a case, the attractive forces (the gravitational and scalar-mediated forces) and the repulsive forces (the electro-static force) between black holes are exactly cancelled in the static limit. In this case, the energy of the system was calculated for small velocities but for small distances between the black holes [6, 7]

In this paper, we investigate the multi-black hole system by adopting the technique of de Vega and Sánchez [2]. Note that a mass-charge relation is satisfied for each individual black hole. Such extreme black holes, or so-called BPS black holes, [6] often appear in string theories.

---

[1] This work is based on [1].

[2] E-mail:b1834@sty.cc.yamaguchi-u.ac.jp

[3] E-mail:shiraish@sci.yamaguchi-u.ac.jp

[4] E-mail:maki@clas.kitasato-u.ac.jp

[5] Actually, the horizon length is a candidate for the cutoff scale in the universe.

[6] In [8], it is shown that they saturate a gravitational analogue of the Bogomol'nyi bound on their mass and charges.

2 "BPS black holes" in slow motion

We consider 'BPS black holes' in $(d+1)$ dimensional Einstein-Maxwell-dilaton theory, which is governed by the action

$$S = \int d^{d+1}x \frac{\sqrt{-g}}{16\pi G}\left[R - \frac{4}{d-1}\nabla_\mu\phi\nabla^\mu\phi - e^{-[4a/(d-1)\phi]}F_{\mu\nu}F^{\mu\nu}\right]. \tag{1}$$

Here R is the scalar curvature and $F_{\mu\nu} = \partial_\mu A_\nu - \partial_\nu A_\mu$ $(\mu,\nu = 0,1,\ldots,d)$, while ϕ is a dilaton field and a is a coupling constant. G denotes the $(d+1)$ dimensional Newton's constant. We set $c = 1$.

This theory admits static multi-centered solutions whose metric and field configurations are given by [5]

$$ds^2 = -V^{-2(d-2)/(d-2+a^2)}dt^2 + V^{2/(d-2+a^2)}d\mathbf{x}^2, \tag{2}$$

$$e^{-[4a/(d-1)\phi]} = V^{2a^2/(d-2+a^2)}, \tag{3}$$

$$A_0(\mathbf{x}) = \sqrt{\frac{d-1}{2(d-2+a^2)}}\left(1 - \frac{1}{V}\right), \tag{4}$$

$$A_i(\mathbf{x}) = 0 \quad (i = 1,\ldots,d), \tag{5}$$

in terms of a harmonic function

$$V(\mathbf{x}) = 1 + \frac{2(d-2+a^2)}{(d-1)(d-2)}\frac{4\pi}{A_{d-1}}G\sum_a \frac{m_a}{|\mathbf{r}_a|^{d-2}}, \tag{6}$$

where $\mathbf{r}_a = \mathbf{x} - \mathbf{x}_a$ is the position vector of 'point particle' a and the labels of 'particles' $a, b, \ldots$ run over $1,\ldots,N$. $A_{d-1} \equiv 2\pi^{d/2}/\Gamma(d/2)$ is the volume of a unit $d-1$ sphere.

The point sources corresponding to the 'particles' can be described by the action

$$I = -\sum_a \int ds_a \left[m_a e^{[2a/(d-1)\phi]} - e_a A_\mu \frac{dx^\mu}{ds_a}\right], \tag{7}$$

with the relation

$$\frac{e_a}{m_a} = \sqrt{\frac{2(d-2+a^2)}{d-1}}. \tag{8}$$

This relation is just the extremity condition for spherically symmetric black holes in the Einstein-Maxwell-dilaton theory [9]. Thus the solution can be viewed as the one for an 'N BPS black hole' system, where the electric forces is cancelled by the forces mediated by the gravitation and the dilaton.

3 The canonical partition function

The canonical partition function for N identical particles at temperature T in d spatial dimensions is

$$Z_N = \frac{1}{N!}\frac{1}{h^{Nd}}\int [dq]\,[dp]\exp(-\beta H), \tag{9}$$

where $[dp] = \Pi_{a=1}^N d^d\mathbf{p}_a$, $[dq] = \Pi_{a=1}^N d^d\mathbf{x}_a$, and $\beta = 1/T$. h is Planck's constant while Boltzmann's constant is set to unity.

Because there are no static forces, the Hamiltonian H for the system of N "BPS black holes" with a common mass m can be written as

$$H = \frac{1}{2}\sum_A\sum_B v^A \mathcal{G}_{AB} v^B, \tag{10}$$

where

$$\mathcal{G}_{(ak)(bl)} = m\left[\delta_{ab}\delta_{kl} + \frac{2}{m}\left(\delta_{kl}\delta^{ij} + \delta^i_k\delta^j_l - \delta^j_k\delta^i_l\right)\partial_{ai}\partial_{bj}L'\right] \equiv m g_{(ak)(bl)}, \tag{11}$$

with

$$L' = -\frac{1}{32\pi G}\int d^d\mathbf{x}\left[V^{2(d-1)/(d-2+a^2)}(\mathbf{x}) - 1 - \frac{4}{d-2}\frac{4\pi}{A_{d-1}}Gm\sum_c \frac{1}{|\mathbf{r}_c|^{d-2}}\right], \tag{12}$$

and

$$V(\mathbf{x}) = 1 + \frac{2(d-2+a^2)}{(d-1)(d-2)}\frac{4\pi}{A_{d-1}}Gm\sum_a \frac{1}{|\mathbf{r}_a|^{d-2}}. \tag{13}$$

The label $\{A\} = \{(ai)\}$ denotes the combination of the label of the particle and the spatial index. Then we obtain the expression for the partition function

$$Z_N = \frac{1}{N!}\left(\frac{2\pi m}{\beta h^2}\right)^{Nd/2}\int [dq]\sqrt{\det g} \equiv \frac{1}{N!}\left(\frac{2\pi m}{\beta h^2}\right)^{Nd/2} \mathcal{Q}, \tag{14}$$

which is proportial to the volume of the moduli space $\mathcal{Q}$.

4 The thermodynamical limit and the equation of state

The pressure P is derived from the free energy F as $P = -\frac{\partial F}{\partial \mathcal{V}}$, where $\mathcal{V} = \int d^d\mathbf{x} = A_{d-1}l^d/d$, l is a radius of a spherical box, thus we find

$$\frac{P\mathcal{V}}{NT} = 1 + \frac{\mathcal{V}}{N}\frac{\partial}{\partial \mathcal{V}}\ln\frac{\mathcal{Q}}{\mathcal{V}^N} = 1 + \frac{l}{Nd}\frac{\partial}{\partial l}\ln\frac{\mathcal{Q}}{\mathcal{V}^N}. \tag{15}$$

Substituting the above result and taking the thermodynamical limit, or in the large-N limit,

$$W = \lim_{N\to\infty}\frac{1}{N}\ln\frac{\mathcal{Q}}{\mathcal{V}^N} = W(y), \tag{16}$$

where the value $\mathcal{Q}/l^{d-2}$ is fixed, we obtain the equation of state

$$\frac{P\mathcal{V}}{NT} = f(y), \tag{17}$$

where

$$y = \frac{1}{d-2}\frac{4\pi}{A_{d-1}}\frac{GmN}{l^{d-2}} \tag{18}$$

is a dimensionless parameter. we estimate $f(y)$ by the Padé approximation and by the mean-field approximation.

5 The Padé approximation

The Padé approximation interpolates between the small and large y regions.

For $y \ll 1$, weakly self-interacting gas, the equation of state reads

$$f(y) = 1 - b_1 y + b_2 y^2 + O(y^3), \tag{19}$$

where

$$b_1 = \frac{d-2}{2}\left[\frac{2(d-a^2)}{d-1}\right]\frac{2d}{d+2}, \tag{20}$$

$$b_2 = d(d-2)\left[\frac{2(d-a^2)}{d-1}\right]^2\left[\left(\frac{2d}{d+2}\right)^2 - \left(1 - \frac{d-2+a^2}{2d(d-a^2)}\right)\frac{d(5d+2)}{(d+2)(d+4)}\right]. \tag{21}$$

In the strong coupling limit $y \gg 1$, we find

$$\frac{\mathcal{Q}}{\mathcal{V}^N} \approx y^{(Nd/2)(d-a^2)/(d-2+a^2)} \times const. \tag{22}$$

Then the Padé approximation shows that

$$\frac{Q}{\mathcal{V}^N} \approx [q_{p1}(y)]^N \equiv (1+\alpha_1 y)^{(Nd/2)(d-a^2)/(d-2+a^2)}, \tag{23}$$

with

$$\alpha_1 = \frac{2(d-2+a^2)}{d-1}\frac{2d}{d+2}. \tag{24}$$

In this approximation, the equation of state reads

$$\frac{P\mathcal{V}}{NT} = f(y) = 1 - \frac{(d-2)(d-a^2)}{d-1}\frac{2d}{d+2}\frac{\alpha_1 y}{1+\alpha_1 y}. \tag{25}$$

At the critical $y = y_c$ [y_c satisfies $f(y_c) = 0$] the gas cannot remain in the normal gaseous phase. [7]

6 The mean-field approximation

In [7] , an effective field theory of "BPS black holes" was constructed. Here we use the effective field theory to obtain the mean-field approximation.

In the mean-field approximation the number density with a chemical potential μ is given by

$$n = \frac{1}{h^d}\int d^d p \exp\left[-\beta\left(\frac{p^2}{2mV^{(d-a^2)/(d-2+a^2)}} - \mu\right)\right] = n_0 V^{d(d-a^2)/2(d-2+a^2)}, \tag{26}$$

with a constant n_0, where the gauge interaction term is discarded.

The mean-field potential V satisfies the following equation [7]:

$$\partial^2 V + 8\pi\frac{d-2+a^2}{d-1}Gmn_0 V^{d(d-a^2)/2(d-2+a^2)} = 0, \tag{27}$$

with the boundary conditions.

The canonical partition function can be expressed as

$$Z_N = \frac{\mathcal{V}^N}{N!}\left[\frac{1}{\mathcal{V}}\int d^d\mathbf{x}\left(\frac{2\pi m}{\beta h^2}V^{(d-a^2)/(d-2+a^2)}\right)^{d/2}\right]^N = \frac{\mathcal{V}^N}{N!}\left(\frac{2\pi m}{\beta h^2}\right)^{Nd/2}[q_{mf}(y)]^N. \tag{28}$$

Then the equation of state reads

$$\frac{P\mathcal{V}}{NT} = f(y) = 1 - \frac{d-2}{d}y\frac{\partial}{\partial y}\ln q_{mf}(y). \tag{29}$$

We evaluate $f(y)$ by a numerical method, since the solution cannot be given analytically in general.

7 Result

In Fig. 1, $f(y)$ obtained by the approximations considered above is shown. All the mean-field and the Padé approximations indicate consistent behavior of the function. The difference appears to be small when $d - a^2$ is small.

[7] In the present approximation scheme, the value of $y = y_c$ is $y_c = \frac{d+2}{2d}\frac{d-1}{(d-2)^2-da^2}$, for $a^2 < a_c^2 \equiv (d-2)^2/d$.

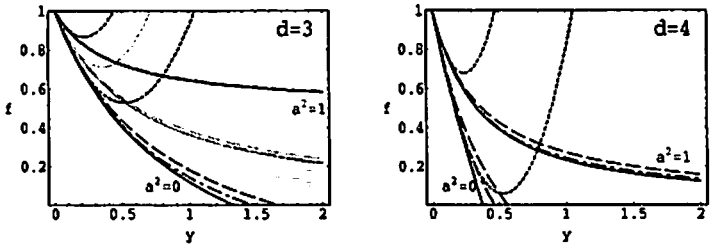

Figure 1: $f(y)$ is plotted against y for $d = 3$ and $d = 4$. The solid line obtained by the mean-field approximation, the dashed line by the lowest-order Padé approximation, the dot-dashed line by the next-to-leading Padé approximation, and the dotted line is the series expansion up to second order.

8 Summary

We have studied a many-body system of "BPS black holes" in d dimensions. The canonical partition function of the system is proportional to the volume of the moduli space of N "BPS black holes" . Therefore the difference from an ideal gas arises through the change of the effective volume of the system: the internal energy and heat capacity at a fixed volume are the same as those of an ideal gas [1].

We estimated the equation of state of the gas by the Padé approximation and the mean-field method. In these approximations, we found that the pressure simply decreases as the value of y increases if the temperature and the density are fixed. This feature is common in the cases for different spatial dimensions and dilaton couplings.

Of course the analytical attempt to describe thermodynamic properties of the "BPS black hole" gas may have been inconclusive and numerical simulations of the self-interacting system may be needed. The present work provides a guideline for such numerical calculations to survey the critical points of the "BPS black hole" gas .

References

[1] N. Kan, T. Maki and K. Shiraishi, *Phys. Rev.* **D 64**, 104009 (2001).

[2] H. J. de Vega and N. Sánchez, *Phys. Lett.* **B 490**, 180 (2000).

[3] K. Shiraishi and T. Maki, *Phys. Rev.* **D 53**, 3070 (1996).

[4] A. Papapetrou, Proc. R. Ir. Acad., Sect. A, *Math. Astron. Phys. Sci.* **51A**, 191 (1947); S. D. Majumdar, *Phys. Rev.* **D 72**, 930 (1947); R. C. Myers, *Phys. Rev.* **D 35**, 455 (1987).

[5] K. Shiraishi, *J. Math. Phys.* **34**, 1480 (1993).

[6] G. W. Gibbons and P. J. Ruback, *Phys. Rev. Lett.* **57**, 1492 (1986); R. C. Ferrell and D. M. Eardley, *Phys. Rev. Lett.* **59**, 1617 (1987); J. Traschen and R. Ferrell, *Phys. Rev.* **D 45**, 2628 (1992); K. Shiraishi, *Nucl. Phys.* **B402**, 399 (1993); K. Shiraishi, *Int. J. Mod. Phys.* **D 2**, 59 (1993).

[7] Y. Degura and K. Shiraishi, *Class. Quantum Grav.* **17**, 4031 (2000).

[8] G. W. Gibbons, D. Kastor, L. A. J. London, P. K. Townsend and J. Traschen, *Nucl. Phys.* **B416**, 850 (1994).

[9] G. W. Gibbons and K. Maeda, *Nucl. Phys.* **B298**, 337 (1982); D. Garfinkle, G. Horowitz and A. Strominger, *Phys. Rev.* **D 43**, 3140 (1991), **45**, 3888(E) (1992).

Noncommutative gravity in three dimensions coupled to point-like sources

Kiyoshi Shiraishi[1]

Faculty of Science, Yamaguchi University,
Yamaguchi-shi, Yamaguchi, 753-8512, Japan

Abstract

Noncommutative gravity in three dimensions with no cosmological constant is reviewed. We find a solution which describes the presence of a torsional source.

1 What does 'noncommutative' mean?

Please see [1] for a review of noncommutative field theory, if you want to study more.

Consider noncommutative coordinates, for example

$$[x, y] = i\theta, \tag{1}$$

where θ is a real constant. Then the 'uncertainty' lies between x and y, namely,

$$\Delta x \Delta y \geq \theta, \tag{2}$$

(where a numerical factor has omitted). This means the existence of the minimal length scale.

If complex combinations of the coordinates, $z = x + iy$ and $z = x - iy$, are introduced, they satisfy

$$[z, z] = 2\theta. \tag{3}$$

There are different representations to describe the noncommutativity; the commutative coordinate formalism with the star product, the Fock space (operator) formalism, *etc.* (see [1] for details). In this talk, we simply use them identically, unless the identification leads to confusions (thus, we do not use $\star$ in this talk). For example, we denote the equalities

$$1 = \sum_{n=0}^{\infty} |n\rangle\langle n|, \qquad z = \sqrt{2\theta}\sum_{n=0}^{\infty} \sqrt{n+1}|n\rangle\langle n+1|, \qquad \bar{z} = \sqrt{2\theta}\sum_{n=0}^{\infty} \sqrt{n+1}|n+1\rangle\langle n|, \tag{4}$$

where ket and bra satisfy $z|0\rangle = 0$, $z|n\rangle = \sqrt{2\theta}\sqrt{n}|n-1\rangle$, $\bar{z}|n\rangle = \sqrt{2\theta}\sqrt{n+1}|n+1\rangle$, and so on.

Another example is

$$2(-1)^m L_m(2r^2/\theta)\, e^{-r^2/\theta} = |m\rangle\langle m|, \tag{5}$$

where $r^2 = x^2 + y^2$ and $L_n(x)$ is the Lagurre polynomial.

For later use, we *define* [2] the inverse of z, $\bar{z}$ as

$$\frac{1}{z} \equiv \frac{1}{\sqrt{2\theta}}\sum_{n=0}^{\infty} \frac{1}{\sqrt{n+1}}|n+1\rangle\langle n|, \quad \frac{1}{\bar{z}} \equiv \frac{1}{\sqrt{2\theta}}\sum_{n=0}^{\infty} \frac{1}{\sqrt{n+1}}|n\rangle\langle n+1|. \tag{6}$$

This definition leads to $z\frac{1}{z} = \frac{1}{\bar{z}}\bar{z} = 1$, however,

$$\frac{1}{z}z = \bar{z}\frac{1}{\bar{z}} = 1 - |0\rangle\langle 0|. \tag{7}$$

[1] E-mail:shiraish@sci.yamaguchi-u.ac.jp

[2] Note that here $\frac{1}{\bar{z}}$ is defined as operator formalism and this may differ from z^{-1} in the usual star product formalism.

Thus the derivative of $\frac{1}{z}$ and $\frac{1}{\bar{z}}$ is

$$\partial_z \frac{1}{z} = \frac{1}{2\theta}\left[z, \frac{1}{z}\right] = \frac{1}{2\theta}|0\rangle\langle 0| = \frac{1}{\theta}e^{-r^2/\theta}, \quad \partial_{\bar{z}} \frac{1}{\bar{z}} = \frac{1}{2\theta}\left[\frac{1}{\bar{z}}, \bar{z}\right] = \frac{1}{2\theta}|0\rangle\langle 0| = \frac{1}{\theta}e^{-r^2/\theta}. \tag{8}$$

Interestingly enough, in the commutative limit, we find

$$\frac{1}{\theta}e^{-r^2/\theta} \xrightarrow{\theta \to 0} \pi\,\delta(x)\delta(y). \tag{9}$$

2 Why 'noncommutative'?

We expect that noncommutative field theory is worth studying, because:

- the fundamental minimal length $\sqrt{\theta}$ may avoid singularities and infinities which arise in usual field theories.
- the effective field theory of string or brane or M-theory in the presence of the background B field can be expressed as a noncommutative field theory.
- the analysis of quantum Hall systems with a constant magnetic field admits the formulation with noncommuting coordinates.

3 Three dimensional noncommutative gravity

...has a long history.

In this talk, we concentrate our attention on noncommutative gravity in three dimensions. [3]

Three dimensional Chern-Simons noncommutative gravity was studied by Bañados *et al.*[3] and more recently by Cacciatori *et al.*[4].

We would like to study noncommutative gravity in three dimensions with no cosmological constant. Further, we wish to find exact solutions whose spatial coordinates are mutually noncommutative.

The signature is taken to be Euclidean, and the coordinates are denoted as

$$x^1 = x, \quad x^2 = y, \quad x^3 = \tau, \qquad \text{where} \quad [x, y] = i\theta. \tag{10}$$

We define a matrix-valued dreibein one-form and a connection one-form as

$$e = e^a J_a + e^4 i, \quad \omega = \omega^a J_a + \omega^4 i, \quad \text{where} \quad J_1 = \frac{i}{2}\sigma_1, \quad J_2 = -\frac{i}{2}\sigma_2, \quad J_3 = \frac{i}{2}\sigma_3. \tag{11}$$

A matrix-valued torsion two-form and a curvature two-form are given by

$$\mathcal{T} = de + \omega \wedge e + e \wedge \omega, \qquad \mathcal{R} = d\omega + \omega \wedge \omega. \tag{12}$$

The vacuum solution of 'Einstein equation' satisfies

$$\mathcal{R} = \mathcal{T} = 0. \tag{13}$$

Unless the Abelian field e^4 and ω^4 vanish, we cannot regard this model as that for noncommutative gravity with an arbitrary value of θ.

[3] See Nair[2] for an extension to the other dimensions.

4 Difficulties in noncommutative gravity I

If we choose the spin connection as

$$\omega = \frac{\alpha}{2}\left(\frac{1}{z}dz - \frac{1}{\bar{z}}d\bar{z}\right)\begin{pmatrix} 1 & 0 \\ 0 & -1 \end{pmatrix}, \tag{14}$$

we obtain the curvature

$$\mathcal{R} = \frac{\alpha}{2\theta}|0\rangle\langle 0|dz\wedge d\bar{z}\begin{pmatrix} 1 & 0 \\ 0 & -1 \end{pmatrix} + \frac{\alpha^2}{4}\left[\frac{1}{z},\frac{1}{\bar{z}}\right]dz\wedge d\bar{z}\begin{pmatrix} 1 & 0 \\ 0 & 1 \end{pmatrix}. \tag{15}$$

In the commutative limit, this can be regarded as the curvature of the spacetime where the point particle with mass $-\alpha/(8G)$ is located at the origin (where G is the Newton constant) [5]. For an arbitrary value of θ, however, the Abelian part remains; its interpretation is difficult, as for a theory of gravity.

5 Difficulties in noncommutative gravity II

In the matrix form, the local Lorentz transformation can be expressed as

$$e' = U^{-1}eU, \qquad \omega' = U^{-1}\omega U + U^{-1}dU, \tag{16}$$

where $UU^{-1} = 1$.

Under these transformation, $\mathcal{T}$ and $\mathcal{R}$ becomes

$$\mathcal{T}' = U^{-1}\mathcal{T}U, \qquad \mathcal{R}' = U^{-1}\mathcal{R}U. \tag{17}$$

Then the equations of motion $\mathcal{T} = \mathcal{R} = 0$ is unchanged.

On the other hand, the local translations can be written as

$$e' = e + d\rho + \omega\rho - \rho\omega, \qquad \omega' = \omega, \tag{18}$$

Under these transformation, $\mathcal{T}$ and $\mathcal{R}$ becomes

$$\mathcal{T}' = \mathcal{T} + \mathcal{R}\rho - \rho\mathcal{R}, \qquad \mathcal{R}' = \mathcal{R}. \tag{19}$$

The equations of motion $\mathcal{T} = \mathcal{R} = 0$ is unchanged also by the translation.

Therefore, we can construct vacuum solutions as pure gauge. The matrices which satisfy $UU^{-1} = 1$ take the form (modulo rigid rotations)

$$U = \begin{pmatrix} S & 0 \\ P & S^{-1} \end{pmatrix}, \qquad U^{-1} = \begin{pmatrix} S^{-1} & P \\ 0 & S \end{pmatrix}, \tag{20}$$

where $SS^{-1} = 1$, $S^{-1}S = 1 - P$, $P^2 = P$, and $SP = PS^{-1} = 0$ are required.

Then the pure-gauge connection is

$$\omega_g = U^{-1}dU = \begin{pmatrix} S^{-1} & P \\ 0 & S \end{pmatrix}\begin{pmatrix} dS & 0 \\ dP & dS^{-1} \end{pmatrix} = \begin{pmatrix} S^{-1}dS + PdP & PdS^{-1} \\ SdP & SdS^{-1} \end{pmatrix}, \tag{21}$$

Unfortunately, this includes the Abelian part in general ($\mathrm{Tr}\omega$). Thus the interpretation of this type of solutions is also unclear in a theory of gravity.

6 A solution with a torsional source

Now we choose

$$e = \frac{i}{2}\left\{d\tau + \frac{GS}{2i}\left(\frac{1}{z}dz - \frac{1}{\bar{z}}d\bar{z}\right)\right\}\begin{pmatrix} 1 & 0 \\ 0 & -1 \end{pmatrix} + \frac{i}{2}\begin{pmatrix} 0 & dz \\ d\bar{z} & 0 \end{pmatrix}, \tag{22}$$

where S is a constant and $\omega = 0$.

Then we obtain

$$\mathcal{T} = \frac{GS}{4\theta} |0\rangle\langle 0| \, d\bar{z} \wedge dz \begin{pmatrix} 1 & 0 \\ 0 & -1 \end{pmatrix}, \qquad \mathcal{R} = 0. \tag{23}$$

In the commutative limit, this corresponds to the solution obtained by Deser, Jackiw and 't Hooft [5] in the case of the mass of the point particle is zero. For a finite θ, the torsional source has a finite extension.

This one-body solution can be generalized to the N-body solution,

$$e = \frac{i}{2}\left\{ d\tau + \sum_{a=1}^{N} \frac{GS_a}{2i}\left(\frac{1}{z - z_a} dz - \frac{1}{\bar{z} - \bar{z}_a} d\bar{z} \right) \right\} \begin{pmatrix} 1 & 0 \\ 0 & -1 \end{pmatrix} + \frac{i}{2} \begin{pmatrix} 0 & dz \\ dz & 0 \end{pmatrix}, \tag{24}$$

where z_a, $\bar{z}_a$ and S_a are constants and $\frac{1}{z-z_a}$ and $\frac{1}{\bar{z}-\bar{z}_a}$ are defined by

$$\frac{1}{z - z_a} = \sum_{m=0}^{\infty} {z_a}^m \left(\frac{1}{z}\right)^{m+1}, \qquad \frac{1}{\bar{z} - \bar{z}_a} = \sum_{m=0}^{\infty} \bar{z}_a^m \left(\frac{1}{\bar{z}}\right)^{m+1}. \tag{25}$$

7 Wave equation

Now we can write down a wave equation for a massless scalar field around one torsional source,

$$\left\{ -\partial_t^2 + 2\left(D_z D_{\bar{z}} + D_{\bar{z}} D_z\right) \right\} \phi = 0, \tag{26}$$

where

$$D_z \equiv \partial_z - \frac{GS}{2i} \frac{1}{z} \partial_t, \qquad D_{\bar{z}} \equiv \partial_{\bar{z}} + \frac{GS}{2i} \frac{1}{\bar{z}} \partial_t. \tag{27}$$

Here we changed the signature into the Lorentzian one.

Solving the noncommutative differential equation, we will analyze the wave scattering by the torsional source. The scattering process is nontrivial for a small impact parameter $\approx \sqrt{\theta}$. The investigation of the wave scattering will be reported elsewhere[6].

8 Open problems

- How can the Abelian fields in this formalism have certain meanings in a theory of gravity?
- How can we obtain 'conical' (*i.e.* massive) solution?
- How can we take global properties of spacetime into account? How and when do we have to use a nonocommutative torus and sphere?

References

[1] M. R. Douglas and N. A. Nekrasov, Rev. Mod. Phys. **73** (2001) 977, `hep-th/0106048`.

[2] V. P. Nair, `hep-th/0112114`.

[3] M. Bañados, O. Chandía, N. Grandi, F. A. Shaposnik, and G. A. Silva, Physical Review **D64** (2001) 084012.

[4] S. Cacciatori, D. Klemm, L. Martucci, and D. Zanon, `hep-th/0201103`.

[5] S. Deser, R. Jackiw, and G. 't Hooft, Annals of Physics (NY) **152** (1984) 220.

[6] K. Shiraishi *et al.*, in preparation.

Nonlinear regime of gravity in brane world

Hideaki, Kudoh [1]

Yukawa Institute for Theoretical Physics, Kyoto University,
Sakyo-ku, Kyoto 606-8502, Japan

Abstract

We investigate the nonlinear regime of the gravity in the Randall-Sundrum two branes model with the radius stabilization mechanism. As the stabilization model, we assume a single scalar field which has the potential in the bulk and the potential on each brane. We develop the formulation of the second order gravitational perturbations under the assumption of the static and axial-symmetric perturbation that is spherically symmetric in the 4-dimensional sense. We discuss the gravity on each brane induced by the matter on its own side, taking the limit of the large coupling of the scalar field interaction term on the branes. It is shown using the Goldberger-Wise stabilization model that the 4-dimensional Einstein gravity is approximately recovered in the second order perturbations.

1 Introduction

Recently, theories with extra-dimensions attract considerable attention from the viewpoint of a solution to the hierarchy problem [1, 2, 3] [4, 5]. The main idea to resolve the large hierarchy is that the large physical volume of extra dimensions generates the small coupling of 4-dimensional gravity. The model that was introduced by Randall and Sundrum (RS) is particularly attractive. The RS two branes model is constructed in a 5-dimensional Anti-de-Sitter (AdS) spacetime [2];

$$ds^2 = dy^2 + e^{-2|y|/\ell}\eta_{\mu\nu}dx^\mu dx^\nu . \tag{1}$$

The fifth coordinate y is compactified on S^1/Z_2, and the positive and the negative tension branes are on the two fixed points. It is assumed that all matter fields are confined on each brane and only the gravity propagates freely in the 5-dimensional bulk. In this model, the hierarchy problem is resolved on the brane with the negative tension if the separation of the branes is about 37 times the AdS radius.

A significant point in discussing the consistency of this model is whether the 4-dimensional Einstein gravity is recovered on the brane from 5-dimensional Einstein gravity in the bulk [6, 7, 8, 9, 10, 11, 12]. Another point is to give a so-called radius stabilization mechanism that works to select the required separation distance between two branes to resolve the hierarchy without fine tunings [13, 14, 15]. The stabilization mechanism is not only important to guarantee the stable hierarchy, but also plays an important roll in the recovery of the 4-dimensional Einstein gravity in the linear order [7, 12] and of the correct cosmological expansion. The discussion on the recovery is almost independent of the detail of the stabilization model. The essence of the recovery in linear perturbations is that the massless mode of the scalar-type gravitational perturbation disappears due to the bulk scalar field, and only the tensor-type perturbation remains to have a massless mode.

Many authors have studied some aspects of the gravity in the brane world model [16, 17, 18, 19, 20, 21, 22, 23] . Although the model does not have a drawback in the linear perturbation, it is not trivial whether the second order gravitational perturbation works as well. As for the second order perturbation in the RS single brane model without bulk scalar field, where the tension of the brane is positive, it was confirmed that there is no observable disagreement with 4-dimensional Einstein gravity [24, 25]. However the setting of the RS two brane model with the stabilization mechanism is quite different from the single brane model, and furthermore we are mainly concerned with the gravity on the negative tension brane. Thus we study the second order gravitational perturbation of the RS two branes model with the stabilization mechanism due to a bulk scalar field. To simplify the analysis, we consider the static

[1] E-mail:kudoh@yukawa.kyoto-u.ac.jp

and axisymmetric configurations, which means that the metric on the branes is spherically symmetric. Furthermore, we take the limit that the coupling of the scalar field interaction term on each brane is very large. In this limit, we find that the 4-dimensional Einstein gravity is approximately recovered.

2 Perturbation Equations

We consider the RS two branes model with a 5-dimensional scalar field introduced to stabilize the distance between the two branes. The unperturbed metric is supposed to be

$$ds^2 = dy^2 + a^2(y)\eta_{\mu\nu}dx^\mu dx^\nu\,, \tag{2}$$

where $\eta_{\mu\nu}$ is the 4-dimensional Minkowski metric with $(-\,+\,+\,+)$ signature. The y direction is bounded by two branes located at $y = y_+$ and $y = y_-$, whose tensions are assumed to be positive and negative, respectively, and we adopt the convention $y_+ < y_-$. To generate the hierarchy between Planck and electroweak scales, we need $a_+/a_- \sim 10^{16}$, where $a_\pm \equiv a(y_\pm)$.

In this paper we investigate the gravity induced by non-relativistic matter fields confined on each brane whose energy-momentum tensor is given in the perfect fluid form

$$T_{\pm\,\nu}^{\ \mu} = a_\pm^{-4}\,\mathrm{diag}\{-\rho_\pm, P_\pm, P_\pm, P_\pm\}. \tag{3}$$

The warp factor in the definition of the energy-momentum tensor (3) is incorporated by the following reason. In the present analysis, we adopt the normalization that any physical quantities are always mapped onto and measured by the length scale at $y = y_+$. Since a length scale is warped by a warp factor $a(y)$, the physical quantities such as ρ_- and P_- are scaled by a factor a_-^{-4}.

To simplify the analysis, we restrict our consideration to the static and axisymmetric spacetime whose axis of symmetry lies along y direction. We denote the perturbed metric by $\tilde{g}_{ab} = g_{ab} + h_{ab}$. The 4-dimensional perturbation $h_{\mu\nu}$ is divided into the trace part and the transverse-traceless (TT) part. According to this decomposition, we assume that the perturbed metric has the diagonal form,

$$ds^2 \;=\; e^{2Y}dy^2 + a^2(y)\left[-e^{A-\psi}dt^2 + e^{B-\psi}dr^2 + e^{C-\psi}r^2d\Omega^2\right]. \tag{4}$$

Here A, B, and C correspond to the TT part, and ψ to the trace part. The TT condition at the linear order is given in terms of A, B, and C as

$$\begin{aligned} A^{(1)}(r,y) &= -\frac{1}{r^2}\partial_r(r^3B^{(1)}(r,y))\,, \\ C^{(1)}(r,y) &= \frac{1}{2r}\partial_r(r^2B^{(1)}(r,y))\,, \end{aligned} \tag{5}$$

where we have expanded the metric functions up to the second order as

$$A = \sum_{J=1,2} A^{(J)}. \tag{6}$$

The other metric functions, Y and ψ, are expanded in the same way. We impose the same conditions as Eq. (5) on $A^{(2)}$, $B^{(2)}$ and $C^{(2)}$ so that $B^{(J)}$ and $C^{(J)}$ are derived from $A^{(J)}$ once it is solved. The second order counter part of the condition (5) does not mean that $A^{(2)}$ is the transverse-traceless perturbation, but we extensively refer to these metric functions as the TT part and ψ as the trace part. By solving the Einstein equations, Y coincides with ψ in the linear perturbation, and then this metric assumption is the same at least in the linear perturbation as the "Newton gauge" condition.

The Lagrangian for the bulk scalar field is

$$\mathcal{L} = -\frac{1}{2}\tilde{g}^{ab}\tilde{\varphi}_{,a}\tilde{\varphi}_{,b} - V_B(\tilde{\varphi}) - \sum_{\sigma=\pm} V_{(\sigma)}(\tilde{\varphi})\delta(y - y_\sigma)\,, \tag{7}$$

where V_B and $V_{(\pm)}$ are the potential in the bulk and that on the respective brane. For most of the present analysis, we do not need to specify the explicit form of the potentials V_B and $V_{(\pm)}$. The scalar field is expanded up to the second order as

$$\tilde{\varphi}(r,y) = \phi_0(y) + \varphi^{(1)}(r,y) + \varphi^{(2)}(r,y)\,, \tag{8}$$

where ϕ_0 is the background scalar field configuration, which depends only on y.

From 5-dimensional Einstein equations with the cosmological term Λ and the equation of motion for the scalar field, we obtain background equations as

$$\begin{aligned} \dot{H}(y) &= -\frac{\kappa}{3}\dot{\phi}_0^2(y), \\ H^2(y) &= \frac{\kappa}{6}\Big(\frac{1}{2}\dot{\phi}_0^2(y) - V_B(\phi_0(y)) - \kappa^{-1}\Lambda\Big), \\ \ddot{\phi}_0(y) &+ 4H(y)\dot{\phi}_0(y) - V_B'(\phi_0(y)) = 0, \end{aligned} \tag{9}$$

where $H(y) := \dot{a}(y)/a(y) (\approx -\sqrt{-\Lambda/6})$ and the 5-dimensional Newton's constant is $G_5 = \kappa/8\pi$. An overdot denotes differentiation with respect to y.

From (r,r), (θ,θ) and (r,y) components of the Einstein equations, we obtain two independent equations:

$$\psi^{(J)}(r,y) = Y^{(J)} + \epsilon^{(J)}\Delta^{-1}S_\psi\,, \tag{10}$$

$$\varphi^{(J)}(r,y) = \frac{3}{2\kappa\dot{\phi}_0 a^2}\partial_y(a^2Y^{(J)}) + \frac{3}{2\kappa\dot{\phi}_0}\epsilon^{(J)}\Big[S_\varphi + \partial_y\Delta^{-1}S_\psi\Big]. \tag{11}$$

where $\Delta \equiv \sum_{i=1}^{3}\partial_i^2$. Here S_ψ and S_φ are the second order source terms that are constructed from the first order quantities [26]. We have introduced a symbol $\epsilon^{(J)}$ that is defined by $\epsilon^{(1)} = 0$ and $\epsilon^{(2)} = 1$ to represent the first and the second order equations in a single expression.

The equations for $A^{(J)}$ and $Y^{(J)}$ are obtained from (r,r) and (y,y) components of Einstein equations as

$$\Big[\frac{1}{a^2}\partial_y a^4 \partial_y \frac{1}{a^2} + \frac{1}{a^2}\Delta\Big](a^2A^{(J)}) = \epsilon^{(J)}S_A\,, \tag{12}$$

$$\Big[a^2\dot{\phi}_0^2\partial_y\frac{1}{a^2\dot{\phi}_0^2}\partial_y a^2 - \frac{2\kappa}{3}a^2\dot{\phi}_0^2 + \Delta\Big]Y^{(J)} = \epsilon^{(J)}S_Y\,. \tag{13}$$

Here S_A and S_Y are the second order source terms.

3 Recovery of the 4D Einstein gravity

We can solve the equations for A and Y by means of the Green function. As for A, the Green function is composed of the massless part and massive (Kaluza-Klein) part, and then the massless mode gives the long-ranged force in contrast to the massive mode that corresponds to the short-ranged force. As for Y, there is no massless mode due to the stabilization mechanism. To evaluate the massive modes for A and Y, we apply a kind of derivative expansion method, in which the typical wavelength of perturbations is supposed to be long. In our configuration, the expansion is valid only when the smallest mass of the KK excitations is sufficiently large. The details of the discussion is given in [26], and we give only the result that we have obtained in the paper.

It is shown that short-ranged mode of $A^{(1)}$ are suppressed by the factor

$$\beta_\pm = \frac{\ell^2}{a_\pm^4 r_\star^2} = \begin{cases} \dfrac{\ell^2}{r_\star^2}, & (y = y_+)\,, \\ \Big(\dfrac{0.1mm}{r_\star}\Big)^2\Big(\dfrac{10^{-16}}{a_-}\Big)^4\Big(\dfrac{\ell}{\ell_{Pl}}\Big)^2, & (y = y_-), \end{cases} \tag{14}$$

where we introduced a typical length scale $r_\star$. We attached a subscript $\pm$ to specify in which case we are working. The suppression factor for the scalar-type perturbation $Y^{(1)}$ is given by

$$\gamma_\pm = \beta_\pm\Big(\frac{1}{\tilde{m}_S\ell}\Big)^2. \tag{15}$$

Here $\tilde{m}_S$ is the radion mass and its order is evaluated as $O(\ell^{-1})$. The correction terms of the second order perturbation are evaluated and represented by using these suppression factors.

It is shown that the 4-dimensional Einstein gravity is approximately recovered even in the second order perturbations. In the isotropic gauge, the temporal component is evaluated on the negative tension brane as

$$\Delta\tilde{A}_{-}^{(2)}(r,y_{-}) = 8\pi G(\rho_{-}^{(2)} + 3P_{-}^{(2)}) - 4\Phi_{-}\Delta\Phi_{-} + O\left(\frac{\beta_{-}\Phi_{-}^{2}}{r_{*}^{2}}\right), \tag{16}$$

and the spatial component is

$$\Delta\tilde{B}^{(2)}(r,y_{-}) = -8\pi G\rho_{-}^{(2)} + 4\Phi_{-}\Delta\Phi_{-} - (\Phi_{-,r})^{2} + O\left(\frac{\beta_{-}\Phi_{-}^{2}}{r_{*}^{2}}\right), \tag{17}$$

where $\Phi_{\pm}(r)$ is the Newton potential. These are identical to the result for the 4-dimensional Einstein gravity in the isotropic coordinates except for the correction term [24]. The analysis of the case with the matter fields on the positive tension brane is also given in [26].

4 Summary

We have considered the second order gravitational perturbations in the RS two branes model with the radius stabilization mechanism. As a model for the radius stabilization, we have assumed a scalar field that has the potential in the bulk and the potential on the brane. From the 5-dimensional Einstein equations, the master equations for the TT part of the metric perturbations and for the scalar-type perturbation are derived assuming static axisymmetric configuration.

We have shown the recovery of the 4-dimensional Einstein gravity in the second order perturbations in the following simplification [26]. First, we assumed that the coupling between the scalar field and the branes is infinitely large. Second, we consider the perturbations induced by the matter fields on one brane where we reside, and neglect the effects caused by the matter fields on the other brane.

When we consider the case in which the matter fields are on the negative tension brane, the correction to the 4-dimensional Einstein gravity appears at the relative order of $O((a_{+}/a_{-})^{4}(\ell/r_{*})^{2})$, where ℓ is the AdS curvature scale, r_{*} is the typical length scale of the perturbation and (a_{+}/a_{-}) is the ratio between the warp factors on the positive and the negative tension branes. When this ratio (a_{+}/a_{-}) is $O(10^{16})$, the hierarchy between Planck and electro-weak scales can be explained. With this choice of the hierarchy, the correction to the metric in the linear perturbation becomes comparable to the usual Newtonian potential when $r_{*} \lesssim 0.1$mm. However, this correction does not give contribution to the force outside the matter distribution. Hence, it seems to be harmless to reproduce the predictions of the 4-dimensional Einstein gravity. We have not confirmed if this feature remains in the second order perturbation, but the correction is suppressed by the above factor compared to the usual post-Newtonian correction. Hence, the effect due to this correction is almost impossible to detect.

When we consider the case in which the matter fields are on the positive tension brane, the correction to the 4-dimensional Einstein gravity in the linear perturbation appears at the relative order of $O((\ell/r_{*})^{2})$. While the correction in the second order perturbation is $O((a_{+}/a_{-})^{2}(\ell/r_{*})^{2})$ compared to the usual post-Newtonian terms. Hence, it seems that the deviation from the 4-dimensional Einstein gravity appears at a larger scale in the second order perturbation. However, this is very likely to be an artifact due to the limitation of our approximation scheme.

To give a complete proof of the recovery of the 4-dimensional Einstein gravity, further extension of the present analysis will be necessary. Here we considered the large coupling limit. It will be interesting to evaluate the correction depending on the coupling strength [27].

References

[1] N. Arkani-Hamed, S. Dimopoulos and G. R. Dvali, Phys. Lett. B **429**, 263 (1998); I. Antoniadis, N. Arkani-Hamed, S. Dimopoulos and G. R. Dvali, Phys. Lett. B **436**, 257 (1998)

[2] L. Randall and R. Sundrum, Phys. Rev. Lett. **83**, 3370 (1999)

[3] L. Randall and R. Sundrum, Phys. Rev. Lett. **83**, 4690 (1999)

[4] J. Lykken and L. Randall, JHEP **0006**, 014 (2000)

[5] S. Mukohyama, Phys. Rev. D **63**, 044008 (2001)

[6] J. Garriga and T. Tanaka, Phys. Rev. Lett. **84**, 2778 (2000)

[7] T. Tanaka and X. Montes, Nucl. Phys. B **582**, 259 (2000)

[8] T. Shiromizu, K. I. Maeda and M. Sasaki, Phys. Rev. D **62**, 024012 (2000)

[9] M. Sasaki, T. Shiromizu and K. I. Maeda, Phys. Rev. D **62**, 024008 (2000)

[10] S. B. Giddings, E. Katz and L. Randall, JHEP **0003**, 023 (2000)

[11] T. Tanaka, Prog. Theor. Phys. **104**, 545 (2000)

[12] S. Mukohyama and L. Kofman, arXiv:hep-th/0112115.

[13] W. D. Goldberger and M. B. Wise, Phys. Rev. Lett. **83**, 4922 (1999)

[14] W. D. Goldberger and M. B. Wise, Phys. Lett. B **475**, 275 (2000)

[15] O. DeWolfe, D. Z. Freedman, S. S. Gubser and A. Karch, Phys. Rev. D **62**, 046008 (2000)

[16] A. Chamblin and G. W. Gibbons, Phys. Rev. Lett. **84**, 1090 (2000).

[17] A. Chamblin, S. W. Hawking and H. S. Reall, Phys. Rev. D **61**, 065007 (2000).

[18] R. Emparan, G. T. Horowitz and R. C. Myers, JHEP**0001**, 007 (2000).

[19] C. Charmousis, R. Gregory and V. A. Rubakov, Phys. Rev. D **62**, 067505 (2000)

[20] C. Germani and R. Maartens, hep-th/0107011.

[21] T. Wiseman, hep-th/0111057.

[22] A. Lewandowski and R. Sundrum, hep-th/0108025.

[23] S. Mukohyama, arXiv:hep-th/0112205.

[24] H. Kudoh and T. Tanaka, Phys. Rev. D **64**, 084022 (2001)

[25] I. Giannakis and H. C. Ren, Phys. Rev. D **63**, 024001 (2001)

[26] H. Kudoh and T. Tanaka, hep-th/0112013.

[27] H. Kudoh and T. Tanaka, In preparation.

Quantum Radiation by Moving Boundary in Brane Universe

Izumi Tanaka[1] and Hideki Ishihara[2]

Department of Physics, Graduate School of Science, Osaka City University, Sumiyoshi, Osaka, 558-8585, Japan

Abstract

Embedded flat Friedmann-Robertson-Walker-brane universe in the five-dimensional anti-de Sitter spacetime is recognized as a moving boundary. The quantum effect of a conformal field resulting from the moving boundary is discussed.

1 Introduction

In this proceedings, we consider a dynamics of brane universe which is embedded in the five dimensional anti-de Sitter(AdS) bulk spacetime in the context of the Randall-Sundrum model with Z_2 symmetry[1]. (see fig.1) We can find Friedmann-Robertson-Walker(FRW) brane solution[2] where great changes of basic properties appear in the cosmological model. [3]

On the Z_2-symmetric brane universe, matter fields are confined to the brane, while gravitaitonal fields and possible scaler fields propagate through all of spacetime. Moreover, the brane evolves on the bulk spacetime through the process of expanding phase of universe. The brane behaves as moving boundary providing certain boundary condition for field living in the bulk spacetime.

If we recognize these brane as moving boundary for a field in the bulk spacetime[4], there are two possible effects. One effect is the observer on the brane may suffer the state of an effective thermal bath which relates to Unruh[5] effect, and the other effect directly corresponds to moving mirror radiation.[6] These effects would have some influence in the cosmology.

2 Brane Dynamics

Let us consider a flat FRW universe embedded in the AdS bulk spacetime with the metric:

$$ds_5^2 = -\frac{r^2}{l^2}dt^2 + \left(\frac{r^2}{l^2}\right)^{-1} dr^2 + r^2 d\Omega_3^2 \,. \tag{1}$$

If matter is confined on the brane, the surface energy-momentum tensor of the brane, S_{ab}, has a form of

$$S_{ab} = -\sigma\gamma_{ab} + T_{ab}, \quad (a,b = 0,1,2,3), \tag{2}$$

where γ_{ab} is the induced metric on brane, σ is a constant which characterizes the brane tension, and T_{ab} is the energy-momentum tensor of matter on brane. Since self-gravitating brane in the five-dimensional bulk spacetime should satisfy the metric junction condition with Z_2 symmetry, the extrinsic curvature of brane, K_{ab}, satisfies

$$K_{ab} = -\kappa^2 \frac{1}{2}(S_{ab} - \frac{1}{3}S\gamma_{ab}), \tag{3}$$

where κ^2 is the five-dimensional gravitational constant. From eq.(3) with eq.(2), we obtain the modified Friedmann equation[2] and the conservation given by

$$\left(\frac{1}{a}\frac{da}{d\tau}\right)^2 = \frac{8\pi}{3}\frac{\kappa^4\sigma}{6}\rho + \frac{\kappa^4}{36}\rho^2 \,, \tag{4}$$

[1] E-mail:itanaka@sci.osaka-cu.ac.jp
[2] E-mail:ishihara@sci.osaka-cu.ac.jp

and

$$\frac{d}{d\tau}\left(\rho a^3\right) + p\frac{d}{d\tau}(a)^3 = 0\,, \tag{5}$$

where τ is proper time along the brane.

From the above equation, flat FRW universe evolves on bulk spacetime. The typical trajectory of FRW universe and Randall Sandrum model are shown together as fig.1.

As shown in fig.1, Randall-Sandrum model has a trajectory of a constant acceleration in AdS. Flat FRW universe has the 3 phases of motion in AdS. In the 1st phase of early stage from the Big bang, the brane starts along null direction. In the 2nd phase, the brane universe evolves with greatly changing acceleration. In the 3rd phase, its motion can be regarded as uniform acceleration.

3 Quantum Radiation by the Brane

We simplify the problem: Consider
(1)2-dimensional bulk spacetime with the metric

$$ds^2 = -\frac{r^2}{l^2}[-dt^2 + d\varsigma^2]\,,\ d\varsigma^2 = \left(\frac{l^2 dr}{r^2}\right)^2\,. \tag{6}$$

(2) Conformal invariant massless scaler field living in the bulk spacetime which satisfying the following equation:

$$\Box\Phi = 0\,. \tag{7}$$

(3) Direchret boundary condition

$$\Phi(t,\ a(t)) = 0\,, \tag{8}$$

on the brane whose motion $\varsigma = a(t)$ is governed by[3]

$$\left(\frac{da}{dt}\right)^2 = \frac{a^4}{l^2}\left[1 - \frac{a^2}{l^2}\left\{\frac{a^2}{l^2} + \alpha^2 a^{-2} + \beta^2 a^{-6}\right\}^{-1}\right]\,, \tag{9}$$

where α and β are constants, and this equation is another expression of (4).

Next we will calculate the energy momentum tensor radiated from the brane. We follow the regularization of the energy-momentum tensor by Fulling and Davies [6].

The solution for eq.(7) satisfying the boundary condition eq.(8) is given as:

$$\psi_k = \exp\left[-ik(t+\varsigma)\right] - \exp\left[-ikp(t-\varsigma)\right]\,, \tag{10}$$

where $p(t-\varsigma)$ is a function which is determined by the boundary trajectory. Then field operator can be expressed as follows:

$$\Phi = \textstyle\sum_k [a_k\psi_k + a_k^\dagger\psi_k^*]\,, \tag{11}$$

where a_k and $a_k^\dagger$ are the annihilation and creation operators, respectively. Here, we set the Randall-Sundrum vacuum where $t = const.$ i.e.

$$a_k\,|\,0\,\rangle = 0 \text{ for } p(t-\varsigma) = t-\varsigma. \tag{12}$$

Then, expectation values of energy momentum tensor is given as follows [6]:

$$\langle 0_{00}\rangle = -\langle 0_{01}\rangle = (12\pi)^{-1}\left[p'(u)\right]^{1/2}\left\{p'(u)^{-1/2}\right\}''\,, u = t-\varsigma \tag{13}$$

The curvature of the bulk spacetime makes vanishing contribution to the energy-momentum tensor.

The solution for eq.(9) is not a simple elementary function. Instead, we consider a model function $z(t) \propto \left\{\frac{1}{2}|-t+\sqrt{t^2+2l^3/\alpha}|\right\}^{-1}$ which has asymptotic behaviors

$$a \approx \frac{\alpha}{l}t,\quad t\to\infty\,, \tag{14}$$

$$a \approx -l\left(\frac{l}{t} - \frac{l^6}{2(2q-1)\beta^2}\left(\frac{t}{l}\right)^{-(2q-1)}\right), \quad t \to -\infty. \tag{15}$$

governed by eq.(9). This simplification might not change qualitative feature of $\langle\theta_{00}\rangle$. Using the model function, time evolution of energy-momentum tensor is given as fig.2. As shown in fig.2, the negative energy radiation phase is followed by positive energy radiation phase.

4 Conclusion

From above calculation, we summarize the results as follows:

In the 1st and the 3rd phases, the brane radiates small amount of energy, In 2nd phase, the brane first radiates the negative energy, and next radiates positive energy. The brane stirs the bulk with energy.

In addition, as l becomes smaller, the time scale of the curve shown in fig.2 becomes larger. This dependence suggests that the larger value of the Λ_5, the smoother the in and out of the heat on the brane.

There are several problem to be solved:

1)We have only made a qualitative evaluation of $\langle\theta_{00}\rangle$. We should make a quantitative evaluation of $\langle\theta_{00}\rangle$, and consider the back reaction.

2)We assume the Direchret boundary condition for simplicity, and for Neumann boundary condition result is qualitatively same. In reality, the boundary depends on the interaction between the brane and the fields living in the bulk spacetime, and we must take this into the consideration.

3)We have to extend our discussion from 2-dim to 5-dim for further understanding.

4)In the above discussion, we evaluate the energy-momentum tensor with conformal invariant vacuum. There might be alternative choice of vacuum. [7]

References

[1] L. Randall and R. Sundrum, Phys. Rev. Lett. **83,** 4690 (1999)

[2] P.Binétruy, C.Deffayet, D.Langlois, Nucl. Phys. B **565**, 269 (2000); C. Csáki, M. Graesser, C. Kolda, J. Terning, Phys. Lett. **B462**, 34 (1999); J.M. Cline, C.Grosjean, G.Servant, Phys. Rev. Lett. **83**, 4245 (1999); P. Binétruy, C. Deffayet, U. Ellwanger and D. Langlois, Phys.Lett. B **477**, 285 (2000); D. Ida, JHEP, **0009**, 014 (2000).

[3] H. Ishihara, Phys. Rev. Lett. **86,** 381 (2001); gr-qc/0107085

[4] D. S. Gorbunov, V. A. Rubakov, and S. M. Sibiryakov, hep-th/0108017; S. Alexander, Y. Ling, and L. Smolin, hep-th/0106097; C. Deffayet, G. Dvali, and G. Gabadadze, astro-ph/0105068; A. Chamblin, A. Karch, and A. Nayeri, hep-th/0007060.

[5] W. G. Unruh. Phys. Rev. **D14,** 870 (1976).

[6] P. C. W. Davies and S. A. Fulling, Proc. R. Soc. London **A348,** 393 (1976); **A354,** 59 (1977); N. D. Birrell and P. C. W. Davies, Quantum Fields in Curved Space (Cambridge University Press, Cambridge, 1982).

[7] S. Deser and O. Levin, Class. Quantum. Grav., **14,** L163 (1997); hep-th/9806223; S. J. Avis, C. J. Isham and D. Storey, Phys. Rev. **D18,**3565 (1978).

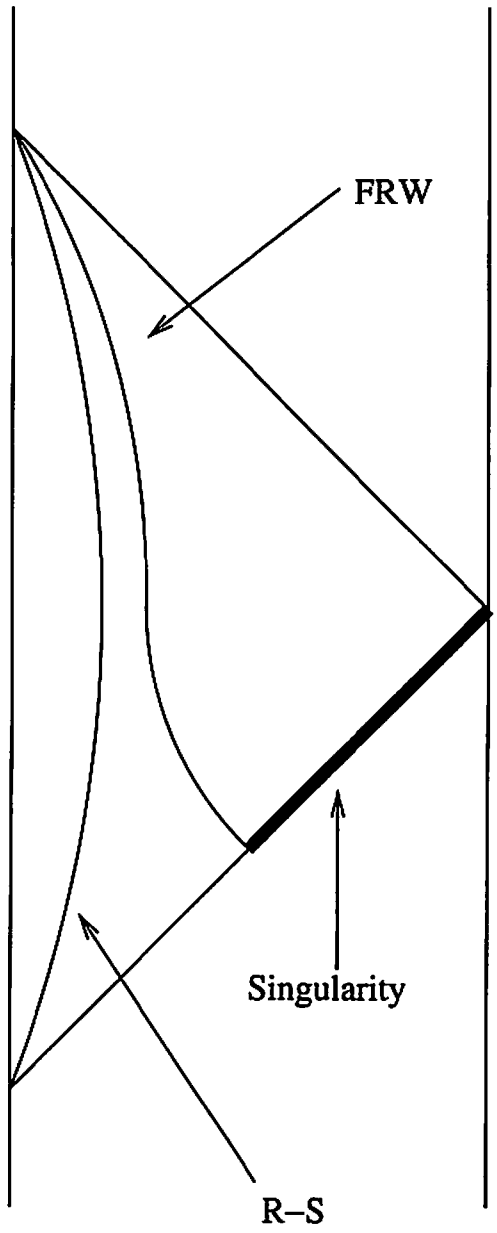

Figure 1: Conformal diagram of brane universe. Randall-Sundrum model and FRW brane universe are embedded in AdS bulk spacetime.

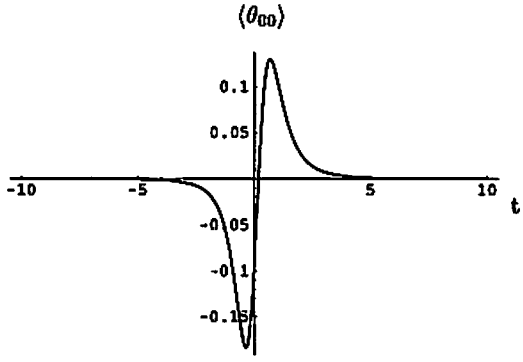

Figure 2: Time evolution of vacuum expectation value of energy momentum tensor.

New Frontiers in String Cosmology
— A Tryptich —

Nemanja Kaloper*

Department of Physics, Stanford University,
Stanford, CA 94305-4060, USA

Abstract

String theory is presently the best candidate for a quantum theory of gravity unified with other forces. It is natural to hope that applications of string theory to cosmology may shed new light on the cosmological conundra, such as singularities, initial conditions, cosmological constant problem and origin of inflation. However there are important conceptual and practical problems which must be addressed before applying string theory to cosmology. This talk concentrates on these problems, loosely having to do with *i*) definition, *ii*) applicability, and *iii*) detectability of string theory in cosmological setting.

1 Introduction

String theory is presently the best candidate for a quantum theory of gravity unified with other forces. It provides us with a framework which is on the one hand manifestly quantum-mechanical, and on the other hand it contains spin-2 massless graviton, and therefore gravitational interaction, among the degrees of freedom comprising the massless spectrum of the theory. Hence the notions of "quantum" and "gravity" peacefully coexist in string theory.

It is therefore natural to hope that applications of string theory to cosmology may shed new light on the open cosmological problems and puzzles, such as singularities, initial conditions, cosmological constant problem and origin of inflation. However the progress in these directions has been slow and difficult. In a manner of speaking, string cosmology is a theory in the making. The main obstacles to more rapid development are important conceptual and practical problems which must be addressed before applying string theory to cosmology. In this talk, we will discuss the problems of background dependence and event horizons as pertaining to *definition* of string theory in cosmology, the *applicability* of string theory at low scales where most of cosmology unravels, and the challenges for *detectability* of short-distance string physics at extremely large distance scales where cosmological observations are normally made.

2 Cosmic Acceleration ... Or Not

• How do we *define* string theory in a cosmological setting?

Thus far we have failed to include interesting cosmological backgrounds within the framework of the controllable mathematics of string theory [1]. In particular no deSitter space backgrounds have been found which could serve as models of the currently accelerating universe [4]. In this section we will discuss a possible reason why accelerating backgrounds have not been found. We will also see the same reasons would preclude eternal quintessence-like behavior. Assuming that these arguments can be put on a firm footing and that observation continues to suggest that the universe is presently accelerating, a serious crisis between theory and observation may materialize. We will discuss one possible way to resolve the crisis, where the universe is really not accelerating, while the observations are accounted for by a quantum-mechanical dimming of distant supernovae.

We stress that we do not want to claim that deSitter space or quintessence is impossible. Rather, the current mathematical framework of string theory may not be the right one for cosmology. Such views

*E-mail:kaloper@stanford.edu

have also been forcefully expressed by Banks [5]. We will argue that this is part of a pattern that effects not only those theories with positive cosmological constants but also any geometry with a future horizon. As we will see this includes quintessence-dominated universes [2, 3].

Just as the degrees of freedom of string theory are specific to each background, so are the "observables" that string theory allows us to compute. In asymptotically flat space-time string theory is a prescription for calculating S-matrix elements relating asymptotically free particle states. As far as we know, these S-matrix elements are the only rigorously defined quantities of the theory. The S-matrix data consists of a list of all the stable objects in the theory and the transition amplitudes between asymptotic states of these objects. One essential requirement for the existence of an S-matrix is to have an asymptotically large space at infinity in which degrees of freedom can separate into a collection of non-interacting particles.

AdS space is another example in which observables of string theory have been identified, namely the boundary correlators of bulk fields. These boundary correlators are very similar to S-matrix elements and again rely on an infinite asymptotic space in which the bulk degrees of freedom can separate into free particles. Neither asymptotically flat space-time nor AdS space provides a realistic framework for cosmology. A more relevant example is the familiar FRW cosmologies, such as in matter- or radiation-dominated universe. It is quite evident that closed FRW spaces which begin and end with singularities, eg bangs and crunches, do not permit asymptotically free particles. Thus, with the present concepts available in string theory it is not known how to formulate the theory in such a background.

Flat-space FRW is not much better in the initial state but the final states are describable in terms of asymptotically free particles. A possible framework for cosmology has been suggested by Witten [6]. The idea is to assume that the initial state of the universe is unique, $|U\rangle$. The final state consisting of free asymptotically well separated particles would be described in terms of a Fock space of asymptotic out-fields. The S-matrix would then be replaced by an S-vector describing the final state amplitudes. In this case correlation functions of (almost) asymptotic fields could be measured by observers stationed at different points. Furthermore in flat FRW space, every set of points has at least one point in the causal future of the set. In other words it is possible to send signals from every point in the set to a common point where the data is collected and correlated. Thus the S-vector would have operational meaning.

On the other hand, if the universe is accelerating, the situation is entirely different. The prototype example is deSitter space. The deSitter geometry has a space-like causal boundary which represents the infinite inflated future (IIF). This leads to fundamental conceptual differences between deSitter and decelerating FRW models. To see this, consider two events or measurements at points a and b in each geometry. If the events are too close to the IIF then the causal futures of these two points do not have any common points. In other words there is no possibility of collecting data from the two measurements. An implication of this is that correlations between quantities at a and at b are unmeasurable by any real observer. For this reason an S-matrix connecting the IIF to the IIP (infinitely inflated past) or to a unique big bang has no observable meaning.

There are related reasons for suspecting that string theory as we know it can not be defined in deSitter . All definitions of string theory involve taking the limit of infinitely many degrees of freedom. For example in its original form, string theory is defined in terms of 2-dimensional conformal field theories (CFTs). These theories can be thought of as the limiting behavior of regulated world sheet theories with finitely many degrees of freedom. The conformal limit is the limit of infinitely many degrees of freedom. Most quantities will not have limits as the regulator is removed. What we have learned is that the observables of string theory are just those quantities, namely on-shell S-matrix elements, which do have limits. Even these quantities will only have limits if the background target space geometry is suitably chosen so as to flow to a non-trivial fixed point. deSitter is not such a fixed point, eg as shown by Maldacena and Nunez [7].

On the other hand, the theory of quintessence [8, 9] has been put forward as an alternative to a positive cosmological constant. According to it the dark energy of the universe is dominated by the potential of a scalar field ϕ which is still rolling to its minimum at $V = 0$. Typically the minimum is at $\phi = \infty$ and the scalar potential may have a form such as

$$V(\phi) \sim \exp(-c\sqrt{\alpha'}\phi) \tag{2.1}$$

where ϕ is a canonically normalized scalar field and c is a numerical constant of order unity. The theory

can also be parameterized by an equation of state of the usual form

$$P = w\epsilon \tag{2.2}$$

where P and ϵ denote pressure and energy density. Recall that a cosmological constant corresponds to $w = -1$, matter domination to $w = 0$ and radiation dominance to $w = 1/3$. Quintessence gives rise to equations of state with $-1 < w < -1/3$. Taken at face value, the observational evidence for a cosmological constant is really a bound on w: $-1 < w_{observed} \lesssim -2/3$. Thus we are not yet forced to postulate a genuine nonvanishing cosmological constant. On the other hand, the eternal quintessence-dominated universes still have future horizons like deSitter space, and are no better suited to an S-matrix or S-vector description.

We now consider the spacetime geometry for $-1 < w < -1/3$ models. For simplicity, we consider in detail only the spatially flat cases ($k = 0$). The conclusions are qualitatively the same for the spatially curved cases as well. It is straightforward to solve the field equations for the $k = 0$ metric, which is

$$ds^2 = -dt^2 + a_0^2 \left(\frac{t}{t_0}\right)^{4/[3(1+w)]} \left(dr^2 + r^2 d\Omega_2\right). \tag{2.3}$$

To determine the causal structure of (2.3) we conformally map it on a part of the Einstein static universe (ESU) [10]. The ESU is a direct product of a spatial sphere S^3 of constant radius and an infinite time axis, with the metric $ds^2 = -d\tau^2 + d\chi^2 + \sin^2(\chi)d\Omega_2$ and so its causal structure is that of an infinite cylinder $R \times S^3$. Since (2.3) has a past singularity and becomes locally flat as $t \to \infty$, its map in ESU is bounded by precisely these regions. The mapping is given by rewriting the metric (2.3) in a form which is explicitly conformal to ESU

$$ds^2 = l^2 \Big(\frac{6(1+w)}{|1+3w|}\Big)^{4/|1+3w|} \frac{[\cos(\frac{\chi-\tau}{2})\cos(\frac{\chi+\tau}{2})]^{4/|1+3w|-2}}{4\,\sin^{4/|1+3w|}(|\tau|)} \Big(-d\tau^2 + d\chi^2 + \sin^2(\chi)d\Omega_2\Big) \tag{2.4}$$

and reading off the images of the boundaries from the transformation of coordinates:

$$\frac{|1+3w|}{6(1+w)} \left(\frac{t}{l}\right)^{|1+3w|/[3(1+w)]} = \Big(\tan(\frac{\chi-\tau}{2}) - \tan(\frac{\chi+\tau}{2})\Big)^{-1} \tag{2.5}$$

Using this, the future limit $t \to \infty$ for any given r maps on the line $\tan(\frac{\chi-\tau}{2}) = \tan(\frac{\chi+\tau}{2})$, which is the latitude circle $\tau = 0$ on the cylinder. The singularity resides in the limit $t \to 0$ for any fixed r, and so it maps onto the line $\tan(\frac{\chi-\tau}{2}) \to \infty$, or therefore $\tau = \chi - \pi$. This is the null semi-circle connecting the points $(-\pi, 0)$ and $(0, \pi)$ on the cylinder. Because the spacetime (2.3) ends there, we must discard the portion of the cylinder outside of these two lines. Unwrapping the remainder, we get the causal structure in Fig. 1.

All those universes which are described by (2.3) descend from a past null singularity, and evolve towards a future spacelike infinity. Any observer must have a future horizon: it is precisely the null line starting in the upper left corner of the diagram and flowing towards the singularity, and corresponds to the portion of the circle $\tau = \pi - \chi$ above the singular circle $\tau = \chi - \pi$. An observer would find the universe at any given finite time to be of finite size - she could only causally explore the interior of the diamond bounded by the horizon and the singularity. However, unlike in deSitter space, she would not lack elbow room in her box. The proper size of the horizon is not constant but grows in time,

$$L_H = a(t) \int_t^\infty \frac{dt'}{a(t')} = \frac{3(1+w)}{|1+3w|} t, \tag{2.6}$$

which shows that the volume of any spacelike hypersurface inside the causal diamond grows extremely large with time! In other words, the proper volume of the region of space near the upper left corner of the diagram in Fig. 1 is tremendously large, and since the horizon is moving away (2.6), it is getting even larger. This is easy to understand intuitively: even though the expansion of the universe (2.3) is accelerating, the acceleration rate decreases with time as $\ddot{a}/a \sim 1/t^2$. Thus at a later time it takes longer for the cosmic acceleration to increase the proper speed between comoving observers to the speed of light.

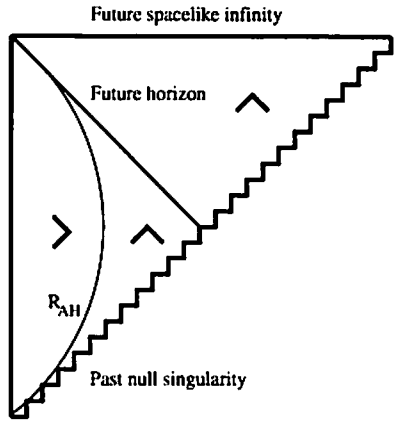

Figure 1: *Causal structure of a spatially flat Universe dominated by* $-1 < w < -1/3$ *matter.*

It is straightforward to show that inclusion of spatial curvature does not alter the structure of infinity which always contains spacelike portions. Hence observers always have future horizons. Further, the borderline case $w = -1/3$ is a hybrid of the previous two cases, in that its past is quintessential, with a past null singularity, and its future is similar to a usual FRW universe with a future null infinity. Since the spacetime has a past null singularity a future null infinity no comoving observer living in it will have a horizon.

Can a conventional string theory relax to a zero-energy supersymmetric vacuum while accelerating? In general this would require an involved analysis, and cannot be easily answered. However, there is a class of supersymmetric theories that can be readily investigated. Suppose that the cosmological evolution of a theory is dominated by a single modulus field, with a stable supersymmetric vacuum. The potential for such a field must satisfy the stability form $V(\phi) = 2(D-2)\left((D-2)(\partial_\phi W)^2 - \kappa^2(D-1)W^2\right)$ and the superpotential W must have a critical point where $\partial_\phi W = 0$ which is the supersmymmetric vacuum of the theory [11, 12]. Here D is the dimension of spacetime. In $4D$, this condition restricts the admissible potentials to the form

$$V = 8(\partial_\phi W)^2 - 12\kappa^2 W^2, \tag{2.7}$$

with $\kappa^2 = 8\pi/M_4^2$. If this potential is to have a zero-energy supersymmetric vacuum and to support $w = const$ quintessence-like evolution, then it must asymptotically have the form $V \sim \exp(-c\kappa\phi)$, where c must obey $|c| < \sqrt{2}$. This is inconsistent with (2.7). Indeed, if the theory is to give rise to an eternal $w = const$ quintessence universe while flowing towards the vacuum, the vacuum must be parameterized by $\phi \to \infty$. The superpotential which leads to such a form and *has* $\partial_\phi W \to 0$ as $\phi \to \infty$ can be expanded in a series of exponentials, with the leading term say

$$W = W_0 \exp(-\alpha\kappa\phi) \tag{2.8}$$

where α is just a number. This gives rise to a potential

$$V = 8W_0^2\kappa^2(\alpha^2 - \frac{3}{2})\exp(-2\alpha\phi), \tag{2.9}$$

with the required asymptotic form. However, potential must be positive, $V > 0$, giving $|\alpha| > \sqrt{\frac{3}{2}}$ and hence

$$|c| = 2|\alpha| > \sqrt{6}. \tag{2.10}$$

Therefore a theory which asymptotically flows towards a supersymmetric stable vacuum $\partial_\phi W = 0$ satisfying (2.7) cannot do so while accelerating!

Note that we could choose the form of V such that accelerated expansion is possible. However superpotentials required for this do not have any critical points $\partial_\phi W = 0$, and so the accelerating theory is not going towards a supersymmetric vacuum where $\partial_\phi W = 0$.

We stress that our analysis does not exclude inflation of the universe as a transient phenomenon. The universe could accelerate for a time and then switch to a stage of decelerated expansion, relaxing to a ground state. In this case the future infinity does not have spacelike portions, and there are no future horizons. Therefore this would not be in conflict with the current lore of string theory, but may require additional fine tunings over and above the current coincidences.

Another way out of this problem is if the universe is not accelerating, but some other phenomenon accounts for the observations [13]. The strongest evidence for the acceleration of the universe comes from the observations of type Ia supernovae at redshifts $0.5 < z < 1.7$, which appear dimmer than they would have been in a matter dominated universe. Hence a possible explanation is to say that at low energies dark energy, such as the cosmological constant or quintessence takes over the control of the evolution, accelerates the expansion and pushes supernovae farther away. An alternative may be to somehow obscure the lines of sight between us at the supernovae, and so prevent all of the light to be detected on Earth. A mechanism for such dimming of supernovae may be provided by an analogue of flavor oscillations. We will discuss here a model with an axion of mass $m \sim 10^{-10}$ eV, which couples to electromagnetism through the usual term $(a/4M)\tilde{F}F$ [13]. Hence this axion cannot be quintessence. Instead it leads to energy-dependent mixing of the photon and the axion in the presence of an external magnetic field B [15]; light traveling in inter-galactic magnetic fields can partially convert into axions, evading detection on Earth. A source would then appear fainter even if the Universe is not accelerating. Some uniform dark energy is still required to satisfy the large scale structure and cosmic microwave background constraints, but it need not lead to cosmological acceleration, e.g. with equation of state $p/\rho = -1/3$. Detailed analysis is given in [13, 14].

The axion-photon coupling is

$$\mathcal{L}_{int} = \frac{a}{M}\vec{E}\cdot\vec{B}\,, \tag{2.11}$$

where the scale M characterizes the strength of the axion-photon interactions. This induces a mixing between the photon and the axion [15, 16] in the presence of a background magnetic field $\vec{B}$, which permeates our Universe [17]. The photon whose electric field is parallel to $\vec{B}$ mixes with the axion, while the photon with electric field orthogonal to $\vec{B}$ remains unaffected by mixing. The evolution equations are, after rotating the coordinate axes such that the propagation is along the y-direction,

$$\left\{\frac{d^2}{dy^2} + \mathcal{E}^2 - \begin{pmatrix} 0 & i\mathcal{E}\frac{B}{M_L} \\ -i\mathcal{E}\frac{B}{M_L} & m^2 \end{pmatrix}\right\}\begin{pmatrix} |\gamma\rangle \\ |a\rangle \end{pmatrix} = 0 \tag{2.12}$$

where we Fourier-transformed the fields to the energy picture $\mathcal{E}$ and introduced the state-vectors $|\gamma\rangle$ and $|a\rangle$ for the photon and the axion. Here $B = \langle\vec{e}\cdot\vec{B}\rangle \sim |\vec{B}|$ is the averaged projection of the extra-galactic magnetic field on the photon polarization $\vec{e}$. We will assume that the averaged value of $\vec{B}$ is close to its observed upper limit, and take for the magnetic field amplitude $|\vec{B}| \sim$ few $\cdot\, 10^{-9}$ G [17, 18]. We can now define the propagation eigenstates by diagonalizing the mixing matrix in Eq. (2.12) and determine the conversion rate of photons into axions along the direction of propagation. In the limit $\mathcal{E}^2 \gg \lambda_i > m^2$, which covers all of the applications of interest to us, the photon survival probability $P_{\gamma\to\gamma} = |\langle\gamma(y_0)|\gamma(y)\rangle|^2$ is

$$P_{\gamma\to\gamma} = 1 - \frac{4\mu^2\mathcal{E}^2}{m^4 + 4\mu^2\mathcal{E}^2}\sin^2\left[\frac{\sqrt{m^4 + 4\mu^2\mathcal{E}^2}}{4\mathcal{E}}\Delta y\right], \tag{2.13}$$

and the mixing angle and the oscillation length are

$$\sin\theta = \frac{\mu\mathcal{E}}{\sqrt{\lambda_+^2 + \mu^2\mathcal{E}^2}}\,, \qquad L_O = \frac{4\pi\mathcal{E}}{\sqrt{m^4 + 4\mu^2\mathcal{E}^2}}\,. \tag{2.14}$$

In the limit $\mathcal{E} \gg m^2/\mu$, the mixing is maximal, while the oscillation length is completely independent of the photon energy: $\sin\theta \sim \frac{1}{\sqrt{2}}$, $L_O \sim \frac{2\pi}{\mu}$. Thus high-energy photons (including optical frequencies $\mathcal{E} \sim 10$ eV as we will see) oscillate achromatically. In contrast, in the low energy limit $\mathcal{E} \ll m^2/\mu$, the mixing is small, and the oscillation length is sensitive to energy: $\sin\theta \sim \frac{\mu\mathcal{E}}{m^2}$, $L_O \sim \frac{4\pi\mathcal{E}}{m^2}$. The oscillations

are very dispersive, but the probability to find axions $P_{\gamma\to a} = 1 - P_{\gamma\to\gamma}$ is tiny, bounded from above by $P_{\gamma\to a} < \sin^2(2\theta) \leq 4\mu^2\mathcal{E}^2/m^4$.

In our Universe the magnetic field is not uniform. Assuming that a typical domain size for the extra-galactic magnetic field is $L_{dom} \sim$ Mpc [17, 18], it is straightforward to numerically solve for the quantum mechanical evolution of unpolarized light in such magnetic domains with uncorrelated field directions. An analytic calculation shows that in the case of maximal mixing, with $\cos(\mu L_{dom}) > -1/3$, the survival probability is monotonically decreasing:

$$P_{\gamma\to\gamma} = \frac{2}{3} + \frac{1}{3}e^{-\Delta y/L_{decay}} \tag{2.15}$$

where in the relevant limit $\mu L_{\rm dom} \ll 1$ the inverse decay length is given by

$$L_{\rm decay} = \frac{8}{3\mu^2 L_{\rm dom}} \,. \tag{2.16}$$

Thus we see that with a random magnetic field the problem becomes essentially classical and after the traversal of many magnetic domains the system is equilibrated between the two photon polarizations and the axion. This leads to the generic prediction that on average one-third of all photons converts to axions after large traversed distances. We can now estimate the axion mass and coupling needed to reproduce SN observations. To take the oscillations into account, in the luminosity-distance v.s. redshift formula we should replace the absolute luminosity $\mathcal{L}$ by an effective one:

$$\mathcal{L}_{eff} = \mathcal{L}\, P_{\gamma\to\gamma} \,. \tag{2.17}$$

The optical photons must oscillate independently of their frequency. For them, the oscillations should reduce the flux of incoming photons by about 20% for SNe at $z \sim 0.5$. This requires $L_{\rm dec} \lesssim H_0^{-1}/2$. Thus the mass scale M for this should be $M \sim 4 \cdot 10^{11}$ GeV. This is within observational bounds for ultralight axions: the strongest bound comes from the SN1987A event, and is given by $M \geq 10^{11}$ GeV [19, 20].

If the microwave photons had fluctuated a lot in the extra-galactic magnetic field, their anisotropy would be very large due to the variations in the magnetic field. To avoid affecting the small primordial CMBR anisotropy, $\Delta T/T \sim 10^{-5}$, the axion mass should be large enough for the mixing between microwave photons and the axion to be small. In this limit, we can ignore the averaging over many random magnetic domains and simply treat each domain as a source of CMBR fluctuation. The photon-axion mixing and the oscillation length in that case are given by $\sin\theta \sim \frac{\mu\mathcal{E}}{m^2}$, $L_O \sim \frac{4\pi\mathcal{E}}{m^2}$. The disturbances of CMBR are controlled by the transition probability into axions $P_{\gamma\to a} \leq 4\frac{B^2\mathcal{E}^2}{m^4M^2}$. For microwave photons $\mathcal{E} \sim 10^{-4}$ eV, and so $P_{\gamma\to a} \leq 2.5 \cdot 10^{-70}(\mathrm{eV})^4/m^4$, and so for $m \sim$ few $\times\, 10^{-16}$ eV we find $P_{\gamma\to a} \leq 10^{-7}$, which is smaller than the observed temperature anisotropy. The oscillation length of microwave photons is $L_O \sim 10^{-4}H_0^{-1}$, which is of order of the coherence length of magnetic domains L_{dom} and so a lot shorter than the horizon size. This is harmless since the oscillation amplitude is so small.

Thus if the axion scales are

$$m \sim 10^{-16}\mathrm{eV}\,, \qquad M \sim 4 \cdot 10^{11}\mathrm{GeV}\,, \tag{2.18}$$

the mixing could produce the desired effect of reducing the flux of light from SNe while leaving the primordial CMBR anisotropy unaffected.

To compare this model with observations, we assume that the constraint on the total energy density of the Universe $\Omega_{tot} \simeq 1$ is satisfied because the Universe contains some form of dark energy which does not clump, but it need not lead to cosmological acceleration. A simple example is dark energy with the equation of state $w = p/\rho = -1/3$ and energy density $\Omega_S = 0.7$, which could originate from a network of frustrated strings with small mass per unit length. Note that because the scale factor a of the universe obeys $\ddot{a}/a = -\frac{4\pi}{3M_{PL}^2}(\rho_{total} + 3p_{total})$, and assuming $\Omega_m = 0.3$ and $\Omega_{dark} = 0.7$, then as long as the ratio $w = p/\rho$ is greater than $-1/2.1 \simeq -0.48$ the Universe would presently not be accelerating. These forms of dark energy do not appear to be excluded either by the position of the first acoustic peak in the CMBR measurements [21] or by combined CMBR+large scale structure fits [22]. In Fig. 2 we have plotted the typical prediction of the oscillation model in a spatially flat Universe with $\Omega_m = 0.3$ and $\Omega_S = 0.7$ against

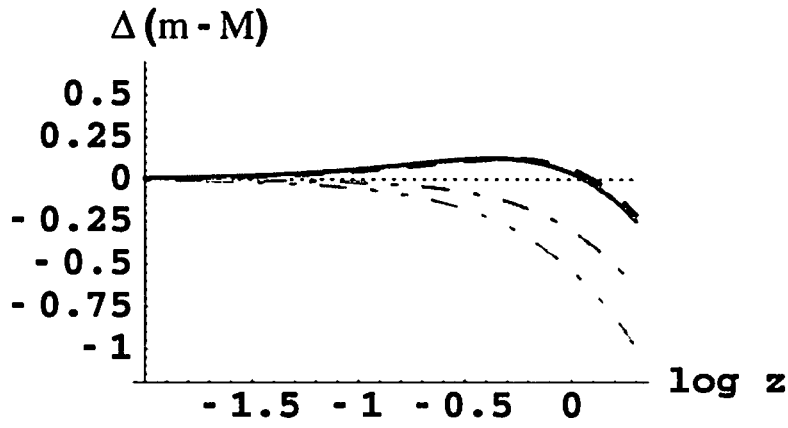

Figure 2: The luminosity-distance vs. redshift curve for several models, relative to the curve with $\Omega_{tot} = 0$ (dotted horizontal line). The dashed curve is a best fit to the supernova data assuming the Universe is accelerating ($\Omega_m = 0.3$, $\Omega_\Lambda = 0.7$); the solid line is the oscillation model with $\Omega_m = 0.3$, $\Omega_S = 0.7$, $M = 4 \cdot 10^{11}$ GeV, $m = 10^{-16}$ eV; the dot-dashed line is $\Omega_m = 0.3$, $\Omega_S = 0.7$ with no oscillations, and the dot-dot-dashed line is for $\Omega_m = 1$ again with no oscillations.

the best fit model for the accelerating Universe with a cosmological constant ($\Omega_m = 0.3$ and $\Omega_\Lambda = 0.7$). The two curves are practically indistinguishable. We note that the oscillation model predicts limited attenuation of the SN luminosities, unlike some other alternatives to the accelerating Universe. The total attenuation is limited to about 1/3 of the initial luminosity, as we have explained above. Since for larger values of z the Universe becomes matter dominated, and the disappearance of photons is saturated in the oscillation model, the two curves will continue lying on top of each other for higher values of z. Thus simply finding higher z supernovae [23] will not distinguish between the two models. The main difference between the two is that the curve for the oscillation model is an averaged curve, with relatively large standard deviations. Therefore it may be much easier to explain outlying events than in the case of the accelerating Universe.

3 Compactifications with Separated Stacks of Branes

• How could string theory be *applicable* at scales much below the string scale?

One of the main challenges for the construction of a unified theory of all forces including gravity is the enormous difference in scales that appear in Nature. On the other hand, string theory has only one dimensionful parameter, the string scale $l_S = M_S^{-1}$, and hence may provide an attractive framework for unification. The question then is, if all forces are characterized by the same fundamental scale, how does the observed difference in scales which characterize their strengths arise? Many scenarios for string phenomenology involve *localized* gauge fields. Perhaps the simplest is the minimal Hořava-Witten theory [24, 25]. Other models use "D-brane" defects on which gauge dynamics occurs [26]. A striking possibility emerging from these ingredients is a new explanation the weakness of gravity [27]. These ideas are providing new avenues for exploring physics beyond the Standard Model, and novel mechanisms for explaining small numbers [28, 29].

Here we will review string phenomenology in a regime which can arise when there are many separated stacks of branes transverse to the compactification manifold M. Their tension curves the space around them. The backreaction is proportional to the sum of brane tensions, and therefore to the total number of branes in some region of space. Hence solitary branes have little effect and their neighborhood is nearly flat. Such case are like "dilute gases", and can be studied by e.g. perturbative string orientifold constructions. In other regimes of couplings where a (super)gravity description is valid, large stacks of branes in the compactification manifold M significantly alter the metric on M. The regions of space where the

branes reside may be viewed as gravitational funnels, or throats. Examples arise in F-theory compactifications on elliptic Calabi-Yau fourfolds [30]. From the 4d point of view the geometry is "warped" - the scale factor of the 4d metric depends on the distance down the throat.

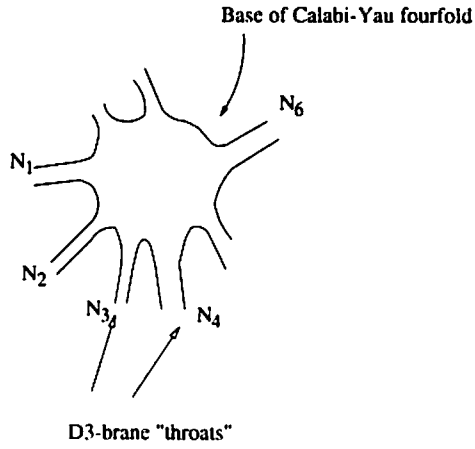

Figure 3: *The Calabi-Yau octopus. N_i is the number of branes in a given region.*

In such models, the ensuing geometry of the compactification resembles an "octopus," where the legs represent throats arising from stacks of branes, as depicted in Fig. 3. The (super)gravity modes in the throat and the low-energy field theory on the branes are dual to each other [31]: the degrees of freedom localized at the ends of the throats are dual to infrared (IR) excitations of the field theory, while the excitations closer to the mouth of the throat are dual to the ultraviolet (UV) degrees of freedom.

This geometry suggests a new mechanism for generating small numbers in 4d physics. The mutual couplings of the IR degrees of freedom residing in different throats are suppressed, as these modes must tunnel through the bulk to communicate. A 5d toy model of Fig. 3 which summarizes the main aspects of the compactification is given in Fig. 4.

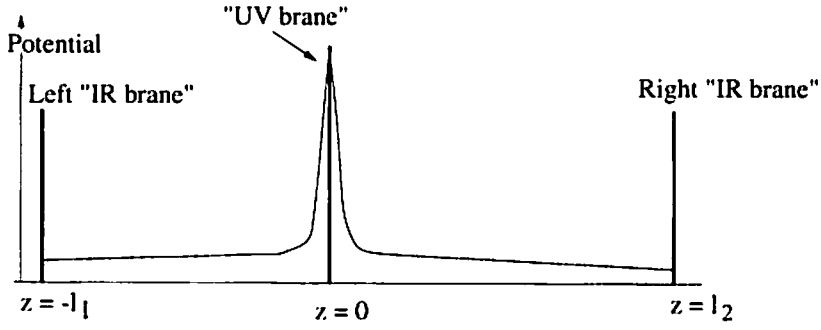

Figure 4: *A simplified picture of two brane throats.*

To get the model depicted in Fig. 2, we choose a 5d metric:

$$ds^2 = \frac{L^2}{(|z| + L)^2}(\eta_{\mu\nu}dx^\mu dx^\nu + dz^2), \qquad -l_1 \le z \le l_2\,. \tag{3.19}$$

Here x^μ are the coordinates of our 4d world, and z is the coordinate down the throat. $l_1 = Le^{R_1/L}$ and $l_2 = Le^{R_2/L}$, and $R_{1,2}$ are the proper distances from the UV brane to the left/right IR branes. To analyze the KK spectrum, define [28]

$$h_{\mu\nu}(x,z) = \sqrt{\frac{L}{|z| + L}}e^{ip\cdot x}\psi_{\mu\nu}(z) \tag{3.20}$$

where $h_{\mu\nu}$ is the 5d graviton. The transverse, traceless modes of $h_{\mu\nu}$ satisfy

$$\partial_z^2\psi + (m^2 - \frac{15}{4(|z|+L)^2})\psi = 0, \qquad -l_1 \leq z \leq l_2 \tag{3.21}$$

with appropriate boundary conditions at the branes, where $p^2 = m^2$ is the 4d KK mass of the mode. This is an effective Schrödinger equation with a potential barrier arising from the warped metric (3.19). The 4d and 5d Planck masses scale out this equation. We expect the low-lying modes in the left/right throat to have masses $\sim 1/l_{1,2}$, so they must tunnel to communicate.

Qualitatively similar barriers arise for any minimally coupled modes in non-AdS backgrounds. The only differences are the explicit relationship between the proper bulk distances and the conformal distances z, and between the parameters of the potential and the bulk scales. Hence our analysis should carry over to those cases.

We would like to analyze the tunneling amplitude, for which the WKB approximation will suffice. The potential in the Schrödinger equation (3.21) is

$$V(z) = \frac{15}{4(|z|+L)^2}\,. \tag{3.22}$$

A precise calculation yields [32]

$$\Gamma \sim m(mL)^4\,. \tag{3.23}$$

The low-energy theory which emerges from such compactifications has an immediate application for constructing a model of dark matter which is not exactly cold. In this model, the role of dark matter is played by the bulk degrees of freedom. Because of the *AdS/CFT* correspondence, these dark matter particles admit a dual interpretation as states in a CFT. While it is fascinating to contemplate that dark matter is described by a CFT, in its simplest form this idea is in conflict with observation. CFT matter would have a relativistic equation of state, acting as hot dark matter (HDM); but the large scale structure of the universe suggests that non-relativistic, cold dark matter (CDM) dominates the dynamics of the universe since $t \sim 10^4$ years. A way to bypass this difficulty is to postulate that the universe has, until recently, been dominated by an unstable CDM particle which decays into CFT matter, with a lifetime of order of the age of the universe. The two-throat model of Fig. 2 provides such a scenario [32]. Suppose the SM is localized on the left IR brane, and that the right throat is dual to a real CFT (i.e. $l_2 \to \infty$). Now introduce a bulk particle, the "bulky," which is distinct from the graviton and which has a bulk parity symmetry under which it changes sign. This symmetry protects it from decay to SM fields. One can show [32] along the lines of [33] that the relic abundance of bulkies today would be

$$\frac{\rho}{\rho_c} \sim 16\pi^2 \times 10^{-2}(M_5 L)^2 \frac{m^2}{TeV^2}\,. \tag{3.24}$$

So if $LM_5 \sim 10$ and $m \sim 100GeV$, then the left bulkies would close the Universe. The left bulkies will decay into their much lighter right cousins with a rate given by Eq. (3.23). A lifetime of the age of the Universe requires $L^{-1} \sim 10^{14}GeV$ and $M_5 \sim 10^{15}GeV$. These scales are of the order of the unification scale and should arise naturally in model building.

In this scenario, the dark matter is slowly decaying into CFT degrees of freedom in our epoch. This can have important observational effects: it can lead to a softening of the dark matter density profile within our galactic halo, by spreading it into extragalactic space, as shown in simulations of decaying CDM performed by Cen [34]. This may help account for the absence of the excess small scale structure predicted in the canonical CDM scenario [34, 35, 36]. A variation of this scenario is to add a right brane with characteristic scale of less than the galactic halo size, $\sim$ 400kpc. This may confine most of the approximately conformal matter within the halo.

This proposal is similar to the scenario of [34] where the CDM particle decays to light, invisible particles, e.g. neutrinos, which escape our galaxy. There it was shown by detailed computer simulations that if a significant fraction (e.g., one-half) of the CDM decays into neutrinos, then at least some of the problems with excess small-scale structure are avoided. The only difference in our case is that the decay product is CFT-matter instead of neutrinos. A potential difficulty of this scenario is that it predicts that younger galaxies should be heavier by an amount which may be too large.

4 Inflation as a Natural Supercollider

• Can we ever *detect* the signatures of <u>really</u> high energy physics?

Observational cosmology provides a window into very early times and hence it may give us a keyhole glimpse of very high energy processes. This has received much more attention recently because of the new experiments underway and being planned to study the cosmic microwave backround radiation (CMBR). The benchmark theory that explains the fluctuations in the CMBR is inflation, which traces them to "thermal" quanta of a scalar inflaton field during a time of exponential expansion of the universe. In the simplest models of inflation the scale of vacuum energy during this period of exponential expansion was $\sim 10^{16}$ GeV and the rate of exponential expansion $H \sim 10^{13} - 10^{14}$ GeV. These enormous energies suggest that during the inflationary epoch various kinds of high energy processes were activated, and further, that they could have left their imprint on the CMBR.

Many authors have drawn attention to this exciting prospect. The first piece of high energy physics to be unraveled could well be dynamics of inflation itself. While it is by no means necessary for the scale of inflation to be as high as $H \sim 10^{13} - 10^{14}$ GeV, as demonstrated by inflationary models where H can be as low as $H \sim 10^3$ GeV [37], the scale of inflation can be experimentally tested. Since gravity couples to mass-energy, the amplitude of gravity waves generated during inflation is directly related to the energy available during inflation. This gravitational radiation imprints itself as a polarized component of the CMBR, whose power is proportional to $(H/m_4)^2$, where m_4 is the (reduced) four dimensional Planck length. So measurements of this power give a direct measurement of H. COBE data already provide the interesting upper bound $H < 10^{14}$ GeV [38], which corresponds to vacuum energies $\sim 10^{16}$ GeV, the supersymmetric unification scale. Here we review the possibility discovering new physics via inflation. The idea, roughly speaking, is to use inflation as a mechanism for projecting, and imprinting, the very short distance physics onto the astrophysical distance scales, observed on the sky. There have been a number of investigations of the signature of high energy scale physics in the CMBR [39, 40, 41, 42, 43, 44, 45]. The analysis of [45] shows that, starting with the usual inflationary vacuum, loop corrections to the inflaton dynamics induce the effects which are of size $\sim H^2/M^2$ relative to the leading order calculations in any theory that is local on momentum scales $\leq H$. Here M is the scale of new high energy physics, and typically is of order of the fundamental Planck scale of the theory. Such an effect may be far too small to observe for a wide range of scales M. Worse yet, the ultimate statistical limit of cosmic variance excludes it from being observed even in principle unless the signal is greater than about a percent of the leading order effect. But, as pointed out in [43], modern string and M theory models allow for the constructions with lower values of the fundamental mass scales, raising the possibility of more favorable ratios H^2/M^2. Below we will review the results of [45] exploring this issue in detail.

The main feature of inflationary dynamics in the slow roll approximation is that we can ignore the acceleration of the scalar field, because the cosmological expansion has the effect of friction and nearly freezes the scalar on the potential slope. The universe is dominated by the scalar field potential energy and undergoes a period of rapid expansion. The usual parameters which characterize the validity of the slow roll approximation are

$$\eta = \frac{\ddot{\phi}}{H\dot{\phi}} \qquad\qquad \epsilon = \frac{3\dot{\phi}^2}{2M^4\mathcal{V}}. \tag{4.25}$$

The slow roll approximation is then formally defined as the regime $|\eta|, |\epsilon| \ll 1$. The relative importance of these parameters depends on the model of inflation. In the slow roll approximation, the field equations become

$$3H^2 = \frac{M^4}{m_4^2}\mathcal{V} \qquad\qquad 3H\dot{\phi} + M^4\frac{\partial\mathcal{V}}{\partial\phi} = 0. \tag{4.26}$$

Using these equations, one readily finds the slow roll parameters in terms of the potential function $\mathcal{V}$, $\eta = \epsilon - m_4^2\frac{\partial_\phi^2\mathcal{V}}{\mathcal{V}}$ and $\epsilon = m_4^2\frac{[\partial_\phi\mathcal{V}]^2}{2\mathcal{V}^2}$. The equations can be integrated, yielding

$$a \simeq a_0 \exp\Big[\frac{1}{m_4^2}\int_\phi^{\phi_0} d\phi\frac{\mathcal{V}}{\partial_\phi\mathcal{V}}\Big] \simeq a_0 \exp\Big[\frac{\mathcal{V}_0\,(\phi_0 - \phi)}{m_4^2\partial_\phi\mathcal{V}_0} + ...\Big]. \tag{4.27}$$

Hence, the universe will undergo rapid expansion while the vev of the inflaton may change only minutely. The space-time geometry is approximated by a future half of de Sitter space during this period. Eventually

the change of the inflaton vev accumulates enough for the inflaton to depart the slow roll regime, and the potential becomes steeper. The inflaton approaches the minimum of the potential, begins to oscillate around it and produce matter particles, reheating the inflated universe back to temperatures which will eventually produce the universe we inhabit.

Let us imagine that at late times the vacuum energy vanishes and inflation terminates such that there are no cosmological event horizons. This avoids conceptual difficulties with quantum gravity in spacetimes with cosmological horizons discussed at great length at the beginning of this review, but suffices to illustrate the main features of inflation in the spacetime language. The causal structure of the universe is then given by the Penrose diagram of Fig. 5.

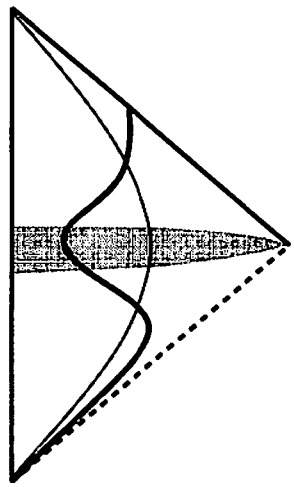

Figure 5: *Causal diagram of an inflationary model. The dashed past null line is the true particle horizon, but it could also be a null singularity. The future null line is the future infinity. The shaded area denotes the region of exit from inflation and reheating. The thin solid line is a worldline of any spacelike separated object from an observer at the center of the space. The bold solid line is the apparent horizon. Its shape is characteristic of inflation in the past, and radiation domination followed by matter domination in the future.*

In the diagram, the region of geometry below the particle horizon (dashed line) is irrelevant for the future evolution as long as the period of inflation was sufficiently long. The future infinity appears as a consequence of our requirement for global exit from inflation. The spacetime below the reheating regime is the inflationary region, while that above it is the postinflationary, decelerating FRW universe. The thin solid line denotes any object spacelike separated from us, and for example is the worldline a distant galaxy follows after it forms. The bold solid line represents the apparent horizon, which plays central role for controlling the dynamics of inflation, as we will now elaborate. During inflation, it starts out almost null and "outward" directed, and then it flips "inward". This reflects that $H \sim$ const. during inflation. It ensures that the apparent horizon plays the role of the causal censor, limiting the amount of information which can fit inside an inflating region. The spacetime will therefore obey cosmic no-hair theorem, and inflation will succeed in getting rid of initial inhomogeneities. This may be viewed as another example of the cosmological variant of the holographic principle [46, 47]. The structure of the spacetime is fully coded on the preferred screen, i.e. the apparent horizon. Its area is small during inflation because H must be large, and hence the Hubble region is censored from excessive outside influence, because only a limited amount of information can fit in the interior. Moreover, most of the objects inside the Hubble region are in the thermal bath of fluctuations located in the region when the apparent horizon is almost null [2], with the cosmological Hawking temperature $T_H = H/2\pi$. Since the inflaton is much lighter than the Hubble scale during inflation, the interactions with the thermal quanta cause its vev and the background metric to fluctuate.

Because of these quantum fluctuations, the inflaton is not exactly frozen to its slowly varying background vev. Instead it hops on the potential around the background value. Thus inside of some regions

of the universe inflation may terminate a little later, because quantum effects push the inflaton a little farther up the plateau. These regions end up a fraction denser than their surroundings, and the matter in them begins to condense sooner, attracting additional matter from the neighborhood and eventually forming clusters and galaxies due to the classical Jeans instability. The fluctuations therefore induce small inhomogeneities on the perfectly smooth geometry left by inflation, which is measured experimentally via its imprint on the cosmic microwave background radiation, $\delta\rho/\rho \sim \delta T/T$, thanks to the Sachs-Wolfe effect. This is directly measured by the COBE [38] satellite, and by the BOOMERanG [48] and MAXIMA [49] experiments, which set the normalization for the inhomogeneities at around $\delta\rho/\rho \sim 10^{-5}$. They further observe that the spectrum of inhomogeneities is nearly scale-independent.

To determine the imprint of the fluctuations quantitatively we can use perturbation theory. In perturbation theory the fluctuations can be decomposed with respect to their transformation properties relative to the residual diffeomorphisms into scalar, vector and tensor modes. The vector modes decouple during inflation. Thus only the scalar and tensor modes are produced. The scalar modes cause density (and therefore CMBR temperature) fluctuations. The tensor modes are primordial gravitational waves produced by inflation, and affect the polarization of CMBR.

A heuristic derivation of the scalar density contrast is as follows: the RMS fluctuation of the field induced by the thermal fluctuations is $\delta\phi = \dot{\phi}\delta\tau$, and that of energy density is $\delta\rho = C\rho H\delta\tau$, where C is a numerical coefficient of order unity, whose precise value depends on the details of postinflationary cosmology. The function $\delta\tau$ is the time delay imprinted by the fluctuations on the vev in different regions of space. Combining these equations, one finds

$$\frac{\delta\rho}{\rho} = C\frac{H}{\dot{\phi}}\delta\phi \tag{4.28}$$

and then one needs to compute the RMS fluctuation of the inflaton $\delta\phi$. Here C is a parameter of order unity, whose precise value depends on the details of reheating. As we will discuss in more detail below, fluctuations of the transverse traceless modes of the graviton (which obey free scalar field equations) also contribute to the density variations.

In order to determine precisely how the quantum fluctuations of these fields evolve into temperature anisotropies in the sky today, one must first compute their effect on the curvature, and then use gauge-invariant gravitational perturbation theory to evolve the perturbation forward to the present era. One can define a gauge-invariant variable ζ, which is well approximated by the right hand side of (4.28) as modes exit from the de Sitter horizon during inflation, and which is approximately constant between this time, and when the mode re-enters the cosmological horizon later. At this later time ζ is well approximated by $\delta\rho/\rho$, establishing (4.28) [50]. This stage in the process is purely classical, because energy scales below H correspond to scales outside the causal horizon, and so coherent quantum fluctuations do not contribute at these wavelengths. The correct procedure is therefore to compute the quantum fluctuation of the inflaton field in de Sitter space, and then use it to evaluate ζ at the time the fluctuation exits the horizon; i.e., at momentum $p = H$. If the slow roll approximation breaks down this procedure will not be accurate, however for the sake of simplicity we consider only models where this is not a concern.

To compute the quantum fluctuation itself, one treats the fluctuating field as a perturbation around the de Sitter background and computes the mean-square variance as the (appropriately normalized) Fourier component of an equal-time two-point function evaluated at 3-momentum $p = H$:

$$(\delta\phi)^2 \sim \langle\phi(p)\phi(-p)\rangle|_{p=H}, \tag{4.29}$$

where ϕ represents either the inflaton or a physical mode of the graviton. The normalization is determined by the more detailed computation we perform below. In standard inflation, this is done assuming the inflaton is a free, minimally coupled scalar. As we will demonstrate in section 3, interactions with massive particles will modify the 2-point function and affect the spectrum of fluctuations. As long as the self-interactions of the inflaton (either in the classical potential, or induced by quantum corrections) are weak at energy scale H, so that a perturbative expansion is valid at this scale, this procedure is well defined. Of course, more general theories will involve strong coupling, but generically will also violate the observed constraints on $\delta\rho/\rho$. This gives $\delta\phi = H/2\pi$, finally yielding

$$\frac{\delta\rho}{\rho} = \frac{C}{2\pi}\frac{H^2}{\dot{\phi}}. \tag{4.30}$$

We can re-express (4.30) in terms of the inflationary potential using the slow roll equations (4.26). It is

$$\frac{\delta\rho}{\rho} = \frac{C}{2\sqrt{3}\pi}\frac{M^2}{m_4^3}\frac{\mathcal{V}^{3/2}}{\partial_\phi \mathcal{V}}. \tag{4.31}$$

This is the familiar formula for scalar fluctuations in inflation. We note that the so-called scalar power spectrum δ_S^2 is related to the density contrast by $\delta_S^2 = (2/5C)^2(\delta\rho/\rho)^2$, and using (4.31) we can express it as

$$\delta_S^2 = \frac{1}{75\pi^2}\frac{M^4}{m_4^6}\frac{\mathcal{V}^3}{[\partial_\phi \mathcal{V}]^2} \tag{4.32}$$

The causal structure of the inflationary spacetime depicted in Fig. 1. provides a straightforward understanding of the emergence of a (nearly) scale-invariant spectrum of fluctuations. A quantum fluctuation which seeds a galaxy is created just before its worldline intersects the apparent horizon. At that instant, it is as big as the Hubble horizon. Then it is expelled outside of the apparent horizon, where it freezes, and remains frozen until horizon reentry in distant future. After reentry the fluctuation becomes dynamical and evolves as dictated by gravitational instability. Scale invariance then follows from causal evolution if $H \simeq$ const., because the fluctuations of very different wavelengths are produced with the same amplitude.

The evolution of the fluctuations can initially be described well by linear perturbation theory. However, nonlinearities eventually develop because of nontrivial interactions with the environment. In the matter dominated era, the fluctuations evolve differently before decoupling than after it. Before decoupling, the universe is opaque and therefore the baryonic matter is influenced by radiation pressure, which competes with gravitational collapse. This results in the emergence of acoustic oscillations, with characteristic peaks imprinted on the CMBR. The peaks appear because the perturbations whose wavelengths are half-integer divisors of the sound horizon (i.e. the largest distance sound can travel within the time of recombination) at decoupling can complete full oscillation cycles. The location and the heights of the peaks measure very accurately the cosmological parameters, in particular the Hubble parameter at decoupling.

Tensor fluctuations are also generated during inflation. These are just the gravitational waves, and correspond to the transverse-traceless metric fluctuations h_{kl}. They obey the linearized field equation $\nabla^2 h^k{}_l = 0$, where the covariant derivatives and raising and lowering of indices is defined relative to the background metric $g_{\mu\nu} = \mathrm{diag}(-1, a^2(t)\delta_{kl})$. Therefore each of the two graviton polarizations obeys the free massless scalar equation, and it is straightforward to quantize them in de Sitter space, in precisely the same way as the inflaton fluctuations. In particular the root mean square fluctuation of the graviton is $\langle \delta h_{kl} \rangle \simeq H/2\pi$. However the formula for the tensor power spectrum is different than for the scalar. It is directly proportional to the fluctuation of the metric,

$$\delta_T^2 = \frac{1}{2\pi^2}\frac{H^2}{m_4^2} = \frac{1}{6\pi^2}\frac{M^4}{m_4^4}\mathcal{V} \tag{4.33}$$

by slow roll equations (4.26). The tensor nature of these fluctuations induce oscillations in the plasma during decoupling which polarize the CMB photons in an observable way [51]. The ratio $\mathcal{R} = \delta_T^2/\delta_S^2$ is a characteristic of the inflationary model, and is given by $\mathcal{R} = \frac{25}{2}\frac{m_4^2[\partial_\phi \mathcal{V}]^2}{\mathcal{V}^2}$. It is straightforward to verify that in terms of the slow roll parameters it is given as $\mathcal{R} = 25\epsilon$.

The fluctuation spectra produced in inflation are not exactly scale-invariant. If the background inflaton vev were exactly frozen, and the geometry precisely de Sitter, the prediction for fluctuations (4.30) (4.33) would have been time-independent, and therefore exactly scale-invariant. In reality, there is weak time-dependence in (4.30) because the inflaton is sliding down the plateau. This time dependence, manifest in the variation of H and $\dot{\phi}$, translates into scale dependence of fluctuations, and produces a spectrum which is not exactly scale-invariant. This departure from scale invariance is a function of the specifics of inflationary model as defined by the potential. Below we will consider the details in the case of modular inflation.

At this point, it is clear how to incorporate interactions into the calculation. We analyze this effect by assuming that string theory at energies $\sim H$ is approximately local. Therefore, if the theory contains a massive field (with mass $M \gg H$) which couples to the inflation, we can integrate it out using standard field theory techniques and obtain an effective potential for the inflaton. As can be seen from the two

point function such a procedure yields–in addition to the ordinary flat space terms terms proportional to H^2/M^2, p^2H^2/M^4, etc. It is important to note that no cutoff or Planck scale comes into these corrections. The highest probe energy available in inflation and later visible in the CMB is H. These assumptions–which rely on low energy locality and renormalization group ideas–are obviously correct in a field theoretic context and also within string perturbation theory around supersymmetric vacua, as well as in the known nonperturbative definitions of string and M theory in supersymmetric backgrounds. However the enduring mystery of the cosmological constant, and the associated mysteries of string theory in de Sitter space, make these assumptions plausible, but not ironclad, in the present context. We will nevertheless retain these assumptions.

All the information about the new physics is then contained in effective field theory for ϕ at the scale H. The scale H is appropriate since that is where we evaluate inflaton correlation functions to compute the size of $\delta\rho/\rho$. Rather than writing a fully generally covariant effective action for ϕ, let us just note that the curvature of de Sitter space is proportional to H^2, and use it as an additional dimensionful parameter in constructing relevant terms. The inflaton interactions must always be very weak to give phenomenologically acceptable values of $\delta\rho/\rho$, and so we will ignore them. Under such conditions the most general Euclidean local action is of the form, assuming $p \gg H$ and using flat space notation for simplicity,

$$\begin{aligned} S_{eff}[\phi] &= \int d^4p\, \phi(p)\phi(-p)\{p^2/2 + H^2/2 + c_0H^2(H^2/M^2) + c_1p^2(H^2/M^2) \\ &\quad + c_2p^4/M^2 + c_3p^4/M^2(H^2/M^2) + c_4p^6/M^4 + \ldots\}. \end{aligned} \tag{4.34}$$

This structure follows from the fact that only even powers of momenta are allowed, and that the curvature is $\sim H^2$. Therefore, no odd powers of M can appear. Information about new physics is contained in the coefficients c_i and in the scale M. From (4.29) we see that measurements of $\delta\rho/\rho$ help determine the value of $\langle\phi(p)\phi(-p)\rangle$ at $p = H$. From (4.34) we find

$$\begin{aligned} \langle\phi(p)\phi(-p)\rangle|_{p=H} &= H^2 + c_0H^2(H^2/M^2) + c_1H^2(H^2/M^2) \\ &\quad + c_2H^4/M^2 + c_3H^2(H^2/M^2)^2 + c_4H^2(H^2/M^2)^2 + \ldots \end{aligned} \tag{4.35}$$

The large M corrections to $\langle\phi(p)\phi(-(p)\rangle|_{p=H}$ organize themselves into a power series in the dimensionless ratio H^2/M^2. We have assumed that this ratio is small, so the only terms that are potentially observable are the ones with coefficients c_1 and c_2. The term with coefficient c_0 is just a renormalization of the potential which we can ignore. The coefficients c_i must be computed, however, and can be much smaller than one, giving effects much smaller than the naive expectation, even in the cases where the fundamental scale $m_{11} \sim M \sim H$.

We now consider some examples. In weakly coupled heterotic string theory models with $g_s^2 \sim .1$, $m_s \sim m_4 \sim 10^{19}$ GeV, the Calabi-Yau compactification radii are hence also of order $1/m_s$. the corrections are $H^2/m_s^2 \sim 10^{-11}$. This is unobservable. To find effects closer to the threshold of detectability we must therefore enter the realm of strongly coupled string theory, where the fundamental mass scale can be much less than m_4. Alternatively, from the point of view of effective $4D$ theory which we use to compute the fluctuations during inflation, we need to have a great number of new degrees of freedom at some high scale, such that because of linear superposition in quantum mechanics their radiative corrections to the inflaton can add up and enahnce the effect.

In particular, if we abandon the requirement of precision grand unification and allow our compactification manifold to get as large as possible, while remaining consistent with the four dimensional character of inflation, we can make the imprint on the CMBR order one, and hence potentially observable. An example is provided by G_2 manifolds, with the fundamental eleven dimensional Planck mass is $m_{11} \gtrsim H \sim 7 \times 10^{13}$ GeV. In this case

$$M \sim m_{11} \sim 8 \times 10^{13}\ \text{GeV} \qquad \frac{H^2}{M^2} \sim 1 \qquad c_1\frac{H^2}{M^2} \sim 0.1\ . \tag{4.36}$$

We emphasize again the imprecision of our estimates; it is easy to imagine gaining or losing an order of magnitude in an explicit model.

We stress that these corrections are in principle observable, if large enough, even if we do not have a detailed knowledge of the inflaton potential. One may be concerned that whatever the corrections, one

can always slightly redefine the inflaton potential to mimick them. If this were the case, disentangling the signatures of new physics from the unknown details of the inflaton potential would be impossible without knowing the full theory. However a differential effect in the scalar and tensor fluctuations due to short distance physics cannot be mimicked by any change of the inflationary potential [52]. Ordinary inflationary fluctuations, without new physics, obey "inflationary consistency conditions" connecting scalar and tensor quantities. New heavy physics predicts a violation of these conditions [52]. This is the unambiguous signal of new physics. However the differencing inherent in the inflationary consistency conditions suppresses the signal by a power of the slow roll parameter ranging in value from $\sim .001 - .06$ in various models. Hence the size of the measurable effect is somewhat smaller than initial estimates suggest. Therefore this unambiguous signal is very challenging to measure. Not only does it require precision data for the scalar fluctuations, but it also requires precision data for the tensor fluctuations, which have not even been observed yet. Forthcoming experiments may be able to observe the tensor fluctuations if inflation occurred at a high scale by observing the B-mode polarization component of the CMBR. To make these observations useful for searching for traces of new physics it would be necessary to carry out cosmic variance limited measurements over a substantial range in wavenumber. This is a formidable experimental challenge. Nevertheless, it might be our only chance to search for <u>really</u> high energy physics, which will otherwise not be accessible to experimentation.

Acknowledgements

The author wishes to express his gratitude to the organizers of the 11^{th} Workshop on GRG for putting together such a stimulating meeting and for their assistance and financial support during the workshop. Particular thanks go to Jun-ichirou Koga, Kei-ichi Maeda, Misao Sasaki and Jun'ichi Yokoyama. It is a great pleasure to thank C. Csaki, S. Dimopoulos, S. Hellerman, S. Kachru, M. Kleban, A. Lawrence, S. Shenker, E. Silverstein, L. Susskind and J. Terning for collaborations which led to the results presented here and which helped shape author's thinking on these subjects. Further thanks go to A. Albrecht, T. Banks, W. Fischler, M. Kaplinghat, L. Knox, A. Linde, P. Steinhardt, S. Thomas, R. Wagoner and J. Yokoyama for very useful discussions. The work reported here was supported in part by NSF grant PHY-9870115.

References

[1] T. Banks, W. Fischler and L. Motl, JHEP **9901** (1999) 019.

[2] S. Hellerman, N. Kaloper and L. Susskind, JHEP **0106** (2001) 003.

[3] W. Fischler, A. Kashani-Poor, R. McNees and S.Paban, JHEP **0107** (2001) 003.

[4] S. Perlmutter et al., Astrophys. J. **483** (1997) 565; A.G. Riess et. al., Astron. J. **116** (1998) 1009; P.M. Garnavich et. al., Astrophys. J. **509** (1998) 74; S. Perlmutter et al., Astrophys. J. **517** (1999) 565.

[5] T. Banks, hep-th/0007146; hep-th/0011255; T. Banks and W. Fischler, hep-th/0102077.

[6] E. Witten, hep-th/0106109.

[7] J. Maldacena and C. Nunez, Int. J. Mod. Phys. **A16** (2001) 822.

[8] B. Ratra and P.J.E. Peebles, Phys. Rev. **D37** (1988) 3406.

[9] R.R. Caldwell, R. Dave and P.J. Steinhardt, Phys. Rev. Lett. **80** (1998) 1582; L. Wang, R.R. Caldwell, J.P. Ostriker and P.J. Steinhardt, Astrophys. J. **530** (2000) 17.

[10] S.W. Hawking and G.F.R. Ellis, *The Large Scale Structure of Space-Time*, Cambridge Univ. Press, Cambridge 1972.

[11] P. Breitenlohner and D.Z. Freedman, Phys. Lett. **B115** (1982) 197; Ann. Phys. **144** (1982) 249.

[12] P.K. Townsend, Phys. Lett. **B148** (1984) 55; K. Skenderis and P.K. Townsend, Phys. Lett. **B468** (1999) 46.

[13] C. Csaki, N. Kaloper and J. Terning, hep-ph/0111311 and hep-ph/0112212.

[14] J. Erlich and C. Grojean, hep-ph/0111335.

[15] P. Sikivie, Phys. Rev. Lett. **51** (1983) 1415 [Erratum-ibid. **52** (1983) 695]; for an overview see G. Raffelt and L. Stodolsky, Phys. Rev. D **37** (1988) 1237.

[16] The possibility of photon oscillations has first been mentioned in H. Georgi, P. Ginsparg and S. L. Glashow, Nature **306** (1983) 765.

[17] P. P. Kronberg, Rept. Prog. Phys. **57** (1994) 325 .

[18] S. Furlanetto and A. Loeb, astro-ph/0110090.

[19] G. G. Raffelt, Ann. Rev. Nucl. Part. Sci. **49** (1999) 163 .

[20] J. W. Brockway, E. D. Carlson and G. G. Raffelt, Phys. Lett. B **383** (1996) 439; J. A. Grifols, E. Masso and R. Toldra, Phys. Rev. Lett. **77** (1996) 2372.

[21] D. Huterer and M. S. Turner, astro-ph/0012510.

[22] S. Perlmutter, M. S. Turner and M. J. White, Phys. Rev. Lett. **83** (1999) 670; M. S. Turner and M. J. White, Phys. Rev. D **56** (1997) 4439.

[23] M. S. Turner and A. Riess, astro-ph/0106051.

[24] P. Hořava and E. Witten, Nucl. Phys. **B460** (1996) 506.

[25] E. Witten, Nucl. Phys. **B471** (1996) 135.

[26] J. Dai, R. G. Leigh and J. Polchinski, Mod. Phys. Lett. **A4** (1989) 2073; P. Horava, Phys. Lett. **B231** (1989) 251; P. Horava, Nucl. Phys. **B327** (1989) 461; G. Pradisi and A. Sagnotti, Phys. Lett. **B216** (1989) 59; J. Polchinski, Phys. Rev. Lett. **75** (1995) 4724.

[27] N. Arkani-Hamed, S. Dimopoulos and G. Dvali, Phys. Lett. **B429** (1998) 263; Phys. Rev. **D59** (1999) 086004; I. Antoniadis, N. Arkani-Hamed, S. Dimopoulos and G. Dvali, Phys. Lett. **B436** (1998) 257.

[28] L. Randall and R. Sundrum, Phys. Rev. Lett. **83** (1999) 3370.

[29] E. Verlinde and H. Verlinde, JHEP **0005** (2000) 034; N. Arkani-Hamed, S. Dimopoulos, N. Kaloper and R. Sundrum, Phys. Lett. **B480** (2000) 193; S. Kachru, M. Schulz and E. Silverstein, Phys. Rev. **D62** (2000) 045021.

[30] H. Verlinde, Nucl. Phys. **B580** (2000) 264.

[31] J. Maldacena, ATMP **2** (1998) 231; S. Gubser, I. Klebanov and A. Polyakov, Phys. Lett. **B428** (1998) 105; E. Witten, ATMP **2** (1998) 253.

[32] S. Dimopoulos, S. Kachru, N. Kaloper, A.E. Lawrence and E. Silverstein, Phys. Rev. **D64** (2001) 121702 and hep-th/0106128.

[33] E. Kolb and M. Turner, *The Early Universe*, Addison-Wesley, Redwood City, 1990.

[34] R. Cen, astro-ph/0005206.

[35] D.N. Spergel and P.J. Steinhardt, Phys. Rev. Lett. **84** (2000) 3760, astro-ph/9909386.

[36] P.J.E. Peebles, astro-ph/0002495.

[37] A. Linde, Phys. Rev. **D49** (1994) 748.

[38] J. C. Mather *et al.*, Astrophys. J. **354** (1990) L37.

[39] D.J.H. Chung, E.W. Kolb, A. Riotto and I. Tkachev, Phys. Rev. **D62** (2000) 043508.

[40] J. Martin and R. H. Brandenberger, Phys. Rev. **D63** (2001) 123501; Mod. Phys. Lett. **A16** (2001) 999; R. H. Brandenberger, S. E. Joras, and J. Martin, hep-th/0112122.

[41] J.C. Niemeyer, Phys. Rev. **D63** (2001) 123502; J. C. Niemeyer and R. Parentani, Phys. Rev. **D64** (2001) 101301.

[42] A. Kempf and J. C. Niemeyer, Phys. Rev. **D64** (2001) 103501.

[43] R. Easther, B. R. Greene, W. H. Kinney, and G. Shiu, Phys. Rev. **D64** (2001) 103502.

[44] R. Easther, B. R. Greene, W. H. Kinney, and G. Shiu, hep-th/0110226.

[45] N. Kaloper, M. Kleban, A.E. Lawrence and S. Shenker, hep-th/0201158.

[46] W. Fischler and L. Susskind, hep-th/9806039.

[47] R. Bousso, JHEP **9907** (1999) 004; JHEP **9906** (1999) 028; Class. Quant. Grav. **17** (2000) 997.

[48] A. E. Lange *et al.*, Phys. Rev. **D63** (2001) 042001.

[49] Balbi, A. *et al.*, Astrophys. J. **545** (2000) L5.

[50] J. Bardeen, P. Steinhardt, and M. Turner, Phys. Rev **D28** (1983) 679.

[51] W. Hu and M.J. White, *New Astron.* **2** (1997) 323.

[52] L. Hui and W. H. Kinney, astro-ph/0109107; see also J. Garriga and V. F. Mukhanov, Phys. Lett. **B458** (1999) 219.

Gravitational energy, dS/CFT and inflation

Tetsuya Shiromizu, Daisuke Ida and Takashi Torii

RESCEU, The University of Tokyo, Tokyo 113-0033, Japan

Abstract

The gravitational energy is examined in asymptotically de Sitter space-times. The positivity will be shown for certain cases. The de Sitter/CFT(dS/CFT) correspondence recently proposed and cosmic no-hair conjecture are testified in the aspect of the gravitational energy. From the holographic renormalization group point of view, the two conjectures are deeply connected with each other.

1 Introduction

The origin of de Sitter entropy is getting to be central issue[1]: From some considerations based on the euclidean quantum gravity or quantum field theory in curved space-times, we obtain the Hawking-Bekenstein formula for the de Sitter space-times[2]. The entropy is proportional to the area of the cosmological horizon. Remember our success on the black hole entropy which is described by the state counting of string[3]. How can we explain the de Sitter entropy in string theory? Apart from an issue of the de Sitter entropy, the fundamental study about the de Sitter space-times is important because our universe has experienced the inflationary phase in very early stage, and the recent observation supports the existence of the positive cosmological constant[4]. The deep understanding of de Sitter geometry will tell us the origin of the vacuum energy.

One way to this end might be given by de Sitter/CFT(dS/CFT) correspondence recently proposed[5] as a possible extension of AdS/CFT correspondence[6]. Then, the de Sitter entropy should be explained by euclidean CFT one. If we do not care details, dS/CFT correspondence is naively expected from formal correspondence to AdS/CFT through double Wick rotations.

For example, the trace anomaly of CFT is easily reproduced[7]. Conversely, this means that things learned in study of the inflationary scenario is useful for AdS/CFT[6], brane-worlds[8] and holographic renormalization group[9].

In this paper, we study the gravitational energy in asymptotically de Sitter space-time, and discuss its significance in the context of dS/CFT correspondence and the cosmic no-hair conjecture. The gravitational energy has been investigated so far in the inflationary universe. As Ashtekar and Das pointed out in AdS/CFT context[11], it is natural to expect that the energy of euclidean CFT is related to the gravitational energy measured on the boundary of the de Sitter space-times. The gravitational energy will also be relevant for the stability of the de Sitter space-times and the corresponding euclidean CFT. As related topics, there is so called cosmic no-hair conjecture[2, 12]. It is widely believed that initial inhomogeneity in our universe is rapidly stretched out and precisely evolve to the de Sitter space-times during the inflation. We can discuss the dynamics of such an evolution in terms of the gravitational energy[13].

The rest of the present paper is organized as follows. In the Sec. 2, we consider the asymptotically de Sitter space-times and their asymptotic behaviors. As an example we examine the n-dimensional Schwarzschild-de Sitter space-time. In the Sec. 3, we discuss the relation of the energy defined by Weyl tensor and the Abbott-Deser(AD) energy[14].

In Sec. 4, we discuss dS/CFT correspondence as an application. Finally, we summarize our study in the Sec. 5.

2 Asymptotically de Sitter space-times

2.1 Conformal infinity

In this section, we briefly give a review of the asymptotically de Sitter space-times following Ref. [15].

Definition: An n-dimensional space-time (M, g) will be said to be *asymptotically de Sitter* if there exists a manifold with boundary, $\hat{M}$, with the metric $\hat{g}$ such that (i) there exists a function Ω on M such that $\hat{g} = \Omega^2 g$ on M, (ii) $\mathcal{I} = \partial\hat{M}$ and $\Omega = 0$ on $\mathcal{I}$, (iii) g satisfies n-dimensional Einstein equation

$$R_{\mu\nu} - (1/2)g_{\mu\nu}R + \Lambda g_{\mu\nu} = 8\pi T_{\mu\nu}, \tag{1}$$

where $\Omega^{-(n-1)}T_\mu{}^\nu$ admits a smooth limit to $\mathcal{I}$ and $\Lambda > 0$ is the positive cosmological constant.

Then, we can show that

$$\hat{g}^{\mu\nu}\partial_\mu\Omega\partial_\nu\Omega = -\frac{2}{(n-1)(n-2)}\Lambda + \frac{\Omega^2}{n(n-1)}\hat{R} + O(\Omega^3) =: -H^2 + \frac{\Omega^2}{n(n-1)}\hat{R} + O(\Omega^3) \tag{2}$$

holds, where a hatted tensor field is regarded as a tensor field on $\hat{M}$. The extrinsic curvature $K_{\mu\nu}$ of the Ω = constant hypersurfaces in (M, g) has the following behavior near the conformal infinity; for the trace part

$$K = (n-1)H - \frac{n+1}{2n(n-1)H}\hat{R}\Omega^2 + O(\Omega^3), \tag{3}$$

and for the trace-free part

$$\sigma^\mu{}_\nu = K^\mu{}_\nu - \frac{1}{n-1}q^\mu{}_\nu K = O(\Omega^2), \tag{4}$$

where $q_{\mu\nu}$ denotes the metric of the Ω = constant hypersurface. The derivation of these asymptotics is similar to that in the asymptotically AdS space-time ($\Lambda < 0$), which is described in Ref. [10].

2.2 Spatial infinity and constant mean curvature slices

In asymptotically flat space-times, there is a natural concept of the total gravitational energy (ADM energy [16]) defined at the spatial infinity i^0. While in asymptotically de Sitter space-times, the conformal infinity $\mathcal{I}$ consists of space-like hypersurface as seen from Eq. (2), so that there are many spatial infinities on $\mathcal{I}$. We shall specify this by considering a flat chart of the de Sitter space-time as a reference background. It is useful because the intrinsic geometry of each constant time hypersurface of asymptotically de Sitter space-time will look like $(n-1)$-dimensional flat space. In order to see this in more detail, it is better to look at the Hamiltonian constraint on a space-like hypersurface Σ:

$${}^{(n-1)}R + K^2 - K_{\mu\nu}K^{\mu\nu} = 16\pi T_{\mu\nu}n^\mu n^\nu + (n-1)(n-2)H^2, \tag{5}$$

where n^μ is the future pointing unit normal vector to Σ. If there is a constant mean curvature slice $K = (n-1)H$ in an asymptotically de Sitter space-time, Eq. (5) becomes

$${}^{(n-1)}R - \sigma_{\mu\nu}\sigma^{\mu\nu} = 16\pi T_{\mu\nu}n^\mu n^\nu, \tag{6}$$

which is exactly the same form as the Hamiltonian constraint on a maximal ($K = 0$) hypersurface in asymptotically flat space-times.

This observation indicates that the asymptotically de Sitter initial data can be formulated in a similar manner to the asymptotically flat case. More precisely, we shall call an initial data set (Σ, q_{ij}, K_{ij}) for the Einstein equation (1) *the asymptotically de Sitter initial data*, if it satisfies

$$q_{ij} = \Big(1 + \frac{2m}{r^{n-3}}\Big)\delta_{ij} + O\Big(\frac{1}{r^{n-2}}\Big) \quad \text{and} \quad K_{ij} = Hq_{ij} + O\Big(\frac{1}{r^{n-2}}\Big), \tag{7}$$

where $r = \sqrt{x^i x^i}$. Let "i^0" be spatial infinity at $r = \infty$. "i^0" is presented by a point of the conformal infinity in the Penrose diagram. When we evaluate the total *finite* energy later, we must impose a stronger condition as follows:

$$K_{ij} = Hq_{ij} + O\Big(\frac{1}{r^{n-1}}\Big). \tag{8}$$

3 Abbott-Deser energy and Weyl tensor

In this section, we show that the conserved Abbott-Deser(AD) energy[14] is identical to that defined by Weyl tensor on the constant mean curvature slices. The latter will play a central role in dS/CFT issue later. The AD energy has the expression [13, 14, 17]

$$E_{\rm AD} = M_{\rm ADM} + \Delta P_{\rm ADM}(\bar{\xi}), \tag{9}$$

$$\Delta P_{\rm ADM}(\bar{\xi}) = P_{\rm ADM}(\bar{\xi}) - \bar{P}_{\rm ADM}(\bar{\xi}) = \frac{1}{8\pi}\oint_{S^{n-2}_\infty} d\bar{S}_i(\pi^i{}_j - \bar{\pi}^i{}_j)\bar{\xi}^j, \tag{10}$$

where $\pi_{ij} = K_{ij} - Kq_{ij}$, $\bar{\pi}_{ij} = -(n-2)Hq_{ij}$ is that defined on the background, $\bar{\xi}^i$ is the space component of the static Killing vector of the background de Sitter space-time in the flat chart. S^{n-2}_∞ denotes the $n-2$-sphere at the spatial infinity "i^{0}".

On the other hand, we may expect that the gravitational energy is measured by the tidal force (the electric part of the Weyl tensor). It is natural to expect a direct relation between the AD energy and the Weyl tensor. In fact, this has been confirmed for the four-dimensional spherically symmetric case [13]. We will extend this to general cases.

The total gravitational energy associated with a slice Σ is defined in terms of the n-dimensional Weyl tensor ${}^{(n)}C_{\mu\alpha\nu\beta}$ by

$$\begin{aligned} E_W &:= -\frac{1}{8\pi}\oint_{S^{n-2}_\infty} ar^{(n)}C_{\mu\alpha\nu\beta}\hat{r}^\mu\hat{r}^\nu n^\alpha n^\beta dS^{n-2} \\ &= M_{\rm ADM} - \frac{(n-3)H}{8\pi}\oint_{S^{n-2}_\infty} ar\Big(k_{\mu\nu} + \frac{1}{n-3}q_{\mu\nu}k\Big)\hat{r}^\mu\hat{r}^\nu dS^{n-2}, \end{aligned} \tag{11}$$

where, S^{n-2}_∞ is regarded as the $(n-2)$-sphere at the spatial infinity (i^0) of Σ, $\hat{r}^\mu$ is the unit outward normal vector to S^{n-2}_∞ (specified by the condition $\hat{r}^\mu n_\mu = 0$) and $k_{\mu\nu} := K_{\mu\nu} - Hq_{\mu\nu}$. Here we used

$$M_{\rm ADM} = -\frac{1}{8\pi}\oint_{S^{n-2}_\infty} ar^{(n-1)}R_{\mu\nu}\hat{r}^\mu\hat{r}^\nu dS^{n-2} = \frac{1}{16\pi}\oint_{S^{n-2}_\infty}(\partial^i q_{ij} - \partial_j q^i{}_i)dS^j, \tag{12}$$

and

$$\begin{aligned} E_{\mu\nu} :&= {}^{(n)}C_{\mu\alpha\nu\beta}n^\alpha n^\beta \\ &= {}^{(n-1)}R_{\mu\nu} + (n-3)H\Big(k_{\mu\nu} + \frac{1}{n-3}q_{\mu\nu}k\Big) + kk_{\mu\nu} - k_\mu{}^\alpha k_{\alpha\nu}. \end{aligned} \tag{13}$$

Those can be derived following the argument of Ref. [18]. If $K = (n-1)H$ holds on Σ, we have $k = 0$ so that Eq. (11) becomes

$$E_W = M_{\rm ADM} - \frac{n-3}{8\pi}\oint_{S^{n-2}_\infty}(Har)k_{\mu\nu}\hat{r}^\mu\hat{r}^\nu dS^{n-2}. \tag{14}$$

In the same way, we obtain the same expression for the AD energy. Here we have required $k_{\mu\nu} = O(1/r^{n-1})$ to make the second term finite.[1] This fall off might be faster than naively expected (See Sec. IIB). However, on $K = (n-1)H$ slices, we have a simple expression: $E_W = E_{\rm AD} = M_{\rm ADM}$.

Here we have one serious and well known problem. AD energy defined here is associated with the static Killing vector. The Killing vector is spacelike outside of the cosmological horizon and evaluate the total energy outside the cosmological horizon. This is not congenial to the term "energy", because the energy must be measured by the *timelike* observers. In the next section, we discuss a new interpretation of the energy which supports the use of the AD energy in asymptotically de Sitter space-times.

Based on the Abbott-Deser energy, we carefully examined the gravitational energy in asymptotically de Sitter space-times so far. In this section as examples we will use the energy to testify dS/CFT correspondence and cosmic no-hair conjecture.

[1] The corresponding term in asymptotically flat space-times is $\int k_{\mu\nu}\hat{r}^\mu\hat{r}^\nu d^{n-2}S$ which is automatically finite because of the absence of the factor, Har.

4 dS/CFT correspondence

Based on the Abbott-Deser energy, we carefully examined the gravitational energy in asymptotically de Sitter space-times so far. In this section as examples we will use the energy to testify dS/CFT correspondence.

Here we shall consider the dS/CFT correspondence in terms of the gravitational energy.

The stress-energy tensor of CFT can be evaluated as [20]

$$\langle T_{\mu\nu}\rangle_{\rm CFT} = (n-2)Hq_{\mu\nu} + K_{\mu\nu} - q_{\mu\nu}K + \frac{1}{(n-3)H}{}^{(n-1)}G_{\mu\nu} + \cdots. \tag{15}$$

The derivation is quite similar to the quasi-local energy proposed by Brown and York[21], who used the Hamilton-Jacobi formalism, so that Eq. (15) has also the concept of the quasi-local energy. Hence we expect that it expresses the total gravitational energy at the conformal infinity. If this expectation is correct, it will be a demonstration of dS/CFT correspondence.

Physically the total energy is measured via the tidal force at the infinity, which is encoded in the electric part of the Weyl tensor:

$$E_{\mu\nu} = {}^{(n-1)}G_{\mu\nu} + (n-3)H(k_{\mu\nu} - q_{\mu\nu}k) + kk_{\mu\nu} - k_{\mu\alpha}k_{\nu}{}^{\alpha} + \frac{1}{2}q_{\mu\nu}(k_{\alpha\beta}k^{\alpha\beta} - k^2). \tag{16}$$

The total gravitational energy can be evaluated with $E_{\mu\nu}$ [18]. As seen in Sec. III the extrinsic curvature $K_{\mu\nu}$ has the asymptotic behavior

$$K_{\mu\nu} = Hq_{\mu\nu} + k_{\mu\nu} \tag{17}$$

where

$$k_{\mu\nu} = O\left(\frac{1}{r^{n-1}}\right) \tag{18}$$

near the conformal infinity.

Accordingly, the stress-energy tensor of CFT is written as

$$\langle T_{\mu\nu}\rangle_{\rm CFT} = \frac{1}{(n-3)H}{}^{(n-1)}G_{\mu\nu} + (k_{\mu\nu} - q_{\mu\nu}k) + \cdots. \tag{19}$$

From Eqs. (16) and (19), we have

$$(n-3)H\langle T_{\mu\nu}\rangle_{\rm CFT} - E_{\mu\nu} = -kk_{\mu\nu} + \cdots = O(1/r^{2n-2}) \tag{20}$$

near the conformal infinity.

Integrating over sphere S^{n-2} at the spatial infinity "i^0" introduced in the previous section, we obtain

$$\oint_{S^{n-2}_{\infty}} dS^{n-2}r\Big[(n-3)H\langle T_{\mu\nu}\rangle_{\rm CFT} - E_{\mu\nu}\Big]\hat{r}^{\mu}\hat{r}^{\nu} = \oint_{S^{n-2}_{\infty}} dS^{n-2}r(-kk_{\mu\nu} + \cdots)\hat{r}^{\mu}\hat{r}^{\nu} = O\Big(\frac{1}{r^{n-2}}\Big), \tag{21}$$

or

$$E_W = (n-3)H\oint_{S^{n-2}_{\infty}} dS^{n-2}r\langle T_{\mu\nu}\rangle_{\rm CFT}\hat{r}^{\mu}\hat{r}^{\nu}. \tag{22}$$

Hence the energy of CFT is identical with the total gravitational energy. This can be contrasted to Ashtekar and Das's claim[11] for AdS/CFT correspondence.

5 Summary

In this paper, we examined Abbott-Deser energy. First we showed that AD energy is identical with the energy defined by the electric part of the Weyl tensor. Since the electric part expresses the tidal force, this is physically desirable result.

We discussed the role of gravitational energy in dS/CFT correspondence. We showed that the CFT energy is same as the gravitational energy. This provides us one evidence for dS/CFT.

References

[1] E. Witten, hep-th/0106109; M. Li, hep-th/0106184; D. Klemm, hep-th/0106247; V. Balasubramanian, P. Horava and D. Minic, JHEP **0105**, 043 (2001); A. Chamblin and N. D. Lambert, Phys. Lett. **B508**, 369 (2001); hep-th/0107031; Y. Gao, hep-th/0107067; J. Bros, H. Epstein and U. Moschella, hep-th/0107091; S. Nojiri and S. D. Odintsov, hep-th/0107134; E. Halyo, hep-th/0107169; I. Sachs and S. N. Solodukhin, hep-th/0107173; A. J. Tolley and N. Turok, hep-th/0108119.

[2] G. W. Gibbons and S. W. Hawking, Phys. Rev. **D15**, 2738 (1977).

[3] A. Strominger and C. Vafa, Phys. Lett. **B379**, 99 (1996).

[4] S. Perlmutter et al, Astrophys. J. **517**, 565 (1999).

[5] A. Strominger, hep-th/0106113.

[6] J. Maldacena, Adv. Theor. Math. Phys., **2**, 231 (1998); O. Aharony, S. S. Gubser, J. Maldacena, H. Ooguri and Y. Oz, Phys. Rep. **323**, 183 (2000).

[7] S. Nojiri and S. D. Odintsov, hep-th/0106191.

[8] L. Randall and R. Sundrum, Phys. Rev. Lett. **83**, 3370 (1999); 4690 (1999).

[9] J. de Boer, E. Verlinde and H. Verlinde, JHEP **0008**, 003 (2000).

[10] T. Shiromizu and D. Ida, Phys. Rev. **D64**, 044015 (2001).

[11] A. Ashtekar and S. Das, hep-th/9911230.

[12] S. W. Hawking and I. Moss, Phys. Lett. **110B**, 35 (1982).

[13] K. Nakao, T. Shiromizu and K. Maeda, Class. Quantum Grav. **11**, 2059 (1994).

[14] L. F. Abbott and S. Deser, Nucl. Phys. **B195**, 76 (1982).

[15] T. Shiromizu, K. Nakao, H. Kodama and K. Maeda, Phys. Rev. **D47**, 3099 (1993).

[16] R. Arnowitt, S. Deser and C.W. Misner, in *Gravitation, an Introduction to Current Research*, edited by L. Witten (Wiley, New York, 1962).

[17] T. Shiromizu, Phys. Rev. **D49**, 5026 (1994); D. Kastor and J. Traschen, Class. Quantum Grav. **13**, 2753 (1996); T. Shiromizu, Phys. Rev. **D60**, 064019 (1999).

[18] A. Ashtekar and R. O. Hansen, J. Math. Phys. **19**, 1542 (1978); A. Ashtekar and A. Magnon, J. Math. Phys. **25**, 2682 (1984).

[19] A. Komar, Phys. Rev. **113**, 934 (1959).

[20] V. Balasubramanian and P. Kraus, Commun. Math. Phys. **208**, 413 (1999).

[21] J. D. Brown and J. W. York, Phys. Rev. **D47**, 1407 (1993).

[22] S. B. Gidding, E. Katz and L. Randall, JHEP **0003**, 023 (2000).

Doubly-gauge-invariant formalism of brane-world cosmological perturbations

Shinji Mukohyama

Department of Physics, Harvard University
Cambridge, MA 02138, USA

Abstract

We review the doubly gauge invariant formalism of cosmological perturbations in the Randall-Sundrum brane world. This formalism leads to four independent equations describing the evolution of scalar perturbations. Three of these equations are differential equations written in terms of gauge invariant variables on the brane only, and the other is an integro-differential equation describing non-locality due to bulk gravitational waves. At low energy the evolution of the scalar-type cosmological perturbations in the brane-world cosmology differs from that in the standard cosmology only by non-local effects due to bulk gravitational waves.

1 Introduction

The idea that our four-dimensional world may be a timelike surface, or a world-volume of a 3-brane, in a higher dimensional spacetime has been attracting a great deal of physical interests. As shown by Randall and Sundrum [1], the 4-dimensional Newton's law of gravity can be reproduced on a 4-dimensional timelike hypersurface with positive tension in a 5-dimensional AdS background despite the existence of the infinite fifth dimension.

Moreover, cosmological solutions in the Randall-Sundrum brane world scenario were found [2, 3, 4, 5]. In these solutions, the standard Friedmann equation is restored at low energy, if a parameter in the solutions is small enough. If the parameter is not small enough, it affects cosmological evolution of our universe as dark radiation [3]. Hence, the parameter should be very small in order that the brane-world scenario should be consistent with nucleosynthesis [2]. On the other hand, in ref. [6], it was shown that 5-dimensional geometry of all these cosmological solutions is the Schwarzschild-AdS (S-AdS) spacetime and that the parameter is equivalent to the mass of the black hole. Therefore, the 5-dimensional bulk geometry should be the S-AdS spacetime with a small mass, which is close to the pure AdS spacetime. Moreover, black holes with small mass will evaporate in a short time scale [7]. Thus, it seems a good approximation to consider the pure AdS spacetime as a 5-dimensional bulk geometry for the brane-world cosmology.

For the AdS bulk spacetime, the brane world scenario can reproduce the standard cosmology as evolution of a homogeneous isotropic universe at low energy. Hence, this scenario may be considered as a realistic cosmology and it seems effective to look for observable consequences of this scenario. For this purpose, cosmic microwave background (CMB) anisotropy is a powerful tool. Therefore, we would like to give theoretical predictions of the brane-world scenario on the CMB anisotropy. There are actually many papers on this subject [8, 9, 10, 11, 12, 13, 14, 15, 16, 17]. However, the calculation of the CMB spectrum is not an easy task. The main difficult problems are the following two: (i) how to give the initial condition; (ii) how to evolve perturbations. As for the first problem, there is essentially the same issue even in the standard cosmology. In this paper we shall concentrate on the problem (ii).

2 Doubly gauge-invariant formalism

In this section we review some important points of the gauge-invariant formalism of gravitational perturbations in the bulk and the doubly gauge-invariant formulation of the perturbed junction condition. For details, see refs. [8, 10].

2.1 Master equation in the bulk

Now let us consider gravitational perturbations in D-dimensional maximally-symmetric spacetimes since in the simple brane world scenario the background bulk geometry is known to be an AdS spacetime, one of three maximally symmetric spacetimes. Since a general motion of homogeneous, isotropic $(D-2)$-brane breaks the symmetry of the D-dimensional maximally symmetric spacetime to that of a $(D-2)$-dimensional constant-curvature space, we consider the following decomposition of the background spacetime.

$$g^{(0)}_{MN} = \gamma_{ab}dx^a dx^b + r^2\Omega_{ij}dx^i dx^j, \tag{1}$$

where Ω_{ij} is a metric of a $(D-2)$-dimensional constant-curvature space, γ_{ab} is a 2-dimensional metric depending only on the 2-dimensional coordinates $\{x^a\}$, and r also depends only on $\{x^a\}$.

Now let us analyze metric perturbations around the maximally symmetric background. First, let us expand metric perturbations by harmonics on the $(D-2)$-dimensional constant-curvature space. Second, let us construct gauge-invariant variables from coefficients of the harmonics expansion. This procedure is done by analyzing the gauge transformation of the coefficients and taking gauge-invariant linear combinations of them. Thirdly, we can solve the constraint equations to obtain master variables from the gauge-invariant variables. The constraint equations are, of course, a part of D-dimensional perturbed Einstein equation. Finally, we can rewrite the remaining components of Einstein equation in terms of the master variables to obtain master equations.

The master equation in general D-dimensions was first obtained in ref.[8] and confirmed in ref. [9][1]. The master equations for generic values of the $(D-2)$-dimensional momentum $\mathbf{k}$ (eg. $\mathbf{k} \neq 0$ for the $K = 0$ case) are of the following form.

$$r^{\alpha+\beta}\nabla^a[r^{-\alpha}\nabla_a(r^{-\beta}\Phi)] - (\mathbf{k}^2 + \gamma K)r^{-2}\Phi = 0, \tag{2}$$

where Φ represents one of master variables $\Phi_{(S)}$, $\Phi_{(V)}$ or $F_{(T)}$, ∇_a is the 2-dimensional covariant derivative compatible with the metric γ_{ab}, and K is the curvature constant of the $(D-2)$-dimensional constant-curvature space. Two equivalent sets of constants (α, β, γ) are listed in Table 1. Master equations for some exceptional values of $\mathbf{k}$ can be found in ref. [8].

Table 1: Two sets of values of (α, β, γ)

Φ	α	β	γ	α	β	γ
$\Phi_{(S)}$	$D-4$	1	0	$-(D-6)$	$D-4$	$2(D-5)$
$\Phi_{(V)}$	$D-2$	0	$-(D-3)$	$-(D-4)$	$D-3$	$D-3$
$F_{(T)}$	D	$-(D-3)$	$-2(D-2)$	$-(D-2)$	2	2

In the next sections we consider the $K = 0$ case only. In this case the exceptional value of $\mathbf{k}$ is $\mathbf{k} = 0$. For $\mathbf{k} = 0$, the corresponding perturbations have the plane symmetry and, thus, the generalized Birkoff's theorem guarantees that the perturbed bulk geometry is a S-AdS spacetime. Hence, the perturbation with $\mathbf{k} = 0$ is actually perturbation of the mass parameter of the S-AdS spacetime around the pure AdS and can be understood as dark radiation on the brane [3]. Hence, we shall concentrate on perturbations with non-zero $\mathbf{k}$. This treatment is, of course, justified by the fact that perturbations with different $\mathbf{k}$ are decoupled from each other at the linearized level.

As an example, let us consider the case with $D = 5$ and $K = 0$. This example is relevant for the 5-dimensional brane world with spatially flat background brane.

In this case we decompose perturbations by harmonics on a 3-dimensional flat space. As shown in Table 2, we have, for example, a gauge-invariant variable which transforms as a 2-dimensional scalar and a 3-dimensional scalar. (In Table 2, Y is a scalar harmonics, $V_{(T)i}$ is a transverse vector harmonics and $T_{(T)ij}$ is a transverse traceless tensor harmonics.) We also have a variable which transforms as a 2-dimensional symmetric tensor and a 3-dimensional scalar. Hence, we have $(1+3)\times 1$ gauge-invariant degrees of freedom

[1] In the latter paper, they extended the master equation of vector and tensor perturbations to more general background without maximal symmetry.

for perturbations which transform as 3-dimensional scalars. Similarly, we have $2\times(3-1)$ and $1\times(6-3-1)$ gauge-invariant degrees of freedom for perturbations which transform as 3-dimensional transverse vectors and transverse traceless tensors, respectively. Therefore, the total number of gauge-invariant degrees of freedom is 10. However, the number of degrees of freedom of gravitons in 5-dimensions is 5. So, we have too much gauge-invariant variables compared to the number of gravitons.

On the other hand, after solving constraint equations, all we have are master variables which transforms as 2-dimensional scalars. Hence, as shown in Table 2, the total number of reduced degrees of freedom is 5. Therefore, the master variables concisely describes gravitons in 5-dimensions.

Table 2: Number of degrees of freedom

	3-D scalar	3-D T vector	3-D TT tensor	# of variables
2-D scalar	$FY\delta_{ij}$		$F_{(T)}T_{(T)ij}$	
2-D vector		$F_aV_{(T)i}$		
2-D tensor (symmetric)	$F_{ab}Y$			
	$(1+3)\times 1$	$2\times(3-1)$	$1\times(6-3-1)$	10
Master variables	$\Phi_{(S)}$	$\Phi_{(V)}$	$F_{(T)}$	
	1×1	$1\times(3-1)$	$1\times(6-3-1)$	5

2.2 Perturbed junction condition

Having the description of the bulk gravitational waves, what we have to do is to investigate Israel junction condition [18].

First, let us represent the world volume of a $(D-2)$-brane in a D-dimensional spacetime by the parametric equations

$$x^M = Z^M(y), \tag{3}$$

where x^M $(M=0,\cdots,D-1)$ and y^μ $(\mu=0,\cdots,D-2)$ are D-dimensional coordinates and $D-1$ parameters, which play a role of $(D-1)$-dimensional coordinates on the brane world-volume. Next, let us consider perturbations of the functions Z^M and the D-dimensional metric g_{MN}. Then, we can calculate perturbations of the induced metric and the extrinsic curvature of the hypersurface as functions of y^μ. Next, we can express the perturbed junction condition in terms of these perturbations and matter perturbations on the brane. Finally, by applying the perturbed junction condition to the homogeneous isotropic background motion of the $(D-2)$-brane and performing the harmonic expansion as in the previous subsections, we can obtain junction conditions for gauge-invariant variables and master variables.

The final expression can be found in refs. [10]. (See also ref. [9].) Here, I would only like to stress one important aspect of the perturbed junction condition.

First, since we are supposed to be living on the brane, physics in our world must not be affected by the following D-dimensional gauge transformation in the higher dimensional bulk.

$$x^M \to x^M + \xi^M(x). \tag{4}$$

On the other hand, all observable quantities in our world must be invariant under the following $(D-1)$-dimensional gauge transformation on the brane.

$$y^\mu \to y^\mu + \zeta^\mu(y). \tag{5}$$

What is important here is that these two kinds of gauge transformations are independent. One might expect that the $(D-1)$-gauge transformation would be a part of the D-gauge transformation. In fact, as explicitly shown in ref. [10], it is not. Therefore, all physical quantities in our world on the brane must be invariant under these two independent gauge transformations. In particular, the junction condition must, and actually can, be written in terms of doubly-gauge-invariant variables only.

3 Integro-differential equation

We already have all basic equations. Namely, we have master equations in the bulk and doubly-gauge-invariant junction condition. The next task we have to do would be to simplify the basic equations to extract physics from them. In this paper we consider scalar perturbations for $D = 5$, $K = 0$.

Before showing the result, let us think about what would be expected. See figure 1. First, let us consider a perturbations localized on the brane. In other words, matter perturbations. By definition, they propagate on the brane. However, at the same time, they can generate gravitational waves. Gravitational waves can, of course, propagate in the bulk spacetime, and may collide with the brane at a spacetime point different from the spacetime point at which the gravitational waves were produced ($t_1 \neq t_2$, $\mathbf{x}_1 \neq \mathbf{x}_2$). When they collide with the brane, they should alter evolution of perturbations localized on the brane. Hence, evolution of perturbations localized on the brane should be non-local. It must, and actually can, be described by some integro-differential equations.

Figure 1: Non-locality due to bulk gravitational waves

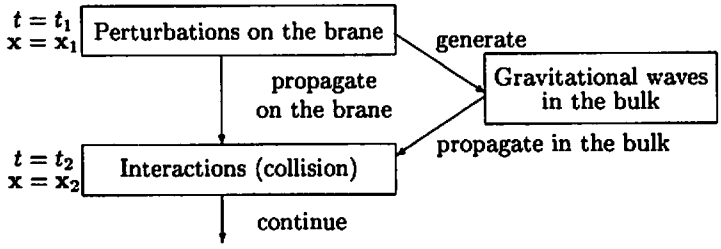

For scalar perturbations, the result of the simplification is three differential equations and an integro-differential equation on the brane [17]. Two of the three differential equations can be understood as the perturbed conservation equation, which is a general consequence of the junction condition. These two are, of course, exactly the same as the corresponding equations in the standard cosmology. The other of the three differential equations differs from the corresponding equation in the standard cosmology only by terms of order $O(\rho/\lambda, p/\lambda)$, where ρ and p are energy density and pressure of the background matter on the brane and λ is the tension of the brane. Therefore, that equation reduces to the equation in the standard cosmology at low energy ($|\rho/\lambda| \ll 1$, $|p/\lambda| \ll 1$).

The last of the four equations is an integro-differential equation of the form

$$\tilde{R}(t) + \int dt' \, K(t,t')S(t') = 0, \tag{6}$$

if we assume that there is no gravitational waves coming from outside of the Poincare patch of the bulk AdS [2], where $\tilde{R}(t)$ is a linear combination of gauge-invariant metric and matter perturbations and their time-derivatives, $S(t)$ is a linear combination of gauge-invariant matter perturbations, and the kernel $K(t,t')$ is constructed from the retarded Green function of the master equation for bulk gravitational waves. Here, we mention that all physical quantities were constructed from coefficients of the 3-dimensional harmonic expansion and that the kernel $K(t,t')$ depends on $\mathbf{k}^2$ quite non-trivially since the master equation depends on $\mathbf{k}^2$, where $\mathbf{k}$ is the 3-dimensional momentum vector. Thus, this equation indeed describes the non-locality due to bulk gravitational waves: the matter perturbation $S(t')$ at the time t' generates gravitational waves and the gravitational waves, in turn, affects the evolution of the perturbation $\tilde{R}(t)$ on the brane at the different time t. The corresponding equation in the standard cosmology is, of course, local and differs from $\tilde{R} = 0$ only by a term of order $O(\rho/\lambda, p/\lambda)$.

Therefore, if we consider a low energy regime, where $|\rho/\lambda| \ll 1$ and $|p/\lambda| \ll 1$, then the four equations for scalar perturbations are almost the same as the corresponding equations in the standard cosmology. The only difference is the non-local term due to bulk gravitational waves. Since a large amount of bulk

[2]For the modification by gravitational waves coming from outside of the Poincare patch, or initial gravitational waves, see ref. [17].

gravitational waves can be produced at an early stage of the brane universe and propagate in the bulk, there may be a possibility that the non-local effect is significant even at a low-energy stage. Further investigation is needed.

References

[1] L. Randall and R. Sundrum, Phys. Rev. Lett. **83**, 4690 (1999) [hep-th/9906064].

[2] P. Binétruy, C. Deffayet, U. Ellwanger and D. Langlois, Phys. Lett. **B477**, 285 (2000) [hep-th/9910219].

[3] S. Mukohyama, Phys. Lett. **B473**, 241 (2000) [hep-th/9911165].

[4] P. Kraus, JHEP **9912**, 011 (1999) [hep-th/9910149].

[5] D. Ida, JHEP **0009**, 014 (2000) [gr-qc/9912002].

[6] S. Mukohyama, T. Shiromizu and K. Maeda, Phys. Rev. **D62**, 024028 (2000), Erratum-ibid. **D63**, 029901 (2001) [hep-th/9912287].

[7] S. W. Hawking, Commun. Math. Phys. **43**, 199 (1975).

[8] S. Mukohyama, Phys. Rev. **D62**, 084015 (2000) [hep-th/0004067].

[9] H. Kodama, A. Ishibashi and O. Seto, Phys. Rev. **D62**, 064022 (2000) [hep-th/0004160].

[10] S. Mukohyama, Class. Quant. Grav. **17**, 4777 (2000) [hep-th/0006146].

[11] R. Maartens, Phys. Rev. **D62**, 084023 (2000) [hep-th/0004166]; C. Gordon and R. Maartens, Phys. Rev. **D63**, 044022 (2001) [hep-th/0009010]; R. Maartens, V. Sahni and T. D. Saini, Phys. Rev. **D63**, 063509 (2001) [gr-qc/0011105].

[12] D. Langlois, Phys. Rev. **D62**, 126012 (2000) [hep-th/0005025]; Phys. Rev. Lett. **86**, 2212 (2001) [hep-th/0010063].

[13] C. van de Bruck, M. Dorca, R. Brandenberger and A. Lukas, Phys. Rev. **D62**, 123515 (2000) [hep-th/0005032].

[14] K. Koyama and J. Soda, Phys. Rev. **D62**, 123502 (2000) [hep-th/0005239].

[15] D. Langlois, R. Maartens and D. Wands, Phys. Lett. **B489**, 259 (2000) [hep-th/0006007].

[16] D. Langlois, R. Maartens, M. Sasaki and David Wands, Phys. Rev. **D63**, 084009 (2001) [hep-th/0012044].

[17] S. Mukohyama, Phys. Rev. **D64**, 064006 (2001) [hep-th/0104185].

[18] W. Israel, Nuovo Cim. **B44**, 1 (1966); Erratum-ibid. **B48**, 463 (1967).

Bubble Instability of the Brane-World

Daisuke Ida,[1] Tetsuya Shiromizu,[2]

Reserch Center for the Early Universe, The University of Tokyo, Tokyo, 113-0033, Japan

Hirotaka Ochiai[3]

Department of Physics, The University of Tokyo, Tokyo, 113-0033, Japan

Abstract

In pure gravity, the Randall-Sundrum two-brane system is semiclassically unstable by creating many small bubbles, which will occupy the Anti-de Sitter five-space. The gravitational instanton describing such instability has been given. This process can also be regarded as the pair annihilation of the positive and negative tension branes.

The possibility of the existence of extra-dimensions is much discussed in recent progress of the unified theory of elementary particles. The extra-dimensions, if exist, should have sufficiently small size such that light Kaluza-Klein modes are not excited, because the current civilization is not aware of them. In other words, the possible maximal size of the extra-dimensions is typically determined by the energy scale of the particle accelerators. On the other hand, there is a new idea that all interactions except for the gravitational interaction are confined to a boundary (brane) of the higher dimensional space-time. Then, the size of the extra-dimensions need not be so small, in which case it is bounded above at most by the length scale of the gravitational experiments verifying the Newton's inverse square law. A simple but consistent model of such brane-worlds was given by Randall and Sundrum, which consists of a single (RSII model) or a pair of (RSI model) four-dimensional Minkowski brane(s) embedded into the five-dimensional Anti-de Sitter space. The brane does not inherit the gravitational interaction of that of five-dimensions, but the right Newton law is realized at least at much larger scale than the AdS radius. Since this model has not yet been excluded even by the latest experiments, it is natural to test its theoretical consistency. In particular, we are interested in its behaviour under the strong gravitation; the stability, the effects on the observational cosmology, black hole physics, and so on. What we shall discuss here is the stability of the Randall-Sundrum model taking quantum gravitational effects into account. Witten showed that the Kaluza-Klein vacuum is unstable under the creation of a bubble, which consists of nothing and expands at nearly the speed of light. This process can be regarded as the effect of the extra-dimension, so that one might expect that the Randall-Sundrum model has similar instability. We shall show that this is the case by constructing an explicit model describing such a semiclassical process.

The Randall-Sundrum model of single brane system (RSII) is given by the metric of the form

$$g = dy^2 + e^{-2|y|/\ell} q_{\mu\nu} dx^\mu dx^\nu, \tag{1}$$

where q is the four-dimensional Minkowski metric. The metric (1) is that of of the five-dimensional AdS space, and the brane is located at $y = 0$ on which

$$K_{\mu\nu} := \frac{1}{2}\pounds_n h_{\mu\nu} = -\frac{1}{\ell} h_{\mu\nu}, \tag{2}$$

is satisfied, where $n = \partial_y$ and $h_{\mu\nu} = e^{-2|y|/\ell} q_{\mu\nu}$ is the unit normal vector and the induced metric of a $y =$ constant hypersurface. If the four-dimensional metric q is replaced by a Ricci-flat metric, then Eq. (1) represents an more generic Einstein metric. Let us write the brane-metric in the form

$$q = -r^2 d\tau^2 + dr^2 + r^2 \cosh^2 \tau d\Omega_2{}^2, \tag{3}$$

[1] E-mail: ida@resceu.s.u-tokyo.ac.jp
[2] E-mail: siromizu@utap.phys.s.u-tokyo.ac.jp
[3] E-mail: ochiai@utap.phys.s.u-tokyo.ac.jp

where $d\Omega_2{}^2$ denotes the standard metric of the unit two-sphere. The metric (3) represents the Rindler space, which is locally flat, but geodesically incomplete at the null hypersurface $r = 0$ (Rindler horizon). Each r = constant hypersurface corresponds to the world sphere in a uniformly accelerated expansion. We here consider another generalization of Eq. (1) with a same asymptotics as Eq. (3) on the brane. This is given by

$$g = \left[\frac{1-(\rho_*/ar)^2}{1+(\rho_*/ar)^2}\right]^2 dy^2 + a^2\left[1+\left(\frac{\rho_*}{ar}\right)^2\right]^2(-r^2d\tau^2 + dr^2 + r^2\cosh^2\tau d\Omega_2{}^2), \tag{4}$$

where $\rho_* > 0$ is a constant and $a := e^{-|y|/\ell}$. The metric (4) solves the five-dimensional Einstein equation with a negative cosmological term and Eq. (2) is also satisfied at every y = constant hypersurface. The coordinate system used here is inappropriate at $ar = \rho_*$, however this is only a coordinate singularity as shown below. The metric (4) is obtained by analytic continuation of the five-dimensional AdS-Schwarzschild space-time, of which metric has the form

$$g = -F(R)dT^2 + F(R)^{-1}dR^2 + R^2(d\chi^2 + \sin^2\chi d\Omega_2{}^2), \tag{5}$$

$$F(R) = 1 - \left(\frac{R_*}{R}\right)^2 + \left(\frac{R}{\ell}\right)^2. \tag{6}$$

This metric can be analytically continued at the totally geodesic surfaces $T = 0$ and $\chi = \pi/2$ by replacement of the coordinates

$$T \mapsto i\Theta, \quad \chi \mapsto \frac{\pi}{2} + i\tau. \tag{7}$$

Then the new metric becomes

$$g = F(R)d\Theta^2 + F(R)^{-1}dR^2 + R^2(-d\tau^2 + \cosh^2\tau d\Omega_2{}^2), \tag{8}$$

which represents the straightforward generalization of the Kaluza-Klein bubble. The (Θ, R)-plane is geodesically incomplete at

$$R = R_h := \ell\left[\frac{1}{2}\left(1+\frac{4R_*^2}{\ell^2}\right)^{1/2} - \frac{1}{2}\right]^{1/2}, \tag{9}$$

which can be removed by making Θ periodic with the period given by the inverse Hawking temperature: $\beta_H := 4\pi/F'(R_h)$. We shall however temporally regard the coordinate Θ as non-periodic. To arrive at the brane-world metric (4), we consider the coordinate transformation given by

$$R = ar\left[1+\left(\frac{\rho_*}{ar}\right)^2\right], \tag{10}$$

$$\Theta = y + \frac{1}{\ell}\int_{R_*}^{R}\frac{R}{F(R)}\left(1-\frac{R_*{}^2}{R^2}\right)^{-1/2}dR, \tag{11}$$

where $\rho_* = R_*/2$ and $a = e^{-y/\ell}$, and the coordinates range over $(-\infty < y < +\infty, ar > \rho_*)$. This chart covers the region $R > R_*$ of the $\{\Theta, R\}$-coordinate system. If we impose the Z_2-boundary condition at $y = 0$ surface, then we will obtain the brane-world model. This however is not sufficient, since $y = 0$ surface is geodesically incomplete at $r = \rho_*$ $[(\Theta, R) = (0, R_*)]$. This can easily be made geodesically complete by reflecting with respect to the surface $\Theta = 0$; If the $y = 0$ surface is given by B_+: $\{\Theta = f(R)\}$, then the reflected surface B_-: $\{\Theta = -f(R)\}$ smoothly continues to B_+ at $R = R_*$. We obtain the brane-world model with the brane at $B = B_+ \cup B_-$ in this way (see Fig. 1).

However, the bulk is geodesically incomplete since it contains the point $R = R_h$, if a *single positive tension* brane is considered. Therefore, the coordinate Θ should be periodic in this case. Then, the brane intersects itself at a point given by $f(R) = \beta_H/2$, where a domain wall (in a four-dimensional sense) should be located. This means that the brane has a spatially compact topology, so that this is not asymptotic to the RSII model.

Next, let us consider a generalization of the Randall-Sundrum model with two branes (RSI), in which a pair of branes with respective positive and negative tension is parallelly located at the boundary of the

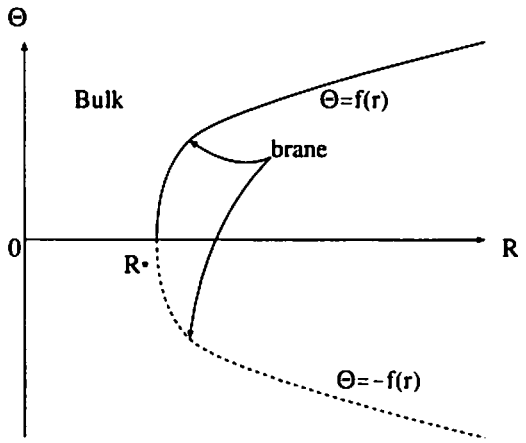

Figure 1: The location of a brane in (R, Θ)-plane for RSII single-brane system.

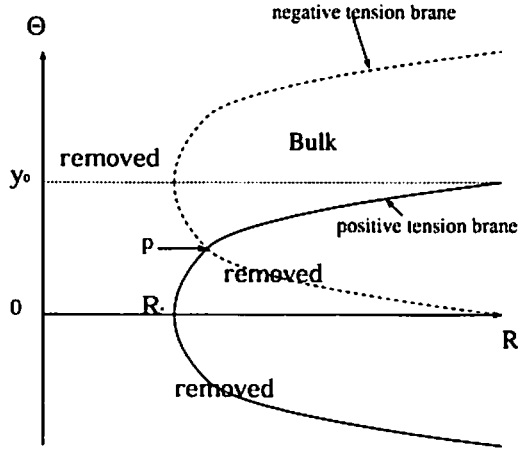

Figure 2: The location of branes in (R, Θ)-plane for RSI two-brane system.

AdS bulk. In the present case, since the (Θ, R)-plane is invariant under the translation in Θ-direction, we can consider many copies of the brane already constructed by such a parallel translation. If the positive tension brane is given by $B = B_+ \cup B_-$, the negative tension brane can be obtained by $\bar{B} = \bar{B}_+ \cup \bar{B}_-$, where $\bar{B}_\pm$: $\{\Theta = \pm f(R) + y_0\}$, and y_0 denotes the separation of branes. Two branes B and $\bar{B}$ intersect at p given by $\Theta = y_0/2$; namely, two branes are connected (see Fig. 2). In the present case, we need not make Θ periodic, since the center $R = R_h$ can be sealed off behind the negative tension brane, so that we can obtain a brane-world model asymptotic to RSI. Note that the induced metric of the brane is smooth at p, where just the embedding of the boundary is singular; In fact, the intrinsic geometry of the brane constructed here is same as that of B in isolation.

Here we shall consider the induced metric h of the brane B. It can be shown that h is given by

$$h = \left[1 + \left(\frac{\rho_*}{r}\right)^2\right]^2 (-r^2 d\tau^2 + dr^2 + r^2 \cosh^2 \tau d\Omega_2{}^2). \tag{12}$$

The coordinate r now ranges all positive value, where the region $r > \rho_*$ corresponds to B_+ and $0 < r < \rho_*$ to B_- [note that the metric (12) is invariant under $r \mapsto \rho_*^2/r$]. Let us introduce null coordinates

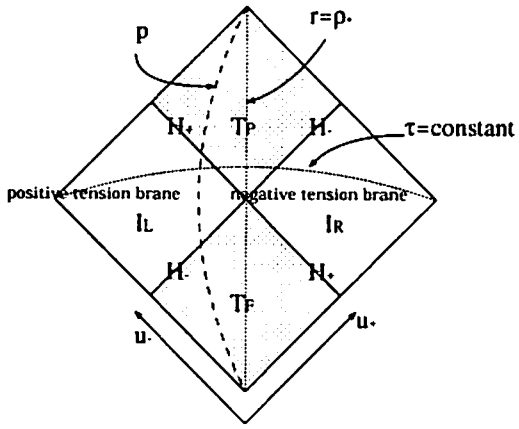

Figure 3: The Penrose diagram for the induced geometry of the brane corresponding to the situation in FIG. 2. The dashed line denotes the surface p connecting two branes.

$u_\pm = \tau \pm \ln(r/\rho_\bullet)$, then the metric (12) becomes

$$h = -{\rho_\bullet}^2 e^{u_+ + u_-} \left(e^{-u_+} + e^{-u_-}\right)^2 du_+ du_- + \mathcal{R}(u_+, u_-)^2 d{\Omega_2}^2, \tag{13}$$

where

$$\mathcal{R}(u_+, u_-) = \frac{\rho_\bullet}{2}(1 + e^{u_+ + u_-})(e^{-u_+} + e^{-u_-}). \tag{14}$$

Then, the expansion rates of the outgoing and the ingoing spherical rays are given by

$$\theta_\pm := \frac{\partial \ln \mathcal{R}}{\partial u_\pm} = \frac{e^{u_\pm} - e^{-u_\pm}}{(1 + e^{u_+ + u_-})(e^{-u_+} + e^{-u_-})}, \tag{15}$$

respectively. There are null hypersurfaces $H_\pm$

$$H_\pm : u_\pm = 0 \tag{16}$$

on which $\theta_\pm$ vanishes, respectively. The brane (B, h) is divided by $H_\pm$ into four regions; (i) I_R: right asymptotic region $u_+ > 0$, $u_- < 0$ $[(\theta_+, \theta_-) = (+, -)]$, (ii) I_L: left asymptotic region $u_+ < 0$, $u_- > 0$ $[(\theta_+, \theta_-) = (-, +)]$, (iii) T_P: past trapped region $u_+ > 0$, $u_- > 0$ $[(\theta_+, \theta_-) = (+, +)]$, (iv) T_F: future trapped region $u_+ < 0$, $u_- < 0$ $[(\theta_+, \theta_-) = (-, -)]$. The Penrose diagram is depicted in Fig. 3.

Each $\tau =$ constant hypersurface has the Einstein-Rosen bridge around $r = \rho_\bullet$. Thus, both of the bulk and the brane has non-trivial topology (simply connected but with non-vanishing second Betti number), which represents the creation of a sort of bubbles (RS bubbles). One however cannot traverse from one side to the other; Once someone steps into T_P, he will never make an exit. Thus, the region T_P is a kind of black holes, though there is much difference from what we know of black holes. In particular, the total gravitational energy vanishes, which indicates that the RSI model might decay by creating RS bubbles semiclassically. A creation of a bubble implies a cross-linking of two branes through a topology changing process of the bulk and the brane. There is negative energy distribution around the RS bubble, which comes from the electric part of the five-dimensional Weyl tensor

$$E_{\mu\nu} = {}^{(5)}C_{\mu\alpha\nu\beta} n^\alpha n^\beta \tag{17}$$

through the effective Einstein equation on the brane

$${}^{(4)}G^\nu_\mu = -E^\nu_\mu = \frac{4\rho_\bullet^2 r^4}{(r^2 + \rho_\bullet^2)^4}(\delta^\tau_\mu \delta^\nu_\tau - 3\delta^\tau_\mu \delta^\nu_\tau + \delta^\vartheta_\mu \delta^\nu_\vartheta + \delta^\varphi_\mu \delta^\nu_\varphi). \tag{18}$$

The energy density observed by r = constant observer therefore becomes

$$\epsilon = -\frac{\rho_*^2 r^4}{2\pi G_4 (r^2+\rho_*^2)^4} < 0, \tag{19}$$

of which amplitude peaks at $r = \rho_*$ with $|\epsilon| = (32\pi G_4 \rho_*^2)^{-1}$, and rapidly dumps as $1/r^4$ ($r \to +\infty$).

Finally, we shall estimate the semiclassical decay probability of the RSI brane-world based on the euclidean path integral approach to the quantum gravity. The corresponding euclidean bounce solution is obtained by the Wick rotation, $\tau \to i\tau_E + \pi/2$, of the metric of Eq (4). The decay occurs at $\tau = 0$ because the 4-dimensional surfaces at $\tau = 0$ is momentary static. As a result the decay probability will be of order $P \sim \exp(-\ell\rho_*^2/G_5)$. Where G_5 is the five-dimensional gravitational constant $G_5 \sim \ell G_4 e^{2y_0/\ell}$, y_0 is the typical coordinate distance between two branes. In the RSI models we often assume $G_5 \sim 1\mathrm{TeV}^{-3}$ and $\ell \sim 1\mathrm{mm}$. For $\rho_* > (G_5/\ell)^{1/2} \sim (10^{11}\mathrm{GeV})^{-1}$, this decay process might be suppressed.

Let us summarise our study. We have constructed an example describing the decay of the Randall-Sundrum brane-world model. The brane geometry has the structure of the Einstein-Rosen bridge. Thus it rather resembles wormhole geometry, which can be regarded as the effect of the negative effective energy induced by the bulk Weyl tensor. In other words, this decay process can be thought of as the pair annihilation of the positive and negative tension branes. Accordingly, it turns out that RSI-type model is realized, but RSII-type model is not. The decay probability of the RSI model has been roughly evaluated. We have discussed taking only the pure gravity into account. However, the introduction of spinor field may be important since it might kinematically forbid this decay process.

References

[1] D. Ida, T. Shiromizu, H. Ochiai, *"Semiclassical Instability of the Brane-World: Randall-Sundrum Bubbles."* Physical Review **D65** (2001) 023504.

Radion fluctuations in Brane Worlds

Kazuya Koyama[1]

Graduate School of Human and Environment Studies, Kyoto University, Kyoto 606-8501, Japan

Abstract

We investigate the effect of the bulk-brane interaction on the cosmological perturbations on the brane in two branes model. At large scales, only the anisotropic perturbations on the brane can interact with the bulk. We find the CMB anisotropy on our brane depends on the matter on a hidden brane and the radion which is the distance from our brane to the hidden brane. If the radion is time varying, the CMB anisotropy is also affected by the brane's own fluctuation

1 Introduction

Recent developments of the particle physics revive the old idea that we are living in 4D brane in higher dimensional spacetime. Since Randall and Sundrum proposed fascinating model for brane world idea, many works have been done about the consistency of their model with observations [1]. The cosmological consequences of the model have been actively investigated. It has been shown that the spatially homogeneous and isotropic universe can be embedded in this model. In order to study further consistency of the model with the observations, it is needed to study the behaviour of the cosmological perturbations [2].

At large scales it is known that the curvature perturbation ζ on uniform density hypersurface can be determined independently of the bulk perturbations. But, the anisotropic perturbation cannot be determined unless bulk geometry is known. This is because the anisotropic perturbations on the brane are coupled to the bulk perturbations. Because the anisotropic perturbations are directly related to the CMB anisotropy, it is important to know how the bulk affects the anisotropic perturbations. In this paper, we consider the two branes model and study the effect of the existence of the hidden brane in the bulk on the CMB anisotropy inside our brane.

Our system is described by the action;

$$S=\frac{1}{2\kappa^2}\int d^5x\sqrt{-g}\left(\mathcal{R}^5+\frac{12}{l^2}\right)+\sum_{i=A,B}\left(-\sigma^i\int d^4x\sqrt{-g_{brane\,i}}+\int d^4x\sqrt{-g_{brane\,i}}\mathcal{L}_{matter^i}\right), \quad (1)$$

where $\mathcal{R}^5$ is the 5D Ricci scalar, l is the curvature radius of the AdS spacetime and $\kappa^2=8\pi G_5$ where G_5 is the Newton's constant in the 5D spacetime. We will assume the 5-dimensional spacetime is S_1/Z_2 compactified. There are two branes (brane A and brane B) sitting at the S_1/Z_2 orbifold fixed points with the tension σ^A and σ^B respectively. The tension of the two branes are taken as

$$\kappa^2\sigma^A=\frac{6}{l},\quad \kappa^2\sigma^B=-\frac{6}{l} \quad (2)$$

in order to ensure that the brane becomes Minkowski spacetime without matter on the brane. The induced metric on the brane i is denoted as $g_{brane\,i}$ and the matter confined to the brane i is described by the lagrangian $\mathcal{L}_{matter^i}$. We are assumed to live in positive tension brane A.

We take the metric for the background spacetime as

$$ds^2=e^{2\gamma(y,t)}dy^2-e^{2\beta(y,t)}dt^2+e^{2\alpha(y,t)}\delta_{ij}dx^idx^j. \quad (3)$$

The y coordinate is compact and runs from $-l$ to l. Furthermore, the identification of (y,t,x^i) with $(-y,t,x^i)$ is made. Thus the space is S_1/Z_2 compactified. Two branes are located at orbifold fixed

[1] E-mail:kazuya@phys.h.kyoto-u.ac.jp

points; the brane A and the brane B are located at $y = 0$ and $y = l$ respectively. The radion is defined as the physical distance between the branes. Thus the radion $d(t)$ is given by

$$d(t) = \int_0^l dy e^{\gamma(y,t)}. \tag{4}$$

We will denote the power series expansion near the branes as

$$\begin{aligned} \alpha(y,t) &= \alpha_0(t) + \alpha_1(t)|y| + \frac{\alpha_2(t)}{2}y^2 + \cdots, \\ \alpha(y,t) &= \alpha_0^B(t) + \alpha_1^B(t)|y - d_*| + \frac{\alpha_2^B(t)}{2}|y - d_*|^2 + \cdots. \end{aligned} \tag{5}$$

2 Cosmological perturbations

We consider the large scale cosmological perturbations in this background spacetime. The perturbed 5D energy-momentum tensor is taken as

$$\delta T_N^M = \begin{pmatrix} 0 & 0 & 0 \\ 0 & -\delta\rho & -(\rho+p)e^{\alpha_0}v_{,i} \\ 0 & (\rho+p)e^{-\alpha_0}v_{,i} & \delta p\,\delta_{ij} \end{pmatrix} \delta(y), \tag{6}$$

where we assume the anisotropic stress vanishes. The perturbed metric at large scales are written as

$$ds^2 = e^{2\gamma}dy^2 - e^{2\beta}(1+2\Phi)dt^2 + e^{2\alpha}\left((1-2\Psi)\delta_{ij} + 2E_{,ij}/k^2\right)dx^i dx^j. \tag{7}$$

The formalism to calculate the cosmological perturbations is complicated. In this paper, we only show the results. The readers who want to know the details can refer to the papers [2]. For simplicity, the low energy universe $\kappa^2 l\rho \ll 1$ will be considered. The metric perturbations and matter perturbations on the brane can be written by two unknown functions; an anisotropic bulk perturbation evaluated at our brane E_0 and a physical fluctuation of the brane φ. The metric perturbations are given by

$$\begin{aligned} \Phi_0 &= -\frac{1}{l}\varphi, \\ \Psi_0 &= \frac{1}{l}\varphi, \\ E_0 &= E_0. \end{aligned} \tag{8}$$

The matter perturbations are given by

$$\begin{aligned} \kappa^2\delta\rho &= -6(\dot{\alpha}_0\dot{\varphi} - \dot{\alpha}_0^2\varphi), \\ \kappa^2\delta p &= 2(\ddot{\varphi} + 2\dot{\alpha}_0\dot{\varphi} - (2\ddot{\alpha}_0 + 3\dot{\alpha}_0^2)\varphi). \end{aligned} \tag{9}$$

The bulk perturbation E should satisfy the wave equation in the bulk

$$E'' - d(t)\frac{4}{l}E' = d(t)^2 e^{2d(t)y/l}\left(\ddot{E} + \left(\frac{\dot{d(t)}}{d(t)} + 3\dot{\alpha}_0 - 2\dot{d(t)}\frac{y}{l}\right)\dot{E}\right), \tag{10}$$

where we used the fact that the background metric at low energies is given by

$$\begin{aligned} \alpha &= -d(t)\frac{y}{l} + \alpha_0(t), \\ \beta &= -d(t)\frac{y}{l}, \\ \gamma &= \log d(t). \end{aligned} \tag{11}$$

The wall fluctuation acts as a source in the junction condition for E at each brane:

$$E_1/k^2 = d(t)e^{-2\alpha_0}\varphi, \quad E_1^B/k^2 = d(t)e^{2d(t)}e^{-2\alpha_0}\varphi^B. \tag{12}$$

From these equations we should solve unknown functions E_0 and φ and determine the behavior of the metric perturbations on the brane.

3 Wall fluctuation

We first derive the solution for wall fluctuation φ. For adiabatic perturbations $\delta p = c_s^2 \delta\rho$, we can obtain the evolution equation for wall fluctuation φ as

$$\ddot{\varphi} + (2 + 3c_s^2)\dot{\alpha}_0\dot{\varphi} - \left(3\dot{\alpha}_0^2 + 2\ddot{\alpha}_0 + 3c_s^2\dot{\alpha}_0^2\right)\varphi = 0. \tag{13}$$

This equation has a conserved quantity

$$\zeta_* = \varphi - \frac{\dot{\alpha}_0^2}{\ddot{\alpha}_0}\left(\frac{1}{\dot{\alpha}_0}\dot{\varphi} - \varphi\right) = const. \tag{14}$$

On the other hand, the curvature perturbation ζ on uniform density hypersurface is defined as

$$\zeta = \Psi_0 - \frac{\dot{\alpha}_0^2}{\ddot{\alpha}_0}\left(\frac{1}{\dot{\alpha}_0}\dot{\Psi}_0 + \Phi_0\right). \tag{15}$$

From (8), we find that the curvature perturbation is conserved

$$\zeta = \zeta_*. \tag{16}$$

Thus, the curvature perturbation is determined independently of the bulk perturbation E. For $w = c_s^2 = const.$ the solution for φ can be easily obtained as

$$\varphi = \frac{3(1+w)}{3w+1}\zeta_* + f(t), \quad f(t) = f_* e^{-\frac{3w+1}{2}\alpha_0}. \tag{17}$$

Physically, the first term of the solution for φ describes the bending of the brane due to the matter perturbation on the brane. The bending of the brane affects the intrinsic curvature of the brane. Then this part of the solution for φ is described by the curvature perturbation. The other solution $f(t)$ describes the brane's fluctuation which does not affect the intrinsic curvature of the brane (see Fig.1). In two branes model, the brane's fluctuation, more precisely the relative difference between the brane's fluctuations of two branes, changes the physical distance between two branes, then it can be called the radion fluctuation. The question is whether observers on the brane can detect the radion fluctuation or not. This question cannot be answered unless we solve the bulk perturbation E.

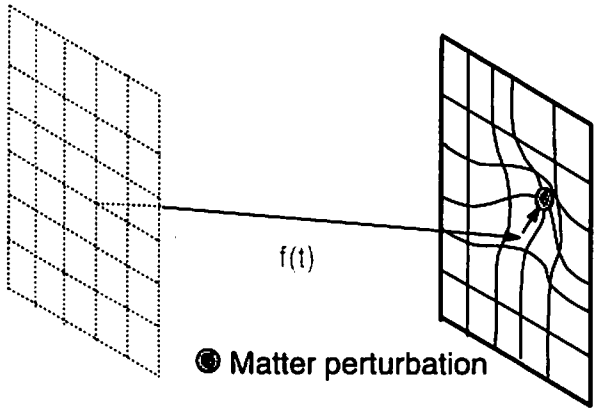

Figure 1: Schematic picture of the wall fluctuation

4 Anisotropic bulk perturbation

It is difficult to solve the wave equation for E for $\dot{d} \neq 0$ exactly. Then we consider the nearly static configuration to assume the time dependence of E is weaker than the y-dependence of E;

$$\left(\frac{\partial_t E}{\partial_y E}\right)^2 = \mathcal{E} \ll 1, \tag{18}$$

and the leading order boundary conditions are given by $E_1 = E_1^B = 0$. Then the solution for E can be written as

$$E = E_0(t) + K(t, y), \tag{19}$$

where $K/E_0 \sim \mathcal{E}$. The next order wave equation in $\mathcal{E}$ gives

$$K'' - d(t)\frac{4}{l}K' = d(t)^2 e^{2d(t)y/l}\left(-\ddot{E}_0 + \left(\frac{\dot{d(t)}}{d(t)} + 3\dot{\alpha}_0 - 2\dot{d(t)}\frac{y}{l}\right)\dot{E}_0\right). \tag{20}$$

The boundary condition for $K(y, t)$ is given by

$$K'(0,t)/k^2 = d(t)e^{-2\alpha_0}\varphi, \quad K'(l,t)/k^2 = d(t)e^{2d}e^{-2\alpha_0}\varphi^B. \tag{21}$$

The general solution for $K'(y, t)$ can be given in terms of E as

$$K'(t,y) = m(t)e^{2d(t)y/l} + n(t)\frac{y}{l}e^{2d(t)y/l} + p(t)e^{4d(t)y/l} \tag{22}$$

where

$$\begin{aligned} n(t) &= l d(t)\dot{d(t)}\dot{E}_0 \\ m(t) &= -\frac{l}{2}d(t)(\ddot{E}_0 + 3\dot{\alpha}_0\dot{E}_0) \end{aligned} \tag{23}$$

and $p(t)$ is arbitrary. The junction conditions give two constraints on the functions $m(t)$, $n(t)$ and $p(t)$;

$$\begin{aligned} m(t) + p(t) &= d(t)e^{-2\alpha_0}\varphi \\ m(t) + n(t) + p(t)e^{2d(t)} &= d(t)e^{-2\alpha_0}\varphi^B. \end{aligned} \tag{24}$$

Then by eliminating $p(t)$ from (24) and using (23) we obtain the evolution equation for E_0 as

$$\ddot{E}_0 + \left(3\alpha_0 + \dot{d(t)}\frac{e^{-d(t)}}{\sinh d(t)}\right)\dot{E}_0 = -\frac{k^2 e^{d(t)}}{\sinh d(t)}e^{-2\alpha_0}l^{-1}(\varphi - e^{-2d(t)}\varphi^B). \tag{25}$$

Using the equation

$$\exp\left(\int \frac{e^{-d(t)}}{\sinh d(t)}\dot{d(t)}\,dt\right) = 2e^{-d(t)}\sinh d(t), \tag{26}$$

the solution for E_0 can be obtained as

$$\dot{E}_0/k^2 = -e^{-3\alpha_0}\left(\frac{e^{d(t)}}{\sinh d(t)}\right)\int e^{\alpha_0}l^{-1}(\varphi - e^{-2d(t)}\varphi^B)\,dt \tag{27}$$

5 CMB anisotropy

Now let us consider the CMB temperature anisotropy. It is convenient to go to the Longitudinal gauge where the induced metric on the brane is given by

$$ds^2_{brane} = -(1 + 2\Phi_0^L)dt^2 + e^{2\alpha_0}(1 - 2\Psi_0^L)\delta_{ij}dx^i dx^j. \tag{28}$$

The metric perturbations in the Longitudinal gauge are obtained as

$$\begin{aligned}\Psi_0^L &= \Psi_0 + \dot{\alpha}_0 e^{2\alpha_0}\dot{E}_0/k^2, \\ \Phi_0^L &= \Phi_0 - e^{2\alpha_0}\ddot{E}_0/k^2 - 2\dot{\alpha}_0 e^{2\alpha_0}\dot{E}_0/k^2.\end{aligned} \tag{29}$$

The CMB anisotropy caused by the ordinary Sachs-Wolfe effect is given by

$$\frac{\Delta T}{T} = -\zeta + \Psi_0^L + \Phi_0^L. \tag{30}$$

First let us consider the limit $d \to \infty$. Then there is effectively a single brane. In this case the solution for the metric perturbations are obtained as

$$\Phi_0^L = \Psi_0^L = \frac{3(1+w)}{3w+5}\zeta_*. \tag{31}$$

This completely agrees with the result of the conventional 4D cosmology. The interesting point is that the brane's fluctuation $f(t)$ cancels out. Now consider the two branes model. For simplicity we take $\varphi^B = 0$. Then the solutions for the metric perturbations are given by

$$\begin{aligned}\Psi_0^L &= \frac{3(1+w)}{3w+1}\left(\frac{3w+1}{3w+5} - \frac{e^{-d(t)}}{\sinh d(t)}\frac{4}{3w+5}\right)\zeta_* - \frac{e^{d(t)}}{2\sinh d(t)}f(t), \\ \Phi_0^L &= \left[\frac{3(1+w)}{3w+1}\left(\frac{3w+1}{3w+5} + \frac{e^{-d(t)}}{\sinh d(t)}\frac{6(1+w)}{3w+5}\right) + \frac{\dot{d}(t)\ t}{\sinh^2 d(t)}\frac{9(1+w)^2}{(3w+1)(3w+5)}\right]\zeta_* \\ &\quad + \left[\frac{e^{-d(t)}}{2\sinh d(t)} - \frac{\dot{d}(t)\ t}{\sinh^2 d(t)}\frac{3(1+w)}{4}\right]f(t).\end{aligned} \tag{32}$$

We find that the CMB anisotropy is affected by the radion $d(t)$. Interestingly the brane's fluctuation $f(t)$ also affects the CMB anisotropy if the radion is time varying. If we include φ^B, the matter perturbation on a hidden brane also affects the CMB anisotropy.

6 Conclusion

In this paper, we investigated the effect of the existence of a hidden brane on the CMB anisotropy inside our brane in two branes model. We found that, at large scales, the curvature perturbation is determined independently of the bulk perturbation. However, anisotropic perturbations on the brane can interact with the bulk perturbation. Thus the CMB anisotropy can be affected by the bulk geometry. We found that, in two branes model, the CMB anisotropy depends on the distance from our brane to a hidden brane, that is, the radion. The matter on a hidden brane also affects the CMB anisotropy. The interesting point is that the brane can fluctuate independently of the matter perturbation on the brane. This fluctuation affects the anisotropic perturbation in the bulk. So it has a possibility to affect the CMB anisotropy. If there is a single brane, the brane's fluctuation cannot be observed. But, in two branes model, we found that the brane's fluctuation affects the CMB anisotropy if the radion is time varying. These modifications from the existence of the hidden brane can be tools to observationaly verify the brane world models.

References

[1] L. Randall and R. Sundrum, Phys. Rev. Lett. **83**, 3370, (1999). see also L. Randall and R. Sundrum, Phys. Rev. Lett. **83**, 4690, (1999).

[2] K. Koyama, J. Soda, Phys. Rev. **D62**, 123502 (2000): Phys. Rev. **D65**, 023514 (2002).

Problems of G and Multidimensional Models

Vitaly N. Melnikov[1], Vladimir D. Ivashchuk[2]

Center for Gravitation and Fundamental Metrology,
VNIIMS, 3-1 M. Ulyanovoy Str., Moscow, 117313, Russia
and
Institute of Gravitation and Cosmology,
Peoples' Friendship University of Russia,
6 Miklukho-Maklaya St., Moscow 117198, Russia

Abstract

Relations for G-dot in multidimensional model with Ricci-flat internal space and multicomponent perfect fluid are obtained. A two-component example: matter (dust) plus 5-brane as quintessence, is also considered and estimations for G-dot are given.

1 Introduction

Dirac's Large Numbers Hypothesis (LNH) is the origin of many theoretical explorations of time-varying G. According to LNH, the value of $\dot{G}/G$ should be approximately the Hubble rate. Although it has become clear in recent decades that the Hubble rate is too high to be compatible with experiment, the enduring legacy of Dirac's bold stroke is the acceptance by modern theories of non-zero values of $\dot{G}/G$ as being potentially consistent with physical reality.

There are three problems related to G, which origin lies mainly in unified models predictions: 1) absolute G measurements, 2) possible time variations of G, 3) possible range variations of G - non-Newtonian, or new interactions. For 1) and 3) see [4].

After the original *Dirac hypothesis* some new ones appeared and also some generalized *theories* of gravitation admitting the variations of an effective gravitational coupling. We may single out three stages in the development of this field:

1. Study of theories and hypotheses with variations of FPC, their predictions and confrontation with experiments (1937-1977).

2. Creation of theories admitting variations of an effective gravitational constant in a particular system of units, analyses of experimental and observational data within these theories [1] (1977-present).

3. Analyses of FPC variations within unified models [4] (present).

Different theoretical schemes lead to temporal variations of the effective gravitational constant:

1. Empirical models and theories of Dirac type, where G is replaced by $G(t)$.

2. Numerous scalar-tensor theories of Jordan-Brans-Dicke type where G depending on the scalar field $\phi(t)$ appears.

3. Gravitational theories with a conformal scalar field arising in different approaches [1].

4. Multidimensional unified theories in which there are dilaton fields and effective scalar fields appearing in our 4-dimensional spacetime from additional dimensions [4]. They may help also in solving the problem of a variable cosmological constant from Planckian to present values and cosmic coincidence problem.

[1]E-mail: melnikov@rgs.phys.msu.su, rgs@com2com.ru
[2]E-mail: ivas@rgs.phys.msu.su

A striking feature of most modern scalar-tensor and unification theories, is that they do not admit a unique and universal constant values of physical constants and of the Newtonian gravitational coupling constant G in particular. In this paper we briefly set out the results of some calculations which have been carried out for various theories, and we discuss various bounds that may be suggested by multidimensional theories. Although the bounds on G-dot and $G(r)$ are in some classes of theories rather wide on purely theoretical grounds as a result of adjustable parameters, we note that observational data concerning other phenomena may place limits on the possible range of these adjustable parameters.

Here we limit ourselves to the problem of G-dot (for $G(r)$ see [1, 2, 3, 4]). We show that the various theories predict the value of $\dot{G}/G$ to be $10^{-12}/yr$ or less. The significance of this fact for experimental and observational determinations of the value of or upper bound on G-dot is the following: any determination with error bounds significantly below 10^{-12} will typically be compatible with only a small portion of existing theoretical models and will therefore cast serious doubt on the viability of all other models. In short, a tight bound on G-dot, in conjunction with other astrophysical observations, will be a very effective "theory killer."

Some estimations for G-dot were done long ago in the frames of general scalar tensor theories using values of cosmological parameters (Ω, H, q etc) known at that time [1, 4]. It is easy to show that for modern values they predict $\dot{G}/G$ at the level of $10^{-12}/yr$ and less (see also recent estimations of A. Miyazaki [5], predicting time variations of G at the level of $10^{-13}yr^{-1}$ for the Machian-type cosmological solution in the Brans-Dicke theory).

The most reliable experimental bounds on $\dot{G}/G$ (radar ranging of spacecraft dynamics [6]) and laser lunar ranging [10] give the limit of $10^{-12}/yr$), so any results at this level or less will be very important for solving the fundamental problem of variations of constants and for discriminating between viable unified theories. So, realization of such multipurpose new generation type space experiments like Satellite Energy Exchange (SEE) for measuring G-dot and also absolute value of G and Yukawa type forces at meters and Earth radius ranges [14] become extremely urgent.

In what follows, we dwell upon some predictions for G-dot from multidimensional models.

2 G-dot in $(4+N)$-dimensional cosmology with multicomponent anisotropic fluid

We consider here a $(4+N)$-dimensional cosmology with an isotropic 3-space and an arbitrary Ricci-flat internal space. The Einstein equations provide a relation between $\dot{G}/G$ and other cosmological parameters.

2.1 The model

Let us consider $(4+N)$-dimensional theory described by the action

$$S_g = \frac{1}{2\kappa^2}\int d^{4+N}x\sqrt{-g}R\,, \tag{1}$$

where κ^2 is the fundamental gravitational constant. Then the gravitational field equations are

$$R_P^M = \kappa^2(T_P^M - \delta_P^M\frac{T}{N+2})\,, \tag{2}$$

where T_P^M is a $(4+N)$-dimensional energy-momentum tensor, $T = T_M^M$, and $M, P = 0, ..., N+3$.

For the $(4+N)$-dimensional manifold we assume the structure

$$M^{4+N} = R \times M_k^3 \times K^N\,, \tag{3}$$

where M_k^3 is a 3-dimensional space of constant curvature,
$M_k^3 = S^3$, R^3, L^3 for $k = +1, 0, -1$, respectively, and K^N is a N-dimensional compact Ricci-flat Riemann manifold.

The metric is taken in the form

$$g_{MN}dx^M dx^N = -dt^2 + a^2(t)g^{(3)}_{ij}(x^k)dx^i dx^j + b^2(t)g^{(N)}_{mn}(y^p)dy^m dy^n \ , \tag{4}$$

where $i,j,k = 1,2,3$; $m,n,p = 4,...,N+3$; $g^{(3)}_{ij}$, $g^{(N)}_{mn}$, $a(t)$ and $b(t)$ are, respectively, the metrics and scale factors for M^3_k and K^N. For T^M_P we adopt the expression of the multicomponent (anisotropic) fluid form

$$(T^M_P) = \sum_{\alpha=1}^{m} diag(-\rho^\alpha(t), p^\alpha_3(t)\delta^i_j, p^\alpha_N(t)\delta^m_n). \tag{5}$$

Under these assumptions the Einstein equations take the form

$$\frac{3\ddot{a}}{a} + \frac{N\ddot{b}}{b} = \frac{\kappa^2}{N+2}\sum_{\alpha=1}^{m}[-(N+1)\rho^\alpha - 3p^\alpha_3 - Np^\alpha_N], \tag{6}$$

$$\frac{2k}{a^2} + \frac{\ddot{a}}{a} + \frac{2\,\dot{a}^2}{a^2} + \frac{N\,\dot{a}\dot{b}}{ab} = \frac{\kappa^2}{N+2}\sum_{\alpha=1}^{m}[\rho^\alpha + (N-1)p^\alpha_3 - Np^\alpha_N], \tag{7}$$

$$\frac{\ddot{b}}{b} + (N-1)\frac{\dot{b}^2}{b^2} + \frac{3\,\dot{a}\dot{b}}{ab} = \frac{\kappa^2}{N+2}\sum_{\alpha=1}^{m}[\rho^\alpha - 3p^\alpha_3 + 2p^\alpha_N]. \tag{8}$$

The 4-dimensional density is

$$\rho^{\alpha,(4)}(t) = \int_K d^N y\sqrt{g^{(N)}}b^N(t)\rho^\alpha(t) = \rho^\alpha(t)b^(t), \tag{9}$$

where we have normalized the factor $b(t)$ by putting

$$\int_K d^N y\sqrt{g^{(N)}} = 1. \tag{10}$$

On the other hand, to get the 4-dimensional gravity equations one should put $8\pi G(t)\rho^{\alpha(4)}(t) = \kappa^2\rho^\alpha(t)$. Consequently, the effective 4-dimensional gravitational "constant" $G(t)$ is defined by

$$8\pi G(t) = \kappa^2 b^{-N}(t) \tag{11}$$

whence its time variation is expressed as

$$\dot{G}/G = -N\dot{b}/b. \tag{12}$$

2.2 Cosmological parameters

Some inferences concerning the observational cosmological parameters can be extracted just from the equations without solving them [9]. Indeed, let us define the Hubble parameter H, the density parameters Ω^α and the "deceleration" parameter q referring to a fixed instant t_0 in the usual way

$$H = \dot{a}/a, \qquad \Omega^\alpha = 8\pi G\rho^{\alpha,(4)}/3H^2 = \kappa^2\rho^\alpha/3H^2, \quad q = -a\ddot{a}/\dot{a}^2 \ . \tag{13}$$

Besides, instead of G let us introduce the dimensionless parameter

$$g = \dot{G}/GH = -Na\dot{b}/\dot{a}b. \tag{14}$$

Then, excluding b from (6) and (8), we get

$$\frac{N-1}{3N}g^2 - g + q - \sum_{\alpha=1}^{m} A^\alpha\Omega^\alpha = 0 \tag{15}$$

with

$$A^\alpha = \frac{1}{N+2}[2N+1+3(1-N)\nu_3^\alpha + 3N\nu_N^\alpha], \tag{16}$$

where

$$\nu_3^\alpha = p_3^\alpha/\rho^\alpha, \quad \nu_N^\alpha = p_N^\alpha/\rho^\alpha, \quad \rho^\alpha > 0\,. \tag{17}$$

When g is small we get from (15)

$$g \approx q - \sum_{\alpha=1}^{m} A^\alpha \Omega^\alpha. \tag{18}$$

Note that (18) for $N=6$, $m=1$, $\nu_3^1 = \nu_6^1 = 0$ (so that $A^1 = 13/8$) coincides with the corresponding relation of Wu and Wang [7] obtained for large times in case $k=-1$ (see also [8]).

If $k=0$, then in addition to (18), one can obtain a separate relation between g and Ω^α, namely,

$$\frac{N-1}{6N}g^2 - g + 1 - \sum_{\alpha=1}^{m}\Omega^\alpha = 0 \tag{19}$$

(this follows from the Einstein equation $R_0^0 - \frac{1}{2}R = \kappa^2 T_0^0$, which is certainly a linear combination of (6)-(8).

The present observational upper bound on g is

$$|\,g\,| \lesssim 0.1 \tag{20}$$

if we take in accord with [6, 10]

$$|\dot{G}/G\,| \lesssim 0.6 \times 10^{-11}(y^{-1}) \tag{21}$$

and $H = (0.7 \pm 0.1) \times 10^{-11}(y^{-1}) \approx 70 \pm 10(km/s.Mpc)$.

2.3 Two-component example: dust + $(N-1)$-brane

Let us consider two component case: $m=2$. Let the first component (called "matter") be a dust, i.e.

$$\nu_3^1 = \nu_N^1 = 0, \tag{22}$$

and the second one (called "quintessence") be a $(N-1)$-brane, i.e.

$$\nu_3^2 = 1, \qquad \nu_N^2 = -1. \tag{23}$$

We remind that as it was mentioned in [11] the multidimensional cosmological model on product manifold $\mathbf{R} \times M_1 \times ... \times M_n$ with fields of forms (for review see [13]) may be described in terms of multicomponent "perfect" fluid [12] with the following equations of state for α-s component: $p_i^\alpha = -\rho^\alpha$ if p-brane worldvolume contains M_i and $p_i^\alpha = \rho^\alpha$ in opposite case. Thus, the field of form matter leads us either to Λ-term, or to stiff matter equations of state in internal spaces.

In this case we get from (18) for small g

$$g \approx q - \frac{2N+1}{N+2}\Omega^1 + 4\frac{N-1}{N+2}\Omega^2, \tag{24}$$

and for $k=0$ and small g we obtain from (19)

$$1 - g \approx \Omega^1 + \Omega^2. \tag{25}$$

Now we illustrate the formulas by the following example when $N=6$ (K^6 may be a Calabi-Yau manifold) and

$$-q = \Omega^1 = \Omega^2 = 0.5. \tag{26}$$

We get from (24)

$$g \approx -\frac{1}{16} \approx -0.06 \tag{27}$$

in agreement with (20).

In this case the second fluid component corresponds to magnetic (Euclidean) $NS5$-brane (in $D=10$ type I, Het or II A string models). Here we consider for simplicity the case of constant dilaton field.

3 Acknowledgements

VNM is grateful to Prof. K.-I. Maeda for the support and hospitality during his stay at the conference in Waseda university.

References

[1] K.P. Staniukovich and V.N. Melnikov, *Hydrodynamics, Fields and Constants in the Theory of Gravitation* (Energoatomizdat, Moscow, 1983) p. 256 (in Russian).

[2] V.N. Melnikov, Int. J. Theor. Phys. **33** (1994) 1569.

[3] V. de Sabbata, V.N. Melnikov and P.I. Pronin, Prog. Theor. Phys. **88** (1992) 623.

[4] V.N. Melnikov, Gravity as a Key Problem of the Millennium. Proc. 2000 NASA/JPL Conference on Fundamental Physics in Microgravity, CD-version, NASA Document D-21522, 2001, p. 4.1-4.17, (Solvang, CA, USA); gr-qc/0007067.

V.N. Melnikov, Gravitation and Cosmology, **6**, N2(22) (2000) 81.

[5] A. Miyazaki, Time-Variation of the Gravitational Constant and the Machian Solution in the Brans-Dicke Theory, gr-qc/0102003.

[6] R. Hellings, Phys. Rev. Lett. **51** (1983) 1609.

E.V. Pitjeva. In: Dynamics and Astrometry of Natural and Artificial Celestial Bodies. Kluwer Acad. Publ. Nethelands, 1997, 251.

[7] Y.-S. Wu and Z. Wang, *Phys. Rev. Lett.* **57** (1986) 1978.

[8] V.D. Ivashchuk and V.N. Melnikov, Nuovo Cimento **B 102**, (1988) 131.

[9] K.A. Bronnikov, V.D. Ivashchuk and V.N. Melnikov, Nuovo Cimento **B 102** (1988) 209.

[10] J.O. Dickey *et al*, Science **265** (1994) 482.

[11] V.D. Ivashchuk and V.N. Melnikov, J. Math. Phys. **41** (2000) 6341-6363; hep-th/9904077.

[12] V.D. Ivashchuk and V.N. Melnikov, Int. J. Mod. Phys. D, **D3** (1994) 795.

[13] V.D. Ivashchuk and V.N. Melnikov, topical review, Class. Quantum Grav. **18** (2001) R1; hep-th/0110274.

[14] A. Sanders and W. Deeds, Phys. Rev. D, **46** (1992) 480.

A. Sanders, V.N. Melnikov et al., Class. Quant. Grav. **17** (2000) 2331.

V.N. Melnikov and A. Sanders, Ciencia Ergo Sum, **8** (2001) 357.

Hoop Conjecture and Cosmic Censorship in the Brane-World

Ken-ichi Nakao[1]

Department of Physics, Graduate School of Science, Osaka City University
Osaka 558-8585, Japan

Kouji Nakamura[2]

Division of Theoretical Astrophysics, National Astronomical Observatory,
Mitaka, Tokyo 181-8588, Japan

Takashi Mishima[3]

Laboratories of Physics, College of Science and Technology, Nihon University,
Narashinodai, Funabashi, Chiba 274-0063, Japan

Abstract

The initial data of gravity for a cylindrical matter distribution confined on the brane is studied in the framework of the single brane Randall-Sundrum scenario. In this scenario, 5-dimensional aspect of gravity appears in the short range gravitational interaction. We found that the sufficiently thin configuration of matter leads to the formation of the marginal surface even if the configuration is infinitely long. This means that the hoop conjecture proposed by Thorne does not hold in the Randall-Sundrum scenario; Even if a mass M does not get compacted into a region whose circumference in every direction is $\mathcal{C} \leq 4\pi GM$, black holes with horizons can form in the Randall-Sundrum scenario.

1 Introduction

Assuming 4-dimensional general relativity and physically reasonable conditions on the matter fields, Thorne has proven that there is no marginal surface in the system of a cylindrical distribution of matter fields[1]. In his proof, the marginal surface means a cylindrically symmetric spacelike 2-surface such that the expansion of the outgoing null normal to this surface vanishes. This result, together with the Newtonian analogy, has led to the so called hoop conjecture for the necessary and sufficient condition on black hole formation: *Black holes with horizons form when and only when a mass M gets compacted into a region whose circumference in every direction is $\mathcal{C} \leq 4\pi GM$*[1]. The converse of the hoop conjecture gives a criterion of naked singularity formation; *If a mass M forms a singularity but does not get compacted into a region whose circumference in every direction is $\mathcal{C} \leq 4\pi M$, then the singularity will be naked.* Then the hoop conjecture is closely related to the cosmic censorship proposed by Penrose[2] which states, roughly speaking, that the gravitational collapse in a physically reasonable situation does not lead to naked singularities. If the hoop conjecture is really true in our universe, and if a singularity formed by physically reasonable gravitational collapse is not confined within a region of $\mathcal{C} \leq 4\pi GM$, it is a counter example for the cosmic censorship.

No counter example for the hoop conjecture has been presented. Indeed, some numerical works have been done to confirm the hoop conjecture. The numerical simulations by Nakamura et al. strongly suggest that a highly elongated axisymmetric cold fluid forms a spindle naked singularity[3]. Later, Shapiro and

[1] E-mail:knakao@sci.osaka-cu.ac.jp
[2] E-mail:kouchan@th.nao.ac.jp
[3] E-mail:tmishima@ns.phys.ge.cst.nihon-u.ac.jp

Teukolsky also showed that the same is true for collisionless particle systems[4]. These numerical works suggest that the hoop conjecture will be true in 4-dimensional general relativity.

However, strictly speaking, we do not know whether general relativity can describe strong gravity in our real universe even for classical situations. We have no experimental evidence for it. If general relativity is inapplicable to the situation of the strong gravity, it again becomes a non-trivial issue whether a highly elongated spindle gravitational collapse could form naked singularities or not.

As an alternative theory of gravity, Randall and Sundrum (RS) recently proposed a scenario of the compactification of a higher dimension without compact manifold[5]. They considered 5-dimensional spacetime with negative cosmological constant $\Lambda < 0$ including a single 3-brane with the positive tension λ. In their scenario, all the physical fields, except for gravity, are assumed to be confined on the brane and the gravity is governed by 5-dimensional Einstein gravity. Using the fine tuning $\sqrt{-6/\Lambda} = 1/\lambda =: l$, they showed that even without a gap in the Kaluza-Klein spectrum, 4-dimensional Newtonian and general relativistic gravity on the brane is reproduced to more than adequate precision. The deviation in the gravitational force from the Newtonian one appears in the short scale less than l. Since experimental tests have already proved the $1/r^2$ corrections to the Newtonian gravitational potential up to the sub-millimeter order, (see e.g.[6]), the length scale of l must be less than millimeter scale.

It is natural to expect that the 5-dimensional aspect in the RS-scenario will appear in the short range force of gravity (the scale less than l). In 5-dimensional Einstein gravity there are so called the black string solutions[7], which are the cylindrically symmetric black holes in 5-dimensional spacetime. The existence of black string solutions in higher dimensional spacetime suggests that the hoop conjecture strongly depends on the spacetime dimension. Due to this higher dimensional effect, the hoop conjecture becomes a highly non-trivial issue in the RS-scenario and this is just the matter in this work[8]. Here we consider a cylindrically symmetric matter distribution on the brane and concentrate only on a time-symmetric initial data which is a 4-dimensional spacelike hypersurface embedded in the whole spacetime with vanishing extrinsic curvature[9].

2 Analisys

We assume that the intrinsic geometry on the initial data is described by the following line element,

$$dl^2 = \phi^2(R,\xi)\left(dR^2 + R^2 d\varphi^2 + dz^2 + e^{2\xi/l}d\xi^2\right). \tag{1}$$

ξ is the coordinate for the extra-dimension, which is chosen so that the brane is located at $\xi = 0$ on this initial data and the brane normal is proportional to $(d\xi)_a$. (R,φ,z) is the spatial cylindrical coordinate system on the 3-dimensional sub-space orthogonal to $(d\xi)_a$.

The conformal factor ϕ is determined by the initial value constraints of 5-dimensional Einstein gravity, i.e., the Hamiltonian constraint and momentum constraints. Since we concentrate on the time symmetric initial data, the momentum constraints are satisfied trivially. On the other hand, the Hamiltonian constraint is given by

$$\left\{ \partial_R^2 + \frac{1}{R}\partial_R + e^{-2\xi/l}\left(\partial_\xi^2 - \frac{1}{l}\partial_\xi\right)\right\}\Omega - \frac{2}{l^2}\Omega\left(\Omega^2 + 3e^{-\xi/l}\Omega + 3e^{-2\xi/l}\right) = 0, \tag{2}$$

where we have introduced a new variable defined by $\Omega := \phi - e^{-\xi/l}$.

The existence of the brane and the matter fields is taken into account by the boundary condition at $\xi = 0$. By the Israel's prescription[10], we can easily see that the extrinsic curvature of the brane in the initial hypersurface has discontinuity which is related to the tension of the brane and the stress-energy tensor of the matter fields. Following the RS-model, we impose Z_2-symmetry with respect to $\xi = 0$[11]. Then the boundary condition on the brane $\xi = 0$ is given by

$$\partial_\xi\left(e^{2\xi/l}\Omega\right) + \frac{\Omega^2}{l} + \frac{4}{3}\pi G_5\rho(R)(\Omega+1)^2 = 0, \tag{3}$$

where $G_5 = Gl$ is the 5-dimensional Newton's gravitational constant[12], $\rho(R)$ is the energy density of the matter fields. The 4-dimensional Minkowski spacetime ($\Omega = 0$) is realized on the brane when $\rho(R) = 0$.

Because of the ambiguity in the original statement by Thorne, there are many proposals and attempts to prove the hoop conjecture[13]. In this letter, we concentrate on the situation in which the support of the energy density $\rho(R)$ is in the infinite cylinder with the coordinate radius R_*. Further, as a definition of the mass, we adopt the total proper mass

$$M := 2\pi \int_0^{R_*} dRR \int_{-L}^{L} dz\phi^3(R,0)\rho(R) \tag{4}$$

within the cylinder of the coordinate radius R_* and a finite coordinate length $2L$. As the definition of the circumference, we adopt the proper length

$$C := 2\int_{-L}^{L} dz\phi(R_*,0) + 4\int_0^{R_*} dR\phi(R,0) \tag{5}$$

of this cylinder. We can easily check that the inequality $C > 4\pi GM$ holds for arbitrary L if and only if the following inequality is satisfied:

$$\frac{4\pi^2 G_5}{l\phi(R_*,0)} \int_0^{R_*} dRR\phi^3(R,0)\rho(R) \leq 1. \tag{6}$$

If the existence of future null infinity similar to the AdS or Minkowski spacetime and further the global hyperbolicity in the causal past of the future null infinity are guaranteed, the formation of a marginal surface in the initial data might mean the formation of a black hole with horizon. Then we may regard that the initial data, in which there is a marginal surface and the inequality (6) holds, as a counter example of the hoop conjecture.

There are two kinds of the marginal surfaces on the initial data: one is defined by the "null" rays confined in the brane and the other is defined by the null rays which propagate in the whole spacetime including the bulk. We call these two marginal surfaces *Brane-MS* and *Bulk-MS*, respectively. As commented in Ref.[9], these two marginal surfaces have different physical meanings from each other. Brane-MS is the marginal surface for all the physical fields confined on the brane. On the other hand, Bulk-MS is for all the physical fields including gravitons which propagate in the whole spacetime. Brane-MS is not concerned with the causal structure of the whole spacetime but Bulk-MS is.

Brane-MS for the cylindrical matter distribution is a cylindrical 2-surface specified by R =constant on the brane where the expansion of the null rays normal to the surface vanishes. In this case, the null rays are defined by the induced metric on the brane. On the time symmetric initial hypersurface, the condition of vanishing expansion of these null rays is equivalent to $\partial_R \left(R\phi^2\right)|_{\xi=0} = 0$. This is the equation for the coordinate radius of the Brane-MS.

On the other hand, Bulk-MS for the cylindrical matter distribution is a cylindrical spacelike 3-surface defined in the whole of a 4-dimensional spacelike hypersurface, on which the expansion of the outgoing null rays normal to the 3-surface vanishes. In this case, the null rays defined by the metric on the whole spacetime. On the time symmetric initial hypersurface, Bulk-MS is expressed by a curve in (R,ξ)-plane, which intersects the axes $R = 0$ and $\xi = 0$. To find this curve, we introduce spherical polar coordinate variables $r := \sqrt{R^2 + l^2(e^{\xi/l} - 1)^2}$ and $\theta := \tan^{-1}\{R/l(e^{\xi/l} - 1)\}$. Then a cylindrical spacelike 3-surface will be specified by the function $r = r(\theta)$. The condition of the vanishing expansion leads to an ordinary differential equation for $r(\theta)$ as

$$\begin{aligned}
\frac{d^2r}{d\theta^2} &= -\frac{3}{r^2}\left(\frac{dr}{d\theta}\right)^3 \partial_\theta \ln\phi + \left(\frac{dr}{d\theta}\right)^2 \left(\frac{2}{r} + 3\partial_r \ln\phi\right) \\
&- 3\frac{dr}{d\theta}\partial_\theta \ln\phi + r + 3r^2\partial_r \ln\phi \\
&+ r\left\{1 + \frac{1}{r^2}\left(\frac{dr}{d\theta}\right)^2\right\}\left(1 - \frac{1}{r}\cot\theta\frac{dr}{d\theta}\right).
\end{aligned} \tag{7}$$

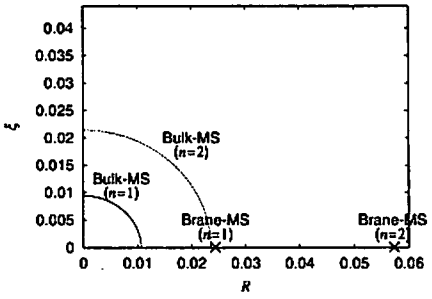

Figure 1: The Bulk-MS and the location of the Brane-MS are depicted. The matter is located within $0 \leq R < 0.01n$ at $\xi = 0$, where $n = 1, 2$.

The boundary conditions both at $\theta = 0$ and at $\pi/2$ to this equation are given by $dr/d\theta = 0$. We search for solutions of Eq.(7) numerically by the shooting method.

We solve Eq.(2) numerically by the finite difference method. The numerically covered region is $0 \leq R \leq R_{\max}$ and $0 \leq \xi \leq \xi_{\max}$. Then we need to specify the boundary conditions at four kinds of numerical boundaries; $R = 0$, $R = R_{\max}$, $\xi = 0$ and $\xi = \xi_{\max}$. We impose $\partial_R \Omega = 0$ at $R = 0$ and Eq.(3) at $\xi = 0$. To fix the boundary conditions at $R = R_{\max}$ and at $\xi = \xi_{\max}$, we assume that the system is isolated, i.e., the space approaches to that of the AdS spacetime for $r \to \infty$. Therefore, the solution should behave as those to linearized Eq.(2) near the numerical boundaries $R = R_{\max}$ and $\xi = \xi_{\max}$. (See [8])

To derive the numerical solutions, we consider the following energy density $\rho(R)$: for $R < R_s$

$$\rho(R)(\Omega + 1)^2|_{\xi=0} = \frac{3\sigma}{\pi R_s^2} \left\{ \left(\frac{R}{R_s} \right)^2 - 1 \right\}^2, \tag{8}$$

while $\rho(R) = 0$ elsewhere, where σ is a constant which corresponds to the line energy density of this system. We choose $l = 1$ (this is regarded as a choice of the unit) and then set the numerical boundaries to be $R_{\max} = \xi_{\max} = 2$. The number of numerical grids for Eq.(2) is 300×300, while that for Eq.(7) is 100. Further, we chose $G_5\sigma/l = 3 \times 10^{-2}n$ and $R_s = 10^{-2}n$, where $n = 1$ or 2. This choice of σ guarantees $|\Omega| \ll 1$ at the numerical boundaries $R = R_{\max}$ and $\xi = \xi_{\max}$.

We have checked our numerical codes for the initial data and for marginal surfaces by comparing the $l = \infty$ numerical solution of the energy density (8) with the $l = \infty$ analytic solution

$$\Omega(R, \xi) = \frac{2G_5\sigma}{3r}. \tag{9}$$

The solution (9) is obtained by solving the Hamiltonian constraint (2) with the boundary condition (3) with a singular line source $\rho(R)(\Omega + 1)^2 = \sigma\delta(R)/(2\pi R)$ under the situation $l \to \infty$.

3 Conclusion

We found both Brane-MS and Bulk-MS as shown in Fig.1. We also confirmed numerically that the inequality (6) holds in these examples. Then we may say that *the Bulk-MS can form even for so highly elongated matter distribution that the inequality $C > 4\pi GM$ is satisfied.* This is our main conclusion. This suggests that massive spindle singularities in the RS scenario will be enclosed by event horizons if the existence of future null infinity and the global hyperbolicity of its causal past are guaranteed, while those in 4-dimensional general relativity do not. Since the cosmological constant does not lead to essential effects in the short range force, as mentioned previously, the 5-dimensional feature in the gravitational interaction appear in sufficiently shorter scales than l in the RS scenario. Then, in a sufficiently shorter

range than l, black string solutions on the brane will be well approximated by 5-dimensional black string solutions in spite of the existence of a timelike singular hypersurface (brane).

We note that the Bulk-MS does not agree with the Brane-MS at the brane in our example. The same result is also obtained in Ref.[9]. To consider this behavior of the Bulk- and Brane-MS, it is instructive to compare with the analytic solutions. In the solution (9), also, the Bulk-MS ($r = G_5\sigma/3$) does not agree with the Brane-MS ($R = 2G_5\sigma/3$) at the brane ($\xi = 0$). On the other hand, in the case of the static black string solution Sch×R[7], the intersection of Bulk-MS with the brane agrees with the Brane-MS. This difference suggest the existence of gravitational waves on the initial data considered here.

Finally it should be note that our result does not necessarily mean that no naked singularity forms in the RS scenario. The pancake-type gravitational collapse might lead to serious naked singularities in the RS scenario although it is not so serious in the framework of 4-dimensional general relativity. This issue is a future problem and will be discussed elsewhere.

We would like to thank M. Yamaguchi and N. Kitazawa for helpful discussions. We are also grateful to D. Ida, A. Ishibashi, H. Ishihara, T. Tanaka, G. Uchida and H. Kodama for their useful comments and discussions. This work was partially supported by the Grant-in-Aid for Creative Basic Research (No. 09NP0801) from the Japanese Ministry of Education, Science, Sports and Culture.

References

[1] K.S. Thorne, in *Magic Without Magic; John Archibald Wheeler*, edited by J. Klauder (Frieman, San Francisco, 1972), p231.

[2] R. Penrose, Riv. Nuovo Cim. 1 (1969) 252.

[3] T. Nakamura, K. Maeda, S. Miyama and M. Sasaki, *Proceedings of the 2nd Marcel Grossmann Meeting on General Relativity* edited by R. Ruffini (Amsterdam: North-Holland), p675 (1982).

[4] S.L. Shapiro, and S.A. Teukolsky, Phys. Rev. Lett. **66**, 994 (1991).

[5] L. Randall and R. Sundrum, Phys. Rev. Lett. **83**, 4690 (1999). J. Garriga and T. Tanaka, *ibid.* **84**, 2778 (2000) M. Sasaki, T. Shiromizu and K. Maeda, Phys. Rev. **D62**, 024008 (2000). T. Shiromizu, K. Maeda and M. Sasaki, *ibid.* **D62**, 024012 (2000).

[6] G.C. Long, H. Chang, and J. Price, Nucl. Phys. **B529**, 23 (1999). C.D. Hoyle, U. Schmidt, B.R. Heckel, E.G. Adelberger, J.H. Gundlach, D.J. Kapner, and H.E. Swanson, Phys. Rev. Lett. **86**, 1418 (2001).

[7] R. Gregory and R. Laflamme, Phys. Rev. Lett. **70**, 2837 (1993). R. Gregory, Class. Quantum Grav. **17**, L125 (2000).

[8] K. Nakao, K. Nakamura, T. Mishima, gr-qc/0112076 (2001).

[9] T. Shiromizu and M. Shibata, Phys. Rev. **D62**, 7502 (2000).

[10] W. Israel, Nuovo Cimento **44B** (1966), 1; W. Israel, *ibid* **48B** (1967), 463; W. Israel, Phys. Rev. **153** (1967), 1388.

[11] M. Yamaguchi, N. Kitazawa, private communications. Z_2-symmetry is often imposed in higher dimensional models in particle physics to avoid a problem of the chirality of the matter fields on the brane.

[12] R. Emparan, G.T. Horowitz, R.C. Myers, J. High Energy Phys. **01**, 007, (2000).

[13] T. Nakamura, S.L. Shapiro, and S.A. Teukolsky, Phys. Rev. **D38**, 2972 (1988). J. Wojtkiewicz, *ibid.* **D41** 1867, (1990). E. Flanagan, *ibid.* **D46**, 1429 (1992). A.M. Abrahams, K.R. Heiderich, S.L. Shapiro, and S.A. Teukolsky, *ibid.* **D46**, 2452 (1992). E. Malec, *ibid.* **67**, 949 (1991). J. Wojtkiewicz, Class. Quantum Grav. **9**, 1255 (1992). T.P. Tod, *ibid.* **9**, 1581 (1992). T. Chiba, T. Nakamura, K. Nakao, and M. Sasaki, *ibid.* **11**, 431 (1994). C. Barrabès, A. Gramain, E. Lesigne, and P.S. Letelier, *ibid.* **9**, L105 (1992).

Future Asymptotic Stability of Compactified LRS Bianchi Type III Vacuum Solutions

Katsuhito Yasuno[1]

Department of Physics, Tokyo Institute of Technology,
2-12-1 Oh-Okayama Meguro-ku, Tokyo 152-8551, Japan

Masayuki Tanimoto[2]

Department of Physics, Yale University,
217 Prospect Street, New Haven, CT 06511, USA

Vincent Moncrief[3]

Departments of Physics and Mathematics, Yale University,
217 Prospect Street, New Haven, CT 06511, USA

Abstract

We study qualitatively the future asymptotic behavior of vacuum solutions linearly perturbed around the spatially compact, locally rotationally symmetric (LRS) Bianchi III vacuum solutions. The underlying topology of spacelike hypersurfaces in the space-time is assumed to be of a trivial circle bundle over the higher genus surface. The main result of our analysis is that the LRS Bianchi III vacuum solutions are stable but not asymptotically stable under inhomogeneous perturbations and U(1)-symmetric perturbations with eigenvalues of the Laplace-Beltrami operator on the higher genus surface being greater than 1/4. We also find that one of the two independent (local) graviational-wave degrees of freedom decays asymptotically in the expanding direction.

1 Introduction

Recent studies of global in time properties of solutions to the Einstein vacuum equations draw attention to the significance of future asymptotic states of eternally expanding, spatially compact vacuum solutions in connection with the geometrization and classification of compact 3-manifolds [1,4-7]. It is suggested that the limiting behavior of the vacuum space-times may reveal the characteristic topological structure of underlying spacelike hypersurfaces. Two possible characteristics have been proposed: the *hyperbolization* and the *conformal volume collapse* (see, e.g. [1, 6] and references therein). The former indeed occurs in the course of evolutions in the expanding direction of constant mean curvature (CMC) small data on compact hyperbolizable 3-manifolds, i.e. compact 3-manifolds which admit a hyperbolic metric of constant negative sectional curvature, provided that a rigidity requirement is satisfied [2, 3]. Namely, nonlinearly perturbed solutions to the Einstein vacuum equations around the spatially compactified (flat) Milne solutions evolve seeking the "background" solution in the expanding direction. The latter is concerned with non-hyperbolizable compact 3-manifolds of Yamabe type -1, i.e. compact 3-manifolds which do not admit any Riemannian metric of non-negative constant scalar curvature and the hyperbolic metric. The compact quotients of the model geometries of Thurstion, Nil, $H^2 \times \mathbb{E}$, $\widetilde{\mathrm{SL}}(2,\mathbb{R})$ and Sol [15] belong to this class. Fischer and Moncrief [7] have shown that the conformal volume collapse indeed occurs in the spatially compact Bianchi models of non-hyperbolizable Yamabe type -1 and that such a collapse

[1] E-mail:kyasuno@th.phys.titech.ac.jp
[2] E-mail:masayuki.tanimoto@yale.edu
[3] E-mail:vincent.moncrief@yale.edu

is caused by the degeneration of the "conformal" metric of scalar curvature -1 totally (Nil) or along the fiber ($H^2 \times \mathbb{E}$, $\widetilde{\mathrm{SL}}(2,\mathbb{R})$ and Sol). We then ask whether such a conformal volume collapse really characterizes the future asymptotics of general solutions to the Einstein vacuum equations. We shall try to examine this issue by studying the small data analysis for compact 3-manifolds of non-hyperbolizable Yamabe type -1. Although we would like to consider the nonlinear analysis eventually, it is natural, as a first step, to begin with studying the linearized perturbations which might give a clue to decide what to be expected in the nonlinear problem.

Our immediate problem is the understanding of the future asymptotic behavior of the linearly perturbed solutions around spatially compact locally homogeneous (and anisotropic) vacuum solutions for which the spacelike hypersurfaces are assumed to be of compact quotients modeled on Nil, Sol, $H^2 \times \mathbb{E}$ and $\widetilde{\mathrm{SL}}(2,\mathbb{R})$. In this paper, we briefly report a part of our results of qualitative analysis of linearly perturbed flows around the spatially compact locally rotationally symmetric (LRS) Bianchi III vacuum solutions whose spatial topology is of a trivial circle bundle over a higher genus surface Σ_g, $g \geq 2$, modeled on $H^2 \times \mathbb{E}$ [18].

2 Qualitative Behavior of Linearly Perturbed Solutions

Here we focus our attention on the *local* dynamical degrees of freedom of perturbations, namely, we do not consider the *Teichmüller deformations* of compact 3-manifolds which are indeed the dynamical degrees of freedom of perturbations with nontrivial dynamics. (For discussions on the global dynamical degrees of freedom of spatially compact locally homogeneous space times, see [11] and references therein.)

It is well known that the linearized Einstein vacuum equations admit the Hamiltonian formulation (see, e.g. [13]). The Hamiltonian system contains the linearized constraints which generate the infinitesimal gauge transformations. We can derive the *gauge-invariant* ordinary (i.e. unconstrained) Hamilton's equations for the gauge-invariant and unconstrained variables that are the true dynamical degrees of freedom of linearized perturbations applying the arguments given by Goldberg, Newman and Rovelli [8].[4] Details of this process will appear elsewhere [14].

To study the qualitative behavior of linearly perturbed solutions, we shall construct an *extended* dynamical system expressed in terms of *dimensionless variables* as in the spatially homogeneous cosmologies (for an extensive review of the dynamical systems approach to cosmology, see the book edited by Wainwright and Ellis [16]) by assembling Hamilton's equations of linearized perturbations and the dynamical system of LRS Bianchi III. Let us write the gauge-invariant and unconstrained perturbation configuration variables by $({}^{S}Q, {}^{V}Q_a)$ which represent two $(\times\infty^3)$ independent degrees of freedom of freely propagating gravitational waves and separate the spatial variables $x \in \Sigma_g \times S^1$ from the time variable $\tau \in \mathbb{R}$ to reduce the partial differential equations to the ordinary differential equations as follows

$$ {}^{S}Q(\tau,x) = \sum_{\lambda,n} {}^{S}Q_{(\lambda,n)}(\tau) S_\lambda \varphi_n \,, \qquad {}^{V}Q_a(\tau,x) = \sum_{\lambda,n} {}^{V}Q_{(\lambda,n)}(\tau)(V_\lambda)_a \varphi_n \,, \tag{1} $$

where S_λ is an eigenfunction of the Laplace–Beltrami operator on Σ_g with eigenvalue $-\lambda < 0$, $(V_\lambda)_a$ is an eigenfunction of the Laplace–Beltrami operator on Σ_g with eigenvalue $-(\lambda+1)$ which is transverse with respect to the standard hyperbolic metric on Σ_g, and φ_n is an eigenfunction of the Laplace–Beltrami operator on S^1 with eigenvalue $-n^2$. Let ${}^{S}P_{(\lambda,n)}$ and ${}^{V}P_{(\lambda,n)}$ be the canonically conjugate momenta of ${}^{S}Q_{(\lambda,n)}$ and ${}^{V}Q_{(\lambda,n)}$, respectively. For each pair of eigenvalues (λ, n), we have a dynamical system of the autonomous ordinary differential equations such that

$$ \begin{aligned} {}^{X}\tilde{Q}'_{(\lambda,n)} &= -2(1+2\Sigma^2) {}^{X}\tilde{Q}_{(\lambda,n)} + {}^{X}f_{(\lambda,n)}(s,\Sigma) {}^{X}P_{(\lambda,n)} \,, \\ {}^{X}P'_{(\lambda,n)} &= -{}^{X}g_{(\lambda,n)}(s,\Sigma) {}^{X}\tilde{Q}_{(\lambda,n)} \,, \end{aligned} \tag{2} $$

$$ \begin{aligned} s' &= 6s(1-s)\Sigma \,, \\ \Sigma' &= (1-\Sigma^2)(1-2\Sigma) \,. \end{aligned} \tag{3} $$

[4] The prescription for the reduction of the Hamiltonian system with first-class constraints given in Ref. [8] has been applied to the cosmological perturbations of inflationary universe by Langlois [12].

Here $X = S, V$, a prime denotes the derivative with respect to the 'dimensionless' time variable τ with range $-\infty < \tau < \infty$ that is defined by $\mathrm{d}t/\mathrm{d}\tau = H^{-1}$, where t is the proper time and $H > 0$ is the Hubble scalar whose evolution is determined by the Raychaudhuri equation [16, Chap. 5], ${}^{X}\tilde{Q}_{(\lambda,n)} = H^{2\,X}Q_{(\lambda,n)}$ are dimensionless configuration variables, and the dimensionless variables $(s,\Sigma) \in \mathbb{R}^2$ forms the LRS Bianchi III (reduced) dynamical system, where $0 < s < 1$ is the curvature variable and $-1 < \Sigma < 1$ is the shear variable. The closure of the LRS Bianchi III invariant set, $\{(s,\Sigma)|0 \leq s \leq 1,\ -1 \leq \Sigma \leq 1\}$, is the closure of the phase subspace of locally homogeneous solutions. ${}^{X}f_{(\lambda,n)}(s,\Sigma)$ and ${}^{X}g_{(\lambda,n)}(s,\Sigma)$ are given by

$$
\begin{aligned}
{}^{S}f_{(\lambda,n)} &= \frac{\mathcal{Z}}{\lambda(\lambda+2)\sqrt{3f_s(1-\Sigma^2)}}\,,\\
{}^{S}g_{(\lambda,n)} &= \frac{\sqrt{3}\lambda(\lambda+2)\sqrt{1-\Sigma^2}}{\sqrt{f_s}\mathcal{Z}^2}\Bigg\{12n^6(1-\Sigma^2)+4n^4f_s\left[9\lambda(1-\Sigma)+2(5-\Sigma)(1+\Sigma)\right]\\
&\quad + n^2(f_s)^2\left[9\lambda^2(4-\Sigma^2)\frac{1-\Sigma}{1+\Sigma}+10\lambda(5\Sigma^2-8\Sigma+5)+32(1+\Sigma)(1-2\Sigma)\right]\\
&\quad + \lambda^2(f_s)^3\frac{2-\Sigma}{1+\Sigma}\left[3\lambda(1-\Sigma)(2-\Sigma)+2(7\Sigma^2-13\Sigma+7)\right]\Bigg\}\,,
\end{aligned}
$$

where $f_s = (1-s)/2s$ and

$$
\mathcal{Z} = 4n^4 + 4n^2f_s\left(\lambda\frac{2-\Sigma}{1+\Sigma}+2\right)+\lambda(f_s)^2\left[\lambda\left(\frac{2-\Sigma}{1+\Sigma}\right)^2+6\frac{1-\Sigma}{1+\Sigma}\right]\,,
$$

and

$$
\begin{aligned}
{}^{V}f_{(\lambda,n)} &= \frac{\Lambda+f_s}{\sqrt{3f_s(1-\Sigma^2)}}\,,\\
{}^{V}g_{(\lambda,n)} &= \frac{9(1+\Sigma)\sqrt{1-\Sigma^2}}{\sqrt{3f_s}(\Lambda+f_s)}\left[\left(n^2+(\lambda+2)f_s\right)(1-\Sigma)-\frac{2}{3}f_s(1+\Sigma)+\frac{4\Lambda f_s\Sigma}{\Lambda+f_s}\right]\,.
\end{aligned}
$$

We fix the time orientation such that τ increases in the expanding direction, thus the late-time regime $\tau \to \infty$ is of our interest.

The phase portrait of the unperturbed LRS Bianchi III subsystem (s,Σ) determined by Eqs. (3) can be easily depicted (Fig. 1). We can show that there exists a future attractor at a point $(s,\Sigma) = (1,1/2)$ corresponding to the Bianchi III form of flat space-time [16, Chap. 9] which has a homothetic vector field [9]. Thus, the LRS Bianchi III vacuum solutions are *asymptotically self-similar*.

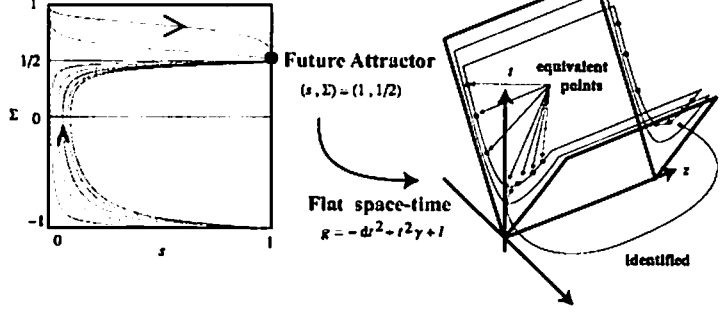

Figure 1: Phase portrait of the LRS Bianchi III subsystem and the flat space-time corresponding to the future asymptotic state. γ_{ab} is the standard hyperbolic metric on Σ_g and ℓ_{ab} is the standard metric on S^1.

The qualitative behavior of the solutions of the extended dynamical system $({}^{X}Q_{(\lambda,n)}, {}^{X}P_{(\lambda,n)}, s, \Sigma) \in \mathbb{R}^6$ obeying Eqs. (2) and (3) are illustrated in Fig. 2 and in Fig. 3. We may determine the existence or absence of equilibrium points of the system by the Bendixon method discussed by Woszczyna [17]. For fully inhomogeneous perturbations with $\lambda > 0$ and $n \neq 0$, there is no equilibrium point at $(s, \Sigma) = (1, 1/2)$ and thus the perturbations exhibit oscillatory behavior. For U(1)-symmetric perturbations with $\lambda > 0$ and $n = 0$, the qualitative behavior changes at the eigenvalue $\lambda = 1/4$: if $\lambda > 1/4$, there is no equilibrium points and thus the perturbations exhibit oscillatory behavior while if $\lambda \leq 1/4$, there exist equilibrium points (accordingly the perturbations lose the wave character) of ${}^{X}\mathcal{U} = {}^{X}Q'/{}^{X}Q$ such that ${}^{V}\mathcal{U} > 0$ so that the perturbations grow and ${}^{S}\mathcal{U} < 0$ so that the perturbations decay. In cases of oscillatory behavior, the numerical results imply that ${}^{S}\tilde{Q}_{(\lambda,n)}$ decays asymptotically as $\tau \to \infty$ while ${}^{V}\tilde{Q}_{(\lambda,n)}$ does not. Finally, we note that the qualitative asymptotic behavior of inhomogeneous perturbations is not sensitive to the values of (λ, n).

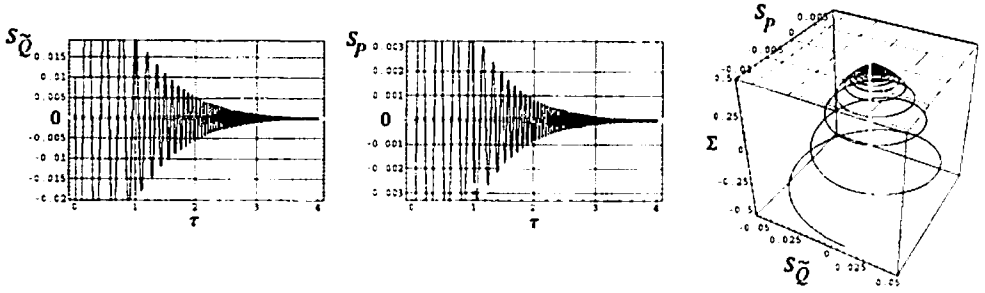

Figure 2: Plots for $(n, \lambda) = (5, 5)$. In the right figure, the vertical line $({}^{S}\tilde{Q}, {}^{S}P) = (0, 0)$ corresponds to the background solution.

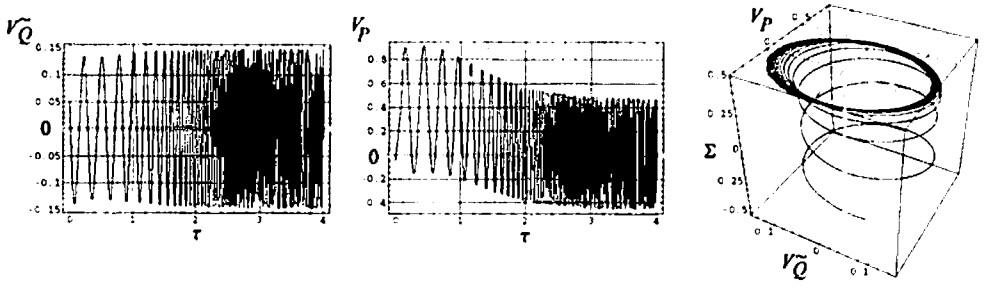

Figure 3: Plots for $(n, \lambda) = (5, 5)$. In the right figure, the vertical line $({}^{V}\tilde{Q}, {}^{V}P) = (0, 0)$ corresponds to the background solution.

3 Conclusion and Discussions

What we have shown is that *the LRS Bianchi III vacuum solutions are stable but not asymptotically stable in the expanding direction under linearized inhomogeneous perturbations* except the U(1)-symmetric perturbations with $\lambda \leq 1/4$ (for definitions of the stability, see, e.g. [10]). Thus, the (future) asymptotic self-similarity of background solutions breaks down for linearly perturbed solutions.

It is worth noting that one of the two independent gravitational-wave degrees of freedom decays asymptotically as $\tau \to \infty$. The implication of this behavior will be understood when we quantify the

linearized analysis, for example, when we study the time evolution of the conformal volume and examining whether the conjectured conformal volume collapse behavior also is realized by the linearly perturbed solutions. It is interesting to study whether that property is universal within the linearized perturbations about other spatially locally homogeneous models with spacelike hypersurfaces are of compact quotients of Nil, $\widetilde{\mathrm{SL}}(2,\mathbb{R})$ and Sol.

More details of the analysis of linearized perturbations around spatially compact LRS Bianchi III vacuum solutions, including the Teichmüller deformations we have not discussed here, will appear elsewhere [18, 19].

Acknowledgments

K.Y. is grateful to Akio Hosoya for continuous encouragement and to Masaru Siino and Tatsuhiko Koike for fruitful discussions. K.Y. is supported by the Japan Society for the Promotion of Science and the Ministry of Education, Science, Sports and Culture. M.T. is supported by a JSPS Postdoctoral Fellowship for Research Abroad.

References

[1] Anderson, M.T.: Commun. Math. Phys. **222**, 533–567 (2001).

[2] Andersson, L.: `gr-qc/9911032`.

[3] Andersson, L. and Moncrief, V.: in preparation.

[4] Fischer, A.E. and Moncrief, V.: Class. Quantum Grav. **16** L79–87 (1999).

[5] Fischer, A.E. and Moncrief, V.: in *Proc. 2nd Samos Meeting on Cosmology, Geometry and Relativity*, ed. S. Cotsakis and G.W. Gibbons (Springer, New York, 2000).

[6] Fischer, A.E. and Moncrief, V.: Class. Quantum Grav. **18** 4493–4515 (2001).

[7] Fischer, A.E. and Moncrief, V.: to appear (2002).

[8] Goldberg, J., Newman, E.T. and Rovelli, C.: J. Math. Phys. **32**, 2739–2743 (1991).

[9] Hewitt, C.G. and Wainwright, J.: Class. Quantum Grav. **10** 99–124 (1993).

[10] Hirsh, M.W. and Smale, S.: *Differential Equations, Dynamical Systems, and Linear Algebra*, (Academic Press, New York, 1974).

[11] Kodama, H.: `gr-qc/0109064`.

[12] Langlois, D.: Class. Quantum Grav. **11** 389–407 (1994).

[13] Moncrief, V.: Phys. Rev. **D12**, 1526–1537 (1975).

[14] Tanimoto, M., Yasuno, K. and Moncrief, V.: in preparation.

[15] Thurston, W.P.: *Three-Dimensional Geometry and Topology*, vol. 1, (Princeton University Press, Princeton, 1997).

[16] Wainwright, J. and Ellis, G.F.R. (ed.): *Dynamical Systems in Cosmology*, (Cambridge University Press, Cambridge, 1997).

[17] Woszczyna, A.: Phys. Rev. **D45**, 1982–1988 (1992).

[18] Yasuno, K.: PhD Thesis, Tokyo Institute of Technology, (2002).

[19] Yasuno, K., Tanimoto, M. and Moncrief, V.: in preparation.

Non-Radial Null Geodesics from Naked Singularity

-Impact parameter of the naked singularity-

Naoki KOBAYASHI,[1] Ken-ichi NAKAO,[2] and Hideki ISHIHARA[3]

Department of Physics, Osaka City University, Sumiyoshi-ku, Osaka, Japan

Abstract

We study null geodesics from naked singularity formed in the self-similar collapse of a marginally bound spherically symmetric dust cloud. We showed the impact parameter of the naked singularity grows as the collapse evolves by integrating numerically the null geodesic equations. The maximal value of the impact parameter is connected with the total mass of the dust cloud, and that is $3\sqrt{3}M$.

1 Introduction

It is known that naked singularities can appear in the classical gravitational collapse of dust spheres, which is described by the Tolman-Bondi solution[1][2]. Null geodesics emanating from the singularity might carry information of very strong gravitational field near the singularity. So, it is interesting to study not only radial null geodesics but also non-radial null geodesics with non-vanishing angular momentum[3][4].

We consider a singularity in marginally bound spherical dust collapse and studied numerically non-radial null geodesics emanating from the singularity using numerical integration's. We show that how a distant observer see the singularity with an apparent impact parameter.

2 Formalism

The marginally bound Tolman-Bondi dust collapse is described by the line element, using comoving coordinates (t, r, θ, ϕ),

$$ds^2 = -dt^2 + R'^2(t,r)dr^2 + R^2(t,r)d\Omega^2, \tag{1}$$

where $d\Omega^2 = d\theta^2 + \sin^2\theta d\phi^2$, and $R(t,r)$ is the areal radius at time t of a shell labeled by r, and prime denotes the partial derivative with respect to r. The Einstein equations which determine the evolution of areal radius $R(t,r)$ are

$$\dot{R}^2 = \frac{F(r)}{R}, \tag{2}$$

$$\frac{F'(r)}{R^2 R'} = \epsilon(t,r), \tag{3}$$

where $\epsilon(t,r)$ is energy density of dust and the dot denotes partial derivative with respect to t. $F(r)$ is an arbitrary function describing the mass within a sphere r.

Hereafter, we consider a model:

$$F(r) = \begin{cases} F_0 r & 0 \le r \le r_c, \\ F_0 r_c & r > r_c, \end{cases} \tag{4}$$

[1] E-mail:covap@sci.osaka-cu.ac.jp
[2] E-mail:knakao@sci.osaka-cu.ac.jp
[3] E-mail:ishihara@sci.osaka-cu.ac.jp

where r_c labels the boundary of the dust cloud, and F_0 is a positive constant. Integration of Eq. (2) gives

$$R^{\frac{3}{2}}(t,r) = \frac{3}{2}\sqrt{F(r)}\,(t_0(r) - t)\,. \tag{5}$$

Choosing an initial scaling of r as $R(0,r) = r$, then we see the integration function $t_0(r)$ becomes $t_0(r) = r/a$, where we have introduced $a \equiv \frac{3}{2}\sqrt{F_0}$. In the region $r \leq r_c$, this solution represents the self-similar collapse. From Eq.(3) $R^2R' = 0$ is the curvature singularity. The time $t = t_0(r)$ corresponds to the time when the mass shell labeled by r meets the singularity. It is known that the singularity at $r = 0$ (usually known as the central shell focusing singularity) is a naked singularity which forms at $t = 0$ in this case.

The geometry of $r > r_c$ is Schwarzschild space-time with the total mass of dust $M \equiv F_0 r_c/2$. The line element is written in a familiar form

$$ds^2 = -\left(1 - \frac{2M}{R}\right)dT^2 + \left(1 - \frac{2M}{R}\right)^{-1}dR^2 + R^2 d\Omega^2. \tag{6}$$

3 Null geodesic equation

We introduce P and ℓ as $\frac{P}{R} \equiv K^t$, $\frac{\ell}{R^2} \equiv K^\phi$, where $K^a = dx^a/d\lambda$ are the tangents to the null geodesics. ℓ is a conserved quantity along null geodesics because of the spherical symmetry. Then null geodesic equations can be written as

$$r\frac{dX}{dr} = \frac{1}{3}\left(X + \frac{2}{\sqrt{X}}\right)\left(1 - \frac{P}{\sqrt{P^2 - \ell^2}}\right) - X, \tag{7}$$

$$r\frac{dP}{dr} = -\frac{\sqrt{F_0\,(P^2 - \ell^2)}}{X^2} + \frac{P}{3}\left(1 + \frac{2}{X^{\frac{3}{2}}}\right), \tag{8}$$

where $X \equiv (1 - a(t/r))^{\frac{2}{3}}$. In case of radial null geodesics, $\ell = 0$, X is determined by Eq.(7) only, but in case of non-radial one, $\ell \neq 0$, Eq.(7) and Eq.(8) are coupled.

For out going geodesics emanate from at least locally naked singularity, X has a positive finite value X_0 at the singularity and P blows up towards the singularity along null geodesics. Asymptotic behavior of P near singularity is

$$P \simeq P_0 r^{-\omega_0}, \tag{9}$$

$$\omega_0 \stackrel{def}{=} \frac{2 - 10X_0^{\frac{3}{2}} - X_0^3}{3X_0^{\frac{3}{2}}\left(X_0^{\frac{3}{2}} + 2\right)}, \tag{10}$$

where P_0 is a constant of integration. Since ω_0 should be positive, X_0 must be in the range

$$0 < X_0 < \left(\frac{2}{26 + 15\sqrt{3}}\right)^{\frac{1}{3}}. \tag{11}$$

It is seen that the existence of null geodesics satisfying Eq.(11) establishes that the singularity would be at least locally naked. Such a locally naked singularity could be globally naked as well. To examine this issue we integrate Eqs.(7) and (8) numerically in the dust cloud and beyond the boundary, and analyze the behavior of null geodesics in the exterior Schwarzschild region using effective potential.

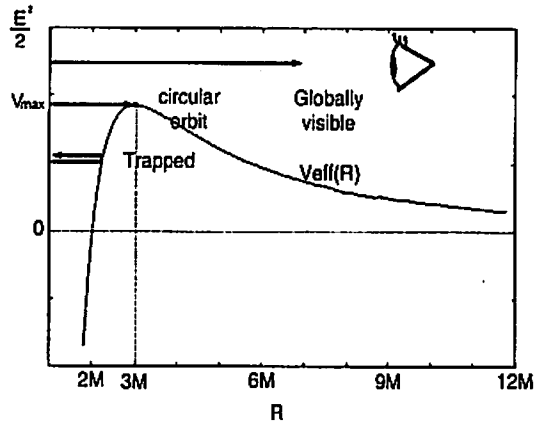

Figure 1: The effective potential, $V_{\rm eff}$, for null geodesics

4 Global behavior

Consider the null geodesics in the exterior Schwarzschild region. We can easily know whether the null geodesics can reach the null infinity or not by null condition $g_{ab}K^aK^b = 0$ which gives

$$\frac{1}{2}\left(\frac{dR}{d\lambda}\right)^2 = \frac{1}{2}E^2 - V_{\rm eff}, \tag{12}$$

$$V_{\rm eff} \stackrel{def}{=} \frac{1}{2}\left(1 - \frac{2M}{R}\right)\frac{\ell^2}{R^2}, \tag{13}$$

where $E \equiv (1 - 2M/R)K^T$ is a constant of motion, and K^T is the time component of null tangent in the static chart (6). As illustrated in Fig.1, the effective potential $V_{\rm eff}$ has the only one maximum $V_{\rm max} \equiv \ell^2/54M^2$ at $R = 3M$. From Eqs.(12) and (13), all null geodesics start from $R > 3M$ can reach null infinity. But in order that the null geodesics from $R < 3M$ reach null infinity $E^2/2$ must be larger than $V_{\rm max}$. If there exist non-radial null geodesics which can reach null infinity, an observer at a distance R who is in the asymptotically flat region detects the light ray from the singularity with a finite angular diameter δ. Then the apparent diameter of the singularity for the very distant observer is defined by $D \equiv R\,\delta$, and that is almost twice the impact parameter of the singularity. The impact parameter is defined by

$$b \stackrel{def}{=} \frac{\ell}{E} \simeq \lim_{R\to\infty} D. \tag{14}$$

Here, we define the areal radius of the dust sphere $R_{\rm exit} \equiv R(t_{\rm exit}, r_c)$, where $t_{\rm exit}$ is the time a null geodesic which comes from the singularity exits the dust cloud.
Hence to classify whether null geodesics from the singularity can reach null infinity or not, we need to know E for each null geodesic at $R_{\rm exit}$. From the continuity of the tangent vector of the null geodesic, we find

$$E = \left(K^t - R'K^r\sqrt{\frac{2M}{R}}\right), \tag{15}$$

where K^t, K^r and R, R' are the values at the boundary $r = r_c$ which can be obtained by numerical integration in the dust cloud for each null geodesic. Thus the information of the null geodesics at the boundary of the dust cloud gives global behavior of null geodesics and the impact parameter of the singularity.

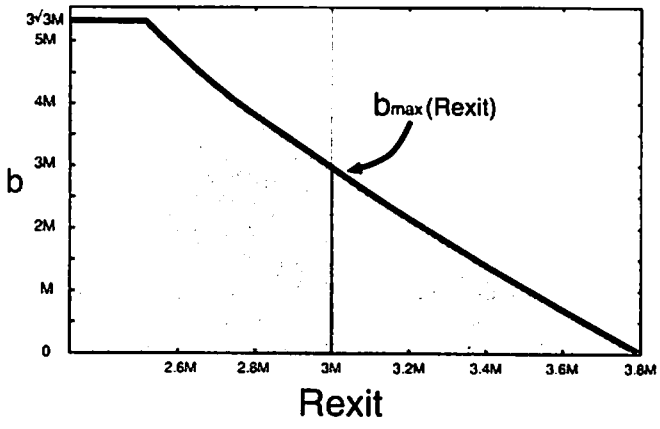

Figure 2: Allowed region of global null geodesics

5 Numerical Results

Fig.2 represents the relation between $R_{\rm exit}$ and the impact parameter of the singularity b. All the geodesics that can reach null infinity are in the gray region of Fig.2. The solid line represents the maximal value of b at a $R_{\rm exit}$. This result shows the smaller $R_{\rm exit}$ makes the larger impact parameter. In other words $b_{\rm max}(R_{\rm exit})$ grows as the collapse evolves. It means $b_{\rm max}(R_{\rm exit})$ grows with time. The numerical result shows that the maximum of the impact parameter of the singularity is given by the non-radial null geodesic $R_{\rm exit} < 3M$, and $max\{b_{\rm max}(R_{\rm exit})\}$ is almost $3\sqrt{3}M$.

6 Summary

We studied the all possible null geodesics including non-radial one from the naked singularity formed in the self-similar gravitational collapse of a marginally bound spherically symmetric dust cloud. We showed numerically that the $b_{\rm max}$ raises 0 to the limiting value $3\sqrt{3}M$ and it conserved until the star goes within its apparent horizon.

Simply, from Eq.(12), we see the possible maximal value of b is at most $3\sqrt{3}M$. It can be concluded that this limiting value of the impact parameter is determined by the exterior geometry of the dust cloud.

References

[1] R.C.Tolman. *Proc.Natl.Acad.Sci.USA*, 20(410), 1934.

[2] H.Bondi. *Mon.Not.Astron.Soc.*. 107(343). 1947.

[3] Filipe C Mena and Brien C Nolan. *Class.Quant.Grav.*, 18:4531 4548, 2001.

[4] I.H.Dwivedi S.S.Deshingkar, P.S.Joshi. Appearrance of the central singularity in spherical collapse. *gr-qc/0111053.*

Correction of Metric Tensor and Variable Cosmological Term

Takao Fukui[1]

Department of Language and Culture, Dokkyo University, Gakuencho, Soka, Saitama, 340-0042, Japan

Abstract

The correction terms of the metric tensor is regarded as a variable cosmological term. Simple solutions of the scale factor and the cosmological term are exactly obtained. The scale factor enables us to make qualitative consideration of the magnitude-redshift relation in an accelerating universe. The equation of state parameter γ is touched.

1 Introduction

One of the probable explanations of the magnitude-redshift relation of type Ia supernovae might be due to an accelerated expansion of the universe. There seems to be two major candidates causing the acceleration. The one candidate is the vacuum energy of the cosmological constant which is left behind from the inflation era to the later eras. It now exceeds the matter density and is essential for the current universe to accelerate [1].

The other candidate is the vacuum energy varing with a scalar field ϕ. It is known as a scalar quintessence which exerts a negative pressure and is in this regard same as the cosmological constant [2]. This scenario can be written in a scalar-tensor theory. Exact solutions in a generalized scalar-tensor theory, for the scale factor and the scalar field are obtained by Fukui et al. [3]. The variable cosmological term also is shown there as a function of ϕ and $\phi_{,i}\phi^{,i}$.

The major difference between the two candidates is the values of the equation of state parameter γ. In the present work, the equation of state is $p = (\gamma - 1)\epsilon$. The cosmological constant strictly gives the value of $\gamma = 0$. On the other hand, the value of the parameter in the quintessence is variable with ϕ and is not always exactly 0. It means that the parameters for the ordinary matter and for the quintessence are not identical.

Recently Fukui [4] presented a new time varying cosmological term only in the metric tensor field. In the cosmological model, if the value of the parameter is exactly 0, the cosmological term is constant and the universe expands exponentially. If the value is less than 2/3, the matter behaves as the quintessence and the cosmological term varies as t^{-2} . Because of the negative pressure due to the entity, the universe accelerates its expansion in a power-law fashion. We present the solutions below in more general forms than those in Ref.[4].

In the present work, we apply the new cosmological term to the accelerated expansion of the universe and see qualitatively its effect on the magnitude-redshift relation.

2 Cosmological Solutions

The Lagrangian density is assumed here as follows by taking the metric tensor corrections into consideration;

$$L = \frac{c^4}{16\pi G}\left[R - 2\lambda_n R^n + 3n(n-1)\lambda_n R_{lm}R^{lm}\right] + L_m, \tag{1}$$

where λ_n is constant and n runs over 0, 1 and 2. The 3rd term in parentheses appears as a quadratic correction in the case of $n = 2$. Another quadratic term $R_{lmst}R^{lmst}$ can be ignored on the basis of the generalized Gauss-Bonnet invariant. The particular combination in the coefficients of the second and

[1] E-mail: tfukui@dokkyo.ac.jp

third terms are determined by the invarint. Here we make the assumption that the second and third terms together are the cosmological term.

$$\Lambda = -\lambda_n \left\{ R^n - \frac{3n(n-1)}{2} R_{lm} R^{lm} \right\}. \tag{2}$$

Hereafter we study only the case of $n = 1$ upon the analysis made in Ref.[4]. The field equation derived from Eq.(1) is solved for the scale factor $a(ct)$ and the cosmological term $\Lambda(ct)$ in the flat Robertson-Walker metric. The conventinonal relation, $\epsilon a^{3\gamma} = const.(\equiv \epsilon_\gamma)$ can be employed because the conservation law of the energy momentum tensor is assured to be valid by the field equation.
(a) $\gamma = 0$: The scale factor is obtained as follows;

$$a = a_0 exp(\sqrt{P_0}t), \tag{3}$$

where $P_0 \equiv 8\pi G\epsilon_0/3(1-2\lambda_1)c^2$, and the deceleration parameter is $q = -1$.
The cosmological term is obtained as follows;

$$\Lambda = \frac{32\pi G\epsilon_0\lambda_1}{c^4(1-2\lambda_1)}. \tag{4}$$

During this era, the cosmological term is constant.
The energy densities and pressures are obtained as follows;

$$\begin{aligned} \epsilon &= -p = \epsilon_0, \\ \epsilon_{vac} &= -p_{vac} = \frac{2\lambda_1\epsilon_0}{1-2\lambda_1}. \end{aligned} \tag{5}$$

Both of them are constant.
(b) $\gamma \neq 0$: The scale factor is obtained as follows;

$$a = \left\{ \frac{6\pi G\epsilon_\gamma \gamma^2}{(1-2\lambda_1)c^2} \right\}^{\frac{1}{3\gamma}} \left(t + \frac{a_\bullet}{Q_\gamma} \right)^{\frac{2}{3\gamma}}, \tag{6}$$

where $Q_\gamma^2 = 8\pi G\epsilon_\gamma/3(1-2\lambda_1)c^2$, and $a_\bullet$ is constant. In Ref.[4], $a_\bullet$ is taken to be 0. From Eqs.(3) and (6), an exponential expansion is restricted strictly to $\gamma = 0$. Otherwise the universe expands in a power-law fashion. The deceleration parameter in (b) is $q = (3\gamma - 2)/2$.
The cosmological term is obtained as follows;

$$\Lambda = -\frac{4(3\gamma-4)\lambda_1}{3\gamma^2} \frac{1}{\{c(t + a_\bullet/Q_\gamma)\}^2}. \tag{7}$$

During these eras, the cosmological term decays as t^{-2}, though $\Lambda = 0$ during the radiation era. From the observation $-1 \leq \gamma - 1 \leq -0.93$ [5], the present scenario leads the universe to accelerate not in an exponential manner but in a power-law fashion with $\gamma < 2/3$.
The energy densities and pressures are obtained as follows;

$$\begin{aligned} p &= (\gamma-1)\epsilon = (\gamma-1)\frac{(1-2\lambda_1)c^2}{6\pi G\gamma^2(t + a_\bullet/Q_\gamma)^2} \\ p_{vac} &= (\gamma-1)\epsilon_{vac} = (\gamma-1)\frac{\lambda_1 c^2}{3\pi G\gamma^2(t + a_\bullet/Q_\gamma)^2}. \end{aligned} \tag{8}$$

3 Evolution of the Universe

Here we assume that the universe evolves in the sense of γ [6], to the current accelerating universe as follows.

era	big bang	inflation	radiation	matter	Inflection	present
γ	γ_b	0	4/3	1	2/3	$\gamma_p < 2/3$
q	q_b	-1	1	1/2	0	$q_p < 0$

At each interface between eras, the junction conditions require that the scale factor $a(ct)$ and its derivative $\dot{a}(ct)$ be continuous. The condition is satisfied at the following epochs.
(I) The transition epoch $t = t_{ir}$ between inflation ($\gamma = 0$) and radiation ($\gamma = 4/3$) is obtained as follows;

$$t_{ir} = \frac{1}{\sqrt{P_0}}\left(\frac{1}{2} \mp \sqrt{\frac{\epsilon_0}{\epsilon_{4/3}}}a_*\right). \tag{9}$$

(II) The other transition epochs (t_{rm}, t_{mI}, t_{Ip}) between γ_1 ($= 4/3, 1, 2/3$) and γ_2 ($= 1, 2/3, \gamma_p < 2/3$) are obtained as follows;

$$t_{12} = \pm\frac{a_*}{\gamma_1 - \gamma_2}\frac{1}{\sqrt{P_0}}\left(\gamma_2\sqrt{\frac{\epsilon_0}{\epsilon_{\gamma 2}}} - \gamma_1\sqrt{\frac{\epsilon_0}{\epsilon_{\gamma 1}}}\right). \tag{10}$$

The double sign in Eqs.(9) and (10) is owing to the sign of Q_γ. Here we include the inflection era as a transition from a deceleration to an acceleration. We might, however, ignore the era as an inflection point for a negligibly short period.

4 Magnitude-Redshift Relation

The magnitude-redshift relation in a flat universe is obtained as follows;

$$m = 5log(1+z)a_R(r_R - r_E) - 2.5logL_i + const., \tag{11}$$

here L_i is an intrinsic luminosity of a source. $(1+z)a_R(r_R - r_E)$ is the luminosity distance to a source of redshift z. The subscriptions R and E denote receiving in the present era and emitting in the matter era respectively. The radial comoving distance $r_R - r_E$ can be derived by using the solution of the scale factor, Eq.(6) as follows;

$$\begin{aligned} r_R - r_E &= \int_{t_E}^{t_R}\frac{c}{a}dt = \int_{t_E}^{t_{mI}}\frac{c}{a_1}dt + \int_{t_{mI}}^{t_{Ip}}\frac{c}{a_{2/3}}dt + \int_{t_{Ip}}^{t_R}\frac{c}{a_{\gamma_p}}dt \\ &= -3c\sqrt{\frac{(1-2\lambda_1)a_R c^2}{6\pi G\epsilon_1}}\frac{1}{\sqrt{1+z}} + 3c\sqrt{\frac{(1-2\lambda_1)a_{mI}c^2}{6\pi G\epsilon_1}} \\ &+ c\sqrt{\frac{3(1-2\lambda_1)c^2}{8\pi G\epsilon_{2/3}}}ln\frac{a_{Ip}}{a_{mI}} \\ &+ \frac{3c}{3\gamma_p - 2}\sqrt{\frac{(1-2\lambda_1)a_R^{3\gamma_p-2}c^2}{6\pi G\epsilon_{\gamma_p}}}\left(1 - \sqrt{\left(\frac{a_{Ip}}{a_R}\right)^{3\gamma_p-2}}\right). \end{aligned} \tag{12}$$

The third term might be small in its effect, or be ignored as is stated above. The last term is essential in the model of an accelerating universe. For the case of the negligible inflection era, i.e. $a_{mI} \sim a_{Ip}(\equiv a_{mp})$, Eq.(12) is approximated as follows;

$$\begin{aligned} r_R - r_E &= -3c\sqrt{\frac{(1-2\lambda_1)a_R c^2}{6\pi G\epsilon_1}}\frac{1}{\sqrt{1+z}} + 3c\sqrt{\frac{(1-2\lambda_1)a_{mp}c^2}{6\pi G\epsilon_1}} \\ &+ \frac{3c}{3\gamma_p - 2}\sqrt{\frac{(1-2\lambda_1)a_R^{3\gamma_p-2}c^2}{6\pi G\epsilon_{\gamma_p}}}\left(1 - \sqrt{\left(\frac{a_{mp}}{a_R}\right)^{3\gamma_p-2}}\right). \end{aligned} \tag{13}$$

Furthermore for $\gamma_p = 1$, i.e. $t_{mI} = t_{Ip} = t_R$, Eq.(12) reduces to the following conventional equation;

$$r_R - r_E = -3c\sqrt{\frac{(1-2\lambda_1)a_R c^2}{6\pi G\epsilon_1}}\frac{1}{\sqrt{1+z}} + 3c\sqrt{\frac{(1-2\lambda_1)a_R c^2}{6\pi G\epsilon_1}} = \frac{2c}{a_R H_R}\left(1 - \frac{1}{\sqrt{1+z}}\right). \tag{14}$$

Therefore the difference $D \equiv \{Eq.(13) - Eq.(14)\}$ will tell us whether the present scenario is sensible or not:

$$D = 3c\sqrt{\frac{(1-2\lambda_1)a_R c^2}{6\pi G\epsilon_1}}\left(\sqrt{\frac{a_{mp}}{a_R}}-1\right)+\frac{3c}{3\gamma_p-2}\sqrt{\frac{(1-2\lambda_1)a_R^{3\gamma_p-2}c^2}{6\pi G\epsilon_{\gamma_p}}}\left(1-\sqrt{\left(\frac{a_{mp}}{a_R}\right)^{3\gamma_p-2}}\right). \quad (15)$$

The first term is negative and the second one is positive. If $D > 0$, then the acceleration works for a larger magnitude. The same tendency of the Hubble diagrams in Ref.[1] has been shown by Fukui in the case of the cosmological models with the cosmological constant containing the interacting matter and radiation [7].

5 Comments

By using Eqs.(9) and (10), the transition epoch t_{lp} is obtained as follows;

$$t_{lp} = \frac{1}{(2-3\gamma_p)\sqrt{P_0}}\left\{\pm 3\gamma_p\sqrt{\frac{\epsilon_0}{\epsilon_{\gamma_p}}}a_* - \sqrt{P_0}(-4t_{ir}+t_{rm}+t_{ml})-2\right\}. \quad (16)$$

For the positive definitness of t_{lp}, the upper sign in Eq.(16) should be taken in the case of $a_* > 0$, and the lower sign in the case of $a_* < 0$. In either case, a_*/Q_γ in Eq.(6) is positive.

According to Rindler [8], if we take $a_* = 0$ in Eq.(6) only for the period $0(s) \le t \le 10^{-37}(s)$, the scale factor is connected smoothly between the big bang and the inflation at the following epoch;

$$t_{bi} = \frac{2}{3\gamma_b}\frac{1}{\sqrt{P_0}}. \quad (17)$$

Since the ratio of the scale factors at t_{ir} and t_{bi} is obtained by Eqs.(3) and (17) as follows;

$$\frac{a_{ir}}{a_{bi}} = exp\left\{\frac{2}{3\gamma_b}\left(\frac{t_{ir}}{t_{bi}}-1\right)\right\},$$

we obtain $\gamma_b \sim 2/3$ for $t_{ir}/t_{bi} \sim 100$ and $a_{ir}/a_{bi} \sim 10^{43}$. Since $q_b \sim 0$, the universe might have begun to expand with a constant speed.

References

[1] A. G. Riess, et al., Astronomical Journal **116** (1998) 1009.
P. M. Garnavich et al., Astrophysical Journal **509** (1998) 74.
S. Perlmutter et al., Astrophysical Journal **517** (1999) 565.

[2] R. R. Caldwell, R. Dave and P. J. Steinhardt, Physical Review Letters **80** (1998) 1582.

[3] T. Fukui, K. Arai and M. Hashimoto, Classical and Quantum Gravity **18** (2001) 2087.

[4] T. Fukui, International Journal of Modern Physics **D10** (2001) 893.

[5] P. S. Corasaniti and E. J. Copeland, Physical Review **D65** (2002) 043004.

[6] M. S. Madsen, J. P. Mimoso, J. A. Butcher and G. F. R. Ellis, Physical Review **D46** (1992) 1399.

[7] T. Fukui, Science Reports of the Tohoku University, Series I **58** (1975) 200.

[8] W. Rindler, *Relativity* (Oxford University Press, Oxford, 2001), p.411.

Quantum Gravity with Minimal Assumptions

Miyuki Nishikawa [1]

Department of Physics, University of Tokyo,
Bunkyo-ku, Tokyo, 113-0033, Japan

Abstract

Several basic results are reviewed on purpose to construct the quantum field theory including gravity, based on physical assumptions as few as possible. Up to now, the work by Steven Weinberg probably suits this purpose the most. Motivated by these results we focus on the fact that the dimension of an operator is not unique unless the operand is identified. This leads to the classification of possible singularities for the relativistic Schrödinger equation.

1 Introduction

We first overview in section 2 a thesis titled 'Quantum Gravity with Minimal Assumptions'[11]. This is mainly the review of quantum gravity from particle point of view. The purpose is to construct the quantum field theory including gravity, based on physical assumptions as few as possible. This consists of 5 subjects, the last of which is an original consideration on the relation between essential singularity and renormalization. This subject is summarized in section 3-5, but please read a preprint[10] for more details.

2 Overview

The first subject, and probably suits this purpose the most is the work by Steven Weinberg, in which he derived the Einstein equation from the Lorentz invariance of the S-matrix. According to his old paper[1], gravity is derived without assuming a curved space-time. Therefore, the general covariance and the geometric property of gravity are possibly subsidiary or mere approximations.

The second subject is that, according to an effective field theory, we can make a prediction without knowing the underlying fundamental theory. For example, John F. Donoghue calculated one loop quantum corrections to the Newtonian potential explicitly, by assuming the Einstein-Hilbert action and fluctuations around the flat metric, and by making use of the result of 't Hooft and Veltman. The potential naturally contains the classical corrections by general relativity[2].

As the third subject, we review what will happen if we loosen the assumption on coordinates in the standard model that all physical coordinates are transformed to the Minkowski space-time by a Poincaré transformation. And we review the troubles and the measures in treating gravitational field under classical approximations assuming a curved space-time[3]. It is known that for the standard model of elementary particles, the anomaly cancellation condition in a curved space-time with torsion is the same as in a flat space-time[4].

As the fourth subject, we clarify the inevitable ambiguities of a theory. For example, the vacuum state in a curved space-time is not unique and there exist several theories those can not be distinguished by the finite times of measurements[3]. This is a theorem on the ambiguity related to the problem of divergence. For another example, a higher-derivative theory includes non-physical solutions those can not be Taylor expanded. This can be the origin of the gauge ambiguity. If we exclude superfluous solutions by imposing the perturbative constraint conditions, it means a gauge fixing and the theory is reduced to local and lower-derivative[5]. This treatment is known to be equivalent to the treatment of a constraint system by Dirac brackets[6].

As the last subject, we consider the following problem. In usual dimensional counting, momentum has dimension one. But a function $f(x)$, when differentiated n times, does not always behave like one

[1] E-mail:nisikawa@hep-th.phys.s.u-tokyo.ac.jp

with its power smaller by n. This inevitable uncertainty may be essential in general theory of renormalization, including quantum gravity. As an example, we classify possible singularities of a potential for the Schrödinger equation, assuming that a potential V has at least one C^2 class eigen function. The result crucially depends on the analytic property of the eigen function near its 0 points.

Notice that neither super-symmetric, higher dimensional, nor grand unification theory is referred to.

3 Renormalization and Essential Singularity

For the rest of this article we are going to focus on the preprint titled Renormalization and Essential Singularity[10]. We consider the relativistic Schrödinger equation assuming a time independent and spherical symmetric $U(1)$ potential $A^\mu := (\phi(r), 0, 0, 0)$. Then, the spherical part of an eigen function satisfies

$$\begin{aligned}[-\frac{1}{r^2}\frac{d}{dr}(r^2\frac{d}{dr}) + \frac{l(l+1)}{r^2}]y &= \frac{(E-e\phi)^2 - m^2c^4}{(h/2\pi)^2c^2}y \\ &=: -V(r)y \end{aligned} \tag{1}$$

From now on, $V(r)$ defined in the R. H. S. is called a potential if and only if there exists a C^2 class eigen function $y(r)$ satisfying (1). The problem is, how singular $V(r)$ can be.

For simplicity we first treat 1 dimensional case with the angular momentum $l = 0$. Then

$$(1) \iff \frac{y''}{y} = V(r) \ , \tag{2}$$

so not $y(r)$ itself but the ratio is important. For example, if $y(r)$ is Taylor expanded, the second derivative of the constant and the linear term vanish. That is,

$$\frac{y''}{y} = \frac{0 + 0 + 2cr + \cdots}{a + br + cr^2 + \cdots} \ .$$

Therefore, the singularity of a potential depends on whether or not $a, b = 0$. In fact there are various kinds of singularities[7][8][9]. For example, we can replace the power of any term of a Taylor series with an arbitrary real number n, or $\log r$. An infinite power is called an essential singularity, and we can make more and more complex singularities by finite times of operations including summations, subtractions, multiplications, divisions, and compositions.

The most general shape of a singularity that is closed in these operations is like

$$\begin{aligned} f(z) &:= (1)_i + (2)_j + \cdots + (m)_k \ , \\ (1)_i &:= \Big(\sum_{n\in\{n\}_i} \sum_{m_1,\cdots,m_{d_i}=-\infty}^{m_{i1},\cdots,m_{id_i}} a_{inm_1\cdots m_{d_i}} z^n (-\log z)^{m_1} (-\log(-z/\log z))^{m_2} \\ &\qquad \cdots (-\log(-z/(-\log(-z/\log\cdots z))))^{m_{d_i}} \Big)_i , \\ (2)_{\pm j} &:= \sum_{i\in\{i\}_j} (\pm) e^{\pm(1)_i} , \\ (3)_{\pm k} &:= \sum_{j\in\{j\}_k} (\pm) e^{\pm(2)_j} , \\ &\vdots \ . \end{aligned} \tag{3}$$

More precise construction and the meaning of this expansion are in [10]. Notice that this has several number of infinite series in one expansion and all the terms are partially ordered in the ascending powers of r. In this case, the domain of the power of $V(r)$ in the limit $r \to +0$ is

$$V(r) \to r^\nu, -2 + \epsilon \lesssim \nu \ ; -1 \le \nu, \tag{4}$$

where ϵ means an infinitesimal positive power like $-(logr)^{-1}$.

Thus we can restrict the shape (i.e. power and sign) of a potential $V(r)$. This is the short distance limit case, but we can also treat the long distance limit case by the change of variables and in dimension N there are 10 possible cases. We can see a shortcut (though not precise) version of the derivation of this main result in the next section.

4 Main Results

Here is the summary of the calculation. If we assume that the eigen function $y(r)$ is a N-dimensional spherical symmetric function $R(r)$ (i.e. orbital angular momentum $l = 0$), and that $R(r)$ is C^2 class, then (5) can be expanded as [2]

$$\begin{aligned} R = a + br \quad &+ \sum_{n=2}^{\infty} a_n r^n \sim + \cdots + \sum_{i<0} (\pm) e^{-b_i r^i \sim \cdots} \cdots \\ &+ \sum_{j<0} (\pm) e^{-c^{c_j r^j \sim \cdots}} \cdots + \sum_{k<0} (\pm) e^{-e^{e^{d_k r^k \sim \cdots \cdots}} \cdots}, \end{aligned} \tag{5}$$

For $a = 0$ and $N \neq 1$, the behavior of $V(r)$ in the limit $r \to +0$ is

$$\begin{aligned} \frac{\Delta R(r)}{R(r)} &= \frac{R''}{R} + \frac{N-1}{r}\frac{R'}{R} \\ &\to \begin{cases} +(N-1)r^{-2} \ (b \neq 0) \\ +n(n+N-2)r^{-2} \ (b = 0 \text{ and } {}^{\exists}a_n \neq 0) \\ +(-ib_i)^2 r^{2i \pm 2\epsilon - 2} \ (b =^{\forall} a_n = 0 \text{ and } {}^{\exists}b_i > 0) \\ +\infty \ (b =^{\forall} a_n =^{\forall} b_i = 0 \text{ and } {}^{\exists}c_j \text{ or } d_k \text{ or } \cdots > 0) \end{cases} \end{aligned} \tag{6}$$

We can extend the results to $r \to +\infty$ case as follows. If we change the variable r to $z := \frac{1}{r}$ and assume that $R(z)$ is C^2 class (expanded like above) (6) is clearly replaced by

$$\begin{aligned} \frac{\Delta R(r)}{R(r)} &= \frac{1}{R(z)} \left\{ \frac{dz}{dr}\frac{d}{dz}\left(\frac{dz}{dr}\frac{dR(z)}{dz}\right) + (N-1)z\frac{dz}{dr}\frac{dR(z)}{dz} \right\} \\ &= z^4 \frac{R''(z)}{R(z)} - z^3(N-3)\frac{R'(z)}{R(z)} \\ &\to \begin{cases} (3-N)\frac{b}{a}z^3 \ (a \neq 0 \text{ and } b \neq 0 \text{ and } N \neq 3) \\ (n-N+2)n\frac{a_n}{a}z^{n+2} \ (a \neq 0 \text{ and } b = 0 \text{ and } {}^{\exists}a_n \neq 0 \text{ and } N \neq 3) \\ (n-1)n\frac{a_n}{a}z^{n+2} \ (a \neq 0 \text{ and } {}^{\exists}a_n \neq 0 \text{ and } N = 3) \\ (\pm)\,0 \ (a \neq 0 \text{ and } b =^{\forall} a_n = 0 \text{ and } {}^{\exists}b_i \text{ or } c_j \text{ or } d_k \text{ or } \cdots > 0) \\ (3-N)z^2 \ (a = 0 \text{ and } b \neq 0 \text{ and } N \neq 3) \\ (n-1)n\frac{a_n}{b}z^{n+1} \ (a = 0 \text{ and } b \neq 0 \text{ and } {}^{\exists}a_n \neq 0 \text{ and } N = 3) \\ (\pm)\,0 \ (a = 0 \text{ and } b \neq 0 \text{ and } {}^{\forall}a_n = 0 \text{ and } {}^{\exists}b_i \text{ or } c_j \text{ or } d_k \text{ or } \cdots > 0 \text{ and } N = 3) \\ (n-N+2)nz^2 \ (a = b = 0 \text{ and } {}^{\exists}a_n \neq 0) \\ +(-ib_i)^2 z^{2i \pm 2\epsilon + 2} \ (a = b =^{\forall} a_n = 0 \text{ and } {}^{\exists}b_i > 0) \\ +\infty \ (a = b =^{\forall} a_n =^{\forall} b_i = 0 \text{ and } {}^{\exists}c_j \text{ or } d_k \text{ or } \cdots > 0) \end{cases} \end{aligned} \tag{7}$$

Noting that $2 \leq n$ and $i < 0$, we conclude that the power of potential $V(r) \to r^{\nu}$ as $r \to \infty$ is $\nu \leq -3$; $-2-\epsilon \lesssim \nu$. There is no reason to assume that $R(z)$ is C^2 class, but more natural normalizability condition that $R(r)$ is a L^2 function leads to small modification $a = b = 0$ and $N < 2n$ (instead of $2 \leq n$) in (5) and (7). Notice that (6) for more general case of N, a can be obtained from (7) by the trivial replacement $N \to 4 - N$ and $z \to r$ with its power smaller by 4. Furthermore, above results show that for a physical dimension $N = 1, 2, 3$, the sign of a potential V must be positive for $\nu \lesssim -2 + \epsilon$ $(r \to 0)$ and $-2 - \epsilon \lesssim \nu$ $(r \to \infty)$, but can be negative for other cases.

[2] The coefficients are all real and $b_i, c_j, d_k, \cdots$ are positive if exist.

We considered here an example of the real scalar field, and the fermion field equation is of course another story. As a future work, I'd like to apply the result to the general theory of renormalization, and renormalons appearing in the perturbative QCD.

5 Discussions

A potential with C^2 class eigen function is only an assumption. The definition of a potential here is local, and valid only in this paper. But my conjecture is that the analyticity of an eigen function is such a property that cannot be distinguished by finite times of measurements. Therefore we assumed that a physical eigen function is C^2 class. This is also only a local constraint and very weak self consistent condition. Therefore it is not a sufficient condition and normalizability is another problem, particularly, in the long distance limit case.

The motivations to introduce such a condition are as follows. The first is that we want to clarify the inevitable ambiguity of a theory. The second is that there are subtle physical problems: which is the more fundamental, a matter field or a potential? Can a potential be measured in the absence of a matter field? It is a future work to clarify the relation between all the different facts that a quantity is realistic, physically measurable, reduced inevitably from other properties, and calculable.

Acknowledgements

I am grateful to Izumi Tsutsui and Toyohiro Tsurumaru for useful discussions. This article is partially based on some implications given by Tsutomu Kambe and Kazuo Fujikawa. I also appreciate Tsutomu Yanagida and Ken-ichi Izawa, and all related people.

References

[1] S. Weinberg, *THE QUANTUM THEORY OF FIELDS. VOL. 1,2* (Cambridge, UK, 1995); Physical Letter **9** (1964) 357; Physical Review **138** (1965) B988.

[2] J.F. Donoghue, Physical Review **D50** (1994) 3874.

[3] R.M. Wald, *Quantum Field Theory in Curved space-time and Black Hole Thermodynamics* (The University of Chicago Press, Chicago, 1994).

[4] A. Dobado, A. Gómez–Nicola, A.L. Maroto, and J.R. Peláez, *Effective Lagrangians for the Standard Model* (Springer, New York, 1997).

[5] J.Z. Simon, Physical Review **D41** (1990) 3720.

[6] P.A.M. Dirac, *Lectures on Quantum Mechanics* (Yeshiva University, New York, 1964).

[7] M.B. Pour-El and J.I. Richards, *Computability in analysis and physics* (Springer, New York, 1989).

[8] R. Penrose, *The emperor's new mind: concerning computers, minds, and the laws of physics* (Oxford University Press, Oxford, 1989).

[9] L.V. Ahlfors, *Complex analysis: an introduction to the theory of analytic functions of one complex variable* (McGraw-Hill, New York, 1953).

[10] M. Nishikawa, preprint hep-th/0110095 (submitted to Progress of Theoretical Physics).

[11] M. Nishikawa, master thesis, 2001.

Quasi-normal modes of D-brane black holes

Yasunari Kurita[1]

Graduate School of Human and Environmental Studies, Kyoto University, Sakyo-ku, Kyoto, 606-8501, Japan

Masa-aki Sakagami,[2]

Faculty of Integrated Human Studies, Kyoto University, Sakyo-ku, Kyoto 606-8501, Japan

Abstract

We obtain the condition equation for quasi-normal modes of a D3-brane black hole in type IIB String theory.

1 Introduction

In string theory, some D-brane systems are thought of as black holes, because they become black hole solutions in Supergravity limit. A few years ago, some physical quantities of black branes, such as entropy and absorption cross section, were compared with those of D-brane. In most cases, they are in exact agreement, which imply AdS/CFT correspondence. If we believe AdS/CFT correspondence, black holes whose near horizon geometry is AdS become D-brane systems or some CFT systems in strong gravity limits. So, for strong gravity physics, such as final states of evaporation, D-brane black holes may be effective. If we consider verification of string theory by black hole physics, Quasi-normal modes(QNM) would be very important.

The absorption cross section of D3-brane black holes were calculated in terms of quantum field theory [1] [2], in which absorption process of a dilaton is its quantum transition into two gauge fields. In black 3-brane cases, absorption probability is given by the solution of scattering problem on black 3-brane background. Two absorption cross sections agree in case of low energy incidental particles. So, classical gravity on black 3-brane background corresponds to quantum fields theory on D3-brane. Then we expect QNM of black 3-brane will agree with those of D3-brane black holes. We, however, don't know how to calculate QNM and their wave functions by quantum field theory on D3-brane. In order to do it, we work out a new method to solve the scattering problem of D-brane black holes.

2 The wave scattering of D3-brane

In this section, we introduce our new calculation method for absorption cross section of D3-brane black hole. It must give the same absorption cross section with quantum field theory. To show it, we consider scattering problem of a D3-brane black hole. The low energy effective action of D3-brane is Dirac-Born-Infeld action, and bulk action with free dilaton in ten dimensions. We take Einstein frame, and consider dilatons as incidental particles, which couple only with gauge fields up to quadratic terms. So, D3-brane is assumed to be flat brane, for simplicity. Then, the action is

$$S = S_{bulk} + S_{DBI} \tag{1}$$

$$= \int d^{10}x \left(-\frac{1}{2}\partial_A\phi\partial^A\phi + \delta^{(6)}(x)(-\frac{1}{4}F_{\mu\nu}F^{\mu\nu} + \frac{\sqrt{2}}{4}\kappa_{10}\phi F_{\mu\nu}F^{\mu\nu}) \right) + \cdots \tag{2}$$

[1] E-mail:kurita@phys.h.kyoto-u.ac.jp
[2] E-mail:sakagami@phys.h.kyoto-u.ac.jp

where $A = 0, 1, 2, \cdots, 9$, and $\mu, \nu = 0, 1, 2, 3$. We take Coulomb gauge for a photon on D3-brane. Then the effective action is

$$S_{eff} = \int d^{10}x \left(-\frac{1}{2}\partial_A \phi \partial^A \phi - \delta^{(6)}(x)\frac{1}{2}(1 - \sqrt{2}\kappa_{10}\phi)\partial_\mu A_i \partial^\mu A^i \right) \tag{3}$$

where $i = 1, 2, 3$. From this action, we see dilaton interact with two photons. In quantum field theory, absorption of dilaton by D3-brane is its quantum transition into two gauge fields. However, we interpret incidental dilaton ϕ as classical wave, and consider D3-brane scattering as wave scattering. In low energy, the dilaton is assumed to be s-wave. $\phi = \phi(t, r)$, $r^2 = x_4^2 + \cdots + x_9^2$. The time evolution of this wave is given by their wave equations,

$$(-\partial_t^2 + \partial_r^2 - \frac{15}{4r^2})\varphi = \delta(r)\frac{\sqrt{2}\kappa_{10}}{\pi^3 r^{5/2}}\partial_\mu A_i \partial^\mu A^i \tag{4}$$

$$\partial_\mu \partial^\mu A^i = \sqrt{2}\kappa_{10}\partial_\mu(\phi \partial^\mu A^i) \tag{5}$$

where $\varphi = r^{5/2}\phi$. We can solve the wave equation by perturbation with respect to interaction with gauge fields, i.e, the coupling constant κ_{10}.

$$\phi = \phi_0 + \kappa_{10}\phi_1 + \kappa_{10}^2\phi_2 + \cdots \tag{6}$$

$$A_i = A_0^i + \kappa_{10}A_1^i + \cdots \tag{7}$$

At lowest order, wave equations are,

$$(-\partial_t^2 + \partial_r^2 - \frac{15}{4r^2})\phi_0 = 0 \tag{8}$$

$$\partial_\mu \partial^\mu A_0^i = 0. \tag{9}$$

Dilaton wave don't interact with D3-brane, and pass through it. So, reflection amplitude is the same as incidental amplitude. And we take negative energy gauge field solutions, which imply Dirac's sea or vacuum on D3-brane. The solutions are,

$$\varphi_0 = ce^{-i\omega t}\sqrt{r}\left[H_2^{(1)}(\omega r) + H_2^{(2)}(\omega r)\right] \tag{10}$$

$$A_0^i = \int \frac{d^3k}{(2\pi)^3}\sqrt{\frac{V_3}{2k_0}}e^{i(k_0 t + \mathbf{k}\cdot\mathbf{x})}\Sigma_\alpha C_\alpha^* \epsilon_{\mathbf{k}}^{(\alpha)\,i}. \tag{11}$$

where, $k_0 = |\mathbf{k}|$, $\epsilon_{\mathbf{k}}^{(\alpha)\,i}$ is polarization vector, and C_α^* is phase.

At first order, wave equations are

$$(-\partial_t^2 + \partial_r^2 - \frac{15}{4r^2})\varphi_1 = -\delta(r)\frac{\sqrt{2}}{\pi^3 r^{5/2}}\partial_\mu A_0^i \partial^\mu A_0^i \tag{12}$$

$$\partial_\mu \partial^\mu A_1^i = -\sqrt{2}\dot{\phi}_0 \dot{A}_0^i. \tag{13}$$

Dilaton wave ϕ_0 interact with only negative energy gauge fields and excite them into positive energy ones on D3-brane. There is no incidental first order dilaton, and negative energy gauge fields cannot create positive energy dilaton. So, there is no first order dilaton. The solutions are,

$$\varphi_1 = 0 \tag{14}$$

$$A_1^i = \frac{\sqrt{2}c\omega^3}{8}\int \frac{d^3k}{(2\pi)^3}\sqrt{\frac{V_3}{2k_0}}e^{-i(\omega - k_0)t}e^{ik_i x^i}\left(\frac{1}{\omega} + \frac{1}{2k_0 - \omega - i\epsilon}\right)\Sigma_\alpha C_\alpha^* \epsilon_k^{(\alpha)\,i}. \tag{15}$$

At second order, dilaton satisfies,

$$(-\partial_t^2 + \partial_r^2 - \frac{15}{4r^2})\varphi_2 = -\delta(r)\frac{2\sqrt{2}}{\pi^3 r^{5/2}}\partial_\mu A_0^i \partial^\mu A_1^i. \tag{16}$$

There is no incidental dilaton at this order, and The excited gauge field A_1^i and negative one A_0^i annihilate to emit a dilaton wave into bulk. This annihilation is interpreted as that of a particle-hole pair. So, we take retarded boundary condition, then,

$$\varphi_2 = -\frac{c\,\omega^8}{32\cdot 64\pi^3}e^{-i\omega t}H_2^{(1)}(\omega r)\sqrt{r}\left(1+\frac{2i}{\pi}\log|\frac{\omega}{\Lambda}|\right) \tag{17}$$

$$=: c\Sigma e^{-i\omega t}H_2^{(1)}(\omega r)\sqrt{r} \tag{18}$$

This dilaton φ_2 corresponds to 1-loop self energy Feynman graph.

Then, dilaton φ is,

$$\varphi = \varphi_0+\kappa_{10}^2\varphi_2+\cdots \tag{19}$$

$$= ce^{-i\omega t}\sqrt{r}\left[(1+\kappa_{10}^2\Sigma+\cdots)H_2^{(1)}(\omega r)+H_2^{(2)}(\omega r)\right] \tag{20}$$

$$\to ce^{-i\omega t}\sqrt{\frac{2}{\pi\omega}}\left[(1+\kappa_{10}^2\Sigma+\cdots)e^{i(\omega r-\frac{5}{4}\pi)}+e^{-i(\omega r-\frac{5}{4}\pi)}\right] \quad (as\ r\to\infty) \tag{21}$$

Reflection coefficient $\mathcal{R}$ is

$$\mathcal{R}=1+\kappa_{10}^2\Sigma+\mathcal{O}(\kappa_{10}^4) \tag{22}$$

Absorption rate $|\mathcal{A}|^2$ is

$$|\mathcal{A}|^2=1-|\mathcal{R}|^2=\frac{\kappa_{10}^2\omega^8}{(32)^2\pi^3}+\mathcal{O}(\kappa_{10}^4) \tag{23}$$

A incidental dilaton is absorbed by D3-brane at this rate. This is lowest absorption process. This dilaton wave is 6-dimensional s-wave, so, the absorption cross section σ is,

$$\sigma=\frac{32\pi^2}{\omega^5}|\mathcal{A}|^2=\frac{\kappa_{10}^2\omega^3}{32\pi}, \tag{24}$$

which agree with the σ of the quantum field theory and that of black 3-brane in supergravity.

3 The condition of QNM

Our new calculation method for D3-brane scattering problem give dilaton's wave functions. Then we can treat the D3-brane scattering problem as wave scattering. Now, we can also obtain the condition of QNM in D3-brane picture as usual wave scattering analysis by treating D3-brane as absorption body. In order to calculate QNM, wave function is summed up to all order, i.e,

$$\varphi = \varphi_0+\kappa_{10}^2\varphi_2+\cdots \tag{25}$$

$$= \varphi_0+ce^{-i\omega t}\sqrt{r}\left[\kappa_{10}^2\Sigma+(\kappa_{10}^2\Sigma)^2+(\kappa_{10}^2\Sigma)^3+\cdots\right]H_2^{(1)}(\omega r) \tag{26}$$

$$= ce^{-i\omega t}\sqrt{r}\left[\frac{1}{1-\kappa_{10}^2\Sigma}H_2^{(1)}(\omega r)+H_2^{(2)}(\omega r)\right] \tag{27}$$

This summation is just as a summation of 1PI Feynman diagrams to all order. Wave function can be normalized as reflection amplitude is equal to one. The normalized wave function φ_{nor} is,

$$\varphi_{nor} = ce^{-i\omega t}\sqrt{r}\left[H_2^{(1)}(\omega r)+(1-\kappa_{10}^2\Sigma)H_2^{(2)}(\omega r)\right] \tag{28}$$

$$\to c'e^{-i\omega t}\left[e^{i(\omega r-\frac{5}{4}\pi)}+(1-\kappa_{10}\Sigma)e^{-i(\omega r-\frac{5}{4}\pi)}\right] \quad (as\ r\to\infty) \tag{29}$$

So, the condition of QNM is no incidental waves,

$$1-\kappa_{10}^2\Sigma = 0 \tag{30}$$

$$1+\frac{\kappa_{10}^2\omega^8}{32\cdot 64\pi^3}+i\frac{\kappa_{10}\omega^8}{(64)^2\pi^4}\log\frac{\omega}{\Lambda} = 0 \tag{31}$$

The frequencies ω, which satisfy this equation, are QNM of D3-brane black hole.

4 Discussion

We obtain the condition of QNM of D3-brane to $\mathcal{O}(\kappa_{10}^2)$.

This condition is expected to agree with that of black 3-brane in supergravity. A scattering problem of massless scalar fields on black 3-brane background can be exactly solved in terms of Mathieu's functions, and the asymptotic form of them gives absorption probability [3]. It also gives the condition of QNM that are decaying modes of no incidental waves.

We can't solve the condition equation of QNM yet and don't compare two QNMs concretely here. Moreover, the fact that the effective parameter region of D-brane black holes is different with that of black branes makes it difficult to compare them. We leave this problem as future work.

References

[1] Igor R.Klebanov, Nucl. Phys. B496 (1997) 231.

[2] Steven S.Gubser et.al., Nucl. Phys. B526 (1998) 393.

[3] Steven S.Gubser, and Akikazu Hashimoto, hep-th/9805140.

Cosmology Based on Hořava-Witten Theory

Shinpei Kobayashi[1] and Kazuya Koyama[2]

Graduate School of Human and Environment Studies, Kyoto University, Yoshidanihonmatsucho, Sakyo-ku, Kyoto, 606-8501, Japan

Abstract

We perturbatively investigated the cosmological evolution of the compactified Hořava-Witten theory when the energy density of the perfect fluid on the brane is much smaller than the tension of the brane. We got the analog of the convensional Friedmann equation and the energy conservation condition on the brane. And we also found the equations for the radion and the bulk scalar field.

1 Introduction

It has been shown that the strongly coupled $E_8 \times E_8$ heterotic string theory can be identified as the eleven-dimensional limit of M-theory conpactified on an $S^1/\mathbb{Z}_2$ orbifold with a set of E_8 gauge supermultiplets on each ten-dimensional orbifold fixed plane [1], [2]. Witten has shown that is a consistent compactification of this M-theory limit on a deformed Calabi-Yau three-fold, which leads to a supersymmetric $\mathcal{N} = 1$ theory in four dimensions and he suggested that there is a substantial regime where the universe appears five-dimensional [3].

Motivated by this "compactified Hořava-Witten theory", Lukas *et al.* derived the five-dimensional effective action of it [4]. They showed that various fields would appear in the bulk and there are E_6 or E_8 matter on each brane. Using this action, they derived the static "vacuum" domain wall solution [5] and the cosmological "vacuum" solution [6].

By the way, the conventional four-dimensional cosomological evolution is usually driven by the matter in the universe. So we would like to put matter on each brane and investigate the cosmological evolution on the branes. Here, for simplicity, we replaced E_6 or E_8 matter with perfect fluid and we introduced the approximation such that the energy density of the perfect fluid on the brane is much smaller than the tension of the brane. Under this approximation we could derive the analog of the conventional Friedmann equation and the energy conservation condition perturbatively. Besides these equations, we also found the equation which determines the behavior of the radion. We are now investigating the profiles of the scale factor, the radion and the bulk scalar field.

The organization of this proceeding is as follows. In Sec.2, we review the setup of our model, derive the equations of motion and introduce the approximation to solve eqations perturbatively. In Sec.3, we give solutions for the background and the perturbation of the first order. And we also show the analog of the conventional Friedmann equation and the energy conservation condition. Sec. 4 is devoted to summary and future works.

[1] E-mail:shinpei@phys.h.kyoto-u.ac.jp
[2] E-mail:kazuya@phys.h.kyoto-u.ac.jp

2 A Model

Based on the action derived by Lukas *et al.* [4], we consider the following action,

$$\begin{aligned} S &= S_{bulk} + S_{brane}, \qquad (1)\\ S_{bulk} &= \frac{1}{2\kappa^2}\int d^5x\sqrt{-g_5}\left(R - \partial_M\phi\partial^M\phi - \frac{1}{3}e^{-2\sqrt{2}\phi}\sigma^2\right)\\ S_{brane} &= -\frac{\sqrt{2}}{\kappa^2}\int_{M_4^{(1)}}\sqrt{-g_4}e^{-\sqrt{2}\phi}\sigma + \int_{M_4^{(1)}}\sqrt{-g_4}e^{\sqrt{2}\phi}\mathcal{L}_m\\ &\quad + \frac{\sqrt{2}}{\kappa^2}\int_{M_4^{(2)}}\sqrt{-g_4}e^{-\sqrt{2}\phi}\sigma + \int_{M_4^{(2)}}\sqrt{-g_4}e^{\sqrt{2}\phi}\tilde{\mathcal{L}}_m. \end{aligned}$$

Here S_{bulk} is the action of the bulk, which includes the potential term and the bulk scalar field, which is called as a breathing mode of the Calabi-Yau volume. Next S_{brane} denotes the action of branes, where σ is the tension of a brane whose value is determined by the volume of Calabi-Yau manifold $\mathcal{L}_m, \tilde{\mathcal{L}}_m$ are the Lagrangian of perfect fluid on each brane, which can be rewritten We can rewritten by the energy density of perfect fluids as

$$\mathcal{L}_m = \Gamma\rho, \quad \tilde{\mathcal{L}}_m = \tilde{\Gamma}\tilde{\rho}. \qquad (2)$$

Finally, we introduce this type of metric,

$$ds^2 = e^{2\gamma(y,t)}dy^2 - e^{2\beta(y,t)}dt^2 + e^{2\alpha(y,t)}\delta_{ij}dx^idx^j. \qquad (3)$$

By using this action and metric, we can find the equations of motion for $\alpha(y,t), \beta(y,t), \gamma(y,t)$ and the bulk scalar $\phi(y,t)$.

Now we would like to solve these equations analitically, but it is difficult to solve them as you know in the case of the Randall-Sundrum model, so we introduce an approximation as follows,

$$\sigma \gg \kappa^2\rho_0, \qquad (4)$$

where ρ_0 is a value of ρ which is evaluated at some reference time. To rewrite the equations under this approximation, we define dimensionless variables as

$$\begin{aligned} Y &\equiv \sigma y \qquad (5)\\ T &\equiv \sqrt{\sigma\kappa^2\rho_0}\, t. \qquad (6) \end{aligned}$$

Now we can write down the equations of motion for $\alpha(y,t), \beta(y,t), \gamma(y,t)$ and $\phi(y,t)$ which explicitly represent the effect of the approximation as follows,
(y,y) :

$$\alpha'^2 + \alpha'\beta' - \varepsilon(\ddot{\alpha} + 2\dot{\alpha}' - \dot{\alpha}\dot{\beta})e^{2(\gamma-\beta)} = \frac{1}{6}\phi'^2 + \varepsilon\frac{1}{6}\dot{\phi}^2e^{2(\gamma-\beta)} - \frac{1}{18}e^{2(\gamma-\sqrt{2}\phi)}. \qquad (7)$$

(t,t) :

$$\begin{aligned} \alpha'' + 2\alpha' - \gamma'\alpha' - \varepsilon(\dot{\alpha}^2 + \dot{\gamma}\dot{\alpha})e^{2(\gamma-\beta)} &= -\frac{1}{6}\phi'^2 - \frac{1}{6}\dot{\phi}^2e^{2(\gamma-\beta)} - \frac{1}{18}e^{2(\gamma-\sqrt{2}\phi)}\\ &\quad + \frac{1}{3}\left(-\sqrt{2}e^{\gamma-\sqrt{2}\phi}\left[\delta(Y) - \delta(Y-R)\right] - \varepsilon e^{\gamma+\sqrt{2}\phi}\left[\frac{\rho}{\rho_0}\delta(Y) + \frac{\tilde{\rho}}{\rho_0}\delta(Y-R)\right]\right). \qquad (8) \end{aligned}$$

(i,j) :

$$\begin{aligned} &2\alpha'' - 2\gamma'\alpha' + 2\alpha'\beta' + 3\alpha'^2 + \beta'' + \beta'^2 - \beta'\gamma'\\ &\quad - \varepsilon(2\ddot{\alpha} + 2\dot{\gamma}\dot{\alpha} - 2\dot{\alpha}\dot{\beta} + 3\dot{\alpha}^2 + \ddot{\gamma} + \dot{\gamma}^2 - \dot{\beta}\dot{\gamma})e^{2(\gamma-\beta)}\\ &\quad = -\frac{1}{2}\phi'^2 + \varepsilon\frac{1}{2}\dot{\phi}^2e^{2(\gamma-\beta)} - \frac{1}{6}e^{2(\gamma-\sqrt{2}\phi)}\\ &\quad - \sqrt{2}e^{\gamma-\sqrt{2}\phi}\left[\delta(Y) - \delta(Y-R)\right] + \varepsilon e^{\gamma+\sqrt{2}\phi}\left[\frac{w\rho}{\rho_0}\delta(Y) + \frac{\tilde{w}\tilde{\rho}}{\rho_0}\delta(Y-R)\right]. \qquad (9) \end{aligned}$$

(y,t) :

$$\dot{\alpha}' - \dot{\gamma}\alpha' + \dot{\alpha}(\beta' - \alpha') = -\frac{1}{3}\dot{\phi}\phi'. \tag{10}$$

ϕ :

$$\phi'' + 3\alpha'\phi' + \beta'\phi' - \gamma'\phi' - \varepsilon(\ddot{\phi} + 3\dot{\alpha}\dot{\phi} - \dot{\beta}\dot{\phi} + \dot{\gamma}\dot{\phi})e^{2(\gamma-\beta)} + \frac{\sqrt{2}}{3}e^{2(\gamma-\sqrt{2}\phi)}$$
$$= 2e^{\gamma-\sqrt{2}\phi}[\delta(Y) - \delta(Y-R)] + \varepsilon e^{\gamma+\sqrt{2}\phi}\left[\frac{\Gamma\rho}{\rho_0}\delta(Y) + \frac{\tilde{\Gamma}\tilde{\rho}}{\rho_0}\delta(Y-R)\right]. \tag{11}$$

Here the prime and the dot denotes the derivative with respect to Y and T respcetively.

We would like to solve these equations perturbatively, so we expanded $\alpha(y,t), \beta(y,t), \gamma(y,t)$ and $\phi(y,t)$ as

$$\alpha(Y,T) = \alpha_{(0)}(Y,T) + \varepsilon\alpha_{(1)}(Y,T) + \varepsilon^2\alpha_{(2)}(Y,T) + \cdots, \tag{12}$$
$$\beta(Y,T) = \beta_{(0)}(Y,T) + \varepsilon\beta_{(1)}(Y,T) + \varepsilon^2\beta_{(2)}(Y,T) + \cdots, \tag{13}$$
$$\gamma(Y,T) = \gamma_{(0)}(Y,T) + \varepsilon\gamma_{(1)}(Y,T) + \varepsilon^2\gamma_{(2)}(Y,T) + \cdots, \tag{14}$$
$$\phi(Y,T) = \phi_{(0)}(Y,T) + \varepsilon\phi_{(1)}(Y,T) + \varepsilon^2\phi_{(2)}(Y,T) + \cdots. \tag{15}$$

If we substitute functions (12)- (15) into eqs.(7) -(11), we can get the equations for each order of ε.

3 Solutions

3.1 Solutions of the Equations of the order ε^0

We decomposed (12)-(15) by the order of ε, and we found the solutions of the equations of the order ε^0 (background solutions) as

$$\alpha_{(0)}(Y,T) = \frac{1}{2}\ln H(Y,T) + \hat{\alpha}(T), \tag{16}$$
$$\beta_{(0)}(Y,T) = \frac{1}{2}\ln H(Y,T) + \hat{\beta}(T), \tag{17}$$
$$\gamma_{(0)}(Y,T) = 2\ln H(Y,T) + \sqrt{2}\hat{\phi}(T) + \ln d(T), \tag{18}$$
$$\phi_{(0)}(Y,T) = \frac{3\sqrt{2}}{2}\ln H(Y,T) + \hat{\phi}(T), \tag{19}$$

where,

$$H(Y,T) \equiv -\frac{\sqrt{2}}{3}d(T)\,|Y| + c_0. \tag{20}$$

Here $\hat{\alpha}(T), \hat{\beta}(T), \hat{\phi}(T)$ and $d(T)$ are arbitrary functions which only have time-dependence. These time-dependenet solutions are different from the static domain wall solutions derived by Lukas et al [5]. $\hat{\alpha}(T)$ and $d(T)$ correspond to the scale factor and the radion, respectively. The radion can be interpreted as the distance between two branes, so it will be important quantity to investigate the stability of double-brane system.

Please note that we can not determine the behavior of $\hat{\alpha}(T), \hat{\beta}(T), \hat{\phi}(T)$ and $d(T)$ from the equations of the order ε^0 due to the approximation we are now using. We are trying to consider cosmological evolution driven by the perfect fluid on the brane, not by the motion of the bulk scalar field ϕ. And at the same time, we are assuming that the energy density of the perfect fluid is very small. Consequently, at the background level, we can not see time-evolution of this system. We will be able to determine time-evolution by the equations of the order of ε.

3.2 Solutions of the Equations of the order ε^1

In this subsection, we show the solutions for the equations of the order ε^1. Substituting the background solutions (16)-(19) into the equations of the order ε^1, we found that there are the following type of particular solutions,

$$\alpha_{(1)}(Y,T) = f_\alpha(T)H^5(Y,T) + g_\alpha(T)H^4(Y,T)Y + h_\alpha(T)H^3(Y,T)Y^2, \tag{21}$$
$$\beta_{(1)}(Y,T) = f_\beta(T)H^5(Y,T) + g_\beta(T)H^4(Y,T)Y + h_\beta(T)H^3(Y,T)Y^2, \tag{22}$$
$$\phi_{(1)}(Y,T) = f_\phi(T)H^5(Y,T) + g_\phi(T)H^4(Y,T)Y + h_\phi(T)H^3(Y,T)Y^2, \tag{23}$$

where $f_\alpha, f_{beta}, \cdots, h_\phi$ are time-dependent functions whose behavior is determined by $\hat{\alpha}, \hat{\beta}, \hat{\phi}$ and d.

From these particular solutions, we can derive the equations which govern the evolution of $\hat{\alpha}, \hat{\beta}, \hat{\phi}$ as follows,

$$\ddot{\hat{\alpha}} + 2\dot{\hat{\alpha}}^2 + \frac{1}{6}\dot{\hat{\phi}}^2 - \dot{\hat{\alpha}}\dot{\hat{\beta}} = \frac{\sqrt{2}}{36}c(1 - 3w - 6\Gamma)\frac{\rho}{\rho_0}, \tag{24}$$

$$\dot{\hat{\alpha}}^2 + \sqrt{2}\dot{\hat{\alpha}}\dot{\hat{\phi}} - \frac{1}{6}\dot{\hat{\phi}}^2 = \frac{2\sqrt{2}}{9}c\frac{\rho}{\rho_0}, \tag{25}$$

$$2\ddot{\hat{\alpha}} + 2\sqrt{2}\dot{\hat{\alpha}}\dot{\hat{\phi}} + 3\dot{\hat{\alpha}}^2 + \sqrt{2}\ddot{\hat{\phi}} + \frac{5}{2}\dot{\hat{\phi}}^2 - \dot{\hat{\alpha}}\dot{\hat{\beta}} - \sqrt{2}\dot{\hat{\beta}}\dot{\hat{\phi}} = -\frac{2\sqrt{2}}{3}cw\frac{\rho}{\rho_0}, \tag{26}$$

$$\ddot{\hat{\phi}} + 3\dot{\hat{\alpha}}\dot{\hat{\phi}} + \sqrt{2}\dot{\hat{\phi}}^2 - \dot{\hat{\beta}}\dot{\hat{\phi}} = \frac{1}{6}c(1 - 3w + 2\Gamma)\frac{\rho}{\rho_0}. \tag{27}$$

And if we take the T derivative of eq.(25) and use eqs.(24)-(27), the analog of the conventional energy consevation condition can be obtained as

$$\dot{\rho} + 3(1+w)\rho\dot{\hat{\alpha}} = -\sqrt{2}(1+\Gamma)\rho\dot{\hat{\phi}} - 2\rho\dot{\hat{\beta}}. \tag{28}$$

Beside these equations, we got the equations for the radion d and the bulk scalar ϕ by comparing the junciton conditions at $Y = 0$ with $Y = R$ as

$$\left(\dot{\hat{\alpha}} - \frac{\sqrt{2}}{12}\frac{R}{\tilde{c}}\dot{d}\right)\dot{d} = \frac{1}{6}\left(c\frac{\rho}{\rho_0} + \tilde{c}\frac{\tilde{\rho}}{\rho_0}\right)\frac{\tilde{c}}{R} \tag{29}$$

$$\ddot{d} + \left(2\sqrt{2}\dot{\hat{\phi}} - \dot{\hat{\beta}} - \frac{7\sqrt{2}}{12}\frac{R}{\tilde{c}}\dot{d}\right)\dot{d} = -\frac{1}{6}\left[c(3w+2)\frac{\rho}{\rho_0} + \tilde{c}(3\tilde{w}+2)\frac{\tilde{\rho}}{\rho_0}\right]\frac{\tilde{c}}{R} \tag{30}$$

$$\left(\dot{\hat{\phi}} - \frac{\sqrt{2}}{6}\dot{\hat{\beta}} - \frac{1}{2}\frac{R}{\tilde{c}}\dot{d}\right)\dot{d} = \frac{\sqrt{2}}{2}\left(c\Gamma\frac{\rho}{\rho_0} + \tilde{c}\tilde{\Gamma}\frac{\tilde{\rho}}{\rho_0}\right)\frac{\tilde{c}}{R} \tag{31}$$

If we set $d(T) = const.$, we find that the following conditions are needed between each perfect fluid.

$$\tilde{\rho} = -\frac{c}{\tilde{c}}\rho, \tilde{w} = w, \ \tilde{\Gamma} = \Gamma. \tag{32}$$

These conditions strongly restrict what kind of perfect fluid can be allowed to exist on the branes.

Behavior of the radion and the bulk scalar field in general case is under investigation.

4 Summary and Future Works

We consider the cosmological model in the context of the compactified Hořava-Witten theory. Under the approximation $\sigma \gg \kappa^2\rho_0$, we derived the equations which describes the cosmological evolution on the brane. Consequently we found that the analog of the conventional Friedmann equation and energy consevation condition in this system.

But note that we use BPS solution as the background solution here. If we use non-BPS solution, we may not be able to derive the Friedmann-like equation and/or the energy conservation condition so easily as in this case. We have to consider both BPS and non-BPS brane for generality.

When we consider the special case $d = const.$, we found that strong conditions $\tilde{\rho} = -\frac{c}{\tilde{c}}\rho, \tilde{w} = w, \tilde{\Gamma} = \Gamma$ are needed. Behavior of the radion d and the bulk scalar ϕ in general case is under investigation. Through this anaysis of the radion and the bulk scalar, we have to verify whether we can reproduce the conventional four-dimensional cosmology. Because, if the bulk scalar is left at sufficiently late time, there exist the possibility that the value of the four-dimensional gravitaional constant would be changed by the bulk scalar.

And we also have to investigate the stability of this system and the confinement of the gravity on the brane to compare this model with Randall-Sundrum ones.

Finally, we would like to include other fields in the bulk and analyze how we should construct the cosmological model with other fields.

References

[1] P. Horava and E. Witten, Nucl. Phys. **B460** (1996) 506.

[2] P. Horava and E. Witten, Nucl. Phys. **B475** (1996) 94.

[3] E. Witten, Nucl. Phys. **B471** (1996) 135.

[4] A. Lukas, B. A. Ovrut, K. S. Stelle and D. Waldram, Nucl. Phys. **B552** (1999) 246.

[5] A. Lukas, B. A. Ovrut, K. S. Stelle and D. Waldram, Phys. Rev. **D59** (1999) 086001.

[6] A. Lukas, B. A. Ovrut, K. S. Stelle and D. Waldram, Phys. Rev. **D60** (1999) 086001.

[7] H. S. Reall, Phys. Rev. **D59** (1999) 103506.

[8] P. M. Cowdall, H. Lü, C. N. Pope, K. S. Stelle and P. K. Townsend, Nucl. Phys. **B 486** (1997) 49.

[9] U. Ellewanger, hep-th/0001126.

New Einstein-Hilbert Type Action for Unification of Spacetime and Matter

Kazunari Shima,[1] Motomu Tsuda[2]

Laboratory of Physics, Saitama Institute of Technology, Okabe-machi, Saitama 369-0293, Japan

Abstract

Based upon the geometrical arguments of nonlinear SUSY in curved higher symmetric (SGM) space-time a new Einstein-Hilbert type action of superon-graviton model(SGM) for space-time and matter is obtained. SGM action is invariant under [global NL SUSY] ⊗ [local GL(4, R)] ⊗ [local Lorentz] ⊗ [global SO(N)].
Some characteristic structures of the gravitational coupling of superons(Nambu-Goldstone fermion) are manifested with some details of the calculations. SGM cosmology is discussed briefly.

1 Introduction

Supersymmetry(SUSY)[1, 2] may be the most promissing gauge symmetry beyond SM, especially for the unification of space-time and matter.
In the previous paper [3] we have introduced a new fundamental constituent with spin-1/2 *superon* and proposed *superon-graviton model*(SGM) equippted with SUSY as a model for unity of space-time and matter. In SGM, the fundamental entities of nature are the graviton with spin-2 and a quintet of superons with spin-1/2. They are the elementary gauge fields corresponding to the local GL(4,R) and the global nonlinear supersymmetry(NL SUSY) with a global SO(10), respectively. Interestingly, the quantum numbers of the superon-quintet are the same as those of the fundamental representation $\underline{5}$ of the matter multiplet of SU(5) GUT[4]. All observed elementary particles including gravity are assigned to a single irreducible massless representation of SO(10) super-Poincaré(SP) symmetry and reveals a remarkable potential for the phenomenology, e.g. they may explain naturally the three-generations structure of quarks and leptons, the stability of proton, various mixings, ..etc[3]. And in SGM except graviton they are supposed to be the (massless) eigenstates of superons of SO(10) SP symmetry [5] of space-time and matter. The uniqueness of N=10 among all SO(N) SP is pointed out. The arguments are group theoretical so far.
In order to obtain the fundamental action of SGM which is invariant at least under local GL(4,R), local Lorentz, global NL SUSY transformations and global SO(10), we have performed the similar geometrical arguments to Einstein genaral relativity theory(EGRT) in the SGM space-time, where the tangent (Riemann-flat) Minkowski space-time is specified by the coset space SL(2,C) coordinates (corresponding to Nambu-Goldstone(N-G) fermion) of NL SUSY of Volkov-Akulov(V-A)[2] in addition to the ordinary Lorentz SO(3,1) coordinates[3], which are locally homomorphic groups [6]. As shown in Ref.[6] the SGM action for the unified SGM space-time is naturally the analogue of Einstein-Hilbert(E-H) action of GR and has the similar concise expression. And interestingly it may be regarded as a kind of a generalization of Born-Infeld action[8]. (The similar systematic arguments are applicable to spin 3/2 N-G case.[7]) As discussed later SGM action may be regarded as an extension of E-H action and Born-Infeld action[8].
In this article, after a brief review of SGM for the self contained arguments, we see some characteristic structures of our model. Finally a potential cosmology, especially the birth of the universe is mentioned briefly.

[1] E-mail:shima@sit.ac.jp
[2] E-mail:tsuda@sit.ac.jp

2 Fundamental action of SGM

In Ref.[6], SGM space-time is defined as the space-time whose tangent(flat) space-time is specified by SO(1,3) Lorentz coordinates x^a and the coset space SL(2,C) coordinates ψ of NL SUSY of Volkov-Akulov(V-A)[2]. The unified vierbein $w^a{}_\mu$ and the unified metric $s_{\mu\nu}(x) \equiv w^a{}_\mu(x) w_{a\nu}(x)$ of SGM space-time are defined by generalizing the NL SUSY invariant differential forms of V-A to the curved space-time[6]. SGM action is given as follows[6]

$$L_{SGM} = -\frac{c^3}{16\pi G}|w|(\Omega + \Lambda), \tag{1}$$

$$|w| = det w^a{}_\mu = det(e^a{}_\mu + t^a{}_\mu), \quad t_a{}^\mu = \frac{\kappa}{2i}\sum_{j=1}^{10}(\bar{\psi}^j \gamma_a \partial^\mu \psi^j - \partial^\mu \bar{\psi}^j \gamma_a \psi^j), \tag{2}$$

where $\kappa(= \kappa_{V-A})$ is an arbitrary constant up now with the dimension of the fourth power of length, $e^a{}_\mu$ and $\psi^j (j = 1, 2, ..10)$ are the fundamental elememtary fields of SGM, i.e. the vierbein of Einstein general relativity theory(EGRT) and the superons of Nambu-Goldstone(N-G) fermion of NL SUSY of Volkov-Akulov[2], respectively. [3] Λ is a cosmological constant which is necessary for SGM action to reduce to V-A model with the first order derivative terms of the superon in the Riemann-flat space-time. Ω is a unified scalar curvature of SGM space-time analogous to the Ricci scalar curvature R of EGRT. SGM action (1) is invariant under the following new SUSY transformations

$$\delta\psi^i(x) = \zeta^i + i\kappa(\bar{\zeta}^j \gamma^\rho \psi^j(x))\partial_\rho \psi^i(x), \tag{3}$$

$$\delta e^a{}_\mu(x) = i\kappa(\bar{\zeta}^j \gamma^\rho \psi^j(x)) D_{[\rho} e^a{}_{\mu]}(x), \tag{4}$$

where $\zeta^i, (i = 1, ..10)$ is a constant spinor parameter, $D_{[\rho} e^a{}_{\mu]}(x) = D_\rho e^a{}_\mu - D_\mu e^a{}_\rho$ and D_μ is a covariant derivative containing a symmetric affine connection. The explicit expression of Ω is obtained by just replacing $e^a{}_\mu(x)$ in Ricci scalar R of EGRT by the unified vierbein $w^a{}_\mu(x) = e^a{}_\mu + t^a{}_\mu$ of the SGM curved space-time, which gives the gravitational interaction of $\psi(x)$ invariant under (3) and (4). The invariance can be easily undestood by observing that under (3) and (4) the new vierbein $w^a{}_\mu(x)$ and the new metric $s_{\mu\nu}(x)$ have general coordinate transformations [6].

$$\delta_\zeta w^a{}_\mu = \xi^\nu \partial_\nu w^a{}_\mu + \partial_\mu \xi^\nu w^a{}_\nu, \tag{5}$$

$$\delta_\zeta s_{\mu\nu} = \xi^\kappa \partial_\kappa s_{\mu\nu} + \partial_\mu \xi^\kappa s_{\kappa\nu} + \partial_\nu \xi^\kappa s_{\mu\kappa}, \tag{6}$$

where $\xi^\rho = i\kappa(\bar{\zeta}^j \gamma^\rho \psi^j(x))$. The overall factor of SGM action is fixed to $\frac{-c^3}{16\pi G}$, which reproduces E-H action of GR in the absence of superons(matter). Also in the Riemann-flat space-time, i.e. $e^a{}_\mu(x) \to \delta^a{}_\mu$, it reproduce V-A action of NL SUSY[2] with $\kappa^{-1}{}_{V-A} = \frac{c^3}{16\pi G}\Lambda$ in the first order derivative terms of the superon. Therefore our model(SGM) predicts a (small) non-zero cosmological constant, provided $\kappa_{V-A} \sim O(1)$, and posesses two mass scales. Furthermore it fixes the coupling constant of superon(N-G fermion) with the vacuum to $(\frac{c^3}{16\pi G}\Lambda)^{\frac{1}{2}}$ (from the low energy theorem viewpoint), which may be relevant to the birth (of the matter and Riemann space-time) of the universe.

It is interesting that our action is the vacuum (matter free) action in SGM space-time as read off from (1) but gives in ordinary Riemann space-time the E-H action with matter(superons) accompanying the spontaneous supersymmetry breaking.

The commutators of new SUSY transformations induces the generalized general coordinate transformations

$$[\delta_{\zeta_1}, \delta_{\zeta_2}]\psi = \Xi^\mu \partial_\mu \psi, \tag{7}$$

$$[\delta_{\zeta_1}, \delta_{\zeta_2}]e^a{}_\mu = \Xi^\rho \partial_\rho e^a{}_\mu + e^a{}_\rho \partial_\mu \Xi^\rho, \tag{8}$$

[3] We use the Minkowski tangent space metric $\frac{1}{2}\{\gamma^a, \gamma^b\} = \eta^{ab} = (+, -, -, -)$ and $\sigma^{ab} = \frac{1}{4}[\gamma^a, \gamma^b]$. Latin $(a, b, ..)$ and Greek $(\mu, \nu, ..)$ are the indices for local Lorentz and general coordinates, respectively.

where Ξ^μ is defined by

$$\Xi^\mu = 2ia(\bar{\zeta}_2\gamma^\mu\zeta_1) - \xi_1^\rho\xi_2^\sigma e_a{}^\mu(D_{[\rho}e^a{}_{\sigma]}). \tag{9}$$

We have shown that our action is invariant at least under[9]

$$[\text{global NL SUSY}] \otimes [\text{local GL}(4,\text{R})] \otimes [\text{local Lorentz}] \otimes [\text{global SO(N)}], \tag{10}$$

which is isomorphic to N=10 extended (global SO(10)) SP symmetry through which SGM reveals the spectrum of all observed particles in the low energy[5]. In contrast with the ordinary SP SUSY, new SUSY may be regarded as a square root of a generalized GL(4,R). The usual local GL(4,R) invariance is obvious by the construction.

The simple expression (1) invariant under the above symmetry may be universal for the gravitational coupling of N-G fermion, for by performing the parallel arguments we obtain the same expression for the gravitational interaction of the spin-3/2 N-G fermion[7].

Now to clarify the characteristic features of SGM we focus on N=1 SGM for simplicity without loss of generality and write down the action explicitly in terms of $t^a{}_\mu$(or ψ) and $g^{\mu\nu}$(or $e^a{}_\mu$). We will see that the graviton and superons(matter) are complementary in SGM and contribute equally to the curvature of SGM space-time. Contrary to its simple expression (1), it has rather complicated and rich structures. By requiring that the unified action of SGM space-time should reduce to V-A in the flat space-time which is specified by x^a and $\psi(x)$ and that the graviton and superons contribute equally to the unified curvature of SGM space-time, it is natural to consider that the unified vierbein $w^a{}_\mu(x)$ and the unified metric $s^{\mu\nu}(x)$ of unified SGM space-time are defined through the NL SUSY invariant differential forms ω^a of V-A[2] as follows:

$$\omega^a = w^a{}_\mu dx^\mu, \tag{11}$$

$$w^a{}_\mu(x) = e^a{}_\mu(x) + t^a{}_\mu(x), \tag{12}$$

where $e^a{}_\mu(x)$ is the vierbein of EGRT and $t^a{}_\mu(x)$ is defined by $t^a{}_\mu(x) = i\kappa\bar{\psi}\gamma^a\partial_\mu\psi$. We can easily obtain the inverse $w_a{}^\mu$ of the vierbein $w^a{}_\mu$ in the power series of $t^a{}_\mu$ as follows, which terminates with t^4(for 4 dimensional space-time):

$$w_a{}^\mu = e_a{}^\mu - t^\mu{}_a + t^\rho{}_a t^\mu{}_\rho - t^\rho{}_a t^\sigma{}_\rho t^\mu{}_\sigma + t^\rho{}_a t^\sigma{}_\rho t^\kappa{}_\sigma t^\mu{}_\kappa. \tag{13}$$

Similarly a new metric tensor $s_{\mu\nu}(x)$ and its inverse $s^{\mu\nu}(x)$ are introduced in SGM curved space-time as follows:

$$\begin{aligned} s_{\mu\nu}(x) &\equiv w^a{}_\mu(x)w_{a\nu}(x) = w^a{}_\mu(x)\eta_{ab}w^b{}_\nu(x) \\ &= g_{\mu\nu} + t_{\mu\nu} + t_{\nu\mu} + t^\rho{}_\mu t_{\rho\nu}, \end{aligned} \tag{14}$$

and

$$\begin{aligned} s^{\mu\nu}(x) &\equiv w_a{}^\mu(x)w^{a\nu}(x) \\ &= g^{\mu\nu} - t^{\mu\nu} - t^{\nu\mu} + t^{\rho\mu}t^\nu{}_\rho + t^{\rho\nu}t^\mu{}_\rho + t^{\mu\rho}t^\nu{}_\rho + \ldots. \end{aligned} \tag{15}$$

We can easily show $w_a{}^\mu w_{b\mu} = \eta_{ab}$, $s_{\mu\nu}w_a{}^\mu w_b{}^\nu = \eta_{ab}$. It is obvious from the above general covariant arguments that (1) is invariant under the ordinaly GL(4,R) and under (3) and (4).

By using (12), (13), (14) and (15) we can express SGM action (1) in terms of $e^a{}_\mu(x)$ and $\psi(x)$, which describes explicitly the fundamental interaction of graviton with superons. The action can be expanded straightforwardly in terms of the power series of κ (or $t^a{}_\mu$) as

$$\begin{aligned} L_{SGM} = &-\frac{c^3\Lambda}{16\pi G}e|w_{V-A}| - \frac{c^3}{16\pi G}eR + \frac{c^3}{16\pi G}e\big[\,2t^{(\mu\nu)}R_{\mu\nu} + \ldots \\ &-2(t^\mu{}_\rho t^{\rho\nu} + t^\nu{}_\rho t^{\rho\mu} + t^{\mu\rho}t^\nu{}_\rho)R_{\mu\nu} - t^{(\mu\sigma)}t^{(\nu\rho)}R_{\mu\nu\rho\sigma} + \ldots \\ &+ \{O(t^3)\} + \{O(t^4)\} + \ldots + \{O(t^{10})\})\big], \end{aligned} \tag{16}$$

where $e = dete^a{}_\mu$, $t^{(\mu\nu)} = t^{\mu\nu} + t^{\nu\mu}$, $t_{(\mu\nu)} = t_{\mu\nu} + t_{\nu\mu}$, and $|w_{V-A}| = detw^a{}_b$ is the flat space V-A action[2] containing up to $O(t^4)$ and R and $R_{\mu\nu}$ are the Ricci curvature tensors of GR. In Ref.[10], we have carried

out the detailed and complete expansion SGM action (in two dimensional space-time) in terms of $e^a{}_\mu(x)$ and $\psi^j(x)$ both from the affine connection formalism and from the spin connection formalism.
Remarkably the first term of (16) can be regarded a s a space-time dependent cosmological term and reduces to V-A action [2] with $\kappa_{V-A}{}^{-1} = \frac{c^3}{16\pi G}\Lambda$ in the Riemann-flat $e_a{}^\mu(x) \to \delta_a{}^\mu$ space-time. The second term of (16) is the familiar E-H action of GR. These expansions show the complementary relation of graviton and (the stress-energy tensor of) superons. The existence of (in the Riemann-flat space-time) NL SUSY invariant terms with the (second order) derivatives of the superons beyond V-A model are manifested. For example, the lowest order of such terms appear in $O(t^2)$ and have the following expressions (up to the total derivative terms)

$$+\epsilon^{abcd}\epsilon_a{}^{efg}\partial_c t_{(be)}\partial_f t_{(dg)}. \tag{17}$$

The existence of such derivative terms in addition to the original V-A model are already pointed out and exemplified in part in [11]. Note that (17) vanishes in 2 dimensional space-time.

Here we just mention that we can consider two types of the flat space in SGM, which are not equivalent. One is SGM-flat, i.e. $w_a{}^\mu(x) \to \delta_a{}^\mu$, space-time and the other is Riemann-flat, i.e. $e_a{}^\mu(x) \to \delta_a{}^\mu$, space-time, where SGM action reduces to $-\frac{c^3\Lambda}{16\pi G}$ and $-\frac{c^3\Lambda}{16\pi G}|w_{V-A}| - \frac{c^3}{16\pi G}(\textit{derivative terms})$, respectively. Note that SGM-flat space-time may allow Riemann space-time, e.g. $t_a{}^\mu(x) \to -e_a{}^\mu + \delta_a{}^\mu$ realizes Riemann space-time *and* SGM-flat space-time. The cosmological implications are mentioned in the discussions.

3 Discussions

We have shown that contrary to its simple expression (1) in unified SGM space-time the expansion of SGM action posesses very complicated and rich structures describing as a whole(not order by order) the graviton-superon interactions (see also Ref.[10]). As mentioned above SGM action is remarkably a free action of E-H type action in unified SGM space-time, the various familiar classical exact solutions of GR may be reinterpreted as those of SGM($w_a{}^\mu(x)$ and metric $s^{\mu\nu}(x)$).

Concerning the abovementioned two inequivalent flat-spaces (i.e. the vacuum of the gravitational energy) of SGM action we can interprete them as follows.

SGM action (1) written by the vierbein $w_a{}^\mu(x)$ and metric $s^{\mu\nu}(x)$ of SGM space-time is invariant under (besides the ordinary local GL(4,R)) the general coordinate transformation[9] with a generalized parameter $i\kappa\bar{\zeta}\gamma^\mu\psi(x)$ (originating from the global supertranslation [2] $\psi(x) \to \psi(x) + \zeta$ in SGM space-time). As proved for E-H action of GR[12], the energy of SGM action of E-H type is expected to be positive (for positive Λ). Regarding the scalar curvature tensor Ω for the unified metric tensor $s^{\mu\nu}(x)$ as an analogue of the Higgs potential for the Higgs scalar, we can observe that (at least the vacuum of) SGM action, (i.e. SGM-flat $w^a{}_\mu(x) \to \delta^a{}_\nu$ space-time,) which allows Riemann space-time and has a positive energy density with the positive cosmological constant $\frac{c^3\Lambda}{16\pi G}$ indicating the spontaneous SUSY breaking, is unstable (,i.e. degenerates) against the supertransformation (3) and (4) with the global spinor parameter ζ in SGM space-time and breaks down spontaneously to Riemann space-time

$$w^a{}_\mu(x) = e^a{}_\mu(x) + t^a{}_\mu(x), \tag{18}$$

with N-G fermions *superons* corresponding to

$$\frac{superGL(4,R)}{GL(4,R)}. \tag{19}$$

(Note that SGM-flat space-time allows Riemann space-time.) Remarkably the observed Riemann space-time of EGRT and matter(superons) appear simultaneously from (the vacuum of) SGM action by the spontaneous SUSY breaking.

The analysis of the structures of the vacuum of Riemann-flat space-time (described by N=10 V-A action with derivative terms similar to (17)) plays an important role to linearlize SGM and to derive SM as the low energy effective theory, which remain to be challenged. The linearlization of the flat-space

N=1 V-A model was already carried out[13, 14]. The linearlization of N=2 V-A model is extremely important from the physical point of view, for it gives a new mechanism generating a (U(1)) gauge field of the linearlized (effective) theory [15]. In our case of SGM the algebra(gauge symmetry) should be changed to broken SO(10) SP(broken SUGRA [16])symmetry by the linearlization which is isomorphic to the initial one (10). The systematic and generic arguments on the relation of linear and nonlinear SUSY are already investigated[17].

Besides the composite picture of SGM it is interesting to consider (elementary field) SGM with the extra dimensions and their compactifications. The compactification of $w^A{}_M = e^A{}_M + t^A{}_M, (A, M = 0, 1, ..D-1)$ produces rich spectrum of particles and (hidden) internal symmetries and may give a new framework for the unification of space-time and matter.

References

[1] J. Wess and B. Zumino, Phys. Lett. **B49** (1974) 52.
SUSY was found independently from the different motivations.
Y.A. Golfand and E.S. Likhtman, JET. Lett. **13** (1971) 323.

[2] D.V. Volkov and V.P. Akulov, Phys. Lett. **B46** (1973) 109.

[3] K. Shima, European Phys. J. **C7** (1999) 341.

[4] H. Georgi and S. L. Glashow, Phys. Rev. Lett. **32** (1974) 32.

[5] K. Shima, Z. Phys. **C18** (1983) 25.

[6] K. Shima, Phys. Lett. **B501** (2001) 237.

[7] K. Shima and M. Tsuda, Phys. Lett. **B521** (2001) 67.

[8] M. Born and L. Infeld, Proc. Roy. Soc.(London) **A144** (1934) 425.

[9] K. Shima and M. Tsuda, Phys. Lett. **B507** (2001) 260.

[10] K. Shima and M. Tsuda, *On Einstein-Hilbert Type Action of Superon-Graviton Model(SGM)*, hep-th/0110102.

[11] S. Samuel and J. Wess, Nucl. Phys. **B221** (1983) 153.

[12] The positive definitness of Einstein-Hilbert action was proved by
E. Witten, Commun. Math. Phys. **80** (1981) 381.

[13] M. Roček, Phys. Rev. Lett. **41** (1978) 451.
E. A. Ivanov and A.A. Kapustnikov, J. Phys. (1982) 167.
T. Uematsu and C.K. Zachos, Nucl. Phys. **B201** (1982) 254.
J. Wess, Karlsruhe University preprint(Festschrift for J. Lopszanski, December,1982).

[14] K. Shima, Y. Tanii and M. Tsuda, Phys. Lett. **B525** (2002) 183.

[15] K. Shima, Plenary talk at the Fourth International Conference on Symmetry in Nonlinear Mathematical Physics, July 7-14, 2001, Kyiv, Ukraine. To appear in the Proceeding.

[16] S. Deser and B. Zumino, Phys. Lett. **B62** (1976) 335.
D. Z. Freedman, P. van Nieuwenhuisen and S. Ferrara, Phys. Rev. **D13** (1976) 3214.

[17] E. A. Ivanov and A.A. Kapustnikov, J. Phys. (1978) 2375.
J. Wess and J. Baggar, *Supersymmetry and Supergravity*, 2nd edition (Princeton University Press 1992).